Understanding the role of Amyloid Beta and Tau protein in neuronal vulnerability in models of sporadic Alzheimer's disease



Féodora Louise Bertherat

New College

University of Oxford

A thesis submitted for the degree of

Doctor of Philosophy

Michaelmas 2025

To my grandmother, Omami.

Acknowledgments

First, I would like to thank Richard, Becky, Nora and Sally for your supervision. Richard, thank you for welcoming me in your lab, and for all the support and advice throughout my PhD. Nora, thank you for agreeing to supervise me despite your move to Spain to start your own group, and for making the tau PFFs. I am very grateful for Bryan, who whilst having a newborn and writing his thesis, taught me how to culture neurons and work with the DFP cell lines. You were very patient with me and have remained available for any questions all the way from Singapore through this whole process. Most importantly, I can't believe how lucky I was that Becky took me under her wing halfway though my PhD. You've been such an wonderful supervisor, and have not only helped me become a better scientist, you've also been an incredible moral support during very hard times. I am forever grateful for all you've done for me.

I'd like to thank the Fondation Professeur Placide Nicod for funding my PhD studentship. This has been an incredible opportunity that would not have been possible without your support. Thank you as well to Alzheimer's Research UK and to the Department of Physiology, Anatomy and Genetics for travel grants which have allowed me to present my work at several international conferences.

I am immensely thankful and indebted to the participants of the Deep and Frequent Phenotyping pilot cohort. Thank you for contributing your time, donating your cells, and going through many, sometimes painful, clinical tests, which have made my research possible and will, hopefully, meaningfully advance dementia research.

I am grateful for Zameel Cader and Noel Buckley who provided invaluable advice during my Transfer of Status and Confirmation of Status, and whose feedback has given me direction and guidance throughout my project.

Thank you to collaborators for helping me along the way: to Dr. Anne Hedegaard

for your help with the DFP iPSCs, and to Helen Rowland for all the advice and help with the DFP neurons.

I have been extremely lucky to be in a lab filled with kind, smart, helpful colleagues, and want to thank all of you for making my work environment a welcoming and friendly one. Thank you to Mari, Rachel, Johanna, Kaitlyn, Billy, Brent, Fangjia, Parnaz, Kaitlyn, Kalina, Naroa, Sandor, Sarah F, Millie, Paula, Iona and Hend for helping me, answering my questions and teaching me how to do things around the lab. I would like to particularly thank Ben and Pete for the help you provided me with all things RNA-seq analysis. Ben, thank you for always taking the time to answer with care and detail, even after my 100th question. Thank you Helen for you help with the Tau RNA sequencing, and for my first experience supervising a student; you taught me a lot. I'd like to thank Ajantha, Rachel, Mari, Billy, Kaitlyn, Sophie F, Iona for your moral support and pep talks; I am grateful to have become friends along the way. Mari, Billy, Harry and Kaitlyn thank you for being my climbing buddies, I appreciate all of you hugely for making the lab a place I get to hang out with friends as well as work. I especially want to thank you, Ajantha for being an incredible friend and colleague throughout these 4 years; thank you for the MANY times you fed my cells, helped me with experimental questions and provided invigorating conversations. I have loved dissecting Ezra Klein's latest episodes and discussing all things politics. Finally, I am very grateful for Sarah P., Charlie, Lorraine and all the RAs, without whom the lab would fall apart. Sarah P, thank you so much for everything you've done for me during my time here. I can't emphasise enough how critical you are to us being able to do our work, and you always do it with patience and kindness.

I'd also like to thank Angela and Uwe for welcoming me in your lab, and to Andressa for supervising a clueless undergrad all these years ago at BU. You gave me my first taste of academic research and you are the reason I wanted to pursue a PhD.

I have many friends here who have made my time in Oxford incredibly special, and want to thank Emma, Nina, Annie, Lucille, Michelle, Hannah, Ziggy, Alyssa, Sophie, Maxime, Lili, Ollie, JB, Ian and so many others. Special shout out to Alyssa– meeting you during my MSc was the highlight of my first year in Oxford, and I am so grateful that we've become such close friends since then. Hannah, Ziggy and Sophie

thank you for being the best housemates and friends; you've seen me during my worst moments of this PhD, and have cheered me on and supported me every step of the way. I truly couldn't have done it without you. Sophie, I'm so happy we met at the tennis social our first year in Oxford, and for becoming my tennis buddy and close friend along the way. Hannah and Ziggy, I am so grateful for your friendship in the last 4 years and for convincing me to move in with you in Observatory Street!! It made my time here so much more joyful and made me feel like I had a home away from home. To Maria, I'm so happy to have knocked on your door on my first day at BU, you've been one of my best friends ever since, and I'm so glad to have you in my life, even if from so far away (P.S. please move to London). To my best friends, Camille and Claudia, thank you for consistently being the most supportive and loving friends since we were 10 years old!!! Having you with me in the UK during this time was invaluable, and I couldn't be more grateful to have you in my life.

But most importantly, I'd like to thank my family. Thank you to my grandmother, Bonne Maman, who as a healthy 95 year old, kept me on track by asking me to "find a cure before I get it". To my sisters Alice, Louise and Constance thank you for being the best sisters one could ever ask for, and thank you for listening to me rant about my PhD for 4 years straight. How lucky am I to have 3 ready-made best friends to grow up with?? Alice, Constance and Annick, moving in with you during my write up was the best decision I could have made; thank you for cooking for me, dealing with my bad moods and mental breakdowns during these last few months.

To my parents: Mami et Papi, merci d'avoir été les meilleurs parents qu'on puisse souhaiter. Je ne pourrai jamais vous remercier assez de m'avoir permis de poursuivre ces études, de m'avoir toujours encouragée à travailler, de m'avoir soutenue, et de m'avoir laissé faire mes propres choix. De Boston à Oxford, en passant par New York, je n'aurais jamais pu avoir ce parcours et ces opportunités sans vous. Je vous aime fort.

Abstract

Alzheimer's disease (AD) is a neurodegenerative disease, and it is the most common form of dementia. AD is characterised by two main pathological hallmarks: the accumulation of extracellular plaques, composed mainly of amyloid beta (Aβ), and of intracellular neurofibrillary tangles (NFTs) containing mostly hyperphosphorylated tau aggregates. Most animal and cellular models to date have focused on fAD, and recapitulate some key pathological features of AD. However, sporadic AD (sAD) models, which are comparatively understudied, are less consistent, likely due to the heterogeneity of sAD. Human induced pluripotent stem cell (iPSC) models provide a promising approach to investigate patient-specific disease mechanisms; however, it remains unclear whether iPSC-derived neurons from sAD patients retain clinically meaningful features of the individuals from whom they originate.

The overarching aim of this thesis was to determine whether iPSC-derived neurons from sAD patients capture donor-specific vulnerability to Alzheimer's disease–relevant pathological insults, and whether in vitro phenotypes relate to clinical measures of disease severity in vivo. To address this, I investigated the effects of the two core pathological hallmarks of AD—amyloid-β oligomers and Tau preformed firbils—across cellular, transcriptional, and molecular levels in a 13 sAD and one fAD patient lines from the Deep and Frequent Phenotyping study.

First, I examined susceptibility to Aβ-induced neurotoxicity across 14 sAD patient-derived cortical neuronal lines. Aβ exposure induced dose-dependent neurite loss and neuronal death across all lines, with significant inter-individual variability. Aβ-induced neurite loss correlated with multiple clinical measures, such as hippocampal volume, providing evidence that sAD iPSC-derived neurons can be used to study individual levels of disease vulnerability.

To investigate mechanisms underlying differential susceptibility to Aβ, I performed bulk RNA sequencing following Aβ exposure in control and patient-derived neurons. Aβ induced substantial transcriptional remodelling in both systems. In control neurons, Aβ altered pathways related to synaptic function, neuronal projection,

and lipid metabolism. Despite strong transcriptional enrichment of cholesterol biosynthesis pathways, genetic and pharmacological suppression of cholesterol synthesis did not mitigate Aβ-induced neurotoxicity, although Aβ exposure induced lipid droplet accumulation. In patient-derived neurons, Aβ induced upregulation of stress response pathways and downregulation of pathways related to cytoskeletal organisation, axonal projection, synaptic function, and oxidative phosphorylation. Although there were no transcriptional differences between resilient vs vulnerable AD patients after Aβ insult, genes that were differentially expressed between both groups correlated with cognition and multiple clinical measures—including cognitive decline and amyloid and tau CSF biomarkers.

This study was then extended to investigating Tau in AD neurons. I show that Tau protein levels are signficantly associated with Tau levels in AD brain and cognition. Tau pre-formed fibril exposure induced neurite loss across patient lines, which correlated with hippocampal volume and amyloid burden. Here, I demonstrate that iPSC-derived neurons from sAD patients retain clinically meaningful donor-specific features and capture inter-individual vulnerability to both amyloid and Tau pathology, supporting their utility for modelling sporadic AD.

Declaration

All the work conducted in this thesis was done by me, with the exception of the Tau PFF preparations, which were done by Dr. Nora Bengoa-Vergniory at the Achucarro Basque Center for Neuroscience. Dr Peter Kilfeather aligned the sequencing reads in Salmon for the first RNA-sequencing experiment described in chapter 4. I supervised Helen Jolly during her DPhil rotations, and she performed the alignment of the sequencing reads, as well as helped with analysis of the Tau RNA sequencing in Chapter 5 of this thesis.
The DFP project is a collaboration between several groups. Dr. Anne Hedegaard, transduced with Ngn2 lentivirus and expanded the original stock of iPSCs from the DFP cohort, and provided me with the protocol and all the necessary instructions to transduce and make new stocks, which was instrumental for me to perform the experiments in this thesis. Dr. Bryan Ng developed the Tau KO-/- cell line and Professor Selina Wray provided me with the P301S exon 10 + 16 cell line used in this thesis.

Contents

Acknowledgments **4**

Abstract **7**

1 Introduction **22**

1.1 Alzheimer's disease 22

1.1.1 Clinical features and neuropathology 23

1.1.1.1 Correlation of Aβ and tau biomarkers with cognitive decline 27

1.1.2 Genetic and non-genetic aetiology 29

1.1.2.1 Familial AD 30

1.1.2.2 Sporadic AD 30

1.1.3 Non-genetic risk factors of Alzheimer's disease 34

1.1.4 Heterogeneity in sAD 36

1.2 Amyloid Beta and Tau 38

1.2.1 Amyloid Beta: formation and disease mechanisms 38

1.2.1.1 Formation of Aβ 38

1.2.1.2 Function of Aβ 39

1.2.2 Tau proteins: function, aggregation, disease mechanisms . . . 40

1.2.2.1 Physiological tau structure and function 40

1.2.2.2 Pathological tau structure and function 41

1.3 Animal models of Alzheimer's disease 44

1.3.1 Familial AD models: Focus on replicating AD pathology . . . 44

1.3.1.1 Knockout mouse models 45

1.3.2 Mouse models of AD genetic risk factors 46

1.4 iPSC-neuronal models of Alzheimer's Disease 47

1.4.1 Familial iPSC models of Alzheimer's disease 49

1.4.2 Sporadic Alzheimer's disease 50

1.4.3 Exogenous Aβ and tau treatment in iPSC-derived neuronal models . . . 50
1.4.4 The Deep and Frequent Phenotyping study . . . 56
1.5 Aims of the thesis . . . 56

2 Materials and Methods **58**
2.1 Deep and Frequent Phenotyping (DFP) study . . . 58
2.2 hiPSC culture . . . 59
2.2.1 Transduction and expansion of DFP iPSCs . . . 60
2.3 Differentiation of iPSC-derived cortical neurons . . . 61
2.3.1 DFP iPSC lines . . . 61
2.3.2 i3 iPSCs . . . 62
2.4 Rat cortical astrocytes maintenance and culture . . . 63
2.5 Lentiviral production . . . 64
2.5.1 Transformation of competent bacteria . . . 64
2.5.2 Lentivirus production . . . 64
2.5.3 Lentiviral titration . . . 65
2.5.3.1 Ngn2 and rtTA viruses . . . 65
2.5.3.2 CRISPRi guides . . . 65
2.5.4 CRISPRi knockdown in i3 neurons . . . 66
2.6 Cell viability assay . . . 67
2.7 Amyloid Beta peptide oligomerization . . . 67
2.8 Tau preformed fibrils production . . . 67
2.9 Lipid droplet visualisation with BODIPY . . . 68
2.10 Immunocytochemistry (ICC) . . . 68
2.11 High-content imaging and analysis . . . 69
2.11.1 Synapse staining . . . 69
2.11.2 Neurite tracing . . . 70
2.11.3 Cleaved Caspase 3 (CC3) staining . . . 70
2.11.4 Lipid droplet imaging . . . 70
2.12 Western Blotting . . . 71
2.13 RNA extraction and cDNA synthesis . . . 72
2.14 Primer design and qPCR . . . 73
2.15 Tau ELISAs . . . 73
2.16 Bulk RNA sequencing . . . 74
2.17 Statistical Analyses . . . 75

3 The effect of $A\beta$ on sporadic AD patient iPSC-derived cortical neurons from the DFP study 76
3.1 Introduction . . . 76
3.1.1 Aims of this chapter . . . 77
3.2 Generation of 14 NgN2-expressing iPSC lines . . . 78
3.3 Characterisation of iPSC-derived cortical neurons . . . 81
3.4 Neurite tracing of Day 7 iPSC-derived cortical neurons from the DFP cohort after $A\beta$ insult . . . 84
3.4.1 Experimental design . . . 84
3.4.2 Amyloid-Beta oligomers . . . 85
3.4.3 Investigating the effect of $A\beta$ on neurite outgrowth in Day 7 iPSC neurons . . . 88
3.4.3.1 $A\beta$1-42 insult . . . 89
3.4.3.2 Aβ25-35 insult . . . 94
3.4.4 Cell viability . . . 99
3.5 Correlation of neurite loss in patient-derived neurons with clinical measures of the same patients . . . 107
3.6 Neurite tracing of Day 70 iPSC-derived cortical neurons from the DFP cohort after $A\beta$ insult . . . 109
3.6.1 Decrease in neurite length and branching after $A\beta$ insult . . . 109
3.6.2 Adenylate Kinase release . . . 115
3.7 Correlation of neurite loss in Day 70 iPSC-derived neurons with clinical measures from the DFP cohort patients . . . 116
3.8 Discussion . . . 119
3.8.1 Choice of timepoints and developmental considerations . . . 120
3.8.1.1 Increased inter-differentiation variability at Day 70 . 120
3.8.1.2 Differences in inter-patient vulnerability between Day 7 and Day 70 . . . 121
3.8.2 Comparison of $A\beta$1-42 and $A\beta$25-35 insults . . . 121
3.8.3 $A\beta$ concentration . . . 122
3.9 Conclusion . . . 122

4 Investigating Aβ-induced transcriptional changes in iPSC-derived cortical neurons 123
4.1 Introduction . . . 123
4.1.1 Aims of this chapter . . . 124

4.2 Bulk-RNA sequencing of i^3 neurons treated with Aβ1-42 124
4.2.1 Experimental design 124
4.2.2 Data quality control 125
4.2.3 Differential Gene Expression analysis overview 127
4.2.4 Gene Set Enrichment analysis overview 130
4.2.5 Analysis of DEGs and enriched pathways 131
4.2.5.1 Upregulated genes and pathways in cells treated with Aβ1-42 compared with Scrambled peptides 131
4.2.5.2 Downregulated genes and pathways in cells treated with Aβ1-42 compared with Scrambled peptides . . . 136
4.3 Investigating the cholesterol synthesis pathways in i^3 neurons treated with Aβ1-42 141
4.3.1 Genetic manipulation of cholesterol synthesis pathways 143
4.3.1.1 CRISPRi Knockdown of SREBP transcription factors 143
4.3.1.2 Neurite outgrowth and cell viability after Aβ1-42 insult 145
4.3.2 Pharmacological inhibition of the cholesterol synthesis pathway 151
4.3.2.1 Mevalonate pathway inhibitors 151
4.3.2.2 Neurite tracing of i3 neurons treated with Aβ and Simvastatin or YM53601 152
4.3.3 Lipid droplet formation after Aβ1-42 insult 157
4.3.4 SREBP protein levels in Aβ1-42 treated neurons 161
4.4 Bulk-RNA sequencing of DFP neurons treated with Aβ1-42 162
4.4.1 Experimental design 162
4.4.2 Data quality control 162
4.4.3 Differential Gene Expression analysis of Aβ treated vs Scrambled iPSC-neurons 163
4.4.4 Fast Gene Set Enrichment Analysis and Over Representation Analysis in the Aβ vs Scrambled comparison 166
4.4.5 Detailed analysis of DEGs and fGSEA 166
4.4.5.1 Upregulated pathways in Aβ vs Scrambled treated neurons 166
4.4.5.2 Downregulated pathways in Aβ vs Scrambled treated neurons 168
4.4.6 Comparison between resilient and vulnerable iPSC-derived neurons from the DFP cohort 170
4.4.6.1 Data quality control 171

4.4.6.2 Differential gene expression and functional gene set enrichment analysis overview . . . 172
4.4.6.3 Detailed analysis of DEGs and enriched pathways in resilient vs vulnerable patients . . . 177
4.4.7 Correlation of significant DEGs between resilient and vulnerable patient lines and clinical measures . . . 179
4.5 Discussion . . . 183
4.5.1 Overview of key findings . . . 183
4.5.2 Cholesterol metabolism and lipid dysregulation in Aβ-treated neurons . . . 184
4.5.3 Translational and proteasomal dysregulation in response to Aβ1-42 . . . 185
4.5.4 Axonal projection, synaptic dysfunction, and neuronal excitability . . . 186
4.5.5 Correlations of DEGs with clinical measures . . . 187
4.5.6 Limitations and future directions . . . 189
4.5.6.1 Differences in transcriptional responses in i^3 and DFP neurons . . . 189
4.5.6.2 Experimental design and vulnerability stratification of DFP neurons in bulk RNA seq . . . 189
4.6 Conclusion . . . 191

5 Investigating the role Tau PFF on sporadic AD patient iPSC-derived cortical neurons from the DFP study 193
5.1 Introduction . . . 193
5.2 Characterisation of Tau expression in iPSC derived cortical neurons . 195
5.2.1 Tau and p-Tau protein expression . . . 195
5.2.2 Tau release in conditioned media . . . 198
5.3 Neurite tracing in iPSC-derived cortical neurons treated with Tau preformed fibrils . . . 201
5.3.1 Co-culture of with astrocytes . . . 201
5.3.1.1 Neurite outgrowth and branching . . . 201
5.3.1.2 Cell viability . . . 205
5.3.2 Cortical neuron monoculture . . . 206
5.3.2.1 Neurite outgrowth and branching . . . 206
5.3.2.2 Cell viability . . . 212

5.3.2.3 Correlation of Tau PFF-induced neurite loss in iPSC-derived cortical neurons with clinical measures of sAD patients . . . 213
5.4 The effect of Tau PFF insult on synaptic density in iPSC-derived cortical neurons from the DFP cohort . . . 217
5.5 Assessing the effect of Tau PFF seeding on Tau phosphorylation in iPSC-derived cortical neurons . . . 221
5.5.1 tTau and astrocyte staining in neuron-astrocyte co-cultures . . 223
5.5.1.1 Cell viability . . . 225
5.6 Bulk RNA sequencing of control iPSC-derived cortical neurons treated with Tau PFFs . . . 227
5.6.1 Quality control of dataset . . . 228
5.6.2 Differential gene expression analysis . . . 228
5.6.3 Functional gene set enrichment analysis (fGSEA) . . . 229
5.7 Discussion . . . 233
5.7.1 Molecular characterisation of Tau in iPSC-derived neurons and correlation with clinical measures . . . 233
5.7.2 Challenges in assessing cellular responses to tau PFF exposure 235
5.7.3 Minimal Transcriptomic Response to Tau PFF Exposure in Bulk RNA Sequencing . . . 237
5.8 Conclusion . . . 237

6 Discussion and Concluding remarks 239
6.1 Thesis overview . . . 239
6.1.0.1 Integration across chapters: patterns and divergences 243
6.2 The use of synthetic protein aggregates to model neurodegeneration . 245
6.3 Modelling resilience and vulnerability in Alzheimer's disease . . . 248
6.4 Concluding remarks and future directions . . . 251

References 253

List of Figures

1.1 Alzheimer Disease amyloid plaques 24
1.2 Neurofibrillary Tangles 25
1.3 Gray matter loss and brain atrophy in Alzheimer's disease 26
1.4 Percent free from Alzheimer's dementia based on *APOE* status . . . 32
1.5 Genetic architecture of AD/dementia highlighting fAD mutations and 81 genome-wide significant loci 34
1.6 Population attributable fraction of potentially modifiable risk factors for dementia 36
1.7 ROSMAP cohort Braak Stages and Cognitive Scores 38
1.8 Alternative splicing of the human MAPT gene 41
1.9 Pathological tau phosphorylation sites and function in the human brain 43

2.1 Differentiation of iPSC derived cortical neurons from the DFP cohort 62
2.2 Differentiation of i3 iPSC derived cortical neurons 63

3.1 Graphical depiction of DFP study design and experimental design of the neurite tracing assay 78
3.2 Transduction efficiency of NgN2 and rttA3 lentiviruses in sAD iPSCs 80
3.3 Expression levels of cortical markers in iPSC-derived neurons by qPCR 82
3.4 Immunostaining of cortical markers in iPSC-derived neurons 83
3.5 Representative images of GFP+ neurons at different steps of the Harmony analysis pipeline 85
3.6 Amyloid Beta oligomerisation 87
3.7 Neurite outgrowth and nuclei count at baseline in Day 7 cortical neurons 89
3.8 Neurite tracing of Day 7 cortical neurons after $A\beta$1-42 insult 91
3.9 $A\beta$1-42 insult impairs neurite outgrowth of Day 7 cortical neuronst . 92
3.10 Aβ1-42 insult impairs branching in Day 7 cortical neurons 94
3.11 Neurite tracing of Day 7 cortical neurons after $A\beta$25-35 insult 96
3.12 Aβ25-35 insult impairs neurite outgrowth in Day 7 cortical neurons . 97

3.13 $A\beta$25-35 insult impairs branching in Day 7 cortical neurons 99
3.14 Quantification of the number nuclei loss in Day 7 cortical neurons due to $A\beta$ insult 101
3.15 Adenylate Kinase Release in Day 7 cortical neurons treated with $A\beta$. 103
3.16 Cleaved Caspase 3 staining in Day 7 cortical neurons treated with $A\beta$1-42 105
3.17 Cleaved Caspase 3 staining in Day 7 cortical neurons treated with $A\beta$25-35 106
3.18 Correlation between clinical measures of the DFP cohort and $A\beta$ induced neurite loss in iPSC-derived cortical neurons 108
3.19 Neurite outgrowth and nuclei count at baseline in Day 70 cortical neurons 110
3.20 Neurite tracing of Day 70 cortical neurons after $A\beta$1-42 insult 112
3.21 Quantification of neurite loss in Day 70 cortical neurons due to $A\beta$1-42 insult 113
3.22 Quantification of the number of nodes in Day 70 cortical neurons due to $A\beta$1-42 insult 114
3.23 Adenylate Kinase Release in Day 70 cortical neurons treated with $A\beta$1-42 116
3.24 Correlation between clinical measures of the DFP cohort and $A\beta$ induced neurite loss in D70 iPSC-derived cortical neurons 118

4.1 Graphical depiction on the RNA sequencing workflow in $\mathbf{i^3}$ neurons . 125
4.2 PCA plot and Euclidian distance heatmap depicting sample clustering of i3 neurons treated with Aβ 126
4.3 MA plot and cortical marker expression in i3 neurons 128
4.4 Volcano plots of DEG between AB-treated and control i3 neurons . . 129
4.5 Top 30 up and downregulated DEGs between Aβ -treated and Scrambled i3 neurons 130
4.6 Top positively enriched pathways in Aβ 5 μM vs Scrambled 5 μM neurons 133
4.7 Top positively enriched pathways in Aβ 10 μM vs Scrambled 10 μM neurons 135
4.8 Over-representation analysis of positively enriched pathways in Aβ 10 μM vs SCR 10 μM treated neurons 136
4.9 Top negatively enriched pathways in Aβ 5 μM vs Scrambled 5 μM neurons 138
4.10 Top negatively enriched pathways in Aβ 10 μM vs Scrambled 10 μM neurons 139

4.11 Over-representation analysis of negatively enriched pathways in Aβ 10 μM vs Scrambled 10 μM neurons 140
4.12 Mevalonate pathway alterations in i3 neurons treated with AB 142
4.13 SREBP lentiviral titration and calculation of CRISPRi KD efficiency 144
4.14 Representative images SREBP1 and 2 KD i3 neurons after Aβ treatment 147
4.15 Quantification of neurites of SREBP1 and 2 KD i3 neurons after Aβ treatment 148
4.16 Quantification of cell viability of SREBP1 and 2 KD i3 neurons after Aβ treatment 150
4.17 Titration of YM53601 and Simvastatin show no increased toxicity between 50 nM and 10 μM of either compound 151
4.18 Representative images i3 neurons treated with Aβ and cholesterol-altering compounds 153
4.19 Quantification of neurite outgrowth and nodes in i3 neurons treated with cholesterol altering compounds in combination with AB 154
4.20 Quantification of cell viability i3 neurons after treatment with Aβ and cholesterol-altering compounds 156
4.21 Analysis pipeline for lipid droplet imaging with BODIPY 158
4.22 Representative images of BODIPY staining of i3 neurons after Aβ treatment 159
4.23 Quantification of lipid droplet formation in i3 neurons after Aβ treatment 160
4.24 SREBP protein levels in Aβ1-42 treated neurons 161
4.25 PCA and Euclidian sample distance map clustering AD-derived neurons gene expression changes after Aβ treatment 163
4.26 Aβ 1-42 causes transcriptional changes in neurons compared to Scrambled 1-42 peptide and untreated control 164
4.27 Analysis of differential gene expression in Aβ vs Scrambled- treated AD patient-derived neurons 165
4.28 Top positively enriched pathways in Aβ 5 μM vs Scrambled 5 μM AD neurons 167
4.29 Top negatively enriched pathways in Aβ 5 μM vs Scrambled 5 μM AD neurons 169
4.30 Flowchart of RNA-sequencing analysis in Resilient vs Vulnerable patient lines 171
4.31 PCA plot of Resilient vs Vulnerable patient iPSC-neurons treated with AB 172

4.32 Representation of DEGs between resilient and vulnerable patient lines, before consistency filtering 173
4.33 Representation of consistently differentially expressed genes in Resilient vs VUlnerable patient neurons 175
4.34 Differentially expressed genes in Resilient vs Vulnerable neurons . . . 176
4.35 Top upregulated pathways in resilient patient-derived neurons compared with vulnerable neurons 178
4.36 Top downregulated pathways in resilient patient-derived neurons compared with vulnerable neurons 179
4.37 Correlation of genes differentially expressed between neurons of resilient and vulnerable patient with their clinical measures 182

5.1 Expression of Tau, p-Tau and GSK3β by iPSC derived cortical neurons 197
5.2 Secretion of Tau and p-Tau by iPSC derived cortical neurons does not correlate with CSF tau and pTau 200
5.3 Representative images of DFP cortical neurons cocultured with astrocytes show no effect of Tau PFFs 203
5.4 Tau PFFs did not induce neurite loss in DFP cortical neurons cocultured with astrocytes 204
5.5 Tau PFFs induce moderate nuclei loss and AK release in DFP cortical neurons co-cultured with astrocytes 206
5.6 Representative images of DFP cortical neurons treated with tau PFFs show neurite loss due to PFFs 208
5.7 Tau PFFs induce neurite loss in DFP cortical neurons 209
5.8 Tau PFFs induce loss of nodes in DFP cortical neurons 211
5.9 Tau PFFs induce nuclei loss and AK release in DFP cortical neurons 213
5.10 Neurite loss in cortical neurons due to Tau PFFs correlates with clinical outcomes of patients 216
5.11 Immunolabeling of Homer 1, Synapsin I/II and MAP2 in Day 75 cortical neurons treated with Tau PFFs 219
5.12 Tau PFF insult does not induce consistent synapse loss in Day 75 DFP cortical neurons 220
5.13 Immunolabelling of p-Tau in cortical neurons shows moderate increase in number of spots after Tau PFF insult 222
5.14 Immunolabelling of tTau and GFAP in cortical neurons after Tau PFF insult. 224

5.15 Tau PFF causes moderate neuronal death in cortical neurons 226
5.16 Clustering and differential gene expression of i3 cortical neurons treated with Tau PFFs 229
5.17 Upregulated pathways in neurons treated with Tau PFFs 231
5.18 Downregulated pathways in neurons treated with Tau PFFs 232

List of Tables

1.1 Alzheimer's disease biomarkers (adapted from Jack et al., 2024 [209]). 29
1.2 hiPSC neuron models used to study Aβ toxicity. 53
1.3 hiPSC neuron models used to study tau pathology. 54

2.1 DFP cohort iPSC line IDs 60
2.2 Composition of Basal Media 64
2.3 List of plasmids used and their functions. 66
2.4 CRISPRi guides 66
2.5 Primary antibodies 69
2.6 Western blot reagents 72
2.7 Primer sequences used for quantitative PCR 73

Chapter 1

Introduction

1.1 Alzheimer's disease

Alzheimer's disease (AD) is the most common age-related neurodegenerative disease, contributing to 60-70% of all dementia cases. It is estimated that about 57 million people worldwide had dementia in 2021, a number that is expected to increase to 139 million by 2050, due to an ageing population [179, 3]. As such, the economic cost of dementia was evaluated at about 1.3 trillion US dollars globally, and is expected to double by 2030 [3]. These figures underscore the pressing need to improve diagnosis, prevention and treatment of AD.

Alzheimer's disease was first described by Alois Alzheimer's in 1907, when a patient, Auguste D., presented with memory impairments [15]. After her death, post mortem histological studies revealed amyloid plaques and neurofibrillary tangles (NFTs) in her brain [164]. Today, more than a century later, the causes of AD, and how to cure it, are still unknown. In 2021 the first disease modifying therapy (DMT), the monoclonal amyloid antibody Aducanumab was approved by the Food and Drug Administration (FDA) in the United States (Biogen has now stopped producing it). Until then, the only available therapies, which reduced symptoms of AD but did not slow progression, were cholinesterase inhibitors (e.g. donezepil) and glutamate regulators (e.g. memantine) [451, 27]. Two other amyloid antibodies have now been approved by the FDA and the European Medical Association (EMA): Lecanemab in 2023 by the FDA and 2024 by the EMA, and then Donanemab in 2024 by the FDA and 2025 by the EMA. These antibodies have been shown to reduce cognitive and functional decline by 20-30% for people living with early AD [430, 479]. They can have serious side effects, including amyloid-related imaging abnormalities (ARIA), a temporary brain swelling that usually resolves over time. These clinical trials have shown that near total removal of amyloid plaques in the brain is not enough to stop

the progression of the disease completely, and there are currently many clinical trials targeting other aspects of AD, including tau and neuroinflammation [194]. In fact, in 2025 there were 182 clinical trials assessing 138 drugs [93].

1.1.1 Clinical features and neuropathology

Alzheimer's disease is characterised by the progressive loss of memory and cognitive functions. Furthermore, neuropsychiatric symptoms such as personality changes, depression, aggression and psychosis, often occur early in the progression of AD, and severely impact the quality of life of both the patients and their caretakers [295]. Many clinical manifestations of AD overlap with other neurodegenerative diseases, such as Frontotemporal dementia (FTD), vascular dementia (VD), and dementia with Lewy Bodies (DLB), which poses a challenge when diagnosing AD. Neuropathologically, AD is defined by the presence of amyloid plaques, which consist mostly of amyloid beta protein (Aβ) (Figure 1.1) and neurofibrillary tangles (NFTs), which consist mostly of hyperphosphorylated tau protein in paired helical filaments (PHF)(Figure 1.2) [287, 236]. Aβ and tau proteins will be discussed in more detail in Section 1.3. These structures used to be visualised via chemical staining methods such as Congo Red, Thioflavin S or silver staining, but are now mostly visualised by immunohistochemistry using anti Aβ or tau antibodies. NFTs are found intracellularly, in the soma and neurites of neurons, while Aβ plaques, which can be diffuse or dense-core, are found extracellularly [287, 236, 252]. Diffuse plaques can be found in the normal aged brain, while dense-core plaques are found mostly in AD brains [419]. Other than these structures, AD brains also present with progressive loss of grey matter, severe brain atrophy and enlarged ventricles compared with healthy brains, though those features are not specific to AD (1.3) [109].

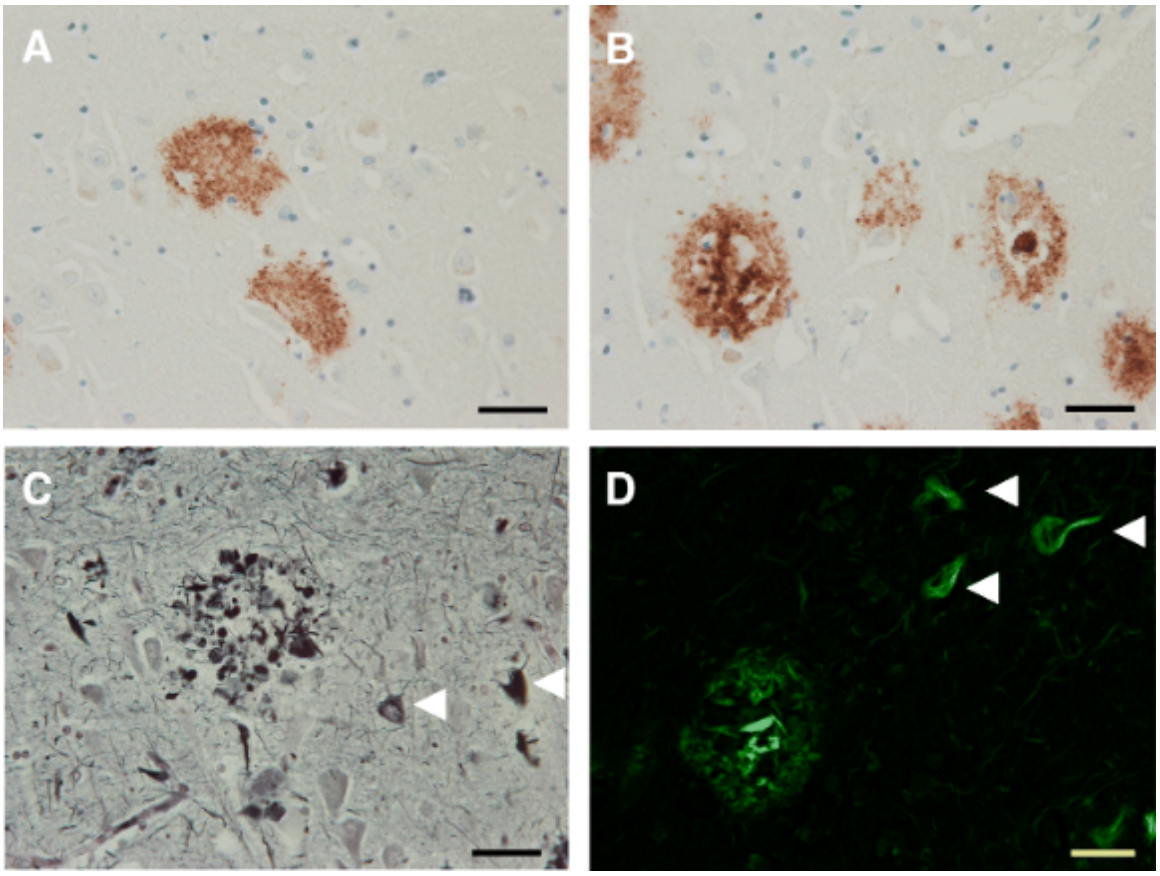


Figure 1.1: **Alzheimer Disease amyloid plaques** Immunohistochemistry of affected Alzheimer's tissues using antibodies directed against Aβ peptides demonstrates the presence of both diffuse (a) and dense core (b) senile plaques. These dense core plaques are often associated with neuritic elements that can stain filamentous tau and correlate with disease severity. Neuritic AD plaques are readily observed using Bielchowsky silver staining (c) or Thioflavin S staining (d). These stains can also label neurofibrillary tangles as shown by the arrowheads. The scale bars are 40 μm. Figure is adapted from [109] with no changes except formatting the caption.

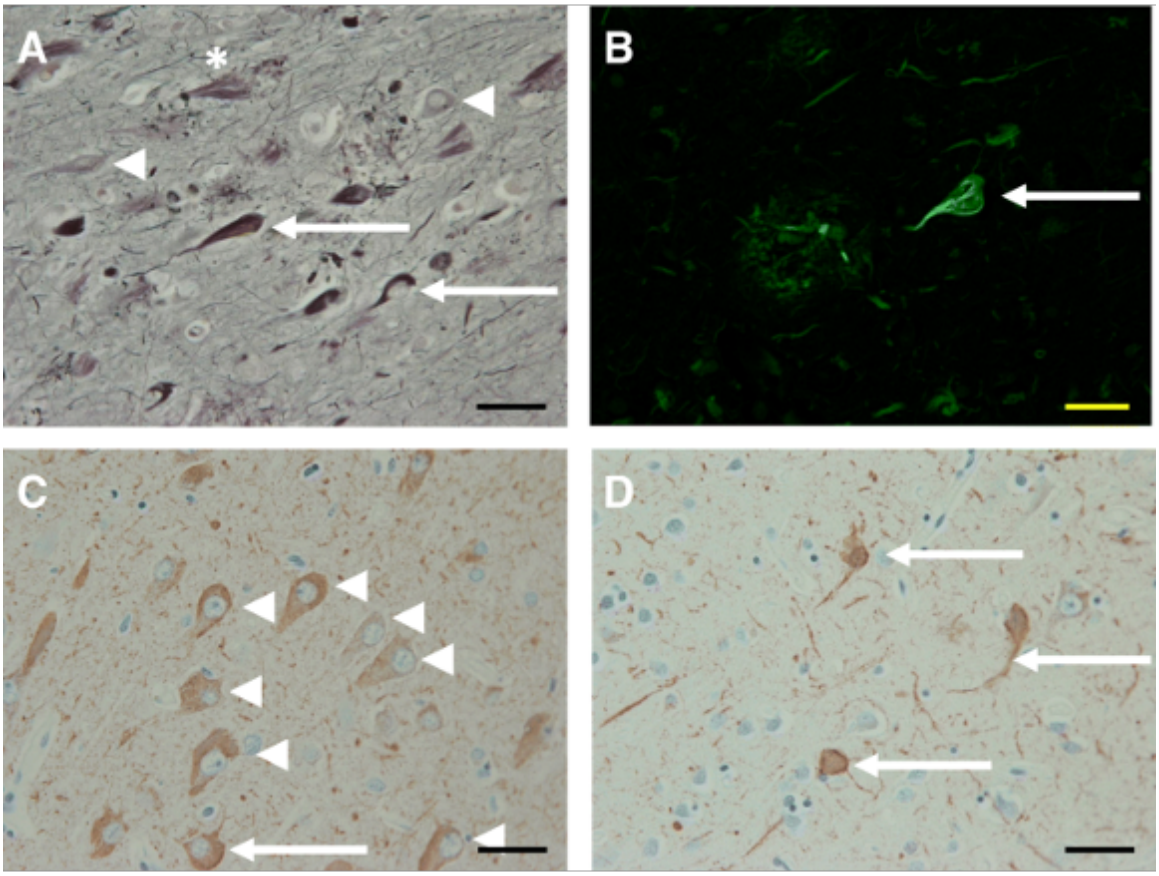


Figure 1.2: **Neurofibrillary Tangles.** Neurofibrillary tangles develop from intracellular pre-tangles containing misfolded tau and small tau aggregates to mature NFTs containing bundles of cross-linked tau filaments before the neuron dies and an extracellular ghost tangle (asterisk) remains. Silver staining (a) and Thioflavin S (b) capture many mature tangles (arrows) and some pre-tangles (arrowheads) along with amyloid plaques and tau neuropil threads. Development of NFTs from the pre-tangles is more easily visualized using tau immunohistochemistry (c,d). This allows the mis-localized somal tau to be distinguished readily from the bundles of PHFs in NFTs in addition to the neuropil threads that can also be pronounced (d). The scale bars are 40 μm. Figure is adapted from [109] with no changes except formatting the caption.

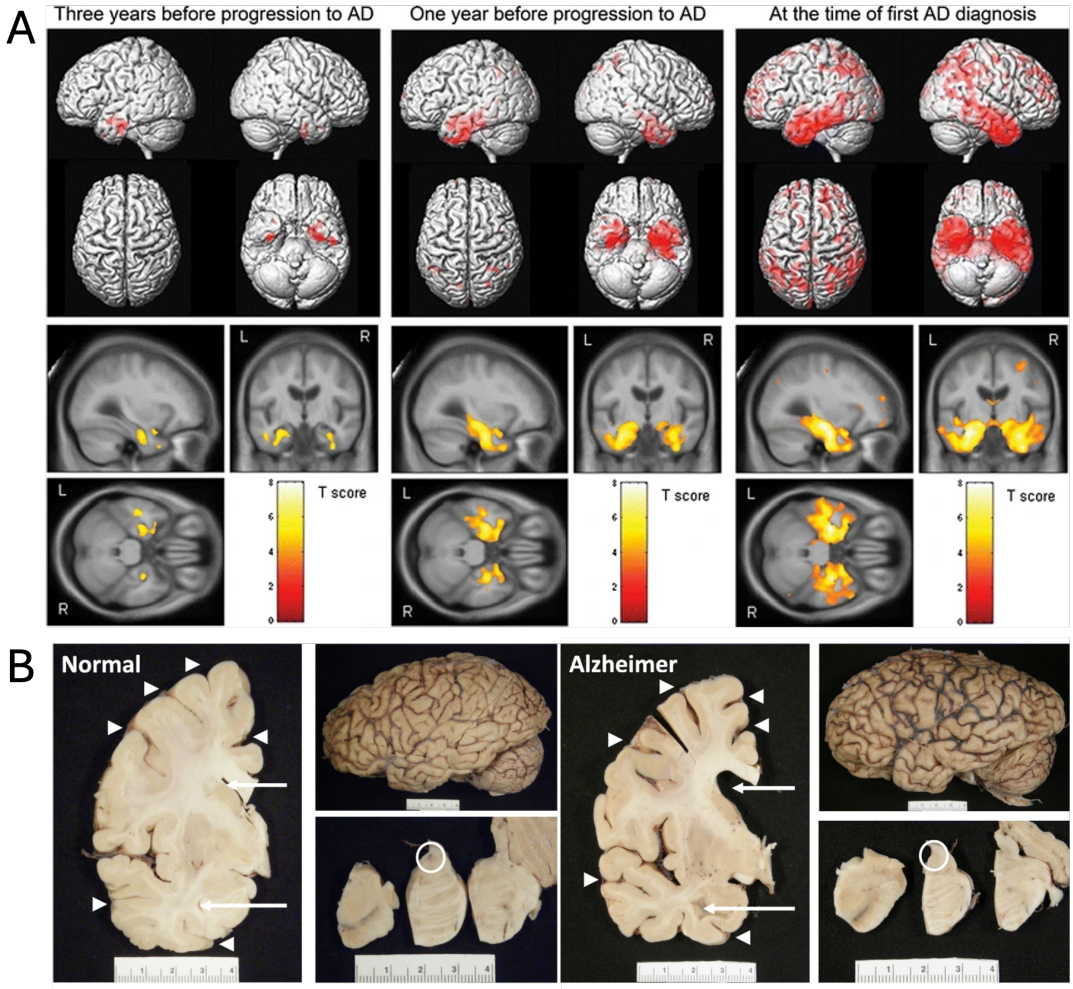


Figure 1.3: **Gray matter loss and brain atrophy in Alzheimer's disease** (A) MRI images showing patterns of gray matter loss in a group of 30 subjects compared to controls, shown at three different time-points in their disease: approximately 3 years before progression to AD while carrying the diagnosis of mild cognitive impairment (MCI), approximately 1 year before progression to AD while still MCI, and at the time of the first AD diagnosis. The results show that atrophy starts in the medial temporal lobes and fusiform gyrus at least 3 years before subjects reach a diagnosis of AD, and then spreads to the posterior temporal lobes and parietal lobes, and then by the time of the first AD diagnosis the pattern becomes more severe and widespread involving the medial temporal lobe, temporoparietal cortices, and the frontal lobe.L:left; R:right. (B) Gross Anatomy of Alzheimer's Brain. Lateral view of an Alzheimer's brain can show widening of sulcal spaces and narrowing of gyri compared to a normal brain. This may be more readily observed in coronal sections as indicated by the arrowheads, and this atrophy is often accompanied by enlargement of the frontal and temporal horns of the lateral ventricles as highlighted by the arrows. Additionally, loss of pigmented neurons in the locus coeruleus is commonly observed in the pontine tegmentum as shown with the open circle. None of these features is exclusive to Alzheimer's disease. Figure is adapted from (A) Whitwell et al. (2010) [506] and (B) DeTure et al. (2019) [109]. Two figures were combined and the figure title was changed accordingly.

In 2011 the National Institute on Aging and Alzheimer's Association (NIA-AA) presented a research framework with recommendations for the diagnosis of AD [11, 295, 441]. Since then, two updates, one in 2018 [210] and one in 2024 [209] have been released. The 2011 report defined diagnostic guidelines for the definition of symptomatic AD, namely mild cognitive impairment (MCI) and AD. In 2018, the framework shifted to a biological definition of AD: AD should now be defined first through the presence of neuropathological burden, while people are asymptomatic, which later leads to the appearance of clinical symptoms. The presence of key AD biomarkers via amyloid Positron Emission Tomography (PET) scans and cerebrospinal fluid (CSF) are reflective of the existence of neuropathology, and can be used to diagnose AD. Before the development of these biomarkers, formerly diagnosing AD was only possible after postmortem analysis and identification of neuropathological burden. In 2018, the NIA-AA group biomarkers into three categories: Amyloid, tau and Neurodegeneration (Neurofilament Light) (AT(N)). Since then, the most significant improvement in diagnostics has been in the development and improvement in accuracy of blood-based biomarkers [209, 345], which were integrated in the new framework, alongside biomarkers related to inflammation (such as GFAP) [209]. These biomarkers are, as of yet, not used for diagnosis in the UK, but are widely used in research. They group biomarkers in three categories: first, biomarkers of AD neuropathologic change, which include Amyloid PET and CSF phospho-tau markers (p-tau 217, p-tau 181, p-tau 231) (Core 1), and tau PET (Core 2); second, biomarkers of non-specific processes involved in AD pathophysiology, including neurodegeneration using CSF neurofilament light (NfL) or structural magneto resonance imaging (MRI) and PET and inflammation (astrocytic activation), using CSF GFAP; third, biomarkers of co-pathology, including vascular brain injury, via infarction on MRI or CT, as well as a-synuclein copathology, using asyn-SAA CSF levels (Table 1.1).

1.1.1.1 Correlation of Aβ and tau biomarkers with cognitive decline

CSF Aβ does not correlate well with cognitive decline, while p-tau concentration correlated better (also in MCI). Consistent with this, tau PET is also a better predictor of cognitive decline. Braak staging of tau propagation in the brain is based on the predictive spread of NFTs throughout the disease, which correlates more closely with disease severity [56, 58]. Nonetheless, Aβ markers remain necessary for the diagnosis of Aβ, as tau pathology is a feature of multiple neurodegenerative diseases. Increasing evidence indicates that phopsho-tau 217 CSF levels are the best

predictor of disease progression, compared to other p-tau species (p-tau 181 and p-tau 231), and correlates well with amyloid pathology [26, 303].
Total tau (tTau), alongside neurofilament light (NfL), is considered a marker of neurodegeneration [183] in various tauopathies, and has been shown to associate with Aβ burden [302, 291, 434], but does not correlate with tau pathology [127, 256]. Recently, tTau was reported to correlate with synaptic degeneration in MCI and AD patients across two independent cohorts [434], further supporting its role as marker of neuronal injury. Complementing fluid biomarkers, neurodegeneration can be detected by assessing brain atrophy using structural MRI. Although brain atrophy is not specific to AD, it correlates well with disease progression and cognitive decline, and therefore offers a non-invasive and more accessible method of detecting neurodegeneration to supplement the diagnosis of AD [142, 483].

Beyond amyloid and tau, a number of additional biomarkers have been shown to associate with AD progression. Synaptic loss, which is one of the earliest manifestation in AD can be detected with synaptic markers such as SNAP25 at preclinical stages of AD [147, 304, 529]. Furthermore, glial fibrillary acidic protein (GFAP), a marker of astrocytic activation, has been shown to correlate with faster cognitive decline and progression severity [13, 40, 484]. Notably, Bellaver et al. (2022) found that Aβ was associated with increased plasma phosphorylated tau only in individuals positive for astrocyte reactivity (Ast+) [40]. Similarly, microglial marker TREM2 was shown to associate with slower amyloid accumulation [129, 308], tau deposition and cognitive decline in A+T+ individuals [360], while associating, alongside GFAP, with synaptic dysfunction [391]. Moreover, PET imaging of translocator protein (TSPO), used as a proxy for microglial activation, correlated hierachically with tau PET, following Braak-like staging. Furthermore, the co-occurrence of Aβ, tau and microglia activation was the strongest predictor of cognitive decline [354], suggesting that microglial activation is a key element linking the effects of Aβ to tau spread, and to downstream cognitive decline.

Intended use / Biomarker	CSF	Plasma	Imaging
Diagnosis			
A (Aβ proteinopathy)	—	—	Amyloid PET
T1 (phosphorylated and secreted AD tau)	—	p-tau217	—
Hybrid ratios	p-tau181/Aβ42, t-tau/Aβ42, Aβ42/40	%p-tau217	—
Staging, prognosis, and indicator of biological treatment effect			
A (Aβ proteinopathy)	—	—	Amyloid PET
T1 (phosphorylated and secreted AD tau)	—	p-tau217	—
Hybrid ratios	p-tau181/Aβ42, t-tau/Aβ42, Aβ42/40	%p-tau217	—
T2 (AD tau proteinopathy)	MTBR-tau243; other p-tau forms (e.g., p-tau205); non-phosphorylated mid-region tau fragments	MTBR-tau243; other p-tau forms (e.g., p-tau205)	tau PET
N (injury, dysfunction, or degeneration of neuropil)	NfL	NfL	Anatomic MRI, FDG PET
I (inflammation; astrocytic activation)	GFAP	GFAP	—
Identification of copathology			
N (injury, dysfunction, or degeneration of neuropil)	NfL	NfL	Anatomic MRI, FDG PET
V (vascular brain injury)	—	—	Infarction on MRI or CT; WMH
S (α-synuclein)	αSyn-SAA	—	—

Table 1.1: Alzheimer's disease biomarkers (adapted from Jack et al., 2024 [209]).

1.1.2 Genetic and non-genetic aetiology

Alzheimer's disease patients can be categorised in two broad subtypes: familial AD (fAD), carrying a inherited, autosomal dominant mutation and sporadic AD (sAD), without a clear genetic cause. fAD is generally early onset (EOAD, < 65 years old [381]), more aggressive in its progression, but only constitutes about 1 % of cases [36]. Most sAD cases are late-onset (LOAD), though a subset of patients, about 10-15%,

have been shown to be early onset [511, 348].

1.1.2.1 Familial AD

fAD develops as a result of mutation in one of three genes: amyloid precursor protein (APP), presinilin 1 (*PSEN1*) and presinilin 2 (*PSEN2*). Mutations in the gene coding for *APP* (chromosome 21) were first identified in 1991 [155, 76, 318], followed by mutations in *PSEN1* (chromosome 14) [67, 423, 459] and *PSEN2* (chromosome 1) [390, 257] in 1995. The discovery that mutations in APP, of which Amyloid Beta is a cleaved product, are found in fAD led to the amyloid cascade hypothesis, which postulates that Aβ deposition in the brain is the initiating factor in the development of AD [176]. This was strengthened by the fact that patients with Down Syndrome, which is caused by a triplication in chromosome 21, have a high chance of developing EOAD [512, 368]. Furthermore, the finding that *PSEN1* and *PSEN2* code for subunits of γ-secretase, which cleaves *APP* to generate Aβ peptides [104, 514], and that mutations in both genes lead to the increased cleavage of *APP* into Aβ1-42 peptides, further supported this theory [117, 414].
Individuals inheriting mutations in *APP* and *PSEN1* are guaranteed to develop AD, while those with a *PSEN2* mutations have a 95% chance [422]. The age of onset of *PSEN1* mutation carriers is generally around 40 years old while *APP* mutation carriers develop symptoms in their fifties [316]. Furthermore *PSEN1* mutation carriers tend to exhibit faster cognitive decline than *APP* and *PSEN2* carriers [394, 222], which tend to have a similar clinical symptoms and neuropathology as sAD [33, 327, 178].

1.1.2.2 Sporadic AD

There are no causative gene mutations in sAD, rather a mix of genetic and environmental risk factors. Nonetheless, the heritability of sAD is high with twin studies estimating it is over 60% [152]. The strongest genetic risk factor is the E4 allele of *APOE*, which codes for apolipoprotein E, a lipid transporter [407]. *APOE* has three alleles: E2, E3 and E4. The *APOE2* allele is protective against the risk of AD, while *APOE4* increases the risk compared to *APOE3*, and decreases the age of onset [91, 405]. Specifically, E2 decreases the risk by 4 [91, 380], while having one or two copies of E4 increases the risk by about 2-4 and 10-15 fold, respectively [92, 450, 135] (Figure 1.4). The risk *APOE4* confers varies depending on ethnicity, with East Asian populations being the most vulnerable compared to Caucasians and African populations [135]. Interestingly, despite African-Americans being at higher

risk of AD, *APOE4* confers much less risk compared to other ethnicities [182, 135]. Importantly, *APOE*4 carriers are at greater risk of developing ARIA, and this has led to the recommendation that genetic testing be done prior to the administration of anti-amyloid drugs [214].

Despite this strong association with AD, the mechanisms by which *APOE* alleles confer different risk to AD remain unclear. However, recent evidence supports the idea that the three alleles alter the biochemical properties of *APOE*, which changes its receptor binding, its structure and downstream lipid metabolism, which then alter disease mechanisms. For instance, an interesting case study reported that a mutation in *APOE3* (Christchurch mutation) conferred protection to AD in a woman with a familial *PSEN1* mutation [22]. While most people with this mutation develop AD in their mid forties, she only developed mild dementia in her mid seventies [22]. Post-mortem analyses of this individual showed reduced tau accumulation and neuroinflammation [418]. This mutation reduces *APOE* receptor binding to heparan sulfate proteoglycan (HSPG), and another mutation in *APOE3* (Jacksonville variant) [246], which prevents APOE oligomerisation and promotes lipid metabolism, was shown to reduce amyloid plaques and neuronal damage [264].
Clinical studies have suggested that *APOE4* accelerates disease progression [371], potentially by accelerating brain atrophy, amyloid and tau deposition [447]. For instance, a recent study in 12,000 participants showed remarkably earlier tau and Aβ positivity in cognitively unimpaired *APOE4* carriers than non-carriers, in a dose-dependent manner (i.e. one or two alleles) [340].

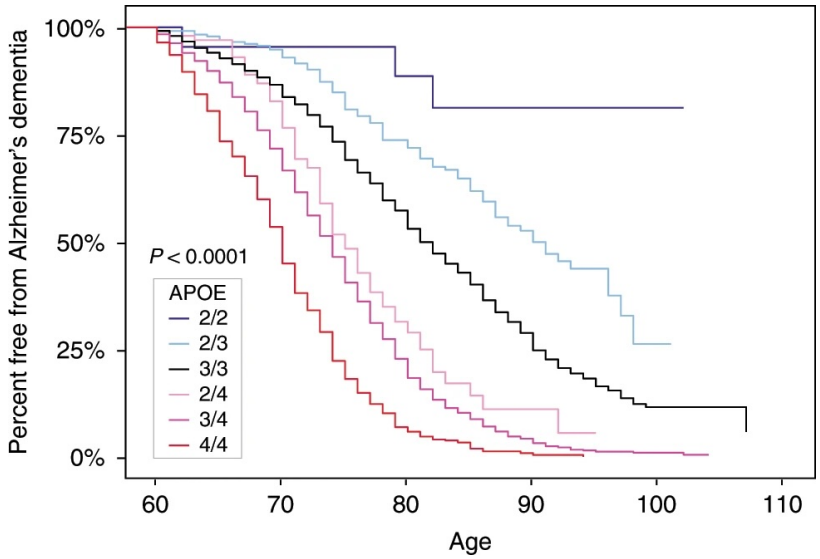


Figure 1.4: **Percent free from Alzheimer's dementia based on *APOE* status**. Kaplan–Meier curves were generated from Alzheimer's dementia cases and cognitively unimpaired non-AD controls in the neuropathologically confirmed group. Y-axis represents the percentage of persons with each *APOE* genotype in the neuropathologically confirmed group who remained free from Alzheimer's dementia. X-axis denotes age at death for controls and age at onset of cases, while replacing with age at death when age at onset was unavailable. Figure adapted from Reiman et al. [380]. No changes were made except the figure title.

Genome-wide Association Studies

Genome-wide association studies (GWAS) have helped uncover other genetic risk variants for AD [41, 213, 508]. Two of the most recent GWAS studies, conduced by Bellenguez et al., and Wightman et al., identified 81 risk loci, 42 of which were novel (Figure 1.5). These studies focused on European databases, and more recent GWAS have started to address the lack of diversity issue by performing cross-ancestry analyses, focusing on East-Asian populations [228] and African Americans [424], which have revealed new associations in these ancestries. The most recent GWAS cross-ancestry study identified 16 novel loci, underscoring the importance of diversity in GWAS studies [509].

The potential genes identified in GWAS studies are related to cholesterol metabolism, endocytosis, the immune system, and amyloid and tau tangle formation. Over 50% of loci contain genes that are involved in microglial function [20, 41], highlighting the importance of glial cells in AD. Notably, one rare variant of *MAPT* (p.A152T) has been associated with AD risk [90, 41], as well as Parkinson's disease and progressive supranuclear palsy (PSP) [251, 221]. Whereas MAPT mutations are causative

in several other tauopathies, none have been shown to cause Alzheimer's disease [363, 513]. Polygenic risk scores can be computed from the multiple risk loci identified in GWAS studies, and provide information on the contribution of genetic factors in the risk of AD. PRS predict AD with around 80% accuracy, and *APOE*4 is the largest contributor to genetic risk [103, 431]. Furthermore, rarer gene variants have larger effect sizes (Figure 1.5) than commonly occurring variants.

Extending on traditional studies, GWAS focusing on neuropathological endophenotypes provide a complementary approach to traditional case–control GWAS by identifying genetic variants associated with specific pathological features of AD. This study has shown that some risk loci are selectively associated with distinct neuropathologies, such as amyloid plaques, neurofibrillary tangles, or other non-AD-related pathologies, while other loci do not associate with any measured pathology [420]. Another approach is to measure cell-type specific PRS scores: one study measured the genetic risk attributed to different cell types in two independent cohorts with 1457 and 2921 individuals, respectively. Cell-type PRS associated with distinct disease mechanisms: astrocytes PRS associated with Aβ diffuse and neuritic plaque, microglia PRS with Aβ neuritic plaque, NFTs, cognitive decline and microglia activation and excitatory neuron PRS associated with PHF-Tau and Aβ PET [519]. This study provides further insight into how genetic risk converges on specific cellular pathways in AD pathogenesis.

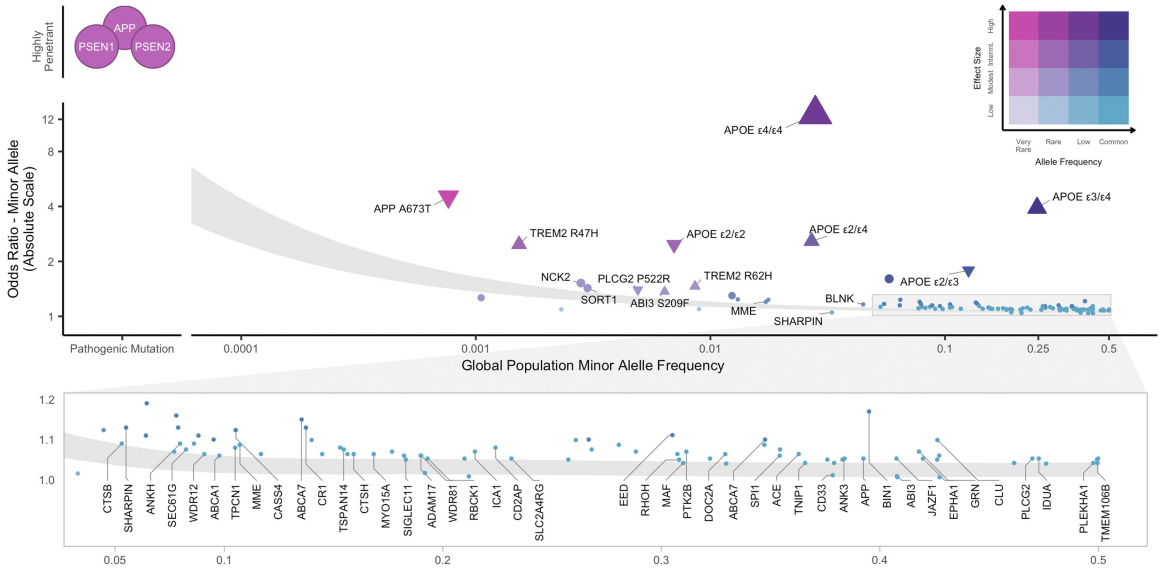


Figure 1.5: **Genetic architecture of AD/dementia highlighting fAD mutations and 81 genome-wide significant loci.** Genetic variants associated with disease are often conceptualized along two dimensions–variant effect size and population minor allele frequency. Highly penetrant mutations in APP, *PSEN1* , *PSEN2* that segregate with autosomal dominant AD are extremely rare and have large effect sizes. Variants discovered by genome-wide associations are mostly common to low-frequency with small effect sizes. To date, AD/dementia GWAS have identified 101 independent AD-associated single nucleotide polymorphisms across 81 genome-wide significant ($p < 5e\text{-}8$) loci. The shaded area illustrates 80% power to detect genome-wide significant association for variants at a given effect size and population frequency between an effective sample size of 382,472 from Bellenguez et al. (2022) (top) and 1 million (bottom), assuming 0.18 AD prevalence. Odds ratios are reported on the absolute scale, with triangles indicating directionality for *APOE* genotypes and rare variants with moderate-high SnpEff impact annotations. Effect sizes for *APOE* genotypes and *APP* Ala673Thr were obtained from Reiman et al.1 and Jonsson et al.,16 respectively. Labeled loci indicate candidate causal genes prioritized by Bellenguez et al. (2022). Variant MAFs and *APOE* genotype frequencies were obtained from the gnomAD global population (GRCh37 v2.1.1). Figure adapted from Andrews et al. [20]. No changes were made to the figure.

1.1.3 Non-genetic risk factors of Alzheimer's disease

Sporadic AD is caused by a combination of genetic and environmental risk factors. In 2020, the Lancet commission on dementia published a report with the different environmental risk factors to AD, which was updated again in 2024 [266]. The commission presents 14 modifiable risk factors, the 2024 update adding 2 new risk factors (vision loss and high cholesterol). They used the largest and most recent worldwide datasets where possible, and used data from the HUNT study, which is

a longitudinal study in 37,000 participants in Norway to estimate communalities (i.e. the clustering of risk factors). Each risk factor has an estimated population attributable fraction (PAF, i.e. the proportion of disease or death in a population is due to a specific risk factor, combining the relative risk and the prevalence). The 14 risk factors are separated by early life (less education), midlife (hearing loss, high LDL cholesterol, depression, traumatic brain injury, physical inactivity, diabetes, smoking, hypertension, obesity, excessive alcohol), and late life (social isolation, air pollution, visual loss), and they amount to a PAF of 45% (Figure 1.6). The largest contributors are education (5%), hearing loss and high cholesterol (7% each), and social isolation (5%).
The analyses focused, where possible on worldwide figures of prevalence, though most large-cohort studies are still performed in high income countries and have a higher proportion of Caucasian participants. Meta-analyses of risk factors in specific countries have found different prevalences of modifiable risk factors [382, 250, 292, 4, 292].

The notion that these risk factors are manageable and preventable led to several studies to establish the effects of lifestyle interventions, as well as guidelines, published by the WHO [2], for risk reduction of dementia. The US POINTER study, which presented their results in July 2025, the UK APPLE-Tree study and the Finnish FINGER study, have all reported that multidomain lifestyle interventions could improve brain health and slow or prevent cognitive decline [29, 108, 324].

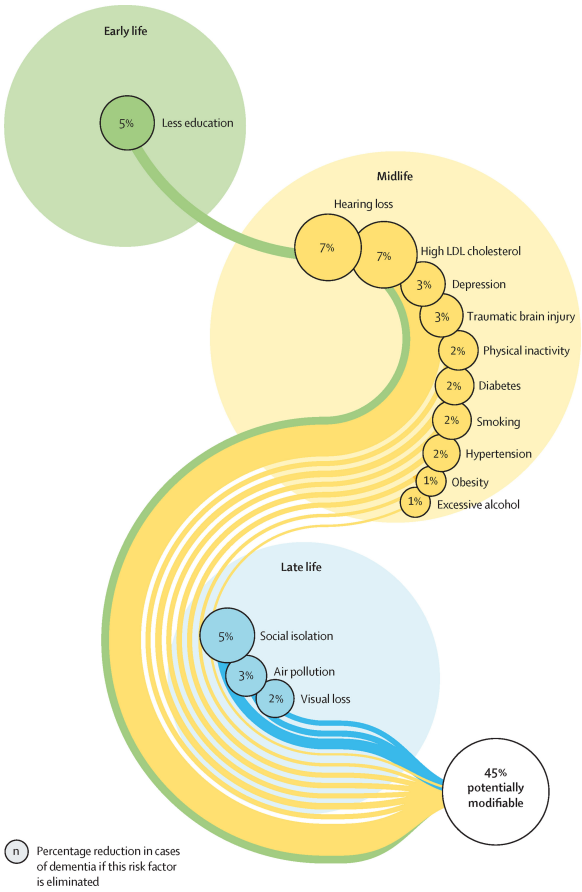


Figure 1.6: Population attributable fraction of potentially modifiable risk factors for dementia. Figure adapted from Livingston et al [266]. No changes were made to the figure.

1.1.4 Heterogeneity in sAD

As discussed above, although AD patients are neuropathologically similar, there is a large heterogeneity in both the rate of clinical progression and the clinical manifestations of AD. The disease can manifest at very different ages (EOAD vs LOAD), which can be due to *APOE* status and fAD mutations, among other factors. EOAD is considered to be a more neuropathologically "pure" version of AD, while LOAD often presents with copathologies. For instance 50% of AD patients also have a-syn pathology [21, 388, 319], which is associated with higher Aβ load, *APOE*4 status and younger age at death [319].

It is important to separate the definitions of resistance and resilience to AD. Resistant individuals are less susceptible to the development of age-related neuropathologic changes. Resilience can be split into two categories: some individuals remain cognitively unimpaired despite severe pathological burden (cognitive resilience (CR)

or cognitive reserve), while others retain better than expected brain structure (i.e. less brain atrophy) given a level of pathology (brain resilience (BR)) [306, 51, 186]. On the other hand, some patients have relatively low burden but quite severe cognitive symptoms; those individuals are defined as vulnerable patients (Figure 1.7).

Clinically, studies have found that women, and younger age were associated with brain resilience to tau pathology [341], while higher education levels and cortical thickness were positively associated with CR to tau pathology [341], and higher education was also associated with CR to amyloid pathology [140]. Additionally, the presence of copathologies significantly reduce CR [8, 319].
Several studies have studied the molecular basis of CR, looking at single cell and bulk sequencing datasets. Using omics datasets from the ROSMAP cohorts, they found that the presence of specific subtypes of parvalbumin and somatostatin positive interneurons is associated with cognitive resilience [337, 74]. These studies suggest that the excitatory-inhibitory balance is a measure of CR. Furthermore, neuroinflammation, as described by increased astrocytosis was associated with lower CR and higher tau pathology; and the genetic risk factor *TMEM106B* is associated with increased Aβ pathology but lower neuronal loss (i.e. it is associated with CR to AD pathology) [337].

Taken together, these studies suggests that both environmental and genetic factors contribute to an individual cognitive resilience. While environmental risk factors can be managed and are, in part, preventable, genetic risk factors are not, and understanding the molecular mechanisms that contribute to cognitive resilience is essential to predict an individuals disease prognostic and determine treatment strategies.

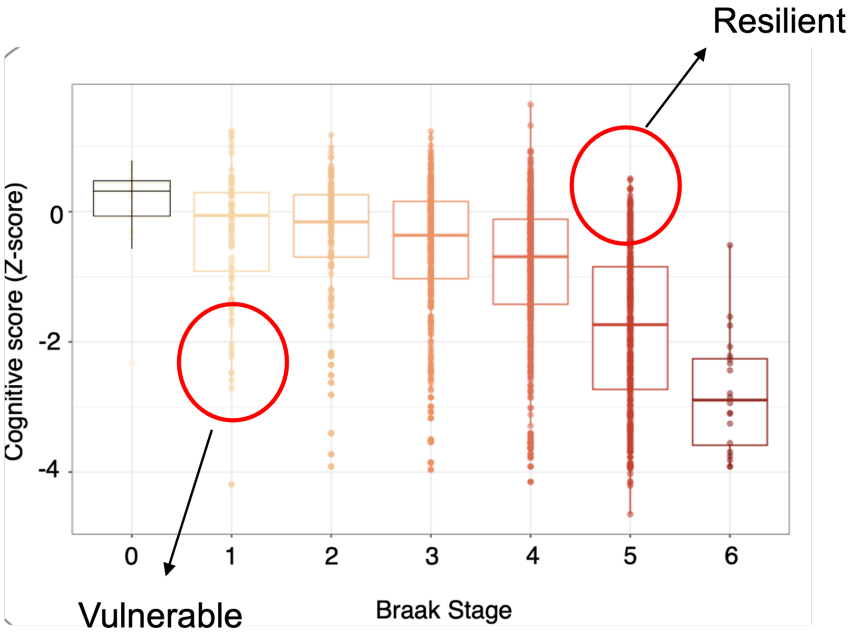


Figure 1.7: **ROSMAP cohort Braak Stages and Cognitive Scores** Boxplot of the ROSMAP cohort's cognitive scores and Braak stages. Some patients have unimpaired cognition at high Braak stages (Stage V) (cognitive resilience), while others have severe cognitive loss with relatively low pathology (Braak Stage I)(vulnerable). The figure was adapted from Dr. Becky Carlyle, and red circles with resilient and vulnerable patients were added by me.

1.2 Amyloid Beta and Tau

1.2.1 Amyloid Beta: formation and disease mechanisms

1.2.1.1 Formation of Aβ

Aβ is one of the products of the sequential cleavage of APP. APP is a transmembrane protein [219], which can be cleaved in two pathways: 1) the sequential cleavage by β-secretase and γ-secretase first into soluble APPβ and the membrane-tethered βc fragment (CTFβ), and then the *APP* intracellular domain (AICD) and Aβ peptides (i.e. amyloidogenic pathway) and 2) cleavage by α-secretase and then γ-secretase into soluble APPα and CTFα, followed by AICD and P3 peptides (i.e. non-amyloidogenic pathway) [161, 433, 432, 77]. Aβ peptides can be between 37 and 49 amino acids depending on the cleavage sites of β- and γ-secretases.

1.2.1.2 Function of Aβ

Physiological functions of Aβ include antimicrobial and antiviral properties [389, 53], helping maintain blood brain barrier (BBB) integrity [28] (note: this is likely why anti-amyloid drugs cause ARIA), and Aβ may regulate synaptic activity [149, 312].
There are two main peptides of Aβ used to describe AD: the primary peptide is Aβ 1-40 and the second is Aβ 1-42; both are produced under physiological conditions [115, 170]. While both Aβ 1-40 and Aβ 1-42 have the ability to aggregate, Aβ 1-42 monomers self-assemble into oligomers, protofibrils and fibrils, eventually leading to the amyloid plaques found in AD brains [491, 524, 244, 77, 208]. Mouse and cell studies harbouring fAD mutations have also demonstrated an increase in Aβ 1-42 production [117, 81, 205], and in vitro studies have shown that a critical concentration of Aβ 1-42 must be reached in order to trigger oligomerisation [329, 200]. In AD patient CSF, there is a decrease of Aβ 1-42 relative to Aβ 1-40 (Aβ 42:40 ratio), due to decreased clearance and increased retention of Aβ 42 in amyloid plaques[293]. The studies suggest that an increase in Aβ 1-42, either due to increased production due to fAD mutations or due to impaired clearance mechanisms [293] leads to the formation of Aβ oligomers and subsequent plaque formation.
Aβ plaques were thought to be the neurotoxic species of Aβ , given their presence in post-mortem AD brains in regions with brain atrophy. However, studies showed that Aβ plaque correlated poorly with cognition [466]. It was later established that soluble Aβ oligomers were likely the neurotoxic species, and correlated better with cognition[5, 296, 272, 224, 331]. This was further supported by mouse studies which showed that synaptic loss preceded Aβ plaque formation [191, 313] and Aβ oligomer treatment caused tau hyperphosphorylation[217] and long-term potentiation deficits[490] and neuronal degeneration [227, 217].
Several other mechanisms have been proposed to explain Aβ oligomer neurotoxicity. Aβ oligomers have been shown to act at the synapse, by binding to the cell surface and disrupting calcium homeostasis [52, 527] and cause hyperactivity in glutamatergic synapses [180], which causes synaptic dysfunction before the appearance of plaques [538], as well as neuronal death [10]. The aggregation of Aβ at the cell surface seems to be mediated by lipid rafts composed of sphingolipids and cholesterol [168, 223]. Furthermore, Aβ oligomers were shown to decrease synapse number [421] and increased oxidative stress [100] in an NMDAR activity-dependent manner, by reducing calcium influx [421]. Finally, Aβ oligomers were shown to cause tau hyperphosphorylation [101, 527], and cause the formation of NFTs in mouse

models [258, 169]. These studies link the function of Aβ1-42 with subsequent tau hyperphosphorylation and aggregation.

1.2.2 Tau proteins: function, aggregation, disease mechanisms

1.2.2.1 Physiological tau structure and function

The gene coding for microtubule-associated protein tau (MAPT, tau) is located on chromosome 17, and has 16 exons [320]. Eight of them are alternatively spliced, and in the adult human brain, 6 main isoforms are expressed, which arise from the alternative splicing of exons 2, 3 and 10 [19, 159]. Tau has a microtubule binding domain, and the inclusion of exon 10 leads to 4 microtubule binding repeats (4R tau), while the exclusion leads to 3 binding repeats (3R tau), which affects the ability of tau to bind microtubules. Furthermore, the inclusion of exons 2 and/or 3 lead to 0, 1 or 2 N-terminal inserts (0N, 1N, 2N), which influence membrane interactions. As such, the 6 tau isoforms are: 0N3R, 0N4R, 1N3R, 1N4R, 2N3R and 2N4R tau (Figure 1.8). The expression of tau isoforms is developmentally regulated: during development, the foetal brain only expresses the shortest tau isoform: 0N3R, while the adult brain expresses all 6 isoforms [237, 458]. The ratio of 3R and 4R tau are roughly equal, while the amounts of 0N, 1N and 2N tau are about 37%, 54% and 9%, respectively [156].

Tau is highly expressed in the human brain, specifically in neurons, and found mostly in axons [47], due to its interaction with microtubules (MTs). Tau promotes microtubule stability, and allows for the rapid assembly and disassembly of MTs, helping maintain and reorganise neuronal cytoskeletal structure [136, 280]. Furthermore, with the help of motor proteins kinesin and dynein, tau enables the transport of organelles and vesicles up an down axons [113, 487]. Interestingly, tau has also been shown to inhibit *APP* transport, leading to its accumulation in the soma, suggesting a link between tau function and *APP* trafficking [444]. During neuronal development, tau is highly phosphorylated and plays an important role in axonal growth [525].

The MT-binding affinity of tau is tightly regulated by phosphorylation, and tau has about 30-40 phosphorylation sites in the brain, most of which are found in the proline rich and c-terminal region of tau and many of which are found in the AD brain [174, 311, 173]. While several phosphorylation sites are associated with tau pathology (discussed in Section 2.2.2.2), tau phosphorylation is an essential component of physiological tau function.

Other than its role in MT stability, tau has been found in small quantities in the nucleus and in dendrites, where it may play a role in maintaining the integrity of DNA [452], and synaptic function [294, 534, 229].

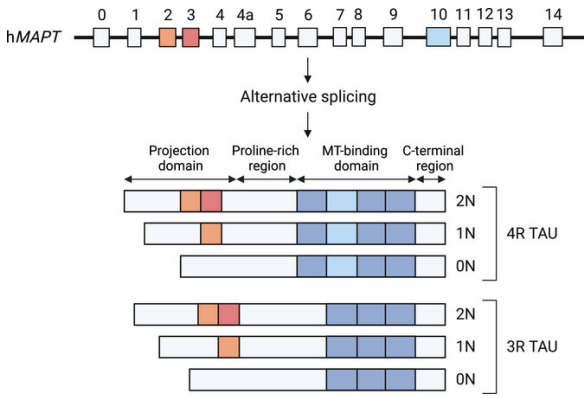


Figure 1.8: **Alternative splicing of the human MAPT gene.** The human MAPT gene encodes for six brain-specific TAU isoforms based on alternative splicing of exons 2, 3, and 10. The TAU protein can be structured into four different domains: The N-terminal projection domain, which projects away from the microtubules (MTs), acts as a spacer and interacts with components of the plasma membrane. The proline-rich region is involved in cellular signalling by interacting with Src-familiy kinases such as Fyn. The MT-binding domain mediates MT polymerization and stability, and the C-terminal region additionally contributes to MT polymerization and TAU's interaction with the plasma membrane. Figure adapted from Buchholz and Zempel [62]. No changes were made.

1.2.2.2 Pathological tau structure and function

Disorders associated with the pathological aggregation of tau are collectively known as tauopathies. Alternative splicing of exon 10 is of particular interest in the context of tauopathies, as the imbalance of 3R:4R ratio leads to the aggregation of specific isoforms of tau: 3R tau aggregates in Pick's disease, 4R tau aggregates in PSP, CBD, FTD with MAPT mutations and argyrophilic grain disease (AGD), and 3R+4R tau aggregates are found in AD and in Primary Age-Related Tauopathy (PART). This is exemplified in FTD, where mutations in exon 10 (P301S, P301L, S305), can cause increased exon 10 inclusion [177, 54] , tau phosphorylation [499] , and increases the propensity of tau to aggregate [305, 86, 130, 160]. Additionally, recent work using cryo-EM has shown that tau adopts disease-specific conformations (tau fold) in AD [139, 132], Pick's [131], CBD [531], AGD and PSP [426], while PART tau has the

same conformation as AD [425]. AD tau PHFs and single filaments (SF) consist of a core of pairs of filaments comprising residues 306-378 on which 3R and 4R tau can be incorporated to grow the filament [139].

As mentioned above, tau is phosphorylated under physiological conditions. However, under pathological conditions, it becomes hyperphosphorylated (Figure 1.9), which alters its MT binding properties and promotes MT disassembly, sequesters other MAPs, including MAP1 and MAP2 and leads to the aggregation of tau [18, 17, 16]. Similarly to Aβ, hyperphosphorylated tau monomers first aggregate into oligomers, then preformed fibrils (PFFs), PHFs, before becoming NFTs [17]. Tau is phosphorylated by a number of kinases, including calmodulin-dependent protein kinase II (CaMKII) [516], cyclic AMP-dependent protein kinase (PKA) [216], glycogen synthase kinase-3β (GSK3β) [359, 356] and cyclin-dependent kinase 5 (cdk5) [358], which have all been associated with tau tangles in the AD brain. Phosphoseryl/phosphothreonyl protein phosphatase-2A (PP-2A) is an enzyme that dephosphorylates abnormal tau [495], and its expression and activity is decreased in the AD brain [489, 460]. Furthermore, it is thought that its inhibition also upregulates the activities of several phosphorylating kinases [496, 357, 470, 453, 43]. As mentioned above, several of these kinases have been shown to act downstream of Aβ [258, 169, 101, 527]. However, the presence of tau aggregates in other tauopathies demonstrates that Aβ is not required for the aggregation of tau. Interestingly, some phosphorylation sites are protective against aggregation [415, 206], and pathological sites in the adult human brain are physiological in the developing brain [60, 157, 290], suggesting that phosphorylation is not always pathogenic and sufficient for its aggregation.

Mechanistically, tau hyperphosphorylation and aggregation leads to the mislocalisation of tau to the soma, dendrites and postsynaptic sites, which leads to synapse dysfunction and loss [189, 469, 455, 190, 499]. Furthermore, studies have shown that tau aggregates act as seeds that can be taken up by cells and promote the phosphorylation and aggregation of normal tau [143, 404, 166]; and this spread seems to be conducted via synapses [82, 265, 119, 111]. The trans-synaptic spread of tau could be due to the degeneration of neurons leading to presynaptic tau seeds leaking and diffusing into the post-synapse, or to the release of seeds via exocytosis or vesicles which are then taken up by the postsynaptic cell [498]. Though this is a convincing mechanism to explain the temporal and spatial spreading of tau observed

in AD [56], other mechanisms, such a microglial-driven spread of tau have also been proposed [282, 492, 25, 259].

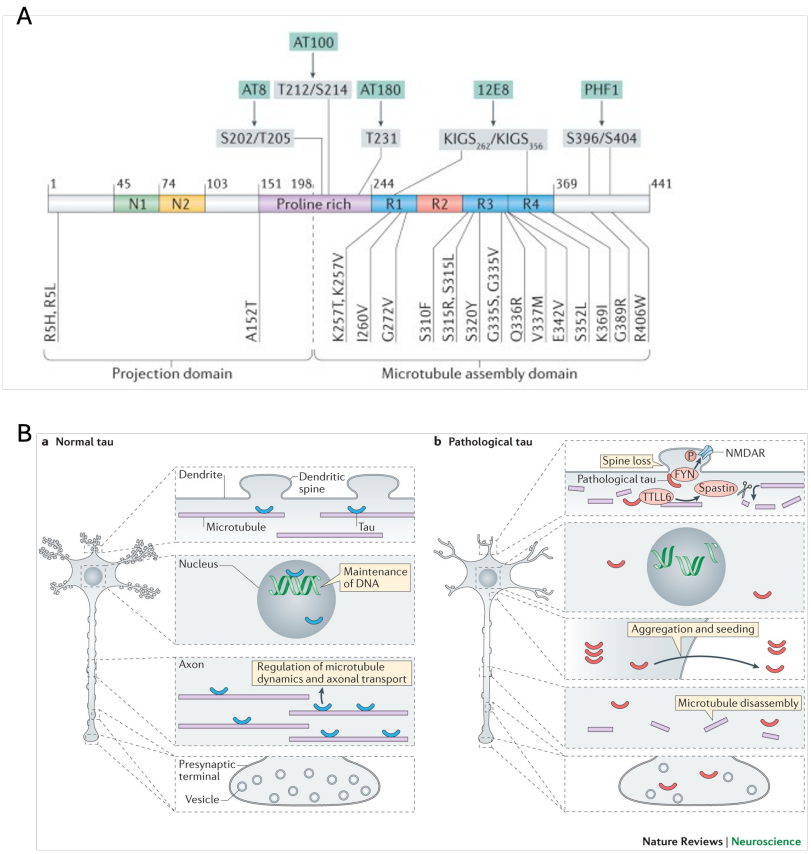


Figure 1.9: **Pathological tau phosphorylation sites and function in the human brain** (A) Phosphorylation sites associated with pathology: tau can be subdivided into two major domains. The assembly domain in the carboxy-terminal section comprises the repeat domains and flanking regions; this domain is responsible for binding to microtubules and for tau aggregation. The projection domain is the amino-terminal section that projects away from microtubules. The middle region of tau (amino acids 151–243) is a Pro-rich domain that contains multiple Thr-Pro or Ser-Pro motifs that are targets of proline-directed kinases such as GSK3β, CDK5, MAPK and JUN N-terminal kinase (JNK). In Alzheimer disease and other tauopathies, these and other motifs become hyperphosphorylated and thereby can be recognized by several well-characterized tau phosphorylation-dependent antibodies (for example, AT8, AT180, AT100, 12E8 and PHF1). Mutations of tau are mostly clustered in or near the repeat domains. (B) Graphical representation of tau functions in (left) physiological conditions and (right) pathological condition. Figure is adapted from Wang and Mandelkow [498]. Images from two figures were combined and caption was adapted to match these changes.

1.3 Animal models of Alzheimer's disease

Numerous rodent models of fAD, and to a lesser extend sAD have been developed. In this section, I will only focus on a few of the most relevant or commonly used ones.

1.3.1 Familial AD models: Focus on replicating AD pathology

Several mouse models of AD have been developed by transgenic introduction of fAD mutations in *APP* [192], *PSEN1* [80, 117] and *PSEN2* [197]. Mice carrying single mutations in *APP* develop amyloid pathology and cognitive impairments; *PSEN1* mutant mice exhibit severe neuronal loss preceding amyloid deposition, though do develop amyloid pathology eventually; and *PSEN2* mice do not develop Aβ pathology, but do show cognitive impairments and increased Aβ1-42. As such, while transgenic mice with single mutations in *APP* are commonly used, *PSEN1* and *PSEN2* models are not. fAD mice expressing several fAD mutations were developed to cause more severe amyloid pathology and cognitive impairments [187]. A very commonly used model is the 5XFAD mouse, which carries three different *APP* and 2 different *PSEN1* mutations [332], which develop AD-related phenotypes earlier than most other mouse models. For instance, amyloid aggregates are seen after 1.5 months and plaques after 2 months vs 4 and 9 months for mice with one mutation in *PSEN1* and *APP* [212].

However, while these mice recapitulate amyloid pathology and some exhibit tau hyperphosphorylation [220, 87, 240], they do not develop tau pathology. This has led researchers to either cross mice with tau mutations associated with FTD (P301S, P301L) with fAD mice or introduce a double mutations in tau and *APP* and/or *PSEN1* to cause the formation of amyloid plaques and NFTs. For example, the 3xTg-AD mouse has a *PSEN1* , an *APP* and a P301L MAPT mutation, and develops amyloid deposits after 6 months, plaques after 12 months and tau aggregates after 12-15 months [335, 37]. These models support the idea that while Aβ pathology occurs prior to tau pathology, both Aβ and tau exacerbate each other's neurotoxic effects. Mouse models expressing both tau and fAD mutations, such as the 3xTg-AD mouse or an APP/Tau P301L mouse [258], develop earlier and more severe Aβ and tau pathology than when the mutation is present alone [37, 258, 362]. Furthermore, as discussed previously, Aβ1-42 fibril injection into a P301L mouse caused the formation of NFTs [169] and Aβ oligomers were also shown to cause tau hyperphosphorylation [101, 527]. On the other hand, several studies in mouse models have reported that

dendritic tau increases Aβ toxicity at postsynaptic sites by stabilising NMDAR and increasing downstream glutamate release [207, 387]. However, it is worth noting that the fibril composition in these mice resembles FTD pathology more closely than AD tau pathology.

Therefore, later studies in mouse models with *APP/PS1* mutations and expressing WT human tau are important to study AD pathology in a more physiological manner. One study showed that introducing WT human tau into a *APP* mutant mouse induced tau pathology that resembled AD tau pathology,[475], others showed decreased synaptic function and increased hyperactivity, which was rescued by lowering tau expression [361, 386] and another showed that human tau increased amyloid plaque size, but not Aβ-mediated synapse loss [211]. Furthermore Aβ-induced impairments of long term potentiation (LTP) was dependent on the expression of human tau [429, 481]. These studies suggest that, at least in rodent models, human tau is required to cause tau pathology.

One of the disadvantages of these transgenic mouse models, is that the overexpression of the *APP* transgene leads to the overproduction of other cleaved products that may have downstream actions that are unphysiological [399]. A solution to this problem is to develop knock-in models, where the mouse *APP* is replaced with a humanized *APP* carrying fAD mutations [399]. Crucially, these models exhibit higher levels of Aβ42:40 without overexpressing APP. In some of these models, amyloid deposition can be seen after 2 months, with plaques seen around 4 months [400], and accumulation of microglia and astrocytes is visible near plaques [500]. However, while some models exhibit cognitive impairments, such as deficits in spatial learning after 8 months[399], most had intact memory until up to 15-18 months of age [399, 500, 400]. Furthermore, while one *APP* model was shown to have increased tau hyperphosphorylation, no model exhibited tau pathology [184].

1.3.1.1 Knockout mouse models

Knockout (KO) of genes involved in AD allow researchers to determine whether removing or reducing the expression of these proteins is protective against AD. The conditional KO of APP[278], *PSEN1* [523] and *PSEN2* did not prove particularly beneficial: they led to cognitive deficits [446, 298] and impairment in synaptic transmission and LTP [446, 298, 523], and even neurodegeneration [409]. However, in mice carrying *APP* mutations, conditional KO of *PSEN1* and *PSEN2* and

β-secretase (BACE1) did lead to rescue of AD phenotype by reducing Aβ production [408, 193]. BACE1 reduction was beneficial when deleted after early development [193], exemplifying that the localised and partial removal or reduction of AD-related proteins can be beneficial, but that the timing is important.

Tau KO mice (*Mapt* -/-) have been used to elucidate tau-dependent mechanisms in neurodegeneration. Four different *Mapt* -/- mouse models elicited no cognitive deficits, learning or memory impairments, though did exhibit age-related motor deficits. These mice did have decreased MT density in axons, though they showed normal axonal development [175], which was likely due to a compensatory mechanisms via the upregulation of MAP1A [175, 474, 145, 98], though this was relevant only in early development . Other *Mapt* -/- mice have shown an impairment in maturation and neurite length in primary neuron cultures [474], and more recent work has reported deficits in neuronal firing of excitatory neurons and alterations in the axonal initial segments (AIS) in cortical slices [75], which is supported by some [6], while others report conflicting results [429, 481]. The inconsistencies in some of the effects of *Mapt* -/- is likely due to the genetic background used as well as other experimental variations: for instance, the improvement of LTP due in *Mapt* -/- seen by Shipton et al (2011) [429], occurs in response to Aβ insult, and this was reversed by the expression of humanised tau in tau KO mice [481]. Similarly, mouse *Mapt* -/- studies have shown that the removal of tau protected primary neurons from Aβ -induced cytotoxicity (via Aβ injections, or in *APP/PS1* mice), rescued working memory deficits, microtubule disassembly, synapse loss and cell death [45, 527, 254, 330, 230, 526, 377]. Two studies directly contradict these results, and show that tau is not required for Aβ-driven toxicity, and in fact, *Mapt* -/- induced axonal degeneration in an *APP/PS1* mouse [369, 99]. Nonetheless, there is significant evidence suggesting a protective effect of tau depletion in AD.

1.3.2 Mouse models of AD genetic risk factors

There have been efforts to establish mouse models of LOAD, which in part have been led by the consortium for Model Organism Development and Evaluation of LOAD (MODEL-AD) [333]. As such, multiple models have been developed with alterations in key risk variants; for example one model which expresses the *TREM2* R47H risk variant and *APOE*4 (LOAD1) [238], and another with *TREM2* R47H + *APOE4* + human *APP* (LOAD2) [239]. LOAD1 demonstrated no amyloid deposition or cognitive impairments at 24 months, though they had altered cytokine levels and

changes in glycolysis [238]. LOAD2, on the other hand, demonstrated neuronal loss, elevated Aβ42 and behavioural deficits on some cognitive tasks at 16 months [239]. Another *TREM2* R47H mouse model showed myelin damage, and when crossed with 5XFAD mice, showed a sex-dependent increase in plaque deposition in female mice, as well as increased Aβ levels [473]. This female-specific *TREM2* effect has been shown in *TREM2* deficient mouse models as well as in *TREM2* R47H mice crossed with the PS19 tauopathy mouse [106, 410].
Recently, an elegant method for studying the roles of different *APOE* alleles was developed: The *APOE*4/*APOE*2 switch model. Mice express *APOE*4, until Cre-recombinase activation switches to the expression of *APOE*2. At the single-cell RNA level, switching to *APOE* induced the most changes on glial and endothelial cells. When crossed with 5XFAD mice, an astrocyte-specific shift to *APOE*2 led to a decreased in amyloid plaques, reduction in microglial activation and improved memory [162]. A microglia specific shift, however, did not elicit any changes in amyloid pathology, though it improved myelination, lessened microgliosis and reduced astrocytic lipid droplets [328].

1.4 iPSC-neuronal models of Alzheimer's Disease

Mouse models are particularly useful in elucidating disease mechanisms *in vivo*. However, there are biological differences between mice and human, as exemplified by the aforementioned differences in the induction of tau pathology with WT human tau vs murine tau in fAD mouse models. Furthermore, mice express 3R tau during foetal and neonatal stages, while in adulthood, they only express 4R tau [458], as opposed to the 6 isoforms seen in humans. Therefore, it is important to complement the work in murine AD models with human cellular models to investigate disease-mechanisms that may be human-specific. Until recently, it was exceedingly difficult to study neurodegenerative disease in human models, and most of the research came from post-mortem brains. While these studies have been and still are essential to studying AD, they only allow for insights at a single timepoint, often when substantial neurodegeneration, atrophy and pathology has developed. While embryonic stem cells have been used in some studies, there are ethical concerns to using human oocytes and embryonic stem cells. In 2007, Yamanaka and Takahashi created induced pluripotent stem cells derived from human skin fibroblasts, and subsequently from blood samples, by overexpressing four transcription factors: OCT4, SOX2, MYC and KLF4 [456, 457].

This discovery provided the opportunity to study neurodegenerative diseases in human neurons derived from individuals who have the disease, with the disease-associated mutations or genetic predispositions, and compared them with healthy human cells. This was previously completely inaccessible without invasive surgeries. Furthermore, while neurons largely do not proliferate, iPSCs do, which also allows for large scale studies, or the differentiation into different cell types, such as cortical neurons [532, 427], dopaminergic [243] neurons, as well as microglia [171], astrocytes [465] and oligodendrocytes [123]. The differentiation and maturation process can be mediated by small molecules such as growth factors, extracellular matrix components, and signalling molecules. These protocols are based on the developmental biology of various neuronal lineages. Another strategy is to induce differentiation via the expression of specific transcription factors, such as, in the case of the cortical neurons used in this thesis, the expression of NgN2 [532]. The neurons produced from iPSCs mature into electrophysiologically active cells, that express neuronal markers specific to the subtype and developmental stage. As such, iPSC-derived neurons (iNeurons) have been used to study Alzheimer's disease *in vitro*.

Furthermore, iPSCs can be genetically modified to, for instance, correct a mutation of interest, creating an isogenic control (i.e. a cell line with the same genetic background except for the corrected mutation), or to modulate the expression of a specific gene. In this regard, clustered regularly interspaced short palindromic repeats-associated protein 9 (CRISPR/Cas9) technology [445] has often been used in iPSCs to model specific disease pathways [88, 378, 277]. It is used in Chapter 4 of this thesis.
CRISPR/Cas9 technology originates from bacteria, in which the CRISPR-cas system provide adaptive immunity [276, 30]. The CRISPR-Cas system is composed of CRISPR RNAs (crRNA), which serve as guides in a complex with trans-activating RNA (tracrRNA), a small RNA that is essential for the maturation of crRNA from pre-crRNA to mature crRNA, as well as with Cas proteins [107, 61]. The CRISPR-Cas9 protein is a dual-RNA-guided endonuclease that uses a guide sequence inside an RNA complex made from a trans-activating RNA and CRISPR RNA (tracRNA:crRNA) to introduce site-specific double-strand breaks (DSB) in a specific DNA target sequence [218, 107]. The RNA complex (tracRNA:crRNA) was then engineered into a single guide RNA, in which the guide sequence can be modified so that Cas9 targets any DNA sequence of interest. DNA target recognition requires both base pairing to the crRNA and the presence of a protospacer motif

(PAM) adjacent to the crRNA on the DNA target sequence [218]. This system was subsequently used successfully in iPSCs, where RNA-guided Cas9 introduced DSBs, which are then repaired by non-homologous end-joining [378, 277].
A modified CRISPR system was then developed where an endonuclease-deficient Cas 9, which contains two mutations (dead Cas9 or dCas9) was used. This system is able to interfere with DNA transcription, therefore repressing a gene of interest without introducing a DSB (CRISPRi) [370, 79]. More recently, the CRISPR system was further modified to allow for the activation of genes (CRISPRa) [181]. These technologies have allowed researchers to regulate genes in control or patient-derived iPSCs that are associated with AD disease mechanisms.

1.4.1 Familial iPSC models of Alzheimer's disease

The first iPSC models of AD were generated from fAD patients carrying *PSEN1* and *PSEN2* mutations, and showed that fAD cortical neurons secrete more Aβ and have a higher Aβ 42:40 ratio than healthy controls, thus demonstrating that iNeurons replicate AD-relevant features [518]. Importantly this was replicated in multiple independent studies with various PSEN mutations, and isogenic controls reversed the increased Aβ production observed [260]. iNeurons harboring fAD *APP* mutations exhibit similar phenotypes, with an increase in secreted Aβ42:40 ratio and furthermore, exhibited increased p-tau and total tau compared to controls [205], which has also been observed in *PSEN1* AD lines [260]. When CRISPR/Cas9 was used to lower *APP* levels down to WT levels, the increase in Aβ42:40 and also in p-tau and tau was reversed. The increase in Aβ secretion and p-tau observed in AD patient neurons is also seen in iPSC neurons derived from patients with Down Syndrome, who carry a third copy of Chromosome 21, and therefore *APP* [428].
Multiple studies have also reported deficits in endosomal pathways in both *APP* and *PSEN1* -mutation carriers: AD neurons with *APP* mutations exhibit greater and larger endosome accumulation, deficits in lipoprotein endocytosis and mitophagy deficits [205, 233, 134], and those with *PSEN1* mutations show defects in mitophagy, autophagy, ubiquitin-proteasome and endo-lysosomal pathways [284, 285, 260, 504, 249]. Furthermore, increased oxidative stress and damage, as well as DNA damage, apoptotic pathways and cell death [284, 336, 504, 520] were observed in *PSEN1* neurons, and impaired mitochondrial dynamics was more severely affected in *PSEN1* and *PSEN2* neurons than *APP* neurons [275].

1.4.2 Sporadic Alzheimer's disease

Several of these phenotypes have also been observed in neurons derived from sAD patients, though less consistently. sAD neurons have been shown to release more Aβ and have increased p-tau levels compared to controls [334, 205]. Furthermore, larger endosomes [205] and defects in mitochondrial function, oxidative and ER stress[233, 48], as well as in activity-induced calcium release [116] have been observed in some but not all sAD patient lines, highlighting the heterogeneity of sAD patients.

The effects of AD risk genes such as *APOE*4 have also been modelled in hiPSC-derived neurons. *APOE*4 neurons have been shown to release more Aβ and have higher tau phosphorylation than *APOE*3, and also had defects in endosomal and mitophagy pathways [262]. *APOE4* astrocytes show impaired Aβ clearance, and increased cholesterol, while *APOE*4 microglia exhibited less Aβ phagocytosis [262]. When corrected to an E3 allele, these phenotypes were rescued. Furthermore, knocking out *APOE* led to phenotypes similar to the E2 and E3 lines, suggesting that the deleterious effects of the *APOE*4 genotype are due to a gain of function of *APOE* [494].
Several SORL1 variants have been identified in AD GWAS, including in patients with EOAD [364]. *SORL1*-KD iPSC-derived neurons had reduced levels of APOE and clusterin (CLU), as well as an increase of Aβ and pTau levels. The expression of SORL1 significantly associated with levels of APOE and CLU in 50 iPSC derived neurons and AD brains from the ROSMAP cohort [247].

1.4.3 Exogenous Aβ and tau treatment in iPSC-derived neuronal models

Importantly, neither fAD nor sAD neurons in 2D cultures present with endogenous Aβ or tau aggregation. As such, another strategy is to mimic AD brain pathophysiology by treating iNeurons with extrinsic Aβ or tau aggregates, and study their effects in cultured neurons. A summary of these studies is found in Tables 1.2 and 1.3.
Aβ oligomer treatment was shown to cause LTP impairment [69, 68], cell death [517, 322, 482, 24], neurite loss [385, 326, 141], synaptic vesicle density reduction [326], synapse loss and EPhys dysfunction [323]. While some studies have reported that fAD neurons are more sensitive to Aβ-induced toxicity, others reported no difference [334, 323]. Furthermore, work from our lab in *Mapt*-/- iNeurons showed that tau depletion reduced Aβ-induced hyperactivity, axonal transport deficits and

neurodegeneration [323], which is consistent with studies conducted in rodent models discussed in section 2.3.1.1.
Furthermore, glycosylated CLU has been shown to exacerbate Aβ neurotoxicity, which was rescued by CRISPR/Cas9 KD of CLU [385, 141]. Aβ has also been shown to induce transcriptomic and proteomic changes in hiPSC neurons: one study compared the effects of Aβ on *APOE*2 and *APOE*3 neurons, showing that while *APOE*2 neurons exhibited increased expression of inflammatory and chemotaxis-related genes [435], while another reported proteomic alterations in control and fAD (*APP* V717I) neurons, related to proteasome and presynaptic vesicles [398]. These studies demonstrated that modelling AD pathology with Aβ oligomers insult replicate findings in rodent models discussed in section 1.3, such as impairment in LTP, neuronal activity and synapse loss.

Most of the work investigating extrinsic tau PFF insult in hiPSC neurons has focused on whether tau PFF could be internalised and seed aggregation in neurons. Many groups have reported that the expression of FTD mutation that increase the aggregation propensity of tau in both iPSC neurons and in the extrinsic tau aggregates used is necessary to induce tau phosphorylation and aggregation [353, 486, 485, 150]. Nonetheless, a few studies have shown that full length 2N4R tau aggregates are internalised by neurons, though one study reported better internalisation of monomers and oligomers than fibrils [476], while another shows that oligomers and fibrils accumulate more quickly, and have different mechanisms of internalisation than monomers [286]. Furthermore, recent work demonstrated that the type of tau insult and the genetic background of the iNeurons is important when evaluating the effects of tau PFFs: they showed that AD brain-derived tau induced more aggregation in wild-type 0N3R neurons than in neurons carrying an FTD mutation in *MAPT* (P301S + exon 10+16 mutations), while treatment with P301L fibrils only elicited aggregation in the FTD neurons. Importantly, they showed no aggregation in tau KO neurons in response to treatment, demonstrating that endogenous tau expression is required for aggregation to occur [281]. Furthermore, cortical inhibitory (Somatostatin +) neurons were shown to be more vulnerable to AD brain-derived tau than hippocampal neurons [501]. One group studied the effects of tau derived from P301L mice on fAD (*PSEN1* L435F) iNeurons, and demonstrated that fAD neurons take up more tau than control neurons, they do not show differences in survival [332].
Multiple studies have reported endosomal and autophagy dysfunction after tau

PFF seeding [353, 501, 485, 476], and that stimulating autophagy reduces tau-PFF effects [485, 476]. Furthermore, tau PFFs induced impaired neuronal activity and calcium release, and neuronal activity was shown to promote tau propagation [353], which supports the work in rodent models that reported tau spread via synapses [82, 265, 119, 111].

Cell type	Model / mutation	Insult	Main findings	Reference
hiPSC neurons	Control	Aβ1–42	Aβ42 oligomers induced LTP impairment, rescued by AD therapeutics	Caneus et al., 2024
hiPSC neurons	Control	Aβ1–42	Compound screen identified a Cdk2 inhibitor that reduced Aβ-induced cell death.	Xu et al., 2013
hiPSC neurons	Control	Aβ1–42	Aβ was more toxic in glutamatergic than GABAergic neurons.	Vazin et al., 2013
hiPSC neurons	Control	Aβ from APP751 mutant cells	Aβ caused reduced vesicle cluster density in neurites and impaired glutamatergic synapse function.	Nieweg et al., 2015
hiPSC neurons	Control	Aβ1–42, tau oligomers, *APP* or tau mouse brain extract	All insults impaired neurite length and LTP induction without causing cell death.	Canneus et al., 2020
hiPSC neurons	Control	AD brain-derived Aβ	Induced transcriptional changes, with JAK/STAT immune/inflammatory pathways most significantly affected.	Colom-Cadena et al., 2024
hiPSC neurons	Control and CLU KO	Aβ1–42, Aβ25–35	Clusterin knockout reduced Aβ-induced neurite loss.	Robbins et al., 2018
hiPSC neurons	Control and CLU exon $2^{-/-}$	Aβ25–35	CLU exon 2 KO altered CLU trafficking and protected neurons from Aβ toxicity; ECM genes downregulated.	Foster et al., 2022
hiPSC neurons	fAD (*APP* V717I)	Aβ1–42	Aβ induced proteomic changes involving proteasome, vesicle pathways, ribonucleoproteins, and increased p-tau S208.	Sackman & Hallbeck, 2020
hiPSC neurons	sAD, fAD (*PSEN1* A246E)	Aβ1–42	fAD neurons secreted more Aβ1–42 and were more sensitive to toxicity than sAD neurons.	Armijo et al., 2017
hiPSC neurons	13 sAD, 1 fAD (APP)	Aβ1–42, Aβ25–35, AD brain Aβ	Neuronal Aβ release correlated with CSF Aβ; synapse loss correlated with clinical severity.	Ng et al., 2022
hiPSC neurons	*APOE* E2/E2 and E3/E3	Aβ1–42	*APOE*3 neurons showed no major pathway changes, while *APOE*2 neurons upregulated inflammation and chemotaxis pathways.	Soladogun & Zhang, 2025
hiPSC neurons	fAD (*PSEN1*) and sAD	Aβ1–42	Increased Aβ release, p-tau, and GSK3B activity; reduced viability compared with controls.	Ochalek et al., 2017

Table 1.2: hiPSC neuron models used to study Aβ toxicity.

Cell type	Model / mutation	Insult	Main findings	Reference
hiPSC neurons	MAPT P301S	K18 P301L tau PFFs	Seeding caused endogenous tau aggregation, endolysosomal dysfunction, and impaired neuronal activity. Neuronal activity promotes tau propagation	Parra-Bravo et al., 2024
hiPSC neurons	Control, MAPT P301S exon 10+16, MAPT$^{-/-}$	AD brain-derived tau, 2N4R P301L PHFs	AD brain tau induced more aggregation in WT neurons, while P301L PHFs induced aggregation only in P301S/E10+16 neurons.	Manos et al., 2022
hiPSC neurons	Control	2N4R tau monomers, oligomers, fibrils	Monomer and aggregate uptake via distinct pathways; LRP1 associated with monomer uptake. Aggregates accumulated more rapidly; oligomers caused some cell death.	Marvian et al., 2024
hiPSC neurons and astrocytes	Control, hetero- and homozygous MAPT S305 mutations	6 tau isoforms	Early 4R tau expression in S305 neurons. 0N isoforms internalised faster by astrocytes. RNA seq of neurons/astros ID mutation specific changes	Bowles et al., 2024
hiPSC neurons	Control	AD brain-derived tau	Cortical inhibitory neurons were more susceptible to tau aggregation than hippocampal neurons; tau seeding caused endosomal dysfunction.	Weilding et al., 2025
hiPSC neurons	MAPT P301L	K18 P301L tau PFFs	Increased AT8 signal and aggregation two weeks post-seeding; reduced by autophagy enhancers.	Verheyen et al., 2015
hiPSC neurons	Exon10+16 ± P301S MAPT	K18 ± P301L tau PFFs	No baseline aggregation. Mutant neurons showed increased apoptosis, Ca^{2+} bursts, and lysosomal pH changes. K18 P301L seeds induced aggregation only in P301S neurons.	Verheyen et al., 2018
hiPSC neurons	Control	FL 2N4R tau monomer, oligomer, fibril	Monomers and oligomers were internalised, but not fibrils. Oligomers caused neurite loss, cell death, and aggregation; autophagy rescued oligomer burden.	Usenovic et al., 2015
hiPSC neurons	fAD (*PSEN1* L435F)	tau seeds from MAPT P301L mice	tau aggregation sensor showed faster tau uptake in fAD neurons without survival differences.	Oakley et al., 2021
hiPSC neurons	MAPT N279K, P301L, E10+16	K18 fibrils	Tau mutants showed increased 4R tau, p-tau, and electrophysiological activity; K18 fibrils induced aggregation and AT8 increase.	Garcia-Leon, 2018

Table 1.3: hiPSC neuron models used to study tau pathology.

As discussed above, the development of iPSC-derived neuronal models has allowed for the study of human neurons in vitro, from patients with the disease of interest. Nonetheless, there are important limitations to these models. Namely, the

reprogramming of fibroblasts or PBMCs into iPSC resets the biological age of the cells, meaning that, despite lengthy differentiation protocols, the neurons studied are in many ways fetal-like, which is an important consideration when modelling an age-related disease like AD. Furthermore, cell culture models lack the complexity, cellular diversity or vasculature of a human brain, and due to these limitations, iPSC-derived neurons do not exhibit any endogenous tau or Aβ aggregation. Although cocultures with glia and neurons, 3D cultures and organoids have started to address some of these limitations, these models remain overly simplistic.

Nonetheless, the work described above has demonstrated that these models are incredibly valuable when studying neurodegeneration, and there have been great strides in establishing reliable models of fAD, and to a lesser extent, sporadic AD. However, iNeurons derived from sAD patients do not consistently reproduce AD-related pathological phenotypes. This is not surprising, given sAD patients, as opposed to fAD patients do not carry mutations that directly increase Aβ production. Recent work, including from our lab, has asked whether iPSC lines derived from sAD patients reflect the clinical measures of the patients they originate from. One study reported that 53 iPSC lines derived from LOAD patients from the ROSMAP cohorts had Aβ and p-tau levels that correlated with Aβ and tau brain pathology, and that there was a high congruence between the iNeurons and the AD brain transcriptomic and proteomic signatures [245], and they observed a similar congruence between iPSC-derived astrocytes and AD brain [248]. Similarly, work from our group showed that sAD neurons from the Deep and Frequent Phenotyping cohort (more details in section 2.4.4) secreted Aβ42 and Aβ40 levels which were correlated with CSF levels. We also reported that sAD patient lines exhibited different levels of vulnerability to extrinsic Aβ insult, as measured by synapse loss and this correlated with clinical measures of the patients. Furthermore, iPSC-derived astrocytes from the same cohort were split in two groups based on their release in CSF of the astrocytic activation marker YKL-40, and the two groups exhibited different morphological changes in response to Aβ insult, which was also associated to their APOE genotype [395].

These studies demonstrated not only that iPSC-derived patient lines replicate key pathological features of the patients they originate from, but line-specific vulnerability to Aβ insult also correlated with patient clinical metrics. The work presented in this thesis will further investigate this question using iPSC-derived neurons from the Deep and Frequent Phenotyping study cohort.

1.4.4 The Deep and Frequent Phenotyping study

The Deep and Frequent Phenotyping (DFP) study is a multicenter study in which patients with MCI were recruited through existing databases. Frequent, repeated measures including cognitive tests, cerebrospinal fluid (CSF), PET imaging, structural and functional MRIs and MEG were collected [242]. A pilot study with 20 patients was first conducted to assess the feasibility of this study design. iPSCs were reprogrammed from PBMCs of 14 patients in the pilot study, which are used in experiments described in this thesis. These include 13 sAD patient, and one fAD patient, which was later found to carry an autosomal dominant APP mutation (accordingly, this patient's iNeurons released more Aβ 42 than the other 13 sAD patients [322]).

The DFP study has several aims. On the clinical front, it is one of the most detailed study of its kind. Although many biomarker studies exist, most only used established measures such as structural imaging or known biomarkers, which are taken relatively infrequently [124, 384, 502]. The DFP study aims to use the varied and frequent measures described above to address the challenges of diagnosing prodromal AD by identifying novel biomarkers.

The experimental branch of the DFP study aims to combine the in-depth, clinical measures described above to cellular phenotypes of iNeurons derived from the same patients, to establish whether individual patients can be modelled *in vitro* (See study design in Chapter 1: Figure 3.1, A). The iPSC work is conducted by several groups, which focus on both neuronal and glial cells, although my work, which is presented here, was conducted on cortical neurons. I aim to continue the work started with DFP iPSC cohort, focusing on both the role of $A\beta$ and tau in patient-specifc vulnerability.

1.5 Aims of the thesis

1. Investigate the effect of Amyloid Beta ($A\beta$) oligomers on neurite outgrowth, and whether it reflects clinical measurements of donor lines.

2. Examine transcriptomic differences in sAD lines in response to Aβ oligomer insult in order to identify what pathways contribute to the vulnerability spectrum observed in sAD patient lines.

3. Explore the effect of tau preformed fibrils (PFF) treatment on various cellular phenotypes, and whether it reflects clinical measurements of donors.

Chapter 2

Materials and Methods

2.1 Deep and Frequent Phenotyping (DFP) study

The DFP study protocol was previously described in great detail in Koychev et al, but will be summarised below [242]. This study took place in 8 recruitment centers across the UK. It is a non-interventional, observational and repeated measures study design, which included 250 male and female participants. A pilot took place beforehand to test for feasibility, and, of this pilot cohort, 14 patients donated PBMCs to make the iPSCs used in this project. The recruited participants were between 56 and 82 years old, 5 females and 9 males, and they had prodromal AD – determined by presence of cognitive impairment and AD pathology but absence of dementia. AD pathology was measured using CSF and PET methods and by using controls that had no cognitive impairment or pathology. All participants went through cognitive testing, which included the Mini Mental State Examination (MMSE), National Adult Reading Test (NART), Clinical Dementia Rating (CDR), Alzheimer's Disease Assessment Scale-Cognitive Sub-scale (ADAS-cog), Bristol Activities of Daily Living Scale (BADLS), Hopkins Verbal Learning Test (HVLT), and the Clock Drawings Tasks 1 and 2 (CLOX1 and CLOX2). MEG recordings (8/14 participants), amyloid PET imaging with [18F] AV45 (0–60 min, 150 ± 24 MBq; 10/14 participants) and tau PET imaging [18F]AV1451 (0–120 min, 163 ± 10 MBq, 9/14 participants) were done once. CSF collection via lumbar puncture was collected twice, 6 months apart, and the measurements were averaged for downstream analyses (12/14 participants). Aβ1-42 was measured by electrochemiluminescence by using a Meso Scale Discovery panel probing for Aβ1-42 with the 6E10 antibody. Total tau (tTau) and phospho tau at Threonine 181 (pTau181) were measured via enzyme-linked immunoassays (ELISA) using the INNOTEST (Fujirebio Europe). An MMSE Score loss rate to measure cognitive decline was determined by dividing the difference in MMSE scores

before first visit and symptom onset by the number of days since both visits. Brain volume was measured at one timepoint for 13/14 patients using MRI.The individual measurements of the patients were not included for confidentiality reasons, however, the mean and range of each measure are described below.

Imaging measures:

Cortical amyloid PET (SUVR) had a mean of 1.43 (range: 1.18–1.63). PET tau had a mean of 1.23 (range: 0.91–1.44). Global MEG recording had a mean of 0.97 (range: 0.94–0.99). Volumetric measures Total brain volume had a mean of 1,436,259.35 (range: 1,200,153.50–1,673,699.00). Hippocampal volume had a mean of 2651.86 (range: 2140.33–3554.75). Corrected hippocampal volume had a mean of 0.00186 (range: 0.00150–0.00244).

Cognitive measures:

MMSE score had a mean of 25.29 (range: 22–29). ADAS-Cog had a mean of 15.57 (range: 3.5-23.5)

CSF biomarkers:

CSF Aβ 1-42 had a mean of 298.54 pg/ml (range: 164.00–450.00 pg/ml). CSF Aβ 40 had a mean of 5740.83 pg/ml (range: 4069.63–8956.72 pg/ml). CSF Aβ 42:40 ratio had a mean of 20.41 (range: 12.75–28.55). CSF total tau had a mean of 753.40 pg/ml (range: 250.56–1232.76 pg/ml). CSF p-tau 181 had a mean of 89.14 pg/ml (range: 39.95–140.45 pg/ml). CSF p-tau:t-tau ratio had a mean of 0.123 (range: 0.099–0.160).

2.2 hiPSC culture

The cell lines used in this project included 13 sporadic AD iPSCs lines and 1 familial AD line from the DFP cohort, as well as i3 iPSCs (i3s). The iPSCs were obtained from peripheral blood mononuclear cells (PBMCs) of Alzheimer's Disease patients recruited through the DFP study and the PBMCs were reprogrammed using Sendai virus, and described previously [322]. Genomic stability of the iPSC lines was checked by karyotyping and SNP array analysis after the last passage before banking. The line IDs are found in Table 2.1.

The i3 line is derived from the WTC11 parental human iPSC line. WTC11 is a well-characterised iPSC line reprogrammed from fibroblasts of a healthy adult male donor (UCSFi001-A; RRID:CVCL_Y803). The i3 line was engineered from WTC11 by stable integration of a doxycycline-inducible NGN2 cassette in Michael Ward's lab at the National Institute of Health and the protocol described below was based

on their published protocol [137, 532, 493].
The cells were maintained in an incubator at 37°C and 5 % CO_2. The iPSCs were plated in mTeSR with ROCK Inhibitor (ROCKi) (1 μM, Tocris Bioscience) and 1 % P/S (Life Technologies) on hESC-qualified 6-well plates for the DFP iPSCs and T75 flasks for the i3s, coated with Matrigel (Corning) or Geltrex (Thermo). ROCKi was removed the next day and media was changed daily. iPSCs were colony-passaged according to confluency using EDTA and replated (1:3-1:6 depending on the proliferation rate of the cell lines). The cells were then frozen down in freezing media (embryonic stem cell grade fetal bovine serum (ES-FBS) and 10 % dimethyl sulfoxide (DMSO)) or used for experiments.

Table 2.1: DFP cohort iPSC line IDs

Patient #	**iPSC ID**
927	BPC-927 03-01
928	BPC-928 03-07
929	BPC-929 03-07
932	BPC-932 03-03
933	BPC-933 03-12
934	BPC-934 03-02
936	BPC-936 03-07
937	BPC-937 03-01
939	BPC-939 03-01
940	BPC-940 03-08
943	BPC-943 03-03
944	BPC-944 03-04-01A
946	BPC-946 04-10
947	BPC-947 04-09

2.2.1 Transduction and expansion of DFP iPSCs

All 14 lines of iPSCs were plated on Matrigel-coated 6 well plates. Once confluent, the cells were passaged using StemPro Accutase Cell Dissociation Reagent (Gibco). They were replated on 6-well plates at 125,000 cells/cm^2 in mTeSR with ROCKi and transduced with lentivirus carrying plasmids for Neurogenin-2 (Ngn2) overexpression (NgN2 and rtTA). The multiplicity of infection (MOI) varied depending on the patient line and had to be optimised for each patient line, but ranged from MOI=4 to MOI=8.

Since the lentiviruses do not express a fluorescent marker, transduction efficiency was determine by inducing differentiation with doxycycline and observing what proportion of cells differentiated successfully.
To create stock, the cells were colony-passaged once 1:6 using EDTA and frozen down in freezing medium once confluent. Excessive passaging was avoided to prevent non-specific differentiation or loss of insertion of the Ngn2 cassette.

2.3 Differentiation of iPSC-derived cortical neurons

2.3.1 DFP iPSC lines

Cells were plated in mTeSR with Rocki on 12-well plates coated with poly-ornithin (PLO) (100 μg/mL) plus laminin (10 μg/mL) (Merck). Both PLO and laminin coatings were incubated O/N at 37°C. Before laminin was added, PLO was aspirated, the plates were rinsed 3x with UltraPure water and left to dry in the hood. The cells were plated at 60,000-120,000 cells/cm^2 depending on the proliferative potential of the cell line. For neurite tracing assay, the cells were transduced with a doxycycline-inducible Ngn2-GFP virus at a concentration of 0.04 μL per 100,000 cells [185] (pLV-TetO-hNGN2-eGFP-Puro). In both cases, the media was changed 5 h later with Ngn2 maturation medium. The cells were selected with puromycin (1.5μg/mL) 2 days later, and replated on the plate format needed for experimental assay on Day 4. The details of the differentiation protocol and media composition can be found in Figure 2.1 and Table 2.2. For most experiments, the cells were replated onto a confluent layer of rat cortical astrocytes (Thermo Fisher) in half-area 96 well plates coated with Poly-D-Lysine (PDL, Thermo). The replating density depended on the assay. Rat cortical astrocytes were introduced to improve neuronal health and morphology, and cell attachment for imaging experiments.

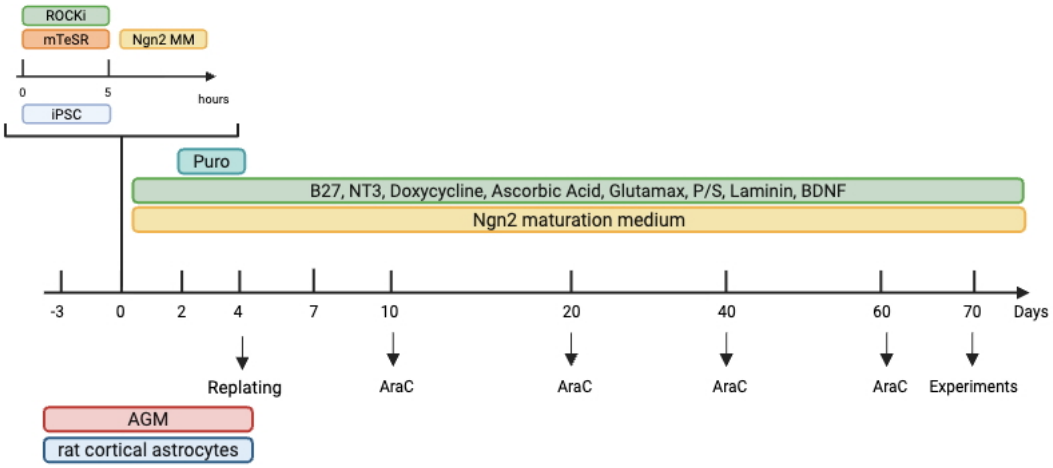


Figure 2.1: Differentiation of iPSC derived cortical neurons from the DFP cohort

2.3.2 i3 iPSCs

The differentiation protocol into i3 neurons is similar to the protocol described above to differentiation the DFP cell lines, as they both use an NgN2 inducible system and is depicted in Figure 2.2. i3s were maintained as iPSCs in mTESR until the desired amount was reached to start differentiating. At that point, on Day 0, the cells were lifted with Accutase, added to a conical tube containing KO-DMEM (Life Technologies) and spun down at 400 g for 5 min. They were plated on T75 flasks coated with Matrigel, at a density of 10 million cells, in induction medium (+ Rocki, 10 μM). The cells were fed daily with induction medium and Rocki was removed on Day 1. For coating of final experimental plates, stock solutions of polyethylenimine (PEI, Sigma) in Borate buffer (20 μL/mL) or PLO (1 mg/mL) were diluted 1:10 in UltraPure water and added onto plates O/N at 37°C. On Day 1, PEI/PLO was removed and the plates were rinsed 4 times with water, and left to dry at RT. On Day 2, the plates were coated with Matrigel and left at 37°C O/N.
On Day 3, the cells were lifted with Accutase, spun down at 300 g for 5 min before being replated on their experimental plates in maturation media + Rocki. The cells were then half-fed twice a week. To avoid peeling, neurons plated on 384 well plates were fed using the CyBio Felix robot (Analytic Jena). Media composition are described in Table 2.2 and cell densities for specific experiments will be described in their respective sections.

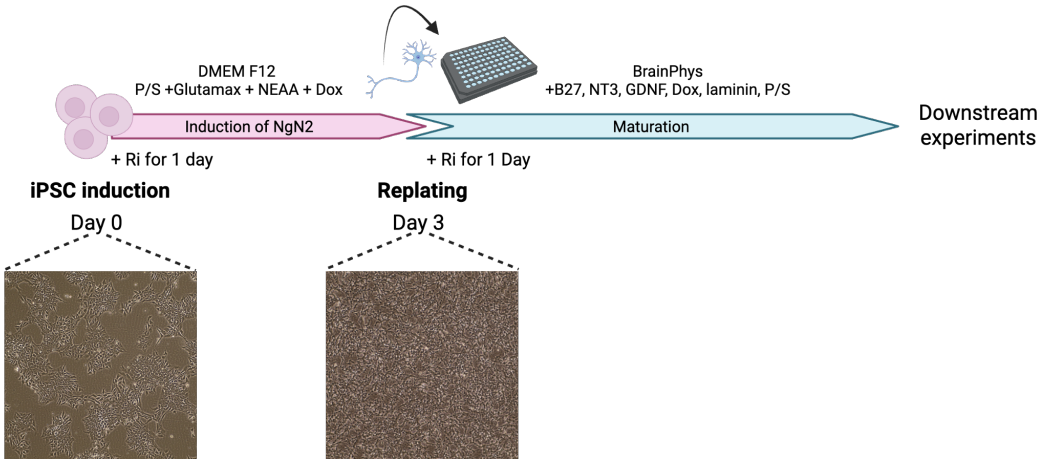


Figure 2.2: Differentiation of i3 iPSC derived cortical neurons

2.4 Rat cortical astrocytes maintenance and culture

For expansion, rat cortical astrocytes were plated on T75 plates and fed every 4 days with Astrocyte Growth Medium (AGM). When confluent, they were passaged 1:7 with using StemProTM AccutaseTM Cell Dissociation Reagent (Gibco), grown to confluency and frozen down in AGM + 10 % DMSO.
For assays, astrocytes were plated on PDL-coated half area 96-well plates at a density of 20,000 cells/cm^2. Cortical neurons were plated on top 7 days later, a confluent monolayer of astrocytes had formed. Once neurons were plated, the cells were fed with Ngn2 maturation media.Media composition is described in Table 2.2

Table 2.2: Composition of Basal Media

Basal Media	Composition
Ngn2 Maturation Medium	Neurobasal medium + 10 ng/mL NT3 supplement + 1X B27 (with vitamin A) supplement + 1 μg/mL Doxycycline + 1X Glutamax + 10 ng/mL BDNF + 200 ng/mL Laminin + 200 μM Ascorbic Acid + 50 μg/mL P/S
Astrocyte Growth Medium	DMEM with high glucose and pyruvate + 15 % FBS + 50 μ/mL P/S + 4mM L-glutamine
i3 Induction Medium	F12 DMEM with 5 mL P/S, Glutamax, N2, Non-essential Amino Acids + 2 μL/mL Doxycycline
i3 Maturation Medium	BrainPhys media with 1X B27, 10 ng/mL NT3 and BDNF, 50 μL/mL P/S, 1 μL/mL Laminin

2.5 Lentiviral production

2.5.1 Transformation of competent bacteria

The guides were designed in SnapGene, assembled and sequence-verified by Dr. Maria Claudia Caiazza, as described previously [71], and the sequences are found in Table 2.4. Ultra competent bacteria were mixed with the guide DNA and spread on Agar plates (Invitrogen) with ampicillin (Sigma, Aldrich, 100 μg/mL). The plates were incubated overnight (O/N) at 37°C, after which a colony was picked and added to LB broth with ampicillin (Invitrogen). The bacteria were then left to shake for 8 hours (h) at 250 RPM at 37°C. Then, 50 mLs of LB broth was spiked with 50 μLs of the bacteria, and left to shake O/N at 250 RPM at 37°C for MIDI prep. The culture was spun down at 3500 RCF for 10 minutes (min) at 4°C, and the DNA was extracted and purified from the pellet using the ZYMO Midi prep kit (Zymo). After elution, DNA concentration was measured using the Nanodrop.

2.5.2 Lentivirus production

Lenti-X HEK293T cells were plated on PLO-coated 15 cm dishes. The cells were transfected the next day. The plasmids and CRISPRi vectors used are described in Table 2.3. A tube containing 2.4 mL Optimem (Life Technologies) and and 30 μL Lipofectamine 3000 (Life Technologies) was added to a tube containing Optimem, 9

μg psPAX6, 3.4 μg pMD2G and 1.4 μg pAdVantage packaging vectors, 80 μL P3000 and 39 μg of the lentiviral vector. It was incubated for 20 min before being added dropwise to the HEK cells. The next day, the medium was changed. Two to three days later, the virus was harvested and concentrated. The media is collected and spun down at 500 x g for 10 min. Except for the NgN2-GFP virus, the viruses were concentrated using the Lenti-X concentrator according to the manufacturer's instructions (Takara Bio). Briefly, the spun-down supernatant is mixed with the Lenti-X concentrator 3:1, mixed by inversion, and incubated at 4°C for 3 days. The samples were centrifuged at 1500 g for 45 min at 4°C. The supernatant was removed without disturbing the pellet, and the pellet was resuspended in 360 μL of PBS and stored at -80°C in 12 μL aliquots. The Ngn2-GFP virus was simply filtered with 0.45 μM steriflip filter (Merck) , then aliquoted and frozen down.

2.5.3 Lentiviral titration

2.5.3.1 Ngn2 and rtTA viruses

The lentiviruses were titrated using a Lenti-X p24 Elisa Kit according to the manufacturer's instruction (Takara Bio). Briefly, lysis buffer was added to each well, followed by the standard curve, supernatant and culture medium samples in their respective wells, and incubated at 37°C for 1 h. After this and each of the following steps the contents of the wells were aspirated and washed 5x with wash buffer. Anti-p24 antibody was added to the wells, incubated for 1 h at 37°C. Streptavidin-HRP was added and incubated at RT for 30 min. Substrate solution was added to each well and incubated in the dark at RT for 30 min. The reaction was stopped by adding Stop Solution, after which the absorbance at 450 nm was measured. Since NgN2-GFP was not concentrated, the virus was tittered on iPSC-derived neurons transduced at Day 4. A transduction efficiency of 1 % was optimal for the purposes of the experiments, and this was achieved by freeze thawing the aliquots once before use (to reduce the titer) and transducing with 0.2 μL per 500,000 cells.

2.5.3.2 CRISPRi guides

The lentiviruses carrying the non-targeting (NT) plasmids or the guides targeting the genes of interest were titrated on i3 neurons by serial dilution. The virus was diluted

in 1:4 in PBS and was added to neurons in volumes of 1500, 1250, 1000, 750, 500, 250, 200, 100, 50 nL. The neurons were transduced upon replating on Day 3. 48 h later, HCS NuclearMask Far Red was added (1:250) and incubated for 15 min at 37°C. The cells were then washed once with PBS, before adding fresh media and live imaging. The transduction efficiency was then determined by looking at BFP colocalisation with HCS NuclearMask Far Red. The guide sequences are found in Table 2.4.

Table 2.3: List of plasmids used and their functions.

Plasmid	**Vector number**	**Function**
psPAX2	Addgene, #12260	Second generation packaging vector
pMD2.G	Addgene, #12259	VSV-G envelope expressing plasmid
pAdVantage	Promega, #E1711	Second generation packaging vector
rtTA (FudeltaGW-rtTA)	Addgene, #19780	Express Transactivator
Ngn2 (pTet-O-Ngn2-puro)	Addgene, #52047	Doxycycline-inducible expression of Ngn2
Ngn2 (pLV-O-hNgn2-eGFP-Puro)	Addgene, #79823	Doxycycline-inducible expression of GFP

Table 2.4: CRISPRi guides

Target	Guide number	Guide sequence
SREBP1	Guide 1	GGAACCAGGGAGGCTCGGTG
	Guide 2	GGCGCCTTGACAGGTGAAGT
SREBP2	Guide 1	GCCGGCACCGCCTCACCGAC
	Guide 2	GTGACCCTGGGAGACATCGA
Non-targeting	Guide 1	GTCCACCCTTATCTAGGCTA
	Guide 2	GGACTAAGCGCAAGCACCTA

2.5.4 CRISPRi knockdown in i3 neurons

The i3 iPSCs are also stably integrated with a CAG-promoter driven dCas9-BFP-KRAB transgene, which allows for rapid CRISPRi mediated knockdown (KD) of genes of

interest [471].
For all CRISPRi experiments, the cells were transduced with 0.375 μL of virus per well on Day 3, upon replating (12,000 cells per well). The media was fully changed the next day to remove viruses and Rocki. The cells were then grown as described above. KD was confirmed by qPCR.

2.6 Cell viability assay

Cell viability was measured using ToxiLight Bioassay Kit (Lonza), which measures the amount of adenylate kinase (AK) in the cell medium. At the end of Aβ and tau treatments, cell medium was collected from wells and AK detection reagents was added 1:5. After a 5 min incubation at RT, the plate was imaged on the Pherastar Plate Reader. Each plate was run twice and the values for each well were averaged and normalised to blank wells (Water + AK reagent).

2.7 Amyloid Beta peptide oligomerization

Lyophilised Aβ 1-42 and treatment control scrambled Aβ 1-42 (Bachem, H-1368 and H7406) were resuspended in 1mM Hexafluoro-2-propanol (HFIP, Merck). They were vortexed for 30 sec then incubated for 1 h at RT, until the liquid looked clear and the Aβ was fully resuspended. The peptide was then aliquoted 20uls aliquots. An additional 50 μL of HFIP was added to each aliquot, left to evaporate, then another 20 μL was added and left to evaporate. They were then dried in the Speed-Vac concentrator for another h to ensure complete evaporation of the HFIP. The Aβ film was stored at -80°C.
To oligomerise, the peptides were first resuspended in DMSO to 5 mM and sonicated in a water bath at RT for 10 min at 20 Hz amplitude, with pulses of 10 sec on, 5 sec off. PBS was then added to 100 μM solution and the peptides were incubated at 4°C for 24 h. The next day, they were centrifuged at 16,000 g for 10 min at 4°C to remove any precipitate or fibrils, then aliquoted and frozen at -80°C until treatment.

2.8 Tau preformed fibrils production

The Tau preformed fibrils were made by Dr. Nora Bengoa-Vergniory. Recombinant human tau (2N4R 441) was obtained from the Oxford Protein Purification Service. Monomer (2 mg/mL) was incubated in Sodium Acetate 100 mM pH 7.0 (Sigma),

0.04 nM Heparin (Sigma), and 2 mM DTT (ThermoFisher) for 28 days at 37 °C with continuous shaking (250 rpm). Fibrils were sonicated (20 % amplitude and 0.25 cycle duty until optimal fragmentation) to yield short fibrils (around 50-100 nm average size). Morphology was verified by TEM in the Microscopy service of the University of the Basque Country. PFFs were aliquoted, and frozen at -80 °C to avoid freeze thawing.

2.9 Lipid droplet visualisation with BODIPY

Lipid droplets were measured using the BODIPY 493/503 dye. The cells were first incubated with NucBlue, a live nuclei stain (2 drops per mL of media) for 15 min at 37°C. Then, BODIPY dye was added to the cells without removing NucBlue at a concentration of 1:500 for 15 min at 37°C. Control wells were treated with the same concentration of DMSO, the solvent for BODIPY. After that the cells were washed gently 3 times with PBS, before adding fresh media. Immediately after, they were live imaged on the Opera Phenix.

2.10 Immunocytochemistry (ICC)

Cortical neurons were fixed in 4 % PFA for 5 min for synapse staining, 20 min for all other staining. They were permeabilized in 0.05 % saponin in PBS for 20 min and blocked with 10 % normal goat serum (NGS) or donkey serum (NDS) with 0.01 % Tween-20 (Merck) in PBS for 1 h. They were incubated O/N at 4°C with primary antibodies in PBS with 1 % NGS and 0.01 % Tween-20 . The next day, they were washed with PBS 3 times, then incubated at RT for 1 h with secondary antibodies in PBS with 1 % NGS or NDS and 0.01 % Tween-20, before washing 3 more times with PBS. All primary antibodies used are described in Table 2.5. All secondaries were goat or donkey Alexa Fluor antibodies (488, 555 or 647, 1:1000, Thermofisher). Dapi (Sigma) was added to secondaries as well (1:10000).

Table 2.5: Primary antibodies

Antibody	**Concentration**	**Species**	**Supplied**
Synapsin I/II	1:500	Guinea Pig	Synaptic Systems
Homer 1	1:500	Rabbit	Synaptic Systems
MAP2	1:1000	Chicken	Abcam
Cleaved Caspase 3	1:1000	Rabbit	Abcam
Human Nuclear Antigen	1:200	Mouse	Abcam
CUX2	1:200	Rabbit	Abcam
CTIP2	1:200	Rat	Abcam
BRN2	1:250	Rabbit	Cell Signalling
B-tubulin	1:500	Rabbit	Abcam
B-tubulin	1:500	Mouse	BioLegend
p-tau (s396)	1:1000	Rabbit	Abcam
AT8	1:500, 1:250	Mouse	ThermoFisher
Tau 12	1:500	Mouse	Merck Millipore
Tau 5	1:500	Mouse	Abcam
S100B	1:500	Mouse	Merck
GFAP	1:500	Chicken	Abcam
SREBP2	1:500	Rabbit	Santa Cruz
SREBP1	1:1000	Mouse	Abcam
TM7SF2	1:250	Mouse	Merck
beta-actin (HRP)	1:10000	Mouse	Abcam

2.11 High-content imaging and analysis

All plates were imaged on the Perkin Elmer Opera Phenix high-content imager and images analysed on the Harmony software v5.2 from Perkin Elmer with customized pipelines.

2.11.1 Synapse staining

Cells were stained with microtubule associated protein 2 (MAP2), Homer 1, Synapsin I/II and DAPI was added to stain nuclei. 23 fields per well were imaged with a 60 X objective with 7 z-stacks (-1 to 5 μm) and a binning value of 1. The synapse pipeline first picks up MAP2 area (0.5 overall threshold). Both Synapsin I/II (presynaptic) and Homer1 (postsynaptic) signals were detected using the "Find Spots" building block (Method A) with threshold values of 0.17 and 0.14, respectively. Spots that were larger than 100 px were filtered out. The synapses were detected by finding

Homer 1 spots in the vicinity of Synapsin I/II spots which were resized by expanding out 5 px.

2.11.2 Neurite tracing

The DFP iPSCs were plated as described above, and transduced with Ngn2 GFP virus. On Day 4 they were replated at a density of 25,000 cells/cm^2 onto rat cortical astrocytes in half area 96-well plate. For i3 iPSCs, the cells were plated at a density of 62,500 cells/cm^2. They were not plated onto rat cortical astrocytes, which is why they were plated at a higher density.
The entire well of a 96 well half area plate was captured with the 488 nm channel, with a 20 X objective, binning value of 1, a z-stack between -3 an 2 μm and standard flatfield correction on the Opera Phenix. Overlap was set to 1 % to enable uninterrupted tracing between fields of view. The Phenix was set to 5 % CO2, 27°C to allow for live imaging. On the first and last day of imaging, Brightfield images were also taken. All analysis was run in the Harmony analysis software. Nuclei were found using “Find Nuclei” (Method B), then filtered by calculating and filtering for their size and roundness, and neurites found using “Find neurites" building blocks.

2.11.3 Cleaved Caspase 3 (CC3) staining

Cells were stained with MAP2, CC3 and Human Nuclear Antigen (HuNu). 15 fields with 4 planes (-4 μm to 2 μm) per well were captured with a 20 X objective, with binning value of 1. The pipeline first picks up MAP2 area (0.5 overall threshold), before finding the Human nuclear antigen positive-nuclei using “Find Nuclei” building block (Method B). Then, nuclei positive for CC3 within the HuNu+ nuclei were found.

2.11.4 Lipid droplet imaging

Lipid droplets were live imaged with BODIPY 493/503 and NucBlue at 63 X magnification on the Opera Phenix (37°C, 5 % CO_2). 41 fields of view were captured with 7 stacks (2-8 μm) and a binning value of 1. The analysis pipeline first identifies nuclei stained with NucBlue using the "Find nuclei" building block, which are then filtered for size and roundness. Then, the droplets are found using the "Find Spots" within the cell area, and their intensity and size are calculated.

2.12 Western Blotting

All samples were lysed with cold RIPA buffer (Thermo) supplemented with 1 x cOmplete(TM), Mini, EDTA-free Protease I inhibitor (Merck) and 1 x Pierce Phosphatase inhibitor (Thermo) (10X stock is made by diluting 1 tablet in 10 mL RIPA). The concentration was determined by BCA assay according to the manufacturers protocol. 4 x LaemmLi Buffer (BioRad) with 1:100 Beta-mercaptoethanol (Sigma) was added to the samples, which were boiled for 5 min at 4°C. In the case of samples being probed for total tau, the samples were lysed without phosphatase inhibitors and were pretreated with Lambda Phosphatase for 1 h before boiling (New England Biolabs). The samples were run on 4-15 % polyacrylamide gels at 100V. The gels were transferred onto a Polyvinylidene fluoride (PVDF) membrane using the TurboBlot fast transfer (BioRad). The blots were then blocked for 1 h, shaking, in 5 % milk in TBST and probed with primary antibodies in 1 % milk in TBST O/N at 4°C, shaking. The next day, the blots were washed in TBST 3 times, probed with secondary antibody (BioRad, 0.2 μL/ mL) in 1 % milk in TBST for 1 h at room temp, washed 3 times with TBST and imaged on the BioRad ChemiDoc. The blots were then stained with beta actin conjugated to HRP (Abcam), which was incubated in 1 % milk for 1h at RT (0.4 μg/mL), washed 3 times before imaging. In cases where the protein of interest was of similar size to beta actin, the blots were first stripped with stripping buffer for 15 min and washed briefly before probing. Details of all buffers and antibodies can be found in Tables 2.5 and 2.6.

Table 2.6: Western blot reagents

Western blot reagents	Concentration
RIPA Buffer	
cOmplete, Mini, EDTA-free Protease Inhibitor Cocktail	1 tablet per 10mL RIPA
Pierce Phosphatase Inhibitor Mini Tablets	1 tablet per 10mL RIPA
4X LaemmLi Buffer	
Beta Mercaptoethanol	1:1000
10X Tris Buffered Saline (TBS)	
MilliQ Water	1L
TRIS 1M pH 7.5	200mL (20mM)
NaCl	88g (150nM)
1X TBS-T	
MilliQ Water	900mL
Tween 20	1mL
10X TBS	100mL
Running Buffer	
MilliQ Water	up to 1L
Tris Base	30.3g
Glycine	144g
SDS	10g

2.13 RNA extraction and cDNA synthesis

Cells were lifted off wells using cold PBS, spun down for 5 min at 500 g. Most of the PBS was then aspirated leaving about 10-20 μL on the pellet before flash freezing them. The cells were then homogenised using buffer RTL with 1:100 Beta-mercaptoethanol .

RNA extraction was performed using the RNAeasy extraction kit following the manufacturer's instructions. A 5 min incubation at RT was added to the protocol following addition of water to the membrane to elute the RNA in order to increase RNA yield. RNA yield was measured using Nanodrop. 100 ng of cDNA was

synthesized from each sample using SuperScript III (Thermo Fisher), following the manufacturer's protocol.

2.14 Primer design and qPCR

Primers were designed on primer blast and all sequences can be found in Table XX. For a 20 μL reaction, the qPCR reagents were used as follows: 10 μL SYBR green master mix, 2 μL cDNA (2ng cDNA), 0.6 μL of 10 μM forward and reverse primers and 6.8 μL of water.

Table 2.7: Primer sequences used for quantitative PCR

Gene	Forward primer	Reverse primer
BRN2	GTTGCCGTTTTGGGGGATTT	ACGAAGAAGGGGCAACACAA
CUX1	CTGGGACACAGGATGCGG	CCGACTTTCAGGCTGGTCTT
GSK3B	GACTAAGGTCTTCCGACCCC	AAGAGTGCAGGTGTGTCTCG
MAPT	ACGAAGCTGCTGGTC	CTTCCAGTCCCGTCTT
SLC17A7 (VGLUT1)	GTCAACAACAGCACCATCCA	CCCGGAATCTGAGTGATGAT
SREBF1	TCCACCCCTGTGTTAGGCTA	ACACTCTGGACCTGGGTGT
SREBF2	CTCCGCAGACGAGGATCATC	TGTACTGTCTGCACCTGCTA
GAPDH	TCATCATCTCTGCCCCCTCT	TCATGGATGACCTTGGCCAG

2.15 Tau ELISAs

The total tau ELISA (Thermofisher) was performed according to the manufacturer's instructions. Conditioned media for cortical neurons was collected and frozen down. Right before use, the samples were spun down at 200 g for 5 min to get rid of debris. All incubations were done at RT. The sample and standards were added to the wells in triplicates and incubated for 2 h. The wells were washed 4 times with 1 X wash buffer. Biotin Conjugate solution was added for 1 h, followed by 4 washes. The Streptavidin HRP solution was added for 30 min, followed by 4 washes. The chromogen solution was added and incubated for 30 min in the dark, followed by the stop solution. The plate was then imaged on the Pherastar (BMG Labtech) at 450 nm wavelength.

The pTAU 181 ELISA (antibodies.com) was performed according to the manufacturers instructions but with a few modifications. The samples of conditioned media were added 3 times for 90 min incubations, instead of one, 2 h incubation. This was to

increase the signal, as the level of secreted ptau181 in the conditioned media was expected to be low.

2.16 Bulk RNA sequencing

3 bulk RNA sequencing experiments were performed. The first and second were performed in i3 neurons treated with Aβ oligomers or tau PFFs, respectively (3 replicates per conditions). The third was performed in the 14 iPSC-derived neuron lines from the DFP cohort treated with Aβ oligomers. Only one replicate per line was included in the experiment due to the considerable number of samples. 2 replica plates were prepared for each experiment and the second was stored for validation experiments.

The second experiment was done as part of a DPhil rotation project by Helen Jolly. The cells were grown, treated, collected and extracted by myself, but the analysis was in large part conducted by Helen. RNA was extracted and quantified as described above. The samples were then sent to Novogene, who performed the library preparation, quality control (QC) and RNA sequencing. 2 samples from the first experiment in i3s did not pass the RNA integrity test, but the samples were still sequenced as the concentration of RNA was sufficient. Briefly, the RNA library preparation included mRNA enrichment with Poly-A capture and fragmentation, cDNA synthesis by reverse transcription and adapter ligation. The libaries were then checked with the Qubit, bioanalyzer and RT-PCR. The Sequencing was done on the Illumina (PE150) platform.

The raw data files were provided in FASTQ files. The reads were first aligned to a reference human transcriptome (Ensembl GRCh38.109) and quantified using Salmon in Terminal. The first experiment was aligned by Dr. Peter Kilfeather, the second by Helen Jolly and the third by myself. All subsequent analysis was done in R (4.3.1) in RStudio (2023.06.0+421). The files generated by Salmon were imported into R using tximport ([436]). The transcripts were then mapped to genes and genes with less than 30 counts were filtered out before differential gene expression analysis was performed using DESeq2 (v.1.42.1) ([270].

Principle component analysis was done using the plotPCA function, after transforming the count matrix using the vst function. To visualise the top differentially expressed genes (DEGs), volcano plots for the $\log_2$ fold change and -$\log_{10}$ p value were generated using ggplot (3.5.2). DEGs with a p value of < 0.05 were highlighted and labelled.

Gene set enrichment analysis (GSEA) and over representation analysis was performed

and visualised using functions written by Dr. Benjamin Vallin (https://github.com/benvallin/rnaseqtools.git), which uses the fgsea (1.28.0) package ([235]). These functions perform pathway enrichment on pathway databases including the Gene Ontology: Biological Process, Cellular Component and Molecular Function, Hallmark pathways, WikiPathways, Reactome Pathways and Kegg Pathways. To perform the analysis, a list of all protein-coding DEGs was generated, ranked by the $\log_2$ fold change times the -$\log_{10}$ p value. This ranking takes into account both the size of the effect and its significance, rather than just the fold change.

2.17 Statistical Analyses

All statistical analyses were performed in Prism or RStudio. The details on each analysis are described in the relevant figure captions.

Chapter 3

The effect of $A\beta$ on sporadic AD patient iPSC-derived cortical neurons from the DFP study

3.1 Introduction

Axonal degeneration is a key early pathological feature of Alzheimer's disease (AD). Dystrophic and degenerating axons are detectable at very early disease stages—appearing even before substantial $A\beta$ or tau deposition, though dystrophic neurites are closely linked to amyloid and tau pathology [241, 366]. Clinical neuroimaging studies further support this, showing axonal and white matter abnormalities in individuals with mild cognitive impairment, as well as reduced hippocampal volume in cognitively normal individuals who are amyloid-positive compared to amyloid-negative controls [352]. These findings suggest that $A\beta$ pathology is tightly linked to early axonal vulnerability in AD.
Mouse models of familial AD similarly demonstrate that synaptic dysfunction and axonal degeneration are early manifestations of the disease, and that changes in white matter integrity coincides with early $A\beta$ accumulation [335, 437, 64]. Furthermore, animal models have shown that $A\beta$ oligomers are likely the more toxic species of $A\beta$, and that they cause LTP deficits [490, 148].

More recently, iPSC models have been shown to recapitulate some features of AD: for instance, neurons derived from fAD patients display elevated $A\beta$ 42 release and APP expression relative to both control and sporadic AD (sAD) neurons, and exhibit increased Tau phosphorylation [334, 339]. $A\beta$ pathology has also been modelled experimentally through the introduction of exogenous $A\beta$ oligomers.

Studies have demonstrated that $A\beta$ oligomers are neurotoxic [122, 326, 482], while fibrils and monomers are not [24]. Furthermore, one study reported that fAD-derived neurons showed heightened vulnerability to $A\beta$ compared to controls [24]. $A\beta$ oligomers impair long-term potentiation and disrupt electrophysiological activity [68, 69], consistent with their synaptotoxic nature. Additional work has implicated Clusterin as a critical mediator of $A\beta$-induced neurite degeneration in both rodent primary cultures and human iPSC-derived neurons [385, 141, 226]. Importantly, work from my lab using sAD iPSC-derived neurons has shown that $A\beta$ exposure can induce synapse loss and deficits in neuronal network activity measured by MEA, highlighting that $A\beta$ toxicity manifests across both familial and sporadic forms of the disease [322].

One of the central aims of the Deep and Frequent Phenotyping (DFP) study is to bridge in-depth clinical measurements from sporadic AD patients with cellular phenotypes observed in iPSC-derived neurons generated from the same individuals (Figure 3.1A). This approach offers the opportunity to test whether patient-specific features of AD can be recapitulated *in vitro*. Recent evidence suggests that such cellular–clinical correspondence is indeed possible. Several studies have shown that iPSC-derived cortical neurons and astrocytes can reflect clinical features of their donors, including measures of amyloid burden, synaptic integrity, and cognitive performance [322, 395, 245, 248]. Two of these studies, conducted within the DFP cohort, found that neuronal phenotypes such as $A\beta$ secretion, synapse density, and electrophysiological activity correlate with clinical readouts including CSF $A\beta$ levels, MEG activity, and cognitive scores.
Building on this evidence, the present chapter continues the investigation into how $A\beta$ exposure affects neurons derived from the DFP cohort, with the goal of determining whether clinically relevant $A\beta$-related vulnerabilities can be captured *in vitro*.

3.1.1 Aims of this chapter

In this chapter, I aimed to:

- Generate NgN2 iPSC lines of 14 patients of the DFP cohort and differentiate them into cortical neurons.
- Investigate whether the $A\beta$ oligomers affect neurite outgrowth of iPSC-derived cortical neurons to a different degree in the 14 patient lines.

- Determine whether the neurite loss caused by $A\beta$ insult is correlated with the clinical measures of those patients.

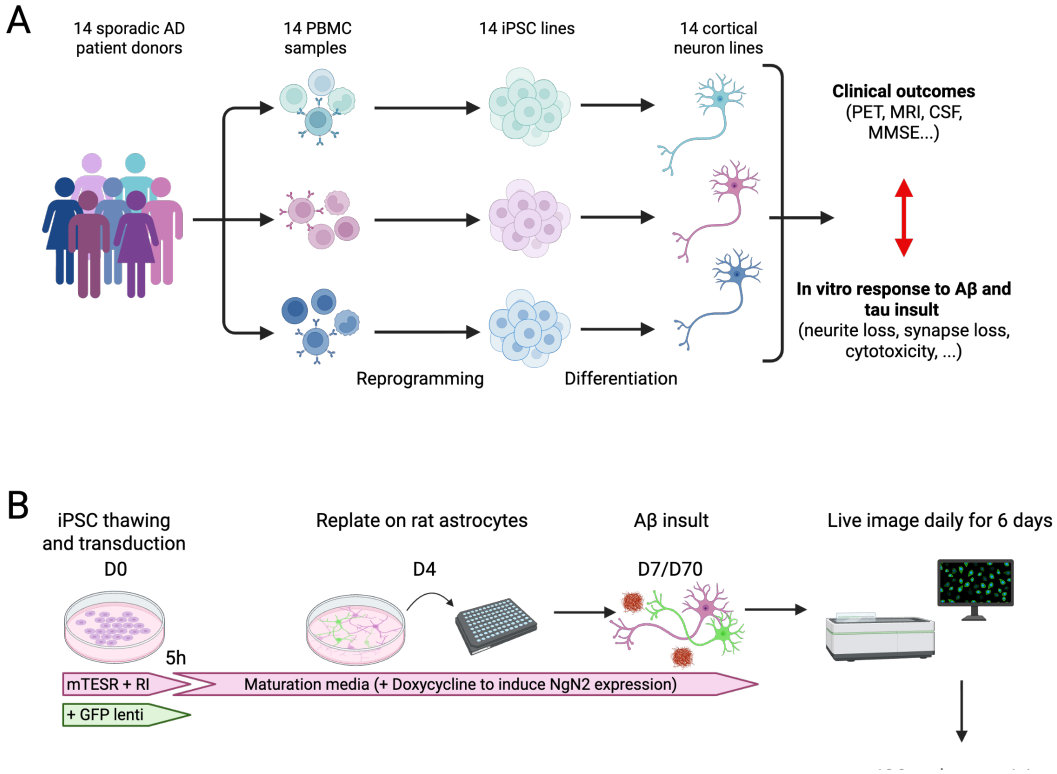


Figure 3.1: **Graphical depiction of DFP study design and experimental design of the neurite tracing assay**(A) Graphical representation of the study design of the experimental arm of the Deep and Frequent Phenotyping Study, (B) Workflow of the GFP neurite tracing assay in the DFP cohort neurons

3.2 Generation of 14 NgN2-expressing iPSC lines

Since this project was originally a collaboration between three groups using the same cells, it was determined that we needed a simple differentiation protocol to reduce the variability between groups. The iPSCs are differentiated into neurons using a NgN2-driven protocol. To do so, I first set out to transduce, expand and bank the iPSC lines of the AD patients according to a previously optimised protocol by Dr. Anne Hedegaard. NgN2 and rttA lentiviruses were produced in HEK293T cells and concentrated. Since the plasmids do not contain a fluorescent marker, the viruses were titered using a p24 ELISA.

Previously, most lines had been transduced at a multiplicity of infection (MOI) of 4 or 6, so I first attempted to repeat this. However, I found that the different cell lines exhibited various levels of transduction efficiency, and I therefore had to optimise the concentration of virus used for each of the 14 lines. The MOI ranged from 4 to 10.
Due to the absence of fluorescent markers, I determined the efficiency by inducing the cells with doxycycline, and seeing how many cells differentiated, and how much cell death was caused by the addition of puromycin, since the plasmids included a puromycin selection sequence (Figure 3.2). I determined that the transduction efficiency was acceptable if no colonies of iPSCs remained after puromycin selection, except for dead colonies which were lifting off the well.
Once the optimal concentration of virus was determined, each line was grown until it could be split on a full 6 well plate and transduced with the appropriate concentration of virus. I then colony-passaged the cells 1:3 before freezing them down for future use. Cells were not expanded for more rounds than this, as this resulted in lower differentiation efficiency and higher rates of spontaneous differentiation. This is likely due to a loss of the transduction cassette caused by excessive passaging.
One line specifically, line 932, tended to spontaneously differentiate easily, and therefore was very challenging to expand and transduce, which is why the cell line was not used in all experiments.

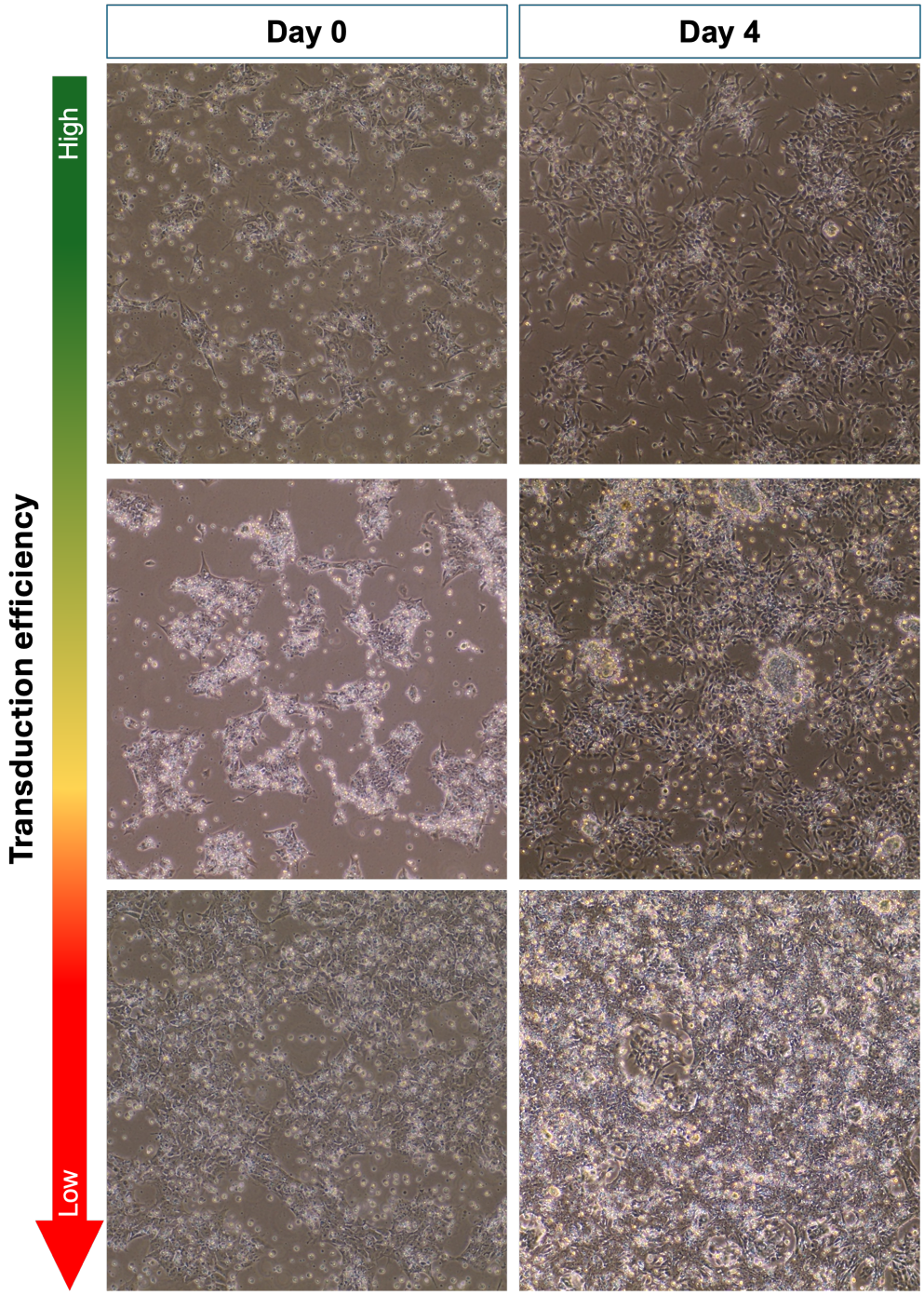


Figure 3.2: **Transduction efficiency of NgN2 and rttA3 lentiviruses in sAD iPSCs**. Representative images of 3 cells lines with (top to bottom) good, acceptable and bad transduction efficiencies at Day 0 (left) and Day 4 (right) after induction with Doxycycline. In the bottom panels large colonies of iPSCs are still visible, even after induction and puromycin selection.)

3.3 Characterisation of iPSC-derived cortical neurons

The DFP cohort cortical neurons have been well characterised in [322]. The NgN2-transducible system leads to rapid and consistent differentiation into glutamatergic cortical neurons [493]. I characterised the neurons by RNA expression using qPCR and protein expression using immunocytochemistry at several timepoints (Figure 3.3, 3.4. The 14 patient lines expressed BRN2 an early upper layer neuronal marker (V), and its RNA expression dropped with time (Figure 3.3, A) [114], while protein levels remained mostly consistent (Figure 3.4, B, E). CUX1 is expressed in layers (II-IV) of the cortex, and is expressed throughout development [325, 537]. It was expressed at similar levels at Day 10, Day 30 and Day 50 in the iPSC-derived neurons (Figure 3.3, B). CTIP2, a deep layer V marker [23], protein expression went up slightly between Day 7 and Day 70 (Figure 3.4, C, F). VGLUT1, which transports glutamate into synaptic vesicles of glutamatergic neurons is expressed in the iPSC-derived neurons [42] (Figure 3.3, C). Its expression goes down with time, which is consistent – along with BRN2 and CUX1 – with other NgN2 neuron protocols [379, 349]. Microtubule-associated protein Tau (Tau) was highly expressed, and increased between Day 10 and Day 30 (Figure 3.3, D).
Cortical neuron markers were expressed in all 14 AD cell lines across multiple timepoint of maturation.

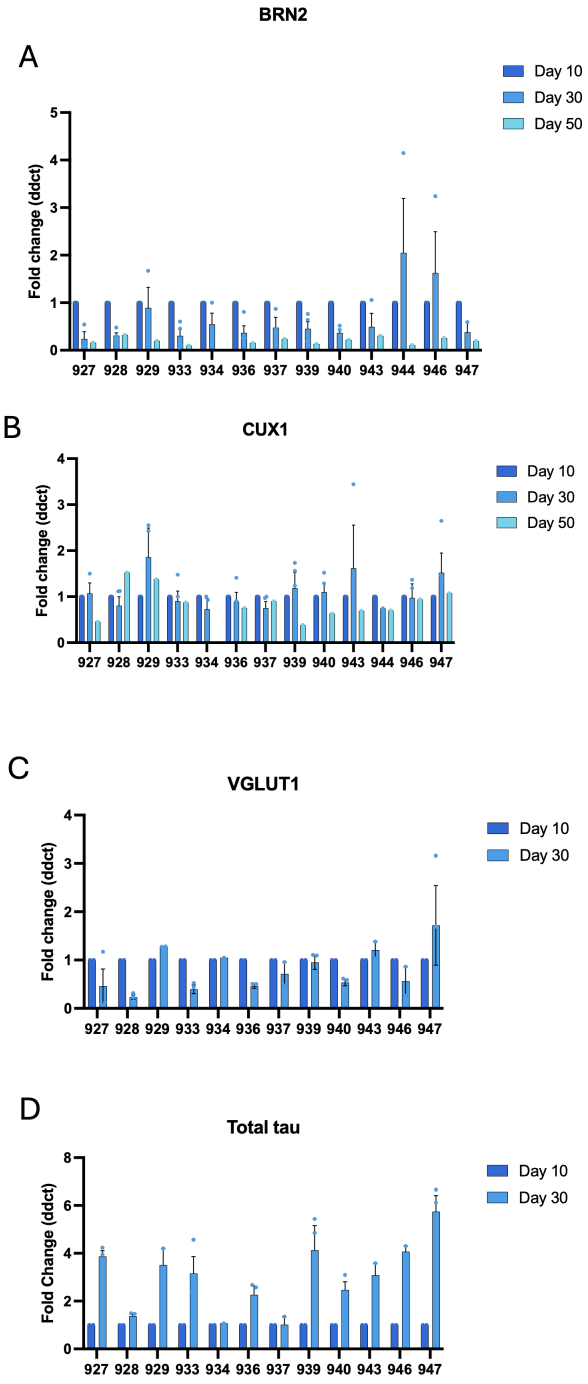


Figure 3.3: **Expression levels of cortical markers in iPSC-derived neurons by qPCR**. (A-D) RNA expression of BRN2, CUX1, VGLUT1 and total Tau at Day 10, Day 30 and day 50 for A-B and Day 10 and 30 for C-D. Expression is normalised to housekeeping gene GAPDH and normalised to Day 10 for each line. Mean ± SEM of 2-3 independent differentiation repeat averaged across 3 technical replicates.

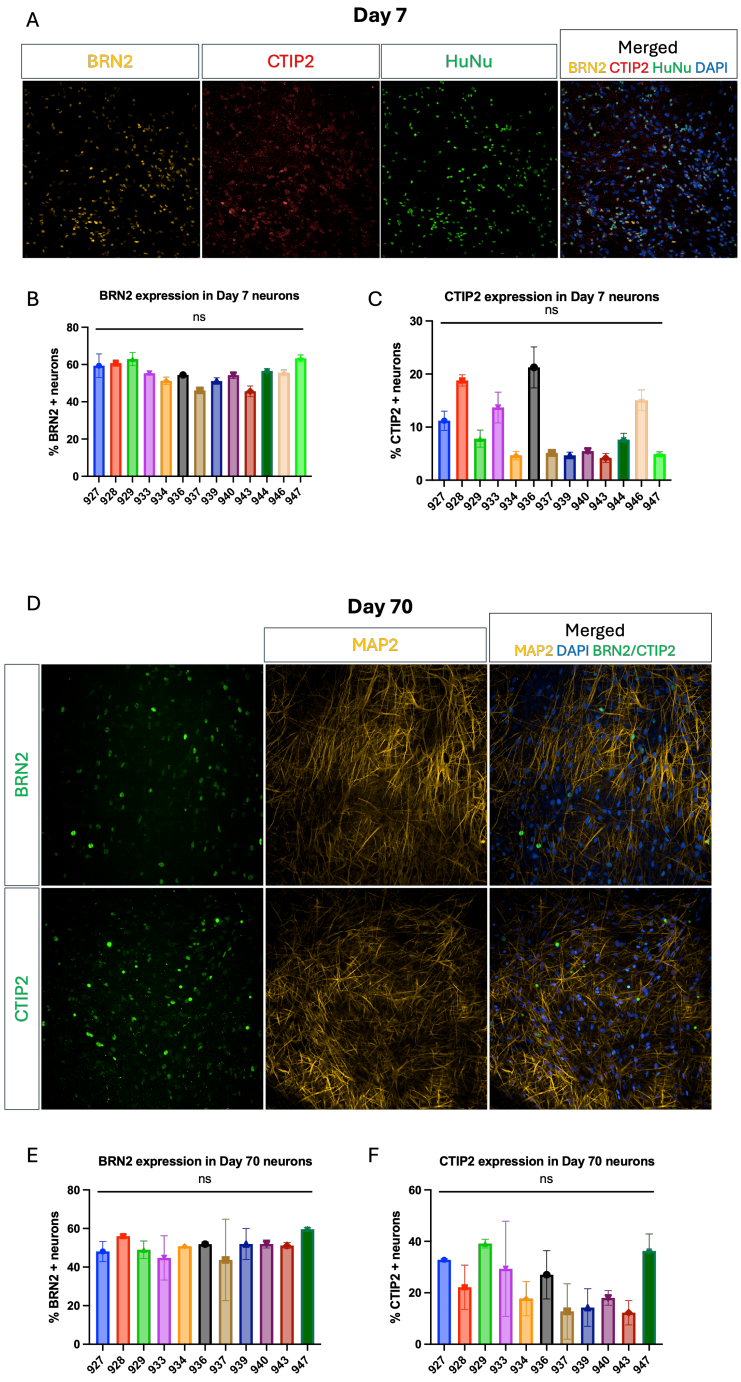


Figure 3.4: **Immunostaining of cortical markers in iPSC-derived neurons**. (A) Representative images HuNu, CTIP2 and BRN2 in Day 7 cortical neurons (B-C) Quantification of the number of neuronal nuclei (HuNu) that are BRN2+ (B) and CTIP2+ (C). (D) Representative images of CTIP2 and BRN2 and MAP2 in Day 70 cortical neurons. (E-F) Quantification of the number of nuclei in MAP2 that are BRN2 + (E) and CTIP2 + (F). Mean ± SEM of 3-4 replicates of 1 differentiation. Kruskal-Wallis test. Each dot is one technical replicate.

3.4 Neurite tracing of Day 7 iPSC-derived cortical neurons from the DFP cohort after $A\beta$ insult

3.4.1 Experimental design

The goal of this experiment was to assess the effect of $A\beta$ oligomers on neurite outgrowth and degeneration in the iPSC-derived neurons from the DFP pilot cohort. As described in Chapter 1, the DFP pilot cohort cells include 13 sAD patient lines, and 1 fAD line carrying an APP mutation. It was previously shown that while this line had a higher secreted $A\beta$42:40 ratio, the effect of $A\beta$ oligomers on this line was within the range of its effect on the other sAD lines [322].

To measure neurite outgrowth, I transduced the neurons with a very low titer of an NgN2-GFP lentivirus, which encodes GFP under the same dox-inducible promoter used to drive NGN2, such that GFP expression confirms doxycycline-induced activation of the differentiation cassette (referred to as NgN2-GFP throughout, see Chapter 2.3 for details) at Day 0 (0.04 μL per 100,000 cells), which transduces about 1 % of cells (Figure 3.5. The cells were plated at a low density (25,000/cm^2), which allowed for accurate tracing of neurites over the course of the live imaging using the Harmony software. Induction of NgN2 overexpression is driven by doxycycline, which was added to the media throughout the differentiation. The iPSC-derived neurons were replated on rat cortical astrocytes 4 days post induction to help with cell adhesion and maturation and maintained until either Day 7 or, as discussed in section 3.5, until Day 70 of maturation before being insulted with $A\beta$ and live imaged daily for 6-13 days (Figure 3.1, B). The NgN2-GFP virus induced expression of GFP in the whole cell, which allowed for the identification of both the nuclei and neurites with the 488 nm channel. The nuclei can be distinguished by filtering for size and morphology in the analysis pipeline (Figure 3.5. The whole well was imaged, with a 2 % overlap between fields of view to enable seamless tracing of the GFP neurons throughout the well.

Rat astrocytes, rather than human were used for several reasons beyond their role in helping with the adhesion of the neurons. Firstly, rat astrocytes were easy to get access to, to expand and to maintain. iPSC-derived human astrocytes have 100+ day differentiation protocols, which are over-complicated for the purposes of this project. Secondly, having a different species of cells meant that for downstream experiments, such as imaging, I could easily discern between human and non-human cells by using human-specific antibodies, if need be.

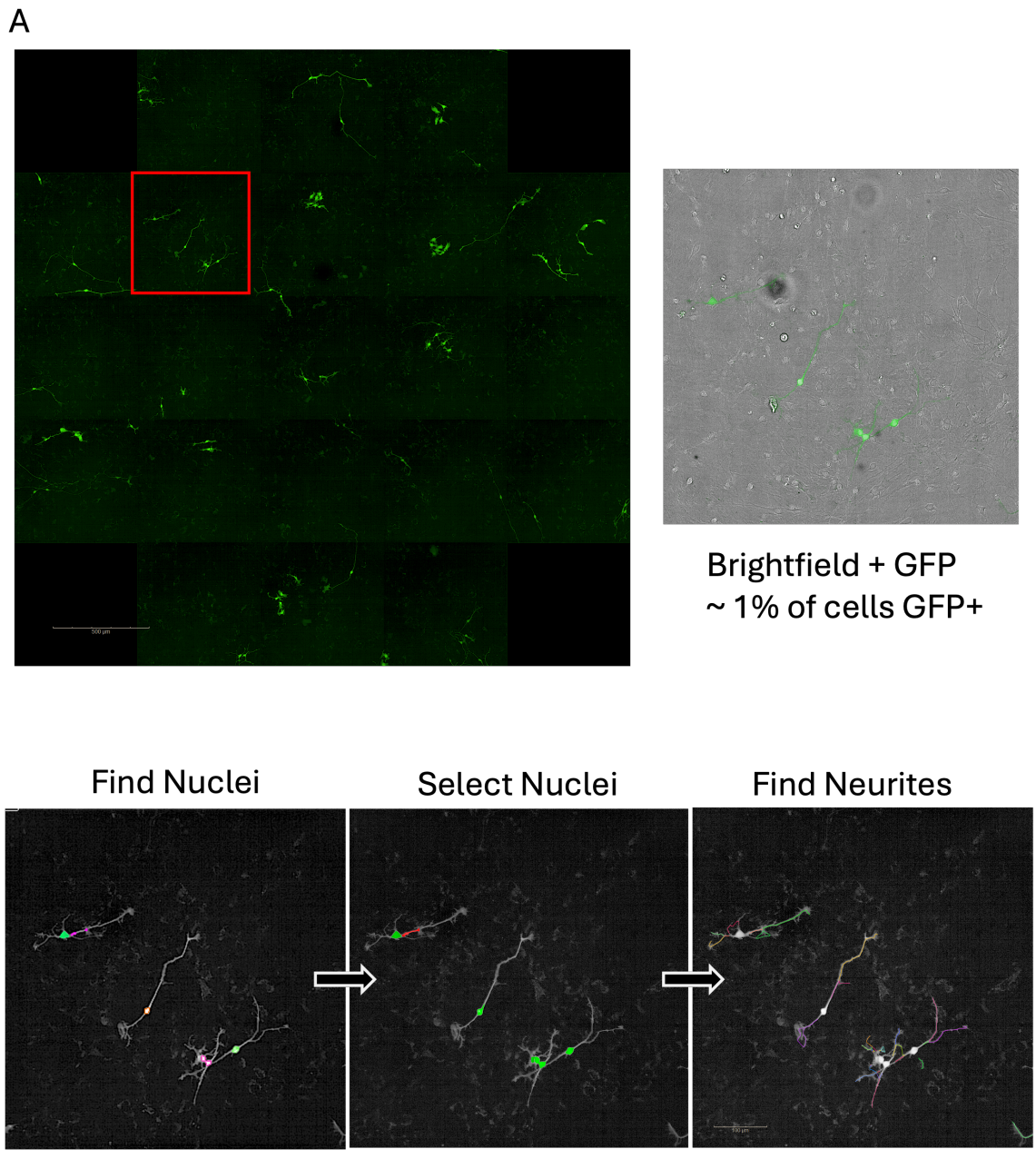


Figure 3.5: **Representative images of GFP+ neurons at different steps of the Harmony analysis pipeline**

3.4.2 Amyloid-Beta oligomers

The neurons were insulted with:

1. $A\beta$ 1-42 oligomers and scrambled peptide control at 5 and 10 μM
2. $A\beta$ 25-35 oligomers and reverse (35-25) peptide control at 10 and 20 μM

I chose these concentrations based on previous experiments on my team showing that

this was the optimal treatment window, as well as to remain consistent with previous work on the DFP lines using Amyloid Beta.

The scrambled and reverse peptides were used to control for the addition of a high concentration of exogenous proteins to the cells. While $A\beta$1-42 peptide is the main component of plaques, and most prone to produce toxic aggregates, I also chose to include another insult in this assay: $A\beta$ 25-35. It is the shortest fragment of $A\beta$ that has large aggregated β-sheet structures that retains toxicity and is therefore thought to be the biologically active region of $A\beta$ [406]. In order to quality control the preps, I ran a western blot probing for $A\beta$ 1-42 before and after oligomerisation (Figure 3.6, A) for every batch I made. Selected batches were sent to the Dunn School for electron microscopy (EM) for more extensive quality control (Figure 3.6, B,C).

The western blots provided a very easy and quick QC. At 0 h, there is only a large monomer band, while at 24 h the monomer band it still visible alongside a smear of oligomers and very few fibrils. The amount of oligomers differs between batches. Interestingly, while the $A\beta$ images show mostly oligomers and monomers and very few fibrils, which agrees with the western blot, the scrambled peptide is much more fibrillar in structure (Figure 3.6, B,C).

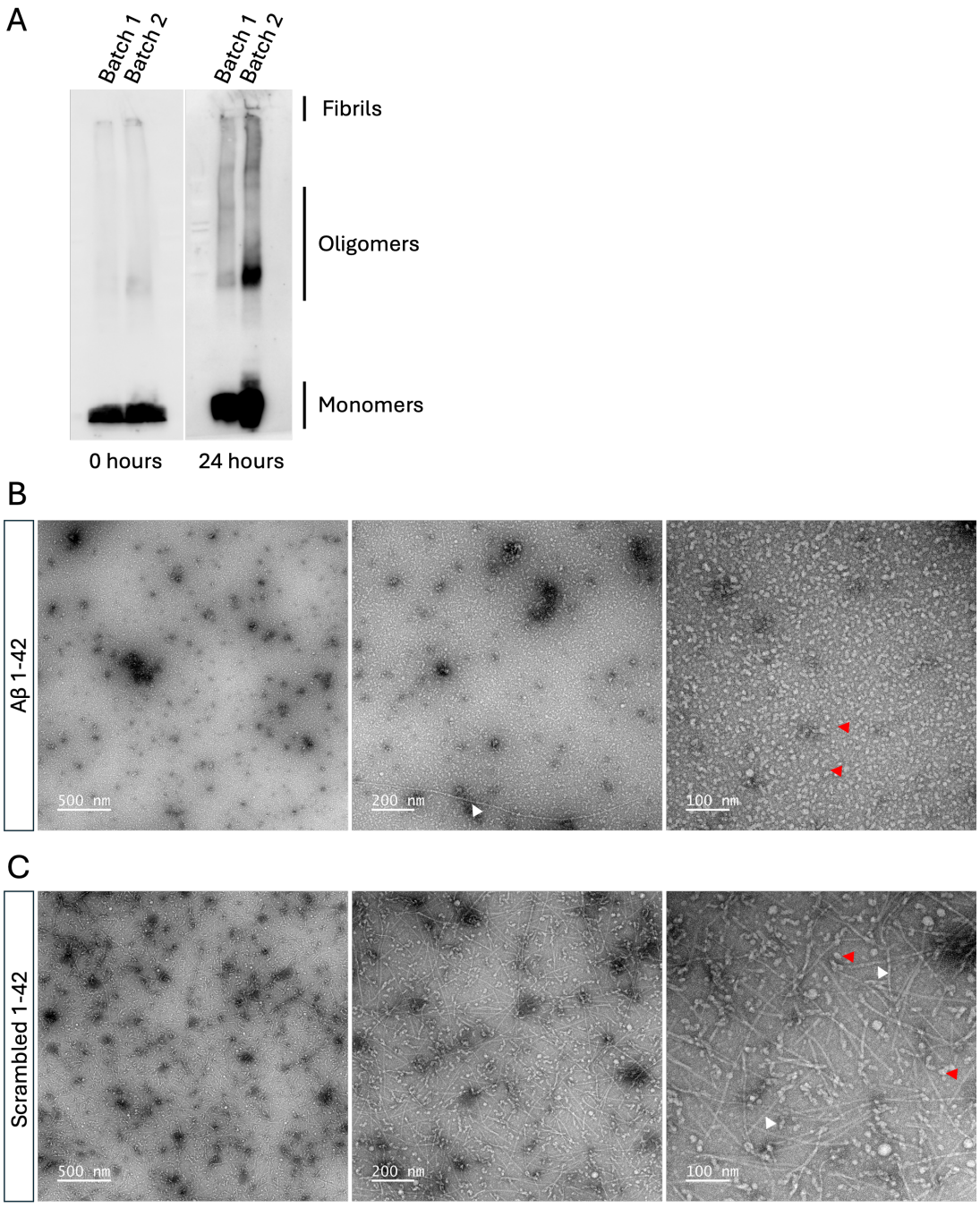


Figure 3.6: **Amyloid Beta oligomerisation.** (A) Western blot of 2 batches $A\beta$ before and after 24 h incubation at 4°C. (B-C) Electron microscopy negative staining of $A\beta$ (B) and Scrambled $A\beta$ (C) peptide at 500 nm, 200 nm and 100 nm. Red arrows point to oligomers, white arrows point to fibrils.

3.4.3 Investigating the effect of $A\beta$ on neurite outgrowth in Day 7 iPSC neurons

This experiment was performed at two timepoints, an early timepoint (Day 7) that is easier to repeat but has potentially quite immature neurons, and a later timepoint (Day 70) where neurons are more mature, but neurite tracing becomes harder due to neurite density (Section 3.5).

To ensure all neurons started with similar baseline neurite growth, I first calculated the total neurite length in each cell line on the first day of treatment. While there were no significant differences between the total neurite length of the 14 lines at Day 0, there were quite large differences between differentiations (each dot is one differentiation, averaged between 9 technical replicates) (Figure 3.7, A). This, however, was mostly due to the difference in the number of cells per well (Figure 3.7, B). When normalised for nuclei number, the variability dropped considerably, and only one line was significantly lower than the rest (line 927) (Figure 3.7, C).

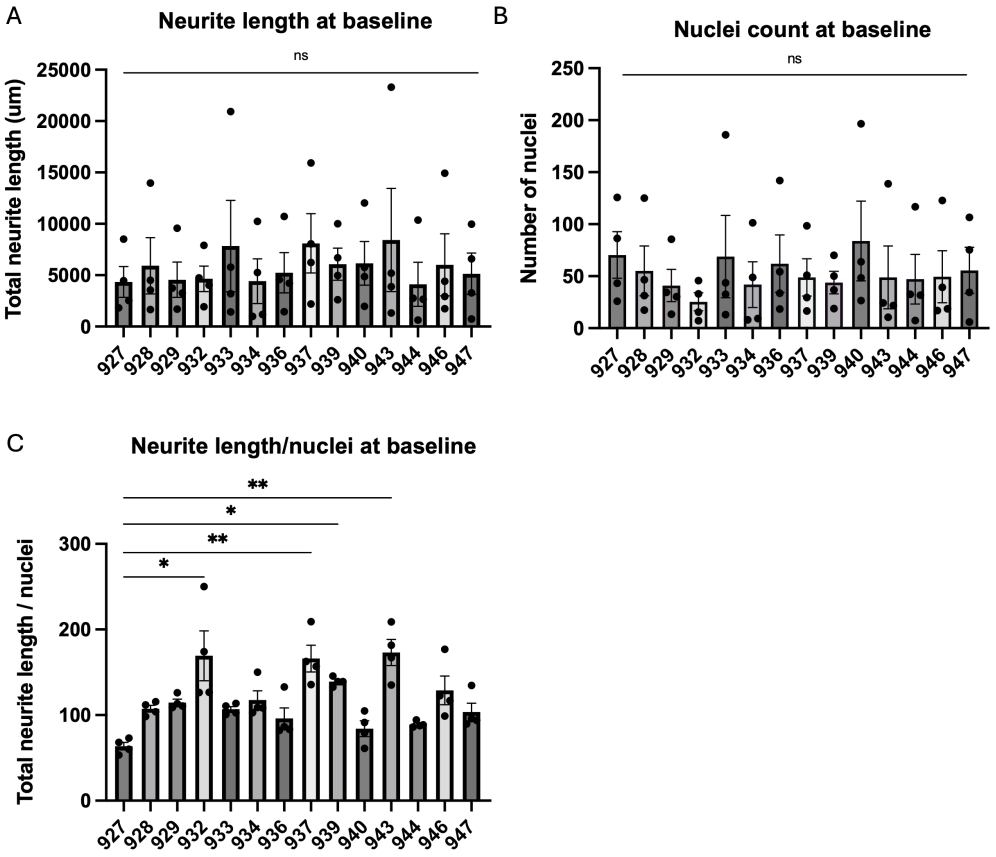


Figure 3.7: **Neurite outgrowth and nuclei count at baseline in Day 7 cortical neurons.** (A) Absolute values of total neurite length (μm) at baseline (Day 0 of imaging, 0 h after treatment). (B) Number of nuclei per well at baseline. (C) Total neurite length normalised by nuclei number at baseline. Mean ± SEM n=4 independent differentiation repeats, averaged across 9 technical replicates. Kruskal Wallis test with Dunn's multiple comparison correction.(A) H(13) = 3.95, (B) H(13) = 6.02,(C) H(13) = 42.75. $p < 0.05$ $(*)$, $p < 0.01$ $(**)$, $p < 0.001$ $(***)$, $p < 0.0001$ $(****)$

3.4.3.1 $A\beta$1-42 insult

Then, I asked whether $A\beta$1-42 oligomers affected neurite outgrowth and branching. To control for differences in seeding densities between wells/cell lines, I normalised the total neurite length and the number of nodes (which represents the number of ramifications, or the branching of the neurites) to the number of nuclei per well. This was important as, even though all lines are plated at the same density, the neurons are still immature and have not stopped proliferating completely.

In all cell lines, $A\beta$ 1-42 at 5 and 10 μM affected neurite outgrowth and the number nodes (Figure 3.8), while the untreated and control peptide conditions showed no

reduction in outgrowth or branching (Figure 3.9, A, Figure 3.10, A). To look at differences between patient lines, I normalised the proportional change in neurite length over time of the $A\beta$ treated condition to the scrambled condition to account for the growth rate of each line and any change of neurite or loss of cells not attributed to the insult. At 10μM, which is a high concentration of $A\beta$, the effect across patient lines was more consistent, with the lines exhibiting between 40 % and 80 % decrease in total neurite length and between 30 % and 75 % decrease in the number of nodes. Accordingly, there was no significant differences between the patient lines (Figure 3.9, C, Figure 3.10, C).

However, in the 5 μM condition, there was a much larger range in vulnerability to $A\beta$ insult. There was a significant difference in neurite loss and decrease of number of nodes between patients, with the decrease ranging between 17 % and 62 % and 8 % and 80 % respectively(Figure 3.9, B, Figure 3.10, B). The neurite loss in the fAD line (line 933) was within the range of the loss observed in the sAD lines. Notably, the neurite loss in each cell line was consistent across treatment concentrations and differentiations (Figure 3.9, D-F).

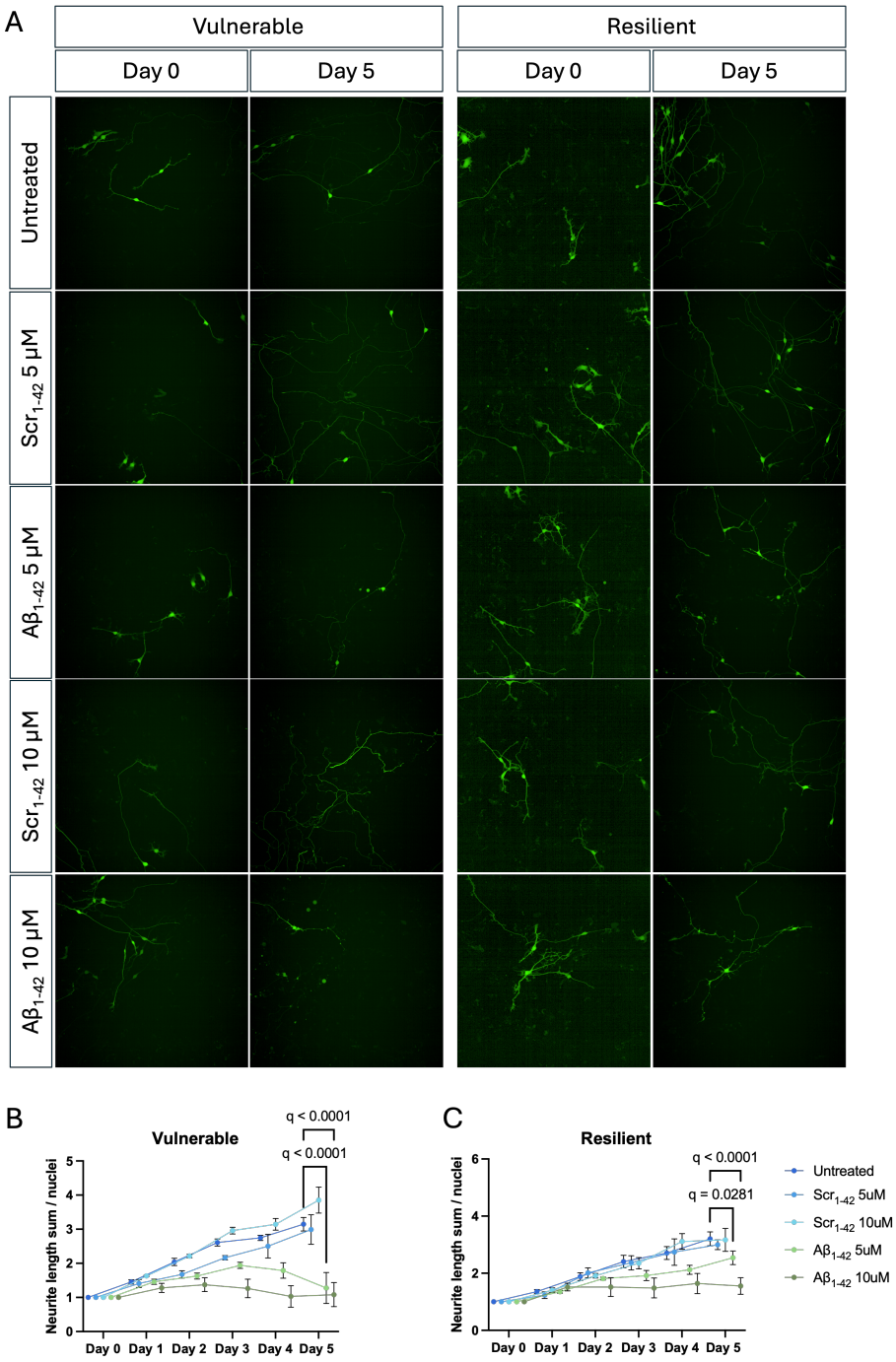


Figure 3.8: **Neurite tracing of Day 7 cortical neurons after $A\beta$1-42 insult.** (A) Representative images of a vulnerable (left) and resilient (right) cell line at Day 0 and Day 5 after addition of $A\beta$. (B-C) Example graphs of a vulnerable (B) and resilient (C) line quantifying the total neurite length (μM), normalised to baseline, over time. Only treatment effect on Day 5 are represented for clarity. Mean ± /SEM, n=4 independent differentiations repeat averaged over 4 technical replicates. Repeated measures mixed model analysis with FDR corrections. (B) Treatment x Time: F (40, 134) = 10.18, p = 0.0001. (C) Treatment x Time: F (40, 114) = 4.712, p = 0.0001.

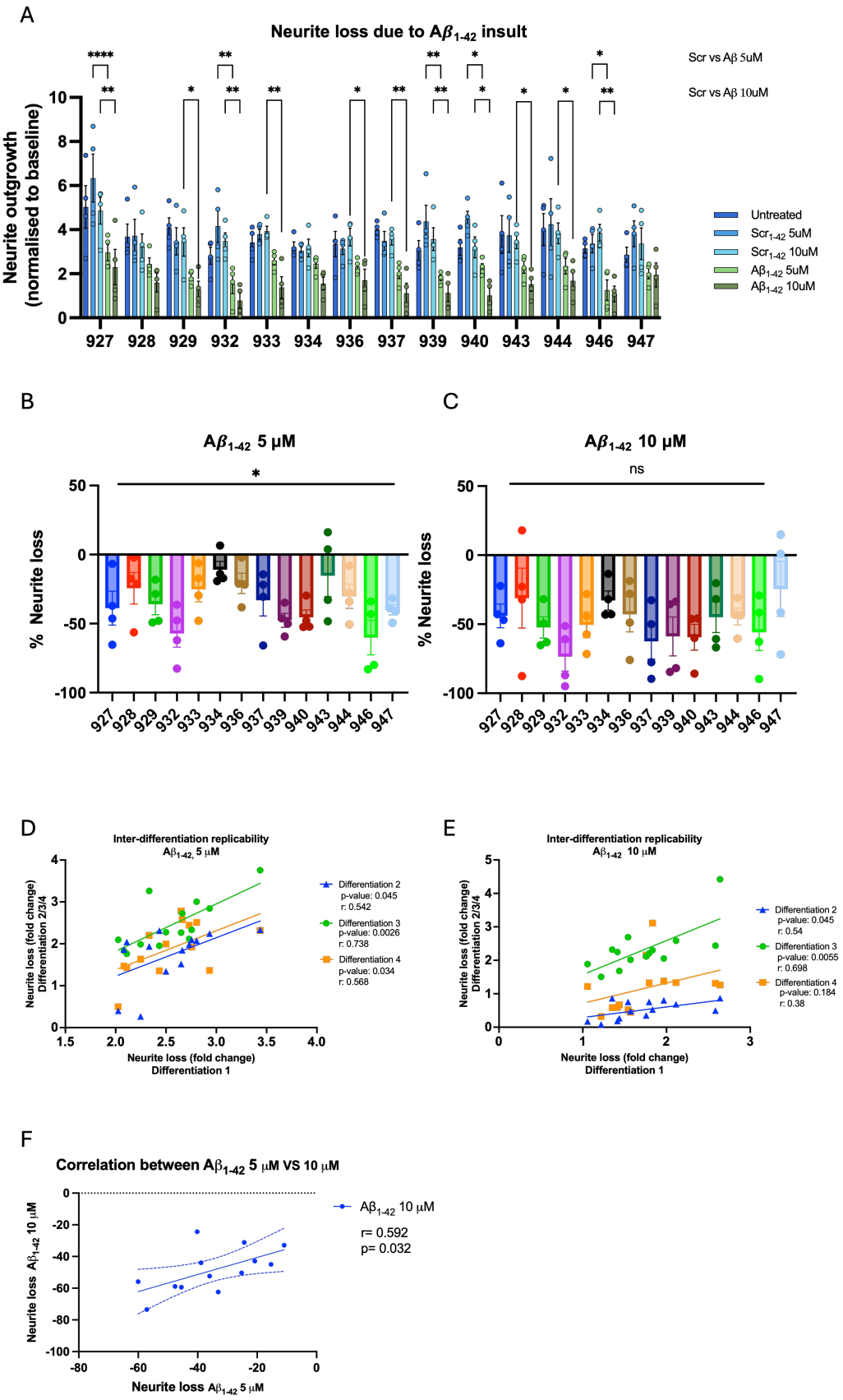


Figure 3.9: *Aβ*1-42 insult impairs neurite outgrowth of Day 7 cortical neurons.

Figure 3.9: continued: (A) Total neurite length on Day 6 of imaging, normalised to baseline (Day 0), in the 14 patient lines. (B-C) % Neurite loss due to $A\beta$1-42 at 5 μM (B) and 10 μM (C) normalised to treatment control . (D-E) Linear regression of neurite loss in each cell line between differentiations in the 5 μM (D) and 10 μM (E) conditions. (F) Linear regression between the neurite loss in 5 μM vs 10 μM conditions. (A) Two-Way ANOVA with Tukey's multiple comparisons test. Treatment effect: F (4, 210) = 66.95, p<0.0001. (B-C) Ordinary One-Way ANOVA with Tukey's multiple comparison's test: (B): F (13, 42) = 2.401, p=0.0161, (C): F (13, 42) = 1.144, p=0.35(D-F) Pearson's correlations with two-tailed p-value and 95 % CI, r and p-value are indicated in each graph. $p < 0.05$ $(*)$, $p < 0.01$ $(**)$, $p < 0.001$ $(***)$, $p < 0.0001$ $(****)$

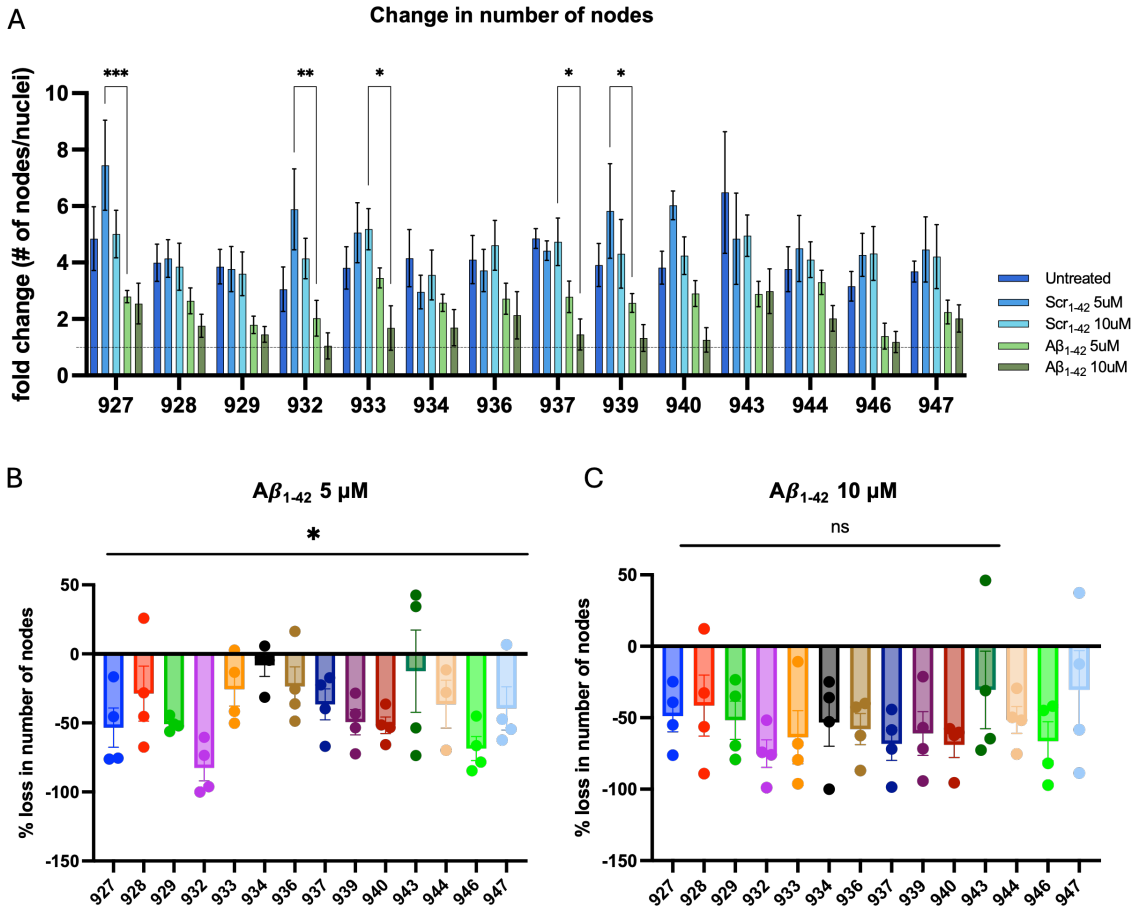


Figure 3.10: **Aβ1-42 insult impairs branching in Day 7 cortical neurons** (A) number of nodes on Day 6 of imaging, normalised to baseline (Day 0), in the 14 patient lines. (B-C) % decrease in number of nodes due to $A\beta$1-42 at 5 μM (B) and 10 μM (C) normalised to treatment control. (A) Two-Way ANOVA with Tukey's multiple comparisons test. Treatment effect: F (4, 210) = 35.44, P<0.0001. (B-C) Ordinary One-Way ANOVA with Tukey's multiple comparison's test: F (13, 41) = 2.142, P=0.0320 (C) F (13, 41) = 0.5871, P=0.8501 $p < 0.05$ (*), $p < 0.01$ (**), $p < 0.001$ (***), $p < 0.0001$ (****)

3.4.3.2 Aβ25-35 insult

Next, I investigated the effect of $A\beta$ 25-35 on neurite outgrowth, and whether it was comparable to $A\beta$ 1-42. Overall, $A\beta$ 25-35 affected neurite outgrowth and branching across all cell lines (Figure 3.11, Figure 3.14, A, Figure 3.13, A), while the reverse peptide $A\beta$ 35-25 had no effect. When compared with 1-42, there was less of a range in the level of neurites that each cell line lost due to the insult. At the 10 μM concentration, neurite loss ranged from 26 and 59 % decrease and for the 20 μM between 42 and 80 % (Figure 3.14, B,C). The change in number of nodes ranged

between 9 and 72 % for the 10 μM and 52 and 81 % for the 20 μM condition (Figure 3.13, B,C). There was no significant difference in neurite loss or number of nodes between the patient lines. In general, $A\beta$25-35 insult seems to lead to quite variable levels of toxicity between differentiations, more so than $A\beta$1-42 (Figure 3.14, E,F).
I then assessed whether the neurite loss due to $A\beta$ was consistent across $A\beta$ species and differentiations. Neurite loss was largely consistent between $A\beta$1-42 and $A\beta$25-35 (Figure 3.13, E). At 10 μM, the effect of $A\beta$25-35 was consistent between differentiation, except for differentiation 4 (Figure 3.13, F), while for at 20μM, $A\beta$25-35 there was no correlation between differentiation, likely due to the high concentration of the insult flattening the dynamic range (Figure 3.13, G).
Here, I have shown that both $A\beta$1-42 and 25-35 caused neurite and branching loss in AD iPSC neurons, and that there were patient-specific differences in vulnerability to $A\beta$. Moreover, the effect of $A\beta$25-35 was less consistent than $A\beta$1-42 between differentiations.

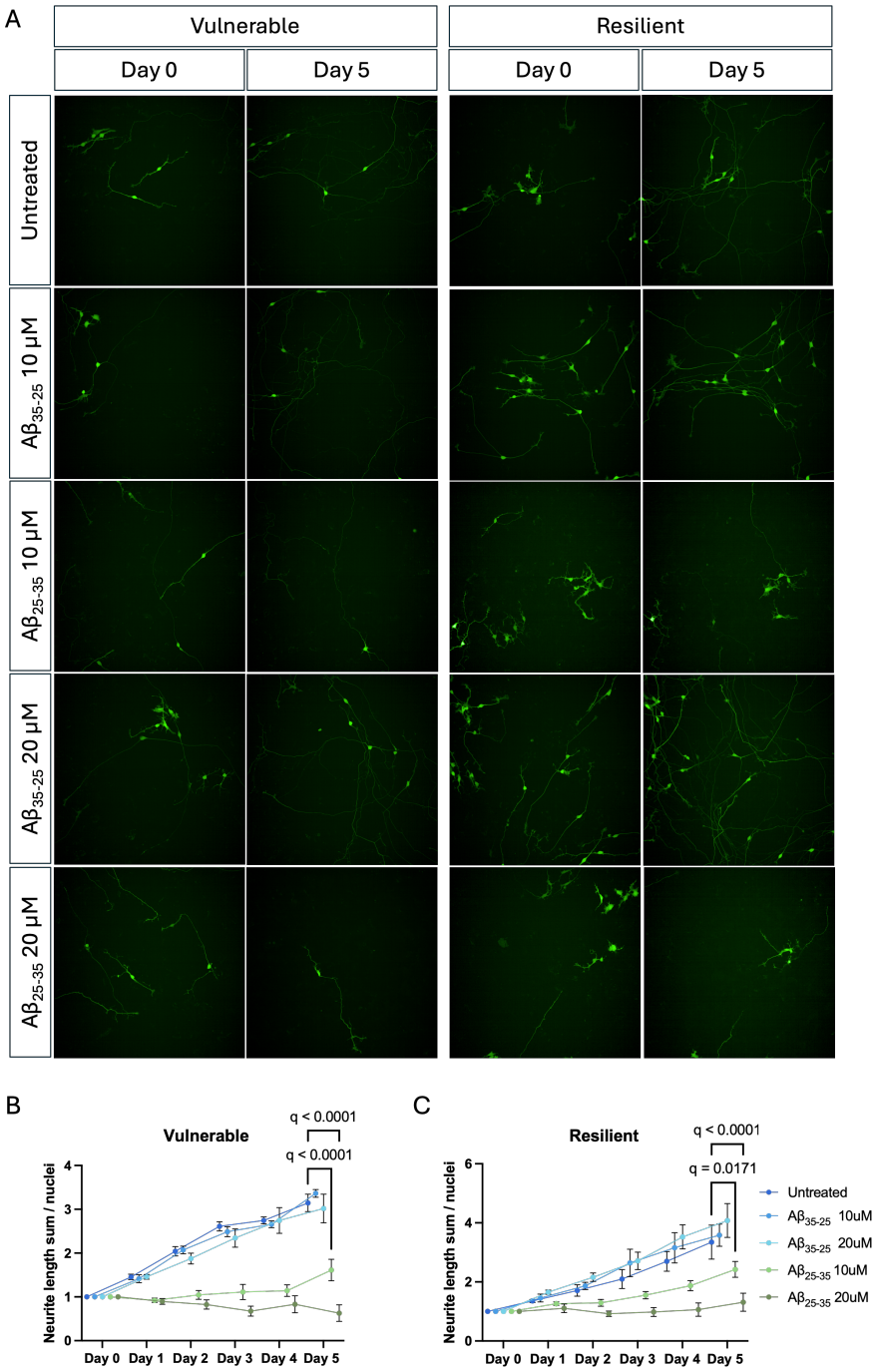


Figure 3.11: **Neurite tracing of Day 7 cortical neurons after $A\beta$25-35 insult**. (A) Representative images of a vulnerable (B) and resilient (C) cell line at Day 0 and Day 5 after addition of $A\beta$ 25-35 and the reverse peptide $A\beta$ 35-25 . (B-C) Quantification of the total neurite length (μM), normalised to baseline, over time. Only treatment effect on Day 5 are represented for clarity. Mean $\pm$ /SEM, n=4 independent differentiations repeat averaged over 4 technical replicates. Repeated measures mixed model analysis with FDR corrections. (B) Treatment x Time: F (40, 134) = 10.18, p = 0.0001 (C) Treatment x Time: F (40, 135) = 4.886, p = 0.0001 (p<0.0001).$p < 0.05$ $(*)$, $p < 0.01$ $(**)$, $p < 0.001$ $(***)$, $p < 0.0001$ $(****)$

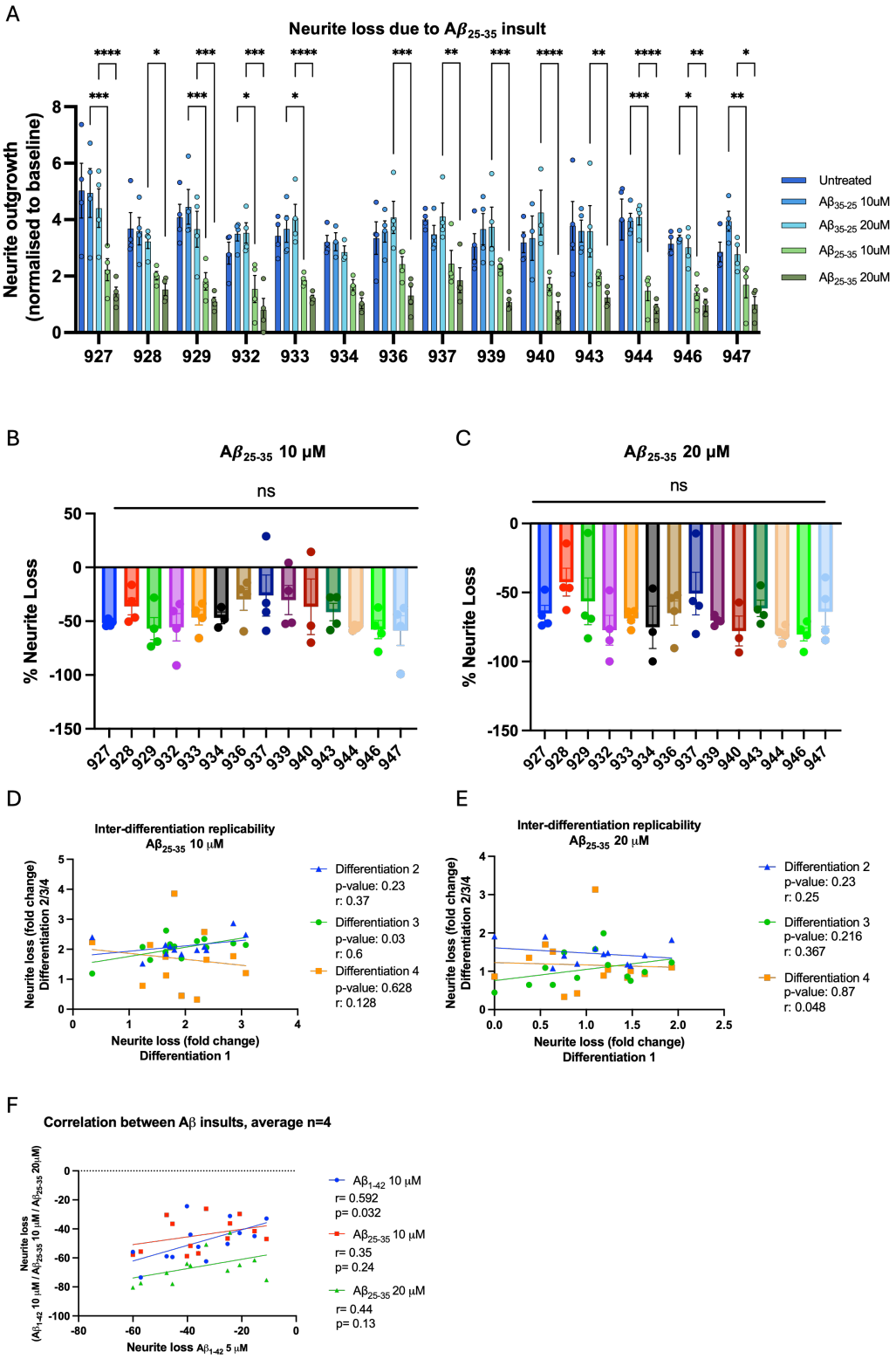


Figure 3.12: **Aβ25-35 insult impairs neurite outgrowth in Day 7 cortical neurons.**

Figure 3.12: Continued: (A) Total neurite length on Day 6 of imaging, normalised to baseline (Day 0), in the 14 patient lines. (B-C) % Neurite loss due to $A\beta$25-35 at 10 μM (B) and 20 μM (C) normalised to treatment control. (D-E) Linear regression of neurite loss in each cell line between differentiations in the 10 μM (D) and 20 μM (E) conditions. (F) Pearson correlation between neurite loss due to $A\beta$1-42 and $A\beta$25-35 insults. (A) Two-Way ANOVA with Tukey's multiple comparisons test. Treatment effect: F (4, 202) = 101.0, P<0.0001 (B-C) Ordinary One-Way ANOVA with Tukey's multiple comparison's test: (B): F (13, 40) = 1.030, P=0.4436, (C): F (13, 40) = 1.364, P=0.2194 (D-F) Pearson's correlation with two-tailed p-value and 95 % CI, r and p-values are indicated in each plot. $p < 0.05$ $(*)$, $p < 0.01$ $(**)$, $p < 0.001$ $(***)$, $p < 0.0001$ $(****)$.

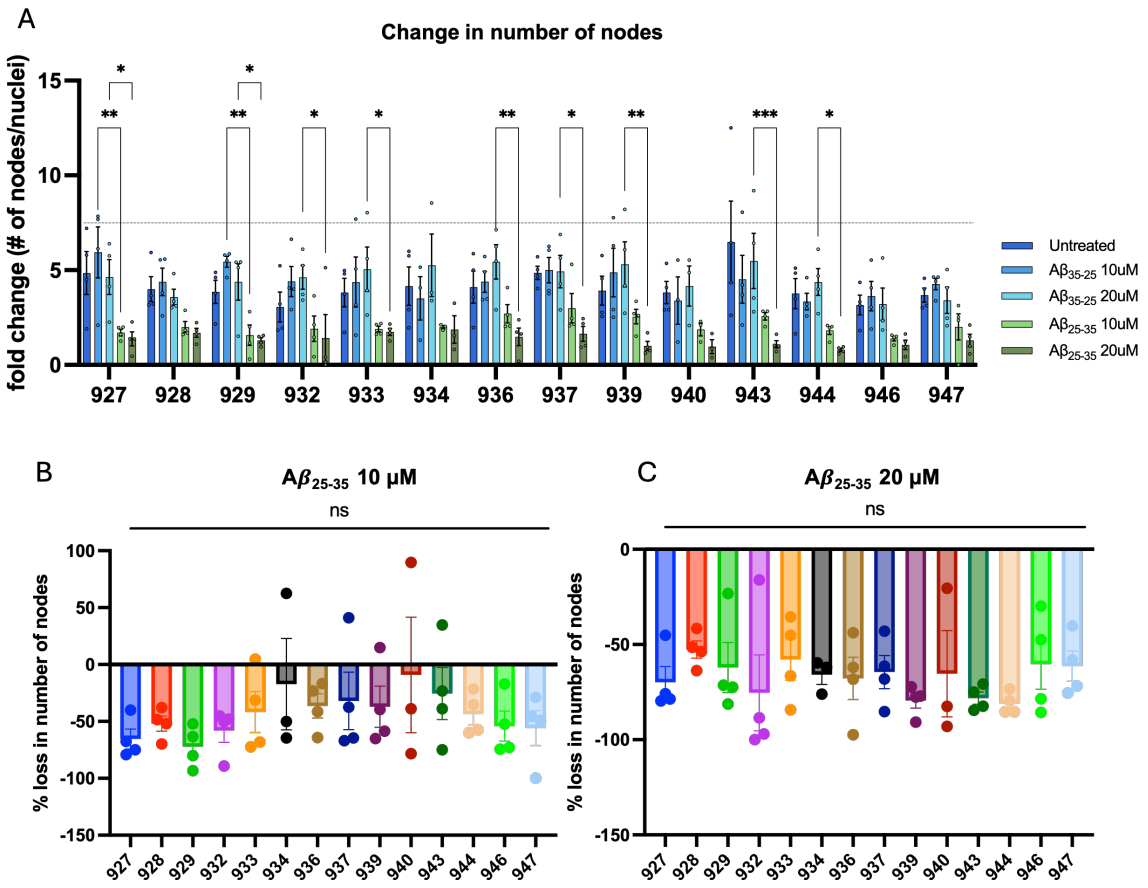


Figure 3.13: *Aβ***25-35 insult impairs branching in Day 7 cortical neurons** (A) number of nodes on Day 6 of imaging, normalised to baseline (Day 0), in the 14 patient lines. (B-C) % decrease in number of nodes due to *Aβ*25-35 at 10 μM (B) and 20 μM (C) normalised to treatment control. (A) Two-Way ANOVA with Tukey's multiple comparisons test. Treatment effect: F (4, 202) = 49.05, P<0.0001. (B-C) Ordinary One-Way ANOVA with Tukey's multiple comparison's test: (B): F (13, 40) = 0.8073, P=0.6493, (C): F (13, 40) = 0.6416, P=0.8044 $p < 0.05$ (∗), $p < 0.01$ (∗∗), $p < 0.001$ (∗ ∗ ∗), $p < 0.0001$ (∗ ∗ ∗∗)

3.4.4 Cell viability

I next looked at whether *Aβ* caused any cytotoxicity and neuronal death, using three approaches. First, I simply looked at nuclei loss between the first and last day of treatment. I then measured adenylate kinase release in the media on the last day of imaging using the Toxilight assay. The advantage of this assay was that it did not require cell lysis, meaning I could still use the neurons for downstream experiment and allowed me to look at cleaved caspase 3 (CC3) staining by ICC. CC3 is the active part of the Caspase 3 enzyme and is a key initiator of apoptosis.

Nuclei loss

On average, there was a 30 % and 46 % reduction in nuclei across all patient lines for the 5 μM and 10 μM condition, respectively, when compared to Day 0 (Figure 3.14, C). There was no change for the three control conditions (between 0-3 % change). In the 5 μM condition there was a large range in how many nuclei were lost per line, ranging from 9 to 47 %, while for the 10 μM it ranged from 21 to 72 % (Figure 3.14, A, B). Interestingly, even though the amount of neurite loss was comparable between $A\beta$1-42 and $A\beta$25-35, there was more nuclei loss in the $A\beta$25-35 conditions than the $A\beta$1-42 conditions. On average the number of nuclei decreased by 60 % and 69 % for the 10 and 20 μM conditions, ranging between 53 % to 70 % and 66 % to 80 %, respectively (Figure 3.14, D, E, F). As with the effect of neurites, $A\beta$25-35 μM was more "consistently" toxic across all cell lines when looking at nuclei number.

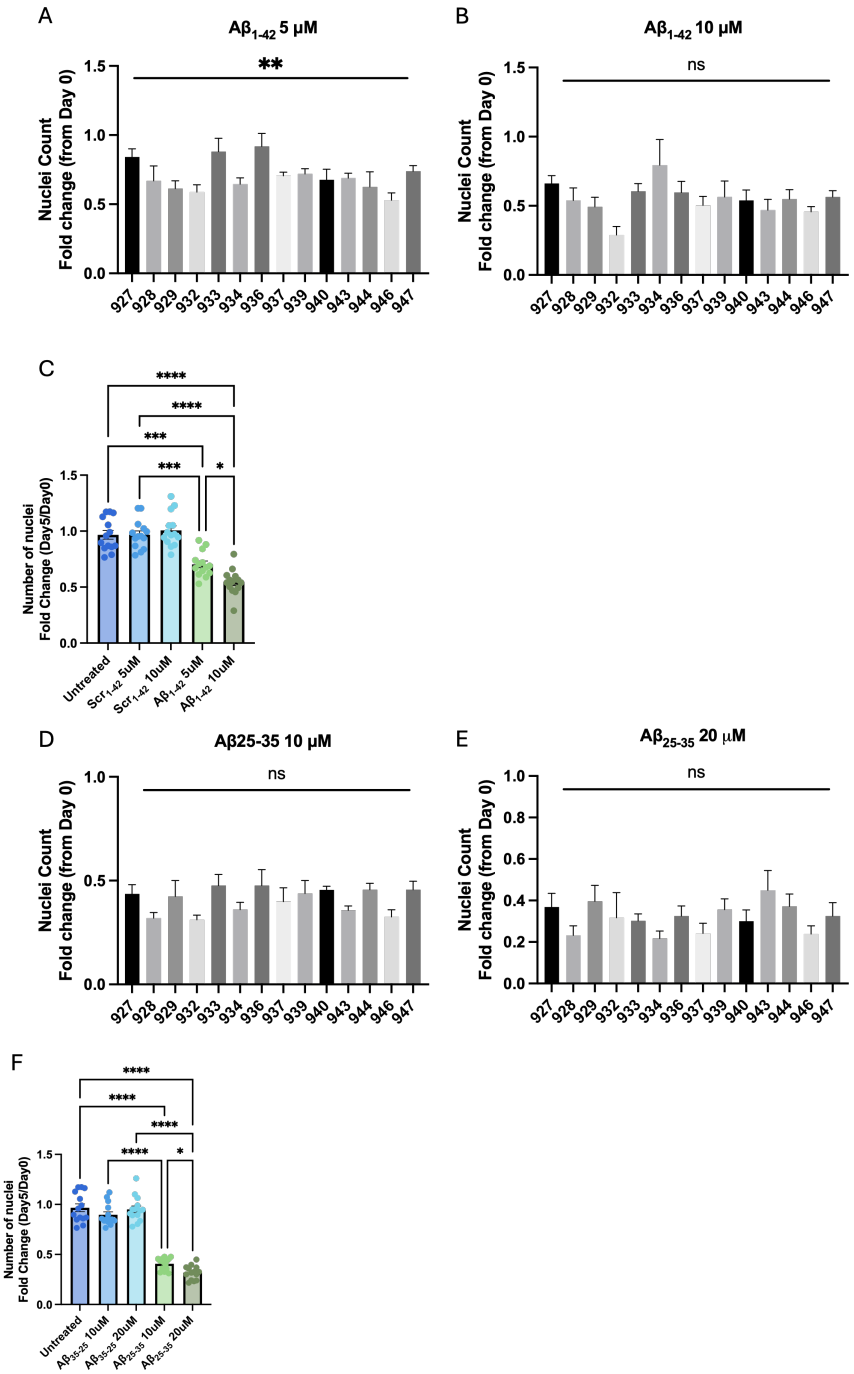


Figure 3.14: **Quantification of the number nuclei loss in Day 7 cortical neurons due to $A\beta$ insult**. (A-B) Nuclei count relative to baseline (Day 0) in neurons treated with 5 μM (A) and 10 μM (B) of $A\beta$1-42 in each line (C) number of nuclei relative to baseline average across all 14 patient lines. (D-E) Nuclei count relative to baseline (Day 0) in neurons treated with 10 μM (D) and 20 μM (E) of $A\beta$25-35 in each line. (F) number of nuclei relative to baseline average across all 14 patient lines.

Figure 3.14: Continued: (A-B, D-E) Ordinary One-way ANOVA with Tukey's , multiple compariasons. (A) F (13, 42) = 2.633, P=0.0089 (B) F (13, 42) = 1.789, P=0.0773 (D) F (13, 40) = 1.530, P=0.1491 (E) F (13, 40) = 1.073, P=0.4079. (C,F) Brown-Forsythe and Welch's ANOVA test: F(8.000, 97.12)= 4.22, P <0.0001. $p < 0.05$ $(*)$, $p < 0.01$ $(**)$, $p < 0.001$ $(***)$, $p < 0.0001$ $(****)$

Adenylate Kinase release

To assess cell viability, cell media was collected on the last day of imaging and adenylate kinase (AK) , which gets released from damaged cells, was measured using the Toxilight assay. $A\beta$1-42 insult caused a significant, dose-dependent increase in AK release compared to untreated and scrambled controls (Figure 3.15, A,B). Unlike the effect on neurite outgrowth or branching, AK levels were quite consistent across patient lines, and there was no significant differences between the lines in either the 5 or 10 μM conditions when corrected with treatment control (Figure 3.15,C).
Similarly to $A\beta$1-42, $A\beta$25-35 also caused a dose-dependent increase in AK release compared to untreated and reverse peptide conditions (Figure 3.15, D, E). There were no significant differences between the patient lines in either the 10 or 20 μM conditions when normalised with treatment control (Figure 3.15,F). The $A\beta$25-35 10 μM had a smaller increase than either of the $A\beta$1-42 conditions, significantly smaller compared with the $A\beta$1-42 10 μM condition, even though it had a higher loss of nuclei (Figure 3.15,G).

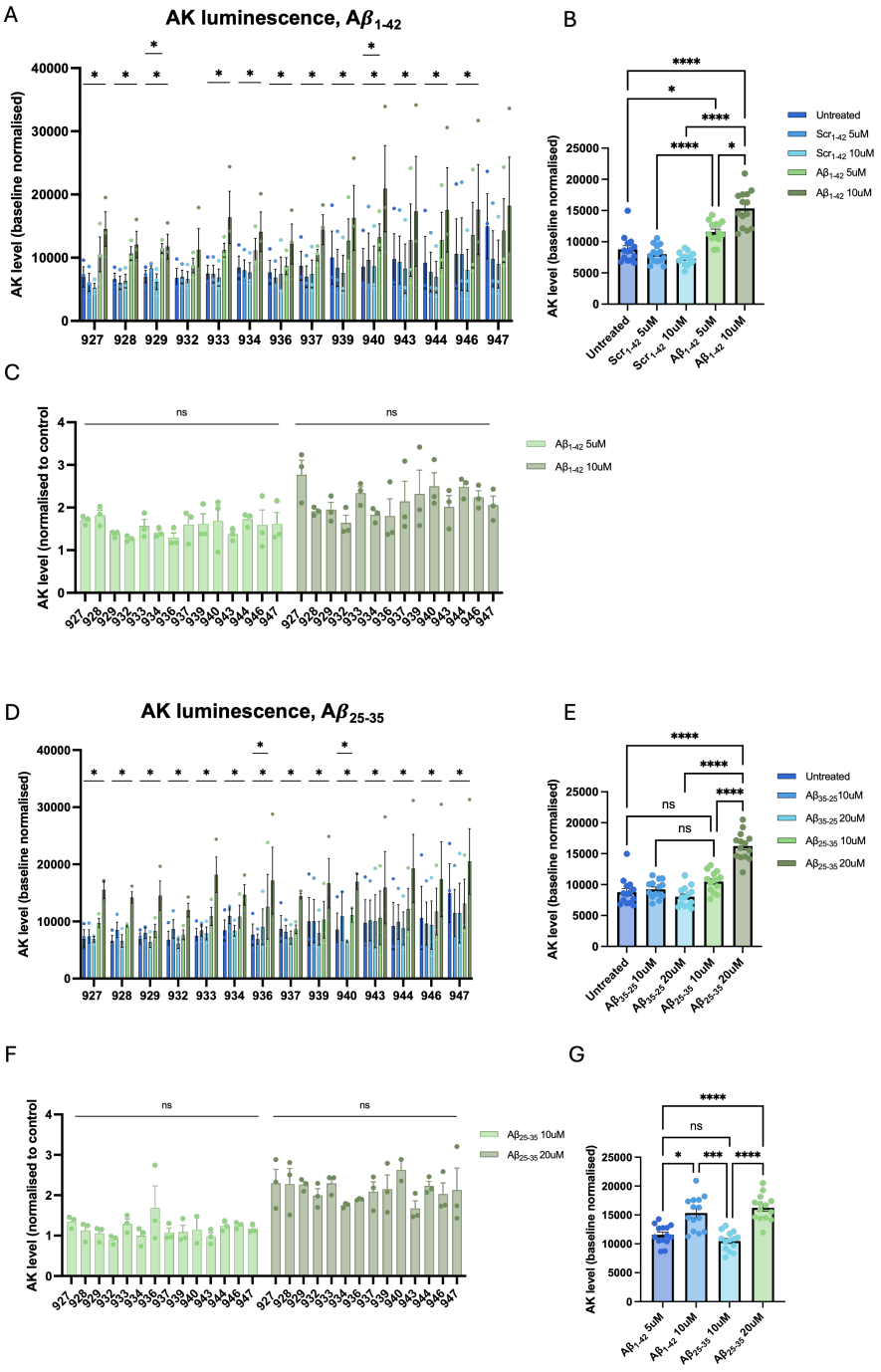


Figure 3.15: **Adenylate Kinase Release in Day 7 cortical neurons treated with $A\beta$.** (A) AK luminescence (blank corrected) in $A\beta$1-42-treated samples.(B) Average AK luminescence in the 14 cell lines. (C) Relative AK luminescence to scrambled $A\beta$1-42 peptide, (5 and 10μM, respectively). (D) AK luminescence (blank corrected) in $A\beta$25-35-treated samples. (E) Average AK luminescence in the 14 cell lines. (F) Relative AK luminescence to reverse $A\beta$35-25 peptide, (10 and 20μM, respectively). Mean ± SEM n=3 independent differentiation repeats, averaged across 3-4 technical replicates.

Figure 3.15: **continued: Adenylate Kinase Release in Day 7 cortical neurons treated with $A\beta$.**. (A,D) 2-Way ANOVA with with Benjamini and Hochberg FDR multiple comparisons correction (q=0.05). F (8, 248) = 10.05, P<0.0001. (B,E,G) Brown-Forsythe and Welch's one-way ANOVA with Dunnett's T3 multiple comparisons test. F (8.000, 84.90)=78.81, p= P<0.0001. (C,F): Ordinary One-way ANOVA with Tukey's multiple comparisons test. (C) $A\beta$ 5μ: F (13, 28) = 0.9633, $A\beta$ 10μ: F (13, 28) = 1.089, P=0.4068. (F) $A\beta$ 10μ: F (13, 27) = 1.058, P=0.4312, $A\beta$ 20μ: F (13, 27) = 1.188, P=0.3389. $p < 0.05$ ($*$), $p < 0.01$ ($**$), $p < 0.001$ ($***$), $p < 0.0001$ ($****$)

Cleaved Caspase 3

In order to discern the human neurons from the rat astrocytes, I stained my cells with Human Nuclear antigen (HuNu), and MAP2 as well as CC3 and looked at the nuclei positive for both CC3 and HuNu. Then, a threshold for what was considered a CC3+ nuclei was set, to remove non-specific background. To do so, CC3 intensity was calculated in every nuclei in the control wells (untreated) for every patient line, individually, and then the threshold was set to 2 standard deviations above the mean for each line.

$A\beta$1-42 at 5 μM did not significantly increase the number of CC3+ HuNu+ nuclei compared to the control conditions, and the spread between cell lines did not differ from the control conditions either, being on average between 2-3 % CC3+ cells (Figure 3.16, C). However, there was a significant difference between the untreated and 10 μM condition. The number of CC3+ cells in between the patient lines ranged from 1.6 to 6.8 %(Figure 3.16, D). Interestingly, the decrease in neurite outgrowth and number of CC3+ wasn't coherent for some cell lines. Line 947 for instance, had the one of the lowest % loss in neurites but highest number of CC3+ cells, though that might be due to the large variability in between differentiation for that particular cell line.

Similarly to the number of nuclei loss, $A\beta$25-35-treated wells had significantly more CC3+ cells than the control conditions (Figure 3.17, C). It ranged from 2 to 7.3 % and 1.5-8.3 % for the 10 and 20 μM conditions respectively, which is comparable to the $A\beta$1-42 10 μM condition. However, there was no dose-dependent increase in CC3+ cells between the 10 and 20 μM condition. In fact, in some cases (such as line 932) there were more CC3+ cells in the lower treatment condition (Figure 3.17,D). Here, I showed that $A\beta$ insult caused neuronal death as demonstrated by a loss of nuclei, an increase in AK release and in CC3. Overall, $A\beta$25-35 was more toxic than $A\beta$1-42.

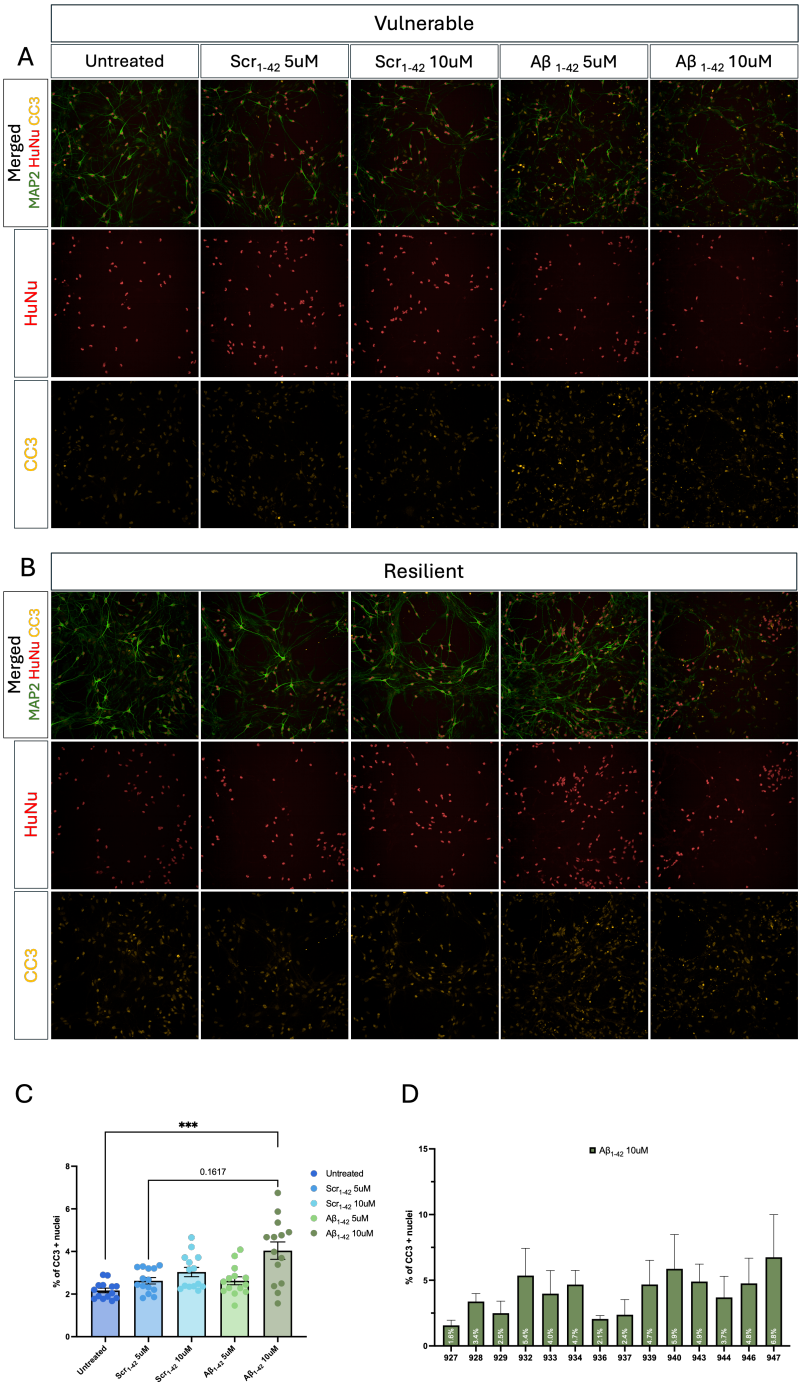


Figure 3.16: **Cleaved Caspase 3 staining in Day 7 cortical neurons treated with $A\beta$1-42** . (A-B) Representative images of a vulnerable (A) and Resilient (B) cell line stained with MAP2 (488), Human Nuclear antigen (647) and CC3 (555) Scale bar: 100nm. (C) Quantification of the %CC3+ HuNu+ nuclei per well in each treatment condition, averaged across the 14 cell lines. (D) Quantification of %CC3+ HuNu+ nuclei per well in each cell line in wells treated with 10 μM of $A\beta$1-42. Mean ± SEM n=4 independent differentiation repeats, averaged across 4 technical replicates. Kruskal Wallis test with Dunn's multiple comparison correction. H (4)=18.5, p=0.001. $p < 0.05$ (*), $p < 0.01$ (**), $p < 0.001$ (***), $p < 0.0001$ (****)

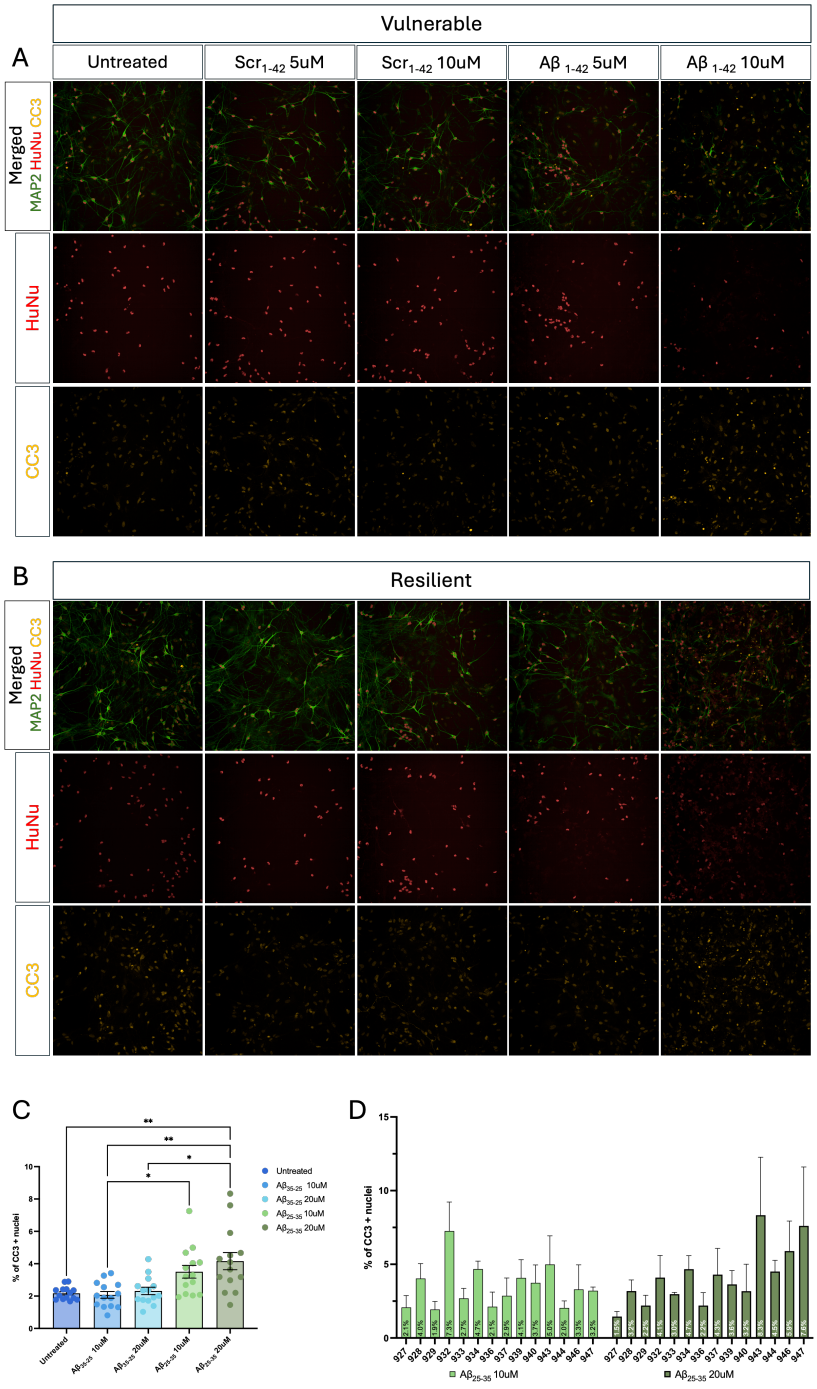


Figure 3.17: **Cleaved Caspase 3 staining in Day 7 cortical neurons treated with $A\beta$25-35** . (A-B) Representative images of a vulnerable (A) and Resilient (B) cell line stained with MAP2 (488), Human Nuclear antigen (647) and CC3 (555) Scale bar: 100nm. (C) Quantification of the %CC3+ HuNu+ nuclei per well in each treatment condition, averaged across the 14 cell lines. (D) Quantification of %CC3+ HuNu+ nuclei per well in each cell line in wells treated with 10 μM or 20 μM of $A\beta$25-35. Mean $\pm$ SEM n=4 independent differentiation repeats, averaged across 3 technical replicates. Kruskal Wallis test with Dunn's multiple comparison correction. H (4) = 22.66, p= 0.0001 $p < 0.05$ $(*)$, $p < 0.01$ $(**)$, $p < 0.001$ $(***)$, $p < 0.0001$ $(****)$

3.5 Correlation of neurite loss in patient-derived neurons with clinical measures of the same patients

The next question I asked was whether the neurite loss due to $A\beta$ in sAD iPSC-derived cortical neurons correlated with clinical measures from those same patients. As mentioned in the introduction to this chapter, one of the main aims for the DFP experimental arm, is to establish whether sporadic AD iPSC models are comparable to the patients they originate from. So here, the aim was to answer whether extrinsic $A\beta$ insult *in vitro* reflect clinical vulnerability to $A\beta$ *in vivo*. In order to capture individual differences in clinical susceptibility to amyloid pathology, I normalised each participant's clinical outcome measures to their respective $A\beta$ burden, as determined by amyloid PET or CSF $A\beta$1–42 levels. This approach provided a measure of clinical impairment per unit of $A\beta$1–42 pathology, enabling direct comparison with the extent of neurite loss observed in patient-derived iPSC neurons exposed to $A\beta$1–42 insult. I was particularly interested in comparing corrected hippocampal volume (the hippocampal volume normalised by total brain volume), since it is an area of neuronal loss in the early stages of AD [57, 477], to neurite loss in iPSC-derived neurons.

There was a significant correlation between higher $A\beta$1-42-induced neurite loss at 5 and 10 μM in iPSC-neurons, and hippocampal volume corrected to CSF $A\beta$42:40 of those patients(Figure 3.18, Bi-Bii). This was also the case when neurite loss was correlated with the hippocampal volume corrected by CSF $A\beta$42, though not significantly for $A\beta$1-42 at 5μM (Figure 3.18, Ci-Cii). Interestingly, unlike $A\beta$1-42, higher neurite loss due to $A\beta$25-35 at 10 μM but not 20 μM was correlated with higher hippocampal volume corrected CSF $A\beta$42:40 and CSF $A\beta$42 (Figure 3.18, Biii-iv, Ciii-iv).

I then generated a correlation matrix of all treatment conditions correlated with all clinical measures, and given the exploratory nature of this analysis, I looked at unadjusted p-values (Figure 3.18, A). Neurite loss due to 5 and 10 μM $A\beta$1-42 treatment also correlated with CSF p-Tau:tau levels (Figure 3.18, Di, Dii). Furthermore, $A\beta$25-35 10 μM condition correlated significantly with hippocampal volume corrected to amyloid PET and $A\beta$25-35 20 μM correlated significantly with Amyloid PET and MEG measurements, though that was not the case for any other treatment condition (Figure 3.18, A).

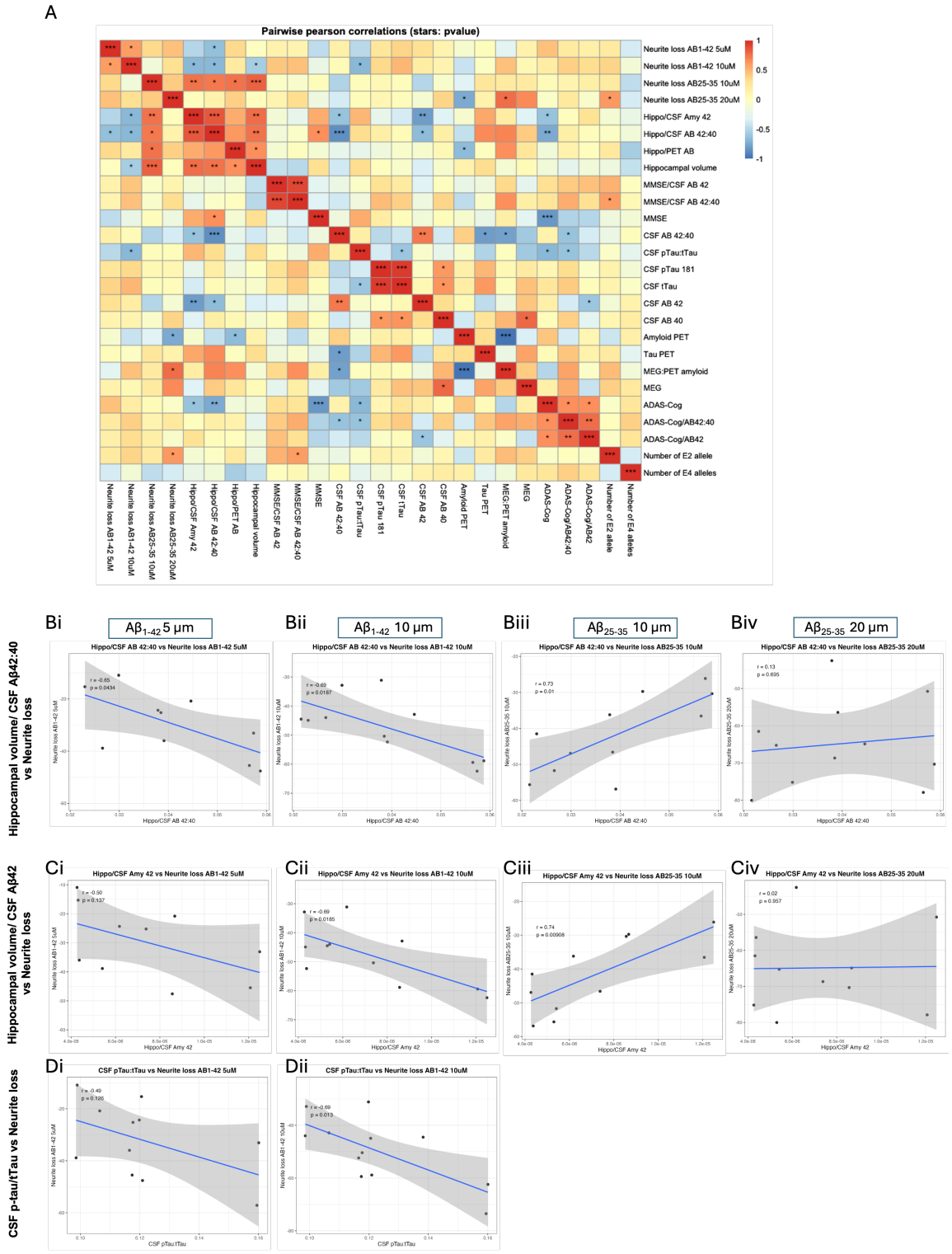


Figure 3.18: **Correlation between clinical measures of the DFP cohort and $A\beta$ induced neurite loss in iPSC-derived cortical neurons.**(A) Correlation matrix of Pearson's correlations between all clinical measures and various $A\beta$ insults. (B-D) Linear regressions of correlations of interest. The y-axis in all graph is % neurite loss due to $A\beta$ and the x-axes are the clinical measures of interest.

Figure 3.18: Continued: (Bi-Biv) Patient corrected hippocampal volume, normalised by their CSF $A\beta$42:40 correlated with neurite loss after $A\beta$1-42 5μM (Bi), $A\beta$1-42 10 μM (Bii), $A\beta$25-35 10μM (Biii), and $A\beta$25-35 20μM (Biv), respectively. (Ci-Civ) Patient corrected hippocampal volume, normalised by their CSF $A\beta$42 correlated with neurite loss after $A\beta$1-42 5μM (Ci), $A\beta$1-42 10 μM (Cii), $A\beta$25-35 10μM (Ciii), and $A\beta$25-35 20μM (Civ) respectively. (Di-Dii) CSF ptau:tau ratio correlated with neurite loss after $A\beta$1-42 5μM (Di), $A\beta$1-42 10μM (Diii). Pearson's correlation with two-tailed p-value and 95 % confidence interval (CI). $p < 0.05$ $(*)$, $p < 0.01$ $(**)$, $p < 0.001$ $(***)$, $p < 0.0001$ $(****)$. p-values, r values are indicated in each graph.

3.6 Neurite tracing of Day 70 iPSC-derived cortical neurons from the DFP cohort after $A\beta$ insult

3.6.1 Decrease in neurite length and branching after $A\beta$ insult

Given that measuring neurite loss at Day 7 corresponds more to a developmental phenotype rather than a degenerative phenotype, I next decided to investigate neurite loss at Day 70, at which point neurons have synchronised firing patterns, synaptic protein localization, and full conversion to OXPHOS metabolism. The choice to look at such an early timepoint when studying and age-related neurodegenerative disease in section 3.3, was due in part to logistical complications: cortical neurons become incredibly branched and complex quite quickly during differentiation, making them too dense to trace, even with a low GFP titer. Nonetheless, I was interested in looking at neurite degeneration in mature neurons and therefore recapitulated the work discussed section 3.3 in Day 70 neurons. I first attempted to repeat the experiment exactly as described above but this led to GFP positive neurites being too dense to trace (data not shown). This is due in large part to the growth of neurites, but also do some remaining proliferation of cells, which increases the number of GFP + cells. Therefore, I decided to only transduce half of the wells with GFP on Day 0, and on Day 4, replate half GFP+/half GFP- cells into every well of the 96 well plate (pre-plated with rat astrocytes).

The first question I asked was whether the 14 lines had the same baseline level of neurites before treatment. The Harmony analysis pipeline was able to detect the majority of neurites, but even with a 3 plane stack, some of the fainter neurites in the background were not detected. Though not significant, there was high variability in the total neurite length at baseline (Figure, 3.19, A), which was partially reduced when normalised with the number of nuclei (Figure,3.19, B, C).

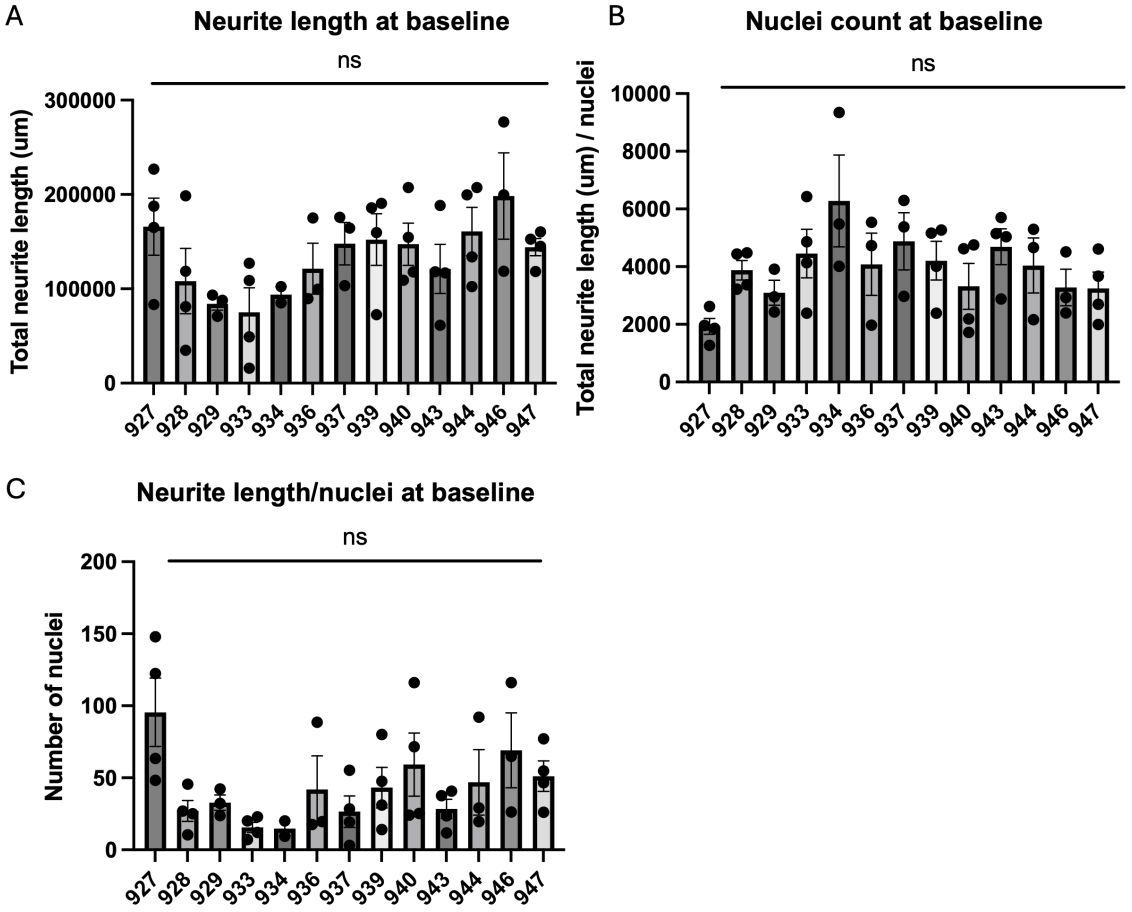


Figure 3.19: **Neurite outgrowth and nuclei count at baseline in Day 70 cortical neurons**. (A) Absolute values of total neurite length (μM) at baseline (Day 0 of imaging, 0h after treatment). (B) Number of nuclei per well at baseline. (C) Total neurite length normalised by nuclei number at baseline. Mean ± SEM n=4 independent differentiation repeats, averaged across 9 technical replicates. Kruskal Wallis test with Dunn's multiple comparison correction.

Then, I investigated whether $A\beta$1-42 oligomers caused neurites to degenerate in Day 70 cortical neurons. As $A\beta$25-35 insult resulted in higher variability between differentiations in Day 7 neurons (section 3.3), I concentrated on replicating experiments with $A\beta$1-42 insult. Moreover, it is less biologically relevant then $A\beta$1-42, as it is not the main component of plaques or oligomers.

I treated the neurons at $A\beta$1-42 at Day 70 and imaged them for 14 days. The longer treatment duration was due to the fact that after 5 days of imaging, I still saw very little decrease in neurites – likely due to the density of neurites in the well – and therefore prolonged the treatment. $A\beta$1-42 caused progressive neurite degeneration in all 14 patient lines (Figure, 3.20, Figure 3.21, A), although some lines exhibited

greater loss than others. While at Day 7, there was a lack of outgrowth due to treatment while the untreated conditions' neurites increased 3-6 fold, at Day 70, while the untreated and control conditions mostly stay stable or grew slightly (-5 to 7 %), the total neurite length of $A\beta$1-42 treated neurons decreased by up to 50 % from baseline. I normalised the neurite length and number of nodes to nuclei, to account for seeding differences and loss of nuclei, as I wanted to look at neurite loss that happens before/independent of cell death. The amount of loss in between patient lines was consistent across treatment concentrations (Figure 3.21, D). On average, the neurons treated with $A\beta$1-42 lost 38 % of neurites for the 5 μM condition and 54 % for the 10 μM condition, while the number of nodes decreased by 48 and 59 %, respectively (Figure 3.21, B,C). Similarly, the loss of branching in neurons decreased due to $A\beta$1-42 in all cells lines. (Figure 3.22, A). Loss of nodes ranged 20 and 80 % in both the 5 and 10 μM conditions. The variability between differentiations at Day 70 was notable, and higher than at Day 7.

Next, I looked at the amount of nuclei loss due to amyloid treatment. Interestingly, I saw a slight, non-significant increase in the number of nuclei when looking at the number of nuclei pooled between the 14 patient lines in the $A\beta$1-42, even though there was significant neurite loss (Figure 3.22, D). This led me to look closely at the analysis pipeline, and I noticed that in some cell lines, where there is some axonal blebbing, the analysis picks up bigger clusters of "blebs" as nuclei, which are not filtered out, and likely lead to the slight increase in nuclei count in the treated wells.

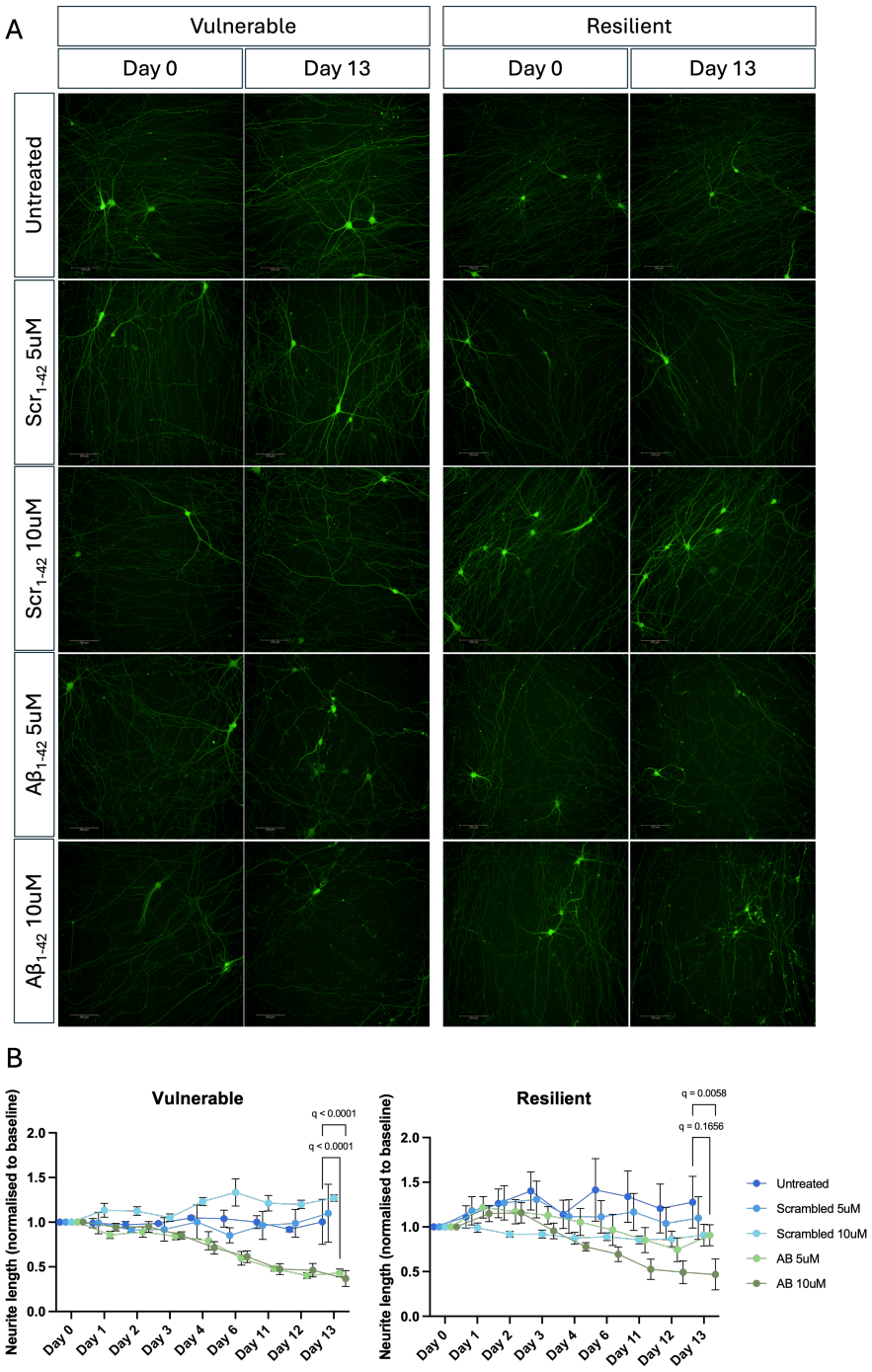


Figure 3.20: **Neurite tracing of Day 70 cortical neurons after $A\beta$1-42 insult**. (A) Representative images of a vulnerable (left) and resilient (right) cell line at Day 0 and Day 13 after addition of $A\beta$. (B) Quantification of the total neurite length (μM), normalised to baseline, over time. +-/SEM N=4 independent differentiations repeat averaged over 4 technical replicates. Repeated measures mixed model analysis with FDR corrections.$p < 0.05$ $(*)$, $p < 0.01$ $(**)$, $p < 0.001$ $(***)$, $p < 0.0001$ $(****)$

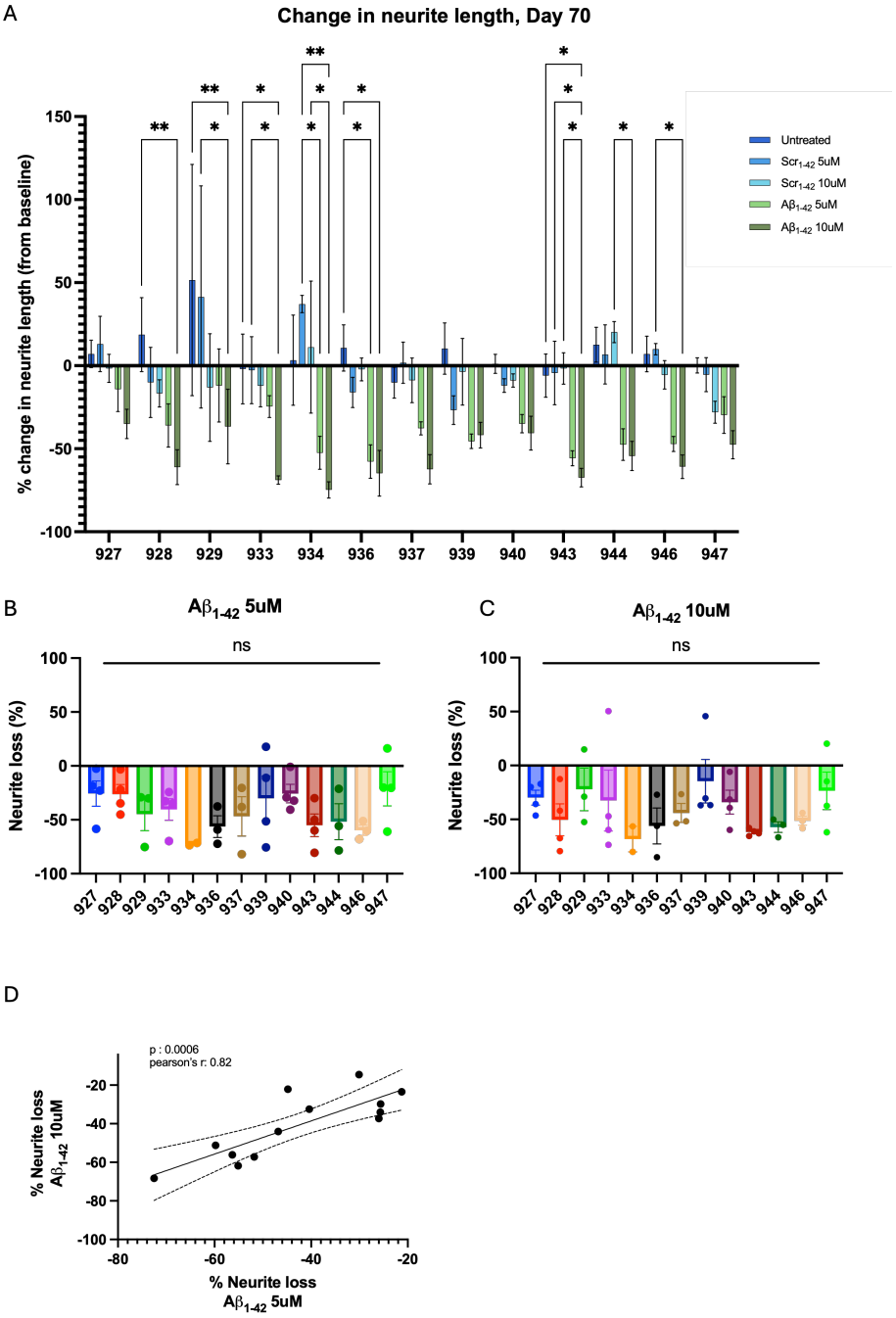


Figure 3.21: **Quantification of neurite loss in Day 70 cortical neurons due to $A\beta$1-42 insult**. (A) Total neurite length on Day 13 of imaging, normalised to baseline (Day 0), in the 14 patient lines. (B-C) % Neurite loss due to $A\beta$1-42 at 5 μM (B) and 10 μM (C) normalised to treatment control . (D) Linear regression between neurite loss at 5 μM vs 10 μM of $A\beta$1-42. (A) 2-Way ANOVA with Tukey's multiple comparison test. (B-C) One-way ANOVA with Tukey's multiple comparison test.(D) Pearson's correlation with two-tailed p-value and 95 % CI. $p < 0.05$ $(*)$, $p < 0.01$ $(**)$, $p < 0.001$ $(***)$, $p < 0.0001$ $(****)$

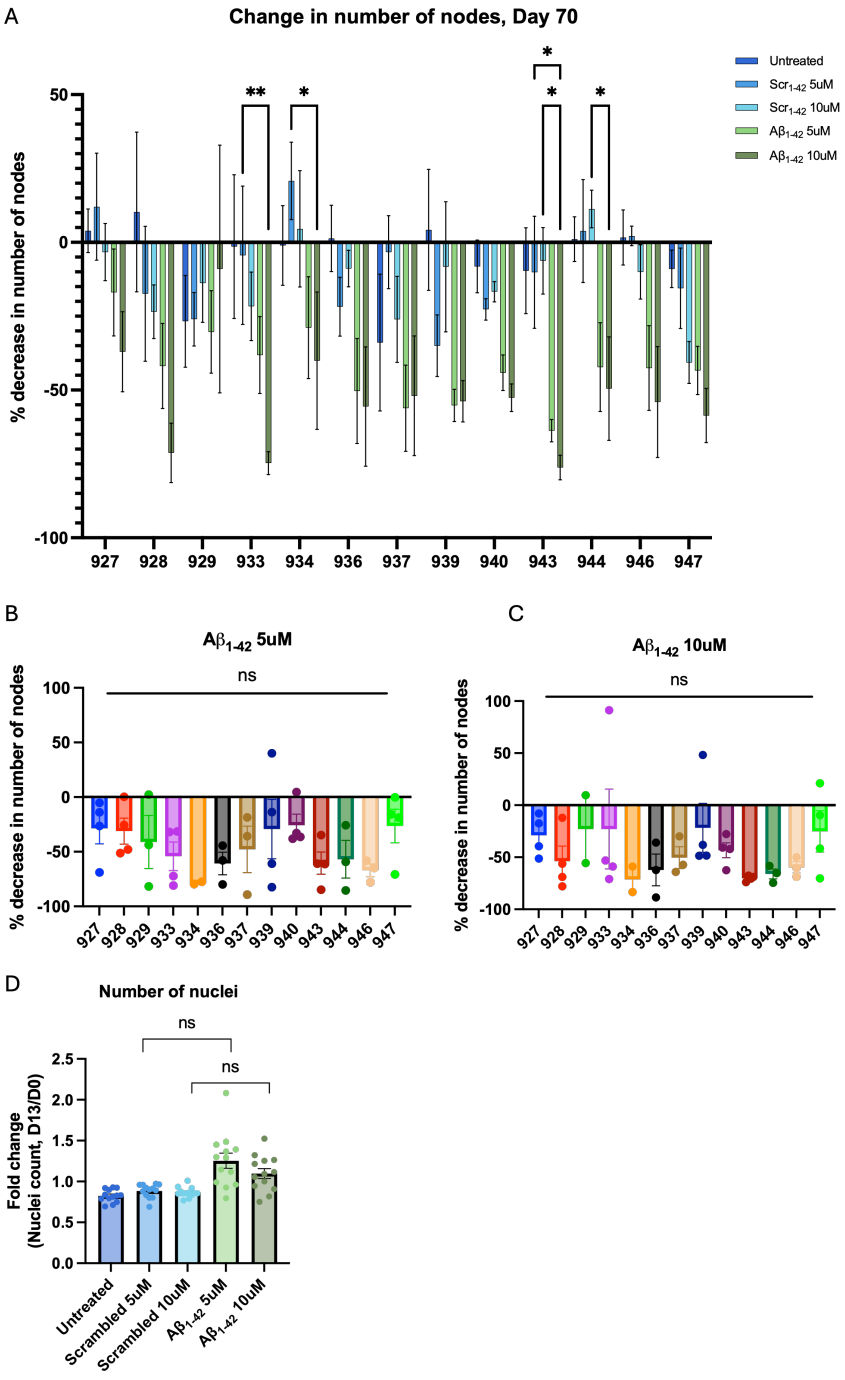


Figure 3.22: **Quantification of the number of nodes in Day 70 cortical neurons due to $A\beta$1-42 insult**. (A) number of nodes on Day 13 of imaging, normalised to baseline (Day 0), in the 14 patient lines. (B-C) % decrease in number of nodes due to $A\beta$1-42 at 5 μM (B) and 10 μM (C) normalised to treatment control. (D) Change in number of nuclei. (A) 2-Way ANOVA with Tukey's multiple comparison test. (B-C) One-way ANOVA with Tukey's multiple comparison test. (D) Kruskal-Wallis test with Dunnett's T3 multiple comparison, $p < 0.05$ ($*$), $p < 0.01$ ($**$), $p < 0.001$ ($***$), $p < 0.0001$ ($****$)

3.6.2 Adenylate Kinase release

To look at cell viability, AK release in the cell supernatant was measured 13 days after $A\beta$1-42 treatment (Day 83) using the Toxilight assay. The neurons were half-fed twice during the treatment, so the media collected for toxilight contained mostly AK released between Day 9 and 14. There was a dose-dependent increase in luminescence in the $A\beta$1-42 treated wells (Figure 3.23, A), which was significant when looking at the AK levels averaged across cell lines (Figure 3.23, B). Given that baseline levels of luminescence were quite different between patient lines, I normalised the luminescence to the treatment controls to look at differences in cell viability between patients (Figure 3.23, C). There were no significant differences in AK release between patient lines.

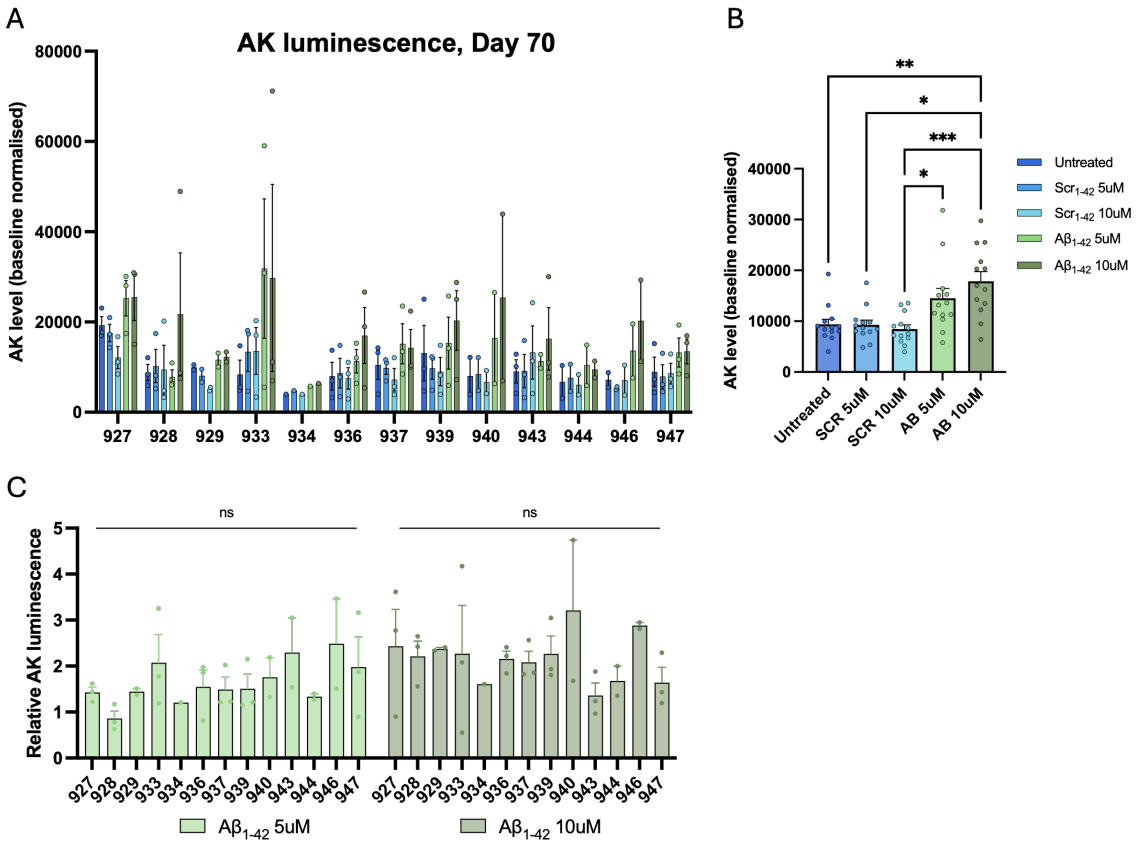


Figure 3.23: **Adenylate Kinase Release in Day 70 cortical neurons treated with $A\beta$1-42.**(A) AK luminescence (blank corrected) in $A\beta$1-42-treated samples.(B) Average AK luminescence in the 14 cell lines. (C) Relative AK luminescence to scrambled $A\beta$1-42 peptide, (5 and 10μM, respectively). Mean ± SEM n=3 independent differentiation repeats, averaged across 3-4 technical replicates. (A,D). 2-Way ANOVA with Benjamini and Hochberg FDR multiple comparisons correction (Q=0.05).(B) Brown-Forsythe and Welch's one-way ANOVA with Dunnett's T3 multiple comparisons test.(C): ordinary One-way ANOVA with Tukey's multiple comparisons test.$p < 0.05$ $(*)$, $p < 0.01$ $(**)$, $p < 0.001$ $(***)$, $p < 0.0001$ $(****)$

3.7 Correlation of neurite loss in Day 70 iPSC-derived neurons with clinical measures from the DFP cohort patients

Finally, I was interested in whether neurite loss in Day 70 cortical neurons correlated with hippocampal volume normalised to CSF $A\beta$ or PET amyloid. Unlike at Day 7, neurite loss did not correlated to hippocampal volume (Figure 3.24, A). I then compared neurite loss with all clinical measures described in Section 3.4, before looking at specific correlations of interest (Figure 3.24, A). Again, here unajdusted

p-values were assessed, due to the exploratory nature of this experiment. Neurite loss due to 5 μM of $A\beta$ correlated significantly with CSF $A\beta$42, while the 10 μM condition correlated significantly with CSF $A\beta$42:40 (Figure 3.24, B-E). There correlations were not significant after correcting for multiple comparisons (Benjamini-Hochberg correction).

I checked whether neurite loss was consistent between lines throughout development, as that could explain why there were no clinical measures that correlated with neurite loss at Day 7 and Day 70. Interestingly, neurite loss at Day 7 due to 5 μM of $A\beta$1-42 negatively correlated with both 5 and 10 μM conditions at Day 70, suggesting that mechanisms of vulnerability at early time-points change as neurons mature. On the other hand, there was no significant correlation between neurite loss at Day 7 with 10 μM of $A\beta$ with either Day 70 conditions (Figure 3.24, F-G).

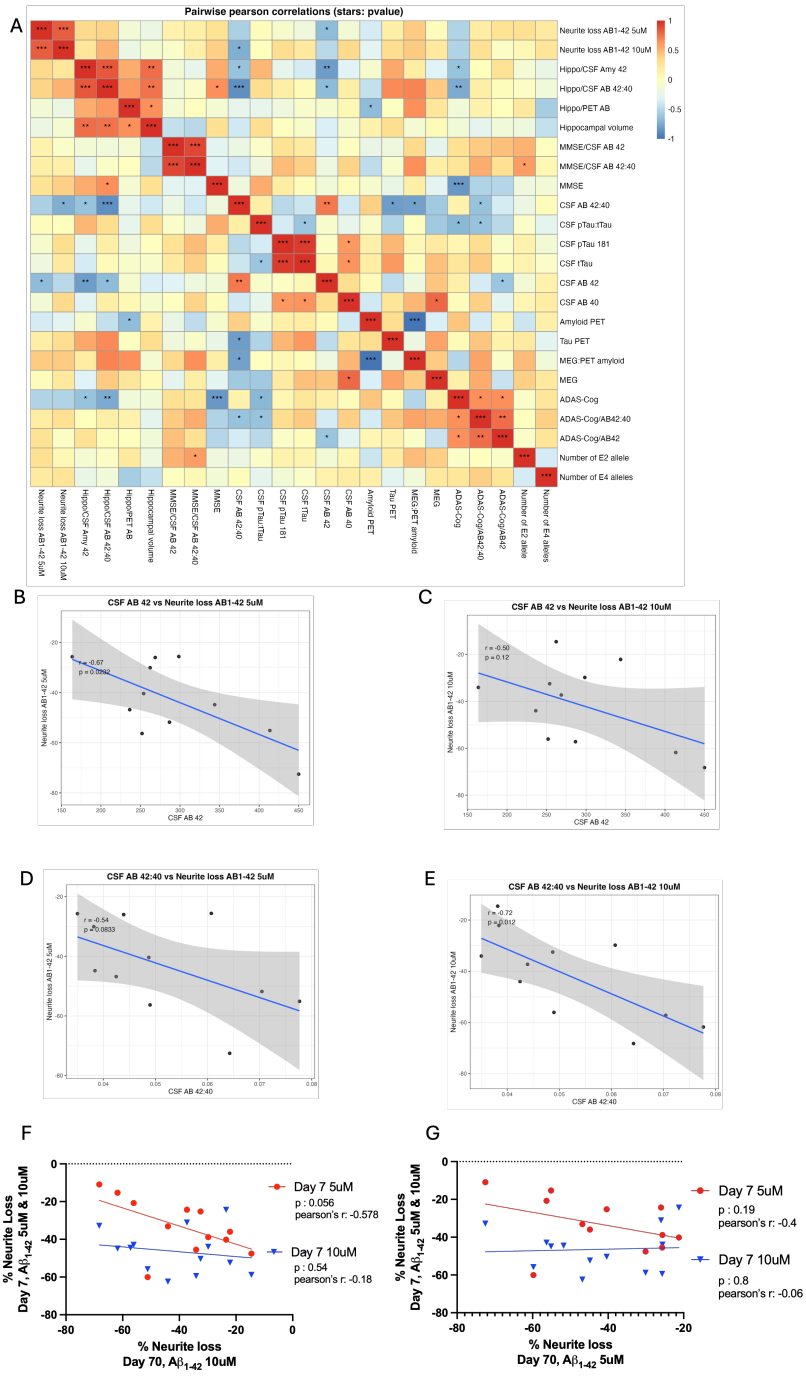


Figure 3.24: **Correlation between clinical measures of the DFP cohort and $A\beta$ induced neurite loss in D70 iPSC-derived cortical neurons**.(A) Correlation matrix of Pearson's correlations between all clinical measures and various $A\beta$ insults. (B-I) Linear regressions of correlations of interest. (B-C) Patient CSF $A\beta$42 correlated with neurite loss after $A\beta$1-42 5μM, $A\beta$1-42 10 μM, respectively. (D-E) Patient CSF $A\beta$42:40 correlated with neurite loss after $A\beta$1-42 5μM, $A\beta$1-42 10μM, respectively. (F-G) Linear regression of correlations between Day 7 and Day 70 neurite loss at 5 μM and 10μM. p-values, r and R^2 values are indicated in each graph. $p < 0.05$ $(*)$, $p < 0.01$ $(**)$, $p < 0.001$ $(***)$, $p < 0.0001$ $(****)$.

3.8 Discussion

In this chapter, I demonstrated that $A\beta$ induces a dose-dependent loss of neurites and branching and an increase in neuronal loss in cortical neurons derived from 14 AD patient iPSCs, at both Day 7 and Day 70. Importantly, neurite loss in response to Aβ was correlated to clinical measures of the patient they originate from, suggesting that sAD iPSC models are able to recapitulate patient-specific susceptibility to pathological insults. Furthermore, patient line–specific vulnerability to $A\beta$ was consistent across two forms of insult ($A\beta$1–42 and $A\beta$25–35) and across independent differentiations, indicating that this phenotype is reproducible and intrinsic to each donor.

I show that neurite loss due to $A\beta$1–42 is associated with hippocampal volume adjusted for CSF $A\beta$ 42:40. The direction of the correlation between neurite loss and hippocampal volume is consistent with the fact that low CSF $A\beta$42:40 indicates high brain deposition; dividing hippocampal volume by a lower CSF value yields a larger ratio. Additionally, higher $A\beta$1-42-driven neurite loss was associated with higher CSF pTau/tTau, which is consistent with studies in AD patients showing that CSF tau biomarkers are associated with amyloid pathology [467, 26, 303]. This correlation has two implications for AD biology. First, the fact that neurite loss correlates more strongly with hippocampal volume normalised to amyloid burden, rather than with absolute amyloid burden alone, suggests that neuronal vulnerability may be more closely tied to how neurons cope with a given level of pathology than to Aβ burden itself. Second, it suggests that the cell-autonomous response of cortical neurons to Aβ — independent of vascular, glial, or immune contributions — already encodes meaningful patient-specific information about disease vulnerability. This is consistent with emerging work showing that iPSC-derived neurons retain donor-specific transcriptional and proteomic signatures [245, 289].
However, the same correlations were not observed in Day 70 neurons, which showed a correlation between higher neurite loss and higher CSF Aβ 42:40 ratio and Aβ 42. This is counter intuitive since higher CSF Aβ 42 levels are associated with lower amyloid burden. Additionally, it was somewhat surprising that hippocampal volume correlated with neurite loss in Day 7 but not Day 70 neurons, as one would expect mature neurons to better reflect age-related hippocampal atrophy. While still controversial [225, 351], increasing evidence supports the presence of adult neurogenesis in the hippocampus [535, 439, 128, 120], which has been shown to drop

sharply in early stages of AD [309, 535, 472]. It is possible then, that immature neurons capture aspects of early-stage vulnerability, which are lost at Day 70.

While having 14 AD patient lines grown in parallel in a single experiment is considered relatively large for an iPSC study, it is small in clinical terms, therefore limiting the strength of the correlations. Due to the small number of data points, some significant correlations should be interpreted with caution, such as those observed at only one concentration of $A\beta$25–35, which may due to chance.

3.8.1 Choice of timepoints and developmental considerations

The use of Day 7 iPSC-derived neurons to measure neurite loss represents a compromise between biological relevance and methodological feasibility. iPSC-derived neurons at this stage are still developmentally immature; they differ from adult neurons in multiple ways, including gene expression profiles (such as Tau isoforms), synaptic maturity, metabolism and overall complexity. However, they do express cortical markers, extend neuritic processes, and display a neuronal morphology. This early timepoint was selected largely for logistical reasons: cortical neurons grow neurites very rapidly and densely, reducing the sensitivity and reproducibility of automated tracing pipelines.

3.8.1.1 Increased inter-differentiation variability at Day 70

- The harmony pipeline is not sensitive enough to pick up all neurites due to the higher density at Day 70, but if the GFP titer was much lower, the number of neurons sampled would become too small.
- Extended time in culture (for 2.5 months) introduces variability that accumulates over time, which is not an issue at Day 7. For instance, slight differences in proliferative rates or seeding densities leads to certain lines having denser cultures, which may impact the metabolic rate of the culture, the health of neurons or their connectivity.
- At Day 70, there was a small increase in nuclei in the $A\beta$ treated condition, which I established was a limitation of the Harmony analysis pipeline, due to the pipeline identifying bigger clumps of axonal blebbing as nuclei. Future studies could address this by transducing neurons with a nuclear BFP lentivirus to improve the accuracy of nuclear counts.

3.8.1.2 Differences in inter-patient vulnerability between Day 7 and Day 70

Surprisingly, Day 7 and Day 70 measurements at 5 μM $A\beta$1–42 were significantly negatively correlated (Figure 3.24 F, G), suggesting there might maturation-dependent shifts in neuronal susceptibility. This is not necessarily surprising given the significant changes neurons experience during maturation, such as the formation of functional synapses or shifting metabolism from glycolysis to oxidative phosphorylation. For instance, LOAD fibroblasts have increased glycolysis [438], and in AD-brains, increased oxidative phosphorylation and decreased glycolysis is associated with resistance to neuropathology [72]. This shift in metabolism, among other maturation -dependent changes, may explain the shift in vulnerability to Aβ observed here.
This negative correlation was not observed at all concentrations, which is partially due to the higher variability discussed above. Additionally, at higher doses, toxicity becomes more severe and more uniform between lines, essentially "flattening" the dynamic range.

3.8.2 Comparison of $A\beta$1-42 and $A\beta$25-35 insults

$A\beta$1–42, unlike other aggregation-prone proteins such as α-synuclein or Tau, aggregates extremely rapidly. Early studies showed that fibrillation is strongly temperature dependent: increasing the temperature from 4°C to 24°C increases the elongation rate 20-fold, and incubating preparations at 37°C for 24 h results in almost exclusively fibrillar species [268, 449]. This inherent instability makes $A\beta$1–42 challenging to work with, as even small deviations in handling can alter the distribution of oligomers and fibrils in a given preparation. Incubating $A\beta$1–42 at 4°C for 24 h slows the aggregation process and generates a more homogeneous oligomeric population [448]. I was therefore extremely careful when preparing these samples, avoiding more than one freeze–thaw cycle and keeping preparations on ice until added to the neurons to minimise unintended aggregation. Nonetheless, as shown by the western blots in 3.6, considerable variability remained in the amount of oligomers present between preps. I suspect that a proportion of the variability observed between differentiations—particularly at Day 7—was due to these differences. For example, preparations containing a higher proportion of fibrils after the 24 h incubation were generally less toxic (data not shown), likely because pre-existing fibrils promoted further fibrillisation of oligomers. Since $A\beta$1–42 fibrils are considered a less toxic

conformation than oligomers [490, 148, 95], increased fibril content results in less toxic preparations [24].
In theory, $A\beta$25–35 should be a more stable peptide and therefore more consistent [49, 141], but this was not the case in my hands: variability was higher between differentiations than for $A\beta$1-42, and range of vulnerability between patient lines were less clear. This could reflect differences in protocols used to make the oligomers, or perhaps be due to the higher concentrations used.

3.8.3 $A\beta$ concentration

The decision to use 5 and 10 μM $A\beta$1-42, and 10-20 μM $A\beta$25-35 was based partly on continuity with previous DFP experiments [395, 322] to be able to compare my work with previous and current experiments, I remained consistent with these concentrations. Moreover, similar concentrations of $A\beta$ have been used in other studies in neuronal models and cellular models [141, 226, 310, 89, 330, 527, 463, 125]. However, these concentrations are clearly supra-physiological. Ideally, neurons would be exposed to low concentrations of $A\beta$ repeatedly over long periods to better mimic *in-vivo* conditions. Practically, this would pose logistical challenges, given the number of cell lines used in this study and the limitations described above of neurite density. It is also worth noting that, while other groups have shown toxicity and neurite loss in iPSC derived neurons at concentrations as low as 1.25 μM of $A\beta$ [385] after 48 hours, I did not observe this at 5 or 10μM.

3.9 Conclusion

Here, I showed that $A\beta$ oligomer–induced neurite loss is patient-specific and reproducible across differentiations and across different types of $A\beta$ insult. $A\beta$ also induced neuronal loss, as demonstrated by AK release, a reduction in nuclei counts, and cleaved caspase 3 staining, and these effects were dose-dependent. Finally, $A\beta$-induced neurite loss correlated with clinical measures from the donor patients, which supports the findings of Ng et al [322] that sAD iPSC-derived neurons retain clinically meaningful features of their donors and that neuronal vulnerability to $A\beta$ *in vitro* reflects aspects of in-vivo susceptibility to $A\beta$ pathology. These findings support the utility of sAD iPSC models for probing patient-specific mechanisms of neurodegeneration.

Chapter 4

Investigating Aβ-induced transcriptional changes in iPSC-derived cortical neurons

4.1 Introduction

Bulk transcriptomic analyses of post-mortem human brain tissue have provided important insights into gene and protein expression changes associated with AD [289, 72, 102]. However, longitudinal studies in sporadic AD have shown that classical pathological markers, such as Aβ and Tau burden, while necessary for diagnosis, do not consistently predict cognitive decline [375, 44]. Some individuals tolerate high levels of pathology with minimal cognitive impairment (resilient individuals), whereas others experience severe cognitive decline despite relatively modest pathological burden (vulnerable individuals), highlighting an incomplete understanding of the molecular basis of vulnerability and resilience.

Patient-derived induced pluripotent stem cell (iPSC) models provide a powerful system for studying disease-associated molecular phenotypes in human neurons while retaining patient-specific genetic backgrounds. Large-scale transcriptomic analyses of sporadic AD iPSC-derived neurons from the ROSMAP cohort by Lagomarsino et al. demonstrated that patient-derived neurons recapitulate key transcriptional features of the donor brain, underscoring the utility of these models for investigating patient heterogeneity in Alzheimer's disease [245].

To date, only a limited number of studies have examined Aβ-induced transcriptional changes in iPSC-derived neuronal systems. Sackmann and Hallbeck investigated Aβ-induced proteomic alterations in long-term neuroepithelial-like stem cells derived from an AD APP mutant donor and APP WT control donor [398]. Colom-Cadena

et al. characterised transcriptional responses to brain-derived Aβ in control iPSC-derived neurons, including modulation by CT1812, a compound that reduces Aβ interactions with transmembrane proteins [85] . More recently, Soladogun and Zhang compared Aβ-induced transcriptional responses in iPSC-derived neurons from an APOE2/E2 and an APOE3/E3 individual [435]. While these studies demonstrate that iPSC-derived neurons mount measurable transcriptional responses to Aβ, they do not address how sporadic AD patient-derived neurons respond to Aβ or how such responses relate to clinical vulnerability and resilience.

In Chapter 3, I established that sporadic AD iPSC-derived neurons exhibit differential vulnerability to Aβ exposure, consistent with findings by Ng et al [322]. However, the molecular pathways and gene expression programs underlying this differential response remain unclear. In this chapter, bulk RNA sequencing was used to characterise Aβ-induced transcriptional responses in iPSC-derived cortical neurons from sporadic Alzheimer's disease patients in the DFP cohort. By integrating patient clinical phenotypes with transcriptomic profiling, this work aims to identify whether differences in transcriptional responses between resilient and vulnerable individuals drive the spectrum of vulnerability observed in morphological experiments, thereby providing new insight into patient-specific mechanisms of disease susceptibility.

4.1.1 Aims of this chapter

In this chapter, I aim to:

- Investigate whether Aβ1-42 elicits transcriptional changes in iPSC-neurons using i^3 cortical neurons
- Validate findings from the transcriptomic analysis of i^3 cortical neurons after Aβ1-42 insult
- Determine whether resilient and vulnerable sAD patient lines exhibit different transcriptional responses to Aβ1-42 insult.

4.2 Bulk-RNA sequencing of i^3 neurons treated with Aβ1-42

4.2.1 Experimental design

In order to assess whether Aβ1-42 caused any transcriptional changes in iPSC-derived cortical neurons before undertaking a bulk RNA-sequencing experiment in the 14

patient lines, I first performed a pilot RNA-seq experiment in i^3 neurons treated with Aβ1-42. The experimental design is depicted in Figure 4.1 and the analysis pipeline is described in section 2.15. The neurons were grown in monoculture and treated at Day 14 with 5 or 10 μM of Aβ1-42 or scrambled peptide, or left untreated, and harvested 6 days later. This timepoint was chosen because i^3 neurons go through significant maturation between Day 7 and 14, during which expression of neural precursor markers such as SOX2, PAX6 and nestin decrease significantly and cortical markers such as *CTIP2, MAP2*, β-tubulin or Tau increase [379, 349]. Neuron samples from three independent differentiations were harvested after Aβ treatment and frozen down so that RNA-extraction could be performed on all samples at the same time, in order to reduce experimental variability.

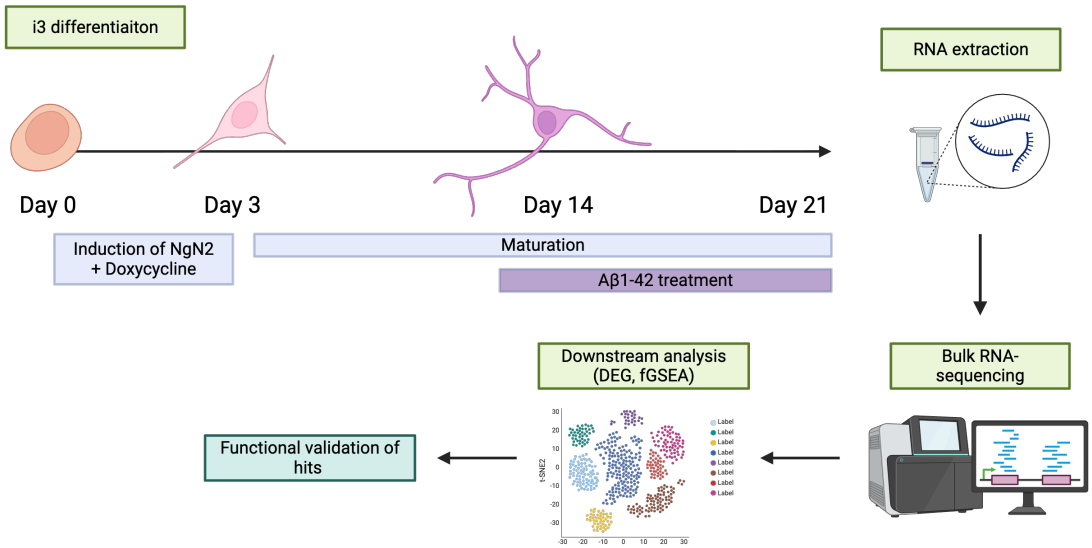


Figure 4.1: **Graphical depiction on the RNA sequencing workflow in i^3 neurons** i^3 neurons were differentiated to Day 14, at which point they were treated with Aβ1-42, Scrambled peptide or left untreated for 6 days, the cells were collected, RNA extracted and sent for sequencing. n=3 independent differentiation for each treatment condition.

4.2.2 Data quality control

After importing the reads into RStudio, the reads were filtered for low counts: genes were kept only if they had more than 30 counts in at least 3 samples, which left 15,465 genes. Principal component analysis (PCA) was performed to look at sample clustering. PC1 separates samples by treatment condition and PC2 by differentiation (Figure 4.2, A). The untreated and scrambled (SCR) treatments

cluster closely together, separately from the Aβ1-42 samples. The sample from the 3rd differentiation treated with 10 μM of Aβ1-42 did not cluster closely with the other Aβ sample. The Euclidean distance heatmap, which computes the pairwise Euclidean distance between every pair of samples using their gene expression profiles, also clearly shows that Aβ1-42 10 μM sample is an outlier (Figure 4.2, B). Furthermore, that sample did not pass the RNA integrity QC performed by Novogene, and therefore, it was not included in downstream analyses.

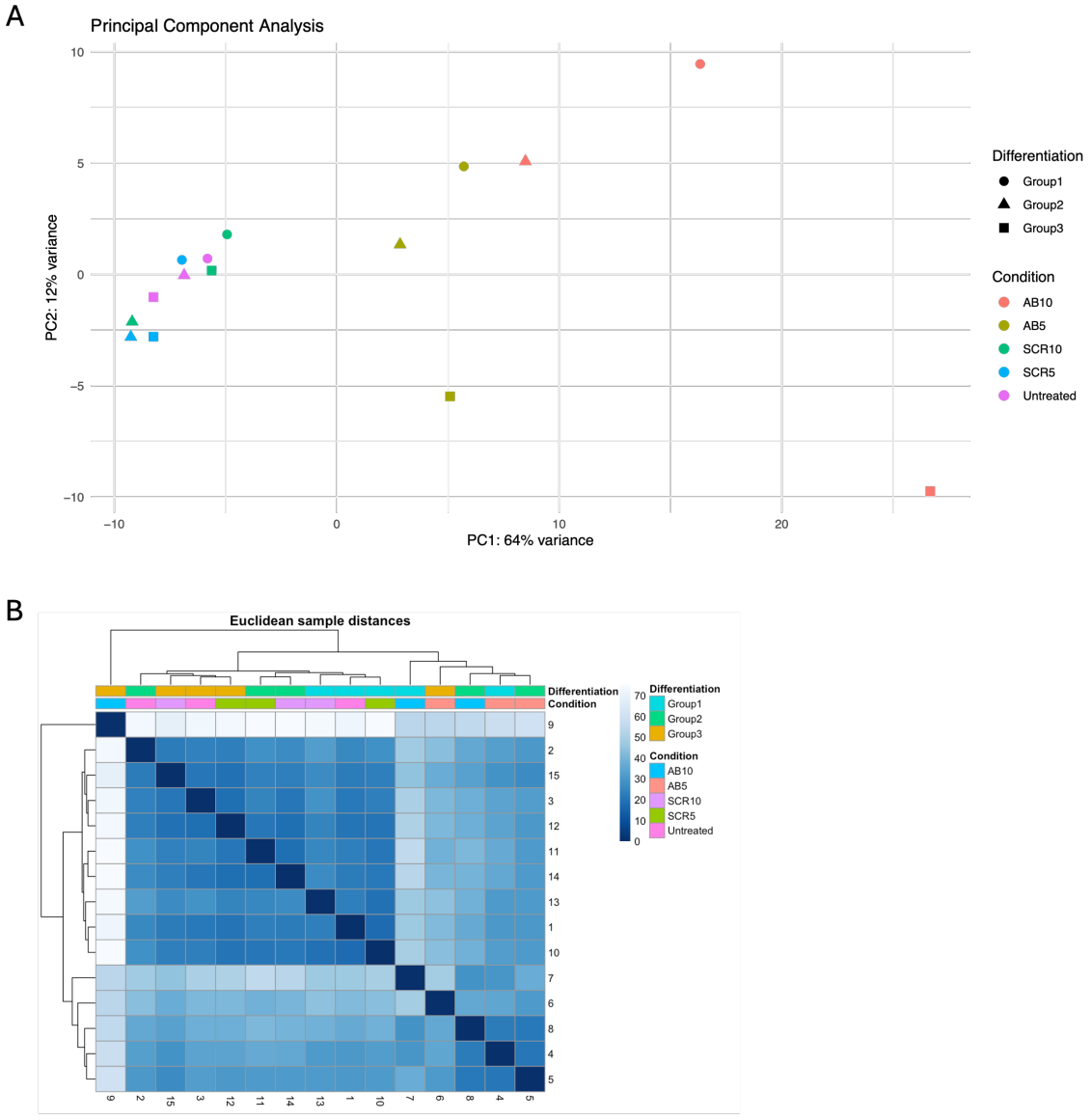


Figure 4.2: **PCA plot and Euclidian distance heatmap depicting sample clustering of i3 neurons treated with Aβ** (A) PCA plot and (B) Euclidian sample distance heatmap of the gene expression i3 neuron samples treated with Aβ at 5 or 10 μM, Scrambled peptide at 5 or 10 μM, or left untreated.

4.2.3 Differential Gene Expression analysis overview

I first plotted the mean of normalised counts of cortical markers across all samples of the i^{3}s neurons (Figure 4.3, A). The i^{3}s expressed high levels of Tau , *MAP2*, β-tubulin, *CUX1* and *CUX2*, moderate levels of *VGLUT1*, *BRN2*, *SATB2* and low levels of *CTIP2*, all of which are consistent with the RNA-sequencing dataset of i^3 neurons published previously [379, 349, 471]. Then differential gene expression analysis was performed using DESeq2, using a linear model that looked at the effect of the treatment while controlling for differences between differentiations (~ Differentiation + Condition). P-values were adjusted for multiple testing using the Benjamini–Hochberg method. MA plots, which plot the normalised counts on the x-axis and the Log_2FoldChange on the y-axis of each gene, were generated to provide an overview of the distribution of the genes for each comparison. Importantly, there were nearly no DEGs between the untreated and scrambled peptide conditions, confirming that the scrambled Aβ1-42 peptide is an appropriate control, and that the effect of Aβ is sequence and structure specific (Figure 4.3, B-D). Furthermore, there was a high correlation between the DEGs in the Aβ 5 μM vs SCR 5 μM and Aβ 10 μM vs SCR 10 μM conditions (r=0.97), confirming that the transcriptional changes due to Aβ are consistent between the two concentrations (Figure 4.3, A). Looking at all DEGs, there were similar numbers of significantly upregulated and downregulated genes in both conditions. In the Aβ 10 μM condition, 2320 genes were significantly upregulated and 2075 genes were significantly downregulated (padj < 0.05) compared to SCR. In the Aβ 5 μM condition, 1393 genes were significantly upregulated and 1448 were significantly downregulated compared to SCR. However, when filtered only for genes with a large effect size (absolute Log_2FoldChange > 1), the number of upregulated genes was higher than the number of downregulated genes (Figure 4.4 A-B). As with the MA plots, the volcano plots show no DEGs between the Untreated and Scr 5 or Scr 10 μM conditions (Figure 4.4 C-D). Significant DEGs dropped to 629 upregulated and 82 downregulated for the Aβ 10 μM condition, and 265 upregulated and only 20 downregulated for the Aβ 5 μM condition. The top genes are depicted in Figure 4.5, B-C. In the list of the top 20 most upregulated genes, 16/20 of the top genes in the Aβ vs SCR 5 μM condition were also in the Aβ vs SCR 10 μM top 20 gene list.

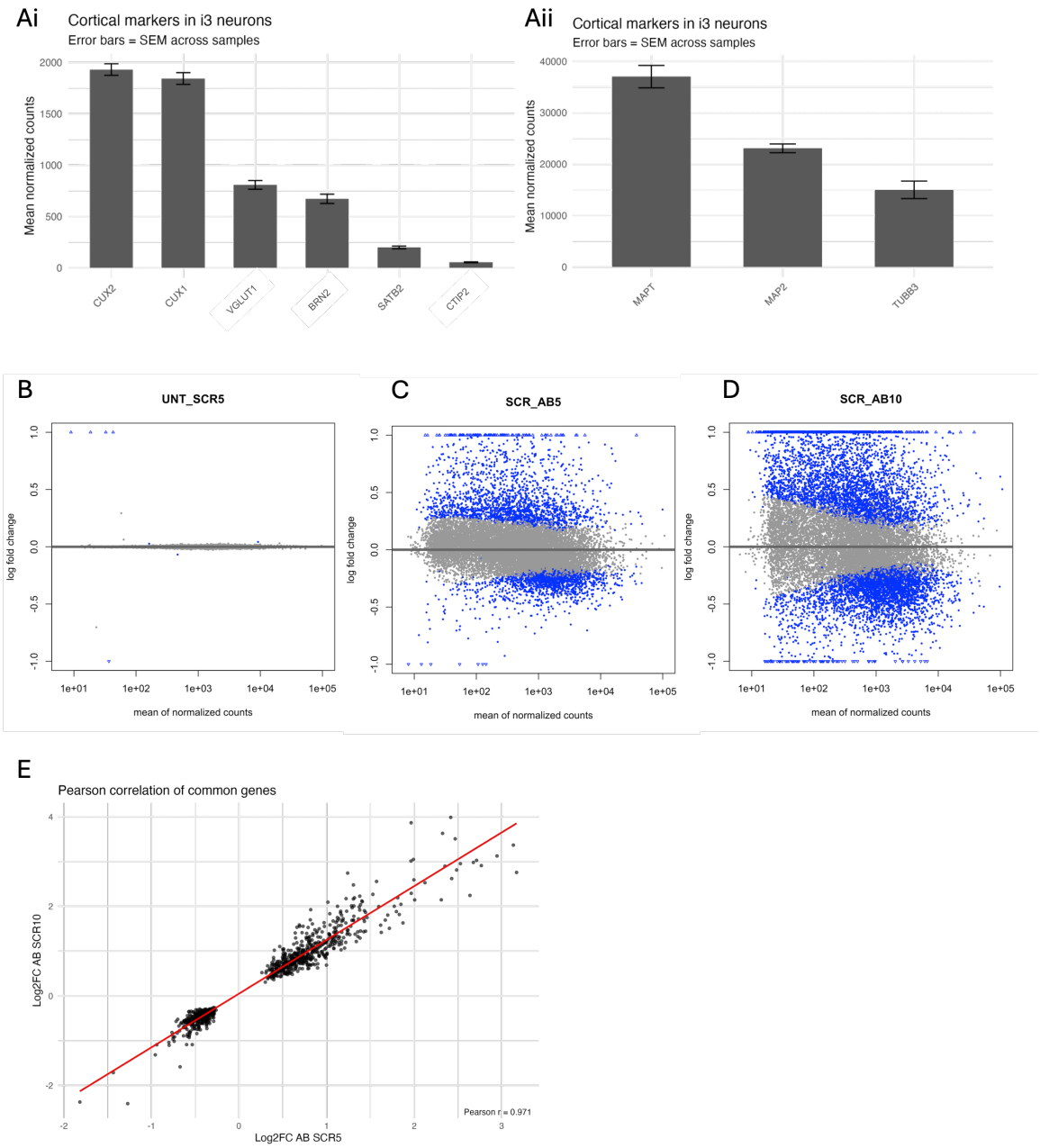


Figure 4.3: **MA plot and cortical marker expression in i3 neurons** (Ai-ii) Bar blot of cortical markers in i3 neurons, averaged across all replicates. Mean +- SEM, n=3 (B-D) MA plots depicting the Log_2FoldChange over the mean of normalised counts of all genes in the Untreated vs Scrambled, Scrambled 5 μM vs Aβ 5 μM, Scrambled 10 μM vs Aβ 10 μM comparisons. (E) Pearson's correlation of all DEGs in the Scrambled vs Aβ condition at 5 μM compared with those in the Scrambled vs Aβ condition at 10 μM . r=0.971

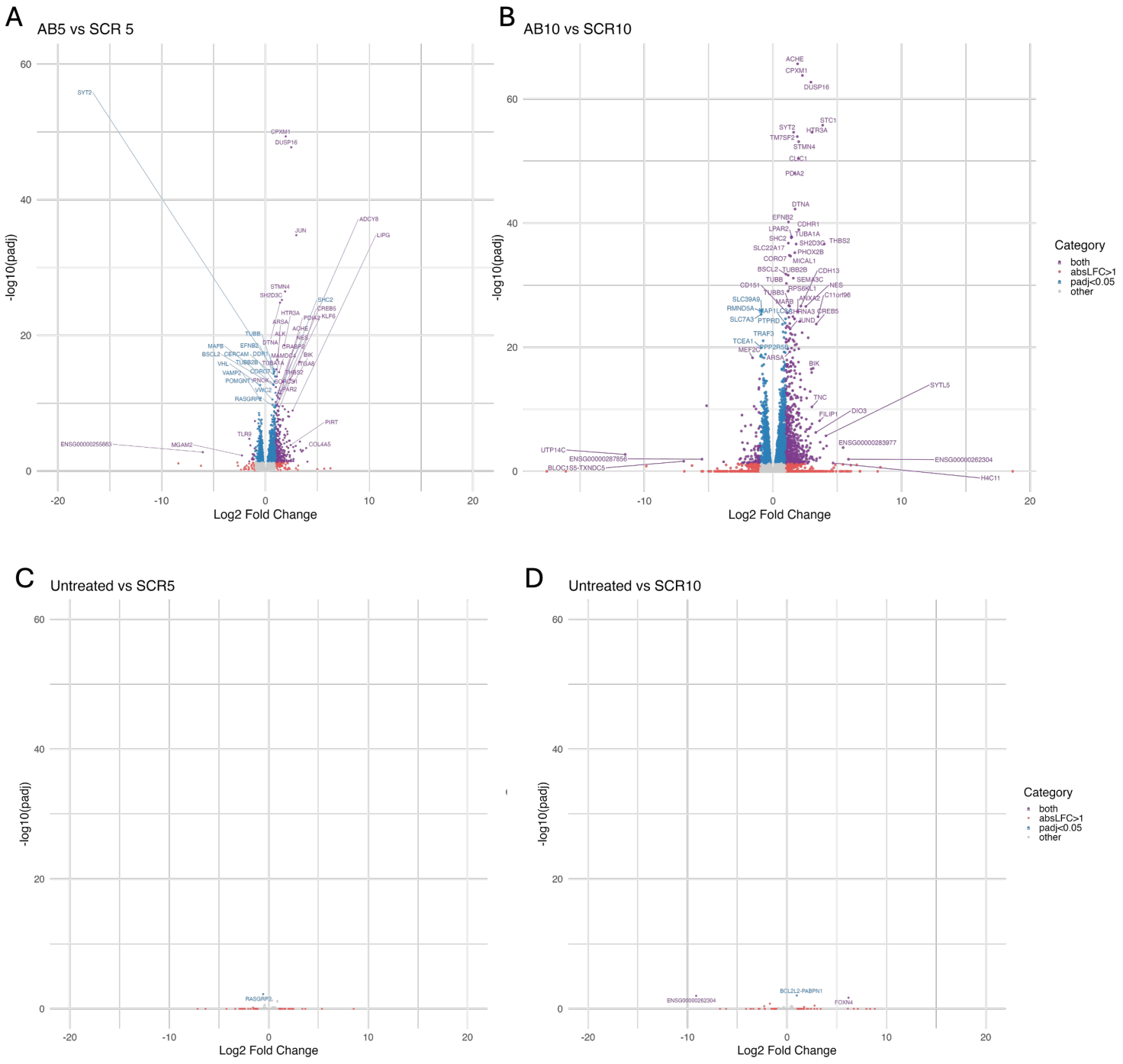


Figure 4.4: **Volcano plots of DEG between AB-treated and control i3 neurons** (A-D) Volcano plots of the DEGs in the (A) Aβ 5 μM vs Scr 5um, (B)Aβ 10 μM vs Scr 10 μM, (C) Untreated vs Scr 5 μM , (D) Untreated vs Scr 10 μM . Blue dots are genes with a padj <0.05, red are genes with absolute Log_2FoldChange > 1, purple are genes that meet both conditions.

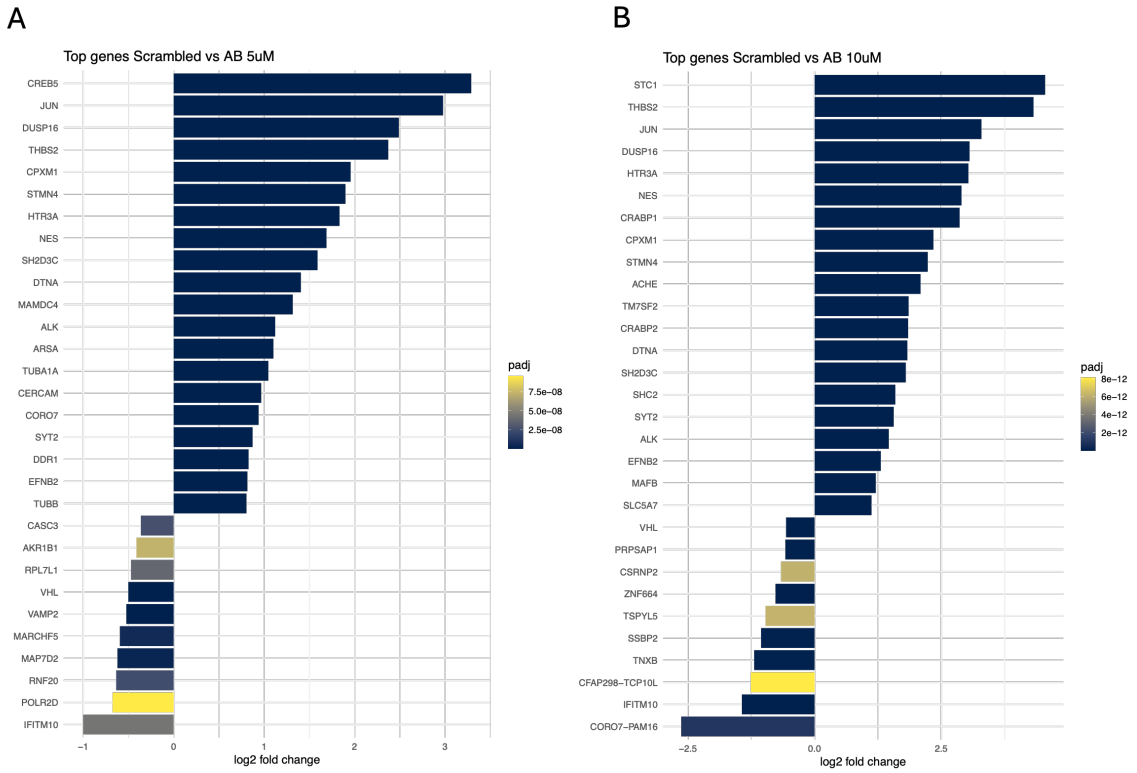


Figure 4.5: **Top 30 up and downregulated DEGs between Aβ -treated and Scrambled i3 neurons** (A) Top 30 DEGs in the Aβ 5 μM condition compared to Scrambled 5 μM condition, (B) Top 30 DEGs in the Aβ 10 μM condition compared to Scrambled 10 μM condition

4.2.4 Gene Set Enrichment analysis overview

Fast Gene Set Enrichment Analysis (fGSEA) was performed to identify groups of genes in the dataset that are enriched in specific pathways. A list of all genes in the dataset, ranked by Log2FoldChange x -Log10 p-value was generated to run fGSEA. This is a more appropriate value to rank genes than Log2FC or p-value alone, as it takes into account both the size of the effect and the significance. This reduces the risk of highly ranked genes coming from genes with large effect size but with very low counts. There are many pathway databases available, including Gene Ontology databases, KEGG, Reactome and Hallmark pathways. Instead of looking at only one or two databases, GSEA was performed on all available pathway databases, and relevant pathways were then analysed in more detail.

4.2.5 Analysis of DEGs and enriched pathways

Following an initial overview of transcriptional changes induced by Aβ1-42 treatment, I conducted a detailed analysis of the differentially expressed genes (DEGs) and enriched pathways in each comparison. Owing to the large number of significant DEGs and pathways detected, this section focuses on the most significant and biologically relevant results. To clarify, when I mention the "5 or 10 μM comparisons", I am referring to the Aβ1-42 5 or 10 μM treated neurons compared to the SCR peptide at 5 or 10 μM.

4.2.5.1 Upregulated genes and pathways in cells treated with Aβ1-42 compared with Scrambled peptides

The top upregulated genes in both the 5 and 10 μM comparisons were involved in axonal projection, guidance and stability such as genes encoding several tubulin proteins (*TUBB3, TUBB2B, TUBA1A*), semaphorins *(SEMA3C, SEMA4A, SEMA5B*), Ephrin B2 (*EFNB2*), Fibronectin Leucine-Rich transmembrane protein (*FLRT3*), statmin 4 (*STMN4*)) and dystrobevin alpha (*DTNA*). Additionally, genes involved in synaptic function such as *ACHE* (acetycholine esterase), *SLC5A7* (solute carrier family 5 member 7), which codes for choline transporter 1, *HTR3A* (5-hydroxytryptamine receptor 3A, a serotonin ion channel), *SYT2* (Synaptotagmin 2), *DRD2* (dopamine receptor D2), *THBS2* (Thrombospondin-2), which plays a role in synaptogenesis. There were a number of genes related to lipid biosynthesis, encoding enzymes responsible for cholesterol synthesis such as *TM7SF2* (Transmembrane 7 Superfamily Member 2), *MVD* (Mevalonate Diphosphate Decarboxylase), *DHCR7* (7-dehydrocholesterol reductase), cholesterol transport such as the Low-Density Lipoprotein Receptor (*LDLR*), and transcription factors, which activate cholesterol pathways *SREBP1* an *SREBP2* (Sterol Regulatory Element-Binding Protein). Genes involved in cell-cell adhesion, such as collagen subunit genes (*COL5A1, COL4A1*), cell-to-cell interaction genes (*ADAM12, THBS2, CDH6*), and other extracellular matrix genes (*TNC, MATN2 and TGFBI*) were also upregulated in both 5 and 10 μM comparisons. Finally, genes involved in stress responses were also upregulated, including *JUN* Proto-Oncogene, *DUSP16* (Dual Specificity Phosphatase 16), *STC1* (Stanniocalcin 1), *SHC2* (SHC-transforming protein 2), *CLU* (Clusterin) and *CREB5* (cAMP responsive element-binding protein 5), which are important players in the *MAPK* and *JNK* signalling pathways (Figure 4.5, A, Figure 4.6, B-E, 4.7, B-E).

Unsurprisingly, fGSEA identified significant positive enrichment for Hallmark and

GO:BP pathways related to the upregulated genes (Figures 4.6, A, 4.7, A). The majority of the enriched terms were involved in axonogenesis (e.g. "GO:BP Neuron Projection Guidance"), followed by lipid biosynthesis pathways (e.g. "GO:BP Sterol Biosynthetic Process"), and smaller subsets were involved in synapse assembly (e.g. "GO:BP Positive regulation of synapse assembly") and cellular stress responses (e.g. "Hallmark Apoptosis", "Hallmark TNFA signalling via NFKB"). The pathways were largely overlapping between the 5 and 10 μM conditions and the size of the enrichments were comparable, although cholesterol pathways were more highly enriched in the 10 μM condition and axon projection pathways were more enriched in the 5 μM condition. Consistent with these findings, subsequent over-representation analysis (ORA) of upregulated significantly differentially expressed genes also identified enrichment in these pathways, with the exception of synaptic pathways, which were not enriched in the fORA. Additionally, in the Aβ vs SCR10 μM condition, the KEGG Lysosome pathways was significantly enriched. The genes in this pathways included *MCOLN1* (Mucolipin-1), *ARSA* (Arylsulfatase A) and *ABCA2* (ABC transporter protein), which are all involved in fat transport and breakdown in the lysosomes. *ARSA* was also one of the top upregulated genes in the Aβ 5 μM vs SCR 5 μM condition (Figure 4.8. While it might seem redundant to run both fGSEA and fORA, when possible (i.e. when a dataset has many significant DEGs, as in this experiment), it is beneficial to perform both, as fGSEA evaluates whether predefined gene sets are overrepresented at the either end of a ranked gene list (it is directional), while fORA — which does not provide an effect size or direction — validates the enrichment of pathways among significantly differentially expressed genes.

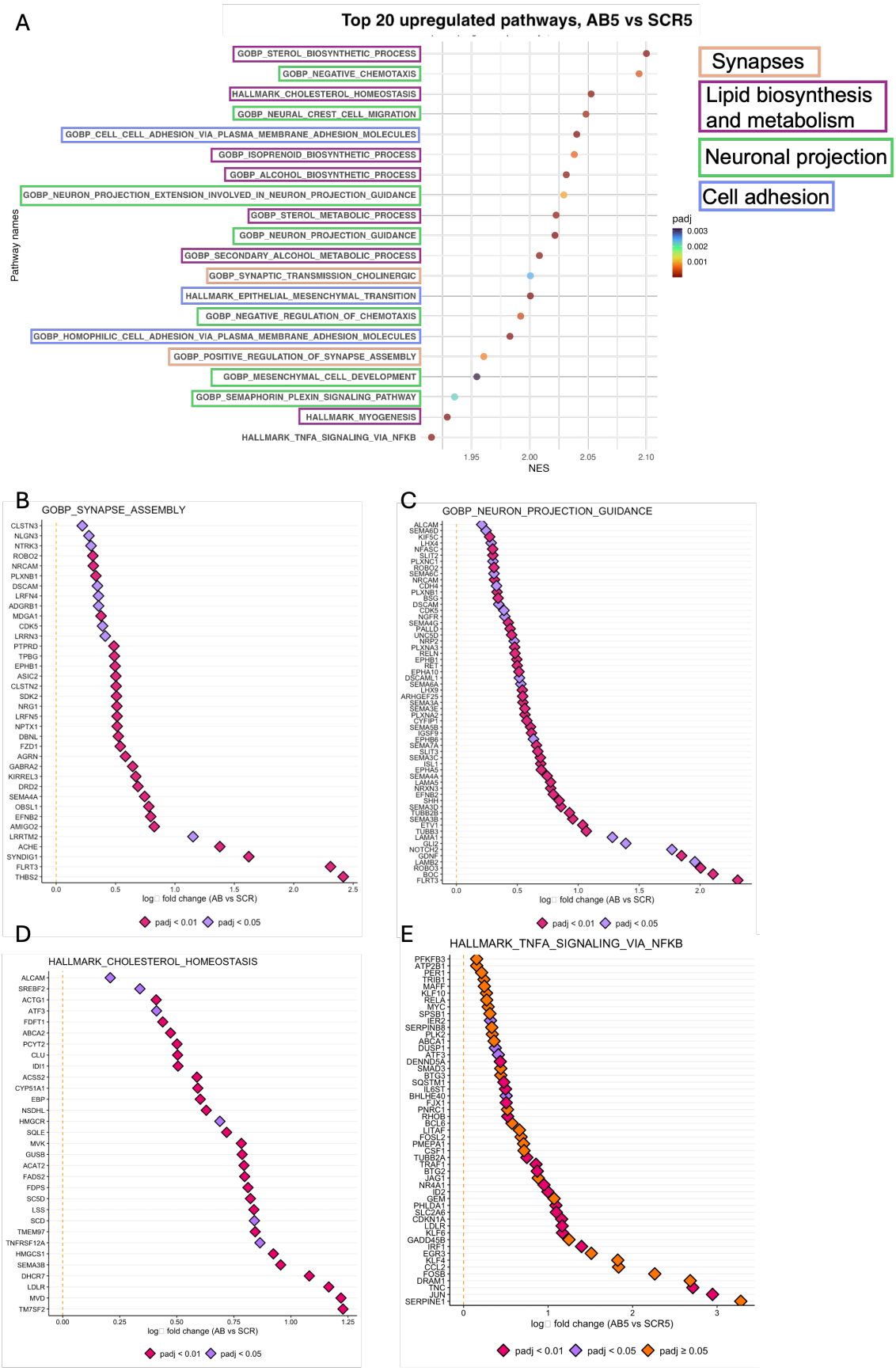

A
Top 20 upregulated pathways, AB5 vs SCR5
GOBP_STEROL_BIOSYNTHETIC_PROCESS
GOBP_NEGATIVE_CHEMOTAXIS
HALLMARK_CHOLESTEROL_HOMEOSTASIS
GOBP_NEURAL_CREST_CELL_MIGRATION
GOBP_CELL_CELL_ADHESION_VIA_PLASMA_MEMBRANE_ADHESION_MOLECULES
GOBP_ISOPRENOID_BIOSYNTHETIC_PROCESS
GOBP_ALCOHOL_BIOSYNTHETIC_PROCESS
GOBP_NEURON_PROJECTION_EXTENSION_INVOLVED_IN_NEURON_PROJECTION_GUIDANCE
GOBP_STEROL_METABOLIC_PROCESS
GOBP_NEURON_PROJECTION_GUIDANCE
GOBP_SECONDARY_ALCOHOL_METABOLIC_PROCESS
GOBP_SYNAPTIC_TRANSMISSION_CHOLINERGIC
HALLMARK_EPITHELIAL_MESENCHYMAL_TRANSITION
GOBP_NEGATIVE_REGULATION_OF_CHEMOTAXIS
GOBP_HOMOPHILIC_CELL_ADHESION_VIA_PLASMA_MEMBRANE_ADHESION_MOLECULES
GOBP_POSITIVE_REGULATION_OF_SYNAPSE_ASSEMBLY
GOBP_MESENCHYMAL_CELL_DEVELOPMENT
GOBP_SEMAPHORIN_PLEXIN_SIGNALING_PATHWAY
HALLMARK_MYOGENESIS
HALLMARK_TNFA_SIGNALING_VIA_NFKB
Pathway names
1.95
2.00
2.05
2.10
NES
padj
0.003
0.002
0.001
Synapses
Lipid biosynthesis and metabolism
Neuronal projection
Cell adhesion
B
GOBP_SYNAPSE_ASSEMBLY
log fold change (AB vs SCR)
padj < 0.01
padj < 0.05
C
GOBP_NEURON_PROJECTION_GUIDANCE
log fold change (AB vs SCR)
padj < 0.01
padj < 0.05
D
HALLMARK_CHOLESTEROL_HOMEOSTASIS
log fold change (AB vs SCR)
padj < 0.01
padj < 0.05
E
HALLMARK_TNFA_SIGNALING_VIA_NFKB
log fold change (AB5 vs SCR5)
padj < 0.01
padj < 0.05
padj ≥ 0.05

Figure 4.6

Figure 4.6: **Top positively enriched pathways in Aβ 5 μM vs Scrambled 5 μM neurons**Continued: (A) Dot plot of the top 20 positively enriched pathways in neurons treated with 5 μM of Aβ compared to Scrambled 5 μM with their normalised enrichment score (NES). Dots are coloured by the pathway's padj. (B-E) Leading edge genes of pathways of interest with their Log_2FoldChanges. Squares are colour by their padj value.

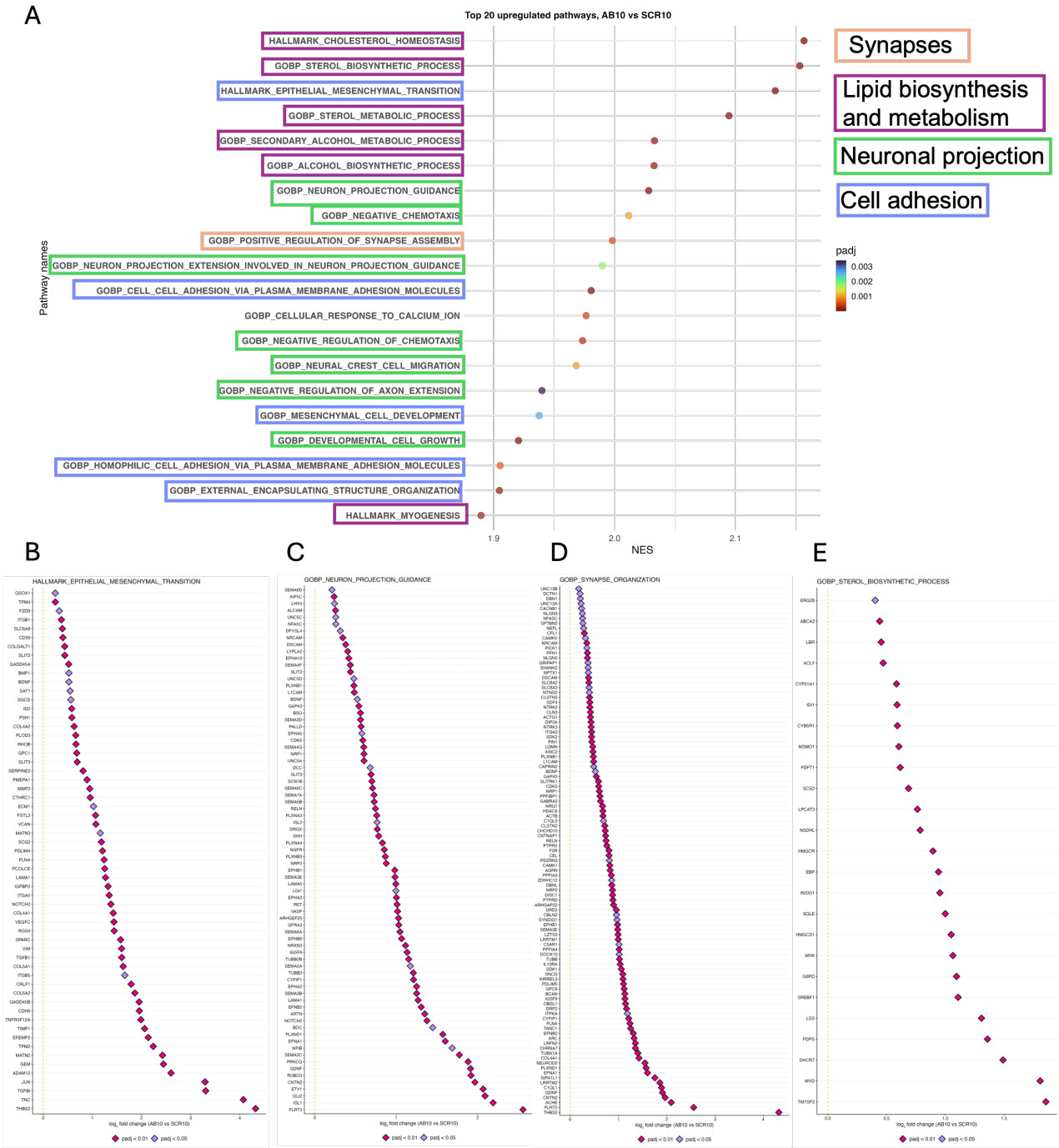


Figure 4.7: **Top positively enriched pathways in Aβ 10 μM vs Scrambled 10 μM neurons** (A) Dot plot of the top 20 positively enriched pathways in neurons treated with 10 μM of Aβ compared to SCR 10 μM with their normalised enrichment score (NES). Dots are coloured by the pathway's padj. (B-E) Leading edge genes of pathways of interest with their Log_2FoldChanges. Squares are colour by their padj value.

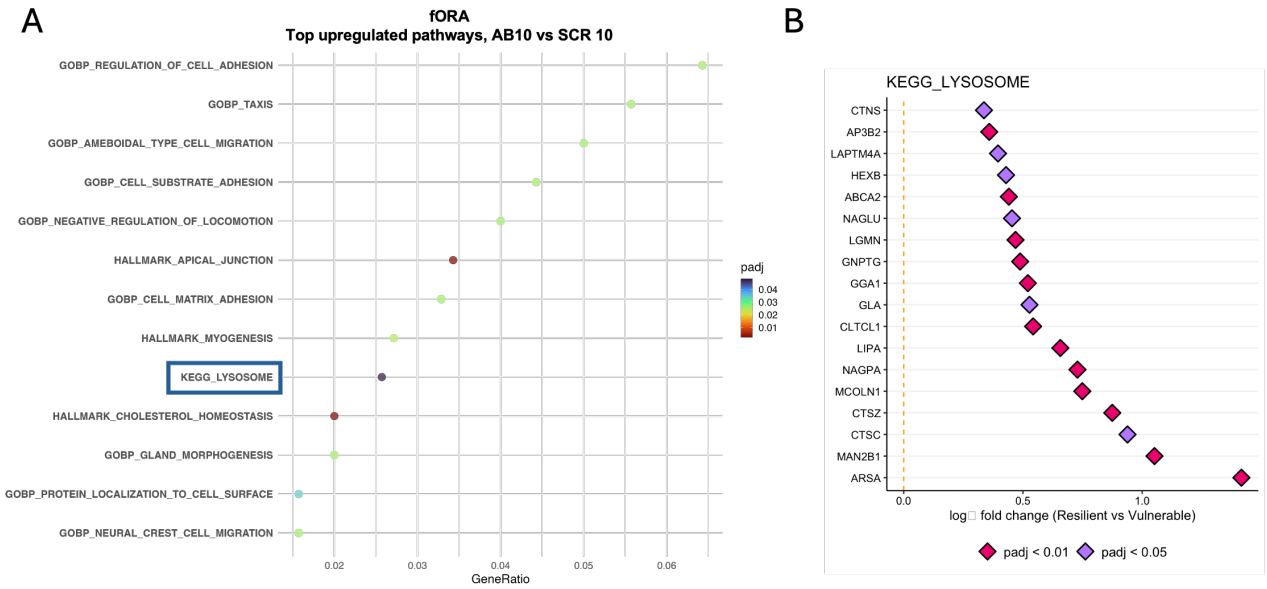


Figure 4.8: **Over-representation analysis of positively enriched pathways in Aβ 10 μM vs SCR 10 μM treated neurons**(A) Dot plot of the top positively enriched pathways, looking at significant DEGS, in neurons treated with 10 μM of Aβ compared to SCR 10 μM with the GeneRatio (i.e. the number of enriched genes/ number of significant DEGs. (B) Leading edge genes of the KEGG Lysosome pathway with their Log_2FoldChanges. Squares are colour by their padj value.Blue boxes represent new pathways not seen in fGSEA.

4.2.5.2 Downregulated genes and pathways in cells treated with Aβ1-42 compared with Scrambled peptides

As mentioned above, although similar numbers of genes were significantly upregulated and downregulated, only 82 and 20 DEGs exhibited a Log_2Fold Change below -1 (i.e. greater than a two fold decrease) in the Aβ vs SCR 10 µM and Aβ vs SCR 5 µM comparisons, respectively. In both the 5 µM and 10 µM conditions, many downregulated genes encoded proteins involved in mRNA processing, translation, and splicing, including *RPL7L1* (Ribosomal Protein L7 Like 1), *CASC3* (Cancer Susceptibility Candidate 3), several RNA polymerase subunits (*POLR2D, POLR2A, POLR2B*), and *SNRPD1* (Small Nuclear Ribonucleoprotein D1 Polypeptide). In the Aβ vs SCR 5 µM condition, a substantial number of genes associated with proteasomal function—specifically components of the 26S proteasome subunit (e.g. *PSMD12, PSMD14, PSMA4, PSMA2*)—were also significantly downregulated, although to a moderate extent (Log_2FoldChange > -1).

Additionally, several genes involved in synaptic vesicle function, including SNARE proteins (*VAMP2, VAMP4, SNAP29*), were downregulated, along with genes

associated with the ubiquitin–proteasome system such as *RNF20* (encoding an E3 ubiquitin ligase) and *VHL* (Von Hippel–Lindau tumour suppressor, which ubiquitinates Hypoxia-Inducible Factor) (Figure 4.5, B, 4.9, B-D, 4.10, B-D). Consistent with these observations, pathways related to ribosome biogenesis, mRNA translation, splicing, and processing showed significant negative enrichment in both the 5 µM and 10 µM conditions (Figure 4.9, A, 4.10, A).

Furthermore, several pathways associated with cellular stress and DNA damage responses were negatively enriched, including cellular response to hypoxia, apoptosis, oxidative phosphorylation, and chromatin disassembly. These pathways encompassed various MAP kinases (*MAPK9, MAPK10, MAPK1*) as well as *XIAP* (X-linked inhibitor of apoptosis protein). Pathways related to protein folding, such as protein folding chaperone, were also negatively enriched and included multiple heat shock proteins (*HSPA9, HSPA13*) and chaperonins (*CCT4, CCT8*), although the genes within these pathways were only moderately downregulated relative to scrambled controls (Log_2FoldChange $>$ -0.5). Proteasomal pathways were significantly negatively enriched in the SCR vs Aβ 5 µM comparison, and to a lesser extent in the SCR vs Aβ 10 µM conditions. Finally, several gene sets involved in protein ubiquitination were negatively enriched in both the 5 µM and 10 µM comparison, with stronger enrichment observed in the SCR vs Aβ 10 µM comparison.

Over-representation analysis of significantly downregulated genes identified pathways largely concordant with those detected by fGSEA, notably pathways associated with mRNA processing and proteasomal function, ubiquitination and MAPK signalling pathways. In addition, the SCR vs Aβ 10 µM comparison revealed significant enrichment of pathways related to exocytosis, endocytosis, and vesicle organisation, which included genes encoding *SNAP29* and several RAB family members (*RAB27B, RAB10, RAB21*) (Figure 4.11 .

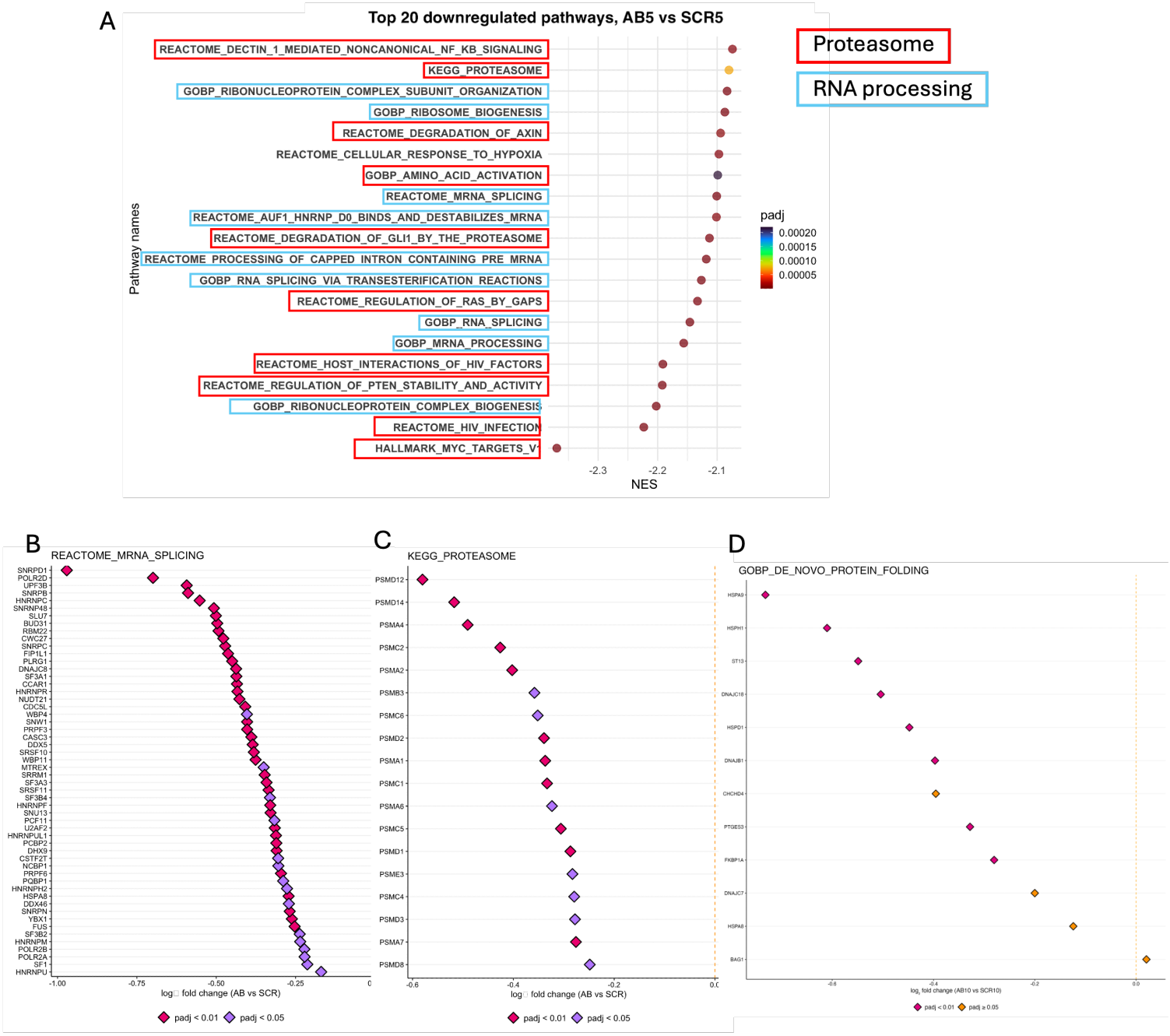


Figure 4.9: **Top negatively enriched pathways in Aβ 5 μM vs Scrambled 5 μM neurons** (A) Dot plot of the top 20 negatively enriched pathways in neurons treated with 5 μM of Aβ compared to Scrambled 5 μM with their normalised enrichment score (NES). Dots are coloured by the pathway's padj. (B-D) Leading edge genes of pathways of interest with their Log_2FoldChanges. Squares are coloured by their padj value.

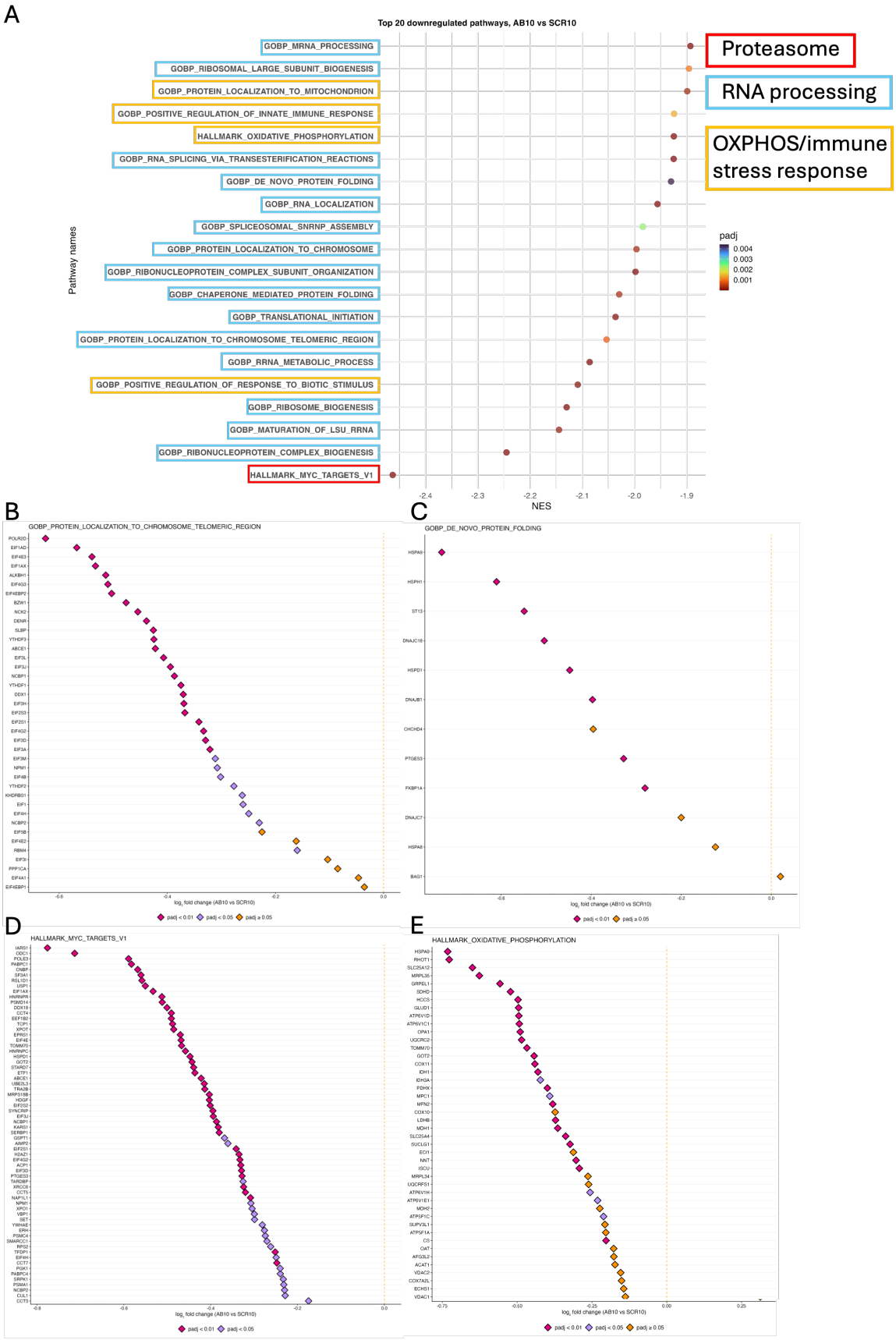

A
Top 20 downregulated pathways, AB10 vs SCR10
GOBP_MRNA_PROCESSING
GOBP_RIBOSOMAL_LARGE_SUBUNIT_BIOGENESIS
GOBP_PROTEIN_LOCALIZATION_TO_MITOCHONDRION
GOBP_POSITIVE_REGULATION_OF_INNATE_IMMUNE_RESPONSE
HALLMARK_OXIDATIVE_PHOSPHORYLATION
GOBP_RNA_SPLICING_VIA_TRANSESTERIFICATION_REACTIONS
GOBP_DE_NOVO_PROTEIN_FOLDING
GOBP_RNA_LOCALIZATION
GOBP_SPLICEOSOMAL_SNRNP_ASSEMBLY
GOBP_PROTEIN_LOCALIZATION_TO_CHROMOSOME
GOBP_RIBONUCLEOPROTEIN_COMPLEX_SUBUNIT_ORGANIZATION
GOBP_CHAPERONE_MEDIATED_PROTEIN_FOLDING
GOBP_TRANSLATIONAL_INITIATION
GOBP_PROTEIN_LOCALIZATION_TO_CHROMOSOME_TELOMERIC_REGION
GOBP_RRNA_METABOLIC_PROCESS
GOBP_POSITIVE_REGULATION_OF_RESPONSE_TO_BIOTIC_STIMULUS
GOBP_RIBOSOME_BIOGENESIS
GOBP_MATURATION_OF_LSU_RRNA
GOBP_RIBONUCLEOPROTEIN_COMPLEX_BIOGENESIS
HALLMARK_MYC_TARGETS_V1
Pathway names
NES
-2.4
-2.3
-2.2
-2.1
-2.0
-1.9
padj
0.004
0.003
0.002
0.001
Proteasome
RNA processing
OXPHOS/immune stress response
B
GOBP_PROTEIN_LOCALIZATION_TO_CHROMOSOME_TELOMERIC_REGION
log2 fold change (AB10 vs SCR10)
padj < 0.01
padj < 0.05
padj ≥ 0.05
C
GOBP_DE_NOVO_PROTEIN_FOLDING
log2 fold change (AB10 vs SCR10)
padj < 0.01
padj ≥ 0.05
D
HALLMARK_MYC_TARGETS_V1
log2 fold change (AB10 vs SCR10)
padj < 0.01
padj < 0.05
E
HALLMARK_OXIDATIVE_PHOSPHORYLATION
log2 fold change (AB10 vs SCR10)
padj < 0.01
padj < 0.05
padj ≥ 0.05

Figure 4.10

Figure 4.10: **Top negatively enriched pathways in Aβ 10 μM vs Scrambled 10 μM neurons** (A) Dot plot of the top 20 negatively enriched pathways in neurons treated with 10 μM of Aβ compared to Scrambled 10 μM with their normalised enrichment score (NES). Dots are coloured by the pathway's padj. (B-D) Leading edge genes of pathways of interest with their Log_2FoldChanges. Squares are coloured by their padj value..

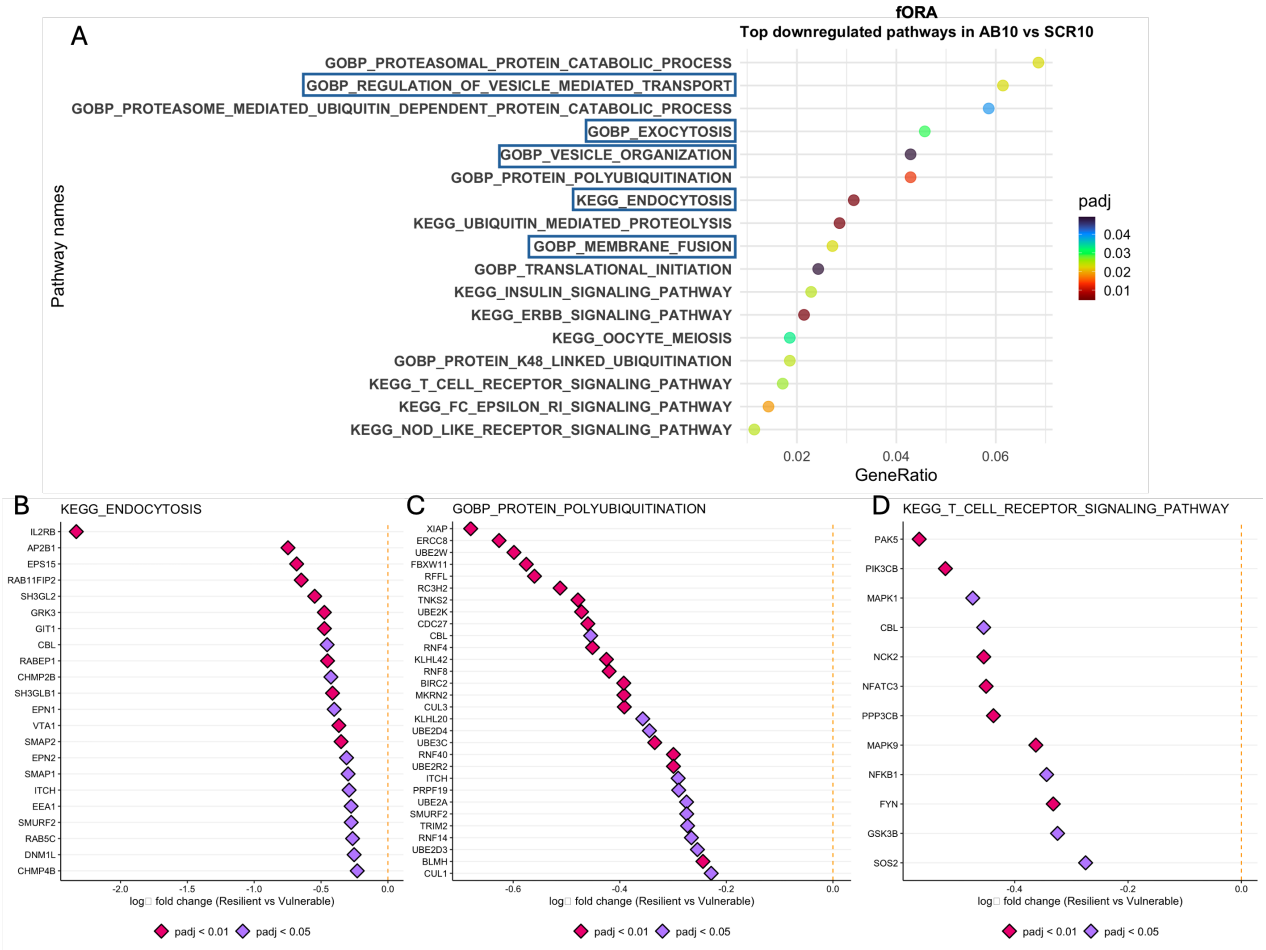


Figure 4.11: **Over-representation analysis of negatively enriched pathways in Aβ 10 μM vs Scrambled 10 μM neurons**(A) Dot plot of the top negatively enriched pathways, looking at significant DEGS, in neurons treated with 10 μM of Aβ compared to Scrambled 10 μM with the GeneRatio (i.e. the number of enriched genes/ number of significant DEGs. (B-D) Leading edge genes of pathways of interest with their Log_2FoldChanges. Squares are colour by their padj value. Blue boxes represent new pathways not seen in fGSEA

4.3 Investigating the cholesterol synthesis pathways in i^3 neurons treated with Aβ1-42

Given cholesterol synthesis pathways were robustly upregulated in the Aβ1-42 treated neurons compared to controls, and have been implicated in AD, I decided to further investigate how cholesterol synthesis is disrupted after Aβ1-42 insult. *SREBP1* and *SREBP2* are transcription factors that activate the mevalonate pathway of cholesterol synthesis, which is depicted in Figure 4.12, A. Both *SREBP1* and *SREBP2* were significantly upregulated in the Aβ treated condition (Figure 4.12, B), and so were the majority of the genes they activated in the mevalonate pathway, which included *HMGCS1, HMGCR, MVD, SQLE, TM7SF2, DHCRH7, FDFT1.*

Therefore, I investigated the effects of manipulating this pathway in two ways: first, via pharmacological inhibition of cholesterol synthesis using Simvastatin and the squalene synthase inhibitor YM53601 (YM), and second, via genetic manipulation of cholesterol synthesis by CRISPR-mediated knockdown of *SREBP1* or *SREBP2*. As a functional output, I measured neurite outgrowth in neurons treated with scrambled or Aβ1-42 oligomers after pharmacological or genetic manipulations. While baseline cholesterol is required for neurite outgrowth [232], excess cholesterol paradoxically rigidifies membranes and disrupts the dynamic lipid raft remodelling required for growth cone motility and neurite extension [138]. Furthermore, Aβ-induced upregulation of *SREBP1* and *SREBP2* and the consequent excess cholesterol accumulation may lead to ER stress and endolysosomal dysfunction, both of which may impair neurite outgrowth. I therefore hypothesised that inhibition of the mevalonate pathway would rescue the neurite outgrowth deficit observed in Chapter 3 following extrinsic Aβ1-42 oligomer insult. Furthermore, I asked whether the increase in lipid synthesis-related genes could be explained by a formation of lipid droplets in the neurons.

A

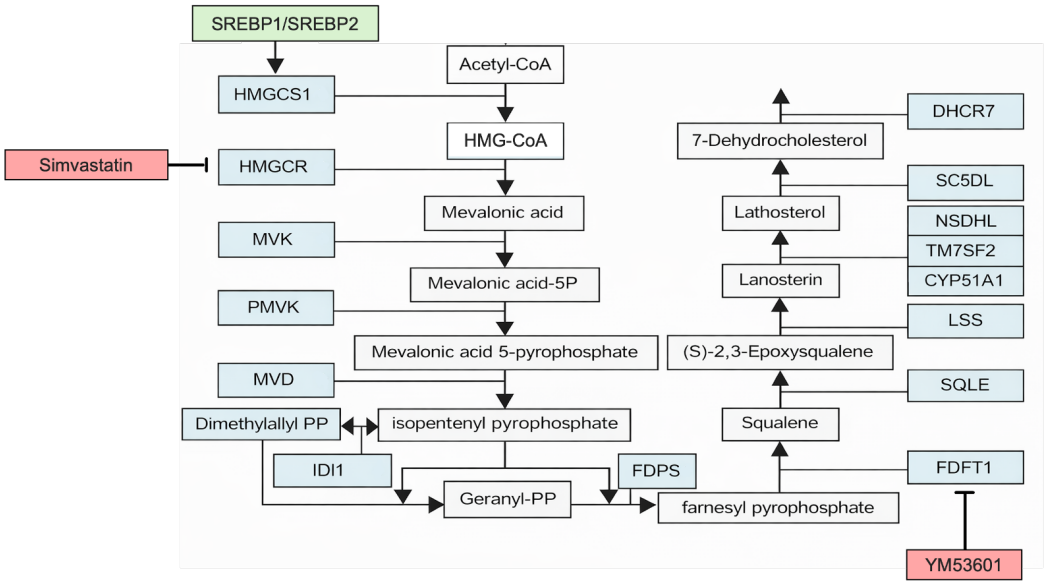


Figure adapted from Mathys et al., 2023 (doi: 10.1016/j.cell.2023.08.039)

B

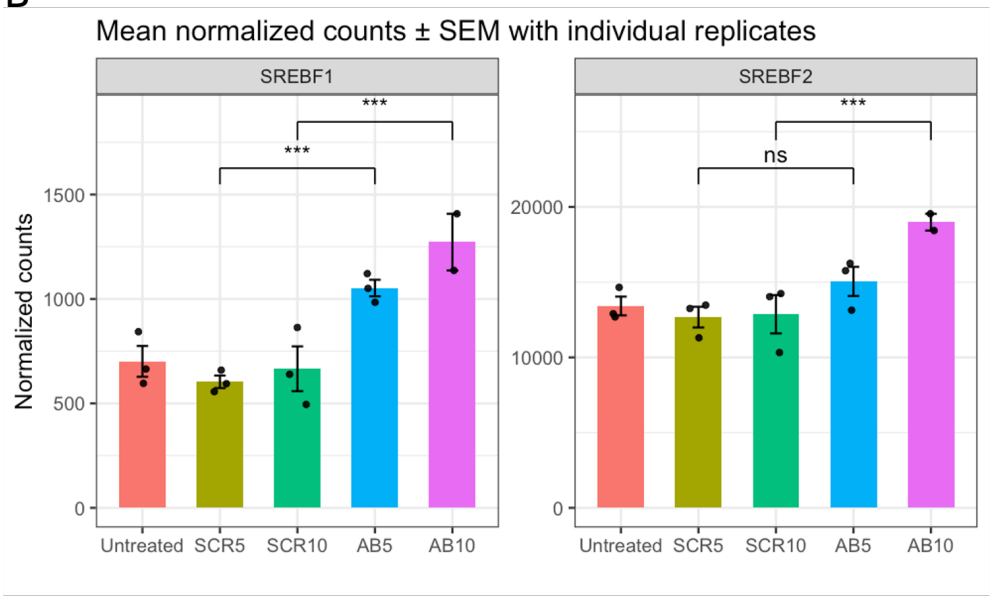


Figure 4.12: **Mevalonate pathway alterations in i3 neurons treated with AB** (A) Graphical depiction of the mevalonate pathway. Cells highlighted in blue were significantly upregulated expressed in AB-treated i3 neurons. Red squares represent cholesterol-altering drugs, and where they take effect. (B) Normalised counts of SREBP1 and SREBP2 in i3 neurons from the RNA sequencing dataset.

4.3.1 Genetic manipulation of cholesterol synthesis pathways

4.3.1.1 CRISPRi Knockdown of SREBP transcription factors

To titer the lentivirus and to verify the KD efficiency, the i^3 neurons were transduced with 2 non-targeting guides (NT-G1, NT-G2), 2 SREBP1 (SREBP1-G1 and -G2) and 2 SREBP2 guides (SREBP2-G1 and -G2), and a full media change was done 24 h post-transduction. The SREBP1 and SREBP2 lentiviruses were first titrated as described in Section 2.5.3.2, by counting the number of BFP+ neurons that co-localised with the number of NucRed + nuclei (Figure 4.13, A, B-D). At 1500 pg/mL, the transduction efficiency ranged between 30-50 %. I therefore doubled the concentration of lentivirus to 3000 pg/ml before checking the KD efficiency by qPCR. 48 h after lentivirus transduction, the neurons were harvested for RNA extraction and CRISPRi knockdown was verified by qPCR (Figure 4.13 E,F). SREBP1-G1 and SREBP1-G2 led to a 57% and 74 % decrease in SREBP1 concentration, respectively. SREBP2-G1 decreased SREBP2 expression by 94 %, but also led to a ~ 80 % decrease in SREBP1 expression as well. SREBP2 guide 2 (G2) on the other hand, only decreased SREBP2 expression by 53 % (Figure 4.13 E,F).

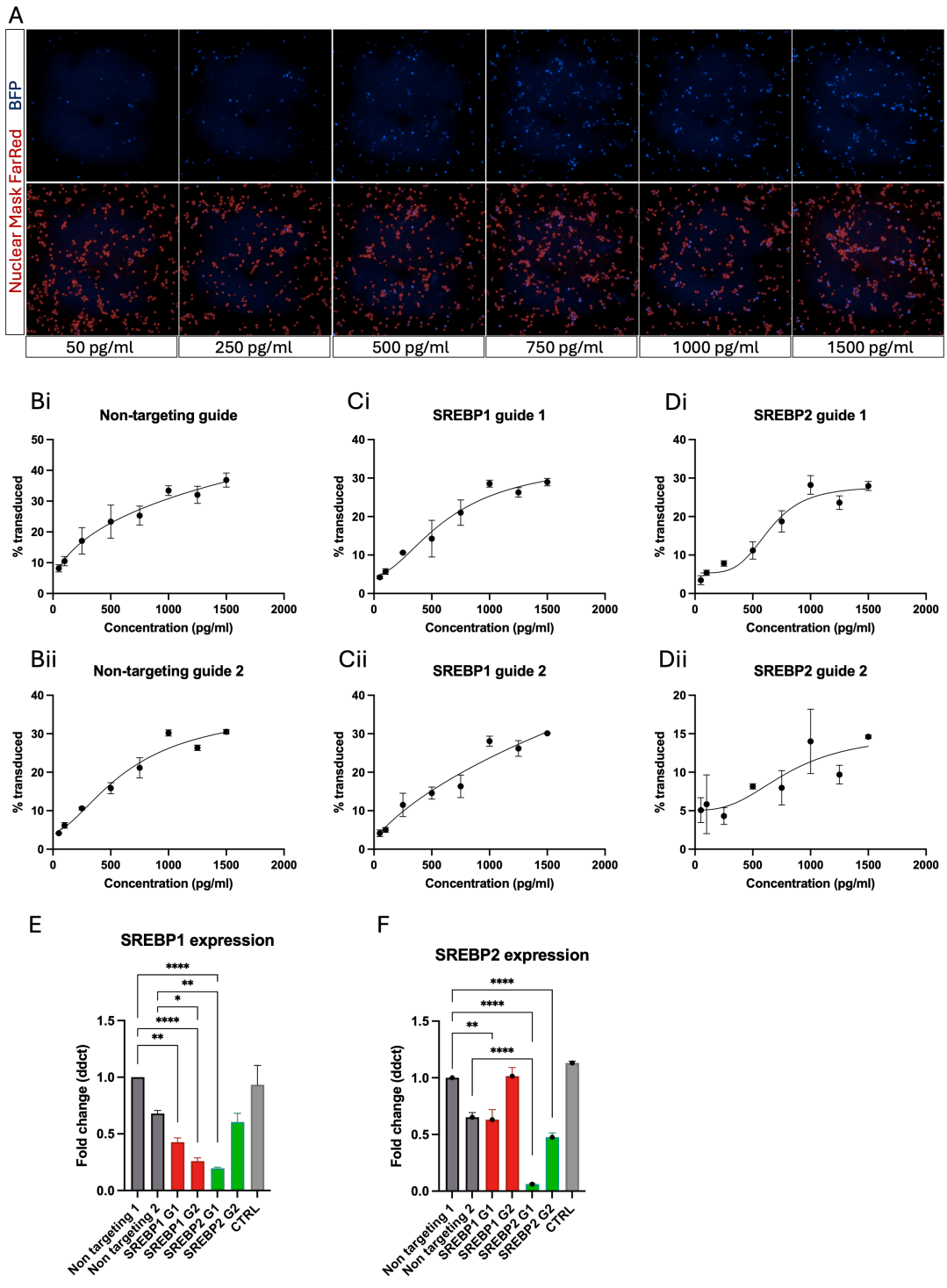


Figure 4.13: **SREBP lentiviral titration and calculation of CRISPRi KD efficiency** (A) Representative images of i3 neuron nuclei after lentivirus transduction, with Nuclear Mask Far Red live stain. (B-D) Titration curves of % BFP + cells are increasing concentration of lentiviruses for (Bi-ii) non-targeting guides 1 and 2, (Ci-ii) SREBP1 guides 1 and 2, and (Di-ii) SREBP2 guides 1 and 2. (E-F) RNA expression of SREBP1 in neurons transduces with non-targeting, SREBP1 or SREBP2 guides.

Figure 4.13: Continued: Mean +- SEM of n=3 technical replicates. Ordinary One-Way ANOVA with Tukey's multiple corrections test. (E): F (6, 14) = 17.66, P<0.0001; (F) F (6, 14) = 57.77, P<0.0001. $p < 0.05$ $(*)$, $p < 0.01$ $(**)$, $p < 0.001$ $(***)$, $p < 0.0001$ $(****)$

4.3.1.2 Neurite outgrowth and cell viability after Aβ1-42 insult

Neurite outgrowth was chosen as an outcome because I have shown that Aβ induces a consistent and robust decrease in neurite outgrowth in iPSC-derived cortical neurons. I hypothesised that SREBP1 and SREBP2 KD, and downstream lipid synthesis downregulation would mitigate Aβ-induced toxicity, as measured by neurite loss.

To remain consistent with the bulk RNA sequencing, I did not include astrocytes for these assays. Due to the lack of astrocytes (which were previously added to help with adhesion) and the neurons being plated at a low density to allow neurite tracing (5'000 per well), I decided to treat the cells with Aβ1-42 at 2.5 and 5 μM instead of keeping the 10 μM concentration used in the Bulk RNA seq, as I had previously noticed that under those conditions the 10 μM concentration led to excessive toxicity and cell death.

Three days post-induction with doxycycline (replating day), the i^{3}s were transduced with NgN2-GFP and with either NT-G1, NT-G2, SREBP1 G1, SREBP1 G2, SREBP2 G1 and SREBP2 G2, and on Day 14, they were treated with Aβ1-42, scrambled control or left untreated. Because the CRISPR guides included a BFP nuclear marker, I selected the GFP neurons that were BFP+ to make sure the analysis was only conducted on neurons that had been successfully transduced. The transduction efficiency was high, and nearly all the GFP neurons were BFP+ (Figure 4.14, A-C).

There was a significant main effect of Aβ treatment on neurite length, whereas knockdown of SREBP1 or SREBP2 had no significant effect, and no interaction between Aβ treatment and SREBP knockdown was detected. Namely, Aβ treatment at 5 µM, but not 2.5 µM, resulted in a significant reduction in neurite length in all conditions (Figure 4.15 A,C). Looking specifically at the Aβ treated neurons normalised to scrambled control, no differences were observed between neurons transduced with non-targeting guides and those with SREBP1 or SREBP2 knockdown (Figure 4.15B,D).

Similarly, Aβ treatment at 5 µM, but not 2.5 µM significantly reduced the number of nodes, (Figure 4.15E,G). However, neither SREBP1 nor SREBP2 knockdown altered

node number in the presence or absence of Aβ, and no interaction effect was observed (Figure 4.15 F,H). Collectively, these findings indicate that SREBP1 and SREBP2 expression are not necessary for Aβ-induced neurite loss.

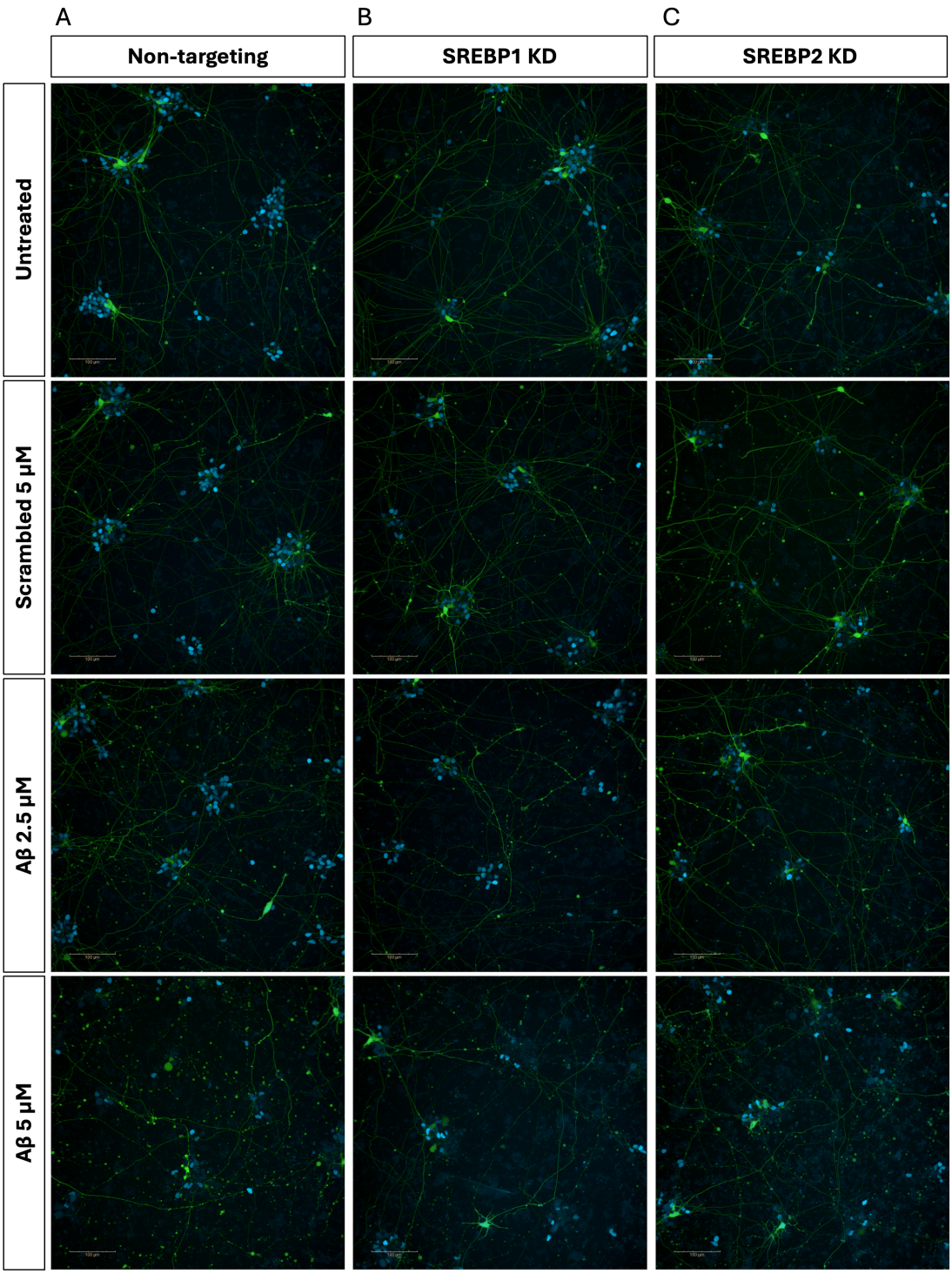


Figure 4.14: **Representative images of SREBP1 and 2 KD GFP i3 neurons after Aβ treatment** (A-C) Neurons transduced with (A) non-targeting guides, (B) SREBP1 guides or (C) SREBP2 guides left untreated or treated with Scrambled 5 μM, Aβ 2.5 μM, or Aβ 5μM.

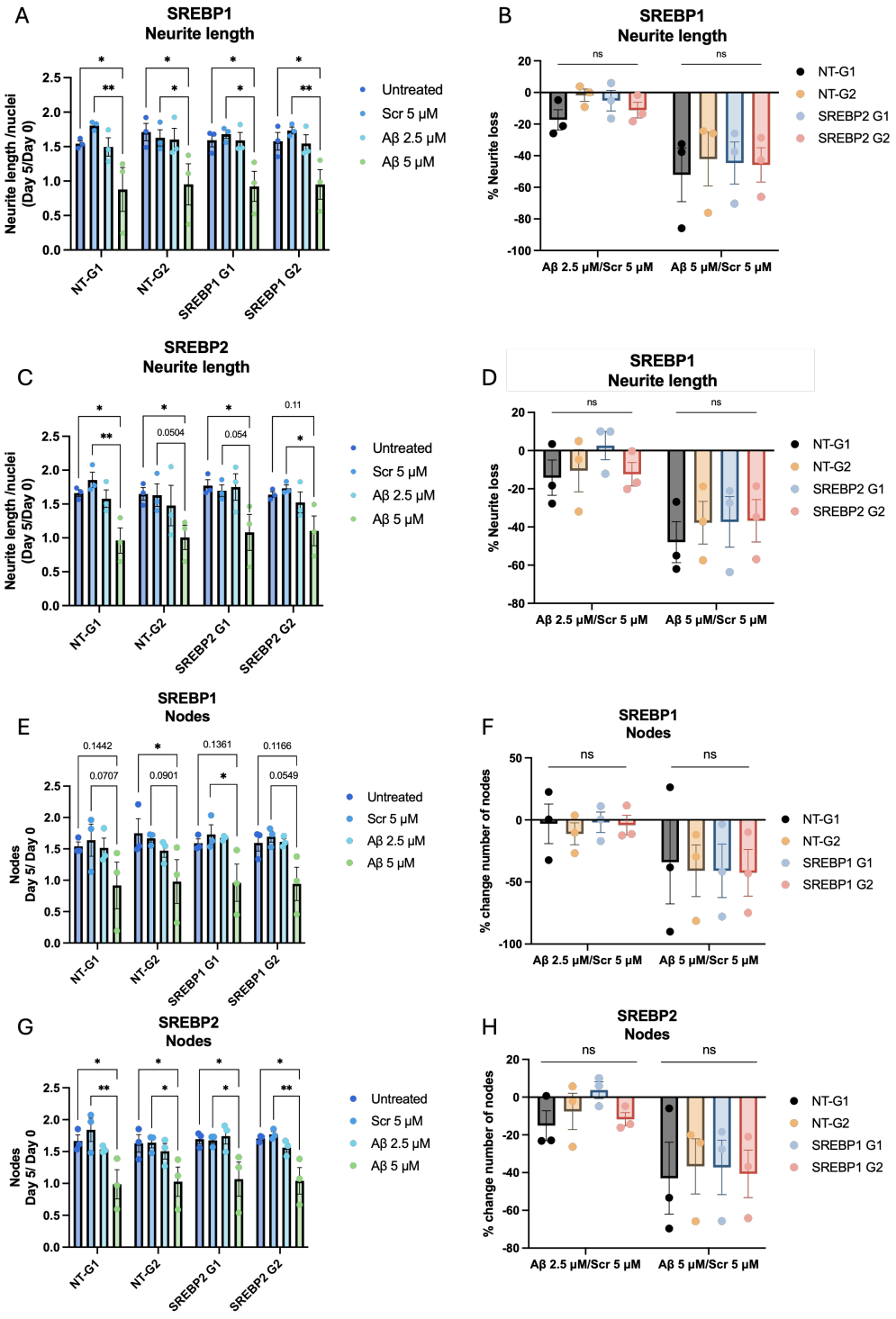


Figure 4.15: **Quantification of neurites of SREBP1 and 2 KD i3 neurons after Aβ treatment** (A,C) Neurite length / nuclei at Day 5 normalised to baseline (Day 0) of (A) SREBP 1 and (C) SREBP2 KD neurons treated with Scrambled 5 μM or Aβ 2.5 and 5 μM. (B, D) % neurite loss in neurons treated with Aβ 2.5 or 5 μM normalised to scrambled peptide.

Figure 4.15: Continued: (E,G) Number of nodes / nuclei at Day 5 normalised to baseline (Day 0) of (E) SREBP 1 and (G) SREBP2 KD neurons treated with Scrambled 5 μM or Aβ 2.5 and 5 μM. (F, H) % neurite loss in neurons treated with Aβ 2.5 or 5 μM normalised to scrambled peptide. Mean +-SEM, n=3 independent differentiation repeats. Each dot represents one differentiation average over 4 replicates. 2-Way ANOVA with Tukey's multiple comparisons test. (A) Treatment effect F (3, 32) = 19.18, P<0.0001; (B) Treatment x Genotype effect F (3, 16) = 0.03676, P=0.9902; (C) Treatment effect F (3, 32) = 15.31, P<0.0001; (D) Treatment x Genotype effect F (3, 16) = 0.2321, P=0.8727; (E) Treatment effect F (3, 32) = 11.60, P<0.0001; (F) Treatment x Genotype effect F (3, 16) = 0.03379, P=0.9913 ; (G) Treatment effect F (3, 32) = 19.71, P<0.0001; (H) Treatment x Genotype effect F (3, 16) = 0.1346, P=0.9380. $p < 0.05$ $(*)$, $p < 0.01$ $(**)$, $p < 0.001$ $(***)$, $p < 0.0001$ $(****)$

Cell viability

Next, I assessed neuronal death by looking at the loss in number of nuclei, counting the change in BFP+ neurons before and after Aβ insult, as well as the release of adenylate kinase (AK). There was no main effect of Aβ treatment at 2.5 or 5 μM or SREBP KD on nuclei number. (Figure 4.16, A-B). On the other hand, there was a significant main effect of Aβ at 5 μM, but not interaction between Aβ and SREBP KD. AK levels were significantly higher in the Aβ 5 μM treated neurons (Figure 4.16, C-D). Aβ-treated neurons transduced with SREBP1-G2 and SREBP2-G1 exhibited a slightly lower — though not significant — release of AK (Figure 4.16, E-F).
These results suggests that the Aβ-induced upregulation of SREBP1 and 2 expression does not mediate Aβ-driven neurite loss or cell death in i3 neurons.

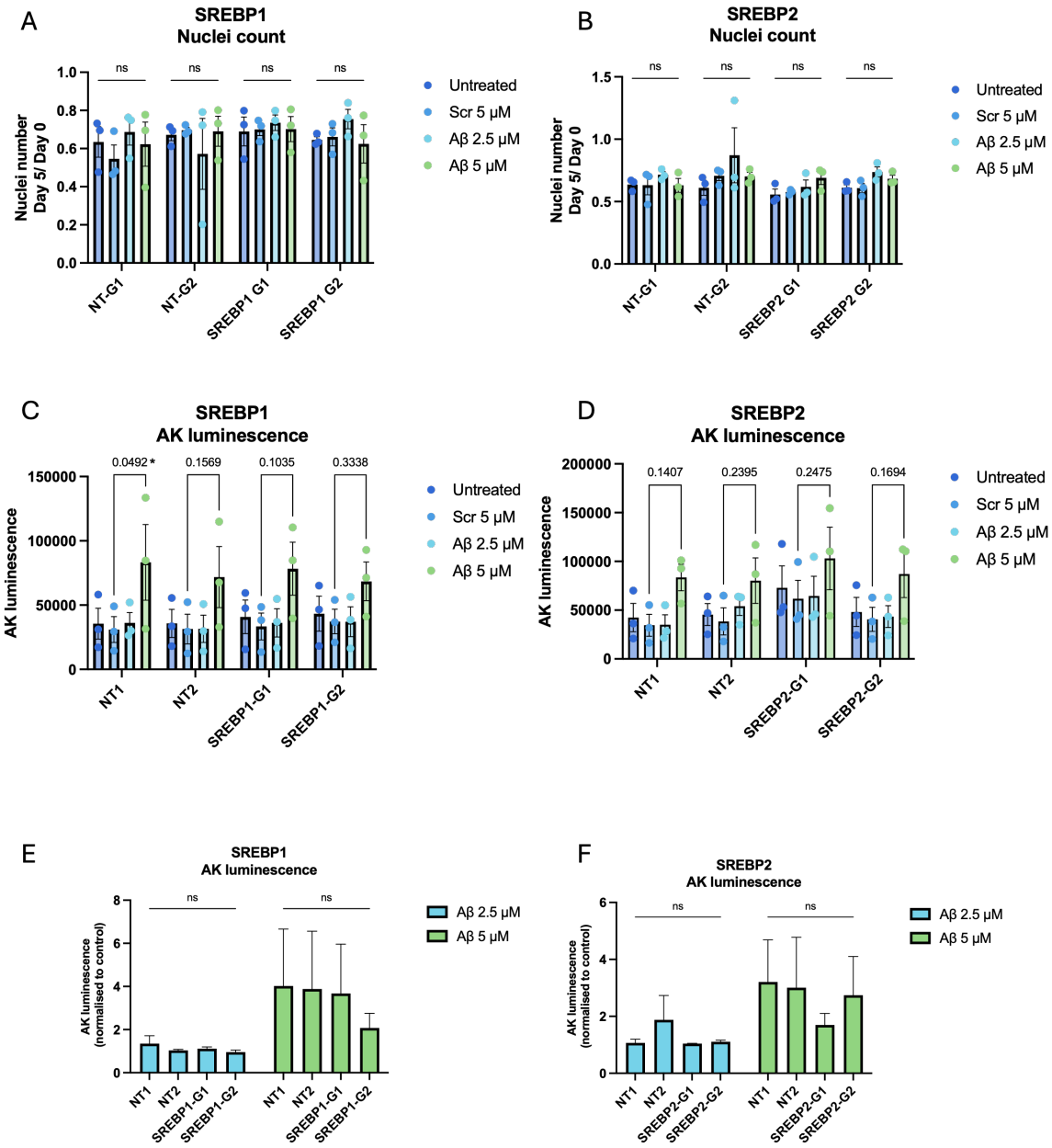


Figure 4.16: **Quantification of cell viability of SREBP1 and 2 KD i3 neurons after Aβ treatment** (A, B) Nuclei count at Day 5 normalised to baseline (Day 0) of (A) SREBP 1 and (B) SREBP2 KD neurons treated with Scrambled 5 μM or Aβ 2.5 and 5 μM. (C, D) AK release in media from neurons treated with Aβ 2.5 or 5 μM, 5 days post treatment. (E,F) Comparison of AK release between NT, (E) SREBP1 and (F) SREBP2 i3 neurons in the 2.5 and 5 μM conditions. Mean +-SEM, n=3 independent differentiation repeats. Each dot represents one differentiation average over 4 replicates. 2-Way ANOVA with Tukey's multiple comparisons test. (A) Treatment effect F (3, 32) = 0.1558, P=0.9252; (B) Treatment effect F (3, 32) = 2.761, P=0.0581 (C) Treatment effect F (3, 32) = 7.140, P=0.0008; (D) Treatment effect F (3, 32) = 5.333, P=0.0043 ; (E) Treatment x Genotype effect F (9, 32) = 0.08334, P=0.9998 ; (G) Treatment x Genotype effect F (9, 32) = 0.06504, P>0.9999. $p < 0.05$ (*), $p < 0.01$ (**), $p < 0.001$ (***), $p < 0.0001$ (****)

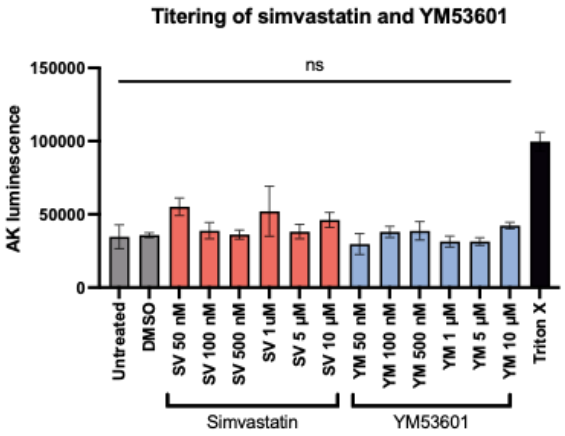


Figure 4.17: **Titration of YM53601 and Simvastatin show no increased toxicity between 50 nM and 10 μM of either compound** AK release of i3 neurons treated with increasing concentrations of Simvastatin and YM53601 to assess toxicity. Mean +-SEM of 3-5 technical replicates. One-way ANOVA with Dunnett's multiple comparison's test F (13, 28) = 1.281, P=0.2810

4.3.2 Pharmacological inhibition of the cholesterol synthesis pathway

4.3.2.1 Mevalonate pathway inhibitors

Simvastatin, which inhibits HMG-CoA reductase (HMGCR), the rate-limiting enzyme in cholesterol biosynthesis, and YM-53601 (YM), a squalene synthase (*FDFT1*) inhibitor, were selected to pharmacologically target the mevalonate pathway (Figure 4.12, A). While statins are widely used cholesterol-lowering agents, they act at an early step in the pathway and consequently affect multiple downstream branches of isoprenoid metabolism. In contrast, YM targets squalene synthase, which is further downstream , thereby providing a more direct and selective inhibition of cholesterol synthesis with reduced impact on upstream non-sterol isoprenoid pathways.

Following titration of both compounds to assess neurotoxicity — measured by AK release — (Figure 4.17, C), which did not show a difference in toxicity between 50 nM and 10 μM of either compound, I decided to use Simvastatin and YM at 1 and 5 μM, which is consistent with the concentration other members of our laboratory use in dopamine and i^3 neurons. The same Aβ concentrations were used as in the CRISPRi experiment described above.

4.3.2.2 Neurite tracing of i3 neurons treated with Aβ and Simvastatin or YM53601

As above, neurite outgrowth was assessed after treatment with Aβ and Simvastatin or YM53601 to test the hypthosesis that cholesterol synthesis inhibition mitigates Aβ-induced neurit loss. i^3 neurons transduced with GFP-NgN2 were treated with Aβ and the compounds on Day 14 post-induction, and imaged daily for 5 days (Figure 4.18).

Two-way ANOVA revealed a significant main effect of Aβ, and no significant interaction between Aβ and Simvastatin or YM. Specifically, neurite length was significantly reduced 5 days after treatment with Aβ at 5 µM, but not 2.5 µM, relative to baseline (Day 0). This reduction was evident in neurons treated with Aβ alone and in the presence of YM at 5 µM, but not in neurons treated with simvastatin (Figure 4.19, Ai).

In the absence of, Aβ there was a slight, but significant, decrease in neurite length in the neurons treated with YM at 1 and 5 μM, suggesting that blocking squalene synthase activity has some inhibitory effects on neurite outgrowth (Figure 4.19 Aii). To account for this effect, changes in neurite length between Day 0 and Day 5 were normalised to untreated controls. Following normalisation, the Aβ-induced decrease in neurite length remained significant (Figure 4.19, Bi). Importantly, within both the Aβ 2.5 µM and 5 µM conditions, neither simvastatin nor YM altered neurite length relative to Aβ treatment alone, consistent with the absence of an interaction effect (Figure 4.19, Bii).

Analysis of neurite branching revealed a similar pattern. Aβ treatment significantly reduced the number of nodes (Figure 4.19, Ci, Di) and YM treatment also reduced branching in the absence of Aβ (Figure 4.19, Cii), consistent with its independent inhibitory effect on neurite growth. However, cholesterol inhibition did not further modify the Aβ-induced reduction in node number, and no differences were observed between neurons treated with Aβ alone or in combination with simvastatin or YM (Figure 4.19, Dii).

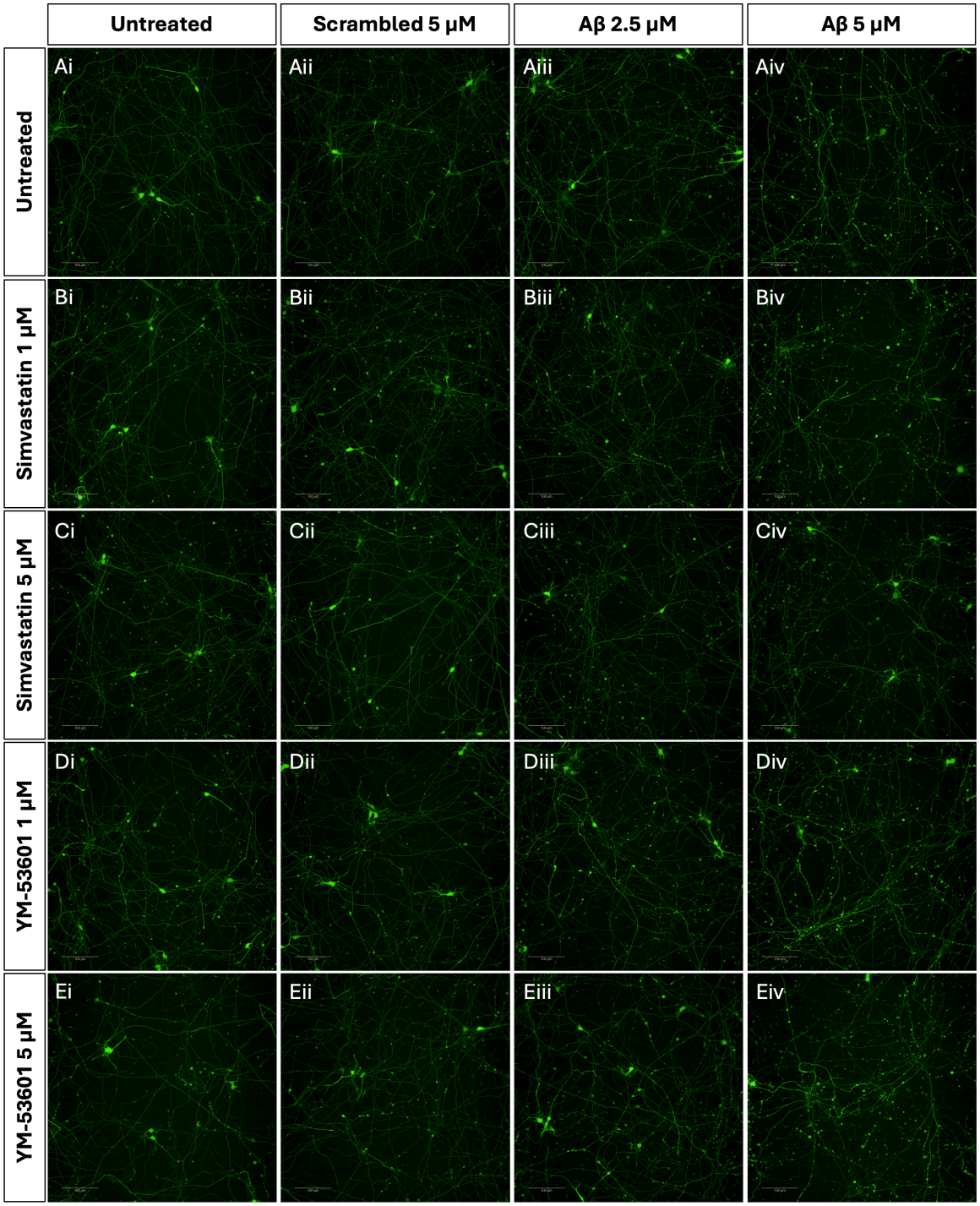


Figure 4.18: **Representative images i3 neurons treated with Aβ and cholesterol-altering compounds** Neurons either left untreated (A) or with (B) 1 μM Simvastatin, (C) 5 μM Simvastatin, (D) 1 μM YM53601, (E) 5μM YM53601. Neurons were also treated with (ii) 5 μM scrambled peptide, (iii) 2.5 μM AB, (iv) 5 μM Aβ peptide.

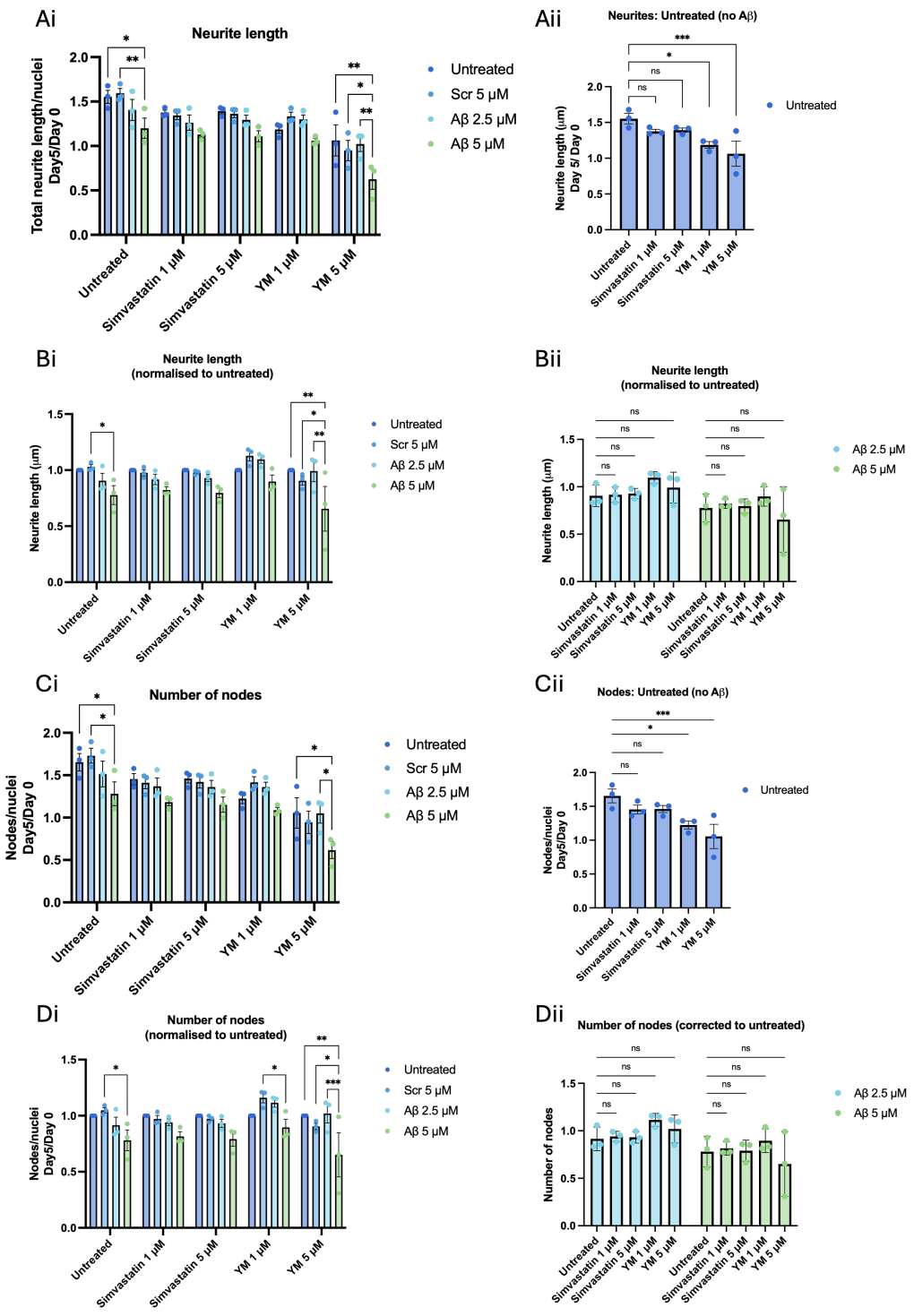


Figure 4.19: **Quantification of neurite outgrowth and nodes in i3 neurons treated with cholesterol altering compounds in combination with AB** (Ai) Neurite length / nuclei at Day 5 normalised to baseline (Day 0) i3 neurons treated with Scrambled 5 μM, Aβ 2.5 or 5 μM. (Aii) Comparison of change in neurite length from baseline in the untreated (no Aβ) condition with simvastatiin or YM53601. (Bi) Change in neurite length from baseline normalised to the untreated (no Aβ + no compound) condition.

Figure 4.19: Continued: (Bii) Comparison of the change in neurite length after treatment with Aβ 2.5 and 5 μM between neurons treated with Simvastatin or YM53601 at 1 or 5 μM. (Di) Number of nodes / nuclei at Day 5 normalised to baseline (Day 0) i3 neurons treated with Scrambled 5 μM, Aβ 2.5 or 5 μM. (Aii) Comparison of change in number of nodes from baseline in the untreated (no AB) condition with Simvastatin or YM53601. (Bi) Change in number of nodes from baseline normalised to the untreated (no Aβ + no compound) condition. (Bii) Comparison of the change in number of nodes after treatment with Aβ 2.5 and 5 μM between neurons treated with Simvastatin or YM53601 at 1 or 5 μM. Mean +-SEM, n=3 independent differentiation repeats. Each dot represents one differentiation average over 4 replicates. 2-Way ANOVA with Tukey's multiple comparisons test. (A) Aβ Treatment effect F (3, 40) = 14.91, P<0.0001; (Aii) Cholesterol inhibitors effect F (4, 40) = 23.16, P<0.0001; (Bi) Treatment effect F (3, 40) = 13.56, P<0.0001; (Bii) Treatments interaction effect F (12, 40) = 0.8272, P=0.6225; (Ci) Treatment effect F (3, 40) = 12.01, P<0.0001; (Cii) Cholesterol inhibitors effect F (4, 40) = 22.46, P<0.0001 ; (Di) Treatment effect F (3, 40) = 14.30, P<0.0001; (H) Treatments interaction effect F (12, 40) = 0.9605, P=0.5005. $p < 0.05$ ($*$), $p < 0.01$ ($**$), $p < 0.001$ ($***$), $p < 0.0001$ ($****$)

Cell viability

I next assessed whether Aβ or cholesterol inhibition induced neuronal death by measuring nuclei loss and AK release. Aβ did not induce any loss of nuclei in any of the conditions (Figure 4.20, A), and despite the decrease in neurite length and number of nodes in the YM conditions without AB, there was no difference in the number of nuclei compared with other untreated (i.e. no Aβ) conditions (Figure 4.20 B). However, there was an increase in AK release in the Aβ 5 μM condition (Figure 4.20 C), though there was no interaction between Aβ and Simvastatin or YM treatment (Figure 4.20 E). In YM-treated neurons without Aβ, consistent with the loss of neurites exhibited in the YM-treated neurons, there was a trend towards an increase in AK release, though it was not significant (Figure 4.20, D). This increase was not observed in the scrambled condition.

In summary, Simvastatin causes no change in neurite outgrowth after Aβ insult, and YM induces a slight decrease in neurite length independent from Aβ insult, which is dose-dependent. Furthermore, Aβ does not induce a loss of nuclei, though it causes an increase in AK release, which stays consistent upon treatment with Simvastatin or YM.

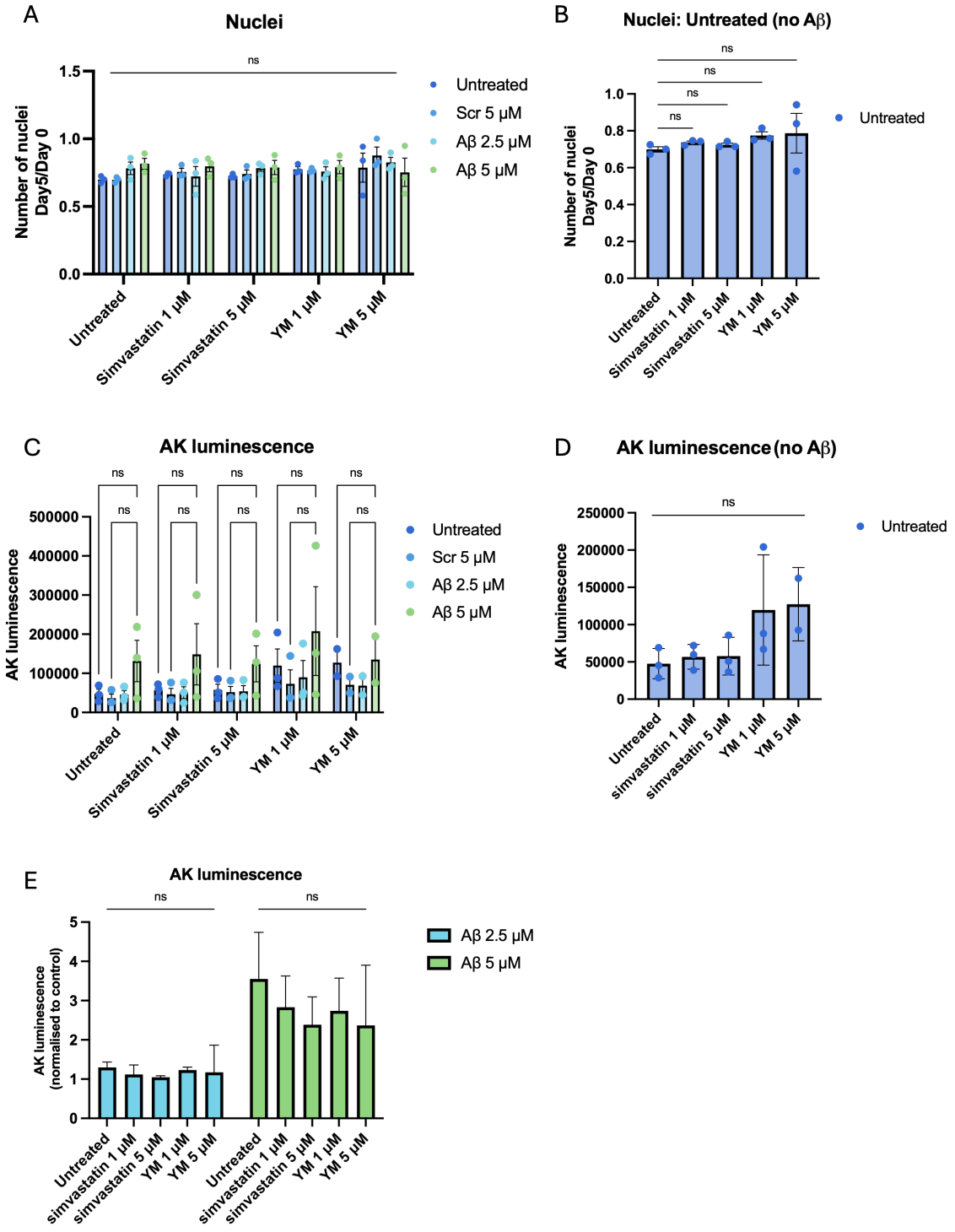


Figure 4.20: **Quantification of cell viability i3 neurons after treatment with Aβ and cholesterol-altering compounds** (A) Nuclei count at Day 5 normalised to baseline (Day 0) of (A) neurons treated with Scrambled 5 μM or Aβ 2.5 and 5 μM + Simvastatin or YM 53601 at 1 or 5 μM (B) Comparison of nuclei count between neurons treated with Simvastatin or YM 53601 at 1 or 5 μM, without AB.

Figure 4.20: Continued: (C) AK release in media from neurons treated with Scrambled 5 μM or Aβ 2.5 and 5 μM + Simvastatin or YM 53601 at 1 or 5 μM , 5 days post treatment (D-E) Comparison of amount of AK release between neurons treated with Simvastatin or YM 53601 at 1 or 5 μM, (D) without AB, or (E) with 2.5 μM or 5μM of AB. Mean +-SEM, n=3 independent differentiation repeats. Each dot represents one differentiation average over 4 replicates. 2-Way ANOVA with Tukey's multiple comparisons test. (A) Aβ treatment effect F (3, 40) = 0.7148, P=0.5490; (B) Interaction effect F (12, 40) = 0.7249, P=0.7188; (C) Treatment effect F (3, 36) = 4.681, P=0.0073; (D-E) Interaction effect F (12, 36) = 0.1377, P=0.9996 $p < 0.05$ $(*)$, $p < 0.01$ $(**)$, $p < 0.001$ $(***)$, $p < 0.0001$ $(****)$

4.3.3 Lipid droplet formation after Aβ1-42 insult

Lipid droplet formation has been shown to be induced by Aβ in mouse studies [94], and I therefore investigated whether the upregulation in cholesterol biosynthesis-related genes was due to an Aβ-induced production of lipid droplets. To answer this, i^3 neurons were stained with BODIPY, a neutral lipid dye, and the live nuclear stain NucBlue every other day for six days following Aβ1-42 exposure. Because BODIPY has a short half-life and NucBlue is mildly neurotoxic with prolonged exposure, all wells were treated with Aβ on Day 14 post-induction, but BODIPY staining was performed on separate sets of neurons treated with Aβ, scrambled peptide, or left untreated at each time point and imaged immediately thereafter (see Section 2.11.4). The Harmony analysis pipeline is outlined in Figure 4.21. Representative images of i^3 neurons at baseline (Day 0), Day 3, and Day 5 of Aβ treatment are shown in Figure 4.22 A-C. Lipid droplet formation was assessed longitudinally rather than at a single endpoint, as lipid droplets are dynamic structures that can form rapidly following stress and may be cleared at later time points.

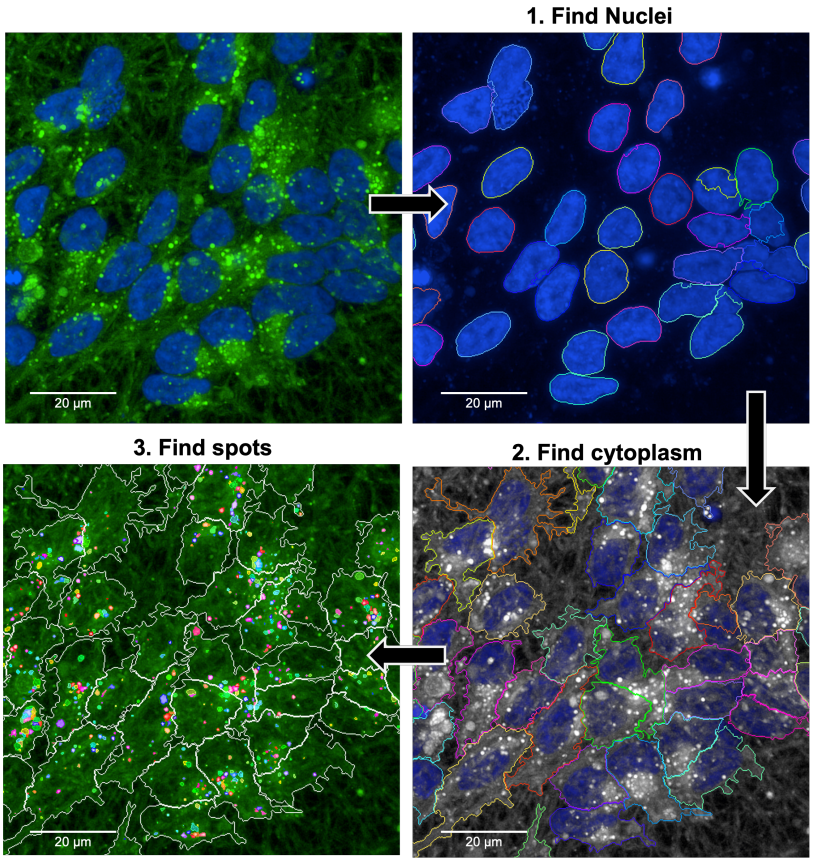


Figure 4.21: **Analysis pipeline for lipid droplet imaging with BODIPY** (1) Find nuclei using Nuc Blue signal, (2) Find cytoplasm, (3) Find spots of Bodipy inside cytoplasm.

Two-way ANOVA revealed a significant main effect of time and Aβ treatment, and there was a significant interaction of time and treatment. Specifically, Aβ induced a time-dependent increase in the number of lipid droplets (as assessed by the number of spots of BODIPY). At baseline (Day 0) and Day 1 post-treatment, no change in droplet number was observed between untreated, scrambled and Aβ-treated neurons. By Day 3, there was a significant increase in the number of droplets, which further increases by Day 5 (Figure 4.23 A). A similar trend is seen in the spot region intensity, though the increase is not significant at Day 3, as well as in the spot size (Figure 4.23 B,C). Consistent with the neurite tracing assays above, there was no change in nuclei number due to Aβ insult (Figure 4.23 D).

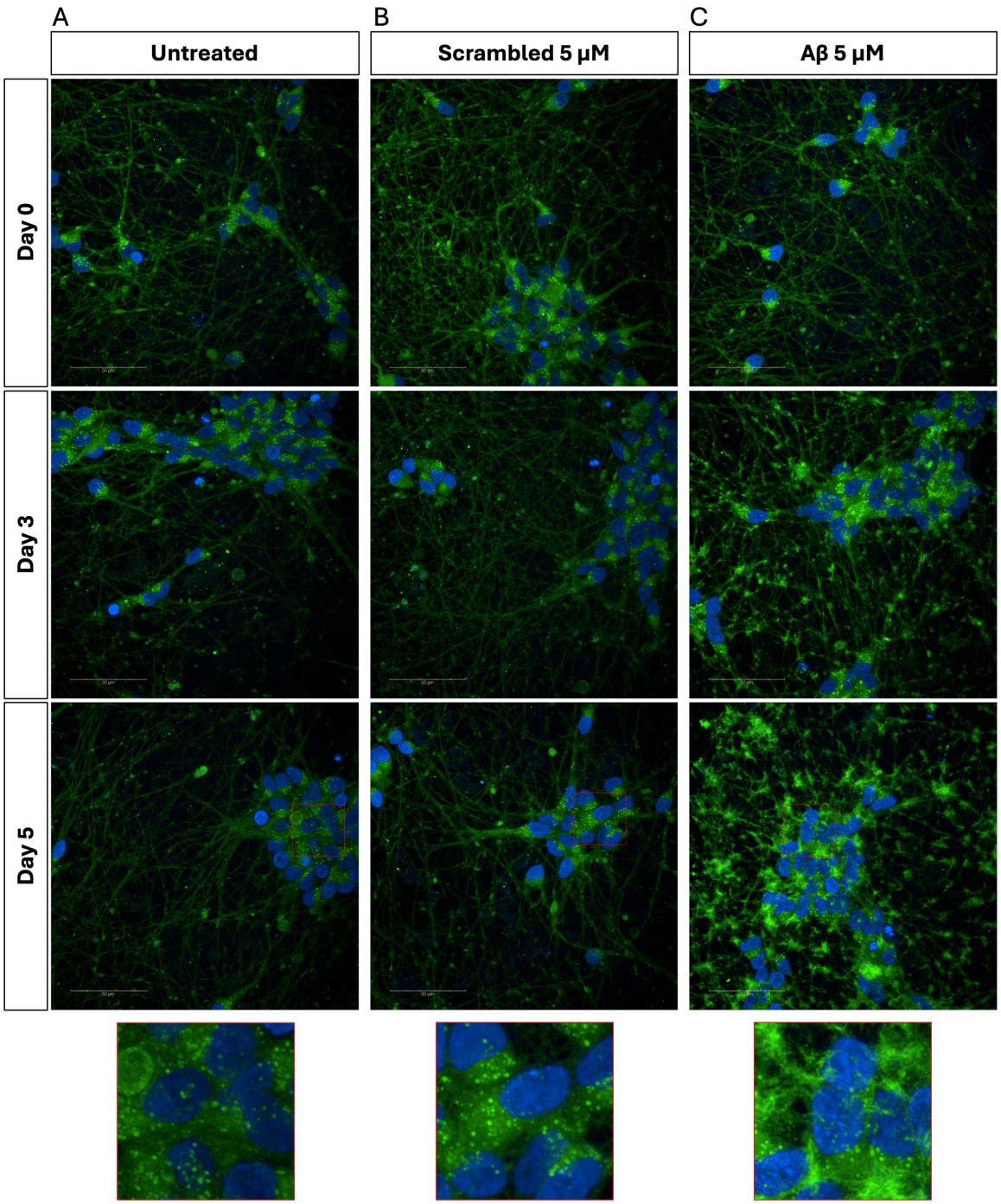


Figure 4.22: **Representative images of BODIPY staining of i3 neurons after Aβ treatment** (A) Untreated, (B) Scrambled 5 μM and (C) Aβ 5μM treated i3 neurons at Day 0 (top), Day 3 (middle) and Day 5 (bottom). Scale bar is 50 μm

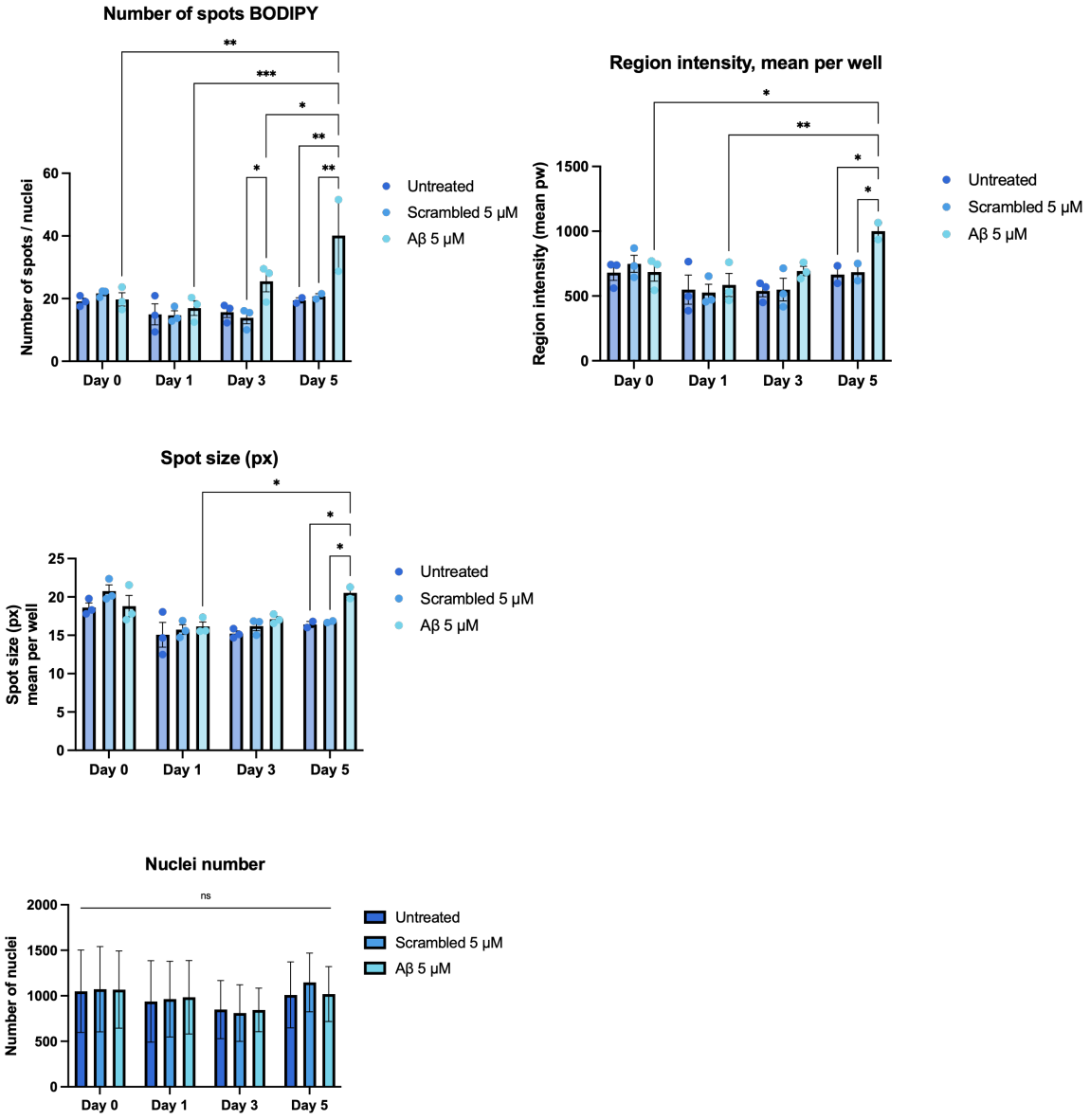


Figure 4.23: **Quantification of lipid droplet formation in i3 neurons after Aβ treatment** Bar plots of (A) Number of spots of Bodipy, (B) BODIPY pot intensity, (C) BODIPY spot size and (D) nuclei number in i3 neurons after treatment with Scrambled 5 μM or Aβ 5 μM over time. Mean +-SEM, n=3 independent differentiation repeats. Each dot represents one differentiation average over 4 replicates. 2-Way ANOVA with Tukey's multiple comparisons test. (A) Treatment effect F (2, 21) = 9.359, P=0.0012, Time effect F (3, 21) = 6.366, P=0.0031; and Time x Interaction effect F (6, 21) = 2.932, P=0.0308. (B) Treatment effect F (2, 21) = 3.611, P=0.0449, Time effect F (3, 21) = 5.399, P=0.0065; (C) Treatment effect F (2, 21) = 4.305, P=0.0271, Time effect F (3, 21) = 12.50, P<0.0001; (D) Treatment x Time effect F (6, 21) = 0.009962, P>0.9999 $p < 0.05$ $(*)$, $p < 0.01$ $(**)$, $p < 0.001$ $(***)$, $p < 0.0001$ $(****)$

4.3.4 SREBP protein levels in Aβ1-42 treated neurons

To validate the change in expression of *SREBP1* and *SREBP2* observed in the bulk RNA-sequencing, I extracted protein from back up samples of i^3 neurons differentiated, treated, and harvested at the same time as the samples sent for RNA sequencing. Surprisingly, there was a dose dependent decrease in SREBP1 and SREBP2 in the Aβ-treated samples (Figure 4.24), which was significant for SREBP1 in the Aβ 5 μM condition compared to the scrambled 5 μM condition (Figure 4.24, B)

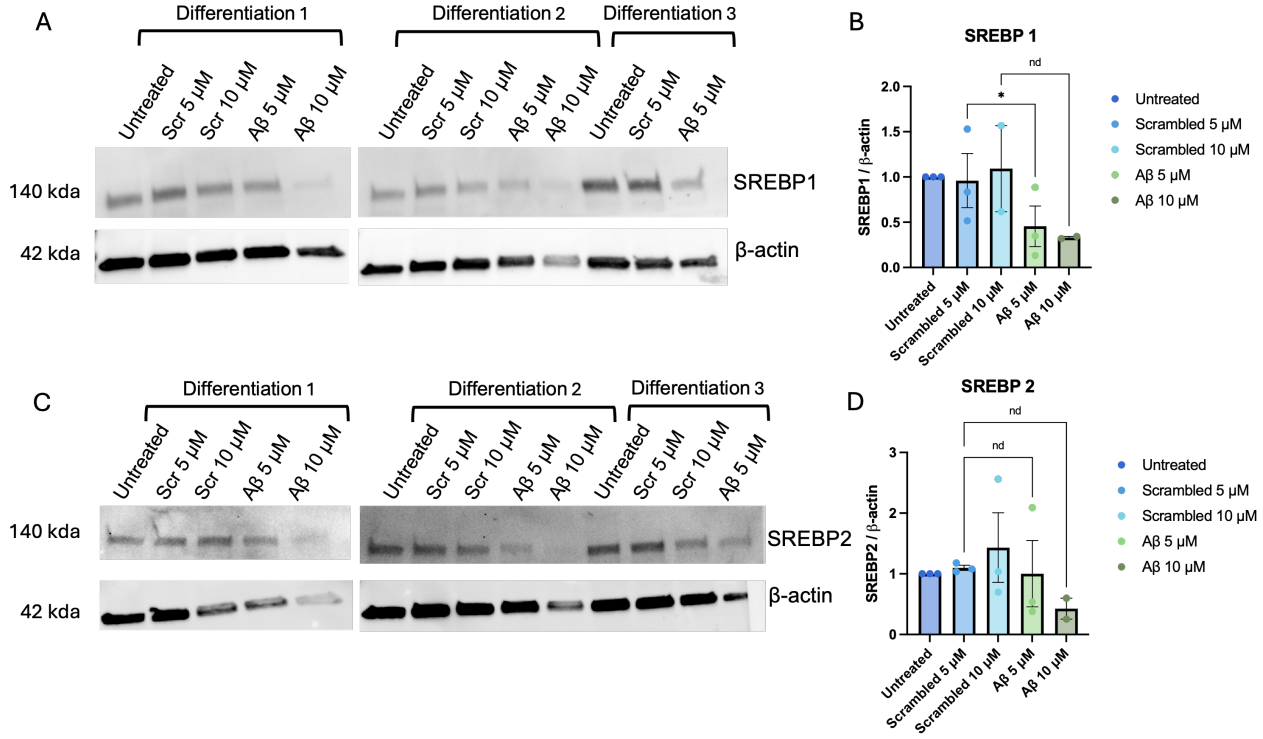


Figure 4.24: **SREBP protein levels in Aβ1-42 treated neurons** (A,C) Immunoblots of (A) SREBP1 and (B) SREBP2 in neurons treated with Scrambled 5 μM or 10 μM, Aβ 5 μM and 10 μM or left untreated. (B, D) Quantification of (B) SREBP1 and (D) SREBP2 protein levels. Mean +- SEM of n =3 independent differentiation repeat. Mixed effect model with Benjamini and Hochberg FDR correction. (B) F (1.095, 1.643) = 3.588, padj value (Scrambled 5 μM vs. Aβ 5 μM) = 0.0436, padj (Scrambled 10 μM vs. Aβ 10 μM) = 0.3485). (D) F (0.9753, 1.707) = 1.221, padj value (Scrambled 5 μM vs. Aβ 5 μM) = 0.8835, padj (Scrambled 10 μM vs. Aβ 10 μM) = 0.3790).$p < 0.05$ $(*)$, $p < 0.01$ $(**)$, $p < 0.001$ $(***)$, $p < 0.0001$ $(****)$.

4.4 Bulk-RNA sequencing of DFP neurons treated with Aβ1-42

4.4.1 Experimental design

The pilot bulk RNA-sequencing experiment in i^3 neurons demonstrated that Aβ exposure induces a robust transcriptional response in iPSC-derived cortical neurons. I extended this analysis to 13 iPSC-derived neuron lines from the DFP cohort, to investigate mechanisms underlying differential susceptibility to Aβ in an unbiased manner. Owing to the number of cell lines included, a single concentration of Aβ (5 µM) and a scrambled peptide control were used, and one biological replicate per line per condition was sequenced. The experimental paradigm was otherwise identical to that used in the i^3 neuron RNA-sequencing experiment described in Section 4.2 and is summarised in Figure 4.1.

This experiment has two primary aims: (1) to assess whether Aβ induces transcriptional changes in AD patient-derived neurons, and (2) to determine whether neurons derived from clinically vulnerable and resilient patients exhibit differential transcriptional responses to Aβ. Specifically, I analysed whether the differences in vulnerability to Aβ can be explained by distinct transcriptomic responses and downstream molecular effects following Aβ exposure.

4.4.2 Data quality control

Principal component analysis was performed to look at sample clustering, and revealed that the individual cell lines clustered mostly together, and not by treatment condition. Line 927 clustered away from the other cell lines, and was therefore removed from further analysis (Figure 4.25 A). When looking at PC3 and PC4, there was a modest separation between the Aβ samples and the untreated and Scrambled samples (Figure 4.25 B). The Euclidean sample distance map further illustrates that individual cell lines clustered closest to other samples from the same cell line (Figure 4.25, C).

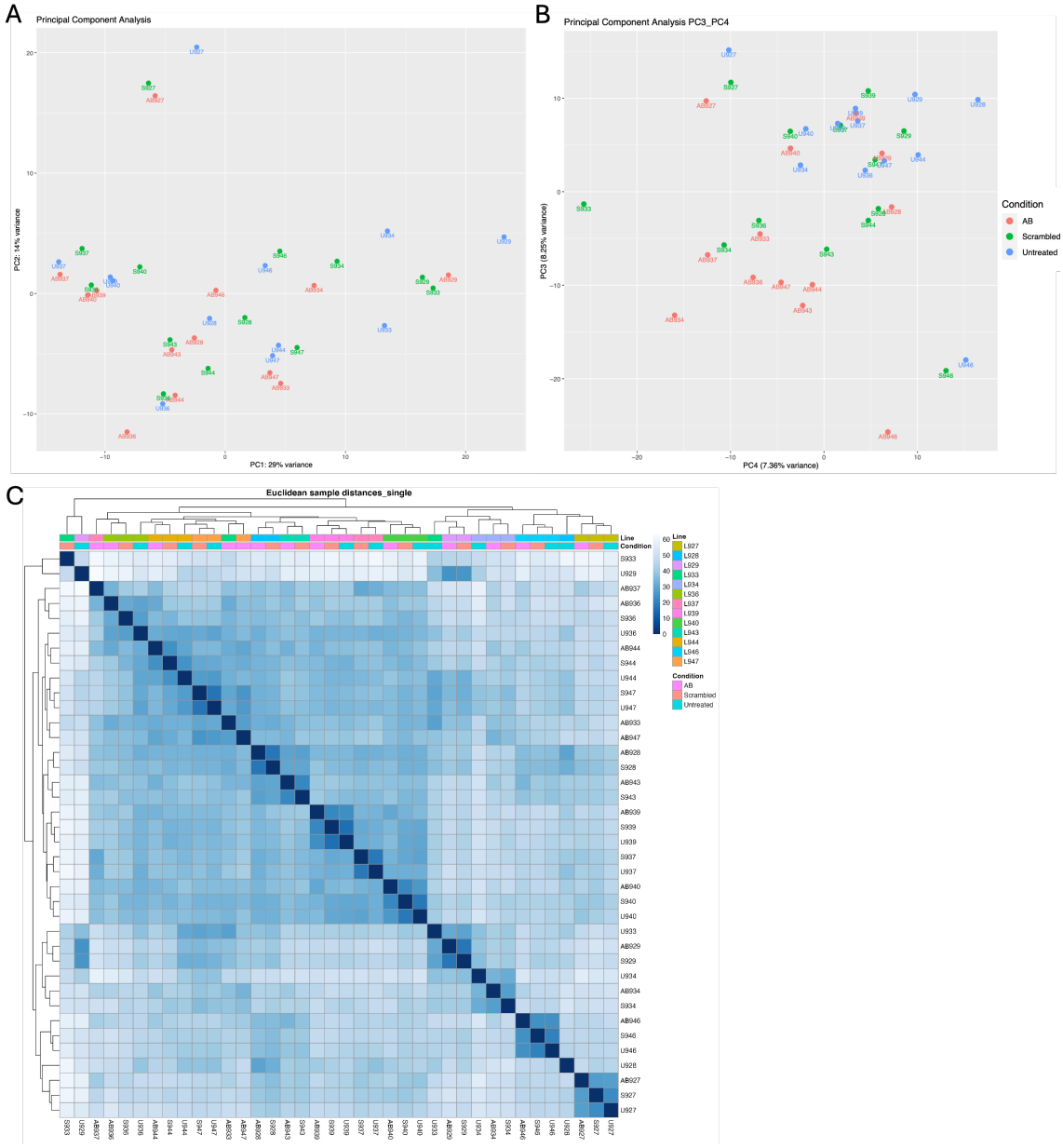


Figure 4.25: **PCA and Euclidian sample distance map clustering AD-derived neurons gene expression changes after Aβ treatment** PCA of (A) PC1 and PC2 and (B) PC3 and PC4 of 13 sAD patient lines treated with AB 5 μM, Scr 5 μM or left untreated. (C) Euclidean sample distance map of 13 sAD patient lines treated with AB 5 μM, Scr 5 μM or left untreated.

4.4.3 Differential Gene Expression analysis of Aβ treated vs Scrambled iPSC-neurons

Next, differential gene expression was performed comparing untreated with scrambled (SCR) samples, SCR with Aβ and Untreated with Aβ samples. Here, all lines

were pooled together to look at the main effect of Aβ across all patients. The model design took into account baseline line-to-line differences (~ Line + Condition). Notably, as in the i^3 RNA-seq experiment, MA plots which look at Log_2FoldChange plotted with mean of normalised counts of each gene showed that the scrambled peptide elicited nearly no transcriptional changes compared with the untreated vs Aβ and scrambled vs Aβ (Figure 4.26, A-C). Furthermore, a Pearson correlation of differentially expressed genes (DEGs) between untreated and Aβ correlated strongly with DEGs in SCR vs Aβ (r=0.98) (Figure 4.26, D). There were 950 significantly upregulated and 1176 significantly downregulated genes in the SCR vs Aβ condition (padj < 0.05). Volcano plots highlighting DEGs in the Aβ vs Scrambled comparison, or lack thereof in the untreated vs Scrambled comparison, and the top 30 DEGs are depicted in Figure 4.27.

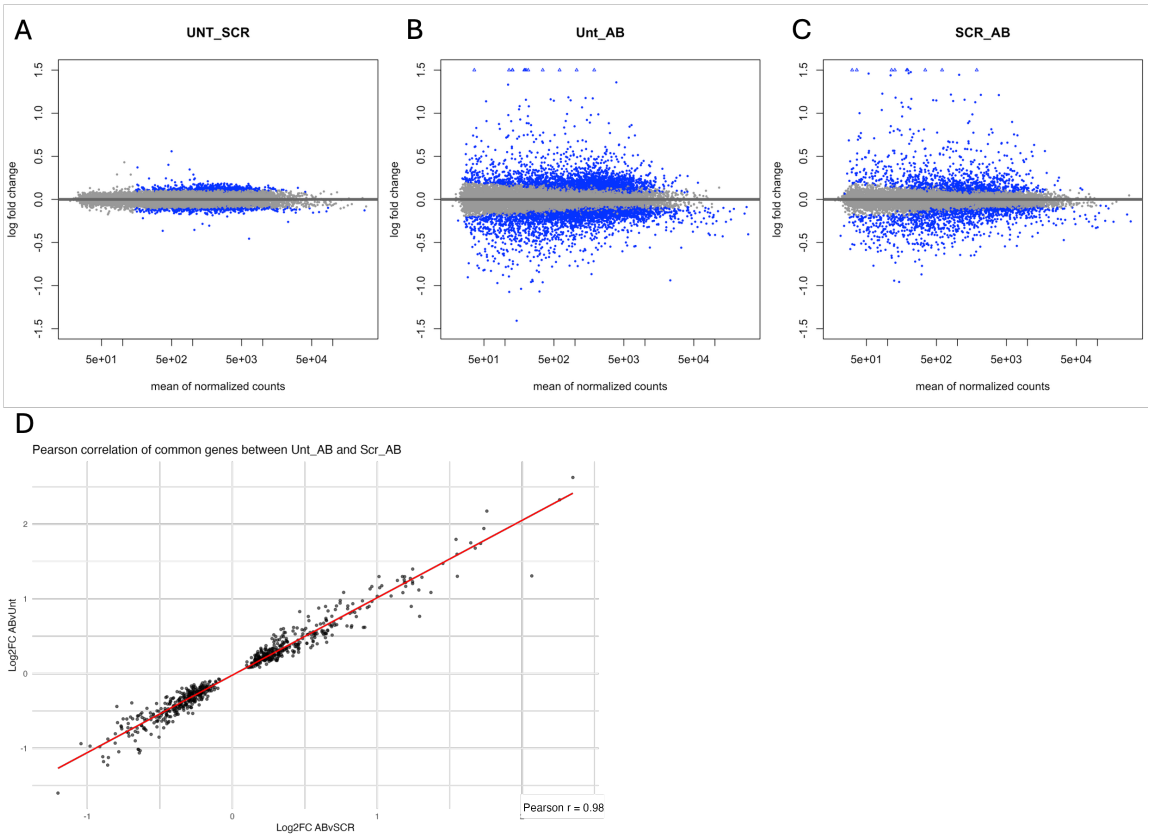
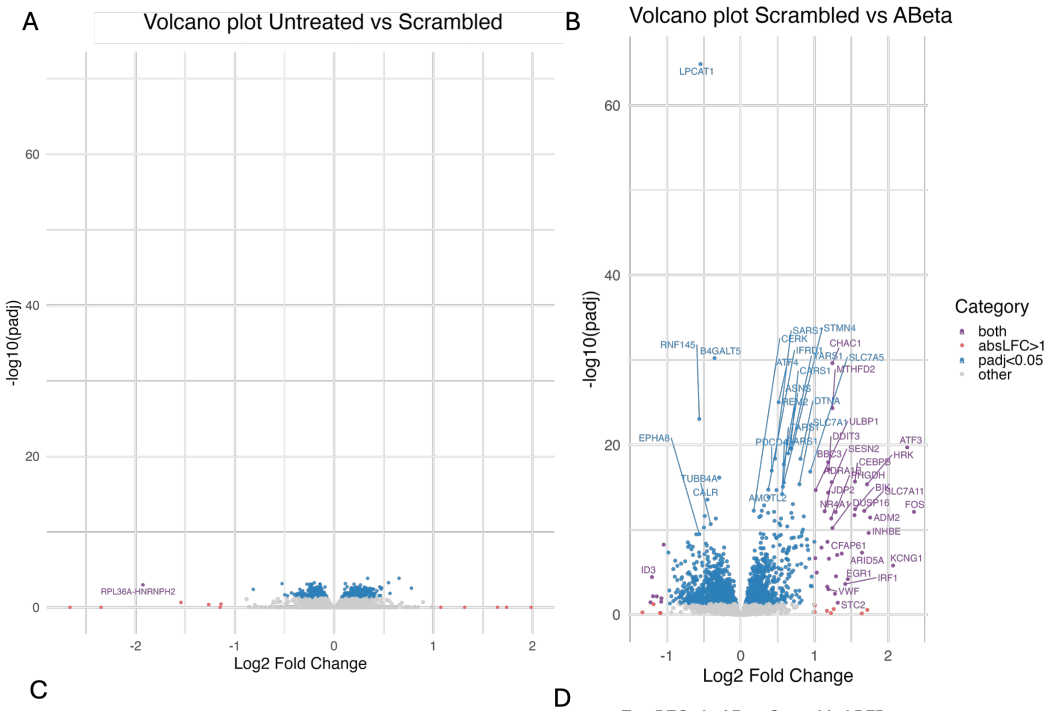
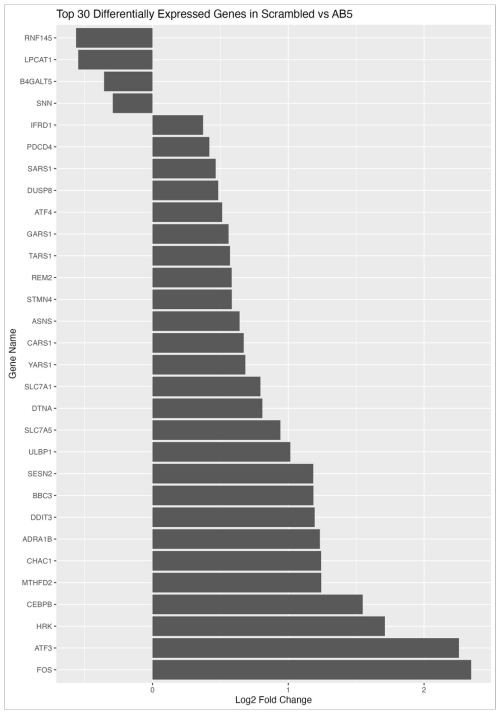


Figure 4.26: **Aβ 1-42 causes transcriptional changes in neurons compared to Scrambled 1-42 peptide and untreated control** (A-C) MA (M, log ratio; A, mean average) plots depicting the Log_2FoldChange over the mean of normalised counts of all genes in the Untreated vs SCR, SCR 5 μM vs Aβ 5 μM, Untreated vs Aβ 5 μM in 13 AD neuron lines. (D) Pearson's correlation of all DEGs in the SCR vs Aβ condition compared with those in the Untreated vs Aβ condition. r=0.98





D

Top DEGs in AB vs Scrambled DFP neurons

Gene	Function
RNF145	E3 ubiquitin ligase; regulates cholesterol metabolism and neuronal membrane homeostasis
LPCAT1	Phospholipid remodeling, specifically cell membrane-related lipids
B4GALT5	Glycosylation enzyme important in membrane-bound sphingolipids, key role in myelin formation and neuronal maturation
SNN	Endo-lysosomal protein, involved in stress response to toxic stimuli
IFRD1	Transcriptional regulator; modulates neuronal growth and differentiation
PDCD4	Translation inhibitor, modulates JUN kinase and EIF4A; role in apoptosis.
SARS1	Serine-tRNA synthetase; essential for neuronal protein synthesis
DUSP8	MAPK phosphatase; modulates neuronal stress and synaptic signalling
ATF4	Integrated stress factor transcription factor, helps cells survive stressors
GARS1	Glycine-tRNA synthetase, essential for protein synthesis
TARS1	Threonine-tRNA synthetase; supports neuronal translation
REM2	RGK GTPase; regulates neuron and synapse development and calcium signalling
STMN4	Stathmin Neuron-specific microtubule regulator; critical for neurite outgrowth
ASNS	Asparagine synthesis; important for neuronal metabolism and protein synthesis.
CARS1	Cysteine-tRNA synthetase; essential for neuronal protein synthesis
YARS1	Tyrosine-tRNA synthetase; protein synthesis. Can also act as a cytokine.
SLC7A1	Cationic amino acid transporter; supports neuronal nitric oxide signaling
DTNA	Dystrobrevin alpha; involved in cytoskeletal stability
SLC7A5	Large neutral amino acid transporter; crucial for brain amino acid supply
ULBP1	Stress-induced ligand; may signal immune activation in the brain
SESN2	Stress response protein; protects neurons from oxidative damage and inflammation
BBC3	Pro-apoptotic factor (PUMA); mediates neuronal cell death under stress by disruption mitochondrial function
DDIT3	ER stress transcription factor (CHOP); promotes neuronal apoptosis
ADRA1B	Adrenergic receptor; modulates neuronal excitability and signaling
CHAC1	Glutathione degradation; involved in neuronal oxidative stress, ferroptosis and unfolded protein response (UPR).
MTHFD2	Mitochondrial enzyme crucial in one-carbon metabolism, important for DNA/RNA production and methylation.
CEBPB	Transcription factor; regulates neuroinflammation via cytokines like Il6 and TNFalpha
HRK	Pro-apoptotic protein; involved in neuronal programmed cell death
ATF3	Immediate early gene; dual role in neuronal apoptosis or survival, neuroinflammation
FOS	Immediate early gene, activated in response to stimuli including stress/inflammation

Upregulated genes in Aβ **Downregulated genes in Aβ**

Figure 4.27: **Analysis of differential gene expression in Aβ vs Scrambled-treated AD patient-derived neurons** (A-B) Volcano plots depicting the significant DEGs between (A) Untreated and SCR comparison and (B) SCR vs Aβ comparison. Blue dots are genes with a padj <0.05, red are genes with absolute Log_2FoldChange > 1, purple are genes that meet both conditions. (C) Bar plot of the top 30 DEGs genes and (D) table describing the function of the top 30 DEGs in the scrambled vs β comparison

4.4.4 Fast Gene Set Enrichment Analysis and Over Representation Analysis in the Aβ vs Scrambled comparison

After identifying significant DEGs, I performed fGSEA to look at enriched pathways in all genes in the sample set, ranked by their Log_2FoldChange x Log_{10} pvalue. There were less positively than negatively enriched pathways identified with fGSEA, with 287 and 472 significantly enriched pathways, respectively. Looking at only significant DEGs, fORA identified 202 positively and 293 negatively enriched pathways.

4.4.5 Detailed analysis of DEGs and fGSEA

4.4.5.1 Upregulated pathways in Aβ vs Scrambled treated neurons

Upregulated genes in the Aβ treated neurons were primarily involved in cell stress responses, including immediate early genes (IEG) (c-*FOS*, *ATF3*, *ATF4*), involved in neuronal apoptosis and survival, genes linked to organelle stress responses such as ER-stress (*DDIT3*) and mitochondrial stress (*SESN2*, *BBC3*, *MTHFD2*), genes involved in neuroinflammation (*ULBP1*, *CEBPB*, *YARS1*). While some of these genes promote apoptosis (*BBC3*, *DDIT3*, *HRK*, *CHAC1*), others support cell survival (*ATF4*, *DUSP8*, *MTHFD2*), or have a dual function depending on the stressor (*ATF3*). As expected, the most upregulated pathways were all involved in cell stress response (e.g. P-53 pathway, TNFA signalling via NFKB, Hypoxia, IL6-JAK-STAT3 signalling pathways). Furthermore, genes linked to protein synthesis were also upregulated, including various tRNA and amino-acid synthetases (*TARS1*, *CARS1*, *YARS1*, *GARS1*, *ASNS*), as well as amino-acid transporters *SLC7A5*,*SLC7A1*). Amino-acid metabolism and activation as well as tRNA biosynthesis were enriched pathways. Finally, multiple phosphatases (*DUSP16*, *DUSP1*, *DUSP8*, *PTPRH*), which a play key role in regulating MAPK/JNK and PI3K/AKT/mTOR signalling pathways, were upregulated (GO:BP Peptidyl Tyrosine Dephosphorylation pathway). The top pathways identified in fGSEA were mostly overlapping with those identified in fORA (Figure 4.28).

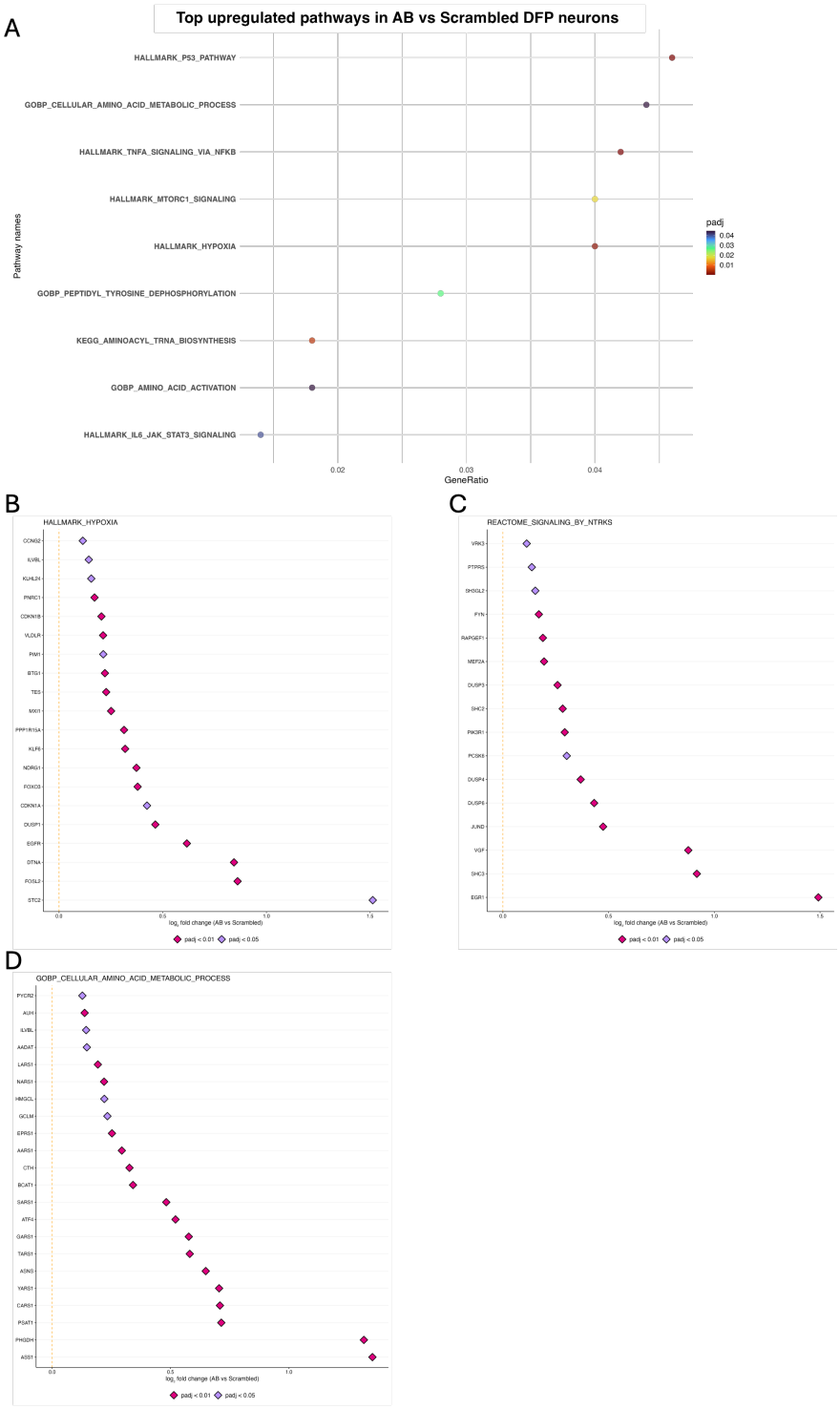


Figure 4.28: **Top positively enriched pathways in Aβ 5 μM vs Scrambled 5 μM AD neurons** (A) Dot plot of the top positively enriched pathways in AD neurons treated with 5 μM of Aβ compared to Scrambled 5 μM with GeneRatio (i.e. the number of positively enriched genes in a pathway/the number of significantly upregulated genes). Dots are coloured by the pathway's padj. (B-D) Leading edge genes of pathways of interest with their Log_2FoldChanges. Squares are coloured by their padj value.

4.4.5.2 Downregulated pathways in Aβ vs Scrambled treated neurons

Although there were more downregulated than upregulated genes and pathways, when looking at the top 30 most DEGs, only 4 were downregulated genes. That included the E3 ubiquitin ligase *RNF145*, which degrades HMG-Coa-Reductase, thereby lowering cholesterol synthesis; *LPCAT1* and *B4GALT5* which are enzymes that regulate cell membrane lipids; and SNN a protein located in endolysosomes, which is involved in stress response to toxic stimuli. Both fGSEA and fORA analyses showed enrichment for pathways related to cytoskeletal structure and axonal projection, synaptic function, and oxidative phosphorylation (OXPHOS) (Figure 4.29). The strongest negative enrichment in the fGSEA were mitochondrial/OXPHOS related pathways, whereas the most enriched pathways in fORA had to do with neuronal differentiation and axonal projections. The genes involved with axonal projection coded for ephrins, sempahorins, and fibronectin, which play a role in axonal guidance (*COBL,EPHA6B, EPHA7, SEMA5A, FN1*) which reorganises the actin cytoskeleton, and myelin-related genes such as *LPCAT1*, which produces myelin lipids and PLP1, which is a main component of myelin. Synaptic related pathways included genes involved in calcium and potassium release (*CALB1*, *KCNA1*), synaptic formation and pruning (*C1QL1*), vesicle docking (*RPH3A*), mu opioid receptor (*OPRM1*), glutamatergic synapses (*SLC2A1*, *SLC1A3*) and genes related to Wnt signalling, which plays an important part in synaptogenesis (*WNT5A, GPC4*). Finally, oxidative phosphorylation related genes included multiple glycolysis enzymes (*PKM, ALDOC, TPI1*), genes coding for proteins, which protect the cell from oxidative stress (*TIGAR*) and mitochondrial enzymes such as *ETFB*, which helps shuttle electrons.

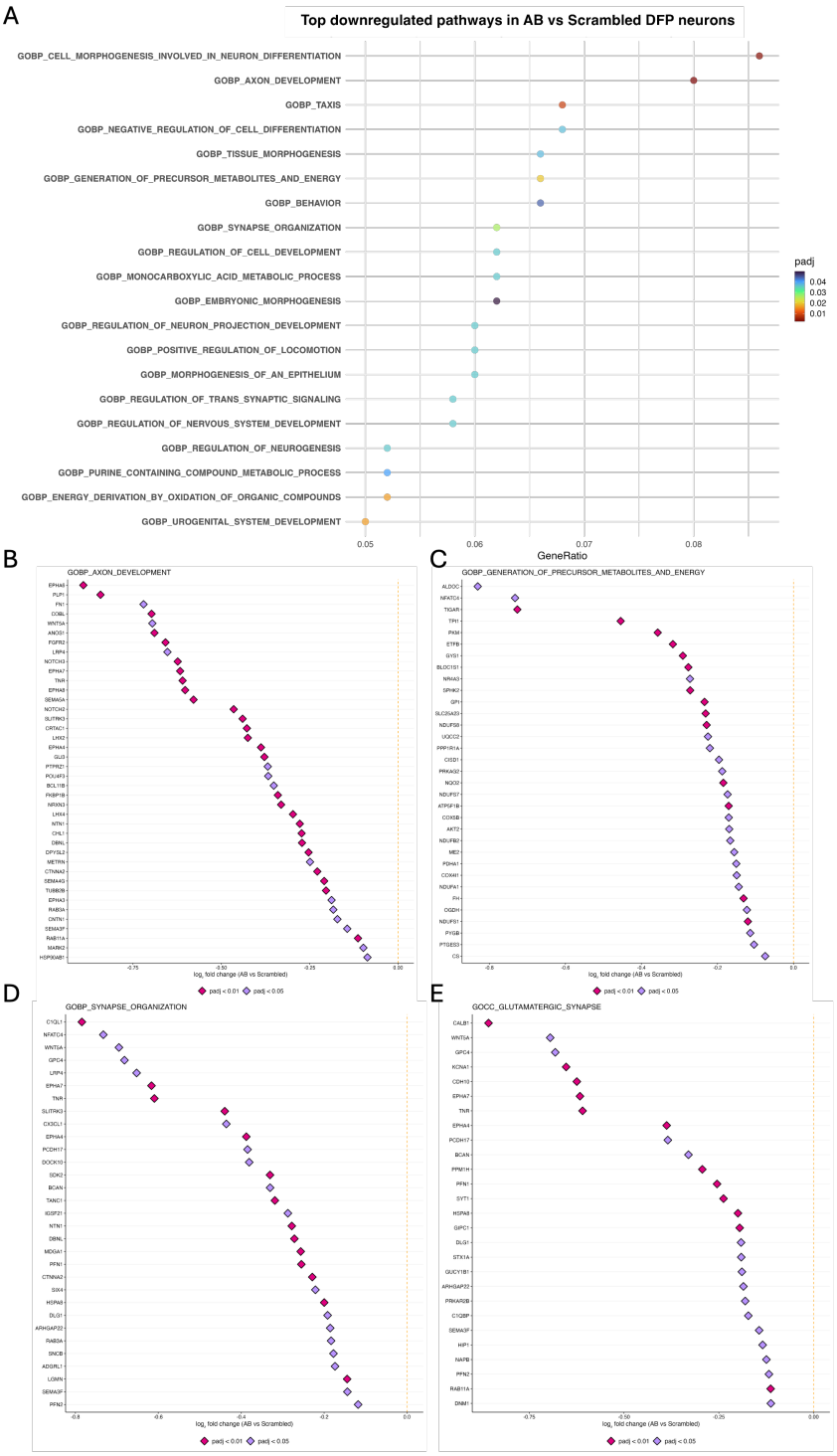


Figure 4.29: **Top negatively enriched pathways in Aβ 5 μM vs Scrambled 5 μM AD neurons** (A) Dot plot of the top negatively enriched pathways in AD neurons treated with 5 μM of Aβ compared to Scrambled 5 μM with GeneRatio (i.e. the number of negatively enriched genes in a pathway/the number of significantly downregulated genes). Dots are coloured by the pathway's padj. (B-D) Leading edge genes of pathways of interest with their Log_2FoldChanges. Squares are coloured by their padj value.

4.4.6 Comparison between resilient and vulnerable iPSC-derived neurons from the DFP cohort

To enable direct comparison between patient-derived clinical phenotypes and their corresponding donor cell lines, I ranked the donor patients by vulnerability based on their Alzheimer's Disease Assessment Scale–Cognitive Subscale (ADAS-Cog) scores [267, 1], and then grouped the cell lines accordingly. The four cell lines derived from the most cognitively resilient patients and the four derived from the most cognitively vulnerable patients were selected for comparison. This decision was motivated by the fact that cognitive decline is the defining clinical manifestation of Alzheimer's disease. Memory impairment and broader cognitive deterioration ultimately determine disease severity and patient vulnerability; therefore, cognitive scores provide a direct and clinically meaningful readout of disease impact. Importantly, the cognitive score used in this study exhibited a wide dynamic range across patients, allowing for clear separation between groups. The four individuals classified as resilient clustered within the unimpaired (0–10) or mild cognitive impairment (11–18) range, whereas the four vulnerable individuals fell within the Alzheimer's disease stage ($\geq$18), enabling unambiguous stratification. The mean of the ages of the resilient and vulnerable groups were similar– 71 and 73 years old, respectively. In contrast, the dynamic range of CSF biomarkers, including Aβ 42 and p-Tau , was smaller across patients and CSF data was missing for two individuals, whereas cognitive scores were available for all patients.

The four resilient and four vulnerable cell lines (based on ADAS-cog score) were pooled by group, resulting in two groups of four lines that were each analysed under Aβ or scrambled control treatment conditions. Direct analysis of gene expression changes across individual cell lines as a function of cognitive vulnerability was not performed because each patient-derived line was measured only once per treatment condition. As a result, differences in cognitive vulnerability attributable to gene expression cannot be separated from inherent differences between individual cell lines. Without replicates within each line, it is not possible to reliably estimate how gene expression varies with vulnerability, independent of baseline line-specific effects. For this reason, differential expression analysis was instead performed at the group level by pooling cell lines into resilient and vulnerable categories.

Differential gene expression was assessed using DESeq2 with a model designed to account for baseline expression differences between individual cell lines while

testing for Aβ-specific effects between resilient and vulnerable groups. The model included main effects of treatment condition (Aβ vs. scrambled), group (resilient vs. vulnerable), and their interaction. A schematic overview of the filtering and analysis workflow is shown in Figure 4.30.

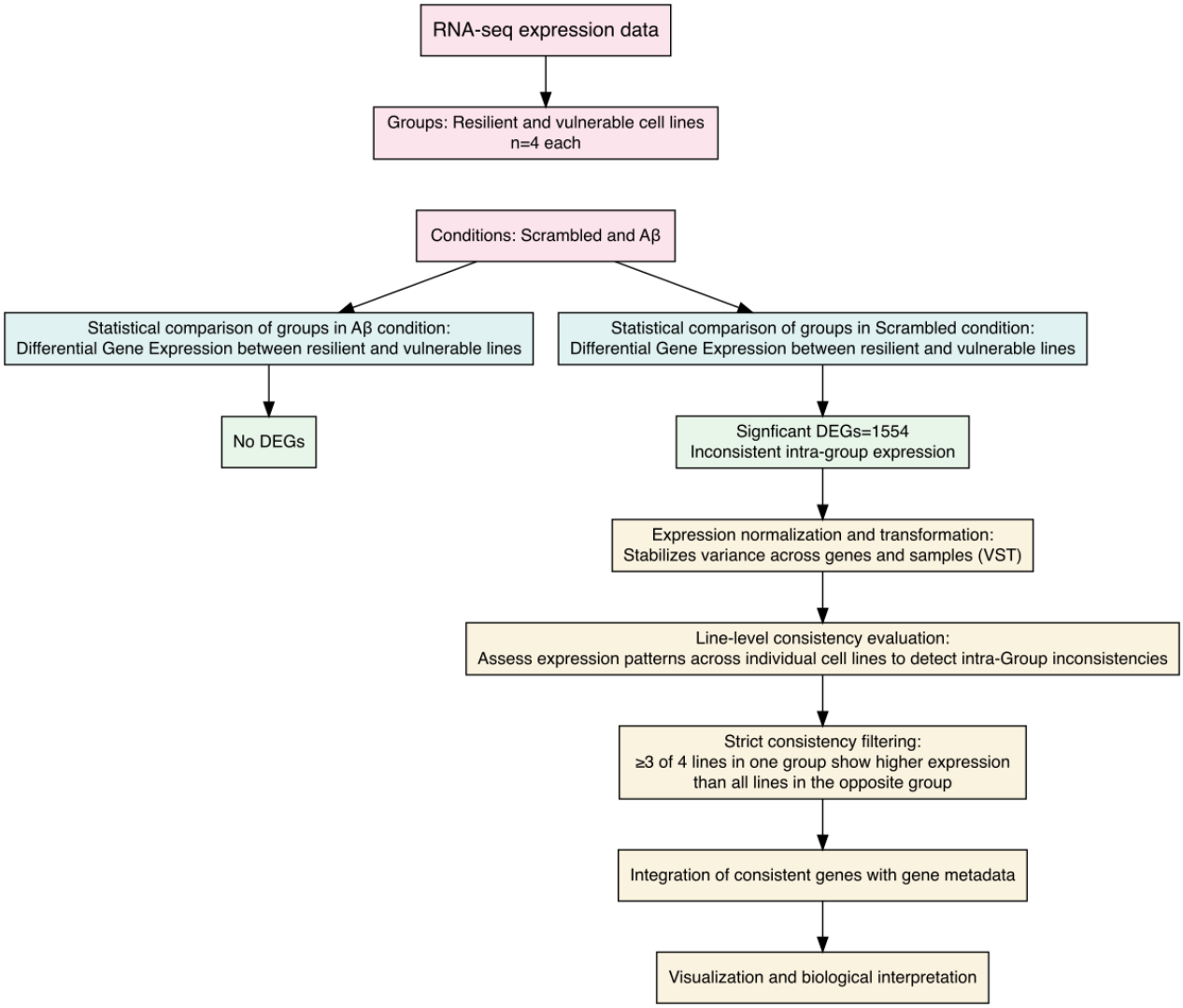


Figure 4.30: **Flowchart of RNA-sequencing analysis in Resilient vs Vulnerable patient lines** Patient lines treated with Aβ were split into groups of Resilient and Vulnerable lines based on their cognitive scores. Baseline gene expression differences between groups went through filtering for consistent genes before further analysis.

4.4.6.1 Data quality control

Principal component analysis (PCA) did not reveal strong separation between resilient and vulnerable samples (Figure 4.31, A). The samples clustered most closely per line.

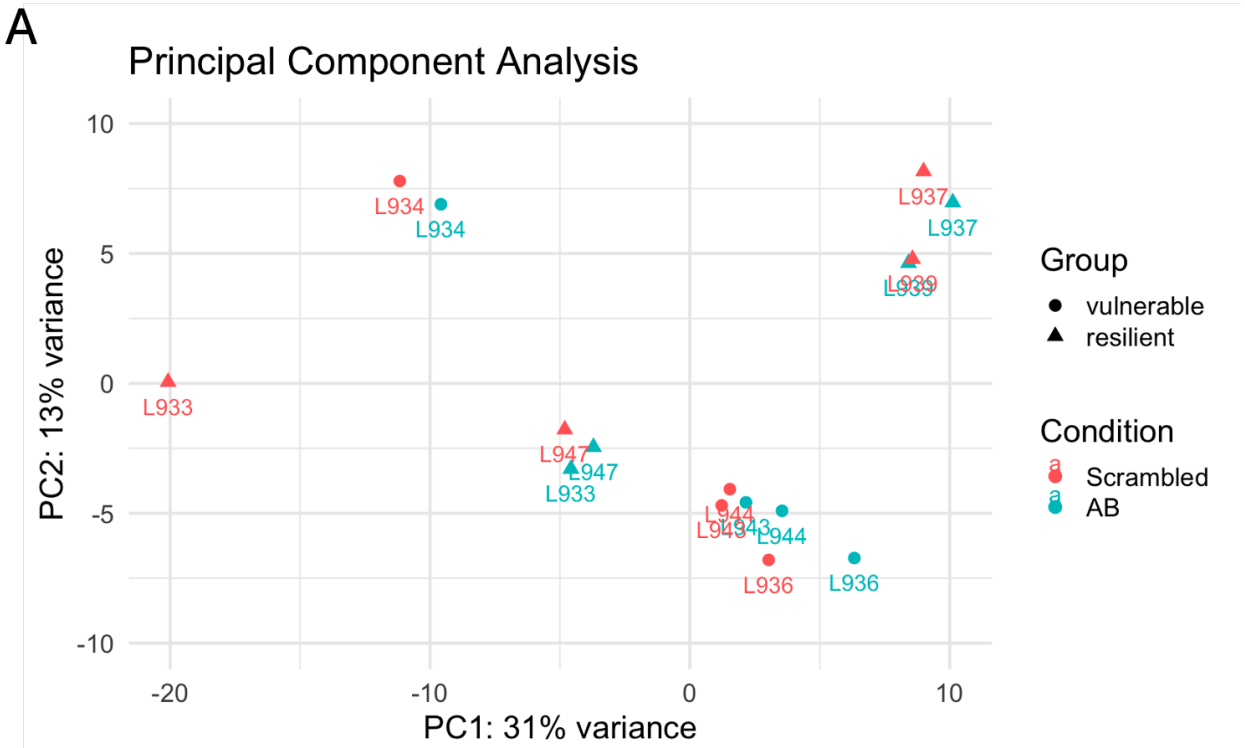


Figure 4.31: **PCA reveals no strong clustering between Resilient vs Vulnerable patient iPSC-neurons** PCA plot of Resilient vs Vulnerable patient iPSC-neurons treated with Aβ or untreated. Colours represent treatment condition and shapes represent group (vulnerable vs resilient).

4.4.6.2 Differential gene expression and functional gene set enrichment analysis overview

I first examined whether there were DEGs between resilient and vulnerable groups within the Aβ-treated neurons, after accounting for any Aβ-independent group differences observed in the scrambled controls. No significant DEGs were detected between resilient and vulnerable lines under Aβ treatment (Figure 4.32, A). Therefore, I assessed whether there were any baseline transcriptional differences between resilient and vulnerable groups in the scrambled condition. This analysis identified 1354 significant DEGs (Figure 4.32, B) . However, closer inspection revealed that many of these genes appeared significant due to inconsistent expression patterns within groups, where differential expression was driven by a single outlier line rather than a consistent group-level effect. Examples of consistent and inconsistent genes are shown in Figure 4.32, C.

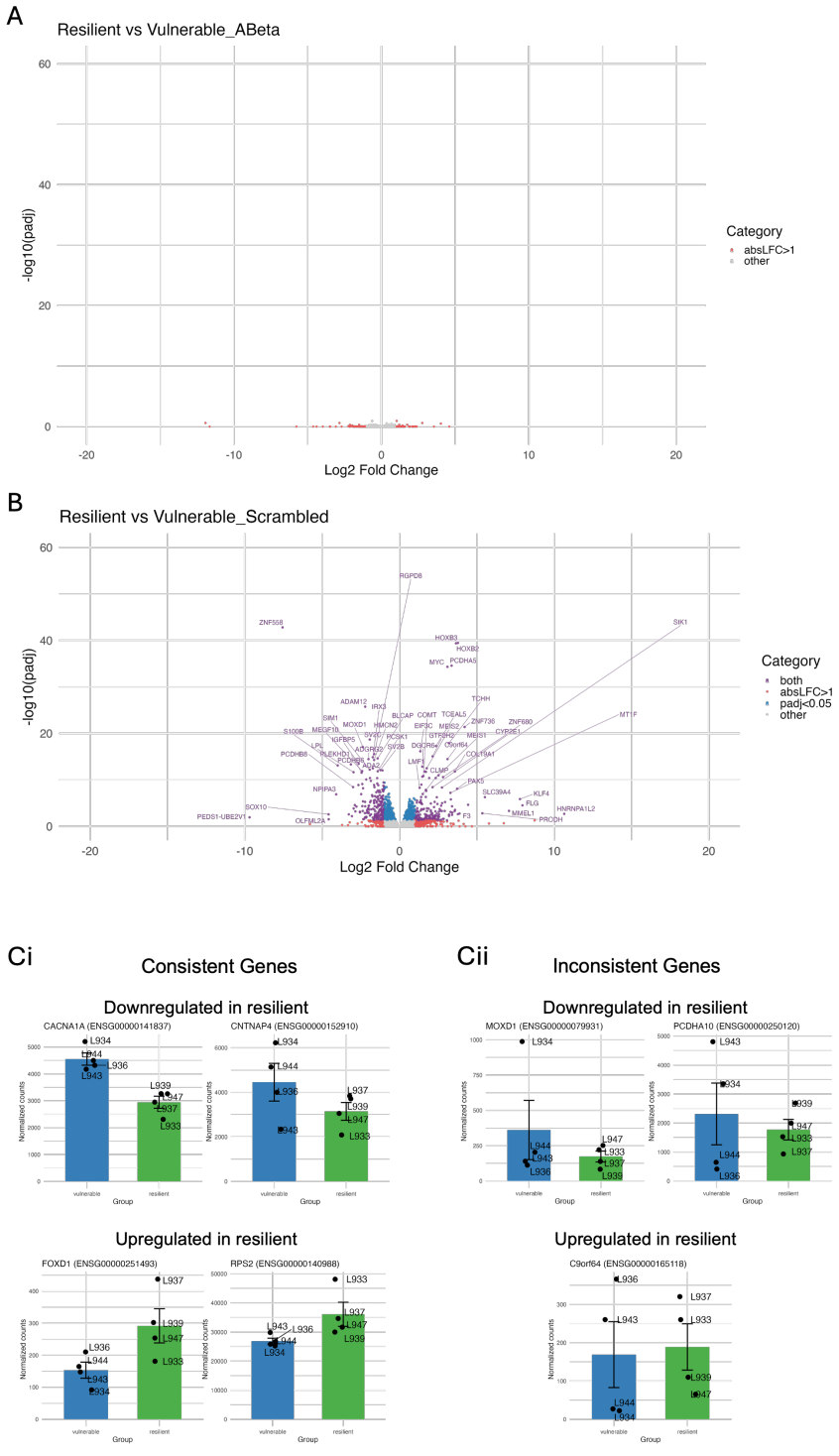


Figure 4.32: **Representation of DEGs between resilient and vulnerable patient lines, before consistency filtering** (A) Volcano plot of DEGs between Resilient vs Vulnerable patient lines due to AB treatment. (B) Volcano plot of DEGs between Resilient vs Vulnerable patient lines at baseline (scrambled condition). (C) Example bar plots of Consistent (Ci) and Inconsistent (Cii) up and down regulated genes in Resilient vs Vulnerable patients. Mean +-SEM of 4 cell lines per group.

To address this, I created a pipeline that filtered out all inconsistent genes (4.30. A gene was defined as consistent if at least three of four cell lines in one group exhibited expression levels that were higher than the maximum expression observed in all cell lines of the opposite group. This filtered down the list of genes to 2294 consistent genes, and 295 significant DEGs. Of those, 131 were upregulated in the resilient lines, and 160 were downregulated in resilient lines compared to vulnerable cell lines (Figure 4.33, A. The result of this filtering can be observed in the heatmap in Figure 4.33 B, which plots all consistent DEGs, where good consistency in direction of regulation between replicates of the vulnerable and resilient groups can be observed. A volcano plot with the consistent genes is depicted in Figure 4.34 A. Finally, functional over-representation analysis (fORA) was performed on all significant, consistent DEGs, which identified 63 significantly positively enriched pathways and 73 significantly negatively enriched pathways.

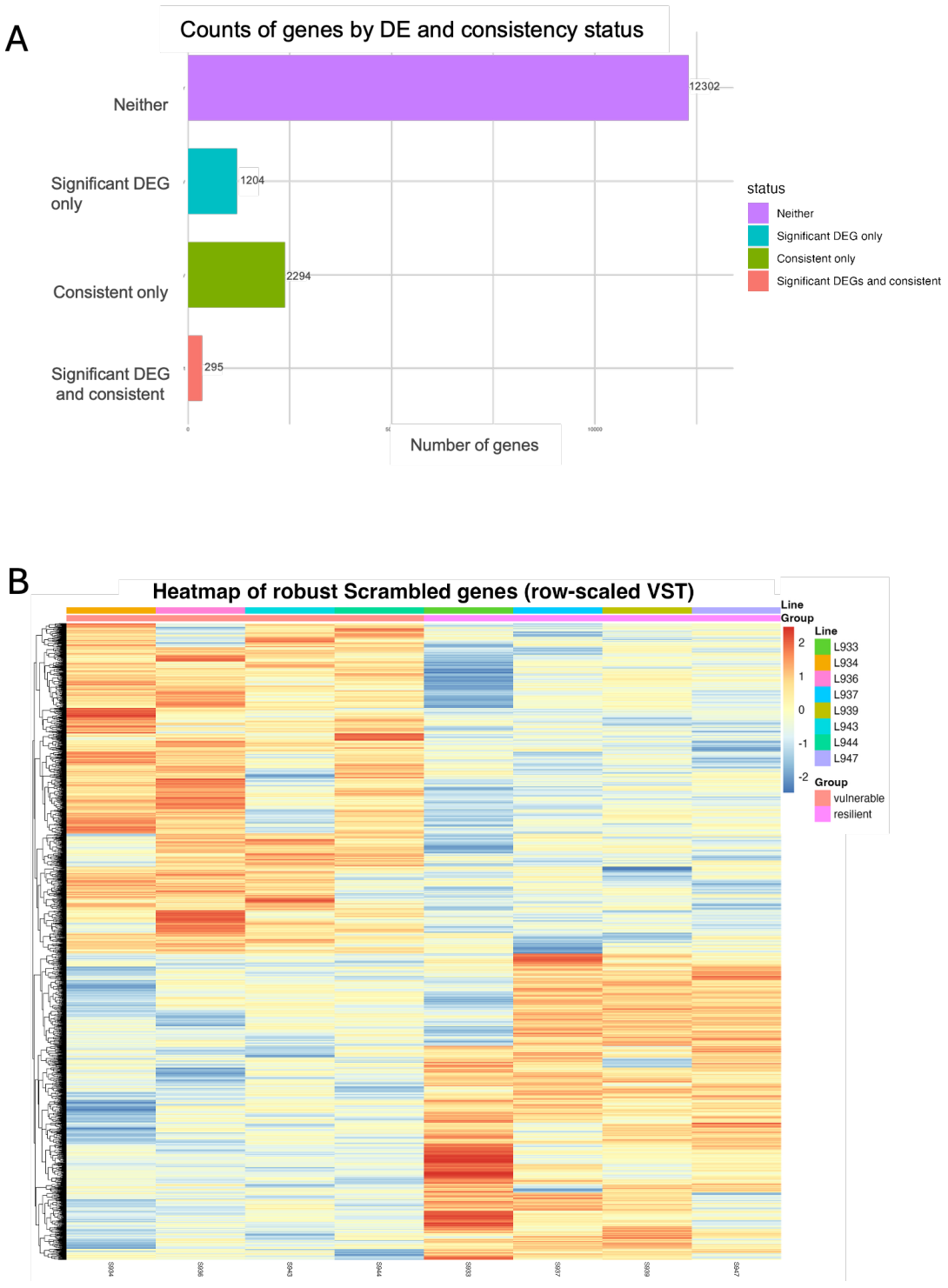
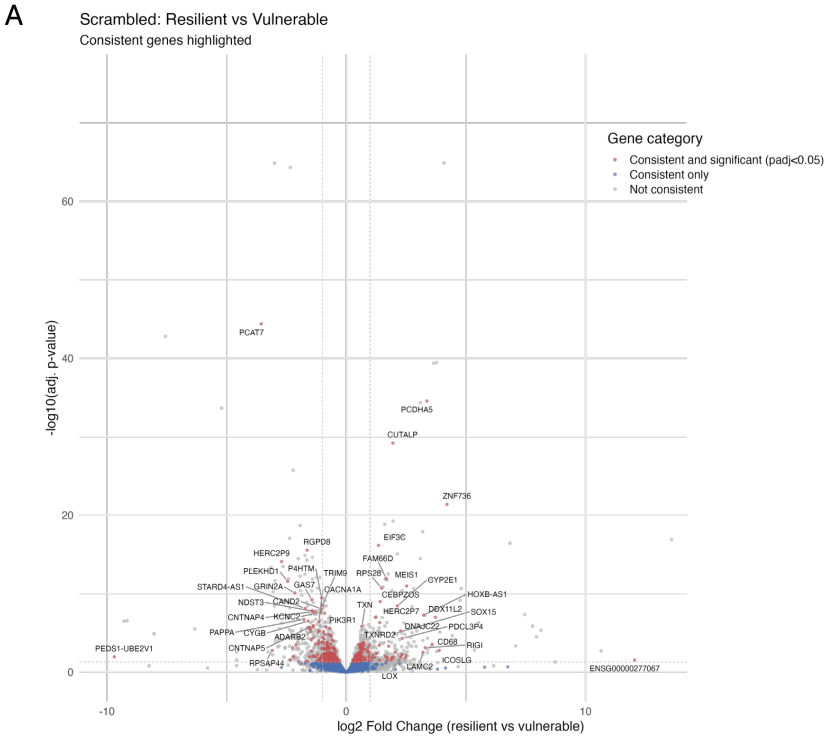
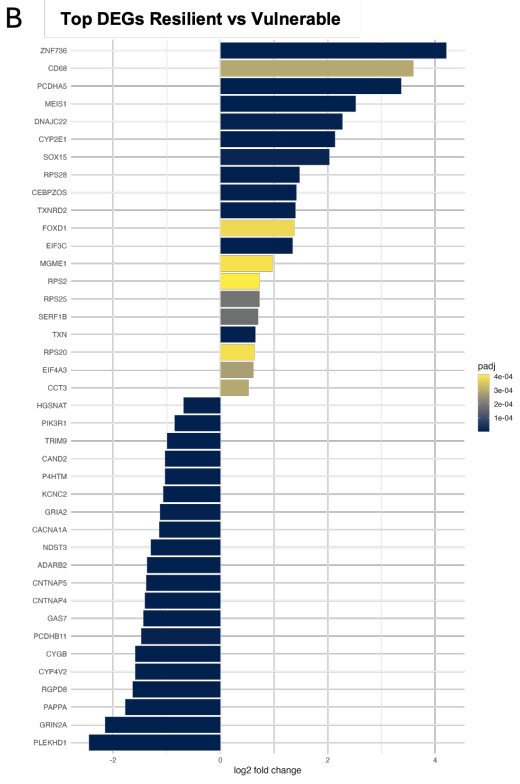


Figure 4.33: **Representation of consistently differentially expressed genes in Resilient vs Vulnerable patient neurons** (A) Bar plot with gene number of all DEGs, Significant DEGs, post-filtering consistent DEGS, and consistent and significant DEGS. (B) Heatmap plotting gene expression (log2FC) of all consistent genes across resilient and patient lines.





C

Top DEGs in Resilient vs Vulnerable DFP cell lines

Gene	Function
FOXD1	Transcription factor involved in brain regionalization
CCT3	Protein folding; essential for neuronal proteostasis
CD68	Microglial marker; involved in neuroinflammation
EIF4A3	mRNA surveillance and splicing; important for neuronal gene expression
RPS25	Ribosomal protein; supports neuronal protein synthesis
SERF1B	Protein aggregation modulation; linked to neurodegeneration
SOX15	Transcription factor; may regulate neural progenitors
DNAJC22	Molecular chaperone; supports neuronal protein folding
TXN	Redox regulation; protects neurons from oxidative stress
TXNRD2	Mitochondrial redox enzyme; neuronal energy balance
CYP20A1	Orphan cytochrome P450; brain-enriched, regulatory roles unclear
CEBPZOS	Regulatory RNA; may influence neuronal gene expression
RPS28	Ribosomal protein; neuronal translation
MEIS1	Transcription factor; involved in neurodevelopment and circadian control
EIF3C	Translation initiation; essential for neuronal protein synthesis
ZNF736	Zinc-finger protein; putative transcriptional regulation
PCDHA5	Protocadherin; mediates neuronal connectivity and synapse specificity
RGPD8	Poorly characterized; may be involved in nuclear transport and gene regulation
PLEKHD1	Associated with neuronal cytoskeleton organization and intracellular signaling
GRIN2A	NMDA receptor subunit; critical for synaptic plasticity, learning, and memory
P4HTM	Regulates hypoxia responses; may influence neuronal metabolism
GAS7	Involved in neurite outgrowth and neuronal differentiation
TRIM9	Regulates axon guidance and synaptic development
CAND2	Modulates protein degradation; linked to neuronal signaling pathways
NDST3	Heparan sulfate modification; important for neurodevelopment
CNTNAP4	Synaptic cell adhesion; regulates GABAergic signaling
KCNC2	Voltage-gated potassium channel; supports fast-spiking interneurons
PAPPA	Regulates IGF signaling; implicated in brain development
CYGB	Oxygen-binding protein; protects neurons from oxidative stress
CACNA1A	Calcium channel subunit; essential for neurotransmitter release
CNTNAP5	Cell adhesion molecule; involved in synapse formation
ADARB2	RNA editing regulator; modulates neuronal transcript diversity
PIK3R1	PI3K signaling; important for neuronal survival and plasticity
CYP4V2	Lipid metabolism; may influence neuronal membrane composition

Upregulated in resilient group **Downregulated in resilient group**

Figure 4.34: **Differentially expressed genes in Resilient vs Vulnerable neurons** (A) Volcano plot of DEGs in resilient neurons compared vulnerable ones. Consistent genes are highlighted. (B) Bar plot of top 30 DEGs in resilient vs vulnerable neurons and (C) Table with top genes and their functions.

4.4.6.3 Detailed analysis of DEGs and enriched pathways in resilient vs vulnerable patients

Upregulated genes in the resilient cell lines were involved in translation (*EIF4A3, EIF3C, RPS28, RPS25*); protein folding (*DNAJC22, CCT3*); as well as with oxidative stress, such as thioredoxin (*TXN*), thioredoxin reductase 2 (*TXNRD2*), which protect neurons from oxidative stress; and with transcription factors, which regulate neuronal differentiation and proliferation (*MEIS1*, *ZN736I*). *PCDHA5* (Protocadherin-alpha 5), a cell-surface protein involved in synapse formation and organisation, as well as neuronal cell adhesion, was also highly upregulated in the resilient group. All positively enriched pathways were involved in translation, protein synthesis and folding (e.g. "GO:BP peptide metabolic process", "GO:BP ribosome biogenesis", "Go:BP positive regulator of translation") (Figure 4.35).

Genes downregulated in resilient cell lines were involved in pathways related to neurite outgrowth and cytoskeletal organisation, including *PLEKHD1*, *GAS7*, and *TRIM9*. Furthermore, there was reduced expression of genes involved in cell–cell adhesion and binding, including contactin-associated proteins (*CNTNAP4*, *CNTNAP5*) and multiple cadherin and cadherin-like genes (*CDH6, CDH11, PCDHB11, PCDHB3*), which mediate calcium-dependent cell adhesion and junction formation, as well as aid in synapse assembly, and contributed to the negative enrichment of pathways such as "GO:BP Biological adhesion". Associated with these changes, genes linked to synaptic formation and organisation pathways were also downregulated, encompassing components of excitatory synapses (*GRIN2A*, *LRRTM3*, *ROBO2*, *SHANK2*), inhibitory (GABAergic) synapses (*GABRA2*, *CLSTN2*), and neurotransmitter release through vesicle docking (*UNC13A*). In addition, several voltage-gated ion channel genes (*CACNB4*, *CACNA1A*, *KCNC2*) showed reduced expression. All of these DEGs drove negative enrichment of pathways such as "GO:BP Cell-cell signalling", "GO:BP ion transport*, or "GO:BP synaptic signalling". Finally, components of the PI3K/Akt signalling pathway (*PAPPA*, *PIK3R1*) were downregulated, aligning with the broader reduction in signalling pathways associated with neuronal structure, connectivity, and synaptic function (Figure 4.36).

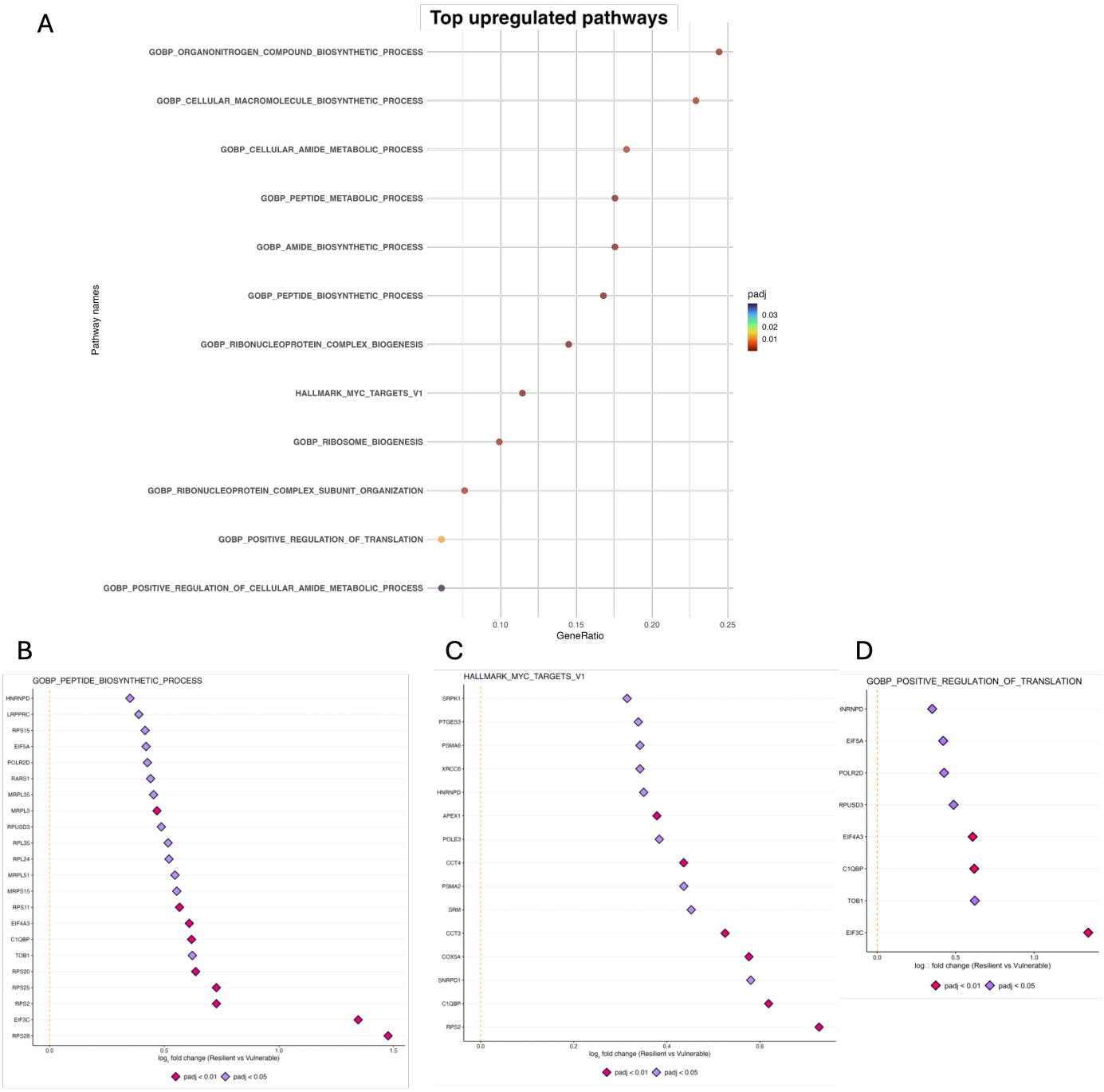


Figure 4.35: **Top upregulated pathways in resilient patient-derived neurons compared with vulnerable neurons** (A) Dot plot of the top upregulated pathways in resilient vs vulnerable patient lines (B) Dot plots of upregulated genes leading the enrichment of these pathways. The dots are coloured according to their p-value.

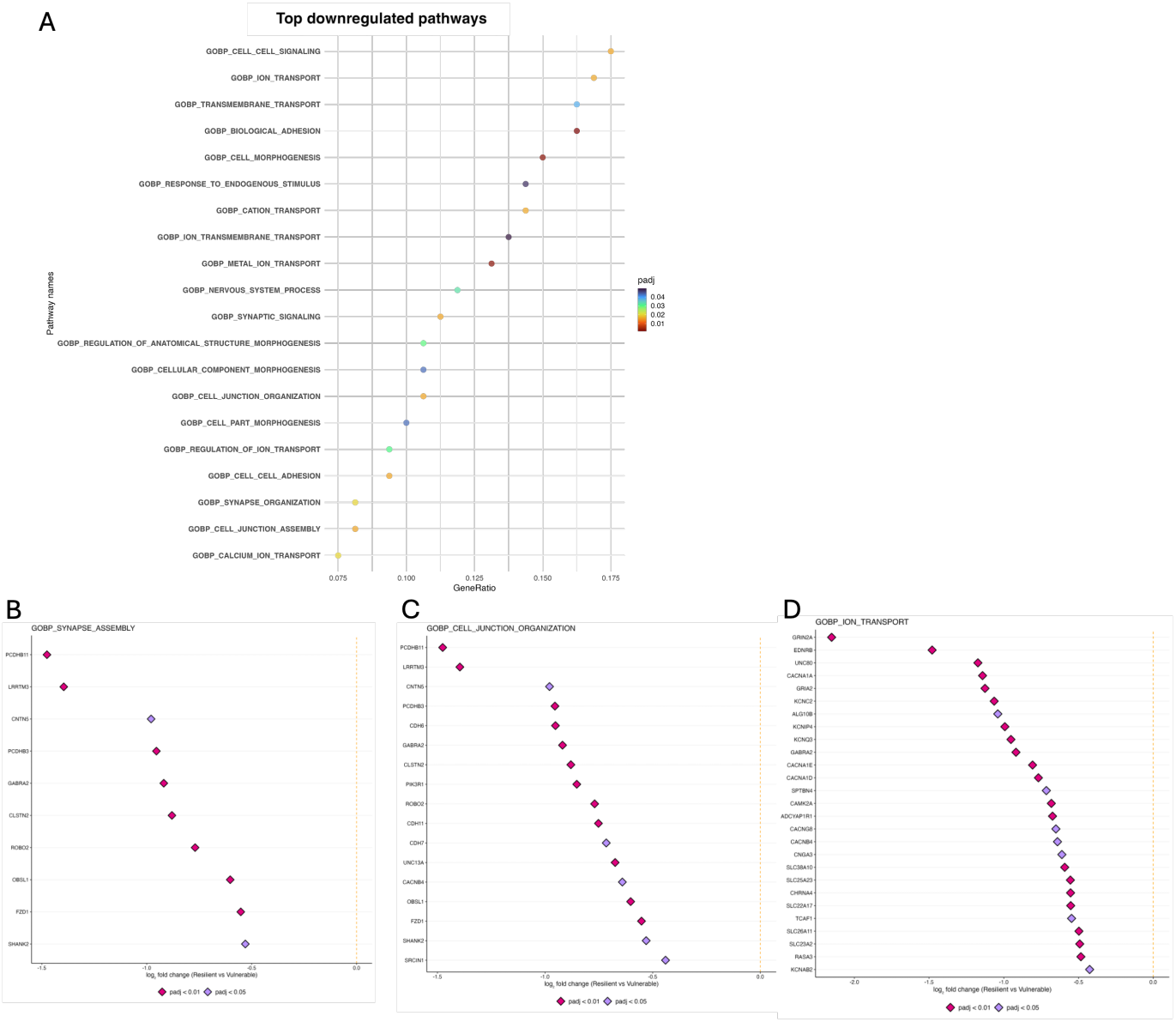


Figure 4.36: **Top downregulated pathways in resilient patient-derived neurons compared with vulnerable neurons** (A) Dot plot of the top downregulated pathways in resilient vs vulnerable patient lines (B) Dot plots of downregulated genes leading the enrichment of these pathways. The dots are coloured according to their p-value.

4.4.7 Correlation of significant DEGs between resilient and vulnerable patient lines and clinical measures

After identifying genes that were consistently and significantly differentially expressed between resilient and vulnerable patient lines, I analysed whether the hits were significantly associated with the clinical measures of the donors. Gene expression

levels (Log2-transformed transcripts per million (TPMs)) were correlated with clinical measures using Spearman's rank correlation coefficient (rho). Given the small sample size and the non-normal distribution of both gene expression and clinical measures, Spearman's rank correlation was appropriate, as it does not assume linearity or normality and is robust to outliers [315].
When adjusting for multiple comparisons (Benjamini-Hochberg (BH) FDR correction), there was only one significantly correlated gene: *COL5A3*– a component of the brain's extracellular matrix– correlated with higher ADAS-cog scores (i.e. worse cognition) (p-value < 0.043, rho$= 0.86$). FDR-BH corrections on such a small sample size is very conservative, and I therefore also analysed genes significant when considering their unadjusted p-value. There were 145 significantly correlated genes (unadjusted p-value<0.05), which decreased to 55 when filtered for strongly correlated genes (absolute rho <0.7)–some of which were correlated with multiple clinical measures (Figure 4.37, A, B). The greatest number of genes strongly correlated with ADAS-Cog scores (12 genes), MEG (13 genes), and CSF Aβ 42:40 and CSF Aβ 42 (8 genes). Looking at other CSF biomarkers, there were 7 genes correlated with p-Tau , 2 with p-Tau:Tau , and 6 with total p-Tau . There were also 3 genes correlated with MMSE scores, and 7 correlated with Tau PET signal (Figure 4.37, C).

Counter-intuitively, the majority of genes correlated with better cognition (i.e. smaller ADAS-cog) were correlated with lower CSF Aβ 42:40 (i.e. more amyloid pathology), while genes correlated with worse cognition (i.e. higher ADAS-cog) were correlated with higher CSF Aβ 42:40 (i.e. less amyloid pathology) (Figure 4.37, A, Bi-ii). Among the genes significantly correlated with better cognition (smaller ADAS-Cog scores) but lower Aβ 42:40 (more amyloid pathology), three genes were related to mitochondrial function: *MRPL14* (associated with cognition) coding for mitochondrial ribosomal subunit, *ATP5MF* (associated with both) and *ATP51FB* (associated with Aβ 42:40), both coding for ATP synthase subunits. On the other hand, *PLD6*, a enzyme which promotes mitochondria fusion was associated with worse cognition and higher CSF Aβ 42:40 (low pathology).
Genes involved in cell–cell adhesion and intracellular trafficking were also associated with cognition and CSF Aβ 42:40. The protocadherin *PCDHA5*, which was upregulated in resilient cell lines, was associated with better cognition, whereas *PCDHGB1* was associated with worse cognition but lower amyloid pathology.
Among endoplasmic reticulum (ER)–related genes, *TAPBP*, involved in MHC class I antigen presentation, was associated with worse cognition and lower amyloid

pathology (higher CSF Aβ 42:40), and *VPS13C*, a lipid transporter between the ER and lysosomes or mitochondria, was also associated with higher CSF Aβ 42:40 levels. Finally, *SPTBN4*, which organises ion channels at the axon initial segment, was correlated with both lower amyloid and tau pathology (higher CSF Aβ 42:40 and low CSF pTau).

Furthermore, nearly every gene significantly correlated with p-Tau was also associated with total Tau levels (Figure 4.37, A, Biii-iv). Of those, *MTERF4*, which was associated with lower CSF p-Tau , tTau, PET Tau and MEG, codes for a protein involved in mitochondrial ribosome assembly, while another mitochondrial ribosome protein, *MRPL51*, was associated with increased CSF p-Tau and Tau (i.e. more tau pathology). Furthermore, four proteins involved in DNA and RNA processing were correlated with higher p-Tau and Tau levels, including *XRCC6*, involved in DNA repair; *POLR2D*, which codes for a subunit of RNA polymerase II; *SNRPD1*, involved in building the spliceosome; and *HNRNPD*, which regulated RNA stability, processing and translation. Here, I identified genes that were significantly differential expressed in resilient vs vulnerable neurons, and showed that a subset of these genes significantly correlated with a range of cognitive and CSF-based clinical measures, with several genes associated with more than one clinical outcome.

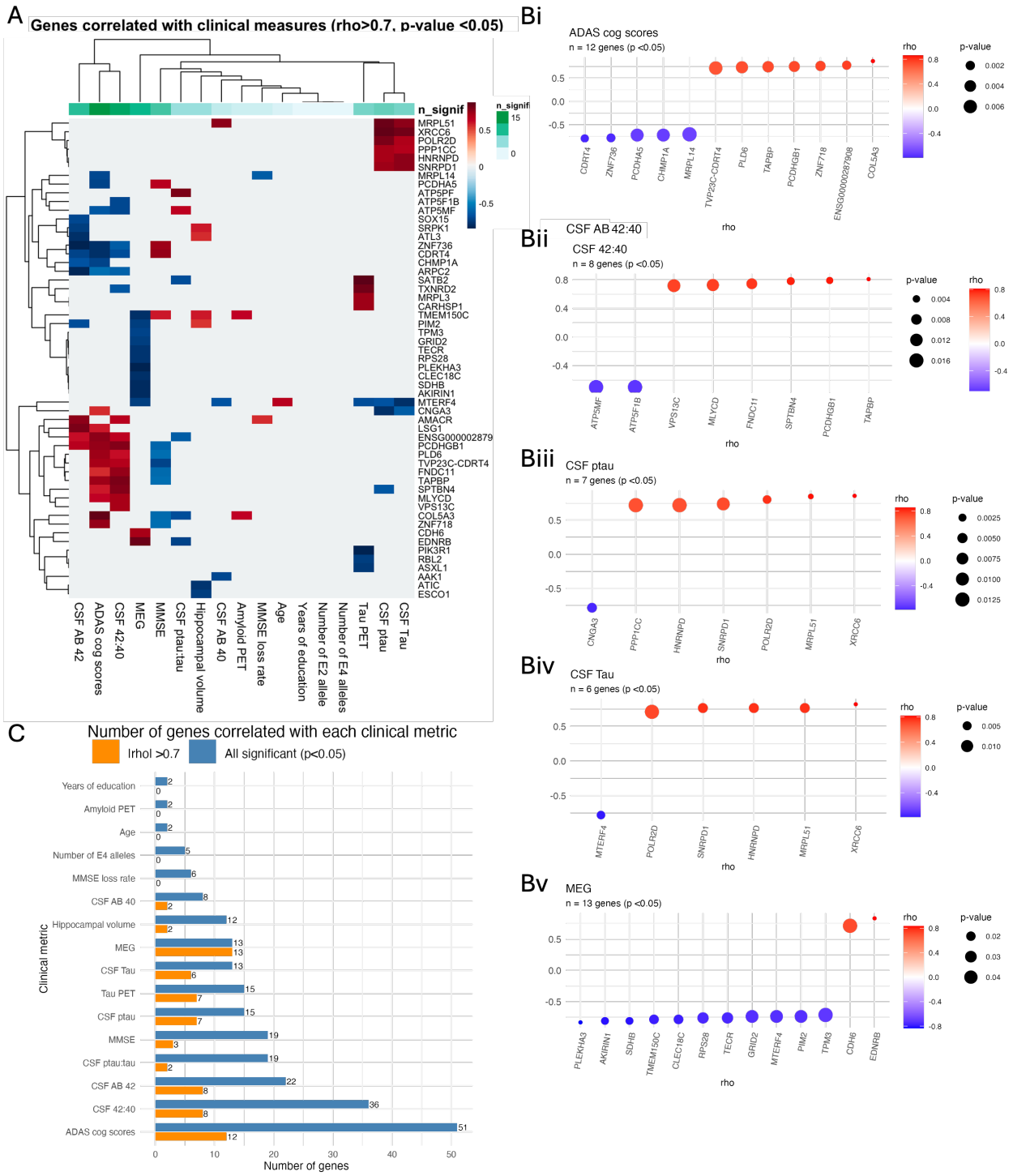


Figure 4.37: **Correlation of genes differentially expressed between iPSC-derived neurons of resilient and vulnerable patient with clinical measures of the donors** (A) Heatmap of genes highly correlated (abs rho $>$ 0.7, p-value $<$0.05) with various clinical metrics. n-signif refers to the number of genes significantly correlated with each metric. (B) Dot plot of genes correlated with each metric (abs rho $>$ 0.7). The size of dots refers to the p-value of the correlation. (C) Number of all significant (blue) or strongly correlated (orange) genes associated with each metric.

4.5 Discussion

4.5.1 Overview of key findings

In this chapter, bulk RNA sequencing was used to investigate Aβ–induced transcriptional changes in both control iPSC-derived neurons (i3 neurons) and AD patient-derived neurons from the DFP cohort. Across both systems, Aβ exposure induced substantial transcriptional remodelling, although the magnitude, directionality, and variability of these responses differed between the homogeneous i^3 model and the genetically heterogeneous patient-derived neurons.

In i^3 neurons, Aβ treatment elicited robust and reproducible transcriptional changes, including positive enrichment of pathways related to synaptic function, neuronal projection, and lipid biosynthesis, alongside negative enrichment of proteasomal and translational pathways. These findings motivated targeted experimental follow-up focused on cholesterol metabolism, including CRISPRi-mediated knockdown of *SREBP1* and *SREBP2*, pharmacological inhibition of cholesterol synthesis, and modulation of lipid droplet formation. Despite transcriptional evidence implicating cholesterol pathways, genetic and pharmacological suppression of cholesterol synthesis did not reduce Aβ-induced neurotoxicity as measured by neurite outgrowth or AK release. Aβ exposure did, however, induce lipid droplet accumulation in a time-dependent manner, suggesting the increase in cholesterol biosynthesis is at least partially driven by this mechanism.

In patient-derived neurons from the DFP cohort, line identity explained a large proportion of transcriptional variance, reflecting substantial inter-individual heterogeneity. Nevertheless, Aβ exposure induced transcriptional changes across lines, including upregulation of stress response pathways, such as immediate early genes associated with neuronal survival and apoptosis, organelle stress responses, and protein synthesis; and downregulation of pathways related to cytoskeletal organisation, axonal projection, synaptic function, and oxidative phosphorylation. Finally, comparison of resilient and vulnerable patient lines revealed baseline transcriptional differences independent of Aβ treatment. Resilient lines showed increased expression of genes involved in translation, protein folding, and oxidative stress protection, while vulnerable lines had upregulated expression of genes associated with synaptic signalling, cell–cell adhesion, and neuronal projections. No significant differences were observed in the transcriptional response to Aβ

between resilient and vulnerable groups. Finally, I identified a set of genes whose expression levels are correlated with multiple clinical measures, including ADAS-Cog, CSF Aβ and Tau biomarkers, and Tau PET signal.

4.5.2 Cholesterol metabolism and lipid dysregulation in Aβ-treated neurons

Cholesterol metabolism has been implicated in Alzheimer's disease, given APOE – the strongest genetic risk factor for sporadic AD– functions as a major lipid transporter, particularly in glial cells. Post-mortem single-cell transcriptomic studies have identified dysregulation of cholesterol-related genes in AD brains, including *TM7SF2*, which was among the most upregulated genes in the Aβ-treated i3 neurons [289]. Experimental studies have further shown that Aβ exposure increases cholesterol and ceramide levels in cultured neurons [94], and that inhibition of cholesterol synthesis can reduce Aβ production and Tau pathology in familial AD iPSC-derived neurons [478]. On the other hand, one paper in iPSC-derived GABAergic neurospheres, showed that Aβ dimer treatment induced a downregulation of cholesterol, perhaps pointing to a cell-type specific response to Aβ [283].

In the present study, reduction of cholesterol synthesis—via genetic knockdown of *SREBP1/2* or pharmacological inhibition using Simvastatin or squalene synthase inhibitor YM53601—did not attenuate Aβ-induced neurotoxicity, which is not consistent with findings from Cutler et al. [94]. Interestingly, Aβ-treated neurons had decreased SREBP protein levels despite increased *SREBP* transcript abundance, suggesting a potential temporal disconnect between transcription and protein turnover. One possibility is that early Aβ-induced suppression of SREBP activity triggers compensatory transcriptional upregulation via feedback mechanisms, which may explain the lack of any effect observed upon cholesterol inhibition. Nonetheless, the difference between RNA and protein levels is striking, and future experiments could involve blocking the proteasome to see whether SREBP1/2 are being rapidly targeted for degradation.

Lipid droplet accumulation in AD has been well described in AD, particularly in glial cells, where Aβ-induced lipid droplet formation impairs plaque clearance, and which has been shown to be exacerbated by APOE4 [172, 365, 488]. Cutler et al. showed that lipid accumulation in AD was only increased compared to controls in vulnerable, pathology-containing, brain areas [94]. Furthermore, studies in cell and mouse models demonstrated Aβ induced accumulation of lipids in neurons, and

that inhibition of cholesterol synthesis reduced Aβ-induced neurotoxicity and Aβ pathology ([94, 195, 196]. In line with these findings, I show Aβ treatment induced lipid droplet accumulation in neurons, although the effect of cholesterol inhibition on lipid droplet formation was not assessed. Future work should determine whether cholesterol modulation alters neuronal lipid droplet accumulation, and clarify the subcellular localisation and functional role of these structures in Aβ-mediated toxicity. Differences between this dataset and post-mortem studies—such as the upregulation of cholesterol-related genes observed here versus downregulation in aged AD brains [289]—are not unexpected, given that these experiments were conducted in relatively young, mono-cultured neurons lacking glial interactions and age-associated pathology.

4.5.3 Translational and proteasomal dysregulation in response to Aβ1-42

Aβ treatment in i^3 neurons induced a downregulation of translation-related genes and pathways. Dysregulated translation has been reported in early AD and is negatively associated with global pathology in post-mortem brain tissue from the ROSMAP cohort [289]. Similar reductions in ribosomal gene expression have been observed in iPSC-derived neurons from AD patients [245] and in transcriptomic analyses of MCI and AD samples from the AddNeuroMed cohort [121]. Notably, in the present study, resilient patient lines from the DFP cohort exhibited positive enrichment of translation-related pathways relative to vulnerable lines, suggesting that maintenance of protein synthesis capacity may contribute to resilience against neurodegenerative stress.

Furthermore, Aβ induced pronounced downregulation of genes encoding both 20S and 26S proteasome subunits, accompanied by negative enrichment of proteasome-related pathways i^3 neurons. Proteasomal dysfunction is a well-established feature of ageing and neurodegenerative disease, and impaired proteasome activity has been documented in AD brains [269, 12, 83, 215]. Experimental studies in mouse and cell culture models have shown that Aβ1-42 can directly inhibit proteasome function by binding to proteasomal subunits, and that enhancing proteasome activity ameliorates Aβ1-42-driven toxicity in cellular and animal models [14, 78, 96, 468].
Interestingly, Hackman and Sallbeck also reported altered expression of proteasome -related genes in response to Aβ in iPSC-derived neural precursor cells, although they observed increased expression of 20S proteasome subunits, in contrast to the decrease

observed in this study [398]. This discrepancy may reflect differences in experimental context, including the use of neural precursor cells, a shorter Aβ exposure (24 h versus 5 days), and potential temporal lags between transcriptional changes and protein turnover, similar to those observed for SREBP expression in this study. Several studies have shown that activation of 26S proteasome activity increased tau clearance in mouse models of AD, and it would be interesting to see whether upregulation of proteasome helped mitigate Aβ-driven toxicity in sAD-derived neurons [413, 412].

4.5.4 Axonal projection, synaptic dysfunction, and neuronal excitability

Axonal degeneration and synaptic dysfunction are hallmark features of Alzheimer's disease, and it was therefore not surprising that pathways related to these processes were prominently altered in response to Aβ1-42. In i^3 neurons, synaptic and axonogenesis-related pathways were positively enriched following Aβ1-42 treatment, whereas in AD patient-derived neurons, these pathways were predominantly downregulated. The latter finding aligns with Aβ1-42-induced neurite loss observed in this thesis and with prior reports of synapse loss in DFP neurons [322].

Several factors likely contribute to this divergent directionality. First, the i^3 model uses a single isogenic line with three independent differentiations per condition, providing high within-system reproducibility but capturing only one genetic background. The DFP dataset, by contrast, comprises 13 genetically distinct AD patient lines with a single replicate per condition, in which between-line variability dominates the transcriptional signal and reduces sensitivity to subtle group-level effects. Second, the i^3 line is a young, healthy control line, whereas the DFP lines derive from patients with established AD; there might therefore be differences in transcriptional state and stress tolerance between the AD patients group and the i^3 line. Third, the apparent positive enrichment of synaptic genes in i^3 neurons may represent a compensatory homeostatic upregulation in response to neurite loss — a pattern also observed in human post-mortem AD transcriptomes [288] and in iPSC-derived AD neurons [245] . Notably, Lagomarsino et al. reported upregulation of synaptic genes in iPSC-derived neurons from AD patients compared to controls.
In line with this, here, comparison of vulnerable and resilient patient lines revealed an upregulation in genes related to synaptic function and activity in the vulnerable individuals. Neuronal hyper-excitability has been documented in early-stage AD

patients [112, 198] and individuals at risk for late-onset AD [32]. Studies in AD mouse models also report hyperactivity, particularly in neurons proximal to Aβ plaques [63, 347, 253], and that reversing abnormal hyper-excitability could reduce Aβ deposition and spread [146]. Whether the transcriptional signatures observed in vulnerable neurons contribute causally to heightened excitability and increased susceptibility to Aβ toxicity remains an important question for future investigation.

4.5.5 Correlations of DEGs with clinical measures

Following the identification of differentially expressed genes between resilient and vulnerable patient-derived neurons, I examined whether the expression of these genes across the 13 patient lines were associated with clinical measures of cognition and Alzheimer's disease pathology. Several of the observed correlations align with existing literature, while others highlight potentially complex or context-dependent relationships between gene expression and clinical phenotypes.

One notable finding was the association between the expression of *PCDHA5*, one of the most upregulated genes in resilient neurons, and better cognitive performance as measured by ADAS-Cog. Although *PCDHA5* itself has not been extensively studied in AD, other protocadherins have been associated with AD-related mechanisms. For example, PCDHGC5 is elevated in 5xFAD mouse brains, and PCDHGC5 deficiency exacerbated Aβ deposition in 5xFAD mice and astrocytic response to Aβ [454]. Yet, another study showed that Aβ increased *PCDHGC5* expression in APP/PS1 mice, and that PCDHGC5 was significantly increased in AD patient CSF [461]. Together, these findings suggest that protocadherin family members may play context-dependent roles in neurodegeneration, warranting further investigation.

Several genes correlated with higher or lower levels of CSF Tau and Aβ have previously been linked to protein aggregation. One gene, *SERF1B*, which was significantly correlated with lower CSF Aβ 42:40 (increased amyloid pathology), has been shown to promote aggregation of amyloidogenic proteins, including Aβ , in vitro and in C.elegans [367, 133, 480]. Its isoform *SERF1A* was also shown to directly interact and increase aggregation in α-synuclein in SHSY-5Y cells [299], supporting a role for SERF proteins in modulating protein aggregation across neurodegenerative diseases.
Additionally, *SPTBN4* (spectrin beta 4), a component of the axonal initial segment (AIS) [522], was correlated with higher CSF Aβ 42:40 and lower p-Tau (less amyloid

and tau pathology), and has previously been reported to be hypermethylated and transcriptionally downregulated in AD brains [403]. Interestingly, the AIS has been implicated in restricting tau localisation under physiological conditions, whereby tau diffuses through the AIS and down the axon, but its retrograde movement is blocked by the AIS. Disruption of AIS integrity allows hyperphosphorylated Tau to mislocalise to somatodendritic compartments [261], suggesting that altered AIS-associated gene expression may influence tau pathology.
Another gene of interest, *VPS13C*, which is implicated in autosomal recessive early-onset parkinsonism [255], was correlated with higher CSF Aβ 42:40 levels in this study. *VPS13C* has also been identified as associated with LOAD risk in a study of the Alzheimer's Disease Neuroimaging Initiative cohort, that compared structural MRIs of AD, MCI and control patients with over 500,000 SNPs [297].

COL5A3 was the only gene that remained significantly correlated with cognition after FDR correction, showing a strong association with worse (higher) ADAS-Cog scores. *COL5A3* was found to be upregulated in AD brains and 5XFAD mice in mixed cortical cultures and astrocytes by single-nucleus and bulk RNA sequencing [464, 536], although its functional role in AD pathophysiology remains unclear.

Finally, multiple genes involved in mitochondrial function (*PLD6, ATP5MF, ATP51FB, MRPL14, MRPL51, MTERF4*) were correlated with cognitive and biomarker measures. Mitochondrial dysfunction—including altered fusion–fission dynamics, impaired oxidative phosphorylation, and defective mitophagy [66, 279, 134]—is a well-established feature of AD and contributes to oxidative stress and neuroinflammation [154, 411, 39]. While MRPL51 has been reported to be downregulated in AD patient blood samples [273], MTERF4 has been shown to increase Aβ production by blocking a-secretase and thereby the non-amyloidogenic cleavage of APP, and was increased in APP/PS1 mice [497]. Furthermore, MTERF4 KD reduced ATP synthesis and mitochondrial DNA copy number, and decreased apoptosis, Aβ 42 release and APP levels in HEK293-APP cells [70]. The positive association between ATP synthases ATP5MF and ATP51FB and better cognition is consistent with previous reports of reduced ATP synthase levels in AD brains, as well as sAD and fAD iPSC models [338, 416, 285].

Notably, many genes associated with better cognitive performance were correlated with lower CSF Aβ 42:40 levels, whereas genes associated with worse cognition

showed the opposite pattern. Although this directionality is counter-intuitive given the established relationship between reduced CSF Aβ 42:40 and increased amyloid pathology, these discordant associations may reflect the influence of outliers (e.g. a single donor with poor cognition but high CSF Aβ 42:40, or vice versa) and limited statistical power in a small cohort, underscoring the need for validation in larger datasets.

4.5.6 Limitations and future directions

4.5.6.1 Differences in transcriptional responses in i^3 and DFP neurons

A striking observation of this chapter is the partial but incomplete overlap between Aβ-induced transcriptional changes in i^3 neurons and in DFP patient-derived neurons. While both systems showed upregulation of stress-response pathways and altered protein homeostasis, several pathways were oppositely regulated: synaptic and axonogenesis-related pathways were positively enriched in i^3 neurons following Aβ treatment, but negatively enriched in DFP neurons; and cholesterol biosynthesis was robustly upregulated in i^3 neurons but not in the DFP cohort. As discussed above, this could be attributed to the experimental design (1 isogenic line vs 13 patient lines) or the disease state (healthy vs AD) of the lines used. These results highlight the challenges– and value– of using both isogenic control models and patient-derived cohorts in parallel: the former provides mechanistic clarity, while the latter captures the inter-individual variation that is central to understanding selective vulnerability in sporadic AD. The limited gene-level overlap between the i3 and the DFP cohorts argues against a single Aβ-induced transcriptional programme, and instead supports a model in which Aβ activates a stress response that is then modulated by the underlying genetic and physiological state of each patient line.

4.5.6.2 Experimental design and vulnerability stratification of DFP neurons in bulk RNA seq

In the bulk RNA-sequencing experiment using neurons derived from AD patients from the DFP cohort, only a single biological replicate per cell line per condition was sequenced, due to practical constraints imposed by the number of patient-derived lines and treatment conditions. Because patient-derived lines are genetically heterogeneous, between-line variability exceeded treatment-induced transcriptional changes, and since each line was profiled only once per condition, within-line

variability could not be assessed, thereby reducing the power to detect robust group level differences. This was exemplified when I analysed resilient vs vulnerable lines, and saw that results could be influenced disproportionately by individual cell lines with extreme expression profiles (defined as "inconsistent genes").

As a result, it was not feasible to model Aβ-induced transcriptional changes across all patient lines using a continuous measure of clinical vulnerability. Instead, vulnerable and resilient lines were pooled to enable group-level comparisons, ranked according to donor ADAS-Cog scores. However, this stratification carries important limitations. First of all, ADAS-Cog was measured at a single timepoint rather than as a longitudinal measure of cognitive trajectory. A single score reflects cumulative disease burden at the time of assessment rather than an individual's rate of decline relative to other patients, meaning that apparent vulnerability could partly reflect differences in disease stage at sampling or accumulated amyloid and tau pathology, rather than intrinsic neuronal susceptibility. Additionally, cognitive performance is shaped by multiple interacting factors — including Aβ and tau burden, age, sex, education, APOE genotype, and time since diagnosis — yet it was not feasible to adjust for these covariates in the present study. With only 14 patients, a multivariable model would lack sufficient independent observations and carry a substantial risk of overfitting, making covariate adjustment statistically inappropriate here.

A related consideration is the use of a "consistency filter" to identify DEGs between resilient and vulnerable lines (Section 4.4.6.2). Genes were retained only if at least 3 of 4 lines in one group exhibited expression above the maximum of the opposite group. While this filter usefully removes genes whose significance is driven by a single outlier, it is a manually-defined criterion with no formal statistical framework: the 3-of-4 threshold was chosen pragmatically, the filter cannot be incorporated into the DESeq2 model, there is no guarantee that the variance it removes is unrelated to the resilient-vs-vulnerable contrast of interest. More statistically appropriate approaches are available for handling unwanted variance in small-cohort RNA-seq experiments. For example, RUVseq [383] estimates factors of unwanted variation from negative control genes or replicate samples and incorporates them as covariates in the differential expression model. Mixed-effects models that explicitly model line as a random effect can also better distinguish between- and within-line variance when multiple replicates per line are available. Applying these approaches in future work — ideally in combination with multiple biological replicates per line — would

be more rigorous and should be considered in the future.

Given these considerations, baseline transcriptional differences between resilient and vulnerable lines could be due to factors other than the vulnerability or resilience of the neurons. First, iPSC-derived neuronal cultures display inter-line variability in differentiation efficiency and expression of cortical markers (as seen in Chapter 3.3), and lines that mature at slightly different rates will show different baseline expression of synaptic, cytoskeletal, and metabolic genes — some of which featured prominently in the resilient-vs-vulnerable comparison. Second, cell-type heterogeneity within the cultures (variable proportions of excitatory neurons, inhibitory neurons, astrocytes, or residual progenitors) can drive apparent differential expression that reflects compositional differences rather than within-cell-type changes. This was not formally assessed here and would benefit from further analysis to determine whether these factors are in part driving the transcriptional differences observed in these groups.

Finally, even with multiple technical replicates, and more robust filtering and stratification methods, 14 cell lines remains a small number to look at clinical vulnerability, and sequencing of a larger cohort of sAD neurons would be more beneficial. Despite these limitations, the paired treatment design enabled within-line comparisons of Aβ response across genetically distinct backgrounds, providing insight into pathways and genes consistently altered by Aβ exposure.
The lack of biological replication and the small number of independent cell lines limit the statistical power and generalisability of baseline expression analyses between resilient and vulnerable patient lines. Nonetheless, several genes and pathways identified here have been independently implicated in Alzheimer's disease in prior studies, supporting the biological relevance of these findings. Accordingly, the findings of this study generate hypotheses that require validation in larger, more deeply replicated cohorts, as well as targeted downstream experiments.

4.6 Conclusion

In this chapter, bulk RNA sequencing was used to characterise Aβ–induced transcriptional changes in control and sporadic Alzheimer's disease patient–derived neurons. Aβ exposure elicited broad transcriptomic remodelling, affecting pathways related to stress responses, protein homeostasis, lipid metabolism, and axonal and

synaptic function. In control neurons, transcriptional changes in cholesterol-related pathways did not translate into reduced Aβ-induced neurotoxicity following genetic or pharmacological inhibition of cholesterol synthesis. Aβ did lead to an increase in lipid droplet formation suggesting that these alterations may reflect downstream stress responses rather than direct mediators of toxicity. In patient-derived neurons, substantial inter-line heterogeneity was observed; nevertheless, Aβ exposure induced significant transcriptional changes, although no Aβ-induced differentially expressed genes were detected between resilient and vulnerable patient groups. Notably, baseline differences in gene expression between resilient and vulnerable lines were identified, highlighting candidate genes and pathways that may contribute to differential vulnerability and warrant further investigation. Overall, these findings provide a foundation for future studies aimed at mechanistically validating the pathways and genes implicated here.

Chapter 5

Investigating the role Tau PFF on sporadic AD patient iPSC-derived cortical neurons from the DFP study

5.1 Introduction

The first two results chapters focused on the role of $A\beta$ on iPSC-derived cortical neurons, and showed that neurons derived from sAD patients reflected clinical measures of the donors they originate from. We focused on $A\beta$, as its accumulation is a major pathological hallmark of AD. Tau accumulation into intracellular fibrils is the other key pathological feature of AD: progression of Tau pathology in the brain has been shown to more reliably predict disease progression, and p-Tau levels in the blood are more reliable earlier biomarkers of the disease [59]. Lagomarsino, et al have shown that protein levels of p-Tau/total Tau (tTau) in iPSC-derived neurons positively associated with pTau/tTau protein in the brain of the corresponding patients. On the other hand, they showed that p-Tau/tTau levels positively associated with cognition [245]. These results suggests that iPSC-derived neurons are able to model the Tau profile of individual patients, and that they associate with clinical outcomes of those patients. However, they did not investigate the effect of Tau insults on iPSC-derived neurons, and whether the response to Tau PFFs correlates with clinical measures of the donors.

Modelling endogenous Tau seeding and aggregation in iPSC-derived neurons is challenging due to absence of 4R isoforms in developing neurons. Even after 100 days in culture, control cortical neurons express mainly 0N3R Tau [443]. In lines expressing pathogenic fronto-temporal dementia (FTD) mutations in Tau (e.g. P301S, P301L, S305 and IVS 10+16) – which can cause increased seeding and

aggregation propensity and increased exon 10 inclusion – 0N4R tau is detected after a few weeks in culture and it takes up to a year to see all 6 Tau isoforms present in the human brain [202, 443, 54]. Multiple groups have shown that no tau inclusions form, even in neurons carrying FTD-causing mutations, after several weeks in culture [353, 485, 486]. Paonessa et al observed changes in Tau phosphorylation and mislocalisation in lines harboring FTD-causing mutations, but no aggregation after 120 days in culture [350].

Another strategy to recapitulate Tau pathology in iPSC models is to treat iPSC-derived cortical neurons with Tau aggregates. In this regard, the majority of the work so far has focused on whether tau aggregates were internalised by neurons and induced phosphorylation of endogenous tau. The results so far are inconsistent: several groups have shown that the inclusion of pathological *MAPT* FTD mutations (e.g. P301s, P301L and Exon 10+16) were required for the aggregation of endogenous Tau after seeding with truncated 4R Tau fibrils (K18) with or without P301L mutations [486, 485, 353]; while two studies reported that full-length 2N4R tau was internalised and increased endogenous tau phosphorylation in control iPSC neurons [476, 286]. Other groups have demonstrated that AD brain derived pathological Tau was internalised by wild-type iPSC neurons in a time- and concentration-dependent manner [281, 501].
Less work has been done to characterise the downstream effect of Tau seeding. Two studies have found that Tau oligomers, specifically, caused neurite degeneration and neuronal loss [476], while monomers and fibrils did not [286], and one study identified calcium release, neuronal activity and endolysosomal trafficking deficits [353]. No research so far has investigated the effect of Tau PFF insult on sporadic AD iPSC-derived cortical neurons and I aim to address this gap using the DFP cohort neurons.

The aims of this chapter are to:

- Characterise Tau expression and Tau release in the iPSC-derived cortical neurons of the DFP cohort.
- Investigate the effect of Tau preformed fibrils (PFF) treatment on various cellular phenotypes, and whether it reflects clinical measurements of the donors.
- Determine whether Tau PFFs induce transcriptomic changes in i3 cortical neurons.

5.2 Characterisation of Tau expression in iPSC derived cortical neurons

5.2.1 Tau and p-Tau protein expression

To characterise Tau expression in iPSC derived neurons from the DFP cohort, neurons were grown in monoculture to Day 30, then harvested for RNA and protein extraction, and the media was saved to measure Tau and p-Tau release (discussed in the next section). Day 30 was the longest I could reliably culture the neurons without astrocytes before the neurons started peeling. Samples from 3 independent differentiations were collected and frozen down so that RNA and protein could be extracted together to minimise variability (Chapter 2.9). Furthermore, for all of the experiments described in this chapter, I also included a *MAPT* -/- line, which retains less than 1 % residual Tau expression [323], and an iPSC-line carrying the Tau P301S and Exon 10+16 mutations (referred to as P301S from now on) [443], as controls for Tau expression and Tau seeding assays.
I examined the RNA expression of Total Tau (tTau) and GSK3β, one of the major enzymes responsible for phosphorylating Tau, which has been shown to be increased in AD neurons (Figure 5.1, A-B) [334]. For protein expression (Figure 5.1, C), I analysed several species of phospho-tau associated with Tau pathology, namely S396, a marker associated with late pathology [344], AT8, which recognises Tau phosphorylated at both Ser202 and Thr205; and AT180, which recognises Tau at phospho-Thr231, both markers of early pathology [26, 55, 158]. When comparing protein and RNA levels, I normalised all values to one reference cell line, (Line 928), to correct for the variability in band intensity between blots, and inter-plate variability for qPCR.

GSK3β and p-GSK3β expression did not differ significantly between cell lines (5.1, A, H, I), whereas both RNA expression and protein levels of tTau were significantly different between patient lines (5.1, B, D). Furthermore, there was a significant difference in protein levels of p-Tau S396 and AT8 between different patient lines, but not AT180 (Figure 5.1, E-G). The lower band in the AT180 blot is faintly visible in the *MAPT* -/- lane, though it seems to be slightly higher than the lower band in the AD lanes. Nonetheless, it is possible that this antibody is not entirely specific for p-Tau Thr231. For S396, AT8 and Tau5, however, there was a clear absence of protein band in the *MAPT* -/- lane (Figure 5.1, C), confirming their specificity for tau. Protein levels of tau and p-tau in P301S neurons were within the

range of the DFP neurons levels. To note, only one differentiation of P301S neurons was included in this analysis due to culturing difficulties.
Next, I looked at the ratio of p-Tau/tTau and p-GSK3β/GSK3β. CSF p-Tau/tTau ratio is also used as a biomarker in AD [31], while a higher p-GSK3β/GSK3β ratio can be indicative of higher increased enzymatic activity and thereby tau phosphorylation. There were no significant differences between the patient neurons in the ratio of any p-Tau/tTau or p-GSK3β/GSK3β (Figure 5.1, J-M), nor were there significant correlation between p-GSK3β/GSK3β and any Tau species (Figure 5.1, N). Of note, the *MAPT* -/- line was not included in these analyses of variance between lines, as it would confound the analysis. It was used as a negative technical control, to demonstrate the specificity of the primers and antibodies used.

I was interested in seeing whether Tau protein levels in the iPSC-neurons reflected those of the patients they originate from, looking at both CSF Tau and Tau PET. There was a strong positive correlation between Tau PET and both total Tau and pTau AT8 protein levels, and a trending positive correlation with pTau S396 (Figure 5.1, O-Q). Furthermore, higher pTauS396:tTau ratio correlated with cognitive decline (MMSE loss rate), though this was strongly driven by one cell line (Figure 5.1, R). On the other hand, there was no correlation between protein levels of tTau, pTau S396, pTau AT8 and p-Tau/tTau (S396 and AT8) with CSF Tau, pTau or p-Tau/tTau ratio, respectively (Figure 5.1, S-W).

Here, I have characterised Tau expression in the AD patient lines, and have found that increased Tau expression reflects PET Tau signal, but not CSF levels in the donor patients, and is correlated positively with cognitive decline.

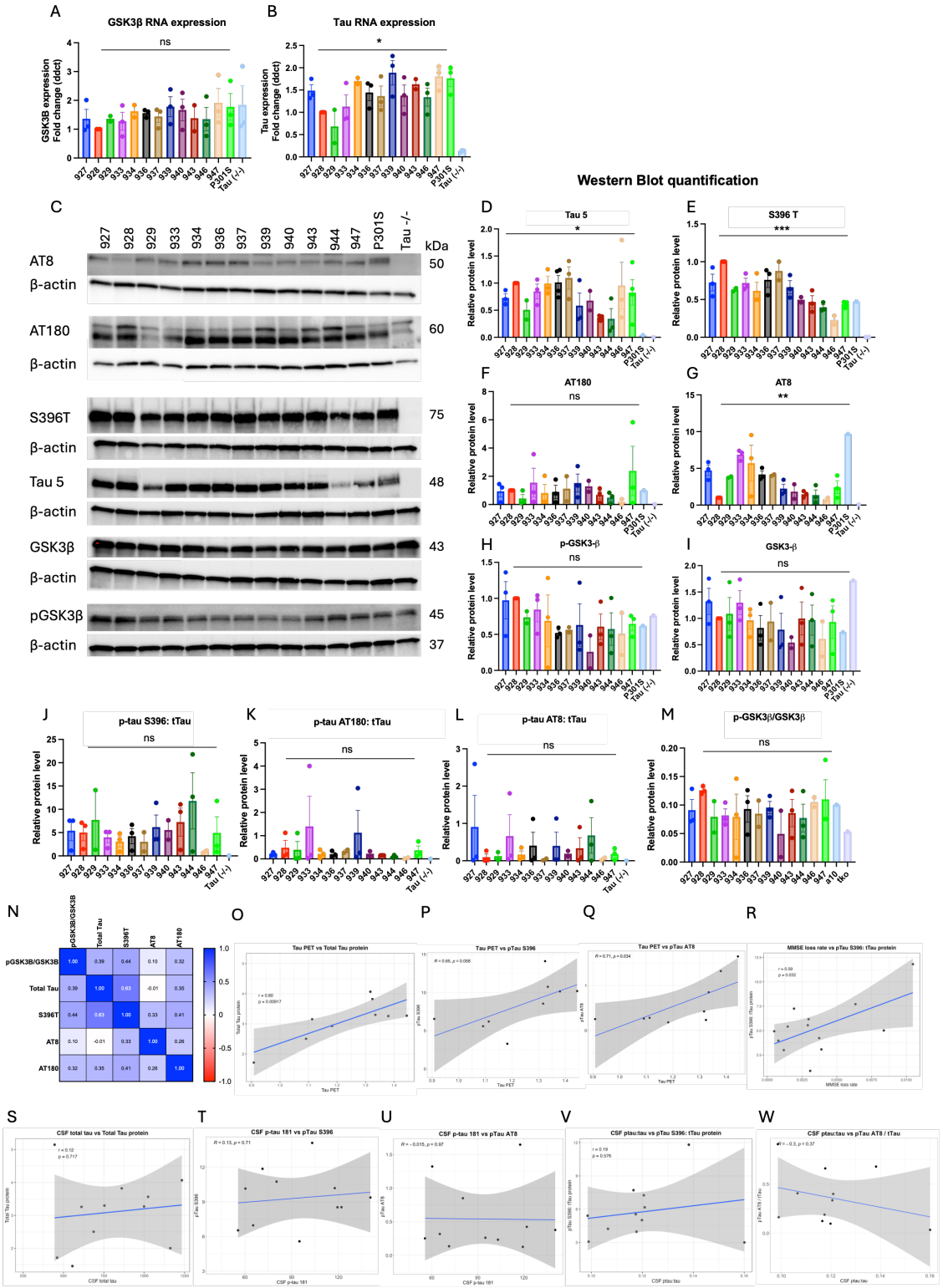


Figure 5.1: **Expression of Tau, p-Tau and GSK3β by iPSC derived cortical neurons**

Figure 5.1: Continued: (A-B) RNA expression of GSK3β (A) and tTau (B) in Day 30 iPSC derived neurons, normalised to GAPDH (ddct). (C) Immunoblots of AT8, AT180, S396T, Tau5, GSK3β and p-GSK3β and with B-actin as control. (D-I) Quantification of protein levels in 13 sAD patient lines, as well as a P301s and a *MAPT -/-* line. Protein levels are normalised to B-actin and do a reference sample (Line 928). (J-L) p-Tau/tTau protein level ratio. (M) p-GSK3β/GSK3β protein level ratio. (N) Correlation matrix (Pearson's) of p-GSK3β/GSK3β with tTau and p-Tau expression. (O-W) Simple linear regressions of p-Tau/tTau and tTau protein levels in iPSC-derived cortical neurons with clinical measures. Mean ± SEM n=3 independent differentiations. (A-M) Ordinary One-Way ANOVA with Tukey's multiple comparisons test. (N-W) Pearson's correlation with two-tailed p-value and 95% CI. $p < 0.05$ ($*$), $p < 0.01$ ($**$), $p < 0.001$ ($***$), $p < 0.0001$ ($****$)

5.2.2 Tau release in conditioned media

Previous work in the DFP cohort has shown that $A\beta42$ release in conditioned media correlated significantly with levels of CSF $A\beta42$ of the patients [322], and I therefore asked whether that was also the case of Tau and p-Tau secretion in conditioned media by ELISA. Of note, this experiment was only performed on cells from one differentiation in triplicates; statistical tests should therefore be considered preliminary. There was a significant difference in tTau secretion between patient lines, but secretion did not correlate with CSF Tau (Figure 5.2, E, H, I). I expected p-Tau levels in conditioned media to be low, and therefore attempted to increase the signal by adding conditioned media for three, 90 min incubations instead of one, 2 h incubation. However, the levels of p-Tau 181 were all situated between the negative control and first standard on the standard curve and were therefore too low to determine the concentration (Figure 5.2, B, F). However, given that the triplicate coefficient of variation for all samples was under 11 %, I decided to use the raw absorbance values for downstream analysis. P-Tau levels were stable across patient lines, and there was a positive but non-significant correlation between levels of secreted p-Tau 181 and CSF p-Tau 181 levels (Figure 5.2 F, J). Next, I calculated the p-Tau to Tau ratio for each cell line using the raw absorbance values, which was significantly different between patient lines (Figure 5.2, G). As with tTau, however, there was no correlation between secreted p-Tau 181:Tau and CSF pTau 181: Tau (Figure 5.2, K). Furthermore, p-Tau and Tau release in conditioned media did not correlate with pTau and Tau protein expression in the neurons (Figure 5.2, L-M).

This experiment demonstrated that levels of secreted tTau were not reflective

of CSF Tau levels of corresponding patient, nor of Tau protein levels in the neurons. Furthermore, p-Tau 181 concentration in media is too low to be reliably measured with the ELISA, and though it correlated positively with CSF p-tau, a more sensitive detection method is required to draw firm conclusions.

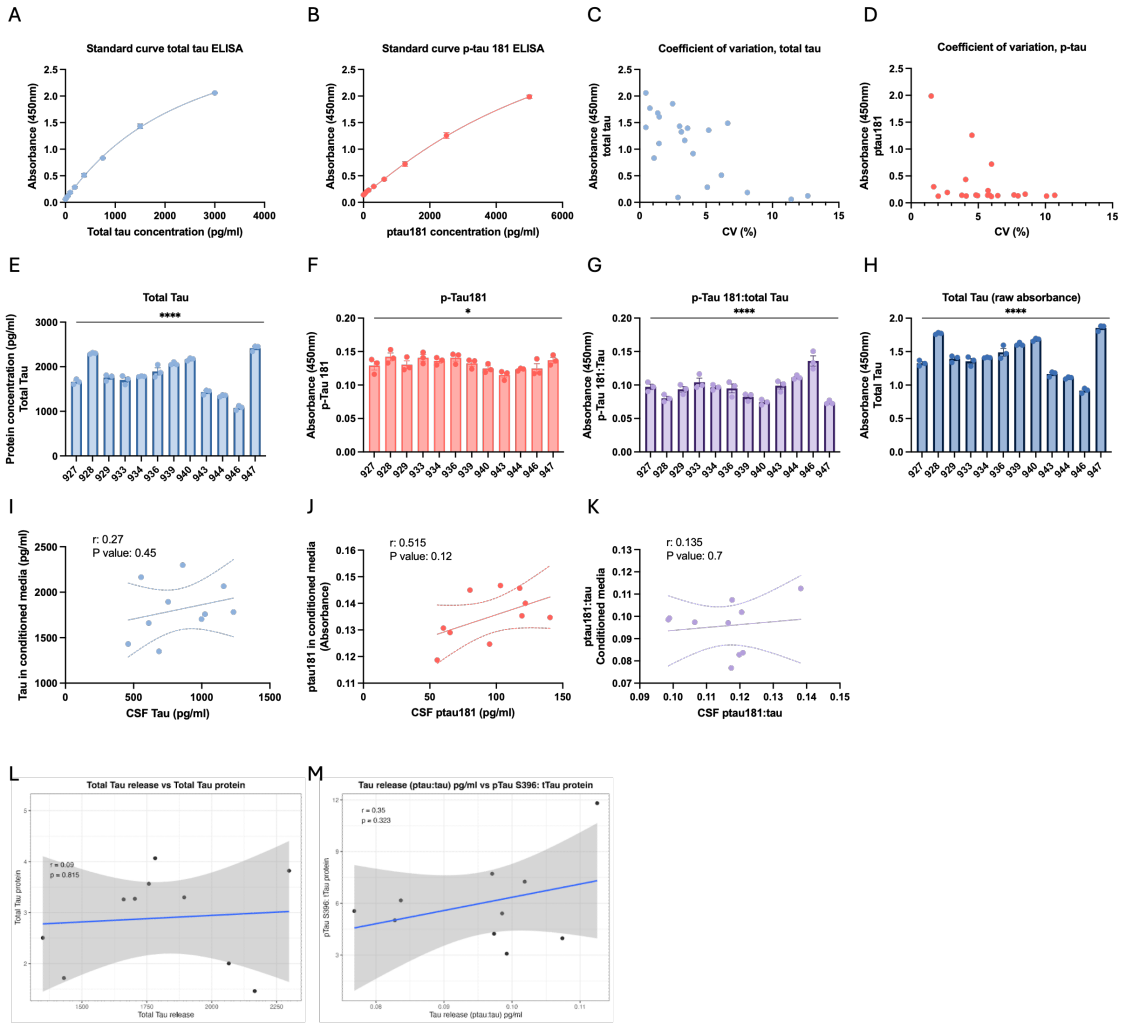


Figure 5.2: **Secretion of Tau and p-Tau by iPSC derived cortical neurons does not correlate with CSF tau and pTau**. (A-B) Standard curve of the Tau (A) and p-Tau 181 (B) ELISAs. (C-D) Coefficient of variation (CV) plot between CV and absorbance values for tTau (C) and p-Tau (D). (E) tTau protein concentration in conditioned media (pg/ml). (F-H) Raw absorbance values for p-Tau (F), p-Tau/tTau (G), and tTau (H). (I-K) Pearson's correlation with linear regression line between secreted tTau (I), p-Tau 181 (J) and p-Tau 181: tTau (K) from iPSC neurons and CSF Tau concentration of the corresponding patients. (L-M) Simple linear regression between p-Tau/tTau release and tTau (L) or p-Tau/tTau (M) protein levels in iPSC-derived cortical neurons. Mean ± SEM n=3 replicates from 1 differentiation. (E-H) Ordinary One-way ANOVA with Tukey's multiple comparisons test. (A) (I-M) Simple linear regression (pearson's correlation) with two-tailed p-value and 95 % CI. $p < 0.05$ (*), $p < 0.01$ (**), $p < 0.001$ (***), $p < 0.0001$ (****).

5.3 Neurite tracing in iPSC-derived cortical neurons treated with Tau preformed fibrils

5.3.1 Co-culture of with astrocytes

5.3.1.1 Neurite outgrowth and branching

Given the greater inter-differentiation consistency and correlation with clinical data observed in Day 7 but not Day 70 in Chapter 3.5, I decided to focus on the Day 7 timepoint to look at the effect of Tau PFFs insult on neurite outgrowth in the DFP iPSC-derived neurons. The same experimental set-up described in Chapter 3 was used here: Neurons transduced with a low titer of NgN2-GFP lentivirus (more details in Chapter 2.3 and Chapter 3.4), co-cultured with astrocytes, were treated with either 1.25, 2.5 to 5 μg/mL of full length 2N4R Tau PFFs and imaged daily for 7 days . 2N4R tau was chosen over other commonly used tau insults , such as K18 PFFS or PFFs carrying FTD mutation, as they are more physiologically relevant to AD than the truncated or mutated forms of tau. Furthermore, 2N4R tau is the longest isoform and therefore contains every domain, and is more aggregation prone than other tau isoforms, due to the presence of 4 microtubule binding repeats.
In this case, the negative control was the PFF vehicle, and I also included a positive control of 2.5 μg/ml PFF with 20 μM of chloroquine (CQ). CQ inhibits lysosomal degradation and therefore should prevent the clearance of fibrils from the cells [231]. The *MAPT -/-* and P301S line were included as negative and positive control to Tau PFF seeding, since the *MAPT -/-* line has nearly no endogenous Tau to seed with and the P301S line has been shown to have increased Tau aggregation upon seeding with fibrils [443, 486].

Unlike with amyloid treatment, Tau PFFs alone caused no neurite loss in the neurons cocultured with astrocytes. The neurites grew consistently between the first and last day of imaging (Figure 5.3, A, Figure 5.4, A,B). 7 days post PFF treatment, most AD lines exhibited a decrease in total neurite length only in the CQ condition (relative to Day 0), which was significant in lines 939 and 944 (Figure 5.4, A). When all cell lines were pooled together, there was significant decrease in neurite length in the cells treated with 2.5 μg/mL PFF + CQ (Figure 5.4, B). The same trend was seen for the number of nodes (Figure 5.4, C-D). Interestingly, there was no difference in the effect of Tau PFF between the sAD patients, the *MAPT -/-* and the P301S lines, suggesting that any toxicity observed was due to the addition

of fibrils rather than seeding and aggregation downstream of insult. Thus, this experiment showed that Tau PFF have minimal effect on neurite outgrowth in Day 7 cortical neurons cocultured with astrocytes, except when paired with CQ. Given that a CQ-only condition was not included in these experiments, it is possible that the effects observed in the Tau PFF+CQ condition are due to CQ-induced toxicity and future experiments should include this control condition.

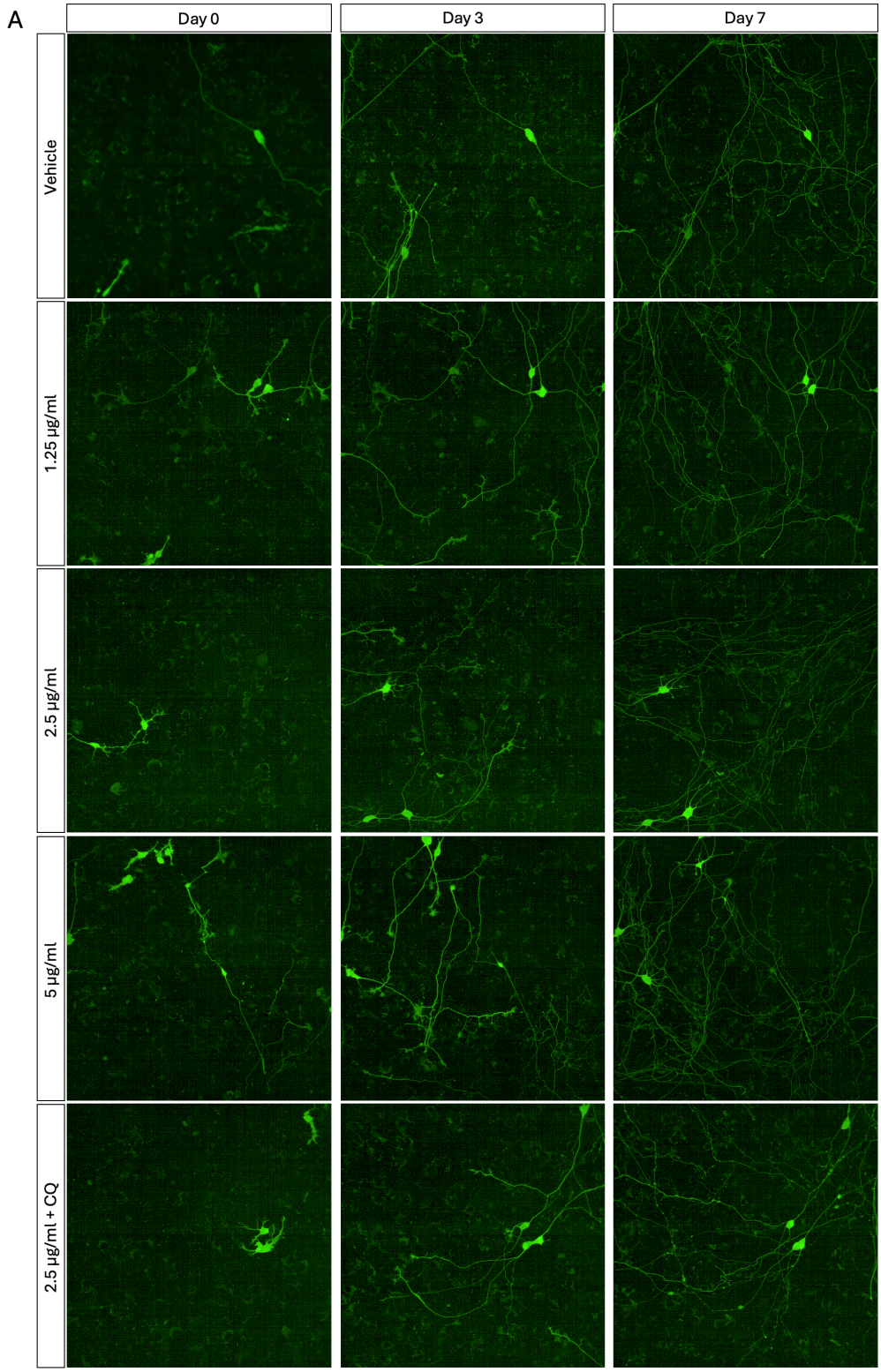


Figure 5.3: **Representative images of DFP cortical neurons cocultured with astrocytes show no effect of Tau PFFs** (A) Representative images of GFP+ neurons at Day 0, Day 3 and Day 7 of imaging (left to right), treated with vehicle, 1.25 μg/mL, 2.5 μg/mL, 5 μg/mL, 2.5 μg/mL + 1 μM CQ. 20X objective, scale bar= 100 μm

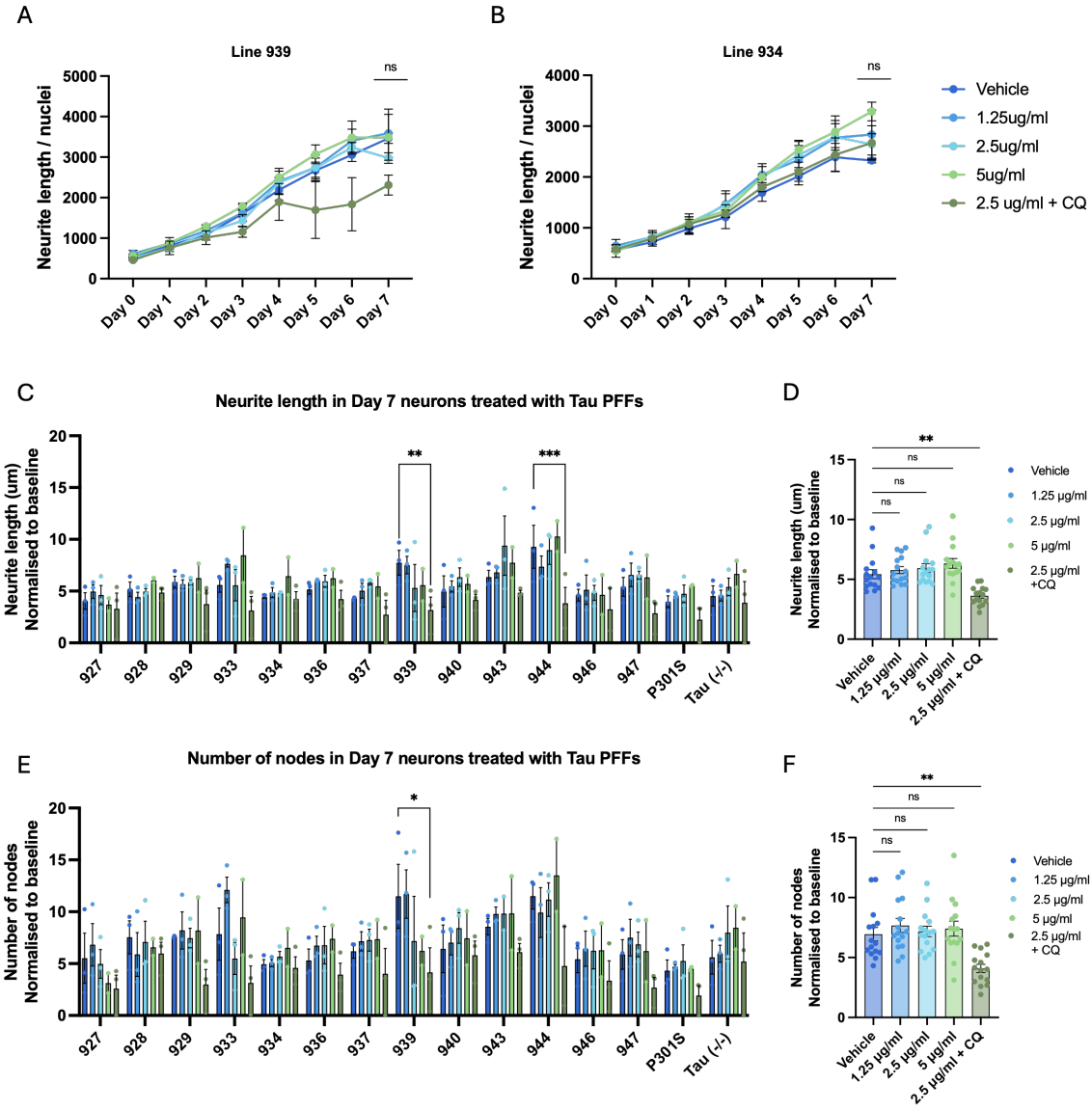


Figure 5.4: **Tau PFFs did not induce neurite loss in DFP cortical neurons cocultured with astrocytes.** (A-B) Representative line graphs of the neurite length (normalised by number of cells) over 7 days in 2 sAD patient lines (939 and 934). No significant change was seen between treatments. (C) Change in neurite length between Day 7 and Day 0 (baseline) in 13 sAD, P301S and *MAPT* -/- lines. Decrease observed in the 2.5 μg/mL + 1 μM CQ was only significant in line 939 and 944. (D) Change in neurite length averaged across all lines. (E) Change in number of nodes between Day 7 and Day 0 (baseline) in 13 sAD, P301S and *MAPT* -/- lines. (F) Change in number of nodes averaged across all lines. Significant decrease between the vehicle and 2.5 μg/mL + 1 μM CQ conditions. Mean ± SEM n=3 independent differentiation repeats averaged over 6 technical replicates.

Figure 5.4: (continued) (A-B) Mixed effect repeated measures model with FDR method of Benjamini and Hochberg corrections for multiple comparisons. (C,E) 2-way ANOVA with Dunnett's multiple comparisons test. (D, F) Kruskal-Wallis test with Dunn's multiple comparisons test.$p < 0.05$ $(*)$, $p < 0.01$ $(**)$, $p < 0.001$ $(***)$, $p < 0.0001$ $(****)$. For all graphs, each dot is one differentiation, except for bar plot averaging across cell lines, where each dot is a cell line.

5.3.1.2 Cell viability

To see whether general cell viability was affected by Tau PFF despite the lack of neurite loss, I looked at nuclei count and AK release in conditioned media. Consistent with the effect on neurite outgrowth, there was no change in nuclei count after 7 days of PFF insult between the treated conditions and the vehicle, except for a significant decrease in nuclei in the 2.5 μg/mL + CQ condition (Figure 5.5, A, B). However, AK release trended upwards in the 2.5 μg/mL condition, and significantly increased in the 1.25 μg/mL, 5 μg/mL, and 2.5 μg/mL PFF + CQ conditions (Figure 5.5, C, D).

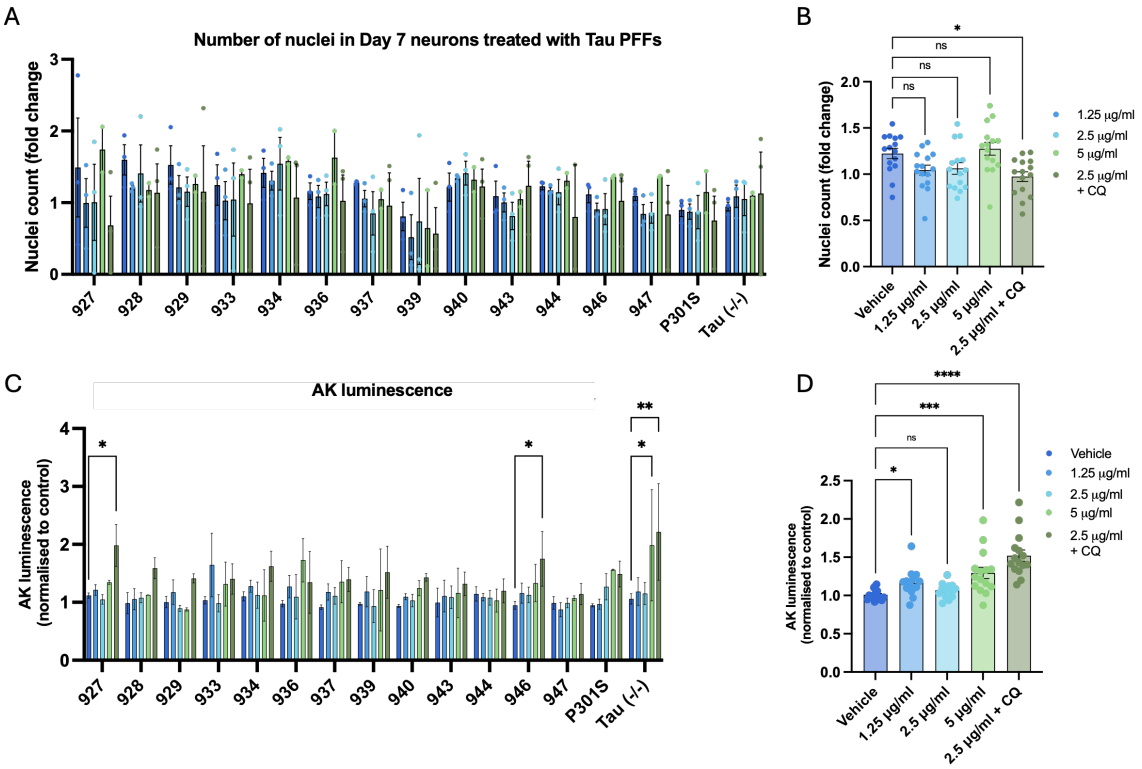


Figure 5.5: **Tau PFFs induce moderate nuclei loss and AK release in DFP cortical neurons co-cultured with astrocytes.** (A-B) Change in number of nuclei after Tau PFF insult between Day 7 and Day 0 (treatment day = baseline) in 13 sAD, P301S and *MAPT* -/- lines (A) or averaged across all lines (B). (C-D) AK release in conditioned media normalised to baseline in 13 sAD, P301S and *MAPT* -/- lines (A) or averaged across all lines. Mean ± SEM n=3 independent differentiations repeat averaged over 6 technical replicates. (A,C) 2-way ANOVA with Dunnett's multiple comparisons test. (B,D) Kruskal-Wallis test with Dunn's mulitple comparisons test.$p < 0.05$ $(*)$, $p < 0.01$ $(**)$, $p < 0.001$ $(***)$, $p < 0.0001$ $(****)$.For all graphs, each dot is one differentiation, except for bar plot averaging across cell lines, where each dot is a cell line.

5.3.2 Cortical neuron monoculture

5.3.2.1 Neurite outgrowth and branching

Given that the astrocytes have been shown to internalise Tau PFFs [54], and help with adhesion of neurons, I wondered whether they might be protecting neurons from any Tau-induced toxicity. Therefore, I next asked whether Tau PFFs induced neurite loss in cortical neurons grown without astrocytes. Indeed, Tau PFF insult caused neurite loss in the DFP neurons, although some patient lines were more vulnerable to Tau PFFs and lost more neurites than others (Figure 5.6, A; Figure 5.7, A-B, D).

Nonetheless, averaging all patient lines, Tau PFF insult caused a decrease in neurite outgrowth (Figure 5.7, E). The *MAPT* -/- neurons had no significant decrease in neurite length, except in the PFF + CQ condition (Figure 5.7, C).
To account for differences in growth rate between cell lines, I normalised the neurite length at Day 7 of the PFF-treated neurons with the vehicle-treated neurons and then compared the % neurite loss between each line. There were marked differences in the amount of neurite loss between patient lines. At 1.25 μg/mL, the decrease ranged from 0.2 % to 55 %, the average loss being about 33 %, and *MAPT* -/- cells lost 7 % neurites relative to control (Figure 5.7,F). At 2.5 μg/mL, it ranged between 12 % and 64 %, the average was 36 % and *MAPT* -/- cells lost 30 % neurites (Figure 5.7,G). At 5 μg/mL, neurite loss ranged from 1.4 % to 56 %, the average was 32 % and *MAPT* -/- cells lost about 30 % as well (Figure 5.7,H). Although, there is a wide range in neurite loss between patient lines, due to the variability between differentiations (such as exhibited by line 940 in Figure 5.7, F, or 933 in 5.7 G and H), this difference was not significant. Furthermore, unlike with the $A\beta$ treatment, where there was a clear dose-dependent effect of treatments, here, the effect was similar between all 3 Tau PFF concentrations. Interestingly, some lines were consistently vulnerable (Line 927, 946) or resilient (Line 936) to both $A\beta$ and tau PFFs (defined by the amount of neurite loss), other patient lines had opposite patterns: Line 934 was one of the most vulnerable to Tau PFF insults (more neurite loss), but was resilient to $A\beta$ insult, while line 940 was resilient to Tau PFF insult (less neurite loss) but vulnerable to $A\beta$ insult.

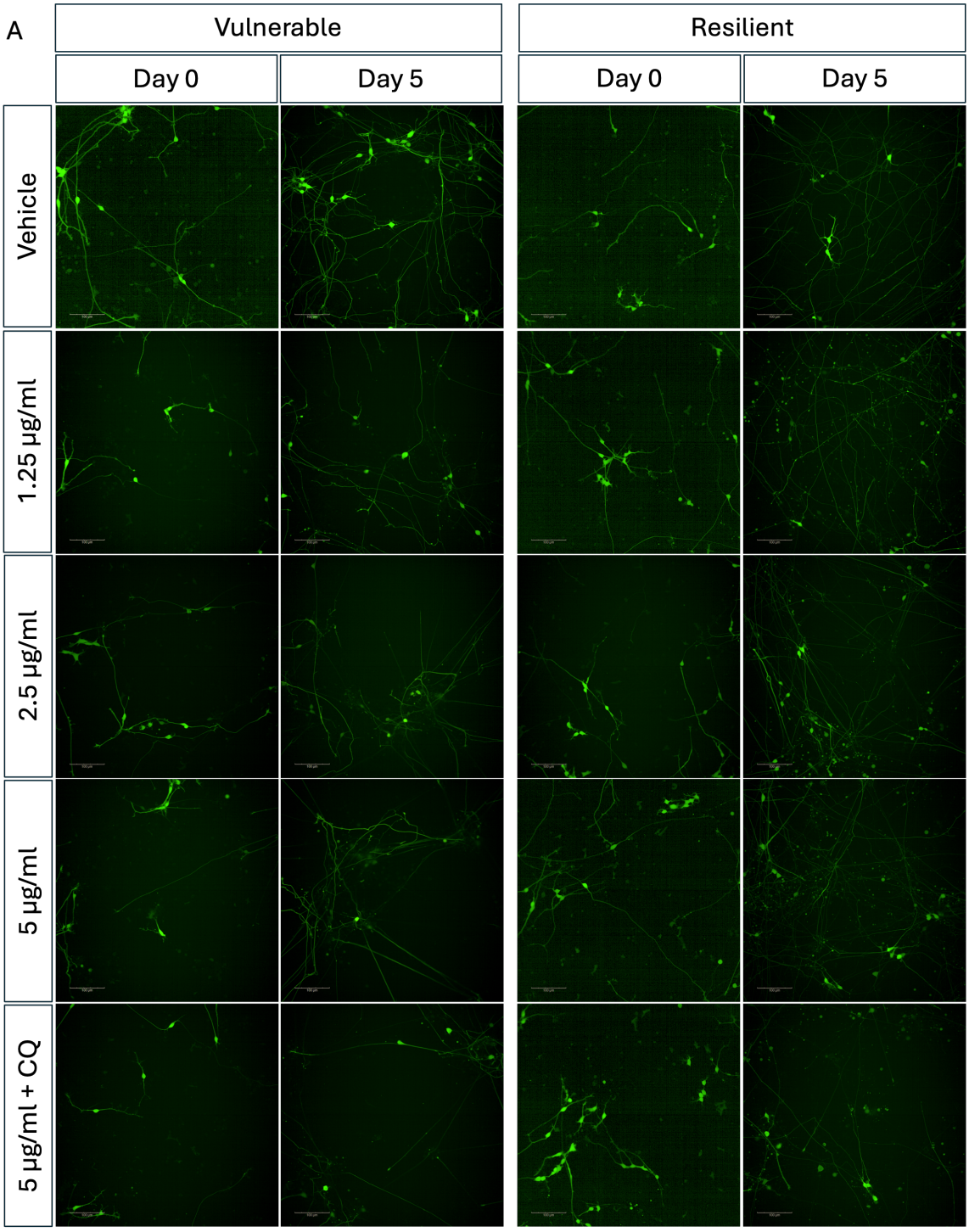


Figure 5.6: **Representative images of DFP cortical neurons treated with tau PFFs show neurite loss due to PFFs** (A-B) Representative images of neurons from vulnerable and resilient lines (defined by amount of neurite loss due to Tau PFFs) at 0 and 6 days after PFF insult (left to right), treated with vehicle, 1.25 μg/mL, 2.5 μg/mL, 5 μg/mL, 2.5 μg/mL + 1 μM CQ. 20X objective, scale bar= 100 μm.

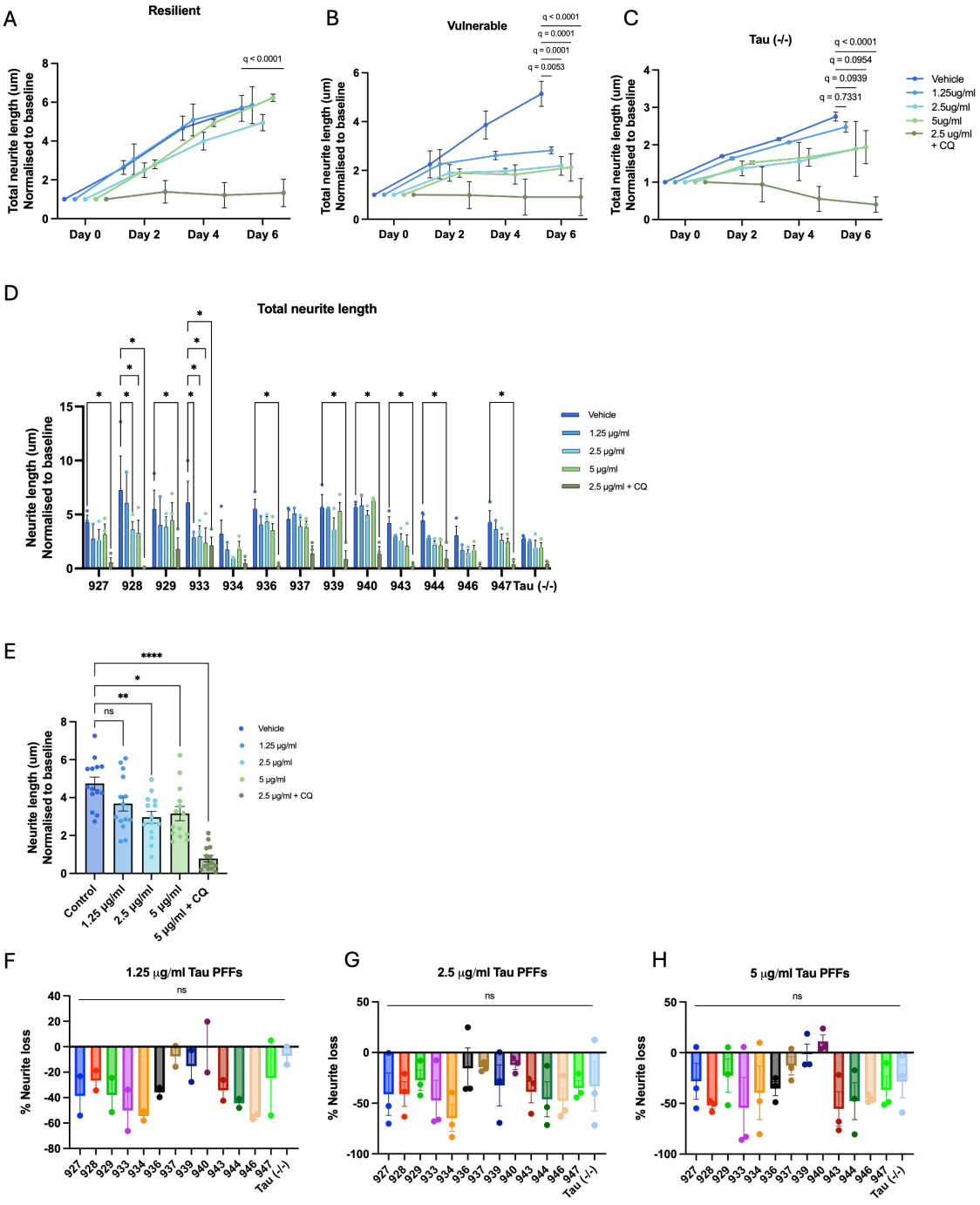


Figure 5.7: **Tau PFFs induce neurite loss in DFP cortical neurons**. (A-C) Representative line graphs of the neurite length (normalised by number of cells) over 6 days in a resilient (A) and vulnerable (B) sAD line and in the *MAPT* -/- line (C). (D) Change in neurite length between Day 6 and Day 0 (baseline) in 13 sAD and *MAPT* -/- lines. (E) Change in neurite length averaged across all lines shows dose dependent, significant decrease in neurite length. (F-H) % change in neurite length 6 day after PFF insult, normalised to control at 1.25 μg/mL (F), 2.5 μg/mL (G) and 5 μg/mL (H). Mean ± SEM n=2-3 independent differentiations repeat averaged over 6 technical replicates.

Figure 5.7: (continued) (A-C) Mixed effect repeated measures model with FDR method of Benjamini and Hochberg corrections for multiple comparisons. (D) 2-way ANOVA with Dunnett's multiple comparisons test. (E-H) Brown-Forsythe and Welch One-way ANOVA tests with Dunnett's T3 multiple comparison test. $p < 0.05$ $(*)$, $p < 0.01$ $(**)$, $p < 0.001$ $(***)$, $p < 0.0001$ $(****)$. For all graphs, each dot is one differentiation, except for bar plot averaging across cell lines, where each dot is a cell line.

Similarly, when looking at branching, Tau PFF caused a loss nodes in the patient neurons, though the effect varied between cell lines (Figure 5.8, A, B). When normalised to vehicle, the % loss in nodes ranged from 2 % and 60 % in the 1.25 μg/mL condition, from a 14 % increase to 60 % decrease in the 2.5 μg/mL condition, and from 2 % to 60 % in the 5 μg/mL condition (Figure 5.8, C-F). The difference in loss of nodes between patient line due 5 μg/mL PFFs was significant.(Figure 5.8, E). Across treatment concentrations, the average loss of nodes was 30 %, except for the 2.5 μg/mL PFF + CQ, which led to a 89 % decrease in nodes. The *MAPT* -/- neurons lost 0 %, 25 % and 12 % of the nodes in the 1.25, 2.5 and 5 μg/mL conditions, respectively.

The PFFs caused neurite and branching loss in the *MAPT* -/- cells as well, though to a lesser extent than some of the sAD lines, especially in the 1.25 μg/mL condition. This suggests that at least some of the loss observed is due to inherent toxicity of fibrils rather than due to downstream seeding. Nonetheless, the effect of Tau PFFs was markedly increased without astrocytes. Whether that is due to the astrocytes internalising fibrils or because they simply help with adhesion and overall health of neurons needs to be further investigated.

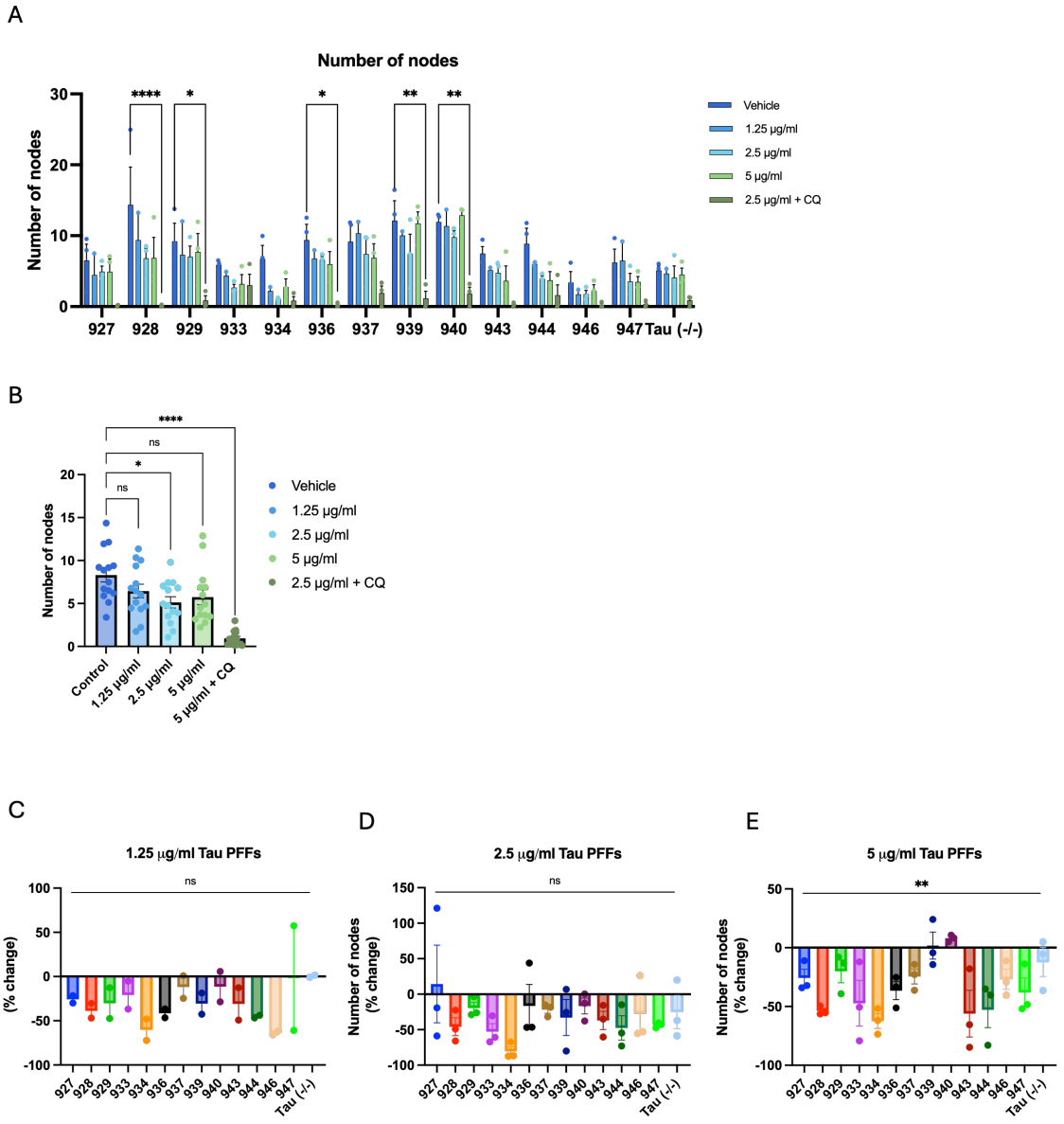


Figure 5.8: **Tau PFFs induce loss of nodes in DFP cortical neurons**. (A) Change in number of nodes between Day 6 and Day 0 (baseline) in 13 sAD and *MAPT -/-* lines. (B) Change in neurite length averaged across all lines shows dose dependent, significant decrease in number of nodes. (C-E) % change in neurite length 6 days after PFF insult, normalised to control at 1.25 μg/mL (C), 2.5 μg/mL (D) and 5 μg/mL (E). Mean $\pm$ SEM n=2-3 independent differentiations repeat averaged over 6 technical replicates. (A) 2-way ANOVA with Dunnett's multiple comparisons test. (B-E) Brown-Forsythe and Welch One-way ANOVA tests with Dunnett's T3 multiple comparison test. $p < 0.05$ $(*)$, $p < 0.01$ $(**)$, $p < 0.001$ $(***)$, $p < 0.0001$ $(****)$. For all graphs, each dot is one differentiation, except for bar plot averaging across cell lines, where each dot is a cell line.

5.3.2.2 Cell viability

Next, I looked at whether Tau PFFs also caused more cell death when neurons are in monoculture by measuring nuclei loss and AK release in the conditioned media. Unsurprisingly, Tau treatment caused a dose dependent decrease in nuclei across all cell lines (Figure 5.9, A, B). However, even though AK luminescence trended towards an increase in treated conditions compared to control, the increase was only significant between the control condition and the 1.25 μg/mL and 2.5 μg/mL + PFF conditions (Figure 5.9, C,D). This is different from what I observed when neurons were co-cultured with astrocytes, where I saw no loss in nuclei (except with PFF + CQ) but a significant increase in AK release across all treatment conditions. In conclusion, sAD neurons cultured without astrocytes are more vulnerable to Tau PFF insult, which leads to a decrease in neurite outgrowth and branching, as well as a cell death.

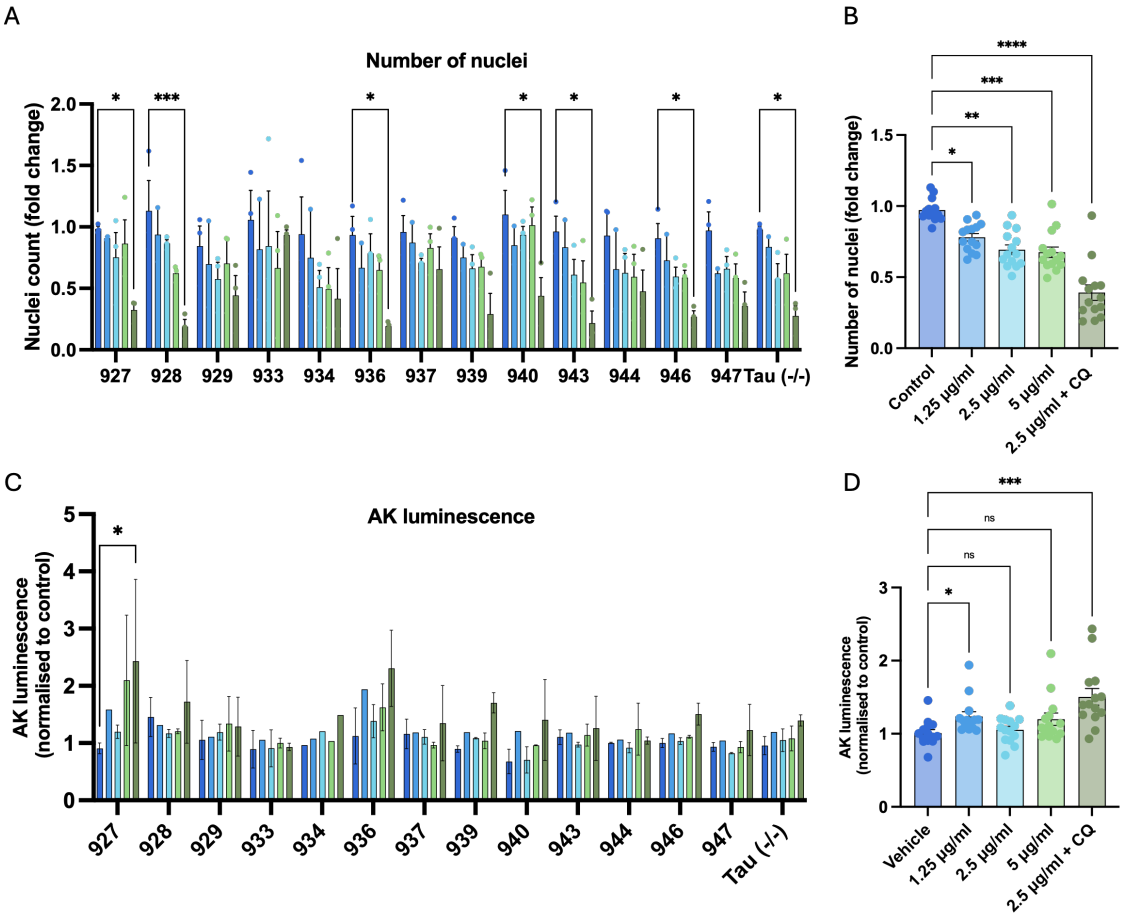


Figure 5.9: **Tau PFFs induce nuclei loss and AK release in DFP cortical neurons .** (A-B) Change in number of nuclei after Tau PFF insult between Day 7 and Day 0 (treatment day = baseline) in 13 sAD, P301S and *MAPT* -/- lines (A) or averaged across all lines (B). (C-D) AK release in conditioned media normalised to baseline in 13 sAD, P301S and *MAPT* -/- lines (A) or averaged across all lines. Mean ± SEM n=2-3 independent differentiations repeat averaged over 6 technical replicates. (A,C) 2-way ANOVA with Dunnett's multiple comparisons test. (B,D) Kruskal-Wallis test with Dunn's mulitple comparisons test. $p < 0.05$ $(*)$, $p < 0.01$ $(**)$, $p < 0.001$ $(***)$, $p < 0.0001$ $(****)$. For all graphs, each dot is one differentiation, except for bar plot averaging across cell lines, where each dot is a cell line.

5.3.2.3 Correlation of Tau PFF-induced neurite loss in iPSC-derived cortical neurons with clinical measures of sAD patients

In Chapter 3, it was established that there are significant correlations between the amount of neurite loss cause by $A\beta$ treatment and several clinical measures of the patients, namely, hippocampal volume corrected by CSF $A\beta$42:40. Furthermore, a study had shown that the level of p-Tau/tTau protein in patient-derived cells

positively correlated with brain pTau/tTau protein levels of the donor patients [245]. On the other hand, they reported a negative association between increased cellular pTau/tTau protein and Tau tangles, which also associated with better cognition.

As described above, while I did not observe a significant correlation between p-Tau/tTau levels in conditioned media with any clinical measure (Figure 5.2), there was a correlation between the increased p-Tau/tTau in cells and cognitive decline, as well as a positive association between pTau (AT8) and tTau with PET amyloid of patients (Figure 5.1). I therefore sought to find out whether neurite loss caused by Tau PFFs in cortical neurons also correlated with clinical measures of patients in the DFP cohort.

I first verified that the amount of loss in each cell line was consistent across differentiations and treatment concentrations. Indeed, there was a positive correlation between the 3 differentiations, and a strong positive correlation between the 3 treatment concentrations (5.10, A-B). Then, the correlations between neurite loss at 1.25 μg/mL, 2.5 μg/mL and 5 μg/mL and clinical measures were calculated. I was particularly interested in whether, as with Aβ insult, Tau PFF-induced neurite loss would be correlated with the corrected hippocampal volume normalised by each participant's Tau burden, as determined by CSF and PET Tau levels. As described in Chapter 3.4.4, this ratio was calculated to consider individual differences in clinical susceptibility to Tau pathology. There was a moderate but significant negative correlation between hippocampal volume normalised to tTau, but not pTau, and neurite loss in 1.25 μg/mL and 2.5 μg/mL conditions, though it was not significant in the 5 μg/mL condition (Figure 5.10, D).

Next, I generated a correlation matrix of all treatment conditions correlated with all clinical measures, and given the exploratory nature of this analysis, I looked at unadjusted p-values (Figure 5.10, C). Higher CSF $A\beta$42:40 was significantly correlated with increased neurite loss at all concentrations (Figure 5.10, E), and this association was also significant between higher CSF $A\beta$42 and higher neurite loss at 1.25 μg/mL and 2.5 μg/mL conditions (Figure 5.10, F). This is counter-intuitive, given higher CSF $A\beta$42:40 is associated with lower disease severity. On the other hand, higher PET Amyloid (i.e. higher amyloid pathology), was associated with more severe neurite loss at 1.25 μg/mL and 2.5 μg/mL conditions (Figure 5.10, G). After Benjamini-Hochberg correction, the correlation between amyloid PET and neurite loss was the only remaining significant correlation (padj=0.03).

Finally, I interrogated whether cellular and secreted pTau and tTau levels were associated with the severity of PFF-induced neurite loss. Interestingly, increased

secreted p-Tau/tTau levels of the cortical neurons was strongly correlated to increased neurite loss at all concentrations of Tau PFFs (Figure 5.10, J), while cellular p-Tau/tTau protein levels in neurons was not (Figure 5.10, K).

Collectively, these results show that greater neurite loss due to Tau PFF insult positively correlates with smaller hippocampal volume normalised by CSF tTau and with higher amyloid burden (Amyloid PET). Even though the effect on individual cell lines is consistent across Tau PFF concentration, the correlations with clinical outcomes were not significant for all concentrations of Tau PFFs. Finally, the amount of Tau released by the neurons is strongly linked to the amount of PFF-induced neurite loss experienced by the neurons.

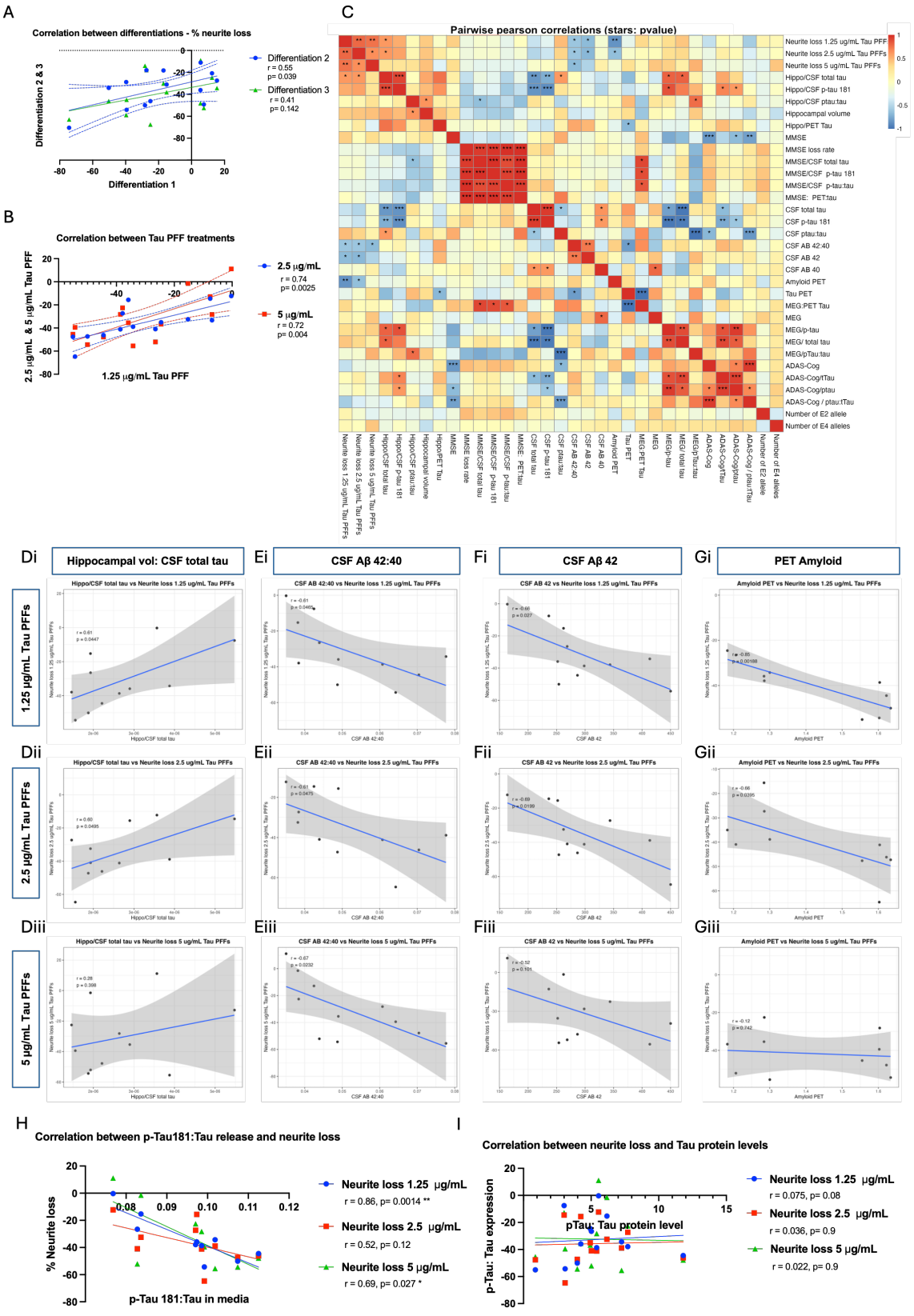


Figure 5.10: **Neurite loss in cortical neurons due to Tau PFFs correlates with clinical outcomes of patients.**

Figure 5.10: Continued: (A) Simple linear regression of % neurite loss across 3 differentiations (B) Simple linear regression of % neurite loss in neurons treated with 1.25 μg/mL, 2.5 μg/mL and 5 μg/mL. (C) Correlation matrix of % neurite loss and clinical outcomes of patients. (D-F) Simple linear regression between neurite loss due to 1.25 μg/mL (i), 2.5 μg/mL (ii) and 5 μg/mL (iii) Tau PFFs and either hippocampal volume corrected for CSF Tau (D), CSF $A\beta$42:40 (E), CSF $A\beta$42 (F) and PET Amyloid (G). (H) Simple linear regression between neurite loss and p-Tau/tTau conditioned media and (J) p-Tau/tTau protein levels in cortical neurons. Mean $\pm$ SEM n=2-3 independent differentiations repeat averaged over 6 technical replicates. For all graphs, Pearson's correlation with two-tailed value and 95 % CI were plotted. Pearson's r and p-values are indicated in each plot. For all graphs, each dot is one patient $p < 0.05$ $(*)$, $p < 0.01$ $(**)$, $p < 0.001$ $(***)$, $p < 0.0001$ $(****)$.

5.4 The effect of Tau PFF insult on synaptic density in iPSC-derived cortical neurons from the DFP cohort

Synaptic dysfunction is one of the early pathological features of Alzheimer's Disease, and cognitive decline has been shown to correlate most closely with synapse loss [466]. Several studies have shown that CSF tTau correlates with synaptic biomarkers such as SNAP 25 and CSF GAP-43 [372, 434, 271]. Furthermore, post-mortem and animal studies have demonstrated that Tau mislocalizes to dendritic spines [189], that synaptic oligomers are found in synapses, even in the absence of plaques [84] and that it causes synaptic dysfunction and loss [234, 534, 207]. Since Tau secretion through presynaptic terminal can be stimulated by neuronal activity [362], and misfolded Tau acts as a seed for Tau propagation [144, 82], it is thought that pathological propagation of Tau may occur through synapses [265, 111].

Our laboratory has previously shown that Aβ oligomers caused synapse loss in sAD patient iPSC-derived neurons, and that this loss correlated with MEG and MMSE scores of patients [322]. However, this has not been studied in the context of Tau. Therefore, I investigated whether Tau PFF induced synapse loss in 75 days old cortical neurons from the DFP cohort, which were co-cultured with rat astrocytes. The cells were treated at Day 70 with 1.25, 2.5, 5 μg/mL of Tau PFFs. Five days later, they were fixed and stained for pre- and post-synaptic markers Synapsin I/II and Homer 1, as well as for MAP2 (Figure 5.11). Synapses were detected by looking for Homer 1 and Synapsin I/II spots that colocalised within the MAP2+ area. The number of synapses was normalised to total MAP2 area to derive

synaptic density, and the number of synapse in the Tau-treated wells was normalised with the vehicle-treated wells to account for differences in synapse number between differentiations.

I first investigated whether Tau PFFs had an effect on synapse density averaged across cell lines. Although there was a slight trend toward a decrease in synapse density, this was not significant. Moreover, when looking at Synapsin I/II and Homer 1 individually to see whether pre- or post-synapses might be differentially affected, no change in Synapsin I/II or Homer 1 spots in Tau-treated wells was observed (Figure 5.12, A-C). However, when looking at the % change between the treated and vehicle conditions for each cell line individually, there was a large range in the change in synapse number due to Tau PFF for all conditions (Figure 5.12, Di-Diii). In the 1.25 μg/mL, the % change ranged from an 80 % increase in synapses to a 40 % decrease (Figure 5.12, Di); in the 2.5 μg/mL, it ranged from a 30 % increase to a 44 % decrease (Figure 5.12, Dii), and in the 5 μg/mL condition, it ranged from a 70 % increase to an 80 % decrease (Figure 5.12, Diii). However, it is important to note that only one differentiation included the 5 μg/mL, due to issues with Tau PFF stocks, and it is therefore challenging to draw firm conclusions from these data points. The difference in synapse density change between patient was significant for the 1.25 μg/mL but not for the 2.5 μg/mL Tau PFF conditions. This likely due to the marked variability in differentiations at the 2.5 μg/mL concentration.
Next, I asked whether the change in synapse density was driven more by pre- or post-synapses. Again, the variability between differentiations makes it difficult to interpret these results with confidence, but nonetheless, Synapsin I/II changes appear to be driving the changes observed in most of the cell lines (Figure 5.12, Ei-Eiii). Tau PFF insult caused around a 50 % decrease in synapse number in the *MAPT -/-* line, and only a 5-10 % decrease in the P301S line.

The number of nuclei and MAP2 area were then measured to determine whether the Tau PFFs were causing neuronal loss. There was a slight decrease in the number of nuclei in the 1.25 and 2.5 μg/mL conditions, which was significant in the 5 μg/mL; and a non-significant decrease in MAP2 area in the 5 μg/mL (Figure 5.12, F, G). In summary, Tau PFF exposure affect synaptic density and leads to a moderate degree of neuronal loss in cortical cultures. However, substantial variability across differentiations limits the strength of these conclusions.

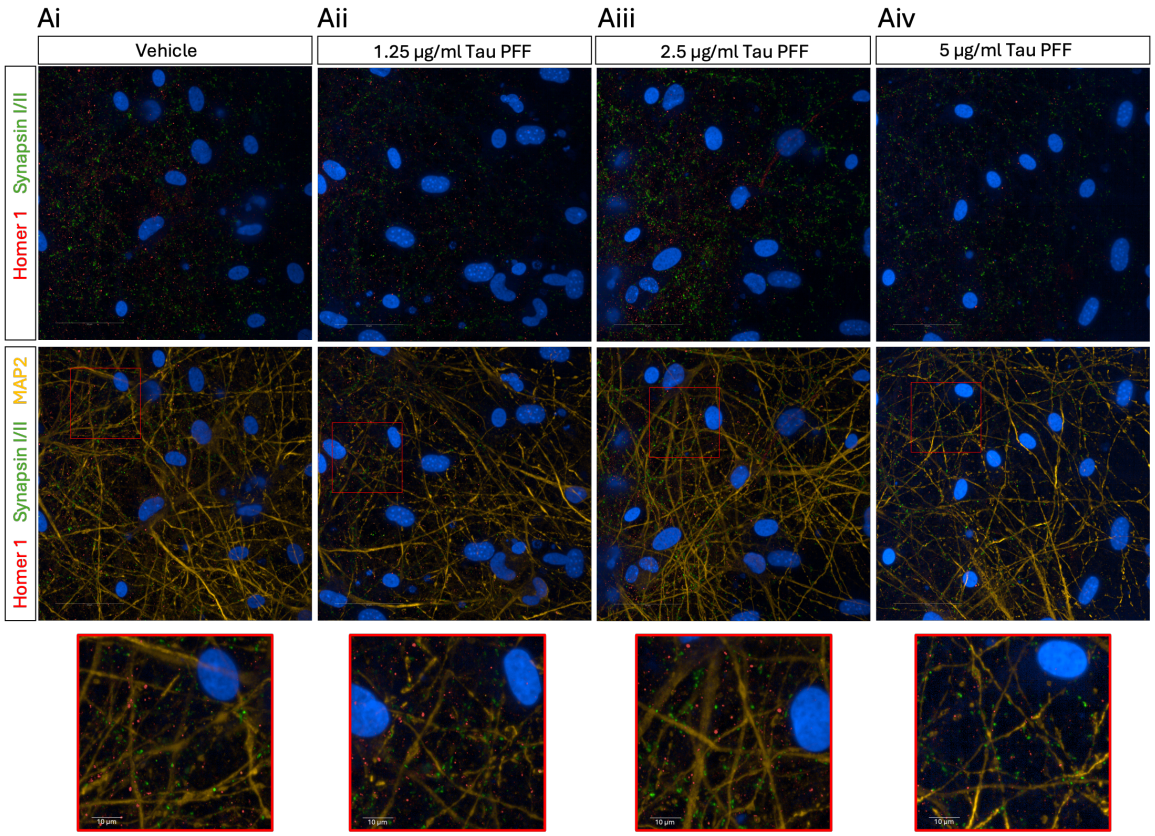


Figure 5.11: **Immunolabeling of Homer 1, Synapsin I/II and MAP2 in Day 75 cortical neurons treated with Tau PFFs.** (Ai-iv) Representative images of Day 75 cortical neurons treated with vehicle (i), 1.25 μg/mL (ii), 2.5 μg/mL (iii) and 5 μg/mL Tau PFFs (iv). They were stained with Homer I (647), Synapsin I/II (555), and MAP2 (488) and Dapi. A 63 X objective was used, scale bars = 50 μm in the top and middle panels, and 10 μm in the bottom panels

.

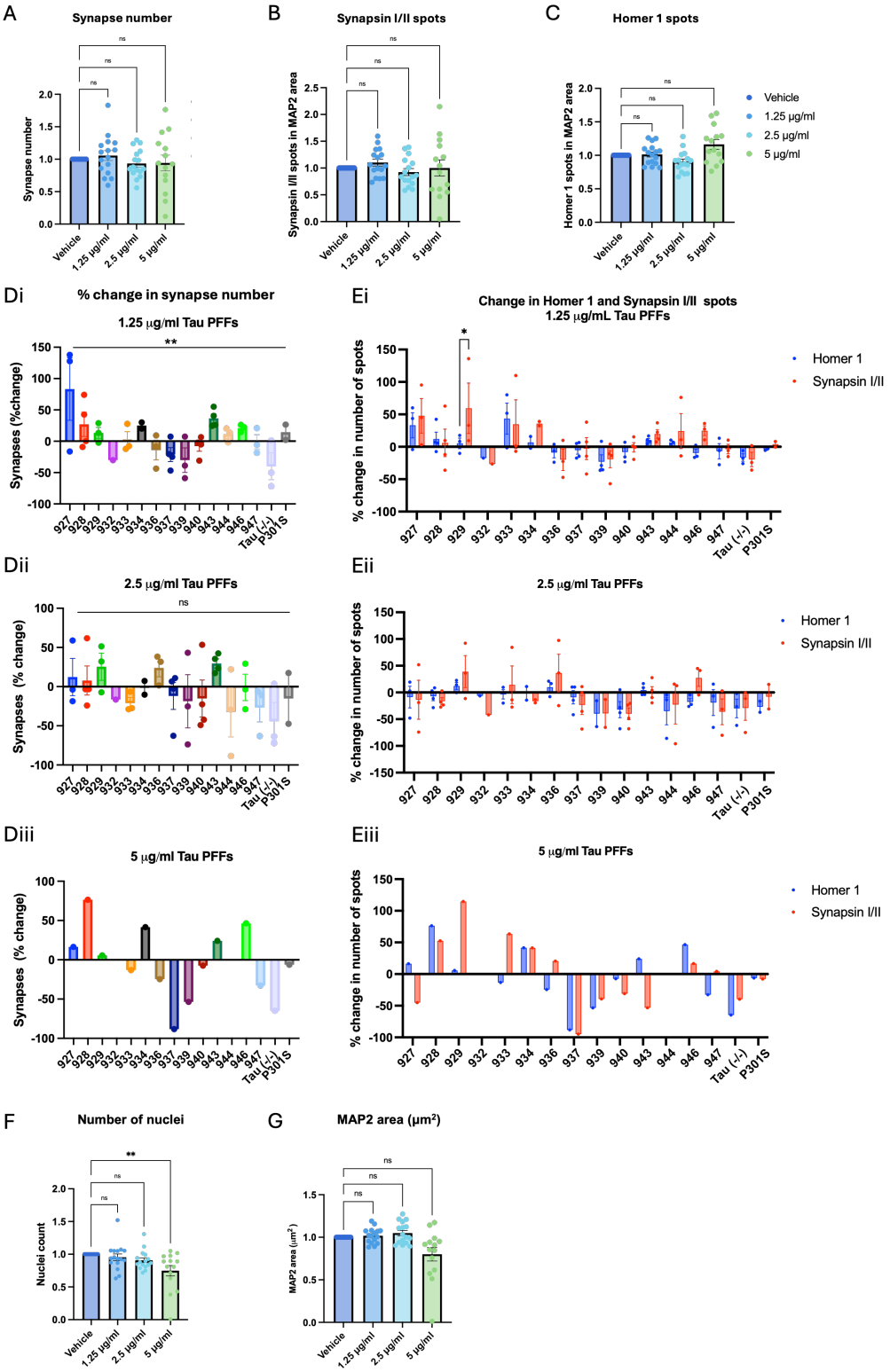


Figure 5.12: **Tau PFF insult does not induce consistent synapse loss in Day 75 DFP cortical neurons** (A-C) Fold change in synapse number (A), Synapsin I/II spots (B) and Homer 1 spots (C) between the vehicle and Tau PFF wells, averaged across all 13 sAD patient, P301S and *MAPT* -/- lines. (Di-Diii) % change in synapse number for each cell line in the 1.25 μg/mL (i), 2.5 μg/mL (ii) and 5 μg/mL Tau PFF (iii) conditions relative to vehicle.

Figure 5.12: (continued) (Ei-iii) % change in Homer 1 and Synapsin I/II spots in MAP2 for each cell line in the 1.25 μg/mL (i), 2.5 μg/mL (ii) and 5 μg/mL Tau PFF (iii) conditions relative to vehicle. (F) Change in nuclei count and (G) MAP2 area between the vehicle and Tau PFF wells, averaged across all 13 sAD patient, P301S and *MAPT* -/- lines. Mean ± SEM n=3 independent differentiations repeat averaged over 3-4 technical replicates (1 differentiation for the 5 μg/mL condition). For all graphs, each dot is one differentiation, except for bar plot averaging across cell lines, where each dot is a cell line. (A-C, F,G) Kruskal-Wallis test with Dunn's multiple comparisons test. (Di-Diii) Ordinary One-Way ANOVA with Tukey's multiple comparisons test. (Ei-Eiii) 2-way ANOVA with Sidak's multiple comparisons test. $p < 0.05$ $(*)$, $p < 0.01$ $(**)$, $p < 0.001$ $(***)$, $p < 0.0001$ $(****)$.

5.5 Assessing the effect of Tau PFF seeding on Tau phosphorylation in iPSC-derived cortical neurons

As mentioned previously, aggregated Tau species can act as seeds that cause other forms of Tau to hyper-phosphorylate, aggregate and thereby spread pathology [82, 144]. Other studies have shown that Tau insult in iPSC-derived cortical neurons are internalised and cause hyperphosphorylation of Tau [443, 486, 476]. Most studies have used mutant *MAPT* lines carrying FTD mutations and truncated Tau fibrils carrying a P301L mutation, which promotes seeding and aggregation; a couple studies have utilised full length 2N4R tau fibrils in control iPSC neurons [476, 286]; but no study has looked at whether full length 2N4R Tau PFF could induce hyperphosphorylation and aggregation of Tau in sporadic AD iPSC-derived neurons.

Using the same Tau concentrations as described in Chapter 5.4, I treated Day 70 neurons co-cultured with astrocytes with Tau PFFs. After 7 Days, I fixed the neurons with 4 % PFA and stained the neurons with p-Tau (AT8) and β Tubulin (β-Tub). There was a high level of AT8 staining, regardless of treatment in the AD and P301S lines (Figure 5.13, Ai). As expected, the *MAPT* -/- cell line had nearly no Tau positive neurites (Figure 5.13, Aii, Figure 5.13, B,D). Despite the high baseline level of AT8, there was a small dose dependent increase in AT8 spots in β-Tubulin area relative to vehicle (Figure 5.13, B, C). Surprisingly, the P301S neurons did not have increased levels of p-Tau between the vehicle and treated wells, nor when compared to the sAD patient lines (Figure 5.13, B).

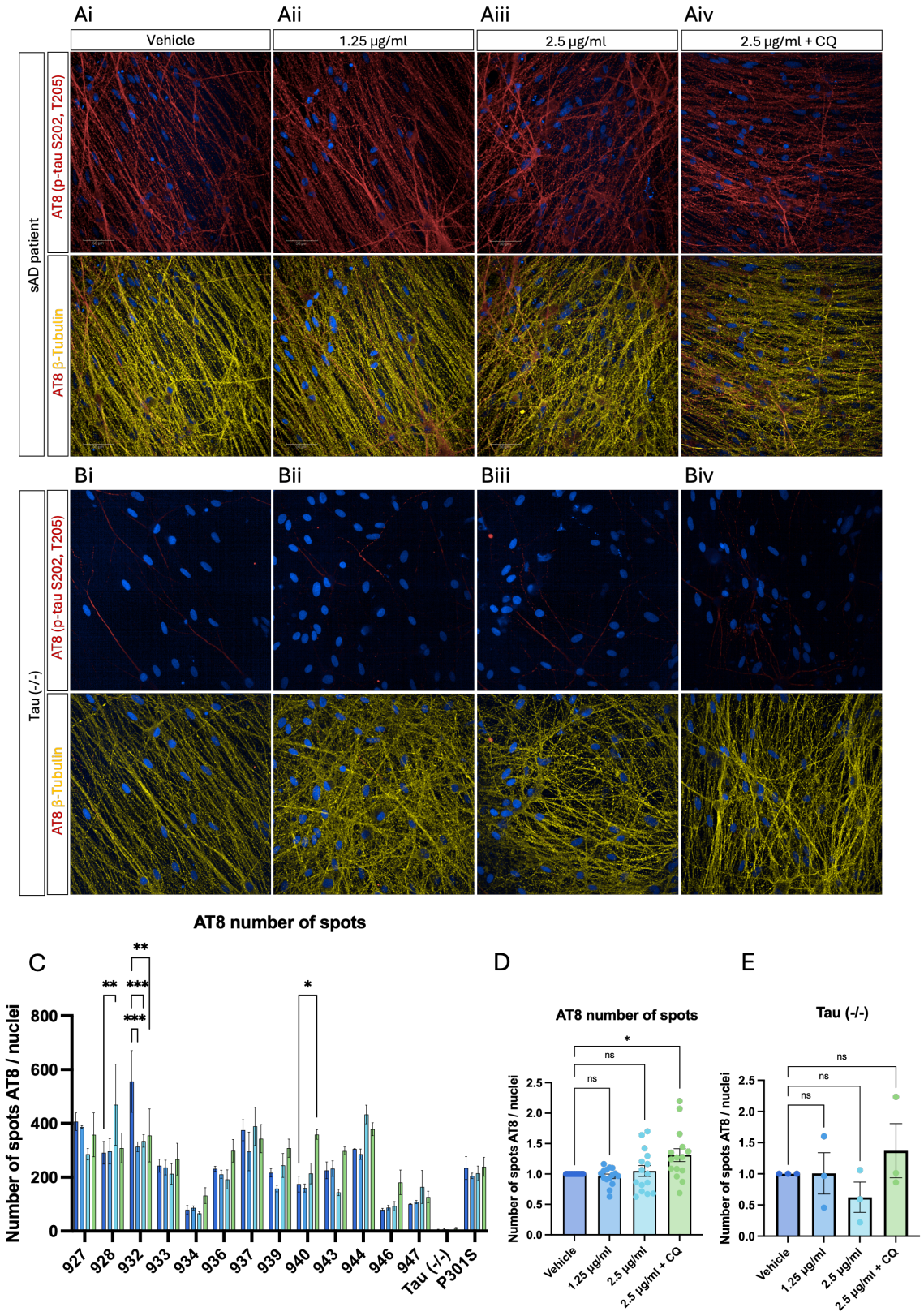


Figure 5.13: **Immunolabelling of p-Tau in cortical neurons shows moderate increase in number of spots after Tau PFF insult.**

Figure 5.13: Continued:(A-B) Representative images of AT8 (647), β-Tub (555) and Dapi staining in sAD patient (A) and *MAPT -/-* (B) neurons. They were treated with Vehicle (i) control, or with 1.25 μg/mL(ii) 2.5 μg/mL (iii) or 2.5 μg/mL + CQ) (iv). Images were taken on 40X objective, scale bar is 50 μm. (C-D) Number of spots of AT8 in β-Tub area, normalised to nuclei in indivual cell lines (C) or averaged across all cell lines (D). (E) Number of spots AT8 in the *MAPT -/-* neurons at all treatment conditions. Mean ± SEM n=3 replicates. (C) 2-Way ANOVA with Dunnett's multiple comparisons test. (D) Kruskal-Wallis test with Dunn's multiple comparisons test. (E) Ordinary One-Way ANOVA with Dunnett's multiple comparisons test.$p < 0.05$ $(*)$, $p < 0.01$ $(**)$, $p < 0.001$ $(***)$, $p < 0.0001$ $(****)$.

5.5.1 tTau and astrocyte staining in neuron-astrocyte co-cultures

Earlier, I hypothesised that the lack of effect in neurite loss when neurons were co-cultured with astrocytes was potentially due to the astrocytes internalising the Tau PFFs. Therefore, in a parallel plate to the one described above, I stained the cells with tTau (Tau 12), β-Tub, and GFAP, an astrocyte maker. I expected that any Tau internalisation would be challenging to visualise in the sAD patient wells, since the baseline level of Tau would be too high, which was indeed the case (Figure 5.14, Ai). However, visualisation of Tau PFFs by staining tTau was possible in the *MAPT -/-* neurons (Figure 5.14, Aii).

Interestingly, there was a dose-dependent decrease in the area of tTau in β-Tub in the Tau PFF conditions in (Figure 5.14, B, C). When averaged across all patient lines, tTau decreased by about 25 % after Tau PFF treatment. There was no change in Tau 12 signal in the *MAPT -/-* neurons (Figure 5.14, D). In the *MAPT -/-* wells, one can clearly see large, Tau 12 + structures, which are absent in the vehicle condition, and are likely remaining PFFs, which are stuck to the plate (white arrows, Figure 5.14 Aii). These structures do not co-localise with astrocytes, and when looking at individual Z-stacks, it is clear that they are not inside cells. Additionally, no Tau 12 signal was observed in the astrocytes. This suggests that either the astrocytes do not internalise the Tau PFFs, or they have already internalised and broken down the PFF 7 days post seeding. There was a slight increase in GFAP area in the Tau PFF + CQ condition, but this was not seen in the wells treated with Tau PFFs alone (Figure 5.14, E).

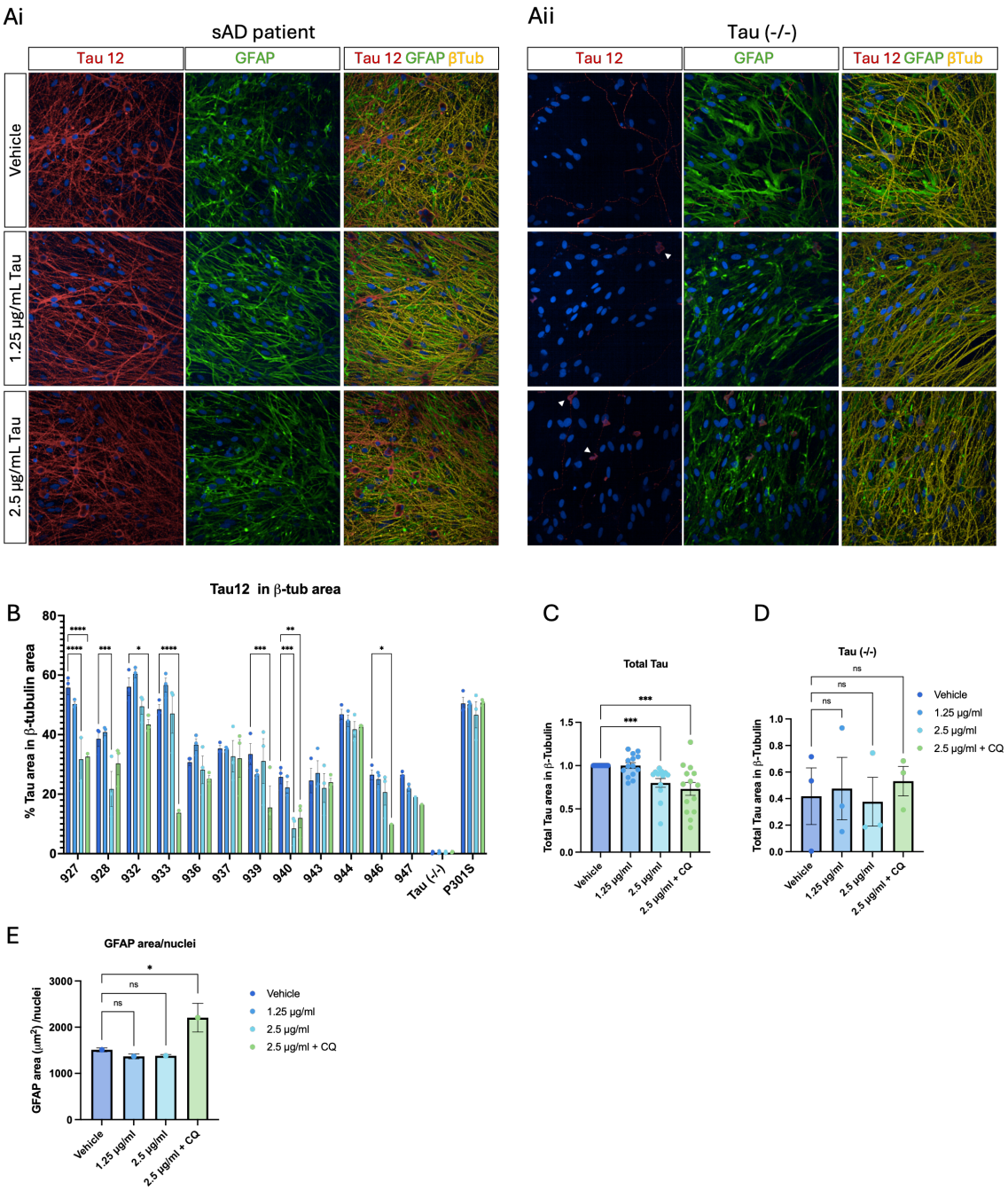


Figure 5.14: **Immunolabelling of tTau and GFAP in cortical neurons after Tau PFF insult.** (A) Representative images of Tau12 (647), β-Tub (555), GFAP (488) and Dapi staining in sAD patient (Ai) and *MAPT* -/- (Aii) neurons. They were treated with Vehicle control, or with 1.25 μg/mL, 2.5 μg/mL or 2.5 μg/mL + CQ). Images were taken on 40X objective. (B-C) Tau 12 + area in β-Tub area in individual cell lines (B) or averaged across all cell lines (C).

Figure 5.14: Continued: (D) Tau 12 area in β-Tub in the *MAPT -/-* neurons at all treatment conditions.(E) GFAP area normalised by nuclei number in all treatment conditions. Mean ± SEM n=3 replicates. (B) 2-Way ANOVA with Dunnett's multiple comparisons test. (C) Kruskal-Wallis test with Dunn's multiple comparisons test. (D-E) Ordinary One-Way ANOVA with Dunnett's multiple comparisons test. $p < 0.05$ $(*)$, $p < 0.01$ $(**)$, $p < 0.001$ $(***)$, $p < 0.0001$ $(****)$.

5.5.1.1 Cell viability

Tau PFF-treated neurons had a decrease in β-tubulin area, indicative of a loss of neurites, in the 2.5 μg/mL and 2.5 μg/mL + CQ condition (Figure 5.15,A,B). This decrease is consistent with the loss of tTau described above (Figure 5.14, B, C). Similar to the effects observed when assessing synapse loss, tau PFF treatment caused a slight decrease in the number of nuclei, which was significant in the 2.5 μg/mL + CQ condition (Figure 5.15, C,D). Moreover, AK release in the media was significantly increased in the 2.5 μg/mL condition, and approached significance in the 2.5 μg/mL + CQ condition. This decrease in cell viability was also seen in the *MAPT -/-* line, which suggests that the loss of neurons is at least partially due to toxic effects of the PFFs themselves, rather than downstream due seeding and aggregation.

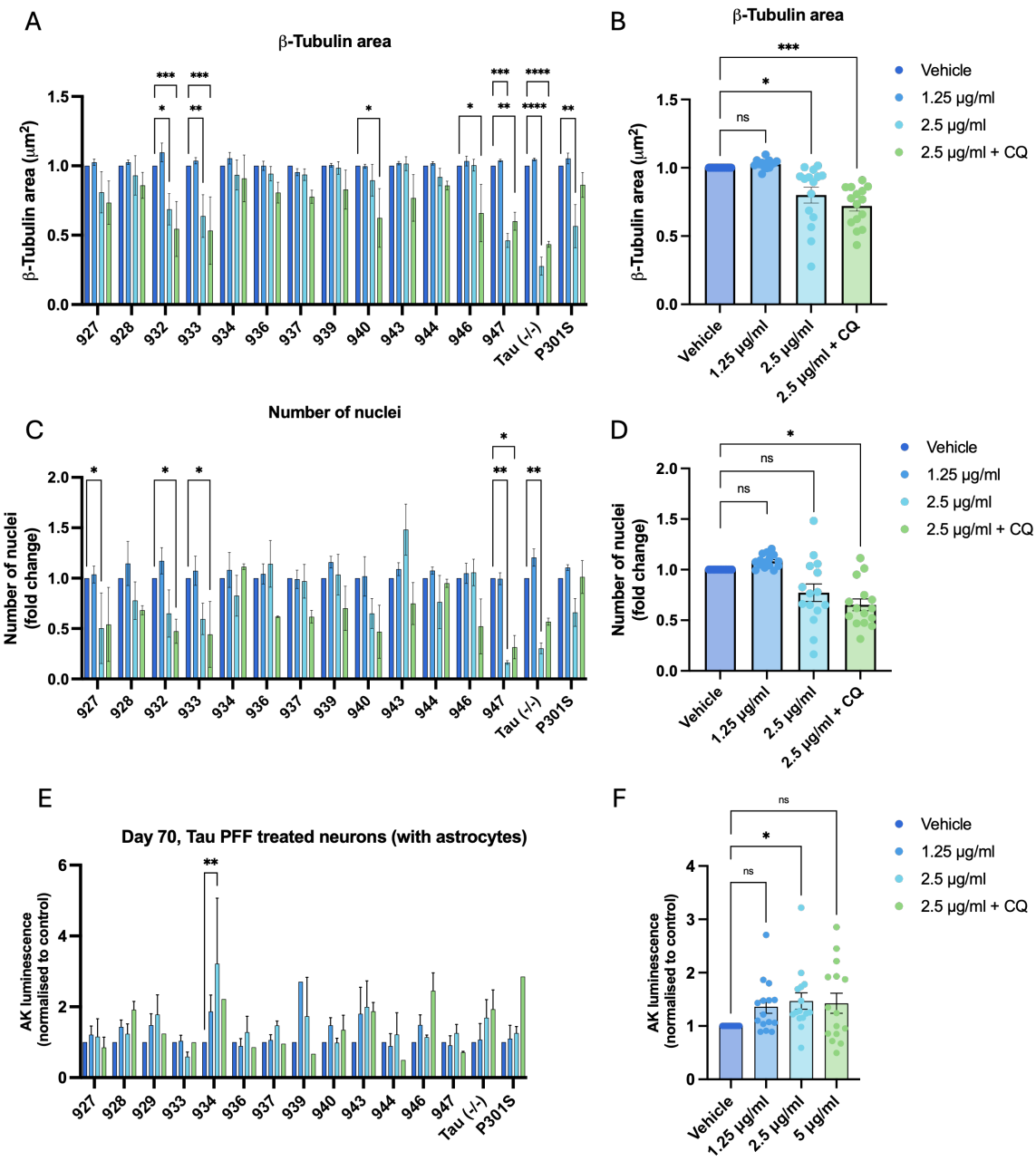


Figure 5.15: **Tau PFF causes moderate neuronal death in Day 70 cortical neurons** (A-B) Change β-Tub area after Tau PFF insult in individual lines (A) or averaged across all cell lines (B). (C-D) Change in number of nuclei after Tau PFF insult in individual lines (C) or averaged across all cell lines (D). (E-F) AK luminescence change (relative to vehicle) in conditioned media of neurons treated with Tau PFFs. (E) Individual Lines (F) Average of all cell lines. Mean ± SEM n=3 replicates. (A,C,E) 2-Way ANOVA with Dunnett's multiple comparisons test. (B,D,F) Kruskal-Wallis test with Dunn's multiple comparisons test. $p < 0.05$ $(*)$, $p < 0.01$ $(**)$, $p < 0.001$ $(***)$, $p < 0.0001$ $(****)$.

5.6 Bulk RNA sequencing of control iPSC-derived cortical neurons treated with Tau PFFs

In my experimental work so far, exposure of iPSC-derived cortical neurons to Tau PFFs produced moderate effects on neuronal phenotypes, including reductions in neurite outgrowth and moderate cell death. These effects were more pronounced in monoculture, though still variable across differentiations, suggesting that additional Tau-induced changes may be occurring but are not readily detected with morphological assays alone.

While Tau uptake, internalisation, and seeding have been well characterised in cell culture models, substantially less is known about the downstream pathways engaged in human neurons following Tau propagation. The study by Parra-Bravo et al. provides an important exception: using P301L fibrils in 4R-P301S neurons, they identified marked endolysosomal dysfunction, impaired neuronal activity, altered calcium handling, and showed that neuronal activity promotes Tau spread [353].

RNA-sequencing offers a valuable and unbiased approach to investigate the molecular effects of Tau PFFs in greater depth, and may uncover pathways impacted by Tau that were not evident from phenotypic assays. In Chapter 3 and 4, I demonstrated that Aβ induced robust neurite loss and transcriptomic changes in the DFP neurons and in control i3 neurons. However, the DFP neurons clustered most closely by line identity rather than by treatment (Figure 4.25), while the i3 neurons clustered by treatment (Figure 4.2). Due to these observations, and the moderate effect of tau PFFs described above, I decided to perform bulk RNA-sequencing on i3 neurons treated with Tau PFFs, as the consistency and purity of i3 cortical neurons across differentiations would make changes due to Tau insult easier to detect. This experiment and the analysis described below were performed alongside a DPhil rotation student, Helen Jolly, who aligned the sequencing reads and helped perform the analysis. Three independent differentiations of i3 neurons were treated with 2.5 μg/mL of Tau PFFs for 5 days. This decision was based on the results of the neurite tracing experiments without astrocytes, where this concentration led to significant loss of neurites. The neurons were treated on Day 14 for 6 days to remain consistent with the RNA-sequencing on Aβ-treated i3s, and enable comparisons (Figure 4.1). As described in Section 4.2.1, i3 neurons go through significant maturation between Day 7 and 14, hence why this timepoint was chosen.

After treatment, RNA was collected and sent for QC and sequencing to Novogene

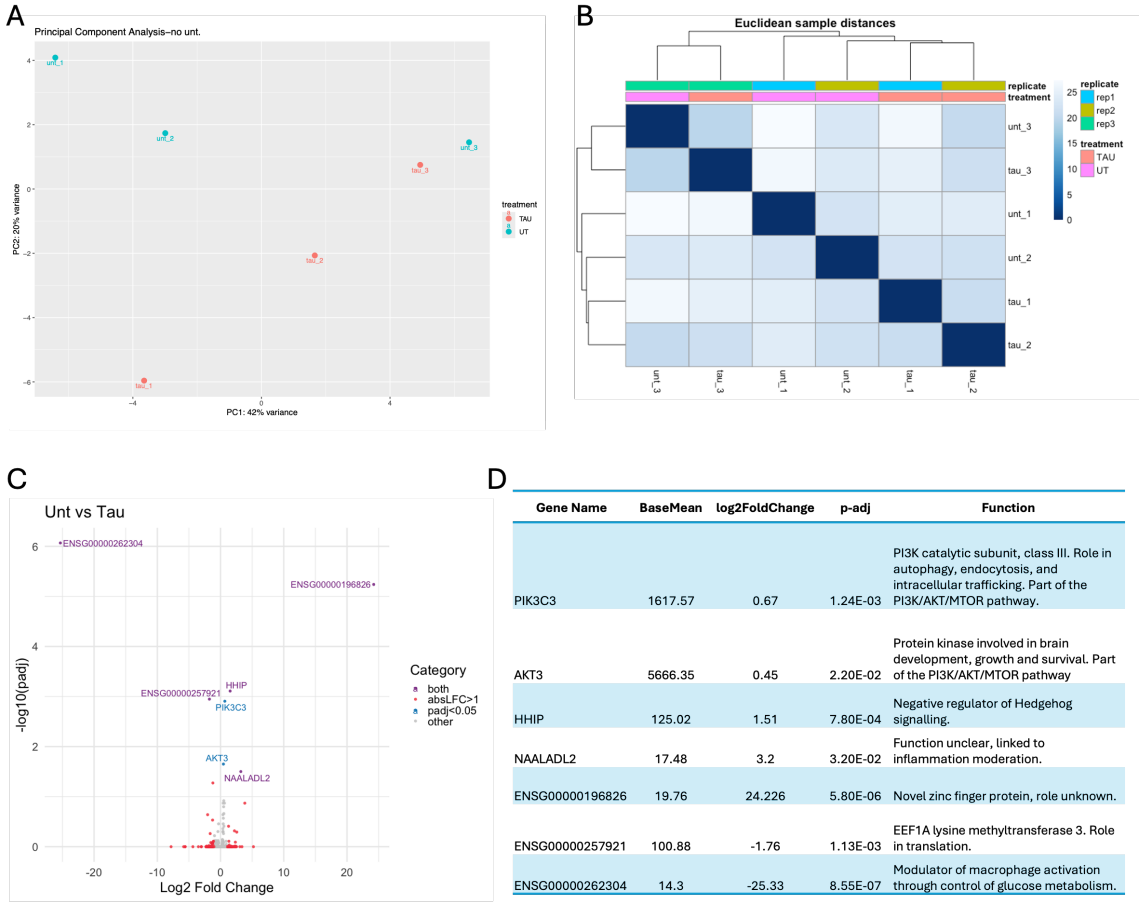
(details found in Chapter 2.2.14). The reads were aligned using Salmon [355], and imported into R using tximport [436]. The genes were filtered for low counts (< 30 counts in at least 2 replicates per condition). This filtered the number of genes to 17,451 genes, which were used to differential gene expression (DEG) analysis using DESEq2 [270]. This result list was filtered for protein coding genes, leaving 14,127 genes.

5.6.1 Quality control of dataset

Principal component of analysis was performed to look at clustering of the samples. This revealed clustering by treatment and by differentiations (rep1, rep2, rep3). Differentiations 1 and 2 had clear separation between untreated (UT) and Tau PFF-treated samples (TAU), while the Tau-treated and untreated sample from differentiation 3 clustered closely together (Figure 5.16, A). Euclidean sample distance heatmap showed a similar clustering (5.16, B).

5.6.2 Differential gene expression analysis

Next, I looked at the number of DEGs in the treated vs untreated condition, which are shown in the volcano plot in Figure 5.16 C. There were only 7 significantly differentially expressed genes (padj < 0.05), which are detailed in Figure 5.16 D. One of the top genes, PIK3C3, which is a class III catalytic subunit of Phosphoinositide 3-kinase (PI3K), is involved in autophagy and endocytosis, by producing the phospholipid PI3P, which is essential to form new autophagosomes and sorting cargo into lysosomes [393, 35]. AKT3 (AKT Serine/Threonine Kinase 3) is a protein kinase involved in cell survival [321]. Importantly, they are both a part of the PI3K/AKT/MTor signalling pathway, which promotes cell survival and neurogenesis [515, 321]. PI3K produces PI3P, which phosphorylates and activates AKT, which in turn leads to the inhibition of GSK3 β [274], a kinase responsible for phosphorylating Tau [440, 188]. However, no other gene in these pathways were significantly differentially expressed, and the fold change of these two genes were 1.6 and 1.36, respectively, which are relatively modest changes in gene expression.



Gene Name	BaseMean	log2FoldChange	p-adj	Function
PIK3C3	1617.57	0.67	1.24E-03	PI3K catalytic subunit, class III. Role in autophagy, endocytosis, and intracellular trafficking. Part of the PI3K/AKT/MTOR pathway.
AKT3	5666.35	0.45	2.20E-02	Protein kinase involved in brain development, growth and survival. Part of the PI3K/AKT/MTOR pathway
HHIP	125.02	1.51	7.80E-04	Negative regulator of Hedgehog signalling.
NAALADL2	17.48	3.2	3.20E-02	Function unclear, linked to inflammation moderation.
ENSG00000196826	19.76	24.226	5.80E-06	Novel zinc finger protein, role unknown.
ENSG00000257921	100.88	-1.76	1.13E-03	EEF1A lysine methyltransferase 3. Role in translation.
ENSG00000262304	14.3	-25.33	8.55E-07	Modulator of macrophage activation through control of glucose metabolism.

Figure 5.16: **Clustering and differential gene expression of i3 cortical neurons treated with Tau PFFs** (A) PCA plot of Untreated (UT) vs Tau treated samples. (B) Euclidean sample distance heatmap. (C) Volcano plot representing the Log_2FoldChange and -Log_{10} p-value of the DEGs in the Tau samples vs the UT samples. Dots represent genes, and are coloured red if their absolute Log_2FoldChange is higher than 1, blue if their p-adj value is < 0.05 and purple if both conditions are met. (D) Table with the significant DEGs and their function.

5.6.3 Functional gene set enrichment analysis (fGSEA)

I then performed fGSEA, and as in Section 4.2, generated a list of all genes in the dataset, ranked by their Log_2FoldChange x -Log_{10} p-value. 1508 pathways had a significant positive enrichment score (i.e enrichment score > 1, upregulated), and 503 had a significant negative enrichment score (i.e enrichment score $<$ -1, downregulation). The top up- and down-regulated pathways with their normalised enrichment score (NES) are depicted in Figure 5.17 A and Figure 5.18 A. Of the 1503 positively enriched pathway, 1356 of them were pathways linked to micro-RNA processing. Although interesting, I did not focus on those pathways for further

analysis. In the list of 152 pathways remaining, pathways of note included dendrite morphogenesis, RNA processing related pathways and, consistent with the significant DEGs, PI3K/AKT signalling cascade (Figure 5.17, B, C, D).

In the downregulated group, pathways linked to mitochondrial function, and to ribosomal function/translation were heavily represented (Figure 5.18 A). Looking more closely at the genes that lead the enrichment (leading edge genes), it is evident that all the genes have very small Log_2FoldChange (i.e. Log_2FoldChange under 0.5, which represents a fold change of 1.4 or smaller) and nearly all have p-adjusted values of >0.05 (Figure 5.18). However, GSEA does not require genes to be individually significant, as it evaluates whether predefined gene sets are overrepresented at the either end of a ranked gene list and identifies consistent directional shifts in the dataset, enabling the detection of biologically relevant pathways that are invisible at the single-gene level. Nonetheless, these represent biologically modest changes, which are more likely to be noisy, and could be due to ranking biases and small sample size.

In conclusion, this RNA sequencing experiment revealed that Tau PFF induces modest changes in transcription, consistent with the mild morphological phenotypes discussed in the first part of the chapter. These changes are related to PI3K/AKT signalling, mitochondrial function and translation.

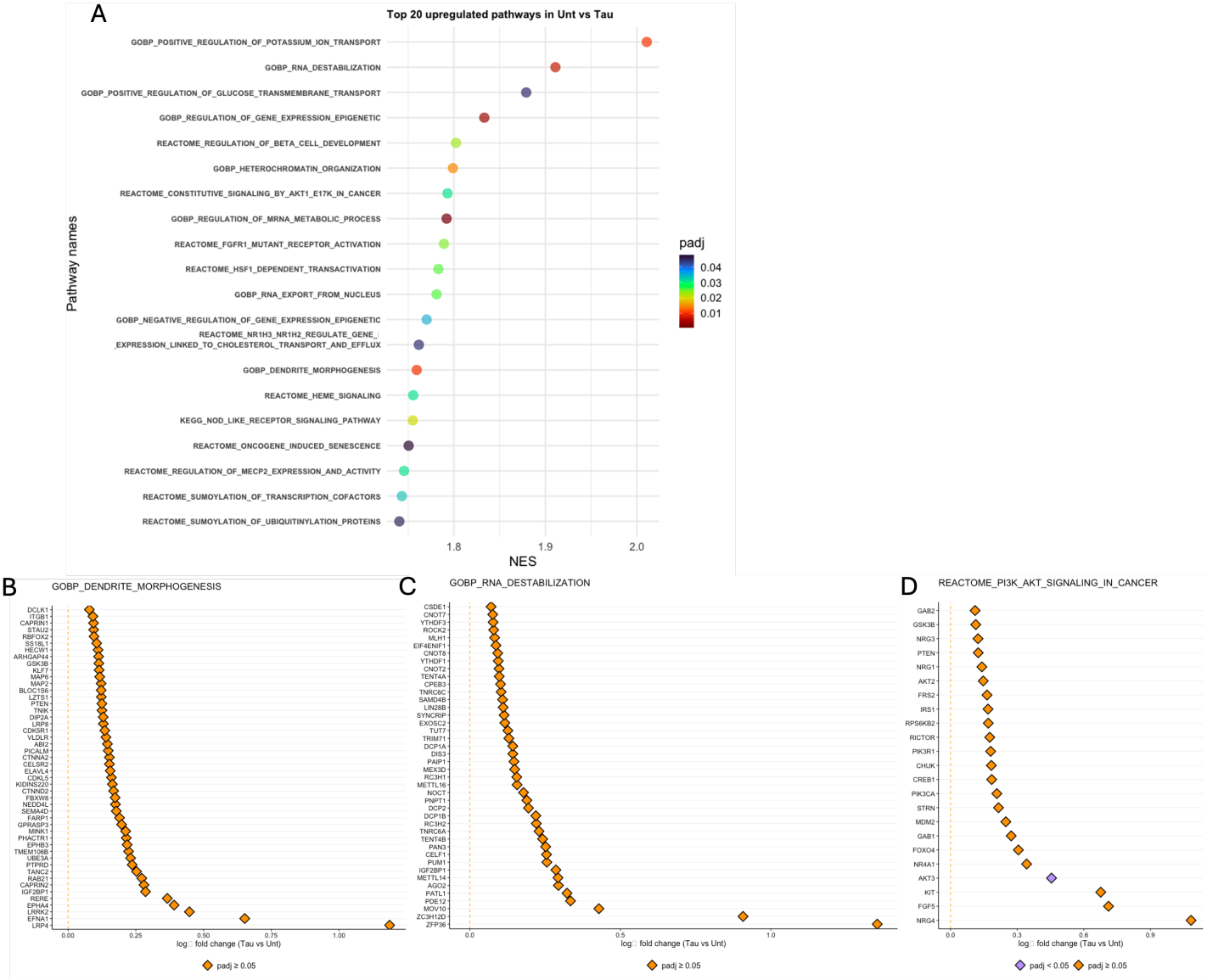


Figure 5.17: **Upregulated pathways in neurons treated with Tau PFFs** (A) Top 20 downregulated pathways with their NES. The colour of the dot is representative of the p-adj value. (B-D) (B) GO:BP Dendrite Morphogenesis, (C) GO:BP RNA Destabilisation, (Di) Reactome PI3_AKT signaling in cancer used as example graphs of leading edge genes in upregulated pathways, plotted in order of their Log2FoldChange. Colour represents their p-adj value.

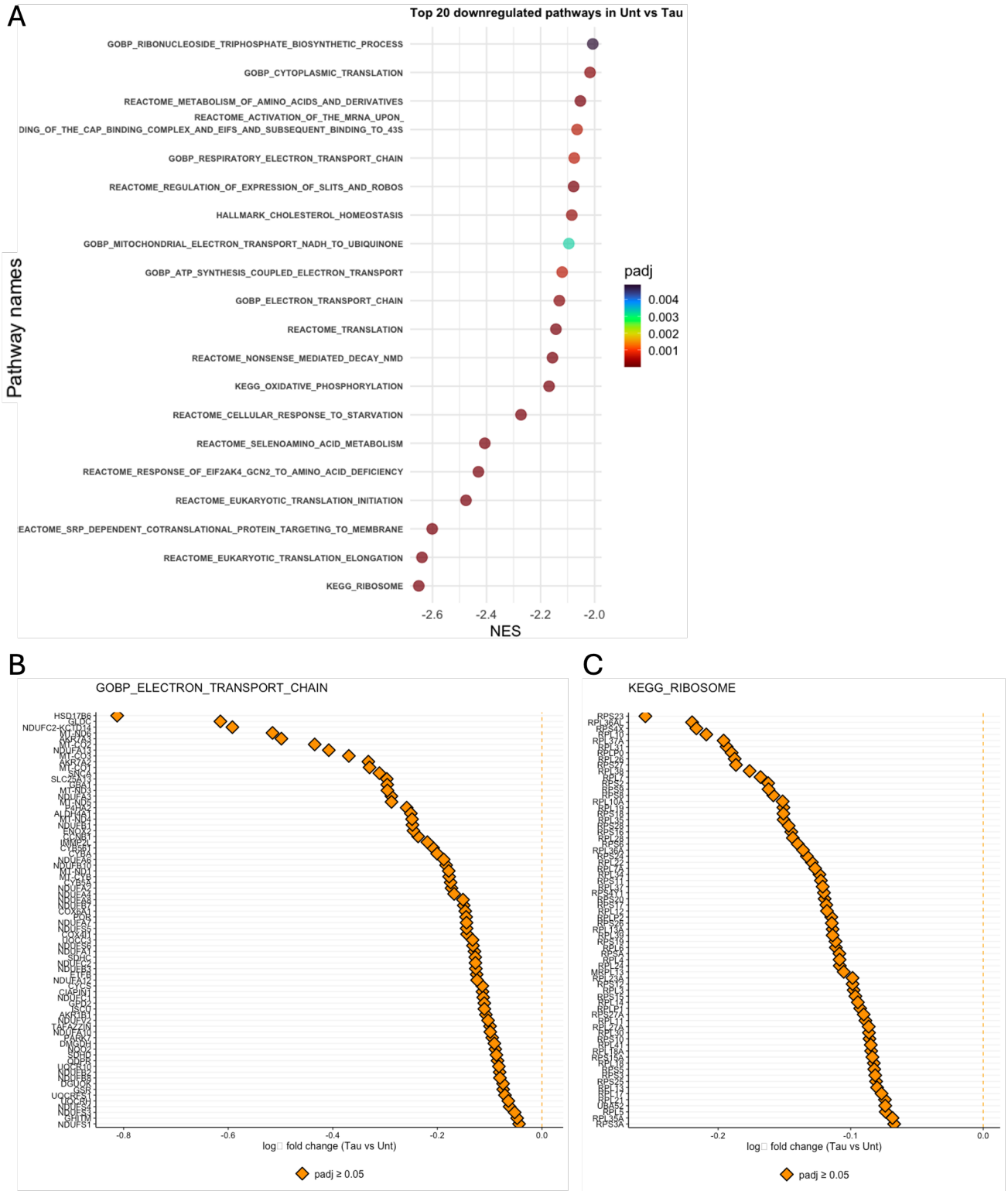


Figure 5.18: **Downregulated pathways in neurons treated with Tau PFFs** (A) Top 20 downregulated pathways with their NES. The colour of the dot is representative of the p-adj value. (B) GO:BP Electron transport chain and (C) KEGG Ribosome used as example graphs of leading edge genes in downregulated pathways, plotted in order of their Log2FoldChange. Colour represents their p-adj value.

5.7 Discussion

5.7.1 Molecular characterisation of Tau in iPSC-derived neurons and correlation with clinical measures

In this chapter, I presented a comprehensive molecular characterisation of Tau, phospho-Tau, and GSK3β expression in sAD iPSC-derived neurons. The analysis revealed substantial heterogeneity in tTau and p-Tau species (e.g., S396, AT8, Tau5; Fig. 5.1) and importantly, cellular tTau and pTau AT8 protein levels significantly correlated with Tau PET signal, a measure of tau pathology. Interestingly, these levels did not correlated with CSF tau or pTau, though differences in tau epitopes measured could explain this result. Another possibility is that cellular tau protein in iPSC-derived neurons, as measured here, captures intra-neuronal tau abundance and phosphorylation state — which is conceptually closer to the brain tau load detected by PET than to the soluble tau released into CSF following neuronal damage.

Secreted total Tau and p-Tau181 from iPSC neurons also did not correlate with CSF total tau and p-Tau181. These results suggest that in iPSC-neurons, cellular tau protein levels, rather than secreted tau are more reflective of tau pathology *in vivo*. Accordingly, higher cellular pTau S396/tTau ratio correlated with greater cognitive decline of the corresponding patients, which is reflective of studies in AD patients demonstrating that CSF and PET Tau correlate with cognitive decline [201, 26]. This finding contrasts with work from Lagomarsino et al., who reported a positive association between cellular p-Tau/tTau and cognition in 53 LOAD patients. However, their analysis used a linear mixed model adjusting for education, gender, and age, and they measured different tau epitopes. Differences in methodology and statistical correction may therefore explain this discrepancy.

To date, most Tau PFF work in iPSC models has been performed in control neurons or neurons carrying FTD mutations, and many have used fibrils which carry mutations that augment their aggregation propensity. In contrast, this study investigated the effects of full-length 2N4R Tau PFFs across multiple timepoints and phenotypes in 12 sporadic and 1 familial AD patient lines, both with and without astrocyte co-culture. The spectrum of neuronal vulnerability, as assessed by neurite loss, significantly correlated with hippocampal volume normalised to CSF total Tau. CSF total tau, unlike CSF pTau is not a measure of tau pathology. However it is closely associated with neuronal injury and axonal loss, and has also been shown

to correlate strongly with early markers of disease, such a synapse degeneration [434, 291, 50]. It is therefore interesting that neurite loss due to Tau PFF insult is associated with hippocampal volume adjusted for CSF total tau levels.

Additionally, enhanced neurite loss due to Tau PFFs correlated with higher amyloid burden (PET amyloid). Confusingly, higher CSF Aβ 42 and 42:40 ratio also correlated with increased neurite loss, while one would expect the opposite, given that CSF Aβ 42:40 is typically highly negatively correlated with PET amyloid. Salvadò et al. (2024), recently established a robust CSF staging model using 5 CSF biomarkers, which predicted the presence of pathology (Amyloid and Tau PET) and aligned with longitudinal changes in other AD biomarkers. They show that once the threshold of Aβ positivity is reached, CSF Aβ 42:40 levels plateau, while pTau levels continue to rise across CSF stages [402]. They also demonstrate that, unlike CSF Aβ 42:40, the level of amyloid PET increased consistently with higher CSF stages. On the other hand, CSF Aβ 42:40 has been shown to detect amyloid pathology before PET amyloid [346]. These results suggest that though CSF Aβ 42:40 is an important biomarker early in the disease, amyloid PET may be a better measure of progression and severity of amyloid pathology.

Finally, I show that neurite loss at all concentrations is significantly correlated with the ratio of secreted ptau/Tau in conditioned media but not cellular ptau:tTau levels (Figure 5.10, H, I). While these results are preliminary, given that the tau ELISAs were only performed on one differentiation, these results indicate that neurons that secrete more pTau are more vulnerable to Tau-PFF induced neurite degeneration. Several explanations could underlie this correlation. Elevated p-Tau secretion may reflect a pre-existing imbalance between tau production and clearance — for instance, impaired autophagic or proteasomal degradation of phospho-tau [498] — which would also leave neurons less able to clear internalised PFFs and prevent templated aggregation. Additionally, secreted tau itself may act as a seed for further tau aggregation [143]. Neurons that secrete more tau may therefore be releasing more potential seed material for the added tau PFFs. Collectively, these findings suggest that iPSC-derived neurons capture patient-specific susceptibility to Tau insult and links vulnerability to Tau PFFs *in vitro* with amyloid pathology *in vivo*.

5.7.2 Challenges in assessing cellular responses to tau PFF exposure

Studying Tau aggregation in iPSC-derived neurons poses inherent challenges, largely due to the developmental immaturity of these models. Reprogramming fibroblasts or PBMCs resets the cellular "biological clock," meaning iPSC-derived neurons resemble fetal rather than adult neurons [237, 458]. This is particularly relevant for Tau, as the adult brain expresses six isoforms, whereas developing neurons express predominantly 0N3R Tau [159]. The adult human brain maintains an approximately 1:1 ratio of 4R to 3R Tau, and disruption of this balance is implicated in tauopathies [442]. In contrast, iPSC-derived cortical neurons typically express only 0N3R Tau unless cultured for almost a year (with the exception of FTD lines).
Moreover, as shown in Sections 5.1 and 5.13, sAD neurons exhibit high endogenous expression of phosphorylated Tau species (e.g., S396, AT180, AT8). Although these epitopes are considered pathological in the adult brain due to their association with PHFs [203, 252, 165, 17], they are physiologically present during brain development without causing aggregation [60, 157, 290]. These developmental differences may limit the utility of iPSC-derived neurons as a model for studying the effects of Tau insult.

Here, I hypothesised that Tau PFFs would cause synapse loss in iPSC derived neurons, given that tau has been shown to mislocalise to dendrites, and cause synapse loss in mouse models of AD and primary neuron cultures [189, 469, 455, 190, 499]. However, I did not observe a consistent decrease in synapse number after Tau PFF insult in the iPSC derived neurons, with some lines exhibiting decreases in synapses, and others increases (Figure 5.12). Several explanations could underlie this results. First, the variability across differentiations– which could be due to differences in the batches of PFF used, or to the extended time in culture introducing more variability in the density or health of the culture– may be hiding Tau PFF-induces changes in synapse number. Second, the synapse density experiments (Section 5.4) were conducted in neurons co-cultured with rat astrocytes, while the more striking neurite loss (Section 5.3.2) was observed in monoculture. This raises the possibility that astrocytes are protecting the neurons from Tau-PFF induced damage by, for instance, internalising the tau PFFs [54] . While monoculture experiments would solve this problem, prolonged culture to Day 70-80 without astrocytes is challenging because they help with neuronal adherence and prevent the neurons from peeling.
This assay has previously been used to measure synapse loss in response to Aβ

in our group [322], but perhaps Aβ induced more robust synaptotoxic effects than tau, hence why they observed consistent changes in synapses. In the future, other methods such as multi-electrode array recordings or calcium imaging could be used to further probe synaptic vulnerability to Tau PFFs.

Furthermore, I was interested in whether Tau PFF insult would induce endogenous phosphorylation of tau in sAD neurons, and whether the DFP patient lines would exhibit differences in their susceptibility to phosphorylate tau after Tau insult. Although there was a small but significant increase in AT8 spots in PFF-treated neurons, the high baseline levels of monomeric p-Tau made it difficult to visualise PFF-induced phosphorylation. While several groups report no such p-Tau signal after PFA fixation [476, 353], others have shown that methanol fixation is required to remove monomeric Tau and reveal seeded inclusions [501, 281]. Furthermore, the absence of signal in the *MAPT -/-* neurons confirmed that this staining was not non-specific binding to other microtubule-associated proteins (Figure 5.13). Attempts to apply methanol fixation using a collaborator's protocol were unsuccessful, as cells detached during fixation. Nevertheless, optimisation of this method will be crucial for future mechanistic studies.

Another important consideration is the treatment duration. Here, PFF exposure was examined after 7 days. While a few studies have reported tau internalisation and endogenous phosphorylation between 24h and 6 days post seeding [281, 476], many studies have reported aggregation in neurons after seeding with fibrils after 2-5 weeks in culture [353, 485, 486], which is a much longer timeframe than what has been done in this thesis. However, differences in the species of tau insults and fixation protocols might explain these discrepancies.

The tau species used in these investigations is an important consideration. I used 2N4R tau PFFs, which two studies have shown get internalised and cause endogenous tau phosphorylation in iPSC-derived neurons [286, 476]. However, others have reported that Tau overexpression or FTD-linked mutations are required for seeding and tau phosphorylation [353, 485, 486].
Given the afore-mentioned studies, it was particularly surprising that P301S neurons did not show elevated p-Tau (AT8) signal after Tau PFF seeding. This could be explained by the considerations mentioned above, namely saturated AT8 signal in developing neurons, short treatment duration or the absence of FTD mutations in

the Tau PFFs. It is possible that P301S neurons are more susceptible to tau seeding and aggregation only when the Tau PFFs themselves also carry FTD mutations, as was observed by Manos et al. [281].
Truncated tau fibrils carrying FTD-associated mutations are arguably less relevant to AD than the full-length 2N4R tau fibrils used in this thesis. Ideally, however, fibrils composed of both 3R and 4R tau would provide the most physiologically accurate model, since tau aggregates in AD are composed of both isoforms. Additionally, AD Tau has a different fold to other tauopathies [139, 132]. Future studies may therefore benefit from incorporating brain-derived tau aggregates. Nonetheless, I have shown that 2N4R Tau PFF-driven neurite loss correlates with clinical measures of AD and with the amount of secreted tau in these neurons, suggesting that this insult relevant to study Tau pathology *in vitro*.

5.7.3 Minimal Transcriptomic Response to Tau PFF Exposure in Bulk RNA Sequencing

Bulk RNA sequencing revealed that Tau PFF exposure induced minimal transcriptomic changes in iPSC-derived neurons. This is consistent with prior observations from our group using α-syn PFFs in astrocytes and dopamine neurons, and with findings by Weidling et al., who similarly detected no differentially expressed genes in cortical inhibitory or hypothalamic neurons seeded with Sarkosyl-insoluble AD brain extract for 72 hours [501]. Importantly, they replicated this absence of transcriptomic change at 1, 2, and 3 weeks post-seeding, despite robust aggregation evidenced by MC1 staining, highlighting that a short treatment timeframe is not the cause behind the lack of transcriptomic changes.
In contrast, single-cell studies have identified transcriptional differences between neurons bearing NFTs and those without them [343, 353]. This suggests that bulk sequencing may dilute or obscure transcriptomic signals arising from the proportion of neurons that internalise PFFs and that single-cell methods -ideally after FACs sorting- might be better suited to investigate Tau PFF mechanisms in iPSC models.

5.8 Conclusion

In summary, this chapter set out to characterise Tau expression and evaluate the effects of Tau PFF exposure in AD iPSC-derived neurons, while also assessing whether neuronal vulnerability to Tau insult reflected clinical features of the donors. I demonstrated that these AD patient-derived neurons express high and variable

levels of Tau and phospho-Tau, and that Tau PFFs consistently induced neurite loss, although this effect was markedly attenuated in the presence of astrocytes. Tau PFFs also caused no significant reduction in synapse density, though variability between differentiations indicates the need for a more robust synaptic assays. Moreover, Tau PFF treatment produced a modest but significant increase in AT8-positive puncta, suggesting potential seeding and endogenous phosphorylation, though alternative staining methods are needed. Finally, bulk RNA sequencing revealed that Tau PFF exposure triggered very few transcriptomic changes in control cortical neurons, reinforcing the idea that Tau PFF insult may not elicit strong responses in this model. Together, these findings provide important insights into Tau biology and PFF-induced vulnerability in sAD iPSC models, while also identifying key limitations to address in future studies.

Chapter 6

Discussion and Concluding remarks

6.1 Thesis overview

The overarching aim of this thesis was to determine whether induced pluripotent stem cell (iPSC) lines derived from patients with sporadic Alzheimer's disease (sAD) retain clinically meaningful features of the individuals from whom they originate. Specifically, this work sought to assess whether iPSC-derived neurons capture patient-specific vulnerability to AD–relevant pathological insults, and whether in vitro phenotypes relate to clinical measures of disease severity in vivo. To address this, the effects of the two core pathological hallmarks of AD—Aβ and tau—were investigated across cellular, transcriptional, and molecular levels.

In Chapter 3, I tested whether iPSC-derived cortical neurons from sAD patients exhibited differential susceptibility to Aβ-induced neurotoxicity, and whether this variability reflects intrinsic, donor-specific properties. I demonstrated that Aβ induces a dose-dependent loss of neurites, reduced branching complexity, and increased neuronal loss across 14 AD patient-derived neuronal lines. Crucially, Aβ-induced neurite loss correlated with clinical measures of disease severity in the donor patients, including hippocampal volume adjusted for amyloid burden. Neurite loss also correlated with CSF p-tau/t-tau levels at Day 7, and with CSF Aβ42:40 and Aβ42 levels at Day 70. Together, these findings provide strong evidence that sAD iPSC-derived neurons can recapitulate patient-specific susceptibility to amyloid toxicity and reflect clinically relevant aspects of disease progression.
Additionally, vulnerability to Aβ was consistent within patient lines across independent differentiations and across two forms of insult (Aβ1–42 and Aβ25–35), demonstrating that susceptibility to Aβ is a reproducible and intrinsic property of each donor rather than an artefact of experimental variability. Neurite loss measured

at Day 7 significantly negatively correlated with neurite loss at Day 70, indicating a maturation-dependent shift in vulnerability. This suggests that vulnerability to Aβ is not a single fixed property of each donor but a context-dependent state that changes with cellular maturation: at Day 7, vulnerability may reflect the capacity of immature neurons to extend neurites under stress, while at Day 70, it may reflect the capacity of more mature neurons to sustain stable synaptic and metabolic function under stress. Some donors may therefore sit at one end of one axis and the opposite end of the other. As discussed in Chapter 3, a potential mechanism for this maturation-dependent change in vulnerability is the metabolic shift from glycolysis to OXPHOS.

Based on the substantial spectrum of vulnerability to Aβ observed in the DFP cohort in Chapter 3, and in prior work [322], Chapter 4 aimed to take an unbiased approach to investigate mechanisms underlying differential susceptibility to Aβ. I performed bulk RNA sequencing following Aβ exposure, first in control neurons (i^3 neurons), and subsequently in patient-derived neurons from the DFP cohort. Across both systems, Aβ exposure induced substantial transcriptional remodelling; however, the magnitude, consistency, and structure of these responses differed between models, as discussed in detail in Chapter 4. In i^3 neurons, Aβ elicited robust and reproducible transcriptional changes, including enrichment of pathways related to synaptic function, neuronal projection, cell adhesion, and lipid biosynthesis, alongside downregulation of proteasomal and translational pathways.
These findings implicated impaired cholesterol metabolism as a potential mediator of Aβ-induced toxicity and motivated targeted experimental interrogation of this pathway. Despite strong transcriptional enrichment of cholesterol biosynthesis pathways, neither genetic suppression of cholesterol synthesis via CRISPRi-mediated knockdown of SREBP1 and SREBP2, nor pharmacological inhibition using the cholesterol-modifying compounds simvastatin and YM53601, mitigated Aβ-induced neurotoxicity as assessed by neurite outgrowth, cell death, and AK release. One possible explanation for this lack of effect is the striking decrease in SREBP1 and SREBP2 protein levels observed following Aβ treatment. I discussed whether this apparent discrepancy between RNA and protein levels could reflect a temporal lag between transcriptional changes and protein synthesis, or whether the observed RNA upregulation represents a compensatory response to earlier inhibition of cholesterol synthesis. However, Aβ exposure did induce time-dependent lipid droplet accumulation, demonstrating that altered lipid metabolism is a prominent cellular

response to Aβ, even if it does not directly modulate neuronal vulnerability in i3 neurons.

In patient-derived neurons, while line identity accounted for a significant proportion of transcriptional variance, Aβ exposure induced gene expression changes across patient lines, including upregulation of stress response pathways and downregulation of pathways related to cytoskeletal organisation, axonal projection, synaptic function, and oxidative phosphorylation. The negative enrichment of axonal projection and synaptic pathways was consistent with my observations of Aβ-induced neurite loss (Chapter 3) and prior observations of synapse loss [322].

The inconsistent direction of pathway enrichment between i^3 and DFP neurons was discussed in Chapter 4, and potential explanations included differences in experimental design, most notably the comparison of a single control line replicated across three differentiations versus 13 genetically heterogeneous AD patient lines; or the fact that i3 neurons are derived from a healthy control while the DFP lines are all derived from patients with established AD, which may lead to differences in their transcriptional responses to Aβ. While these are likely drivers, subtle differences in media composition and differentiation protocols may also influence neuronal subtype composition, maturation state, or metabolic profile. For instance, the DFP neurons are grown in neurobasal media, while the i3s are grown in BrainPhys media, and while the supplements in each are similar, DFP media contains Ascorbic Acid (AA), which the i3 media does not. AA is involved in the synthesis of neurotransmitter, has been shown to increase β-tubulin expression and promote synaptic maturation [401]. One study comparing BrainPhys vs Neurobasal media in i3s showed differences in gene expression (iNeuron RNA-Seq App, [471]). For example, CTIP2, a marker of deep-layer cortical neurons, is robustly expressed in DFP neurons (Figure 3.4) but expressed at very low levels in i^3 neurons in both my dataset (Figure 4.3) and other studies [471, 379, 349].

Finally, comparison of resilient and vulnerable patient lines, ranked by ADAS-cog scores, revealed no significant differences in the transcriptional response to Aβ exposure between groups. However, there were baseline transcriptional differences independent of Aβ exposure between resilient and vulnerable patients. The expression of those genes in the 13 AD lines was then correlated with clinical metrics, which revealed significant associations with multiple clinical measures, including cognitive decline and CSF amyloid and tau biomarkers. Notably, genes that were positively correlated with better cognitive scores largely correlated with worse amyloid

pathology (lower CSF Aβ42:40), while genes associated with worse cognition correlated with lower amyloid pathology (high CSF Aβ42:40). The reasons for this counterintuitive observation remain unclear. One possibility is that some genes are only significant due to one or two lines driving the correlation. Performing influential point analysis—which asks whether a result would remain significantly altered if a specific data point was removed—on a per-gene, per-line basis would be a meaningful next step to understand this discrepancy and better interpret these findings.

In Chapter 5, I extended this investigation to patient-specific vulnerability to tau pathology, the second major pathological hallmark of Alzheimer's disease. I characterised protein levels of total tau, phosphorylated tau, and GSK3β expression in iPSC-derived neurons from the DFP cohort, revealing substantial inter-individual heterogeneity. Importantly, total tau levels significantly correlated with tau PET signal, providing further evidence that iPSC-derived neurons retain clinically meaningful donor-specific features. The cellular p-tau/t-tau protein ratio positively correlated with patient MMSE decline rate. This relationship differed from some prior reports [245], potentially reflecting differences in cohort composition and analytical approach.

Using full-length 2N4R tau pre-formed fibrils (PFFs), this study represents one of the most extensive analyses of tau-induced neurotoxicity in sporadic AD patient-derived neurons to date. Tau PFF exposure induced neurite loss across patient lines, an effect mitigated by the addition of rat astrocytes. The degree of vulnerability to tau PFFs correlated with hippocampal volume normalised to CSF total tau, mirroring the correlation observed between Aβ-induced neurite loss and hippocampal volume normalised to CSF Aβ42:40. Enhanced neurite loss in response to tau PFFs also correlated with markers of amyloid pathology, including CSF Aβ42:40 ratios and amyloid PET signal, paralleling relationships observed for Aβ-induced neurite loss in Chapter 3. In contrast to Aβ exposure, tau PFF treatment induced minimal transcriptional changes in i^3 neurons, suggesting that tau-mediated neurotoxicity may operate through mechanisms distinct from widespread transcriptional reprogramming. Together, these findings suggest that vulnerability to tau insult in vitro is linked to amyloid burden in vivo, supporting a model in which amyloid and tau pathologies are mechanistically intertwined rather than independent.

6.1.0.1 Integration across chapters: patterns and divergences

Cellular vulnerability is patient-specific across multiple insults, but the same lines are not uniformly vulnerable. Aβ-induced neurite loss (Chapter 3) and tau-PFF-induced neurite loss (Chapter 5) both show substantial inter-line variability, but the rank order of lines is not preserved across the two insults. A line near the top of the Aβ vulnerability ranking is not reliably near the top of the tau ranking, and neither ranking maps cleanly onto the ADAS-Cog-based clinical stratification used to define resilient and vulnerable groups in Chapter 4. While the limitations of the vulnerability ranking in Chapter 4 were discussed extensively already, this argues against a single "fragility" property of each donor and instead supports a model in which patient-specific vulnerability is multidimensional, with distinct molecular pathways conferring susceptibility to different pathological insults.

This is also supported by the bulk RNA-sequencing experiments in Chapters 4 and 5. The minimal transcriptional response to tau PFFs was hard to reconcile with the substantial neurite loss observed in monoculture. And it contrasts sharply with the broad transcriptional remodelling induced by Aβ (Chapter 4). I discussed in Chapter 5 that two possible interpretations of this result could be that tau-PFF-induced toxicity operates predominantly through post-translational mechanisms, and that bulk RNA sequencing dilutes single-cell transcriptional responses occurring only in the small subset of neurons that internalise PFFs– which is supported by the literature which showed no transcriptional changes in iPSC derived neurons [501], unless the neurons were FACs sorted to only include neurons with NFTs [343, 353]. Either way, the divergence between the morphological and transcriptional readouts is itself a finding: it implies that the mechanisms by which Aβ and tau damage neurons are different, even when the downstream phenotype (neurite loss) is similar, hence why different cell lines are vulnerable to tau and Aβ insult.

Furthermore, the baseline transcriptional differences between resilient and vulnerable lines identified in Chapter 4—elevated translation, protein folding, and oxidative stress protection in resilient lines; elevated synaptic signalling, adhesion, and projection programmes in vulnerable lines—are mechanistically coherent with the morphological phenotypes measured in Chapters 3 and 5. High baseline proteostatic capacity may plausibly protect against the proteotoxic stress imposed by both Aβ and tau aggregates, while elevated neuronal activity may plausibly exacerbate activity-dependent damage. This also agrees with findings from other groups which find that proteosomal genes are downregulated in AD brains and iPSC neurons from AD patients [245, 289], and that enhancing proteosome activity ameliorates Aβ and

tau pathology [96, 468].

The results presented in this thesis extend previous work demonstrating that iPSC-derived neurons retain clinically meaningful, donor-specific features [322, 395, 245, 248]. While earlier studies established concordance between iPSC-derived neuronal phenotypes and AD biomarkers or brain transcriptomic profiles, this work directly links cellular vulnerability to extrinsic Aβ and tau insults with in vivo measures of neurodegeneration and clinical severity. Building on prior work in our lab, this thesis demonstrates that Aβ-induced neurite loss correlates with hippocampal volume normalised to amyloid burden, and provides the most extensive transcriptomic analysis to date of Aβ exposure in iPSC-derived neurons. Whereas only two prior studies have examined transcriptional responses to Aβ insult—one limited to three control lines [84] and the other comparing a single APOE2 and APOE3 line [435]—this work analyses Aβ-induced transcriptional changes across a cohort of 13 sporadic AD patient-derived neuronal lines, enabling assessment of both shared and inter-individual responses.
In addition, this thesis demonstrates that tau protein levels in iPSC neurons reflect tau pathology in the donor brain and shows, for the first time, that cellular vulnerability to tau PFFs correlates with clinical measures of disease vulnerability in patients, demonstrating the feasibility of modelling patient-specific vulnerability to Tau pathology *in vitro* .

Two specific points of divergence with prior work are worth noting. First, the directionality of the association between cellular p-Tau/tTau and cognitive decline observed here differs from that reported by Lagomarsino et al. in the ROSMAP cohort. As discussed in Chapter 5 , methodological differences (different phospho-epitopes, different statistical models, different adjustment for covariates) may account for some of this, but the possibility that the DFP and ROSMAP cohorts differ in clinically meaningful ways—DFP containing only sAD patients, ROSMAP being a community-based cohort with many cognitively normal donors, donors with AD, and resilient donors with AD pathology but no cognitive decline—should not be dismissed.
Second, the failure of cholesterol synthesis inhibition to rescue Aβ-induced neurite loss in i^3 neurons (Chapter 4) diverges from work in mouse cortical neurons [94] and in familial AD iPSC neurons [478] showing that cholesterol modulation reduces Aβ-induced neurotoxicity. The discrepancy may reflect differences in cell type, timing

of inhibition, donor patient (fAD vs sAD), but it is informative: it suggests that the contribution of cholesterol to Aβ-induced toxicity may be context-dependent rather than universal, with implications for whether cholesterol-modulating drugs are likely to be uniformly effective across AD subtypes.

Collectively, these findings support the utility of iPSC models for capturing patient-specific susceptibility to both amyloid and tau pathology. sAD is a genetically complex disease, and this work adds to the growing body of evidence that demonstrates the value of iPSC models for studying patient-specific disease mechanisms in the brain. These findings have several implications for AD research. First, patient-derived iPSC neurons can be used to test hypotheses about individual-level disease mechanisms in ways that post-mortem tissue cannot, because the cells can be repeatedly differentiated, perturbed, and profiled while still reflecting meaningful aspects of the donor's biology. For instance, the baseline transcriptional differences identified between resilient and vulnerable lines — in translation, protein folding, and oxidative stress protection — point to candidate pathways that could be targeted pharmacologically, and tested for their ability to shift vulnerable neurons toward a more resilient state in cells matched to the patient. Furthermore, the observation that different donors appear to be vulnerable to different insults supports the idea that sAD is not a single disease but a set of partially overlapping subtypes, distinguishable not only by their vulnerability to amyloid and tau pathology but also by the underlying cellular processes that determine how neurons respond to those insults — including proteostatic capacity, neuronal excitability, and lipid handling. As larger iPSC cohorts become available, this kind of cellular subtyping could contribute to precision medicine approaches in AD by complementing clinical and biomarker-based stratification, and informing which patients are most likely to benefit from which therapies.

6.2 The use of synthetic protein aggregates to model neurodegeneration

In this thesis, synthetic Aβ and tau protein aggregates were used to model AD pathology. However, the concentrations required to induce neurite loss and cell death are supraphysiological, with reported CSF concentrations of approximately 1 pM for Aβ, 300-700 ng/ml for total tau, around 80ng/mL for pTau 181 [199, 528], compared with 5-10 μM Aβ and 1.25-5μg/mL Tau PFFs used here. These concentrations

were used to model the effects of pathological burden over a short experimental timeframe, compressing processes that occur over years in vivo. Although truly recapitulating the gradual formation of pathology is not currently feasible in cell models, in retrospect, treatment paradigms where neurons are insulted over weeks at lower concentrations may have more closely mimicked physiological mechanisms, and should be used in the future, where feasible.

Furthermore, synthetic aggregates do not replicate the species present in the human brain. In vitro–generated Aβ oligomers and fibrils differ structurally from those isolated AD brains [307, 507], as well as having different aggregation dynamics [392]. Interestingly, isolation of Aβ from AD brains, revealed that sAD and fAD Aβ filaments had different structures from one another [521]. On the other hand, synthetic Aβ oligomers have been shown to have similar functional effects as brain derived-AB. Both induced neurite loss, synapse loss and cell death [322, 217], both were shown to cause tau hyperphosphorylation in hippocampal neurons [217]. Furthermore synthetic Aβ oligomer also binds NMDAR receptors, promoting calcium influx [110, 73], which in fAD mouse models, as discussed in Chapter 1, has been shown to cause hyperactivity and induce synapse loss. Therefore, despite structural difference in Aβ aggregates, which should be considered carefully, synthetic Aβ aggregates retain many of the functions that endogenous Aβ aggregates have, making them an appropriate insult to study AD pathology in cell models.
Similarly, synthetic tau filaments differ from those found in AD [530]. The tau PFFs used here consisted of unphosphorylated full-length 2N4R tau, whereas AD brain tau aggregates comprise a mixture of phosphorylated 3R and 4R tau adopting the characteristic AD fold described in Chapter 1 [139]. I have discussed previously that recombinant full length Tau PFFs are internalised by iPSC neurons and can trigger hyperphosphorylation of endogenous tau [476], however, other studies have demonstrated differences between recombinant tau and brain-derived tau oligomers [281]. It has been shown that synthetic tau and AD or control brain-derived tau aggregates are both internalised, but not degraded by astrocytes, and that they can both spread between cells. However, AD-brain tau elicit a stronger reaction state in astrocytes compared to control brains, and only astrocyte medium from astrocytes treated with AD-brain tau fibrils cause synaptotoxicity [126]. Furthermore, tau derived from brains of patients with various tauopathies are internalised via different routes in primary cortical neurons. These results highlight that while recombinant tau can recapitulate several disease relevant mechanisms, these structural differences

are an important consideration when interpreting the relevance of the cellular and transcriptomic changes observed in this thesis.

The use of brain-derived Aβ and tau oligomers thereby may be a more physiologically relevant alternative to study tau insult in vitro. However, such preparations suffer from low yield, scalability challenges, and batch-to-batch variability. For instance, one study reported marked differences in the species of tau oligomers in different AD brains. There were differences in their phosphorylation sites, which were associated with their seeding propensities, which in turn correlated to the rate of disease progression. Notably, soluble tau from different AD brains also respond differently to a panel anti-tau antibodies [118]. While these results obviously have important implications to understand the differences in progression of tau pathology between patients, as well as for potential anti-tau therapeutics, they also pose important logistical complications when considering using brain-derived tau oligomers in iPSC models, where replicability and consistency across experiments and differentiations are essential to draw relevant conclusions. Although, as discussed in Chapter 3, synthetic oligomers also exhibit variability, I demonstrated that Aβ- and tau-induced neurite loss was consistent across experiments at several timepoints, and correlated with clinical measures of vulnerability. In conclusion, despite their limitations, synthetic aggregates remain valuable tools for interrogating AD-relevant mechanisms in iPSC models, although improvement of yield and replicability of brain-derived tau oligomers for use in iPSC-derived neuronal models would be highly beneficial, and should be pursued in the future.

To bypass extrinsic aggregate addition altogether, 3D culture systems could be considered, with or without co-culture of other cell types. These models are particularly well suited to studying later disease stages characterised by the accumulation of Aβ and tau, as time-dependent inclusion of Aβ and Tau in organoids has been demonstrated previously [376, 163]. However, current 3D culture systems also bring about complications: organoids develop a necrotic core due to the lack of vascularisation [153], and also suffer from lack of reproducibility [374, 373], although recent studies introducing vascular-like structures into brain organoids [65, 417], and improvements in protocols which increase reproducibility [46, 7] have begun to address some of these limitations. Nonetheless, given the number of patient lines used in this project, the complexity and length of 3D culture protocols would

be logistically challenging, and these systems may be better suited to smaller scale studies.

6.3 Modelling resilience and vulnerability in Alzheimer's disease

Increasing evidence in imaging and biomarker studies in the human brain suggest that amyloid-beta pathology precedes tau deposition in cognitively unimpaired individuals (CU). Tau pathology, in turn, is more closely related to cognitive decline. Amyloid and Tau positive (A+T+) individuals have a greater risk of future cognitive decline than (A+T-) individuals [342]. Nonetheless, a substantial proportion of A+T+ individuals remain cognitively unimpaired for more than 3.5 years, indicating considerable heterogeneity in clinical progression even within this high-risk group. The observation that tau pathology and subsequent cognitive decline can occur independently of amyloid in other tauopathies has raised questions regarding the relevance of the amyloid cascade hypothesis. This has led to the suggestion that the strong emphasis on Aβ in research and therapeutic development is driven largely by the fact that familial AD (fAD) is caused by mutations that increase Aβ production, and may therefore be less relevant to sporadic AD (sAD).

However, findings from this thesis together with other studies support a central role for Aβ in sAD pathogenesis. Aβ has been shown to be neurotoxic in rodent and cellular models, and recent studies in iPSC-derived neurons from late onset AD patients demonstrate that CSF Aβ42:40 correlates with cognitive decline and polygenic risk scores (PRS). In addition, genome-wide association studies have identified multiple AD risk genes involved in Aβ clearance and APP processing. APOE, for example, mediates Aβ clearance in astrocytes, with efficiency decreasing from APOE2 to APOE3 to APOE4 [105, 38]. Other risk genes, including PICALM and CLU have also been implicated in Aβ clearance [38, 533], and CLU has been shown to modulate Aβ toxicity in iPSC-derived neurons [385, 141]. Furthermore, rodent studies discussed in chapter 1 demonstrated that Aβ exacerbates tau pathology. Together with the findings from the DFP cohort, these data support a model in which individuals with sAD exhibit varying susceptibility to Aβ accumulation, likely driven by genetic factors affecting clearance or inflammation, among others, causing cellular stress which in turn promote tau phosphorylation and aggregation, ultimately leading to the development of cognitive symptoms.

iPSC modelling provides a powerful platform to interrogate these mechanisms of vulnerability in patient-derived cells carrying different genetic risk factors. An important limitation of iPSC-based approaches is the loss of environmental and age-related risk factors during reprogramming, which are known to contribute to the risk of developing sAD. While direct differentiation from fibroblasts or PBMCs is now possible, these approaches present challenges in scalability, as the iPSC stage enables cell expansion prior to differentiation [300, 151]. Nonetheless, sAD has high heritability, and GWAS indicate that a substantial proportion of disease risk is genetically mediated, making iPSC models well suited to isolating and experimentally examining key aspects of this genetic susceptibility without environmental confounds. This is exemplified by the observations in this thesis, supported by other work in the DFP [322, 395] and ROSMAP cohorts [245, 248], which show that iPSC derived from sAD patients, which have lost environmental risk factors, retain clinically meaningful, patient-specific features. This suggests that a large subset of sAD is still (poly)genetically driven.

This thesis, together with previous studies [245, 322] supports the relevance of studying cortical neurons when modelling vulnerability and resilience in neurodegeneration. Neurons in the limbic and forebrain region are more vulnerable to pathological depositions and degeneration than more caudal brain regions [503, 505]. This selective vulnerability has been recapitulated in iPSC-derived fAD neurons, where iPSC-derived cortical neurons (both inhibitory and excitatory neurons) exhibited increased cellular total Tau and pTau and higher secreted Aβ42:40 than neurons from caudal regions (e.g. hindbrain, spinal cord neurons). These cortical neurons were also vulnerable to treatment with AD-brain extract, while caudal neurons were unaffected [317].
Selective neuronal vulnerability is perhaps most clearly illustrated in Parkinson's disease, in which dopaminergic neurons of the substantia nigra preferentially degenerate. This phenomenon has been demonstrated in vitro, including in studies from our lab, which show that iPSC-derived dopamine neurons are more vulnerable to a-synuclein PFFs than other neuronal subtypes [9, 501, 34].
Cholinergic neuron loss is an early pathological feature of AD [314, 301], and iPSC-derived cholinergic neurons have been shown to be particularly vulnerable to glutamate-mediated cell death [116]. In contrast, cholinergic neurons were found to have less Aβ42:40 than glutamatergic neurons derived from the same patients, and Aβ oligomers induced greater tau phosphorylation and abnormal

electrophysiological activity in glutamatergic—but not cholinergic—neurons [462]. These findings highlight the importance of modelling multiple neuronal subtypes to dissect disease-relevant pathways.
While this thesis focused on excitatory cortical neurons, other studies have identified inhibitory interneuron populations [501, 337, 74], as being selectively vulnerable in AD. Indeed, somatostatin expression is decreased in AD brains [97], and several studies have reported that the loss of somatostatin and parvalbumin positive interneurons is associated with cognitive decline [337, 74]. Additionally, in iPSC-derived neurons, somatostatin interneurons were more vulnerable to brain derived tau oligomers than excitatory hippocampal neurons [501].

Furthermore, substantial evidence indicates that other cell types—including astrocytes, microglia, and oligodendrocytes— might be an important contributor in conferring increased vulnerability to disease progression. More than 50% of AD GWAS hits are most highly expressed in microglia, and APOE4, the strongest genetic risk factor for AD, is expressed at relatively low levels in neurons. A study published in January 2026 estimated that the fraction of AD risk attributable to APOE genotype ranged from 71.5% to 92% across four large cohorts [510]. If these estimates are accurate, mechanisms driving vulnerability to Aβ and tau pathology must be investigated in other brain cell types. Consistent with this, Bellaver et al. demonstrated that Aβ was associated with increased tau phosphorylation and tangle accumulation only in individuals exhibiting astrogliosis (2023) [40]. Rodent studies further show that injection of fibrillar Aβ-containing brain homogenates induces tau pathology via activation of the microglial NLRP3 inflammasome [204]. Studies have shown that iPSC-derived astrocytes derived from patient with high or low levels of inflammation in the CSF have differential responses to Aβ insult [395], and that iPSCs-derived from resilient individuals have elevated secretion of interferon gamma. Accordingly, higher PRS scores were associated with lower levels of interferon proteins in iPSC-derived astrocytes [248].
In my study, I did not observe transcriptional differences in neuronal responses to Aβ between resilient and vulnerable Aβ+ individuals. While the small number of individuals and replicates likely contributed, it would be informative to assess whether glial cells derived from these same individuals exhibit differential responses to Aβ.

Large-scale co-culture models incorporating patient-derived neurons and glia would

be particularly valuable but at a scale would require substantial optimisation and collaborative effort. With this in mind, Lish et al. have demonstrated that the use of transcription factor-driven protocols, such as NgN2-driven cortical neuron differentiation or SOX9/NFIB driven astrocyte differentiation, while also establishing cryopreservation steps for each cell type, enables cocultures in 20 days post thawing [263]. This is considerably easier and shorter than other coculture protocols which are often 90+ days long, and represent significant logistical challenges [167, 396, 397].

6.4 Concluding remarks and future directions

The results of this thesis strengthen existing evidence that iPSC-derived neurons retain clinically meaningful features of the patients from whom they are derived. This work also demonstrates that sAD patient-derived neurons are differentially vulnerable to both Aβ and tau insults, and that this vulnerability correlates with *in vivo* clinical measures. In addition, this thesis identified several genes and pathways that are altered after Aβ insult, and that are differentially regulated between resilient and vulnerable individuals. Future work will focus on validating key findings from the RNA sequencing analyses through targeted mechanistic studies. An additional 35 iPSC lines from the DFP cohort have now been generated, enabling validation of identified genes and pathways in a larger cohort.

Further investigation of tau PFF–induced phenotypes is warranted. Given variability in synaptic staining, alternative approaches such as multi-electrode array recordings or calcium imaging could be employed to probe synaptic vulnerability. Optimisation of methanol-based staining protocols to look at tau phosphorylation will also be important to assess whether specific sAD neurons exhibit increased propensity for tau hyperphosphorylation. Finally, comparing phenotypes induced by synthetic tau PFFs with those elicited by brain-derived tau oligomers, even at smaller scale, would provide valuable insight into the physiological relevance of synthetic tau PFFs. Furthermore, expanding this work to include other cell types, establishing coculture systems with astrocytes and microglia, and comparing the transcriptomic signatures of these cell types in response to Aβ or tau insult will be important in determining drivers of vulnerability in sAD.

Finally, the demonstration that iPSC-derived neurons recapitulate donor-specific susceptibility raises the possibility of precision medicine approaches, whereby

therapeutic targets and treatment efficacy could be assessed in patient-specific models. As larger cohorts of sAD iPSC lines become available, this approach may enable identification of subtypes of sporadic AD, and prediction of individual responses to therapy, informing optimal treatment strategies in the future.

References

[1] A new rating scale for Alzheimer's disease. *American Journal of Psychiatry*, 141(11):1356–1364, November 1984.

[2] *Risk Reduction of Cognitive Decline and Dementia: WHO Guidelines*. WHO Guidelines Approved by the Guidelines Review Committee. World Health Organization, Geneva, 2019.

[3] World Health Organisation: Ageing and Health. Technical report, World Health Organisation, January 2025.

[4] Simon Adelman, Martin Blanchard, Greta Rait, Gerard Leavey, and Gill Livingston. Prevalence of dementia in African–Caribbean compared with UK-born White older people: two-stage cross-sectional study. *British Journal of Psychiatry*, 199(2):119–125, August 2011.

[5] Mahiuddin Ahmed, Judianne Davis, Darryl Aucoin, Takeshi Sato, Shivani Ahuja, Saburo Aimoto, James I Elliott, William E Van Nostrand, and Steven O Smith. Structural conversion of neurotoxic amyloid-β1–42 oligomers to fibrils. *Nature Structural & Molecular Biology*, 17(5):561–567, May 2010.

[6] Tariq Ahmed, Ann Van Der Jeugd, David Blum, Marie-Christine Galas, Rudi D'Hooge, Luc Buee, and Detlef Balschun. Cognition and hippocampal synaptic plasticity in mice with a homozygous tau deletion. *Neurobiology of Aging*, 35(11):2474–2478, November 2014.

[7] Giuseppe Aiello, Mohamed Nemir, Barbora Vidimova, Cindy Ramel, Joanna Viguie, Arianna Ravera, Krzysztof Wrzesinski, and Claudia Bagni. Increased reproducibility of brain organoids through controlled fluid dynamics. *EMBO Reports*, 26(24):6209–6239, November 2025.

[8] Erin J. Aiello Bowles, Paul K. Crane, Rod L. Walker, Jessica Chubak, Andrea Z. LaCroix, Melissa L. Anderson, Dori Rosenberg, C. Dirk Keene, and Eric B.

Larson. Cognitive Resilience to Alzheimer's Disease Pathology in the Human Brain. *Journal of Alzheimer's Disease*, 68(3):1071–1083, April 2019.

[9] Ajantha Abey. *Investigating Selective Neuronal Vulnerability in Alzheimer's and Parkinson's Disease with Induced Pluripotent Stem Cells*. PhD thesis, University of Oxford, 2024.

[10] Elena Alberdi, Mª Victoria Sánchez-Gómez, Fabio Cavaliere, Alberto Pérez-Samartín, José Luis Zugaza, Ramón Trullas, María Domercq, and Carlos Matute. Amyloid β oligomers induce Ca2+ dysregulation and neuronal death through activation of ionotropic glutamate receptors. *Cell Calcium*, 47(3):264–272, March 2010.

[11] Marilyn S. Albert, Steven T. DeKosky, Dennis Dickson, Bruno Dubois, Howard H. Feldman, Nick C. Fox, Anthony Gamst, David M. Holtzman, William J. Jagust, Ronald C. Petersen, Peter J. Snyder, Maria C. Carrillo, Bill Thies, and Creighton H. Phelps. The diagnosis of mild cognitive impairment due to Alzheimer's disease: Recommendations from the National Institute on Aging-Alzheimer's Association workgroups on diagnostic guidelines for Alzheimer's disease. *Alzheimer's & Dementia*, 7(3):270–279, May 2011.

[12] Amani Alghamdi, Julie Vallortigara, David R. Howlett, Martin Broadstock, Tibor Hortobágyi, Clive Ballard, Alan J. Thomas, John T. O'Brien, Dag Aarsland, Johannes Attems, Paul T. Francis, and David R. Whitfield. Reduction of RPT6/S8 (a Proteasome Component) and Proteasome Activity in the Cortex is Associated with Cognitive Impairment in Lewy Body Dementia. *Journal of Alzheimer's Disease*, 57(2):373–386, March 2017.

[13] Madeline Ally, Michael A. Sugarman, Henrik Zetterberg, Kaj Blennow, Nicholas J. Ashton, Thomas K. Karikari, Hugo J. Aparicio, Brandon Frank, Yorghos Tripodis, Brett Martin, Joseph N. Palmisano, Eric G. Steinberg, Irene Simkin, Lindsay A. Farrer, Gyungah R. Jun, Katherine W. Turk, Andrew E. Budson, Maureen K. O'Connor, Rhoda Au, Lee E. Goldstein, Neil W. Kowall, Ronald Killiany, Robert A. Stern, Thor D. Stein, Ann C. McKee, Wei Qiao Qiu, Jesse Mez, and Michael L. Alosco. Cross-sectional and longitudinal evaluation of plasma glial fibrillary acidic protein to detect and predict clinical syndromes of Alzheimer's disease. *Alzheimer's & Dementia: Diagnosis, Assessment & Disease Monitoring*, 15(4):e12492, October 2023.

[14] Claudia G. Almeida, Reisuke H. Takahashi, and Gunnar K. Gouras. β-Amyloid Accumulation Impairs Multivesicular Body Sorting by Inhibiting the Ubiquitin-Proteasome System. *The Journal of Neuroscience*, 26(16):4277–4288, April 2006.

[15] Alois Alzheimer. Über eine eigenartige Erkrankung der Hirnrinde. *Allgemeine Zeitschrift fur Psychiatrie und Psychisch-gerichtliche Medizin.*, (64:146-8.), January 1907.

[16] Alejandra del C. Alonso, Inge Grundke-Iqbal, and Khalid Iqbal. Alzheimer's disease hyperphosphorylated tau sequesters normal tau into tangles of filaments and disassembles microtubules. *Nature Medicine*, 2(7):783–787, July 1996.

[17] Alejandra Del C. Alonso, Tanweer Zaidi, Michal Novak, Inge Grundke-Iqbal, and Khalid Iqbal. Hyperphosphorylation induces self-assembly of τ into tangles of paired helical filaments/straight filaments. *Proceedings of the National Academy of Sciences*, 98(12):6923–6928, June 2001.

[18] Alejandra del C. Alonso, Inge Grundke-Iqbal, Héctor S. Barra, and Khalid Iqbal. Abnormal phosphorylation of tau and the mechanism of Alzheimer neurofibrillary degeneration: Sequestration of microtubule-associated proteins 1 and 2 and the disassembly of microtubules by the abnormal tau. *Proceedings of the National Academy of Sciences*, 94(1):298–303, January 1997.

[19] Athena Andreadis. Tau gene alternative splicing: expression patterns, regulation and modulation of function in normal brain and neurodegenerative diseases. *Biochimica et Biophysica Acta (BBA) - Molecular Basis of Disease*, 1739(2-3):91–103, January 2005.

[20] Shea J. Andrews, Alan E. Renton, Brian Fulton-Howard, Anna Podlesny-Drabiniok, Edoardo Marcora, and Alison M. Goate. The complex genetic architecture of Alzheimer's disease: novel insights and future directions. *eBioMedicine*, 90:104511, April 2023.

[21] Yasushi Arai, Mineo Yamazaki, Osamu Mori, Hiromi Muramatsu, Goro Asano, and Yasuo Katayama. α-Synuclein-positive structures in cases with sporadic Alzheimer's disease: morphology and its relationship to tau aggregation. *Brain Research*, 888(2):287–296, January 2001.

[22] Joseph F. Arboleda-Velasquez, Francisco Lopera, Michael O'Hare, Santiago Delgado-Tirado, Claudia Marino, Natalia Chmielewska, Kahira L. Saez-Torres, Dhanesh Amarnani, Aaron P. Schultz, Reisa A. Sperling, David Leyton-Cifuentes, Kewei Chen, Ana Baena, David Aguillon, Silvia Rios-Romenets, Margarita Giraldo, Edmarie Guzmán-Vélez, Daniel J. Norton, Enmanuelle Pardilla-Delgado, Arabiye Artola, Justin S. Sanchez, Juliana Acosta-Uribe, Matthew Lalli, Kenneth S. Kosik, Matthew J. Huentelman, Henrik Zetterberg, Kaj Blennow, Rebecca A. Reiman, Ji Luo, Yinghua Chen, Pradeep Thiyyagura, Yi Su, Gyungah R. Jun, Marcus Naymik, Xiaowu Gai, Moiz Bootwalla, Jianling Ji, Lishuang Shen, John B. Miller, Leo A. Kim, Pierre N. Tariot, Keith A. Johnson, Eric M. Reiman, and Yakeel T. Quiroz. Resistance to autosomal dominant Alzheimer's disease in an APOE3 Christchurch homozygote: a case report. *Nature Medicine*, 25(11):1680–1683, November 2019.

[23] Paola Arlotta, Bradley J. Molyneaux, Jinhui Chen, Jun Inoue, Ryo Kominami, and Jeffrey D. Macklis. Neuronal Subtype-Specific Genes that Control Corticospinal Motor Neuron Development In Vivo. *Neuron*, 45(2):207–221, January 2005.

[24] Enrique Armijo, Cesar Gonzalez, Mohammad Shahnawaz, Andrea Flores, Brian Davis, and Claudio Soto. Increased susceptibility to Aβ toxicity in neuronal cultures derived from familial Alzheimer's disease (PSEN1-A246E) induced pluripotent stem cells. *Neuroscience Letters*, 639:74–81, February 2017.

[25] Hirohide Asai, Seiko Ikezu, Satoshi Tsunoda, Maria Medalla, Jennifer Luebke, Tarik Haydar, Benjamin Wolozin, Oleg Butovsky, Sebastian Kügler, and Tsuneya Ikezu. Depletion of microglia and inhibition of exosome synthesis halt tau propagation. *Nature Neuroscience*, 18(11):1584–1593, November 2015.

[26] Nicholas J. Ashton, Andréa L. Benedet, Tharick A. Pascoal, Thomas K. Karikari, Juan Lantero-Rodriguez, Wagner S. Brum, Sulantha Mathotaarachchi, Joseph Therriault, Melissa Savard, Mira Chamoun, Erik Stoops, Cindy Francois, Eugeen Vanmechelen, Serge Gauthier, Eduardo R. Zimmer, Henrik Zetterberg, Kaj Blennow, and Pedro Rosa-Neto. Cerebrospinal fluid p-tau231 as an early indicator of emerging pathology in Alzheimer's disease. *eBioMedicine*, 76:103836, February 2022.

[27] Alireza Atri, José L. Molinuevo, Ole Lemming, Yvonne Wirth, Irena Pulte, and David Wilkinson. Memantine in patients with Alzheimer's disease receiving donepezil: new analyses of efficacy and safety for combination therapy. *Alzheimer's Research & Therapy*, 5(1):6, 2013.

[28] Craig S. Atwood, Richard L. Bowen, Mark A. Smith, and George Perry. Cerebrovascular requirement for sealant, anti-coagulant and remodeling molecules that allow for the maintenance of vascular integrity and blood supply. *Brain Research Reviews*, 43(1):164–178, September 2003.

[29] Laura D. Baker, Mark A. Espeland, Rachel A. Whitmer, Heather M. Snyder, Xiaoyan Leng, Laura Lovato, Kathryn V. Papp, Melissa Yu, Miia Kivipelto, Ashley S. Alexander, Susan Antkowiak, Maryjo Cleveland, Claire Day, Richard Elbein, Sarah Tomaszewski Farias, Deborah Felton, Katelyn R. Garcia, Darren R. Gitelman, Sarah Graef, Marjorie Howard, Jeffrey Katula, Katherine Lambert, Olivia Matongo, Anne Marie McDonald, Valory Pavlik, Rema Raman, Stephen Salloway, Christy Tangney, Jennifer Ventrelle, Sharon Wilmoth, Benjamin J. Willliams, Rena Wing, Nancy Woolard, and Maria C. Carrillo. Structured vs Self-Guided Multidomain Lifestyle Interventions for Global Cognitive Function: The US POINTER Randomized Clinical Trial. *JAMA*, 334(8):681, August 2025.

[30] Rodolphe Barrangou, Christophe Fremaux, Hélène Deveau, Melissa Richards, Patrick Boyaval, Sylvain Moineau, Dennis A. Romero, and Philippe Horvath. CRISPR Provides Acquired Resistance Against Viruses in Prokaryotes. *Science*, 315(5819):1709–1712, March 2007.

[31] Nicolas R. Barthélemy, Benjamin Saef, Yan Li, Brian A. Gordon, Yingxin He, Kanta Horie, Erik Stomrud, Gemma Salvadó, Shorena Janelidze, Chihiro Sato, Vitaliy Ovod, Rachel L. Henson, Anne M. Fagan, Tammie L. S. Benzinger, Chengjie Xiong, John C. Morris, Oskar Hansson, Randall J. Bateman, and Suzanne E. Schindler. CSF tau phosphorylation occupancies at T217 and T205 represent improved biomarkers of amyloid and tau pathology in Alzheimer's disease. *Nature Aging*, 3(4):391–401, March 2023.

[32] Susan Spear Bassett, David M. Yousem, Catherine Cristinzio, Ivana Kusevic, Michael A. Yassa, Brian S. Caffo, and Scott L. Zeger. Familial risk for Alzheimer's disease alters fMRI activation patterns. *Brain*, 129(5):1229–1239, May 2006.

[33] Randall J Bateman, Paul S Aisen, Bart De Strooper, Nick C Fox, Cynthia A Lemere, John M Ringman, Stephen Salloway, Reisa A Sperling, Manfred Windisch, and Chengjie Xiong. Autosomal-dominant Alzheimer's disease: a review and proposal for the prevention of Alzheimer's disease. *Alzheimer's Research & Therapy*, 3(1):1, 2010.

[34] Armin Bayati, Riham Ayoubi, Adriana Aguila, Cornelia E. Zorca, Ghislaine Deyab, Chanshuai Han, Sherilyn Junelle Recinto, Emmanuelle Nguyen-Renou, Cecilia Rocha, Gilles Maussion, Wen Luo, Irina Shlaifer, Emily Banks, Ian McDowell, Esther Del Cid Pellitero, Xue Er Ding, Behrang Sharif, Philippe Séguéla, Moein Yaqubi, Carol X.-Q. Chen, Zhipeng You, Narges Abdian, Heidi M. McBride, Edward A. Fon, Jo Anne Stratton, Thomas M. Durcan, Patrick C. Nahirney, and Peter S. McPherson. Modeling Parkinson's disease pathology in human dopaminergic neurons by sequential exposure to α-synuclein fibrils and proinflammatory cytokines. *Nature Neuroscience*, 27(12):2401–2416, December 2024.

[35] Wibke Bechtel, Martin Helmstädter, Jan Balica, Björn Hartleben, Betina Kiefer, Fatima Hrnjic, Christoph Schell, Oliver Kretz, Shuya Liu, Felix Geist, Dontscho Kerjaschki, Gerd Walz, and Tobias B. Huber. Vps34 Deficiency Reveals the Importance of Endocytosis for Podocyte Homeostasis. *Journal of the American Society of Nephrology*, 24(5):727–743, May 2013.

[36] Lynn M. Bekris, Chang-En Yu, Thomas D. Bird, and Debby W. Tsuang. Review Article: Genetics of Alzheimer Disease. *Journal of Geriatric Psychiatry and Neurology*, 23(4):213–227, December 2010.

[37] Ramona Belfiore, Alexis Rodin, Eric Ferreira, Ramon Velazquez, Caterina Branca, Antonella Caccamo, and Salvatore Oddo. Temporal and regional progression of Alzheimer's disease-like pathology in 3xTg-AD mice. *Aging Cell*, 18(1):e12873, February 2019.

[38] Robert D Bell, Abhay P Sagare, Alan E Friedman, Gurrinder S Bedi, David M Holtzman, Rashid Deane, and Berislav V Zlokovic. Transport Pathways for Clearance of Human Alzheimer's Amyloid β-Peptide and Apolipoproteins E and J in the Mouse Central Nervous System. *Journal of Cerebral Blood Flow & Metabolism*, 27(5):909–918, May 2007.

[39] Simon M. Bell, Hollie Wareing, Francesco Capriglia, Rachel Hughes, Katy Barnes, Alexander Hamshaw, Liam Adair, Allan Shaw, Alicja Olejnik, Suman De, Elizabeth New, Pamela J. Shaw, Matteo De Marco, Annalena Venneri, Daniel J. Blackburn, Laura Ferraiuolo, and Heather Mortiboys. Increasing hexokinase 1 expression improves mitochondrial and glycolytic functional deficits seen in sporadic Alzheimer's disease astrocytes. *Molecular Psychiatry*, 30(4):1369–1382, April 2025.

[40] Bruna Bellaver, Guilherme Povala, Pamela C. L. Ferreira, João Pedro Ferrari-Souza, Douglas T. Leffa, Firoza Z. Lussier, Andréa L. Benedet, Nicholas J. Ashton, Gallen Triana-Baltzer, Hartmuth C. Kolb, Cécile Tissot, Joseph Therriault, Stijn Servaes, Jenna Stevenson, Nesrine Rahmouni, Oscar L. Lopez, Dana L. Tudorascu, Victor L. Villemagne, Milos D. Ikonomovic, Serge Gauthier, Eduardo R. Zimmer, Henrik Zetterberg, Kaj Blennow, Howard J. Aizenstein, William E. Klunk, Beth E. Snitz, Pauline Maki, Rebecca C. Thurston, Ann D. Cohen, Mary Ganguli, Thomas K. Karikari, Pedro Rosa-Neto, and Tharick A. Pascoal. Astrocyte reactivity influences amyloid-β effects on tau pathology in preclinical Alzheimer's disease. *Nature Medicine*, 29(7):1775–1781, July 2023.

[41] Céline Bellenguez, Fahri Küçükali, Iris E. Jansen, Luca Kleineidam, Sonia Moreno-Grau, Najaf Amin, Adam C. Naj, Rafael Campos-Martin, Benjamin Grenier-Boley, Victor Andrade, Peter A. Holmans, Anne Boland, Vincent Damotte, Sven J. Van Der Lee, Marcos R. Costa, Teemu Kuulasmaa, Qiong Yang, Itziar De Rojas, Joshua C. Bis, Amber Yaqub, Ivana Prokic, Julien Chapuis, Shahzad Ahmad, Vilmantas Giedraitis, Dag Aarsland, Pablo Garcia-Gonzalez, Carla Abdelnour, Emilio Alarcón-Martín, Daniel Alcolea, Montserrat Alegret, Ignacio Alvarez, Victoria Álvarez, Nicola J. Armstrong, Anthoula Tsolaki, Carmen Antúnez, Ildebrando Appollonio, Marina Arcaro, Silvana Archetti, Alfonso Arias Pastor, Beatrice Arosio, Lavinia Athanasiu, Henri Bailly, Nerisa Banaj, Miquel Baquero, Sandra Barral, Alexa Beiser, Ana Belén Pastor, Jennifer E. Below, Penelope Benchek, Luisa Benussi, Claudine Berr, Céline Besse, Valentina Bessi, Giuliano Binetti, Alessandra Bizarro, Rafael Blesa, Mercè Boada, Eric Boerwinkle, Barbara Borroni, Silvia Boschi, Paola Bossù, Geir Bråthen, Jan Bressler, Catherine Bresner, Henry Brodaty, Keeley J. Brookes, Luis Ignacio Brusco, Dolores Buiza-Rueda, Katharina Bûrger, Vanessa Burholt, William S. Bush, Miguel Calero, Laura B.

Cantwell, Geneviève Chene, Jaeyoon Chung, Michael L. Cuccaro, Ángel Carracedo, Roberta Cecchetti, Laura Cervera-Carles, Camille Charbonnier, Hung-Hsin Chen, Caterina Chillotti, Simona Ciccone, Jurgen A. H. R. Claassen, Christopher Clark, Elisa Conti, Anaïs Corma-Gómez, Emanuele Costantini, Carlo Custodero, Delphine Daian, Maria Carolina Dalmasso, Antonio Daniele, Efthimios Dardiotis, Jean-François Dartigues, Peter Paul De Deyn, Katia De Paiva Lopes, Lot D. De Witte, Stéphanie Debette, Jürgen Deckert, Teodoro Del Ser, Nicola Denning, Anita DeStefano, Martin Dichgans, Janine Diehl-Schmid, Mónica Diez-Fairen, Paolo Dionigi Rossi, Srdjan Djurovic, Emmanuelle Duron, Emrah Düzel, Carole Dufouil, Gudny Eiriksdottir, Sebastiaan Engelborghs, Valentina Escott-Price, Ana Espinosa, Michael Ewers, Kelley M. Faber, Tagliavini Fabrizio, Sune Fallgaard Nielsen, David W. Fardo, Lucia Farotti, Chiara Fenoglio, Marta Fernández-Fuertes, Raffaele Ferrari, Catarina B. Ferreira, Evelyn Ferri, Bertrand Fin, Peter Fischer, Tormod Fladby, Klaus Fließbach, Bernard Fongang, Myriam Fornage, Juan Fortea, Tatiana M. Foroud, Silvia Fostinelli, Nick C. Fox, Emlio Franco-Macías, María J. Bullido, Ana Frank-García, Lutz Froelich, Brian Fulton-Howard, Daniela Galimberti, Jose Maria García-Alberca, Pablo García-González, Sebastian Garcia-Madrona, Guillermo Garcia-Ribas, Roberta Ghidoni, Ina Giegling, Giaccone Giorgio, Alison M. Goate, Oliver Goldhardt, Duber Gomez-Fonseca, Antonio González-Pérez, Caroline Graff, Giulia Grande, Emma Green, Timo Grimmer, Edna Grünblatt, Michelle Grunin, Vilmundur Gudnason, Tamar Guetta-Baranes, Annakaisa Haapasalo, Georgios Hadjigeorgiou, Jonathan L. Haines, Kara L. Hamilton-Nelson, Harald Hampel, Olivier Hanon, John Hardy, Annette M. Hartmann, Lucrezia Hausner, Janet Harwood, Stefanie Heilmann-Heimbach, Seppo Helisalmi, Michael T. Heneka, Isabel Hernández, Martin J. Herrmann, Per Hoffmann, Clive Holmes, Henne Holstege, Raquel Huerto Vilas, Marc Hulsman, Jack Humphrey, Geert Jan Biessels, Xueqiu Jian, Charlotte Johansson, Gyungah R. Jun, Yuriko Kastumata, John Kauwe, Patrick G. Kehoe, Lena Kilander, Anne Kinhult Ståhlbom, Miia Kivipelto, Anne Koivisto, Johannes Kornhuber, Mary H. Kosmidis, Walter A. Kukull, Pavel P. Kuksa, Brian W. Kunkle, Amanda B. Kuzma, Carmen Lage, Erika J. Laukka, Lenore Launer, Alessandra Lauria, Chien-Yueh Lee, Jenni Lehtisalo, Ondrej Lerch, Alberto Lleó, William Longstreth, Oscar Lopez, Adolfo Lopez De Munain, Seth Love, Malin Löwemark, Lauren Luckcuck, Kathryn L. Lunetta, Yiyi Ma, Juan Macías,

Catherine A. MacLeod, Wolfgang Maier, Francesca Mangialasche, Marco Spallazzi, Marta Marquié, Rachel Marshall, Eden R. Martin, Angel Martín Montes, Carmen Martínez Rodríguez, Carlo Masullo, Richard Mayeux, Simon Mead, Patrizia Mecocci, Miguel Medina, Alun Meggy, Shima Mehrabian, Silvia Mendoza, Manuel Menéndez-González, Pablo Mir, Susanne Moebus, Merel Mol, Laura Molina-Porcel, Laura Montrreal, Laura Morelli, Fermin Moreno, Kevin Morgan, Thomas Mosley, Markus M. Nöthen, Carolina Muchnik, Shubhabrata Mukherjee, Benedetta Nacmias, Tiia Ngandu, Gael Nicolas, Børge G. Nordestgaard, Robert Olaso, Adelina Orellana, Michela Orsini, Gemma Ortega, Alessandro Padovani, Caffarra Paolo, Goran Papenberg, Lucilla Parnetti, Florence Pasquier, Pau Pastor, Gina Peloso, Alba Pérez-Cordón, Jordi Pérez-Tur, Pierre Pericard, Oliver Peters, Yolande A. L. Pijnenburg, Juan A. Pineda, Gerard Piñol-Ripoll, Claudia Pisanu, Thomas Polak, Julius Popp, Danielle Posthuma, Josef Priller, Raquel Puerta, Olivier Quenez, Inés Quintela, Jesper Qvist Thomassen, Alberto Rábano, Innocenzo Rainero, Farid Rajabli, Inez Ramakers, Luis M. Real, Marcel J. T. Reinders, Christiane Reitz, Dolly Reyes-Dumeyer, Perry Ridge, Steffi Riedel-Heller, Peter Riederer, Natalia Roberto, Eloy Rodriguez-Rodriguez, Arvid Rongve, Irene Rosas Allende, Maitée Rosende-Roca, Jose Luis Royo, Elisa Rubino, Dan Rujescu, María Eugenia Sáez, Paraskevi Sakka, Ingvild Saltvedt, Ángela Sanabria, María Bernal Sánchez-Arjona, Florentino Sanchez-Garcia, Pascual Sánchez Juan, Raquel Sánchez-Valle, Sigrid B. Sando, Chloé Sarnowski, Claudia L. Satizabal, Michela Scamosci, Nikolaos Scarmeas, Elio Scarpini, Philip Scheltens, Norbert Scherbaum, Martin Scherer, Matthias Schmid, Anja Schneider, Jonathan M. Schott, Geir Selbæk, Davide Seripa, Manuel Serrano, Jin Sha, Alexey A. Shadrin, Olivia Skrobot, Susan Slifer, Gijsje J. L. Snijders, Hilkka Soininen, Vincenzo Solfrizzi, Alina Solomon, Yeunjoo Song, Sandro Sorbi, Oscar Sotolongo-Grau, Gianfranco Spalletta, Annika Spottke, Alessio Squassina, Eystein Stordal, Juan Pablo Tartan, Lluís Tárraga, Niccolo Tesí, Anbupalam Thalamuthu, Tegos Thomas, Giuseppe Tosto, Latchezar Traykov, Lucio Tremolizzo, Anne Tybjærg-Hansen, Andre Uitterlinden, Abbe Ullgren, Ingun Ulstein, Sergi Valero, Otto Valladares, Christine Van Broeckhoven, Jeffery Vance, Badri N. Vardarajan, Aad Van Der Lugt, Jasper Van Dongen, Jeroen Van Rooij, John Van Swieten, Rik Vandenberghe, Frans Verhey, Jean-Sébastien Vidal, Jonathan Vogelgsang, Martin Vyhnalek, Michael Wagner, David Wallon, Li-San Wang, Ruiqi Wang, Leonie Weinhold, Jens Wiltfang, Gill

Windle, Bob Woods, Mary Yannakoulia, Habil Zare, Yi Zhao, Xiaoling Zhang, Congcong Zhu, Miren Zulaica, EADB, Jan Laczo, Vaclav Matoska, Maria Serpente, Francesca Assogna, Fabrizio Piras, Federica Piras, Valentina Ciullo, Jacob Shofany, Carlo Ferrarese, Simona Andreoni, Gessica Sala, Chiara Paola Zoia, Maria Del Zompo, Alberto Benussi, Patrizia Bastiani, Mari Takalo, Teemu Natunen, Tiina Laatikainen, Jaakko Tuomilehto, Riitta Antikainen, Timo Strandberg, Jaana Lindström, Markku Peltonen, Richard Abraham, Ammar Al-Chalabi, Nicholas J. Bass, Carol Brayne, Kristelle S. Brown, John Collinge, David Craig, Pangiotis Deloukas, Nick Fox, Amy Gerrish, Michael Gill, Rhian Gwilliam, Denise Harold, Paul Hollingworth, Jarret A. Johnston, Lesley Jones, Brian Lawlor, Gill Livingston, Simon Lovestone, Michelle Lupton, Aoibhinn Lynch, David Mann, Bernadette McGuinness, Andrew McQuillin, Michael C. O'Donovan, Michael J. Owen, Peter Passmore, John F. Powell, Petra Proitsi, Martin Rossor, Christopher E. Shaw, A. David Smith, Hugh Gurling, Stephen Todd, Catherine Mummery, Nathalie Ryan, Giordano Lacidogna, Ad Adarmes-Gómez, Ana Mauleón, Ana Pancho, Anna Gailhajenet, Asunción Lafuente, D. Macias-García, Elvira Martín, Esther Pelejà, F. Carrillo, Isabel Sastre Merlín, L. Garrote-Espina, Liliana Vargas, M. Carrion-Claro, M. Marín, Ma Labrador, Mar Buendia, María Dolores Alonso, Marina Guitart, Mariona Moreno, Marta Ibarria, Mt Periñán, Nuria Aguilera, P. Gómez-Garre, Pilar Cañabate, R. Escuela, R. Pineda-Sánchez, R. Vigo-Ortega, S. Jesús, Silvia Preckler, Silvia Rodrigo-Herrero, Susana Diego, Alessandro Vacca, Fausto Roveta, Nicola Salvadori, Elena Chipi, Henning Boecker, Christoph Laske, Robert Perneczky, Costas Anastasiou, Daniel Janowitz, Rainer Malik, Anna Anastasiou, Kayenat Parveen, Carmen Lage, Sara López-García, Anna Antonell, Kalina Yonkova Mihova, Diyana Belezhanska, Heike Weber, Silvia Kochen, Patricia Solis, Nancy Medel, Julieta Lisso, Zulma Sevillano, Daniel G. Politis, Valeria Cores, Carolina Cuesta, Cecilia Ortiz, Juan Ignacio Bacha, Mario Rios, Aldo Saenz, Mariana Sanchez Abalos, Eduardo Kohler, Dana Lis Palacio, Ignacio Etchepareborda, Matias Kohler, Gisela Novack, Federico Ariel Prestia, Pablo Galeano, Eduardo M. Castaño, Sandra Germani, Carlos Reyes Toso, Matias Rojo, Carlos Ingino, Carlos Mangone, David C. Rubinsztein, Stefan Teipel, Nathalie Fievet, Vincent Deramerourt, Charlotte Forsell, Håkan Thonberg, Maria Bjerke, Ellen De Roeck, María Teresa Martínez-Larrad, Natividad Olivar, GR@ACE, Nuria Aguilera, Amanda Cano, Pilar Cañabate, Juan Macias, Olalla Maroñas, Raúl Nuñez-Llaves, Clàudia

Olivé, Ester Pelejá, DEGESCO, Astrid D. Adarmes-Gómez, María Dolores Alonso, Guillermo Amer-Ferrer, Martirio Antequera, Juan Andrés Burguera, Fátima Carrillo, Mario Carrión-Claro, María José Casajeros, Marian Martinez De Pancorbo, Rocío Escuela, Lorena Garrote-Espina, Pilar Gómez-Garre, Saray Hevilla, Silvia Jesús, Miguel Angel Labrador Espinosa, Agustina Legaz, Sara López-García, Daniel Macias-García, Salvadora Manzanares, Marta Marín, Juan Marín-Muñoz, Tamara Marín, Begoña Martínez, Victoriana Martínez, Pablo Martínez-Lage Álvarez, Maite Mendioroz Iriarte, María Teresa Periñán-Tocino, Rocío Pineda-Sánchez, Diego Real De Asúa, Silvia Rodrigo, Isabel Sastre, Maria Pilar Vicente, Rosario Vigo-Ortega, Liliana Vivancos, EADI, Jacques Epelbaum, Didier Hannequin, Dominique Campion, Vincent Deramecourt, Christophe Tzourio, Alexis Brice, Bruno Dubois, GERAD, Amy Williams, Charlene Thomas, Chloe Davies, William Nash, Kimberley Dowzell, Atahualpa Castillo Morales, Mateus Bernardo-Harrington, James Turton, Jenny Lord, Kristelle Brown, Emma Vardy, Elizabeth Fisher, Jason D. Warren, Martin Rossor, Natalie S. Ryan, Rita Guerreiro, James Uphill, Nick Bass, Reinhard Heun, Heike Kölsch, Britta Schürmann, André Lacour, Christine Herold, Janet A. Johnston, Peter Passmore, John Powell, Yogen Patel, Angela Hodges, Tim Becker, Donald Warden, Gordon Wilcock, Robert Clarke, Panagiotis Deloukas, Yoav Ben-Shlomo, Nigel M. Hooper, Stuart Pickering-Brown, Rebecca Sussams, Nick Warner, Anthony Bayer, Isabella Heuser, Dmitriy Drichel, Norman Klopp, Manuel Mayhaus, Matthias Riemenschneider, Sabrina Pinchler, Thomas Feulner, Wei Gu, Hendrik Van Den Bussche, Michael Hüll, Lutz Frölich, H-Erich Wichmann, Karl-Heinz Jöckel, Michael O'Donovan, Michael Owen, Demgene, Shahram Bahrami, Ingunn Bosnes, Per Selnes, Sverre Bergh, FinnGen, Aarno Palotie, Mark Daly, Howard Jacob, Athena Matakidou, Heiko Runz, Sally John, Robert Plenge, Mark McCarthy, Julie Hunkapiller, Meg Ehm, Dawn Waterworth, Caroline Fox, Anders Malarstig, Kathy Klinger, Kathy Call, Tim Behrens, Patrick Loerch, Tomi Mäkelä, Jaakko Kaprio, Petri Virolainen, Kari Pulkki, Terhi Kilpi, Markus Perola, Jukka Partanen, Anne Pitkäranta, Riitta Kaarteenaho, Seppo Vainio, Miia Turpeinen, Raisa Serpi, Tarja Laitinen, Johanna Mäkelä, Veli-Matti Kosma, Urho Kujala, Outi Tuovila, Minna Hendolin, Raimo Pakkanen, Jeff Waring, Bridget Riley-Gillis, Jimmy Liu, Shameek Biswas, Dorothee Diogo, Catherine Marshall, Xinli Hu, Matthias Gossel, Robert Graham, Beryl Cummings, Samuli Ripatti, Johanna Schleutker, Mikko Arvas,

Olli Carpén, Reetta Hinttala, Johannes Kettunen, Arto Mannermaa, Jari Laukkanen, Valtteri Julkunen, Anne Remes, Reetta Kälviäinen, Jukka Peltola, Pentti Tienari, Juha Rinne, Adam Ziemann, Jeffrey Waring, Sahar Esmaeeli, Nizar Smaoui, Anne Lehtonen, Susan Eaton, Sanni Lahdenperä, Janet Van Adelsberg, John Michon, Geoff Kerchner, Natalie Bowers, Edmond Teng, John Eicher, Vinay Mehta, Padhraig Gormley, Kari Linden, Christopher Whelan, Fanli Xu, David Pulford, Martti Färkkilä, Sampsa Pikkarainen, Airi Jussila, Timo Blomster, Mikko Kiviniemi, Markku Voutilainen, Bob Georgantas, Graham Heap, Fedik Rahimov, Keith Usiskin, Tim Lu, Danny Oh, Kirsi Kalpala, Melissa Miller, Linda McCarthy, Kari Eklund, Antti Palomäki, Pia Isomäki, Laura Pirilä, Oili Kaipiainen-Seppänen, Johanna Huhtakangas, Apinya Lertratanakul, Marla Hochfeld, Nan Bing, Jorge Esparza Gordillo, Nina Mars, Margit Pelkonen, Paula Kauppi, Hannu Kankaanranta, Terttu Harju, David Close, Steven Greenberg, Hubert Chen, Jo Betts, Soumitra Ghosh, Veikko Salomaa, Teemu Niiranen, Markus Juonala, Kaj Metsärinne, Mika Kähönen, Juhani Junttila, Markku Laakso, Jussi Pihlajamäki, Juha Sinisalo, Marja-Riitta Taskinen, Tiinamaija Tuomi, Ben Challis, Andrew Peterson, Audrey Chu, Jaakko Parkkinen, Anthony Muslin, Heikki Joensuu, Tuomo Meretoja, Lauri Aaltonen, Johanna Mattson, Annika Auranen, Peeter Karihtala, Saila Kauppila, Päivi Auvinen, Klaus Elenius, Relja Popovic, Jennifer Schutzman, Andrey Loboda, Aparna Chhibber, Heli Lehtonen, Stefan McDonough, Marika Crohns, Diptee Kulkarni, Kai Kaarniranta, Joni A. Turunen, Terhi Ollila, Sanna Seitsonen, Hannu Uusitalo, Vesa Aaltonen, Hannele Uusitalo-Järvinen, Marja Luodonpää, Nina Hautala, Stephanie Loomis, Erich Strauss, Hao Chen, Anna Podgornaia, Joshua Hoffman, Kaisa Tasanen, Laura Huilaja, Katariina Hannula-Jouppi, Teea Salmi, Sirkku Peltonen, Leena Koulu, Ilkka Harvima, Ying Wu, David Choy, Pirkko Pussinen, Aino Salminen, Tuula Salo, David Rice, Pekka Nieminen, Ulla Palotie, Maria Siponen, Liisa Suominen, Päivi Mäntylä, Ulvi Gursoy, Vuokko Anttonen, Kirsi Sipilä, Justin Wade Davis, Danjuma Quarless, Slavé Petrovski, Eleonor Wigmore, Chia-Yen Chen, Paola Bronson, Ellen Tsai, Yunfeng Huang, Joseph Maranville, Elmutaz Shaikho, Elhaj Mohammed, Samir Wadhawan, Erika Kvikstad, Minal Caliskan, Diana Chang, Tushar Bhangale, Sarah Pendergrass, Emily Holzinger, Xing Chen, Åsa Hedman, Karen S. King, Clarence Wang, Ethan Xu, Franck Auge, Clement Chatelain, Deepak Rajpal, Dongyu Liu, Katherine Call, Tai-he Xia, Matt Brauer, Mitja Kurki, Juha Karjalainen,

Aki Havulinna, Anu Jalanko, Priit Palta, Pietro Della Briotta Parolo, Wei Zhou, Susanna Lemmelä, Manuel Rivas, Jarmo Harju, Arto Lehisto, Andrea Ganna, Vincent Llorens, Hannele Laivuori, Sina Rüeger, Mari E. Niemi, Taru Tukiainen, Mary Pat Reeve, Henrike Heyne, Kimmo Palin, Javier Garcia-Tabuenca, Harri Siirtola, Tuomo Kiiskinen, Jiwoo Lee, Kristin Tsuo, Amanda Elliott, Kati Kristiansson, Kati Hyvärinen, Jarmo Ritari, Miika Koskinen, Katri Pylkäs, Marita Kalaoja, Minna Karjalainen, Tuomo Mantere, Eeva Kangasniemi, Sami Heikkinen, Eija Laakkonen, Csilla Sipeky, Samuel Heron, Antti Karlsson, Dhanaprakash Jambulingam, Venkat Subramaniam Rathinakannan, Risto Kajanne, Mervi Aavikko, Manuel González Jiménez, Pietro Della Briotta Parola, Arto Lehistö, Masahiro Kanai, Mari Kaunisto, Elina Kilpeläinen, Timo P. Sipilä, Georg Brein, Ghazal Awaisa, Anastasia Shcherban, Kati Donner, Anu Loukola, Päivi Laiho, Tuuli Sistonen, Essi Kaiharju, Markku Laukkanen, Elina Järvensivu, Sini Lähteenmäki, Lotta Männikkö, Regis Wong, Hannele Mattsson, Tero Hiekkalinna, Teemu Paajanen, Kalle Pärn, Javier Gracia-Tabuenca, ADGC, Erin Abner, Perrie M. Adams, Alyssa Aguirre, Marilyn S. Albert, Roger L. Albin, Mariet Allen, Lisa Alvarez, Liana G. Apostolova, Steven E. Arnold, Sanjay Asthana, Craig S. Atwood, Gayle Ayres, Clinton T. Baldwin, Robert C. Barber, Lisa L. Barnes, Sandra Barral, Thomas G. Beach, James T. Becker, Gary W. Beecham, Duane Beekly, Jennifer E. Below, Penelope Benchek, Bruno A. Benitez, David Bennett, John Bertelson, Flanagan E. Margaret, Thomas D. Bird, Deborah Blacker, Bradley F. Boeve, James D. Bowen, Adam Boxer, James Brewer, James R. Burke, Jeffrey M. Burns, Will S. Bush, Joseph D. Buxbaum, Nigel J. Cairns, Chuanhai Cao, Christopher S. Carlson, Cynthia M. Carlsson, Regina M. Carney, Minerva M. Carrasquillo, Scott Chasse, Marie-Francoise Chesselet, Alessandra Chesi, Nathaniel A. Chin, Helena C. Chui, Jaeyoon Chung, Suzanne Craft, Paul K. Crane, David H. Cribbs, Elizabeth A. Crocco, Carlos Cruchaga, Michael L. Cuccaro, Munro Cullum, Eveleen Darby, Barbara Davis, Philip L. De Jager, Charles DeCarli, John DeToledo, Malcolm Dick, Dennis W. Dickson, Beth A. Dombroski, Rachelle S. Doody, Ranjan Duara, Nilüfer Ertekin-Taner, Denis A. Evans, Thomas J. Fairchild, Kenneth B. Fallon, Martin R. Farlow, John J. Farrell, Victoria Fernandez-Hernandez, Steven Ferris, Matthew P. Frosch, Brian Fulton-Howard, Douglas R. Galasko, Adriana Gamboa, Marla Gearing, Daniel H. Geschwind, Bernardino Ghetti, John R. Gilbert, Thomas J. Grabowski, Neill R. Graff-Radford, Struan F. A. Grant,

Robert C. Green, John H. Growdon, Jonathan L. Haines, Hakon Hakonarson, James Hall, Ronald L. Hamilton, Oscar Harari, Lindy E. Harrell, Jacob Haut, Elizabeth Head, Victor W. Henderson, Michelle Hernandez, Timothy Hohman, Lawrence S. Honig, Ryan M. Huebinger, Matthew J. Huentelman, Christine M. Hulette, Bradley T. Hyman, Linda S. Hynan, Laura Ibanez, Gail P. Jarvik, Suman Jayadev, Lee-Way Jin, Kim Johnson, Leigh Johnson, M. Ilyas Kamboh, Anna M. Karydas, Mindy J. Katz, Jeffrey A. Kaye, C. Dirk Keene, Aisha Khaleeq, Ronald Kim, Janice Knebl, Neil W. Kowall, Joel H. Kramer, Pavel P. Kuksa, Frank M. LaFerla, James J. Lah, Eric B. Larson, Chien-Yueh Lee, Edward B. Lee, Alan Lerner, Yuk Yee Leung, James B. Leverenz, Allan I. Levey, Mingyao Li, Andrew P. Lieberman, Richard B. Lipton, Mark Logue, Constantine G. Lyketsos, John Malamon, Douglas Mains, Daniel C. Marson, Frank Martiniuk, Deborah C. Mash, Eliezer Masliah, Paul Massman, Arjun Masurkar, Wayne C. McCormick, Susan M. McCurry, Andrew N. McDavid, Stefan McDonough, Ann C. McKee, Marsel Mesulam, Jesse Mez, Bruce L. Miller, Carol A. Miller, Joshua W. Miller, Thomas J. Montine, Edwin S. Monuki, John C. Morris, Amanda J. Myers, Trung Nguyen, Sid O'Bryant, John M. Olichney, Marcia Ory, Raymond Palmer, Joseph E. Parisi, Henry L. Paulson, Valory Pavlik, David Paydarfar, Victoria Perez, Elaine Peskind, Ronald C. Petersen, Jennifer E. Phillips-Cremins, Aimee Pierce, Marsha Polk, Wayne W. Poon, Huntington Potter, Liming Qu, Mary Quiceno, Joseph F. Quinn, Ashok Raj, Murray Raskind, Eric M. Reiman, Barry Reisberg, Joan S. Reisch, John M. Ringman, Erik D. Roberson, Monica Rodriguear, Ekaterina Rogaeva, Howard J. Rosen, Roger N. Rosenberg, Donald R. Royall, Mark A. Sager, Mary Sano, Andrew J. Saykin, Julie A. Schneider, Lon S. Schneider, William W. Seeley, Susan H. Slifer, Scott Small, Amanda G. Smith, Janet P. Smith, Yeunjoo E. Song, Joshua A. Sonnen, Salvatore Spina, Peter St George-Hyslop, Robert A. Stern, Alan B. Stevens, Stephen M. Strittmatter, David Sultzer, Russell H. Swerdlow, Rudolph E. Tanzi, Jeffrey L. Tilson, John Q. Trojanowski, Juan C. Troncoso, Debby W. Tsuang, Otto Valladares, Vivianna M. Van Deerlin, Linda J. Van Eldik, Robert Vassar, Harry V. Vinters, Jean-Paul Vonsattel, Sandra Weintraub, Kathleen A. Welsh-Bohmer, Patrice L. Whitehead, Ellen M. Wijsman, Kirk C. Wilhelmsen, Benjamin Williams, Jennifer Williamson, Henrik Wilms, Thomas S. Wingo, Thomas Wisniewski, Randall L. Woltjer, Martin Woon, Clinton B. Wright, Chuang-Kuo Wu, Steven G. Younkin, Chang-En Yu, Lei Yu, Yuanchao Zhang, Yi Zhao,

Xiongwei Zhu, CHARGE, Hieab Adams, Rufus O. Akinyemi, Muhammad Ali, Nicola Armstrong, Hugo J. Aparicio, Maryam Bahadori, James T. Becker, Monique Breteler, Daniel Chasman, Ganesh Chauhan, Hata Comic, Simon Cox, Adrienne L. Cupples, Gail Davies, Charles S. DeCarli, Marie-Gabrielle Duperron, Josée Dupuis, Tavia Evans, Frank Fan, Annette Fitzpatrick, Alison E. Fohner, Mary Ganguli, Mirjam Geerlings, Stephen J. Glatt, Hector M. Gonzalez, Monica Goss, Hans Grabe, Mohamad Habes, Susan R. Heckbert, Edith Hofer, Elliot Hong, Timothy Hughes, Tiffany F. Kautz, Maria Knol, William Kremen, Paul Lacaze, Jari Lahti, Quentin Le Grand, Elizabeth Litkowski, Shuo Li, Dan Liu, Xuan Liu, Marisa Loitfelder, Alisa Manning, Pauline Maillard, Riccardo Marioni, Bernard Mazoyer, Debora Melo Van Lent, Hao Mei, Aniket Mishra, Paul Nyquist, Jeffrey O'Connell, Yash Patel, Tomas Paus, Zdenka Pausova, Katri Raikkonen-Talvitie, Moeen Riaz, Stephen Rich, Jerome Rotter, Jose Romero, Gena Roshchupkin, Yasaman Saba, Murali Sargurupremraj, Helena Schmidt, Reinhold Schmidt, Joshua M. Shulman, Jennifer Smith, Hema Sekhar, Reddy Rajula, Jean Shin, Jeannette Simino, Eeva Sliz, Alexander Teumer, Alvin Thomas, Adrienne Tin, Elliot Tucker-Drob, Dina Vojinovic, Yanbing Wang, Galit Weinstein, Dylan Williams, Katharina Wittfeld, Lisa Yanek, Yunju Yang, Lindsay A. Farrer, Bruce M. Psaty, Mohsen Ghanbari, Towfique Raj, Perminder Sachdev, Karen Mather, Frank Jessen, M. Arfan Ikram, Alexandre De Mendonça, Jakub Hort, Magda Tsolaki, Margaret A. Pericak-Vance, Philippe Amouyel, Julie Williams, Ruth Frikke-Schmidt, Jordi Clarimon, Jean-François Deleuze, Giacomina Rossi, Sudha Seshadri, Ole A. Andreassen, Martin Ingelsson, Mikko Hiltunen, Kristel Sleegers, Gerard D. Schellenberg, Cornelia M. Van Duijn, Rebecca Sims, Wiesje M. Van Der Flier, Agustín Ruiz, Alfredo Ramirez, and Jean-Charles Lambert. New insights into the genetic etiology of Alzheimer's disease and related dementias. *Nature Genetics*, 54(4):412–436, April 2022.

[42] Elizabeth E. Bellocchio, Richard J. Reimer, Robert T. Fremeau, and Robert H. Edwards. Uptake of Glutamate into Synaptic Vesicles by an Inorganic Phosphate Transporter. *Science*, 289(5481):957–960, August 2000.

[43] Malika Bennecib, Cheng-Xin Gong, Inge Grundke-Iqbal, and Khalid Iqbal. Inhibition of PP-2A upregulates CaMKII in rat forebrain and induces hyperphosphorylation of tau at Ser 262/356. *FEBS Letters*, 490(1-2):15–22, February 2001.

[44] D. A. Bennett, J. A. Schneider, Z. Arvanitakis, J. F. Kelly, N. T. Aggarwal, R. C. Shah, and R. S. Wilson. Neuropathology of older persons without cognitive impairment from two community-based studies. *Neurology*, 66(12):1837–1844, June 2006.

[45] María Berrocal, Alberto Alvarez-Barrientos, and Ana M. Mata. Neurotoxic amyloid β-peptide and tau produce cytokine-like effects on PMCA in glioblastoma cell lines, enhancing its activity and isoforms expression. *FEBS Open Bio*, 15(8):1350–1364, August 2025.

[46] Taylor Bertucci, Kathryn R. Bowles, Steven Lotz, Le Qi, Katherine Stevens, Susan K. Goderie, Susan Borden, Laura Maria Oja, Keith Lane, Ryan Lotz, Hailey Lotz, Rebecca Chowdhury, Shona Joy, Brigitte L. Arduini, David C. Butler, Michael Miller, Heide Baron, Carl Alexander Sandhof, M. Catarina Silva, Stephen J. Haggarty, Celeste M. Karch, Daniel H. Geschwind, Alison M. Goate, and Sally Temple. Improved Protocol for Reproducible Human Cortical Organoids Reveals Early Alterations in Metabolism with *MAPT* Mutations, July 2023.

[47] L I Binder, A Frankfurter, and L I Rebhun. The distribution of tau in the mammalian central nervous system. *The Journal of cell biology*, 101(4):1371–1378, October 1985.

[48] Julian H. Birnbaum, Debora Wanner, Anton F. Gietl, Antje Saake, Thomas M. Kündig, Christoph Hock, Roger M. Nitsch, and Christian Tackenberg. Oxidative stress and altered mitochondrial protein expression in the absence of amyloid-β and tau pathology in iPSC-derived neurons from sporadic Alzheimer's disease patients. *Stem Cell Research*, 27:121–130, March 2018.

[49] I. Blasko, M. Wagner, N. Whitaker, B. Grubeck-Loebenstein, and P. Jansen-Dürr. The amyloid β peptide Aβ (25–35) induces apoptosis independent of p53. *FEBS Letters*, 470(2):221–225, March 2000.

[50] K. Blennow, A. Wallin, H. Ågren, C. Spenger, J. Siegfried, and E. Vanmechelen. tau protein in cerebrospinal fluid: A biochemical marker for axonal degeneration in Alzheimer disease? *Molecular and Chemical Neuropathology*, 26(3):231–245, December 1995.

[51] Diana I. Bocancea, Anna C. Van Loenhoud, Colin Groot, Frederik Barkhof, Wiesje M. Van Der Flier, and Rik Ossenkoppele. Measuring Resilience and Resistance in Aging and Alzheimer Disease Using Residual Methods: A Systematic Review and Meta-analysis. *Neurology*, 97(10):474–488, September 2021.

[52] David C. Bode, Mark D. Baker, and John H. Viles. Ion Channel Formation by Amyloid-β42 Oligomers but Not Amyloid-β40 in Cellular Membranes. *Journal of Biological Chemistry*, 292(4):1404–1413, January 2017.

[53] Karine Bourgade, Hugo Garneau, Geneviève Giroux, Aurélie Y. Le Page, Christian Bocti, Gilles Dupuis, Eric H. Frost, and Tamàs Fülöp. β-Amyloid peptides display protective activity against the human Alzheimer's disease-associated herpes simplex virus-1. *Biogerontology*, 16(1):85–98, February 2015.

[54] Kathryn R. Bowles, Chiara Pedicone, Derian A. Pugh, Laura-Maria Oja, Filipa H. Sousa, Lois K. Keavey, Brian Fulton-Howard, Sarah A. Weitzman, Yiyuan Liu, Jonathan L. Chen, Matthew D. Disney, and Alison M. Goate. Development of MAPT S305 mutation human iPSC lines exhibiting elevated 4R tau expression and functional alterations in neurons and astrocytes. *Cell Reports*, 43(12):115013, December 2024.

[55] F. Braak, H. Braak, and E. M. Mandelkow. A sequence of cytoskeleton changes related to the formation of neurofibrillary tangles and neuropil threads. *Acta Neuropathologica*, 87(6):554–567, June 1994.

[56] H. Braak and E. Braak. Neuropathological stageing of Alzheimer-related changes. *Acta Neuropathologica*, 82(4):239–259, September 1991.

[57] H. Braak and E. Braak. Evolution of neuronal changes in the course of Alzheimer's disease. In K. Jellinger, F. Fazekas, and M. Windisch, editors, *Ageing and Dementia*, volume 53, pages 127–140. Springer Vienna, Vienna, 1998. Series Title: Journal of Neural Transmission. Supplementa.

[58] Heiko Braak, Kelly Del Tredici, Udo Rüb, Rob A.I De Vos, Ernst N.H Jansen Steur, and Eva Braak. Staging of brain pathology related to sporadic Parkinson's disease. *Neurobiology of Aging*, 24(2):197–211, March 2003.

[59] Matthew R. Brier, Brian Gordon, Karl Friedrichsen, John McCarthy, Ari Stern, Jon Christensen, Christopher Owen, Patricia Aldea, Yi Su, Jason Hassenstab, Nigel J. Cairns, David M. Holtzman, Anne M. Fagan, John C. Morris, Tammie L. S. Benzinger, and Beau M. Ances. Tau and Aβ imaging, CSF measures, and cognition in Alzheimer's disease. *Science Translational Medicine*, 8(338), May 2016.

[60] Jean-Pierre Brion, Carthage Smith, Anne-Marie Couck, Jean-Marc Gallo, and Brian H. Anderton. Developmental Changes in τ Phosphorylation: Fetal τ Is Transiently Phosphorylated in a Manner Similar to Paired Helical Filament-τ Characteristic of Alzheimer's Disease. *Journal of Neurochemistry*, 61(6):2071–2080, December 1993.

[61] Stan J. J. Brouns, Matthijs M. Jore, Magnus Lundgren, Edze R. Westra, Rik J. H. Slijkhuis, Ambrosius P. L. Snijders, Mark J. Dickman, Kira S. Makarova, Eugene V. Koonin, and John Van Der Oost. Small CRISPR RNAs Guide Antiviral Defense in Prokaryotes. *Science*, 321(5891):960–964, August 2008.

[62] Sarah Buchholz and Hans Zempel. The six brain-specific TAU isoforms and their role in Alzheimer's disease and related neurodegenerative dementia syndromes. *Alzheimer's & Dementia*, 20(5):3606–3628, May 2024.

[63] Marc Aurel Busche, Gerhard Eichhoff, Helmuth Adelsberger, Dorothee Abramowski, Karl-Heinz Wiederhold, Christian Haass, Matthias Staufenbiel, Arthur Konnerth, and Olga Garaschuk. Clusters of Hyperactive Neurons Near Amyloid Plaques in a Mouse Model of Alzheimer's Disease. *Science*, 321(5896):1686–1689, September 2008.

[64] Yan Cai, Xue-Mei Zhang, Lauren N. Macklin, Huaibin Cai, Xue-Gang Luo, Salvatore Oddo, Frank M. LaFerla, Robert G. Struble, Gregory M. Rose, Peter R. Patrylo, and Xiao-Xin Yan. BACE1 Elevation is Involved in Amyloid Plaque Development in the Triple Transgenic Model of Alzheimer's Disease: Differential Aβ Antibody Labeling of Early-Onset Axon Terminal Pathology. *Neurotoxicity Research*, 21(2):160–174, February 2012.

[65] Bilal Cakir, Yangfei Xiang, Yoshiaki Tanaka, Mehmet H. Kural, Maxime Parent, Young-Jin Kang, Kayley Chapeton, Benjamin Patterson, Yifan Yuan, Chang-Shun He, Micha Sam B. Raredon, Jake Dengelegi, Kun-Yong Kim, Pingnan Sun, Mei Zhong, Sangho Lee, Prabir Patra, Fahmeed Hyder, Laura E.

Niklason, Sang-Hun Lee, Young-Sup Yoon, and In-Hyun Park. Engineering of human brain organoids with a functional vascular-like system. *Nature Methods*, 16(11):1169–1175, November 2019.

[66] M. J. Calkins, M. Manczak, P. Mao, U. Shirendeb, and P. H. Reddy. Impaired mitochondrial biogenesis, defective axonal transport of mitochondria, abnormal mitochondrial dynamics and synaptic degeneration in a mouse model of Alzheimer's disease. *Human Molecular Genetics*, 20(23):4515–4529, December 2011.

[67] Dominique Campion, Jean-Michel Flaman, Alexis Brice, Didier Hannequin, Bruno Dubois, Cosette Martin, Viviane Moreau, Françoise Charbonnier, Olivier Didierjean, Sandrine Tardieu, Christiane Penet, Michèle Puel, Florence Pasquier, François Le Doze, Gil Bellis, Alphonse Calenda, Roland Heilig, Maria Martinez, Jacques Mallet, Michel Bellis, Françoise Clerget-Darpoux, Yves Agid, and Thierry Frebourg. Mutations of the *presenilin I* gene in families with early-onset Alzheimer's disease. *Human Molecular Genetics*, 4(12):2373–2377, 1995.

[68] Julbert Caneus, Nesar Akanda, John W. Rumsey, Xiufang Guo, Max Jackson, Christopher J. Long, Frank Sommerhage, Sanya Georgieva, Nicholas M. Kanaan, David Morgan, and James J. Hickman. A human induced pluripotent stem cell-derived cortical neuron human-on-a chip system to study $A\beta_{42}$ and tau-induced pathophysiological effects on long-term potentiation. *Alzheimer's & Dementia: Translational Research & Clinical Interventions*, 6(1):e12029, January 2020.

[69] Julbert Caneus, Kaveena Autar, Nesar Akanda, Marcella Grillo, Christopher J. Long, Max Jackson, Sarah Lindquist, Xiufang Guo, Dave Morgan, and James J. Hickman. Validation of a functional human AD model with four AD therapeutics utilizing patterned ipsc-derived cortical neurons integrated with microelectrode arrays. *Scientific Reports*, 14(1):24875, October 2024.

[70] Zijun Cao, Xue Feng, Li Wang, and Xiaoliang Wang. Inhibition of MTERF4 disrupts mitochondrial function and attenuates amyloidogenic APP processing in HEK293-APPswe cells via HSDL2-mediated apoptosis and autophagy. *Journal of Radiation Research and Applied Sciences*, 18(3):101839, September 2025.

[71] Phillippa J Carling, Brent J Ryan, William McGuinness, Shikha Kataria, Stewart W Humble, Stefan Milde, James A Duce, Nirav Kapadia, William J Zuercher, John B. Davis, Elena Di Daniel, and Richard Wade-Martins. Multiparameter phenotypic screening for endogenous TFEB and TFE3 translocation identifies novel chemical series modulating lysosome function. *Autophagy*, 19(2):692–705, February 2023.

[72] Becky C. Carlyle, Savannah E. Kandigian, Johannes Kreuzer, Sudeshna Das, Bianca A. Trombetta, Yikai Kuo, David A. Bennett, Julie A. Schneider, Vladislav A. Petyuk, Robert R. Kitchen, Robert Morris, Angus C. Nairn, Bradley T. Hyman, Wilhelm Haas, and Steven E. Arnold. Synaptic proteins associated with cognitive performance and neuropathology in older humans revealed by multiplexed fractionated proteomics. *Neurobiology of Aging*, 105:99–114, September 2021.

[73] Roberta Cascella, Elisa Evangelisti, Alessandra Bigi, Matteo Becatti, Claudia Fiorillo, Massimo Stefani, Fabrizio Chiti, and Cristina Cecchi. Soluble Oligomers Require a Ganglioside to Trigger Neuronal Calcium Overload. *Journal of Alzheimer's Disease*, 60(3):923–938, October 2017.

[74] Isabel Castanho, Pourya Naderi Yeganeh, Carles A. Boix, Sarah L. Morgan, Hansruedi Mathys, Dmitry Prokopenko, Bartholomew White, Larisa M. Soto, Giulia Pegoraro, Saloni Shah, Athanasios Ploumakis, Nikolas Kalavros, David A. Bennett, Christoph Lange, Doo Yeon Kim, Lars Bertram, Li-Huei Tsai, Manolis Kellis, Rudolph E. Tanzi, and Winston Hide. Molecular hallmarks of excitatory and inhibitory neuronal resilience to Alzheimer's disease. *Molecular Neurodegeneration*, 20(1):103, October 2025.

[75] Che-Wei Chang, Mark D. Evans, Xinxing Yu, Gui-Qiu Yu, and Lennart Mucke. Tau reduction affects excitatory and inhibitory neurons differently, reduces excitation/inhibition ratios, and counteracts network hypersynchrony. *Cell Reports*, 37(3):109855, October 2021.

[76] Marie-Christine Chartier-Harlin, Fiona Crawford, Henry Houlden, Andrew Warren, David Hughes, Liana Fidani, Alison Goate, Martin Rossor, Penelope Roques, John Hardy, and Mike Mullan. Early-onset Alzheimer's disease caused by mutations at codon 717 of the β-amyloid precursor protein gene. *Nature*, 353(6347):844–846, October 1991.

[77] Guo-fang Chen, Ting-hai Xu, Yan Yan, Yu-ren Zhou, Yi Jiang, Karsten Melcher, and H Eric Xu. Amyloid beta: structure, biology and structure-based therapeutic development. *Acta Pharmacologica Sinica*, 38(9):1205–1235, September 2017.

[78] E. Sandra Chocron, Erin Munkácsy, Harper S. Kim, Przemyslaw Karpowicz, Nisi Jiang, Candice E. Van Skike, Nicholas DeRosa, Andy Q. Banh, Juan P. Palavicini, Paweł Wityk, Leszek Kalinowski, Veronica Galvan, Pawel A. Osmulski, Elzbieta Jankowska, Maria Gaczynska, and Andrew M. Pickering. Genetic and pharmacologic proteasome augmentation ameliorates Alzheimer's-like pathology in mouse and fly APP overexpression models. *Science Advances*, 8(23):eabk2252, June 2022.

[79] Eira Choudhary, Preeti Thakur, Madhu Pareek, and Nisheeth Agarwal. Gene silencing by CRISPR interference in mycobacteria. *Nature Communications*, 6(1):6267, February 2015.

[80] De-Hua Chui, Hiroshi Tanahashi, Kazuharu Ozawa, Sachiya Ikeda, Frédéric Checler, Otoya Ueda, Hiroshi Suzuki, Wataru Araki, Haruhisa Inoue, Keiro Shirotani, Keikichi Takahashi, Ferenc Gallyas, and Takeshi Tabira. Transgenic mice with Alzheimer presenilin 1 mutations show accelerated neurodegeneration without amyloid plaque formation. *Nature Medicine*, 5(5):560–564, May 1999.

[81] Martin Citron, David Westaway, Weiming Xia, George Carlson, Thekla Diehl, Georges Levesque, Kelly Johnson-wood, Michael Lee, Peter Seubert, Angela Davis, Dora Kholodenko, Ruth Motter, Robin Sherrington, Billie Perry, Hong Yao, Robert Strome, Ivan Lieberburg, Johanna Rommens, Soyeon Kim, Dale Schenk, Paul Fraser, Peter St George Hyslop, and Dennis J. Selkoe. Mutant presenilins of Alzheimer's disease increase production of 42-residue amyloid β-protein in both transfected cells and transgenic mice. *Nature Medicine*, 3(1):67–72, January 1997.

[82] Florence Clavaguera, Tristan Bolmont, R. Anthony Crowther, Dorothee Abramowski, Stephan Frank, Alphonse Probst, Graham Fraser, Anna K. Stalder, Martin Beibel, Matthias Staufenbiel, Mathias Jucker, Michel Goedert, and Markus Tolnay. Transmission and spreading of tauopathy in transgenic mouse brain. *Nature Cell Biology*, 11(7):909–913, July 2009.

[83] Gregory M. Cole and Paola S. Timiras. Ubiquitin-protein conjugates in Alzheimer's lesions. *Neuroscience Letters*, 79(1-2):207–212, August 1987.

[84] Martí Colom-Cadena, Caitlin Davies, Sònia Sirisi, Ji-Eun Lee, Elizabeth M. Simzer, Makis Tzioras, Marta Querol-Vilaseca, Érika Sánchez-Aced, Ya Yin Chang, Kristjan Holt, Robert I. McGeachan, Jamie Rose, Jane Tulloch, Lewis Wilkins, Colin Smith, Teodora Andrian, Olivia Belbin, Sílvia Pujals, Mathew H. Horrocks, Alberto Lleó, and Tara L. Spires-Jones. Synaptic oligomeric tau in Alzheimer's disease — A potential culprit in the spread of tau pathology through the brain. *Neuron*, 111(14):2170–2183.e6, July 2023.

[85] Martí Colom-Cadena, Jamie Toombs, Elizabeth Simzer, Kristjan Holt, Robert McGeachan, Jane Tulloch, Rosemary J. Jackson, James H. Catterson, Maxwell P. Spires-Jones, Jamie Rose, Lora Waybright, Anthony O. Caggiano, Declan King, Francesco Gobbo, Caitlin Davies, Monique Hooley, Sophie Dunnett, Robert Tempelaar, Soraya Meftah, Makis Tzioras, Mary E. Hamby, Nicholas J. Izzo, Susan M. Catalano, Claire S. Durrant, Colin Smith, Owen Dando, and Tara L. Spires-Jones. Transmembrane protein 97 is a potential synaptic amyloid beta receptor in human Alzheimer's disease. *Acta Neuropathologica*, 147(1):32, June 2024.

[86] Benjamin Combs and T. Chris Gamblin. FTDP-17 Tau Mutations Induce Distinct Effects on Aggregation and Microtubule Interactions. *Biochemistry*, 51(43):8597–8607, October 2012.

[87] Júlia Companys-Alemany, Andreea L. Turcu, Marion Schneider, Christa E. Müller, Santiago Vázquez, Christian Griñán-Ferré, and Mercè Pallàs. NMDA receptor antagonists reduce amyloid-β deposition by modulating calpain-1 signaling and autophagy, rescuing cognitive impairment in 5XFAD mice. *Cellular and Molecular Life Sciences*, 79(8):408, August 2022.

[88] Le Cong, F. Ann Ran, David Cox, Shuailiang Lin, Robert Barretto, Naomi Habib, Patrick D. Hsu, Xuebing Wu, Wenyan Jiang, Luciano A. Marraffini, and Feng Zhang. Multiplex Genome Engineering Using CRISPR/Cas Systems. *Science*, 339(6121):819–823, February 2013.

[89] A. Copani, F. Condorelli, A. Caruso, C. Vancheri, A. Sala, A. M. Giuffrida Stella, P. L. Canonico, F. Nicoletti, and M. A. Sortino. Mitotic signaling

by β-amyloid causes neuronal death. *The FASEB Journal*, 13(15):2225–2234, December 1999.

[90] Giovanni Coppola, Subashchandrabose Chinnathambi, Jason JiYong Lee, Beth A. Dombroski, Matt C. Baker, Alexandra I. Soto-Ortolaza, Suzee E. Lee, Eric Klein, Alden Y. Huang, Renee Sears, Jessica R. Lane, Anna M. Karydas, Robert O. Kenet, Jacek Biernat, Li-San Wang, Carl W. Cotman, Charles S. DeCarli, Allan I. Levey, John M. Ringman, Mario F. Mendez, Helena C. Chui, Isabelle Le Ber, Alexis Brice, Michelle K. Lupton, Elisavet Preza, Simon Lovestone, John Powell, Neill Graff-Radford, Ronald C. Petersen, Bradley F. Boeve, Carol F. Lippa, Eileen H. Bigio, Ian Mackenzie, Elizabeth Finger, Andrew Kertesz, Richard J. Caselli, Marla Gearing, Jorge L. Juncos, Bernardino Ghetti, Salvatore Spina, Yvette M. Bordelon, Wallace W. Tourtellotte, Matthew P. Frosch, Jean Paul G. Vonsattel, Chris Zarow, Thomas G. Beach, Roger L. Albin, Andrew P. Lieberman, Virginia M. Lee, John Q. Trojanowski, Vivianna M. Van Deerlin, Thomas D. Bird, Douglas R. Galasko, Eliezer Masliah, Charles L. White, Juan C. Troncoso, Didier Hannequin, Adam L. Boxer, Michael D. Geschwind, Satish Kumar, Eva-Maria Mandelkow, Zbigniew K. Wszolek, Ryan J. Uitti, Dennis W. Dickson, Jonathan L. Haines, Richard Mayeux, Margaret A. Pericak-Vance, Lindsay A. Farrer, Owen A. Ross, Rosa Rademakers, Gerard D. Schellenberg, Bruce L. Miller, Eckhard Mandelkow, and Daniel H. Geschwind. Evidence for a role of the rare p.A152T variant in MAPT in increasing the risk for FTD-spectrum and Alzheimer's diseases. *Human Molecular Genetics*, 21(15):3500–3512, August 2012.

[91] E. H. Corder, A. M. Saunders, N. J. Risch, W. J. Strittmatter, D. E. Schmechel, P. C. Gaskell, J. B. Rimmler, P. A. Locke, P. M. Conneally, K. E. Schmader, G. W. Small, A. D. Roses, J. L. Haines, and M. A. Pericak-Vance. Protective effect of apolipoprotein E type 2 allele for late onset Alzheimer disease. *Nature Genetics*, 7(2):180–184, June 1994.

[92] E. H. Corder, A. M. Saunders, W. J. Strittmatter, D. E. Schmechel, P. C. Gaskell, G. W. Small, A. D. Roses, J. L. Haines, and M. A. Pericak-Vance. Gene Dose of Apolipoprotein E Type 4 Allele and the Risk of Alzheimer's Disease in Late Onset Families. *Science*, 261(5123):921–923, August 1993.

[93] Jeffrey L. Cummings, Yadi Zhou, Garam Lee, Kate Zhong, Jorge Fonseca, Amanda M. Leisgang-Osse, and Feixiong Cheng. Alzheimer's disease drug development pipeline: 2025. *Alzheimer's & Dementia: Translational Research & Clinical Interventions*, 11(2):e70098, April 2025.

[94] Roy G. Cutler, Jeremiah Kelly, Kristin Storie, Ward A. Pedersen, Anita Tammara, Kimmo Hatanpaa, Juan C. Troncoso, and Mark P. Mattson. Involvement of oxidative stress-induced abnormalities in ceramide and cholesterol metabolism in brain aging and Alzheimer's disease. *Proceedings of the National Academy of Sciences*, 101(7):2070–2075, February 2004.

[95] Karie N. Dahlgren, Arlene M. Manelli, W. Blaine Stine, Lorinda K. Baker, Grant A. Krafft, and Mary Jo LaDu. Oligomeric and Fibrillar Species of Amyloid-β Peptides Differentially Affect Neuronal Viability. *Journal of Biological Chemistry*, 277(35):32046–32053, August 2002.

[96] Kanisa Davidson, Mehar Bano, Danitra Parker, Karl Rodriguez, Pawel Osmulski, Maria Gaczynska, and Andrew M. Pickering. β-Amyloid impairs Proteasome structure and function. Proteasome activation mitigates amyloid induced toxicity and cognitive deficits, October 2024.

[97] Peter Davies, Robert Katzman, and Robert D. Terry. Reduced somatostatin-like immunoreactivity in cerebral cortex from cases of Alzheimer disease and Alzheimer senile dementa. *Nature*, 288(5788):279–280, November 1980.

[98] Hana N. Dawson, Adriana Ferreira, Michele V. Eyster, Nupur Ghoshal, Lester I. Binder, and Michael P. Vitek. Inhibition of neuronal maturation in primary hippocampal neurons from tau deficient mice. *Journal of Cell Science*, 114(6):1179–1187, March 2001.

[99] H.N. Dawson, V. Cantillana, M. Jansen, H. Wang, M.P. Vitek, D.M. Wilcock, J.R. Lynch, and D.T. Laskowitz. Loss of tau elicits axonal degeneration in a mouse model of Alzheimer's disease. *Neuroscience*, 169(1):516–531, August 2010.

[100] Fernanda G. De Felice, Pauline T. Velasco, Mary P. Lambert, Kirsten Viola, Sara J. Fernandez, Sergio T. Ferreira, and William L. Klein. Aβ Oligomers Induce Neuronal Oxidative Stress through an N-Methyl-D-aspartate Receptor-dependent Mechanism That Is Blocked by the Alzheimer Drug Memantine. *Journal of Biological Chemistry*, 282(15):11590–11601, April 2007.

[101] Fernanda G. De Felice, Diana Wu, Mary P. Lambert, Sara J. Fernandez, Pauline T. Velasco, Pascale N. Lacor, Eileen H. Bigio, Jasna Jerecic, Paul J. Acton, Paul J. Shughrue, Elizabeth Chen-Dodson, Gene G. Kinney, and William L. Klein. Alzheimer's disease-type neuronal tau hyperphosphorylation induced by Aβ oligomers. *Neurobiology of Aging*, 29(9):1334–1347, September 2008.

[102] Philip L. De Jager, Yiyi Ma, Cristin McCabe, Jishu Xu, Badri N. Vardarajan, Daniel Felsky, Hans-Ulrich Klein, Charles C. White, Mette A. Peters, Ben Lodgson, Parham Nejad, Anna Tang, Lara M. Mangravite, Lei Yu, Chris Gaiteri, Sara Mostafavi, Julie A. Schneider, and David A. Bennett. A multi-omic atlas of the human frontal cortex for aging and Alzheimer's disease research. *Scientific Data*, 5(1):180142, August 2018.

[103] Itziar De Rojas, Sonia Moreno-Grau, Niccolo Tesi, Benjamin Grenier-Boley, Victor Andrade, Iris E. Jansen, Nancy L. Pedersen, Najada Stringa, Anna Zettergren, Isabel Hernández, Laura Montrreal, Carmen Antúnez, Anna Antonell, Rick M. Tankard, Joshua C. Bis, Rebecca Sims, Céline Bellenguez, Inés Quintela, Antonio González-Perez, Miguel Calero, Emilio Franco-Macías, Juan Macías, Rafael Blesa, Laura Cervera-Carles, Manuel Menéndez-González, Ana Frank-García, Jose Luís Royo, Fermin Moreno, Raquel Huerto Vilas, Miquel Baquero, Mónica Diez-Fairen, Carmen Lage, Sebastián García-Madrona, Pablo García-González, Emilio Alarcón-Martín, Sergi Valero, Oscar Sotolongo-Grau, Abbe Ullgren, Adam C. Naj, Afina W. Lemstra, Alba Benaque, Alba Pérez-Cordón, Alberto Benussi, Alberto Rábano, Alessandro Padovani, Alessio Squassina, Alexandre De Mendonça, Alfonso Arias Pastor, Almar A. L. Kok, Alun Meggy, Ana Belén Pastor, Ana Espinosa, Anaïs Corma-Gómez, Angel Martín Montes, Ángela Sanabria, Anita L. DeStefano, Anja Schneider, Annakaisa Haapasalo, Anne Kinhult Ståhlbom, Anne Tybjærg-Hansen, Annette M. Hartmann, Annika Spottke, Arturo Corbatón-Anchuelo, Arvid Rongve, Barbara Borroni, Beatrice Arosio, Benedetta Nacmias, Børge G. Nordestgaard, Brian W. Kunkle, Camille Charbonnier, Carla Abdelnour, Carlo Masullo, Carmen Martínez Rodríguez, Carmen Muñoz-Fernandez, Carole Dufouil, Caroline Graff, Catarina B. Ferreira, Caterina Chillotti, Chandra A. Reynolds, Chiara Fenoglio, Christine Van Broeckhoven, Christopher Clark, Claudia Pisanu, Claudia L. Satizabal, Clive Holmes, Dolores Buiza-Rueda, Dag Aarsland, Dan Rujescu, Daniel

Alcolea, Daniela Galimberti, David Wallon, Davide Seripa, Edna Grünblatt, Efthimios Dardiotis, Emrah Düzel, Elio Scarpini, Elisa Conti, Elisa Rubino, Ellen Gelpi, Eloy Rodriguez-Rodriguez, Emmanuelle Duron, Eric Boerwinkle, Evelyn Ferri, Fabrizio Tagliavini, Fahri Küçükali, Florence Pasquier, Florentino Sanchez-Garcia, Francesca Mangialasche, Frank Jessen, Gaël Nicolas, Geir Selbæk, Gemma Ortega, Geneviève Chêne, Georgios Hadjigeorgiou, Giacomina Rossi, Gianfranco Spalletta, Giorgio Giaccone, Giulia Grande, Giuliano Binetti, Goran Papenberg, Harald Hampel, Henri Bailly, Henrik Zetterberg, Hilkka Soininen, Ida K. Karlsson, Ignacio Alvarez, Ildebrando Appollonio, Ina Giegling, Ingmar Skoog, Ingvild Saltvedt, Innocenzo Rainero, Irene Rosas Allende, Jakub Hort, Janine Diehl-Schmid, Jasper Van Dongen, Jean-Sebastien Vidal, Jenni Lehtisalo, Jens Wiltfang, Jesper Qvist Thomassen, Johannes Kornhuber, Jonathan L. Haines, Jonathan Vogelgsang, Juan A. Pineda, Juan Fortea, Julius Popp, Jürgen Deckert, Katharina Buerger, Kevin Morgan, Klaus Fließbach, Kristel Sleegers, Laura Molina-Porcel, Lena Kilander, Leonie Weinhold, Lindsay A. Farrer, Li-San Wang, Luca Kleineidam, Lucia Farotti, Lucilla Parnetti, Lucio Tremolizzo, Lucrezia Hausner, Luisa Benussi, Lutz Froelich, M. Arfan Ikram, M. Candida Deniz-Naranjo, Magda Tsolaki, Maitée Rosende-Roca, Malin Löwenmark, Marc Hulsman, Marco Spallazzi, Margaret A. Pericak-Vance, Margaret Esiri, María Bernal Sánchez-Arjona, Maria Carolina Dalmasso, María Teresa Martínez-Larrad, Marina Arcaro, Markus M. Nöthen, Marta Fernández-Fuertes, Martin Dichgans, Martin Ingelsson, Martin J. Herrmann, Martin Scherer, Martin Vyhnalek, Mary H. Kosmidis, Mary Yannakoulia, Matthias Schmid, Michael Ewers, Michael T. Heneka, Michael Wagner, Michela Scamosci, Miia Kivipelto, Mikko Hiltunen, Miren Zulaica, Montserrat Alegret, Myriam Fornage, Natalia Roberto, Natasja M. Van Schoor, Nazib M. Seidu, Nerisa Banaj, Nicola J. Armstrong, Nikolaos Scarmeas, Norbert Scherbaum, Oliver Goldhardt, Oliver Hanon, Oliver Peters, Olivia Anna Skrobot, Olivier Quenez, Ondrej Lerch, Paola Bossù, Paolo Caffarra, Paolo Dionigi Rossi, Paraskevi Sakka, Patrizia Mecocci, Per Hoffmann, Peter A. Holmans, Peter Fischer, Peter Riederer, Qiong Yang, Rachel Marshall, Rajesh N. Kalaria, Richard Mayeux, Rik Vandenberghe, Roberta Cecchetti, Roberta Ghidoni, Ruth Frikke-Schmidt, Sandro Sorbi, Sara Hägg, Sebastiaan Engelborghs, Seppo Helisalmi, Sigrid Botne Sando, Silke Kern, Silvana Archetti, Silvia Boschi, Silvia Fostinelli, Silvia Gil, Silvia Mendoza, Simon Mead, Simona Ciccone, Srdjan Djurovic, Stefanie

Heilmann-Heimbach, Steffi Riedel-Heller, Teemu Kuulasmaa, Teodoro Del Ser, Thibaud Lebouvier, Thomas Polak, Tiia Ngandu, Timo Grimmer, Valentina Bessi, Valentina Escott-Price, Vilmantas Giedraitis, Vincent Deramecourt, Wolfgang Maier, Xueqiu Jian, Yolande A. L. Pijnenburg, EADB contributors, A. David Smith, Aldo Saenz, Alessandra Bizzarro, Alessandra Lauria, Alessandro Vacca, Alina Solomon, Anna Anastasiou, Anna Richardson, Anne Boland, Anne Koivisto, Antonio Daniele, Antonio Greco, Arnaoutoglou Marianthi, Bernadette McGuinness, Bertrand Fin, Camilla Ferrari, Carlo Custodero, Carlo Ferrarese, Carlos Ingino, Carlos Mangone, Carlos Reyes Toso, Carmen Martínez, Carolina Cuesta, Carolina Muchnik, Catharine Joachim, Cecilia Ortiz, Céline Besse, Charlotte Johansson, Chiara Paola Zoia, Christoph Laske, Costas Anastasiou, Dana Lis Palacio, Daniel G. Politis, Daniel Janowitz, David Craig, David M. Mann, David Neary, Deckert Jürgen, Delphine Daian, Diyana Belezhanska, Eduardo Kohler, Eduardo M. Castaño, Effrosyni Koutsouraki, Elena Chipi, Ellen De Roeck, Emanuele Costantini, Emma R. L. C. Vardy, Fabrizio Piras, Fausto Roveta, Federica Piras, Federico Ariel Prestia, Francesca Assogna, Francesca Salani, Gessica Sala, Giordano Lacidogna, Gisela Novack, Gordon Wilcock, Håkan Thonberg, Heike Kölsch, Heike Weber, Henning Boecker, Ignacio Etchepareborda, Irene Piaceri, Jaakko Tuomilehto, Jaana Lindström, Jan Laczo, Janet Johnston, Jean-François Deleuze, Jenny Harris, Jonathan M. Schott, Josef Priller, Juan Ignacio Bacha, Julie Snowden, Julieta Lisso, Kalina Yonkova Mihova, Latchezar Traykov, Laura Morelli, Luis Ignacio Brusco, Malik Rainer, Mari Takalo, Maria Bjerke, Maria Del Zompo, Maria Serpente, Mariana Sanchez Abalos, Mario Rios, Markku Peltonen, Martin J. Herrman, Mary H. Kosmidis, Matias Kohler, Matias Rojo, Matthew Jones, Michela Orsini, Nancy Medel, Natividad Olivar, Nick C. Fox, Nicola Salvadori, Nigel M. Hooper, Pablo Galeano, Patricia Solis, Patrizia Bastiani, Peter Passmore, Reinhard Heun, Riitta Antikainen, Robert Olaso, Robert Perneczky, Sandra Germani, Sara López-García, Seth Love, Shima Mehrabian, Silvia Bagnoli, Silvia Kochen, Simona Andreoni, Stefan Teipel, Stephen Todd, Stuart Pickering-Brown, Teemu Natunen, Thomas Tegos, Tiina Laatikainen, Timo Strandberg, Tuomo M. Polvikoski, Vaclav Matoska, Valentina Ciullo, Valeria Cores, Vincenzo Solfrizzi, Viviana Lisetti, Zulma Sevillano, The GR@ACE study group, C. Abdelnour, N. Aguilera, E. Alarcon, M. Alegret, A. Benaque, M. Boada, M. Buendia, P. Cañabate, A. Carracedo, A. Corbatón-Anchuelo, I. De Rojas, S. Diego, A. Espinosa,

A. Gailhajenet, P. García-González, S. Gil, M. Guitart, A. González-Pérez, I. Hernández, M. Ibarria, A. Lafuente, J. Macias, O. Maroñas, E. Martín, M. T. Martínez, M. Marquié, A. Mauleón, L. Montrreal, S. Moreno-Grau, M. Moreno, A. Orellana, G. Ortega, A. Pancho, E. Pelejá, A. Pérez-Cordon, J. A. Pineda, S. Preckler, I. Quintela, L. M. Real, M. Rosende-Roca, A. Ruiz, M. E. Sáez, A. Sanabria, M. Serrano-Rios, O. Sotolongo-Grau, L. Tárraga, S. Valero, L. Vargas, DEGESCO consortium, A. D. Adarmes-Gómez, E. Alarcón-Martín, M. D. Alonso, I. Álvarez, V. Álvarez, G. Amer-Ferrer, M. Antequera, C. Antúnez, M. Baquero, M. Bernal, R. Blesa, M. Boada, D. Buiza-Rueda, M. J. Bullido, J. A. Burguera, M. Calero, F. Carrillo, M. Carrión-Claro, M. J. Casajeros, J. Clarimón, J. M. Cruz-Gamero, M. M. De Pancorbo, I. De Rojas, T. Del Ser, M. Diez-Fairen, R. Escuela, L. Garrote-Espina, J. Fortea, E. Franco-Macías, A. Frank-García, J. M. García-Alberca, S. Garcia Madrona, G. Garcia-Ribas, P. Gómez-Garre, I. Hernández, S. Hevilla, S. Jesús, M. A. Labrador Espinosa, C. Lage, A. Legaz, A. Lleó, A. Lopez De Munain, S. López-García, D. Macias-García, S. Manzanares, M. Marín, J. Marín-Muñoz, T. Marín, M. Marquié, A. Martín Montes, B. Martínez, C. Martínez, V. Martínez, P. Martínez-Lage Álvarez, M. Medina, M. Mendioroz Iriarte, M. Menéndez-González, P. Mir, J. L. Molinuevo, P. Pastor, J. Pérez Tur, T. Periñán-Tocino, R. Pineda-Sanchez, G. Piñol-Ripoll, A. Rábano, D. Real De Asúa, S. Rodrigo, E. Rodríguez-Rodríguez, J. L. Royo, A. Ruiz, R. Sanchez Del Valle Díaz, P. Sánchez-Juan, I. Sastre, S. Valero, M. P. Vicente, R. Vigo-Ortega, L. Vivancos, IGAP (ADGC, CHARGE, EADI, GERAD), C. Macleod, C. McCracken, Carol Brayne, Catherine Bresner, Detelina Grozeva, Eftychia Bellou, Ewen W. Sommerville, F. Matthews, Ganna Leonenko, Georgina Menzies, Gill Windle, Janet Harwood, Judith Phillips, K. Bennett, Lauren Luckuck, Linda Clare, Robert Woods, Salha Saad, Vanessa Burholt, PGC-ALZ consortia, Iris E. Jansen, Arvid Rongve, Patrick Gavin Kehoe, Guillermo Garcia-Ribas, Pascual Sánchez-Juan, Pau Pastor, Jordi Pérez-Tur, Gerard Piñol-Ripoll, Adolfo Lopez De Munain, Jose María García-Alberca, María J. Bullido, Victoria Álvarez, Alberto Lleó, Luis M. Real, Pablo Mir, Miguel Medina, Philip Scheltens, Henne Holstege, Marta Marquié, María Eugenia Sáez, Ángel Carracedo, Philippe Amouyel, Gerard D. Schellenberg, Julie Williams, Sudha Seshadri, Cornelia M. Van Duijn, Karen A. Mather, Raquel Sánchez-Valle, Manuel Serrano-Ríos, Adelina Orellana, Lluís Tárraga, Kaj Blennow, Martijn Huisman, Ole A.

Andreassen, Danielle Posthuma, Jordi Clarimón, Mercè Boada, Wiesje M. Van Der Flier, Alfredo Ramirez, Jean-Charles Lambert, Sven J. Van Der Lee, and Agustín Ruiz. Common variants in Alzheimer's disease and risk stratification by polygenic risk scores. *Nature Communications*, 12(1):3417, June 2021.

[104] Bart De Strooper, Paul Saftig, Katleen Craessaerts, Hugo Vanderstichele, Gundula Guhde, Wim Annaert, Kurt Von Figura, and Fred Van Leuven. Deficiency of presenilin-1 inhibits the normal cleavage of amyloid precursor protein. *Nature*, 391(6665):387–390, January 1998.

[105] Rashid Deane, Abhay Sagare, Katie Hamm, Margaret Parisi, Steven Lane, Mary Beth Finn, David M. Holtzman, and Berislav V. Zlokovic. apoE isoform–specific disruption of amyloid β peptide clearance from mouse brain. *Journal of Clinical Investigation*, 118(12):4002–4013, December 2008.

[106] Argyro Thalia Delizannis, Annelies Nonneman, Wangchen Tsering, An De Bondt, Ilse Van Den Wyngaert, Bin Zhang, Emily Meymand, Modupe F. Olufemi, Pyry Koivula, Shaniya Maimaiti, John Q. Trojanowski, Virginia M.-Y. Lee, and Kurt R. Brunden. Effects of microglial depletion and TREM2 deficiency on Aβ plaque burden and neuritic plaque tau pathology in 5XFAD mice. *Acta Neuropathologica Communications*, 9(1):150, December 2021.

[107] Elitza Deltcheva, Krzysztof Chylinski, Cynthia M. Sharma, Karine Gonzales, Yanjie Chao, Zaid A. Pirzada, Maria R. Eckert, Jörg Vogel, and Emmanuelle Charpentier. CRISPR RNA maturation by trans-encoded small RNA and host factor RNase III. *Nature*, 471(7340):602–607, March 2011.

[108] Harriet Demnitz-King, Mariam Adeleke, Julie A Barber, Michaela Poppe, Jessica Budgett, Sweedal Alberts, Larisa Duffy, Anne-Marie Minihane, Rachel Gillings, Hannah Chapman, Rosario Isabel Espinoza Jeraldo, Oliver Kelsey, Malvika Muralidhar, Sedigheh Zabihi, Elisa Aguirre, Nicholas Bass, Anna Betz, Henry Brodaty, Alexandra Burton, Paul Higgs, Rachael Maree Hunter, Jonathan Huntley, Helen C Kales, Iain Lang, Natalie L Marchant, Sarah Morgan-Trimmer, Penny Rapaport, Miguel Rio, Irene Petersen, Zuzana Walker, Kate Walters, Sube Banerjee, Joanne Rodda, Marina Palomo, and Claudia Cooper. Remote, lower-intensity, multidomain lifestyle intervention for subjective cognitive decline or mild cognitive impairment (APPLE-Tree):

a multicentre, single-masked, randomised controlled trial. *The Lancet Healthy Longevity*, 6(10):100777, October 2025.

[109] Michael A. DeTure and Dennis W. Dickson. The neuropathological diagnosis of Alzheimer's disease. *Molecular Neurodegeneration*, 14(1):32, December 2019.

[110] I. Dewachter, R.K. Filipkowski, C. Priller, L. Ris, J. Neyton, S. Croes, D. Terwel, M. Gysemans, H. Devijver, P. Borghgraef, E. Godaux, L. Kaczmarek, J. Herms, and F. Van Leuven. Deregulation of NMDA-receptor function and down-stream signaling in APP[V717I] transgenic mice. *Neurobiology of Aging*, 30(2):241–256, February 2009.

[111] Alix de Calignon, Manuela Polydoro, Marc Suárez-Calvet, Christopher William, David H. Adamowicz, Kathy J. Kopeikina, Rose Pitstick, Naruhiko Sahara, Karen H. Ashe, George A. Carlson, Tara L. Spires-Jones, and Bradley T. Hyman. Propagation of Tau Pathology in a Model of Early Alzheimer's Disease. *Neuron*, 73(4):685–697, February 2012.

[112] B. C. Dickerson, D. H. Salat, D. N. Greve, E. F. Chua, E. Rand-Giovannetti, D. M. Rentz, L. Bertram, K. Mullin, R. E. Tanzi, D. Blacker, M. S. Albert, and R. A. Sperling. Increased hippocampal activation in mild cognitive impairment compared to normal aging and AD. *Neurology*, 65(3):404–411, August 2005.

[113] Ram Dixit, Jennifer L. Ross, Yale E. Goldman, and Erika L. F. Holzbaur. Differential Regulation of Dynein and Kinesin Motor Proteins by Tau. *Science*, 319(5866):1086–1089, February 2008.

[114] Martin H. Dominguez, Albert E. Ayoub, and Pasko Rakic. POU-III Transcription Factors (Brn1, Brn2, and Oct6) Influence Neurogenesis, Molecular Identity, and Migratory Destination of Upper-Layer Cells of the Cerebral Cortex. *Cerebral Cortex*, 23(11):2632–2643, November 2013.

[115] Harry F. Dovey, Susanna Suomensaari-Chrysler, Ivan Lieberburg, Sukanto Sinha, and Pam S. Keim. Cells with a familial Alzheimer s disease mutation produce authentic β-peptide. *NeuroReport*, 4(8):1039–1042, August 1993.

[116] Lishu Duan, Bula J Bhattacharyya, Abdelhak Belmadani, Liuliu Pan, Richard J Miller, and John A Kessler. Stem cell derived basal forebrain cholinergic neurons from Alzheimer's disease patients are more susceptible to cell death. *Molecular Neurodegeneration*, 9(1):3, 2014.

[117] Karen Duff, Chris Eckman, Cindy Zehr, Xin Yu, Cristian-Mihail Prada, Jordi Perez-tur, Mike Hutton, Luc Buee, Yasuo Harigaya, Debra Yager, David Morgan, Marcia N. Gordon, Leigh Holcomb, Lawrence Refolo, Brenda Zenk, John Hardy, and Steven Younkin. Increased amyloid-β42(43) in brains of mice expressing mutant presenilin 1. *Nature*, 383(6602):710–713, October 1996.

[118] Simon Dujardin, Caitlin Commins, Aurelien Lathuiliere, Pieter Beerepoot, Analiese R. Fernandes, Tarun V. Kamath, Mark B. De Los Santos, Naomi Klickstein, Diana L. Corjuc, Bianca T. Corjuc, Patrick M. Dooley, Arthur Viode, Derek H. Oakley, Benjamin D. Moore, Kristina Mullin, Dinorah Jean-Gilles, Ryan Clark, Kevin Atchison, Renee Moore, Lori B. Chibnik, Rudolph E. Tanzi, Matthew P. Frosch, Alberto Serrano-Pozo, Fiona Elwood, Judith A. Steen, Matthew E. Kennedy, and Bradley T. Hyman. Tau molecular diversity contributes to clinical heterogeneity in Alzheimer's disease. *Nature Medicine*, 26(8):1256–1263, August 2020.

[119] Simon Dujardin, Katia Lécolle, Raphaëlle Caillierez, Séverine Bégard, Nadège Zommer, Cédrick Lachaud, Sébastien Carrier, Noëlle Dufour, Gwennaëlle Aurégan, Joris Winderickx, Philippe Hantraye, Nicole Déglon, Morvane Colin, and Luc Buée. Neuron-to-neuron wild-type Tau protein transfer through a trans-synaptic mechanism: relevance to sporadic tauopathies. *Acta Neuropathologica Communications*, 2(1):14, December 2014.

[120] Ionut Dumitru, Marta Paterlini, Margherita Zamboni, Christoph Ziegenhain, Sarantis Giatrellis, Rasool Saghaleyni, Åsa Björklund, Kanar Alkass, Mathew Tata, Henrik Druid, Rickard Sandberg, and Jonas Frisén. Identification of proliferating neural progenitors in the adult human hippocampus. *Science*, 389(6755):58–63, July 2025.

[121] Simone D'Angiolini, Agnese Gugliandolo, Gabriella Calì, and Luigi Chiricosta. Early Dysregulation of RNA Splicing and Translation Processes Are Key Markers from Mild Cognitive Impairment to Alzheimer's Disease: An In Silico Transcriptomic Analysis. *International Journal of Molecular Sciences*, 26(15):7303, July 2025.

[122] Philip J. Ebenezer, Adam M. Weidner, Harry LeVine, William R. Markesbery, M. Paul Murphy, Le Zhang, Kalavathi Dasuri, Sun Ok Fernandez-Kim, Annadora J. Bruce-Keller, Elena Gavilán, and Jeffrey N. Keller. Neuron Specific

Toxicity of Oligomeric Amyloid-β: Role for JUN-Kinase and Oxidative Stress. *Journal of Alzheimer's Disease*, 22(3):839–848, November 2010.

[123] Marc Ehrlich, Sabah Mozafari, Michael Glatza, Laura Starost, Sergiy Velychko, Anna-Lena Hallmann, Qiao-Ling Cui, Axel Schambach, Kee-Pyo Kim, Corinne Bachelin, Antoine Marteyn, Gunnar Hargus, Radia Marie Johnson, Jack Antel, Jared Sterneckert, Holm Zaehres, Hans R. Schöler, Anne Baron-Van Evercooren, and Tanja Kuhlmann. Rapid and efficient generation of oligodendrocytes from human induced pluripotent stem cells using transcription factors. *Proceedings of the National Academy of Sciences*, 114(11), March 2017.

[124] Kathryn A Ellis, Ashley I Bush, David Darby, Daniela De Fazio, Jonathan Foster, Peter Hudson, Nicola T. Lautenschlager, Nat Lenzo, Ralph N. Martins, Paul Maruff, Colin Masters, Andrew Milner, Kerryn Pike, Christopher Rowe, Greg Savage, Cassandra Szoeke, Kevin Taddei, Victor Villemagne, Michael Woodward, and David Ames. The Australian Imaging, Biomarkers and Lifestyle (AIBL) study of aging: methodology and baseline characteristics of 1112 individuals recruited for a longitudinal study of Alzheimer's disease. *International Psychogeriatrics*, 21(4):672–687, August 2009.

[125] Richard J. Elsworthy, Mattea J. Finelli, Sarah Aqattan, Connor Dunleavy, Marianne King, Adele Ludlam, Marta A. Tarczyluk, Sophie L. Allen, Sophie Prosser, Rui Chen, Sandra Martinez Jarquin, Dong H. Kim, James Brown, H. R. Parri, Sarah Aldred, and Eric J. Hill. Altered metabolic function induced by Aβ-oligomers and PSEN1 mutations in iPSC -derived astrocytes. *Journal of Neurochemistry*, 169(1):e16267, January 2025.

[126] Khalid Eltom, Tobias Mothes, Sylwia Libard, Martin Ingelsson, and Anna Erlandsson. Astrocytic accumulation of tau fibrils isolated from Alzheimer's disease brains induces inflammation, cell-to-cell propagation and neuronal impairment. *Acta Neuropathologica Communications*, 12(1):34, February 2024.

[127] S. Engelborghs, K. Sleegers, P. Cras, N. Brouwers, S. Serneels, E. De Leenheir, J.-J. Martin, E. Vanmechelen, C. Van Broeckhoven, and P. P. De Deyn. No association of CSF biomarkers with APOE 4, plaque and tangle burden in definite Alzheimer's disease. *Brain*, 130(9):2320–2326, September 2007.

[128] Peter S. Eriksson, Ekaterina Perfilieva, Thomas Björk-Eriksson, Ann-Marie Alborn, Claes Nordborg, Daniel A. Peterson, and Fred H. Gage. Neurogenesis in the adult human hippocampus. *Nature Medicine*, 4(11):1313–1317, November 1998.

[129] Michael Ewers, Gloria Biechele, Marc Suárez-Calvet, Christian Sacher, Tanja Blume, Estrella Morenas-Rodriguez, Yuetiva Deming, Laura Piccio, Carlos Cruchaga, Gernot Kleinberger, Leslie Shaw, John Q Trojanowski, Jochen Herms, Martin Dichgans, the Alzheimer's Disease Neuroimaging Initiative (ADNI), Matthias Brendel, Christian Haass, and Nicolai Franzmeier. Higher CSF sTREM2 and microglia activation are associated with slower rates of beta-amyloid accumulation. *EMBO Molecular Medicine*, 12(9):e12308, September 2020.

[130] Benjamin Falcon, Annalisa Cavallini, Rachel Angers, Sarah Glover, Tracey K. Murray, Luanda Barnham, Samuel Jackson, Michael J. O'Neill, Adrian M. Isaacs, Michael L. Hutton, Philip G. Szekeres, Michel Goedert, and Suchira Bose. Conformation Determines the Seeding Potencies of Native and Recombinant Tau Aggregates. *Journal of Biological Chemistry*, 290(2):1049–1065, January 2015.

[131] Benjamin Falcon, Wenjuan Zhang, Alexey G. Murzin, Garib Murshudov, Holly J. Garringer, Ruben Vidal, R. Anthony Crowther, Bernardino Ghetti, Sjors H. W. Scheres, and Michel Goedert. Structures of filaments from Pick's disease reveal a novel tau protein fold. *Nature*, 561(7721):137–140, September 2018.

[132] Benjamin Falcon, Wenjuan Zhang, Manuel Schweighauser, Alexey G. Murzin, Ruben Vidal, Holly J. Garringer, Bernardino Ghetti, Sjors H. W. Scheres, and Michel Goedert. Tau filaments from multiple cases of sporadic and inherited Alzheimer's disease adopt a common fold. *Acta Neuropathologica*, 136(5):699–708, November 2018.

[133] S. Fabio Falsone, N. Helge Meyer, Evelyne Schrank, Gerd Leitinger, Chi L.L. Pham, Michelle T. Fodero-Tavoletti, Mats Holmberg, Martin Dulle, Benjamin Scicluna, Bernd Gesslbauer, Hanna-Marie Rückert, Gabriel E. Wagner, David A. Merle, Ellen A. Nollen, Andreas J. Kungl, Andrew F. Hill, Roberto Cappai, and Klaus Zangger. SERF Protein Is a Direct Modifier of Amyloid Fiber Assembly. *Cell Reports*, 2(2):358–371, August 2012.

[134] Evandro F. Fang, Yujun Hou, Konstantinos Palikaras, Bryan A. Adriaanse, Jesse S. Kerr, Beimeng Yang, Sofie Lautrup, Md Mahdi Hasan-Olive, Domenica Caponio, Xiuli Dan, Paula Rocktäschel, Deborah L. Croteau, Mansour Akbari, Nigel H. Greig, Tormod Fladby, Hilde Nilsen, M. Zameel Cader, Mark P. Mattson, Nektarios Tavernarakis, and Vilhelm A. Bohr. Mitophagy inhibits amyloid-β and tau pathology and reverses cognitive deficits in models of Alzheimer's disease. *Nature Neuroscience*, 22(3):401–412, March 2019.

[135] Lindsay A. Farrer. Effects of Age, Sex, and Ethnicity on the Association Between Apolipoprotein E Genotype and Alzheimer Disease: A Meta-analysis. *JAMA*, 278(16):1349, October 1997.

[136] Stuart C. Feinstein and Leslie Wilson. Inability of tau to properly regulate neuronal microtubule dynamics: a loss-of-function mechanism by which tau might mediate neuronal cell death. *Biochimica et Biophysica Acta (BBA) - Molecular Basis of Disease*, 1739(2-3):268–279, January 2005.

[137] Michael S. Fernandopulle, Ryan Prestil, Christopher Grunseich, Chao Wang, Li Gan, and Michael E. Ward. Transcription Factor–Mediated Differentiation of Human iPSCs into Neurons. *Current Protocols in Cell Biology*, 79(1):e51, June 2018.

[138] Eduardo J. Fernández-Pérez, Fernando J. Sepúlveda, Christian Peters, Denisse Bascuñán, Nicolás O. Riffo-Lepe, Juliana González-Sanmiguel, Susana A. Sánchez, Robert W. Peoples, Benjamín Vicente, and Luis G. Aguayo. Effect of Cholesterol on Membrane Fluidity and Association of Aβ Oligomers and Subsequent Neuronal Damage: A Double-Edged Sword. *Frontiers in Aging Neuroscience*, 10:226, August 2018.

[139] Anthony W. P. Fitzpatrick, Benjamin Falcon, Shaoda He, Alexey G. Murzin, Garib Murshudov, Holly J. Garringer, R. Anthony Crowther, Bernardino Ghetti, Michel Goedert, and Sjors H. W. Scheres. Cryo-EM structures of tau filaments from Alzheimer's disease. *Nature*, 547(7662):185–190, July 2017.

[140] for the Alzheimer's Disease Neuroimaging Initiative, Dominik Wolf, Florian U. Fischer, and Andreas Fellgiebel. Impact of Resilience on the Association Between Amyloid-β and Longitudinal Cognitive Decline in Cognitively Healthy Older Adults. *Journal of Alzheimer's Disease*, 70(2):361–370, July 2019.

[141] Evangeline M. Foster, Marco Fernandes, Adria Dangla-Valls, Philip Hublitz, Menelaos Pangalos, Simon Lovestone, Elena M. Ribe, and Noel J. Buckley. Glycosylated clusterin species facilitate Aβ toxicity in human neurons. *Scientific Reports*, 12(1):18639, November 2022.

[142] Giovanni B. Frisoni, Nick C. Fox, Clifford R. Jack, Philip Scheltens, and Paul M. Thompson. The clinical use of structural MRI in Alzheimer disease. *Nature Reviews Neurology*, 6(2):67–77, February 2010.

[143] Bess Frost, Rachel L. Jacks, and Marc I. Diamond. Propagation of Tau Misfolding from the Outside to the Inside of a Cell. *Journal of Biological Chemistry*, 284(19):12845–12852, May 2009.

[144] Bess Frost, Julian Ollesch, Holger Wille, and Marc I. Diamond. Conformational Diversity of Wild-type Tau Fibrils Specified by Templated Conformation Change. *Journal of Biological Chemistry*, 284(6):3546–3551, February 2009.

[145] Katsunori Fujio, Mahito Sato, Takefumi Uemura, Takashi Sato, Reiko Sato-Harada, and Akihiro Harada. 14-3-3 proteins and protein phosphatases are not reduced in tau-deficient mice. *NeuroReport*, 18(10):1049–1052, July 2007.

[146] Rebecca Gail Canter, Wen-Chin Huang, Heejin Choi, Jun Wang, Lauren Ashley Watson, Christine G. Yao, Fatema Abdurrob, Stephanie M. Bousleiman, Jennie Z. Young, David A. Bennett, Ivana Delalle, Kwanghun Chung, and Li-Huei Tsai. 3D mapping reveals network-specific amyloid progression and subcortical susceptibility in mice. *Communications Biology*, 2(1):360, October 2019.

[147] Douglas Galasko, Meifang Xiao, Desheng Xu, Denis Smirnov, David P. Salmon, Nele Dewit, Jeroen Vanbrabant, Dirk Jacobs, Hugo Vanderstichele, Eugeen Vanmechelen, Alzheimer's Disease Neuroimaging Initiative (ADNI), and Paul Worley. Synaptic biomarkers in CSF aid in diagnosis, correlate with cognition and predict progression in MCI and Alzheimer's disease. *Alzheimer's & Dementia: Translational Research & Clinical Interventions*, 5(1):871–882, January 2019.

[148] Sam Gandy, Adam J. Simon, John W. Steele, Alex L. Lublin, James J. Lah, Lary C. Walker, Allan I. Levey, Grant A. Krafft, Efrat Levy, Frédéric Checler, Charles Glabe, Warren B. Bilker, Ted Abel, James Schmeidler, and Michelle E.

Ehrlich. Days to criterion as an indicator of toxicity associated with human Alzheimer amyloid-β oligomers. *Annals of Neurology*, 68(2):220–230, August 2010.

[149] Ana Garcia-Osta and Cristina M. Alberini. Amyloid beta mediates memory formation. *Learning & Memory*, 16(4):267–272, April 2009.

[150] Juan Antonio García-León, Alfredo Cabrera-Socorro, Kristel Eggermont, Ann Swijsen, Joke Terryn, Raheem Fazal, FatemehArefeh Nami, Laura Ordovás, Ana Quiles, Frederic Lluis, Lutgarde Serneels, Keimpe Wierda, Annerieke Sierksma, Mohamed Kreir, Francisco Pestana, Philip Van Damme, Bart De Strooper, Lieven Thorrez, Andreas Ebneth, and Catherine M. Verfaillie. Generation of a human induced pluripotent stem cell–based model for tauopathies combining three microtubule-associated protein TAU mutations which displays several phenotypes linked to neurodegeneration. *Alzheimer's & Dementia*, 14(10):1261–1280, October 2018.

[151] Sergio Gascón, Elisa Murenu, Giacomo Masserdotti, Felipe Ortega, Gianluca L. Russo, David Petrik, Aditi Deshpande, Christophe Heinrich, Marisa Karow, Stephen P. Robertson, Timm Schroeder, Johannes Beckers, Martin Irmler, Carsten Berndt, José P. Friedmann Angeli, Marcus Conrad, Benedikt Berninger, and Magdalena Götz. Identification and Successful Negotiation of a Metabolic Checkpoint in Direct Neuronal Reprogramming. *Cell Stem Cell*, 18(3):396–409, March 2016.

[152] Margaret Gatz, Chandra A. Reynolds, Laura Fratiglioni, Boo Johansson, James A. Mortimer, Stig Berg, Amy Fiske, and Nancy L. Pedersen. Role of Genes and Environments for Explaining Alzheimer Disease. *Archives of General Psychiatry*, 63(2):168, February 2006.

[153] Stefano L. Giandomenico, Susanna B. Mierau, George M. Gibbons, Lea M. D. Wenger, Laura Masullo, Timothy Sit, Magdalena Sutcliffe, Jerome Boulanger, Marco Tripodi, Emmanuel Derivery, Ole Paulsen, András Lakatos, and Madeline A. Lancaster. Cerebral organoids at the air–liquid interface generate diverse nerve tracts with functional output. *Nature Neuroscience*, 22(4):669–679, April 2019.

[154] E. Giraldo, A. Lloret, T. Fuchsberger, and J. Viña. Aβ and tau toxicities in Alzheimer's are linked via oxidative stress-induced p38 activation: Protective role of vitamin E. *Redox Biology*, 2:873–877, 2014.

[155] Alison Goate, Marie-Christine Chartier-Harlin, Mike Mullan, Jeremy Brown, Fiona Crawford, Liana Fidani, Luis Giuffra, Andrew Haynes, Nick Irving, Louise James, Rebecca Mant, Phillippa Newton, Karen Rooke, Penelope Roques, Chris Talbot, Margaret Pericak-Vance, Allen Roses, Robert Williamson, Martin Rossor, Mike Owen, and John Hardy. Segregation of a missense mutation in the amyloid precursor protein gene with familial Alzheimer's disease. *Nature*, 349(6311):704–706, February 1991.

[156] M. Goedert and R. Jakes. Expression of separate isoforms of human tau protein: correlation with the tau pattern in brain and effects on tubulin polymerization. *The EMBO Journal*, 9(13):4225–4230, December 1990.

[157] M Goedert, R Jakes, R A Crowther, J Six, U Lübke, M Vandermeeren, P Cras, J Q Trojanowski, and V M Lee. The abnormal phosphorylation of tau protein at Ser-202 in Alzheimer disease recapitulates phosphorylation during development. *Proceedings of the National Academy of Sciences*, 90(11):5066–5070, June 1993.

[158] M. Goedert, R. Jakes, and E. Vanmechelen. Monoclonal antibody AT8 recognises tau protein phosphorylated at both serine 202 and threonine 205. *Neuroscience Letters*, 189(3):167–170, April 1995.

[159] M. Goedert, M.G. Spillantini, R. Jakes, D. Rutherford, and R.A. Crowther. Multiple isoforms of human microtubule-associated protein tau: sequences and localization in neurofibrillary tangles of Alzheimer's disease. *Neuron*, 3(4):519–526, October 1989.

[160] Michel Goedert, Ross Jakes, and R.Anthony Crowther. Effects of frontotemporal dementia FTDP-17 mutations on heparin-induced assembly of tau filaments. *FEBS Letters*, 450(3):306–311, May 1999.

[161] Todd E. Golde, Steven Estus, Linda H. Younkin, Dennis J. Selkoe, and Steven G Younkin. Processing of the Amyloid Protein Precursor to Potentially Amyloidogenic Derivatives. *Science*, 255(5045):728–730, February 1992.

[162] Lesley R. Golden, Dahlia S. Siano, Isaiah O. Stephens, Steven M. MacLean, Kai Saito, Georgia L. Nolt, Jessica L. Funnell, Akhil V. Pallerla, Sangderk Lee, Cathryn Smith, Jing Chen, Haining Zhu, Clairity Voy, Callie M. Whitus, Gabriela Hernandez, Brandon C. Farmer, Kumar Pandya, Dale O. Cowley, Shannon L. Macauley, Scott M. Gordon, Josh M. Morganti, and Lance A. Johnson. APOE4 to APOE2 allelic switching in mice improves Alzheimer's disease-related metabolic signatures, neuropathology and cognition. *Nature Neuroscience*, 28(12):2461–2475, December 2025.

[163] Cesar Gonzalez, Enrique Armijo, Javiera Bravo-Alegria, Andrea Becerra-Calixto, Charles E. Mays, and Claudio Soto. Modeling amyloid beta and tau pathology in human cerebral organoids. *Molecular Psychiatry*, 23(12):2363–2374, December 2018.

[164] M. B. Graeber, S. Kösel, E. Grasbon-Frodl, H. J. Möller, and P. Mehraein. Histopathology and APOE genotype of the first Alzheimer disease patient, Auguste D. *neurogenetics*, 1(3):223–228, March 1998.

[165] I Grundke-Iqbal, K Iqbal, Y C Tung, M Quinlan, H M Wisniewski, and L I Binder. Abnormal phosphorylation of the microtubule-associated protein tau (tau) in Alzheimer cytoskeletal pathology. *Proceedings of the National Academy of Sciences*, 83(13):4913–4917, July 1986.

[166] Jing L. Guo and Virginia M.-Y. Lee. Seeding of Normal Tau by Pathological Tau Conformers Drives Pathogenesis of Alzheimer-like Tangles. *Journal of Biological Chemistry*, 286(17):15317–15331, April 2011.

[167] Sudha R. Guttikonda, Lisa Sikkema, Jason Tchieu, Nathalie Saurat, Ryan M. Walsh, Oliver Harschnitz, Gabriele Ciceri, Marjolein Sneeboer, Linas Mazutis, Manu Setty, Paul Zumbo, Doron Betel, Lot D. De Witte, Dana Pe'er, and Lorenz Studer. Fully defined human pluripotent stem cell-derived microglia and tri-culture system model C3 production in Alzheimer's disease. *Nature Neuroscience*, 24(3):343–354, March 2021.

[168] Karen Hoppens Gylys, Jeffrey A. Fein, Fusheng Yang, Carol A. Miller, and Gregory M. Cole. Increased cholesterol in Aβ-positive nerve terminals from Alzheimer's disease cortex. *Neurobiology of Aging*, 28(1):8–17, January 2007.

[169] J. Götz, F. Chen, J. Van Dorpe, and R. M. Nitsch. Formation of Neurofibrillary Tangles in P301L Tau Transgenic Mice Induced by Aβ42 Fibrils. *Science*, 293(5534):1491–1495, August 2001.

[170] Christian Haass, Michael G. Schlossmacher, Albert Y. Hung, Carmen Vigo-Pelfrey, Angela Mellon, Beth L. Ostaszewski, Ivan Lieberburg, Edward H. Koo, Dale Schenk, David B. Teplow, and Dennis J. Selkoe. Amyloid β-peptide is produced by cultured cells during normal metabolism. *Nature*, 359(6393):322–325, September 1992.

[171] Walther Haenseler, Stephen N. Sansom, Julian Buchrieser, Sarah E. Newey, Craig S. Moore, Francesca J. Nicholls, Satyan Chintawar, Christian Schnell, Jack P. Antel, Nicholas D. Allen, M. Zameel Cader, Richard Wade-Martins, William S. James, and Sally A. Cowley. A Highly Efficient Human Pluripotent Stem Cell Microglia Model Displays a Neuronal-Co-culture-Specific Expression Profile and Inflammatory Response. *Stem Cell Reports*, 8(6):1727–1742, June 2017.

[172] Michael S. Haney, Róbert Pálovics, Christy Nicole Munson, Chris Long, Patrik K. Johansson, Oscar Yip, Wentao Dong, Eshaan Rawat, Elizabeth West, Johannes C. M. Schlachetzki, Andy Tsai, Ian Hunter Guldner, Bhawika S. Lamichhane, Amanda Smith, Nicholas Schaum, Kruti Calcuttawala, Andrew Shin, Yung-Hua Wang, Chengzhong Wang, Nicole Koutsodendris, Geidy E. Serrano, Thomas G. Beach, Eric M. Reiman, Christopher K. Glass, Monther Abu-Remaileh, Annika Enejder, Yadong Huang, and Tony Wyss-Coray. APOE4/4 is linked to damaging lipid droplets in Alzheimer's disease microglia. *Nature*, 628(8006):154–161, April 2024.

[173] Diane P. Hanger, Joanna C. Betts, Thérèse L. F. Loviny, Walter P. Blackstock, and Brian H. Anderton. New Phosphorylation Sites Identified in Hyperphosphorylated Tau (Paired Helical Filament-Tau) from Alzheimer's Disease Brain Using Nanoelectrospray Mass Spectrometry. *Journal of Neurochemistry*, 71(6):2465–2476, December 1998.

[174] Diane P. Hanger, Helen L. Byers, Selina Wray, Kit-Yi Leung, Malcolm J. Saxton, Anjan Seereeram, C. Hugh Reynolds, Malcolm A. Ward, and Brian H. Anderton. Novel Phosphorylation Sites in Tau from Alzheimer Brain Support a Role for Casein Kinase 1 in Disease Pathogenesis. *Journal of Biological Chemistry*, 282(32):23645–23654, August 2007.

[175] A. Harada, K. Oguchi, S. Okabe, J. Kuno, S. Terada, T. Ohshima, R. Sato-Yoshitake, Y. Takei, T. Noda, and N. Hirokawa. Altered microtubule organization in small-calibre axons of mice lacking tau protein. *Nature*, 369(6480):488–491, June 1994.

[176] John A. Hardy and Gerald A. Higgins. Alzheimer's Disease: The Amyloid Cascade Hypothesis. *Science*, 256(5054):184–185, April 1992.

[177] Masato Hasegawa, Michael J Smith, Masaaki Iijima, Takeshi Tabira, and Michel Goedert. FTDP-17 mutations N279K and S305N in tau produce increased splicing of exon 10. *FEBS Letters*, 443(2):93–96, January 1999.

[178] Martin Haupt, Alexander Kurz, Stefan Pollmann, and Barbara Romero. Alzheimer's disease: identical phenotype of familial and non-familial cases. *Journal of Neurology*, 239(5):248–250, May 1992.

[179] Liesi E. Hebert, Jennifer Weuve, Paul A. Scherr, and Denis A. Evans. Alzheimer disease in the United States (2010–2050) estimated using the 2010 census. *Neurology*, 80(19):1778–1783, May 2013.

[180] Audrey Hector and Jonathan Brouillette. Hyperactivity Induced by Soluble Amyloid-β Oligomers in the Early Stages of Alzheimer's Disease. *Frontiers in Molecular Neuroscience*, 13:600084, January 2021.

[181] Amy J. Heidersbach, Kristel M. Dorighi, Javier A. Gomez, Ashley M. Jacobi, and Benjamin Haley. A versatile, high-efficiency platform for CRISPR-based gene activation. *Nature Communications*, 14(1):902, February 2023.

[182] Hugh C. Hendrie, Jill Murrell, Olusegun Baiyewu, Kathleen A. Lane, Christianna Purnell, Adesola Ogunniyi, Frederick W. Unverzagt, Kathleen Hall, Christopher M. Callahan, Andrew J. Saykin, Oye Gureje, Ann Hake, Tatiana Foroud, and Sujuan Gao. APOE ε4 and the risk for Alzheimer disease and cognitive decline in African Americans and Yoruba. *International Psychogeriatrics*, 26(6):977–985, June 2014.

[183] Camilla Hesse, Lars Rosengren, Eugeen Vanmechelen, Hugo Vanderstichele, Christer Jensen, Pia Davidsson, and Kaj Blennow. Cerebrospinal Fluid Markers for Alzheimer's Disease Evaluated after Acute Ischemic Stroke. *Journal of Alzheimer's Disease*, 2(3-4):199–206, October 2000.

[184] Yu Hirota, Yasufumi Sakakibara, Kyoko Ibaraki, Kimi Takei, Koichi M Iijima, and Michiko Sekiya. Distinct brain pathologies associated with Alzheimer's disease biomarker-related phospho-tau 181 and phospho-tau 217 in *App* knock-in mouse models of amyloid-β amyloidosis. *Brain Communications*, 4(6):fcac286, November 2022.

[185] Seok-Man Ho, Brigham J. Hartley, Julia Tcw, Michael Beaumont, Khalifa Stafford, Paul A. Slesinger, and Kristen J. Brennand. Rapid Ngn2-induction of excitatory neurons from hiPSC-derived neural progenitor cells. *Methods*, 101:113–124, May 2016.

[186] Timothy J. Hohman, Donald G. McLaren, Elizabeth C. Mormino, Katherine A. Gifford, David J. Libon, Angela L. Jefferson, For the Alzheimer's Disease Neuroimaging Initiative, Alzheimer's Disease Neuroimaging Initiative, Michael W. Weiner, Ron Petersen, Paul Aisen, Clifford Jack, William Jagust, Leslie M. Shaw, John Trojanowski, Laurel Beckett, Art Toga, Andrew Saykin Psy.D, John C. Morris, Tom Montine, and Robert Green. Asymptomatic Alzheimer disease: Defining resilience. *Neurology*, 87(23):2443–2450, December 2016.

[187] Leigh Holcomb, Marcia N. Gordon, Eileen McGowan, Xin Yu, Stan Benkovic, Paul Jantzen, Kristal Wright, Irene Saad, Ryan Mueller, Dave Morgan, Sunny Sanders, Cindy Zehr, Kassandra O'Campo, John Hardy, Cristian-Mihail Prada, Chris Eckman, Steve Younkin, Karen Hsiao, and Karen Duff. Accelerated Alzheimer-type phenotype in transgenic mice carrying both mutant amyloid precursor protein and presenilin 1 transgenes. *Nature Medicine*, 4(1):97–100, January 1998.

[188] Ming Hong and Virginia M.-Y. Lee. Insulin and Insulin-like Growth Factor-1 Regulate Tau Phosphorylation in Cultured Human Neurons. *Journal of Biological Chemistry*, 272(31):19547–19553, August 1997.

[189] Brian R. Hoover, Miranda N. Reed, Jianjun Su, Rachel D. Penrod, Linda A. Kotilinek, Marianne K. Grant, Rose Pitstick, George A. Carlson, Lorene M. Lanier, Li-Lian Yuan, Karen H. Ashe, and Dezhi Liao. Tau Mislocalization to Dendritic Spines Mediates Synaptic Dysfunction Independently of Neurodegeneration. *Neuron*, 68(6):1067–1081, December 2010.

[190] Lenka Hromadkova, Chae Kim, Tracy Haldiman, Lihua Peng, Xiongwei Zhu, Mark Cohen, Rohan De Silva, and Jiri G. Safar. Evolving prion-like tau conformers differentially alter postsynaptic proteins in neurons inoculated with distinct isolates of Alzheimer's disease tau. *Cell & Bioscience*, 13(1):174, September 2023.

[191] Albert Y. Hsia, Eliezer Masliah, Lisa McConlogue, Gui-Qiu Yu, Gwen Tatsuno, Kang Hu, Dora Kholodenko, Robert C. Malenka, Roger A. Nicoll, and Lennart Mucke. Plaque-independent disruption of neural circuits in Alzheimer's disease mouse models. *Proceedings of the National Academy of Sciences*, 96(6):3228–3233, March 1999.

[192] Karen Hsiao, Paul Chapman, Steven Nilsen, Chris Eckman, Yasuo Harigaya, Steven Younkin, Fusheng Yang, and Greg Cole. Correlative Memory Deficits, Aβ Elevation, and Amyloid Plaques in Transgenic Mice. *Science*, 274(5284):99–103, October 1996.

[193] Xiangyou Hu, Brati Das, Hailong Hou, Wanxia He, and Riqiang Yan. BACE1 deletion in the adult mouse reverses preformed amyloid deposition and improves cognitive functions. *Journal of Experimental Medicine*, 215(3):927–940, March 2018.

[194] Li-Kai Huang, Yi-Chun Kuan, Ho-Wei Lin, and Chaur-Jong Hu. Clinical trials of new drugs for Alzheimer disease: a 2020–2023 update. *Journal of Biomedical Science*, 30(1):83, October 2023.

[195] Birgit Hutter-Paier, Henri J. Huttunen, Luigi Puglielli, Christopher B. Eckman, Doo Yeon Kim, Alexander Hofmeister, Robert D. Moir, Sarah B. Domnitz, Matthew P. Frosch, Manfred Windisch, and Dora M. Kovacs. The ACAT Inhibitor CP-113,818 Markedly Reduces Amyloid Pathology in a Mouse Model of Alzheimer's Disease. *Neuron*, 44(2):227–238, October 2004.

[196] Henri J. Huttunen, Daniel Havas, Camilla Peach, Cory Barren, Stephan Duller, Weiming Xia, Matthew P. Frosch, Birgit Hutter-Paier, Manfred Windisch, and Dora M. Kovacs. The Acyl-Coenzyme A: Cholesterol Acyltransferase Inhibitor CI-1011 Reverses Diffuse Brain Amyloid Pathology in Aged Amyloid Precursor Protein Transgenic Mice. *Journal of Neuropathology & Experimental Neurology*, 69(8):777–788, August 2010.

[197] Dae Y. Hwang, Kab R. Chae, Tae S. Kang, Jin H. Hwang, Chae H. Lim, Hyun K. Kang, Jun S. Goo, Mi R. Lee, Hwa J. Lim, Sae H. Min, Jun Y. Cho, Jin T. Hong, Chi W. Song, Sang G. Paik, Jung S. Cho, and Yong K. Kim. Alterations in behavior, amyloid p-42, caspase-3, and Cox-2 in mutant PS2 transgenic mouse model of Alzheimer's disease. *The FASEB Journal*, 16(8):805–813, June 2002.

[198] Anne Hämäläinen, Maija Pihlajamäki, Heikki Tanila, Tuomo Hänninen, Eini Niskanen, Susanna Tervo, Pasi A. Karjalainen, Ritva L. Vanninen, and Hilkka Soininen. Increased fMRI responses during encoding in mild cognitive impairment. *Neurobiology of Aging*, 28(12):1889–1903, December 2007.

[199] Mikko Hölttä, Oskar Hansson, Ulf Andreasson, Joakim Hertze, Lennart Minthon, Katarina Nägga, Niels Andreasen, Henrik Zetterberg, and Kaj Blennow. Evaluating Amyloid-β Oligomers in Cerebrospinal Fluid as a Biomarker for Alzheimer's Disease. *PLoS ONE*, 8(6):e66381, June 2013.

[200] Marija Iljina, Gonzalo A. Garcia, Alexander J. Dear, Jennie Flint, Priyanka Narayan, Thomas C. T. Michaels, Christopher M. Dobson, Daan Frenkel, Tuomas P. J. Knowles, and David Klenerman. Quantitative analysis of co-oligomer formation by amyloid-beta peptide isoforms. *Scientific Reports*, 6(1):28658, June 2016.

[201] Konstantinos Ioannou, Marco Bucci, Antonios Tzortzakakis, Irina Savitcheva, Agneta Nordberg, Konstantinos Chiotis, and for the Alzheimer's Disease Neuroimaging Initiative. Tau PET positivity predicts clinically relevant cognitive decline driven by Alzheimer's disease compared to comorbid cases; proof of concept in the ADNI study. *Molecular Psychiatry*, 30(2):587–599, February 2025.

[202] Mariangela Iovino, Sylvia Agathou, Ana González-Rueda, Martin Del Castillo Velasco-Herrera, Barbara Borroni, Antonella Alberici, Timothy Lynch, Sean O'Dowd, Imbisaat Geti, Daniel Gaffney, Ludovic Vallier, Ole Paulsen, Ragnhildur Thóra Káradóttir, and Maria Grazia Spillantini. Early maturation and distinct tau pathology in induced pluripotent stem cell-derived neurons from patients with *MAPT* mutations. *Brain*, 138(11):3345–3359, November 2015.

[203] Khalid Iqbal, Tanweer Zaidi, GuangY. Wen, Inge Grundke-Iqbal, PatriciaA. Merz, SadiaS. Shaikh, HenrykM. Wisniewski, Irina Alafuzoff, and Bengt Winblad. DEFECTIVE BRAIN MICROTUBULE ASSEMBLY IN ALZHEIMER'S DISEASE. *The Lancet*, 328(8504):421–426, August 1986.

[204] Christina Ising, Carmen Venegas, Shuangshuang Zhang, Hannah Scheiblich, Susanne V. Schmidt, Ana Vieira-Saecker, Stephanie Schwartz, Shadi Albasset, Róisín M. McManus, Dario Tejera, Angelika Griep, Francesco Santarelli, Frederic Brosseron, Sabine Opitz, James Stunden, Maximilian Merten, Rakez Kayed, Douglas T. Golenbock, David Blum, Eicke Latz, Luc Buée, and Michael T. Heneka. NLRP3 inflammasome activation drives tau pathology. *Nature*, 575(7784):669–673, November 2019.

[205] Mason A. Israel, Shauna H. Yuan, Cedric Bardy, Sol M. Reyna, Yangling Mu, Cheryl Herrera, Michael P. Hefferan, Sebastiaan Van Gorp, Kristopher L. Nazor, Francesca S. Boscolo, Christian T. Carson, Louise C. Laurent, Martin Marsala, Fred H. Gage, Anne M. Remes, Edward H. Koo, and Lawrence S. B. Goldstein. Probing sporadic and familial Alzheimer's disease using induced pluripotent stem cells. *Nature*, 482(7384):216–220, February 2012.

[206] Arne Ittner, Sook Wern Chua, Josefine Bertz, Alexander Volkerling, Julia Van Der Hoven, Amadeus Gladbach, Magdalena Przybyla, Mian Bi, Annika Van Hummel, Claire H. Stevens, Stefania Ippati, Lisa S. Suh, Alexander Macmillan, Greg Sutherland, Jillian J. Kril, Ana P. G. Silva, Joel P. Mackay, Anne Poljak, Fabien Delerue, Yazi D. Ke, and Lars M. Ittner. Site-specific phosphorylation of tau inhibits amyloid-β toxicity in Alzheimer's mice. *Science*, 354(6314):904–908, November 2016.

[207] Lars M. Ittner, Yazi D. Ke, Fabien Delerue, Mian Bi, Amadeus Gladbach, Janet Van Eersel, Heidrun Wölfing, Billy C. Chieng, MacDonald J. Christie, Ian A. Napier, Anne Eckert, Matthias Staufenbiel, Edna Hardeman, and Jürgen Götz. Dendritic Function of Tau Mediates Amyloid-β Toxicity in Alzheimer's Disease Mouse Models. *Cell*, 142(3):387–397, August 2010.

[208] T. Iwatsubo, T. C. Saido, D. M. Mann, V. M. Lee, and J. Q. Trojanowski. Full-length amyloid-beta (1-42(43)) and amino-terminally modified and truncated amyloid-beta 42(43) deposit in diffuse plaques. *The American Journal of Pathology*, 149(6):1823–1830, December 1996.

[209] Clifford R. Jack, J. Scott Andrews, Thomas G. Beach, Teresa Buracchio, Billy Dunn, Ana Graf, Oskar Hansson, Carole Ho, William Jagust, Eric McDade, Jose Luis Molinuevo, Ozioma C. Okonkwo, Luca Pani, Michael S. Rafii, Philip Scheltens, Eric Siemers, Heather M. Snyder, Reisa Sperling, Charlotte E. Teunissen, and Maria C. Carrillo. Revised criteria for diagnosis and staging of Alzheimer's disease: Alzheimer's Association Workgroup. *Alzheimer's & Dementia*, 20(8):5143–5169, August 2024.

[210] Clifford R. Jack, David A. Bennett, Kaj Blennow, Maria C. Carrillo, Billy Dunn, Samantha Budd Haeberlein, David M. Holtzman, William Jagust, Frank Jessen, Jason Karlawish, Enchi Liu, Jose Luis Molinuevo, Thomas Montine, Creighton Phelps, Katherine P. Rankin, Christopher C. Rowe, Philip Scheltens, Eric Siemers, Heather M. Snyder, Reisa Sperling, Contributors, Cerise Elliott, Eliezer Masliah, Laurie Ryan, and Nina Silverberg. NIA-AA Research Framework: Toward a biological definition of Alzheimer's disease. *Alzheimer's & Dementia*, 14(4):535–562, April 2018.

[211] Rosemary J. Jackson, Nikita Rudinskiy, Abigail G. Herrmann, Shaun Croft, JeeSoo Monica Kim, Veselina Petrova, Juan Jose Ramos-Rodriguez, Rose Pitstick, Susanne Wegmann, Monica Garcia-Alloza, George A. Carlson, Bradley T. Hyman, and Tara L. Spires-Jones. Human tau increases amyloid β plaque size but not amyloid β-mediated synapse loss in a novel mouse model of Alzheimer's disease. *European Journal of Neuroscience*, 44(12):3056–3066, December 2016.

[212] Joanna L Jankowsky, Hilda H Slunt, Victoria Gonzales, Nancy A Jenkins, Neal G Copeland, and David R Borchelt. APP processing and amyloid deposition in mice haplo-insufficient for presenilin 1. *Neurobiology of Aging*, 25(7):885–892, August 2004.

[213] Iris E. Jansen, Jeanne E. Savage, Kyoko Watanabe, Julien Bryois, Dylan M. Williams, Stacy Steinberg, Julia Sealock, Ida K. Karlsson, Sara Hägg, Lavinia Athanasiu, Nicola Voyle, Petroula Proitsi, Aree Witoelar, Sven Stringer, Dag Aarsland, Ina S. Almdahl, Fred Andersen, Sverre Bergh, Francesco Bettella, Sigurbjorn Bjornsson, Anne Brækhus, Geir Bråthen, Christiaan De Leeuw, Rahul S. Desikan, Srdjan Djurovic, Logan Dumitrescu, Tormod Fladby, Timothy J. Hohman, Palmi V. Jonsson, Steven J. Kiddle, Arvid Rongve, Ingvild Saltvedt, Sigrid B. Sando, Geir Selbæk, Maryam Shoai, Nathan G. Skene,

Jon Snaedal, Eystein Stordal, Ingun D. Ulstein, Yunpeng Wang, Linda R. White, John Hardy, Jens Hjerling-Leffler, Patrick F. Sullivan, Wiesje M. Van Der Flier, Richard Dobson, Lea K. Davis, Hreinn Stefansson, Kari Stefansson, Nancy L. Pedersen, Stephan Ripke, Ole A. Andreassen, and Danielle Posthuma. Genome-wide meta-analysis identifies new loci and functional pathways influencing Alzheimer's disease risk. *Nature Genetics*, 51(3):404–413, March 2019.

[214] So Yeong Jeong, Chong Hyun Suh, Jae-Sung Lim, Woo Hyun Shim, Hwon Heo, Yangsean Choi, Ho Sung Kim, Sang Joon Kim, and Jae-Hong Lee. Incidence of Amyloid-Related Imaging Abnormalities in Phase III Clinical Trials of Anti-Amyloid-β Immunotherapy: An Updated Meta-Analysis. *Neurology*, 104(8):e213483, April 2025.

[215] Shan Jiang, Malavika Srikanth, Rossana Serpe, Shadi Yavari, Pallavi Gaur, Galen Andrew Collins, Rajesh Soni, Vilas Menon, and Natura Myeku. Early proteasome downregulation and dysfunction drive proteostasis failure in Alzheimer's disease. *Brain*, 148(12):4372–4388, December 2025.

[216] Gregory A. Jicha, Charles Weaver, Eric Lane, Cintia Vianna, Yvonne Kress, Julia Rockwood, and Peter Davies. cAMP-Dependent Protein Kinase Phosphorylations on Tau in Alzheimer's Disease. *The Journal of Neuroscience*, 19(17):7486–7494, September 1999.

[217] Ming Jin, Nina Shepardson, Ting Yang, Gang Chen, Dominic Walsh, and Dennis J. Selkoe. Soluble amyloid β-protein dimers isolated from Alzheimer cortex directly induce Tau hyperphosphorylation and neuritic degeneration. *Proceedings of the National Academy of Sciences*, 108(14):5819–5824, April 2011.

[218] Martin Jinek, Krzysztof Chylinski, Ines Fonfara, Michael Hauer, Jennifer A. Doudna, and Emmanuelle Charpentier. A Programmable Dual-RNA–Guided DNA Endonuclease in Adaptive Bacterial Immunity. *Science*, 337(6096):816–821, August 2012.

[219] Jie Kang, Hans-Georg Lemaire, Axel Unterbeck, J. Michael Salbaum, Colin L. Masters, Karl-Heinz Grzeschik, Gerd Multhaup, Konrad Beyreuther, and Benno Müller-Hill. The precursor of Alzheimer's disease amyloid A4 protein resembles a cell-surface receptor. *Nature*, 325(6106):733–736, February 1987.

[220] Takeshi Kanno, Ayako Tsuchiya, and Tomoyuki Nishizaki. Hyperphosphorylation of Tau at Ser396 occurs in the much earlier stage than appearance of learning and memory disorders in 5XFAD mice. *Behavioural Brain Research*, 274:302–306, November 2014.

[221] Eleanna Kara, Helen Ling, Alan M. Pittman, Karen Shaw, Rohan De Silva, Roberto Simone, Janice L. Holton, Jason D. Warren, Jonathan D. Rohrer, Georgia Xiromerisiou, Andrew Lees, John Hardy, Henry Houlden, and Tamas Revesz. The MAPT p.A152T variant is a risk factor associated with tauopathies with atypical clinical and neuropathological features. *Neurobiology of Aging*, 33(9):2231.e7–2231.e14, September 2012.

[222] Simantini J. Karve, John M. Ringman, Albert S. Lee, Kevin O. Juarez, and Mario F. Mendez. Comparison of clinical characteristics between familial and non-familial early onset Alzheimer's disease. *Journal of Neurology*, 259(10):2182–2188, October 2012.

[223] Takeshi Kawarabayashi, Mikio Shoji, Linda H. Younkin, Lin Wen-Lang, Dennis W. Dickson, Tetsuro Murakami, Etsuro Matsubara, Koji Abe, Karen Hsiao Ashe, and Steven G. Younkin. Dimeric Amyloid β Protein Rapidly Accumulates in Lipid Rafts followed by Apolipoprotein E and Phosphorylated Tau Accumulation in the Tg2576 Mouse Model of Alzheimer's Disease. *The Journal of Neuroscience*, 24(15):3801–3809, April 2004.

[224] Rakez Kayed, Elizabeth Head, Jennifer L. Thompson, Theresa M. McIntire, Saskia C. Milton, Carl W. Cotman, and Charles G. Glabe. Common Structure of Soluble Amyloid Oligomers Implies Common Mechanism of Pathogenesis. *Science*, 300(5618):486–489, April 2003.

[225] Gerd Kempermann, Fred H. Gage, Ludwig Aigner, Hongjun Song, Maurice A. Curtis, Sandrine Thuret, H. Georg Kuhn, Sebastian Jessberger, Paul W. Frankland, Heather A. Cameron, Elizabeth Gould, Rene Hen, D. Nora Abrous, Nicolas Toni, Alejandro F. Schinder, Xinyu Zhao, Paul J. Lucassen, and Jonas Frisén. Human Adult Neurogenesis: Evidence and Remaining Questions. *Cell Stem Cell*, 23(1):25–30, July 2018.

[226] R Killick, E M Ribe, R Al-Shawi, B Malik, C Hooper, C Fernandes, R Dobson, P M Nolan, A Lourdusamy, S Furney, K Lin, G Breen, R Wroe, A W M To, K Leroy, M Causevic, A Usardi, M Robinson, W Noble, R Williamson,

K Lunnon, S Kellie, C H Reynolds, C Bazenet, A Hodges, J-P Brion, J Stephenson, J Paul Simons, and Simon Lovestone. Clusterin regulates β-amyloid toxicity via Dickkopf-1-driven induction of the wnt–PCP–JNK pathway. *Molecular Psychiatry*, 19(1):88–98, January 2014.

[227] Hyeon-Jin Kim, Soo-Cheon Chae, Dae-Kwon Lee, Brett Chromy, Sam Cheol Lee, Yeong-Chul Park, William L. Klein, Grant A. Krafft, and Seong-Tshool Hong. Selective neuronal degeneration induced by soluble oligomeric amyloid beta-protein. *The FASEB Journal*, 17(1):118–120, January 2003.

[228] Jun Pyo Kim, Sang-Hyuk Jung, Beomjin Jang, Minyoung Cho, Minku Song, Jaeyoung Kim, Beomsu Kim, Hyunwoo Lee, Daeun Shin, Eun Hye Lee, Hyemin Jang, Bo-Hyun Kim, Hongki Ham, Dokyoon Kim, Towfique Raj, Carlos Cruchaga, Hee Jin Kim, Duk L. Na, Sang Won Seo, and Hong-Hee Won. Cross-ancestry genome-wide association study identifies implications of SORL1 in cerebral beta-amyloid deposition. *Nature Communications*, 16(1):3150, April 2025.

[229] Tetsuya Kimura, Daniel J. Whitcomb, Jihoon Jo, Philip Regan, Thomas Piers, Seonghoo Heo, Christopher Brown, Tsutomu Hashikawa, Miyuki Murayama, Heon Seok, Ioannis Sotiropoulos, Eunjoon Kim, Graham L. Collingridge, Akihiko Takashima, and Kwangwook Cho. Microtubule-associated protein tau is essential for long-term depression in the hippocampus. *Philosophical Transactions of the Royal Society B: Biological Sciences*, 369(1633):20130144, January 2014.

[230] Michelle E. King, Ho-Man Kan, Peter W. Baas, Alev Erisir, Charles G. Glabe, and George S. Bloom. Tau-dependent microtubule disassembly initiated by prefibrillar β-amyloid. *The Journal of Cell Biology*, 175(4):541–546, November 2006.

[231] Daniel J Klionsky, Kotb Abdelmohsen, Akihisa Abe, Md Joynal Abedin, Hagai Abeliovich, Abraham Acevedo Arozena, Hiroaki Adachi, Christopher M Adams, Peter D Adams, Khosrow Adeli, Peter J Adhihetty, Sharon G Adler, Galila Agam, Rajesh Agarwal, Manish K Aghi, Maria Agnello, Patrizia Agostinis, Patricia V Aguilar, Julio Aguirre-Ghiso, Edoardo M Airoldi, Slimane Ait-Si-Ali, Takahiko Akematsu, Emmanuel T Akporiaye, Mohamed Al-Rubeai,

Guillermo M Albaiceta, Chris Albanese, Diego Albani, Matthew L Albert, Jesus Aldudo, Hana Algül, Mehrdad Alirezaei, Iraide Alloza, Alexandru Almasan, Maylin Almonte-Beceril, Emad S Alnemri, Covadonga Alonso, Nihal Altan-Bonnet, Dario C Altieri, Silvia Alvarez, Lydia Alvarez-Erviti, Sandro Alves, Giuseppina Amadoro, Atsuo Amano, Consuelo Amantini, Santiago Ambrosio, Ivano Amelio, Amal O Amer, Mohamed Amessou, Angelika Amon, Zhenyi An, Frank A Anania, Stig U Andersen, Usha P Andley, Catherine K Andreadi, Nathalie Andrieu-Abadie, Alberto Anel, David K Ann, Shailendra Anoopkumar-Dukie, Manuela Antonioli, Hiroshi Aoki, Nadezda Apostolova, Saveria Aquila, Katia Aquilano, Koichi Araki, Eli Arama, Agustin Aranda, Jun Araya, Alexandre Arcaro, Esperanza Arias, Hirokazu Arimoto, Aileen R Ariosa, Jane L Armstrong, Thierry Arnould, Ivica Arsov, Katsuhiko Asanuma, Valerie Askanas, Eric Asselin, Ryuichiro Atarashi, Sally S Atherton, Julie D Atkin, Laura D Attardi, Patrick Auberger, Georg Auburger, Laure Aurelian, Riccardo Autelli, Laura Avagliano, Maria Laura Avantaggiati, Limor Avrahami, Suresh Awale, Neelam Azad, Tiziana Bachetti, Jonathan M Backer, Dong-Hun Bae, Jae-sung Bae, Ok-Nam Bae, Soo Han Bae, Eric H Baehrecke, Seung-Hoon Baek, Stephen Baghdiguian, Agnieszka Bagniewska-Zadworna, Hua Bai, Jie Bai, Xue-Yuan Bai, Yannick Bailly, Kithiganahalli Narayanaswamy Balaji, Walter Balduini, Andrea Ballabio, Rena Balzan, Rajkumar Banerjee, Gábor Bánhegyi, Haijun Bao, Benoit Barbeau, Maria D Barrachina, Esther Barreiro, Bonnie Bartel, Alberto Bartolomé, Diane C Bassham, Maria Teresa Bassi, Robert C Bast, Alakananda Basu, Maria Teresa Batista, Henri Batoko, Maurizio Battino, Kyle Bauckman, Bradley L Baumgarner, K Ulrich Bayer, Rupert Beale, Jean-François Beaulieu, George R. Beck, Christoph Becker, J David Beckham, Pierre-André Bédard, Patrick J Bednarski, Thomas J Begley, Christian Behl, Christian Behrends, Georg Mn Behrens, Kevin E Behrns, Eloy Bejarano, Amine Belaid, Francesca Belleudi, Giovanni Bénard, Guy Berchem, Daniele Bergamaschi, Matteo Bergami, Ben Berkhout, Laura Berliocchi, Amélie Bernard, Monique Bernard, Francesca Bernassola, Anne Bertolotti, Amanda S Bess, Sébastien Besteiro, Saverio Bettuzzi, Savita Bhalla, Shalmoli Bhattacharyya, Sujit K Bhutia, Caroline Biagosch, Michele Wolfe Bianchi, Martine Biard-Piechaczyk, Viktor Billes, Claudia Bincoletto, Baris Bingol, Sara W Bird, Marc Bitoun, Ivana Bjedov, Craig Blackstone, Lionel Blanc, Guillermo A Blanco, Heidi Kiil Blomhoff, Emilio Boada-Romero, Stefan Böckler, Marianne Boes, Kathleen Boesze-Battaglia, Lawrence H

Boise, Alessandra Bolino, Andrea Boman, Paolo Bonaldo, Matteo Bordi, Jürgen Bosch, Luis M Botana, Joelle Botti, German Bou, Marina Bouché, Marion Bouchecareilh, Marie-Josée Boucher, Michael E Boulton, Sebastien G Bouret, Patricia Boya, Michaël Boyer-Guittaut, Peter V Bozhkov, Nathan Brady, Vania Mm Braga, Claudio Brancolini, Gerhard H Braus, José M Bravo-San Pedro, Lisa A Brennan, Emery H Bresnick, Patrick Brest, Dave Bridges, Marie-Agnès Bringer, Marisa Brini, Glauber C Brito, Bertha Brodin, Paul S Brookes, Eric J Brown, Karen Brown, Hal E Broxmeyer, Alain Bruhat, Patricia Chakur Brum, John H Brumell, Nicola Brunetti-Pierri, Robert J Bryson-Richardson, Shilpa Buch, Alastair M Buchan, Hikmet Budak, Dmitry V Bulavin, Scott J Bultman, Geert Bultynck, Vladimir Bumbasirevic, Yan Burelle, Robert E Burke, Margit Burmeister, Peter Bütikofer, Laura Caberlotto, Ken Cadwell, Monika Cahova, Dongsheng Cai, Jingjing Cai, Qian Cai, Sara Calatayud, Nadine Camougrand, Michelangelo Campanella, Grant R Campbell, Matthew Campbell, Silvia Campello, Robin Candau, Isabella Caniggia, Lavinia Cantoni, Lizhi Cao, Allan B Caplan, Michele Caraglia, Claudio Cardinali, Sandra Morais Cardoso, Jennifer S Carew, Laura A Carleton, Cathleen R Carlin, Silvia Carloni, Sven R Carlsson, Didac Carmona-Gutierrez, Leticia Am Carneiro, Oliana Carnevali, Serena Carra, Alice Carrier, Bernadette Carroll, Caty Casas, Josefina Casas, Giuliana Cassinelli, Perrine Castets, Susana Castro-Obregon, Gabriella Cavallini, Isabella Ceccherini, Francesco Cecconi, Arthur I Cederbaum, Valentín Ceña, Simone Cenci, Claudia Cerella, Davide Cervia, Silvia Cetrullo, Hassan Chaachouay, Han-Jung Chae, Andrei S Chagin, Chee-Yin Chai, Gopal Chakrabarti, Georgios Chamilos, Edmond Yw Chan, Matthew Tv Chan, Dhyan Chandra, Pallavi Chandra, Chih-Peng Chang, Raymond Chuen-Chung Chang, Ta Yuan Chang, John C Chatham, Saurabh Chatterjee, Santosh Chauhan, Yongsheng Che, Michael E Cheetham, Rajkumar Cheluvappa, Chun-Jung Chen, Gang Chen, Guang-Chao Chen, Guoqiang Chen, Hongzhuan Chen, Jeff W Chen, Jian-Kang Chen, Min Chen, Mingzhou Chen, Peiwen Chen, Qi Chen, Quan Chen, Shang-Der Chen, Si Chen, Steve S-L Chen, Wei Chen, Wei-Jung Chen, Wen Qiang Chen, Wenli Chen, Xiangmei Chen, Yau-Hung Chen, Ye-Guang Chen, Yin Chen, Yingyu Chen, Yongshun Chen, Yu-Jen Chen, Yue-Qin Chen, Yujie Chen, Zhen Chen, Zhong Chen, Alan Cheng, Christopher Hk Cheng, Hua Cheng, Heesun Cheong, Sara Cherry, Jason Chesney, Chun Hei Antonio Cheung, Eric Chevet, Hsiang Cheng Chi, Sung-Gil Chi, Fulvio Chiacchiera, Hui-Ling Chiang, Roberto Chiarelli, Mario Chiariello,

Marcello Chieppa, Lih-Shen Chin, Mario Chiong, Gigi Nc Chiu, Dong-Hyung Cho, Ssang-Goo Cho, William C Cho, Yong-Yeon Cho, Young-Seok Cho, Augustine Mk Choi, Eui-Ju Choi, Eun-Kyoung Choi, Jayoung Choi, Mary E Choi, Seung-Il Choi, Tsui-Fen Chou, Salem Chouaib, Divaker Choubey, Vinay Choubey, Kuan-Chih Chow, Kamal Chowdhury, Charleen T Chu, Tsung-Hsien Chuang, Taehoon Chun, Hyewon Chung, Taijoon Chung, Yuen-Li Chung, Yong-Joon Chwae, Valentina Cianfanelli, Roberto Ciarcia, Iwona A Ciechomska, Maria Rosa Ciriolo, Mara Cirone, Sofie Claerhout, Michael J Clague, Joan Clària, Peter Gh Clarke, Robert Clarke, Emilio Clementi, Cédric Cleyrat, Miriam Cnop, Eliana M Coccia, Tiziana Cocco, Patrice Codogno, Jörn Coers, Ezra Ew Cohen, David Colecchia, Luisa Coletto, Núria S Coll, Emma Colucci-Guyon, Sergio Comincini, Maria Condello, Katherine L Cook, Graham H Coombs, Cynthia D Cooper, J Mark Cooper, Isabelle Coppens, Maria Tiziana Corasaniti, Marco Corazzari, Ramon Corbalan, Elisabeth Corcelle-Termeau, Mario D Cordero, Cristina Corral-Ramos, Olga Corti, Andrea Cossarizza, Paola Costelli, Safia Costes, Susan L Cotman, Ana Coto-Montes, Sandra Cottet, Eduardo Couve, Lori R Covey, L Ashley Cowart, Jeffery S Cox, Fraser P Coxon, Carolyn B Coyne, Mark S Cragg, Rolf J Craven, Tiziana Crepaldi, Jose L Crespo, Alfredo Criollo, Valeria Crippa, Maria Teresa Cruz, Ana Maria Cuervo, Jose M Cuezva, Taixing Cui, Pedro R Cutillas, Mark J Czaja, Maria F Czyzyk-Krzeska, Ruben K Dagda, Uta Dahmen, Chunsun Dai, Wenjie Dai, Yun Dai, Kevin N Dalby, Luisa Dalla Valle, Guillaume Dalmasso, Marcello D'Amelio, Markus Damme, Arlette Darfeuille-Michaud, Catherine Dargemont, Victor M Darley-Usmar, Srinivasan Dasarathy, Biplab Dasgupta, Srikanta Dash, Crispin R Dass, Hazel Marie Davey, Lester M Davids, David Dávila, Roger J Davis, Ted M Dawson, Valina L Dawson, Paula Daza, Jackie De Belleroche, Paul De Figueiredo, Regina Celia Bressan Queiroz De Figueiredo, José De La Fuente, Luisa De Martino, Antonella De Matteis, Guido Ry De Meyer, Angelo De Milito, Mauro De Santi, Wanderley De Souza, Vincenzo De Tata, Daniela De Zio, Jayanta Debnath, Reinhard Dechant, Jean-Paul Decuypere, Shane Deegan, Benjamin Dehay, Barbara Del Bello, Dominic P Del Re, Régis Delage-Mourroux, Lea Md Delbridge, Louise Deldicque, Elizabeth Delorme-Axford, Yizhen Deng, Joern Dengjel, Melanie Denizot, Paul Dent, Channing J Der, Vojo Deretic, Benoît Derrien, Eric Deutsch, Timothy P Devarenne, Rodney J Devenish, Sabrina Di Bartolomeo, Nicola Di Daniele, Fabio Di Domenico, Alessia

Di Nardo, Simone Di Paola, Antonio Di Pietro, Livia Di Renzo, Aaron DiAntonio, Guillermo Díaz-Araya, Ines Díaz-Laviada, Maria T Diaz-Meco, Javier Diaz-Nido, Chad A Dickey, Robert C Dickson, Marc Diederich, Paul Digard, Ivan Dikic, Savithrama P Dinesh-Kumar, Chan Ding, Wen-Xing Ding, Zufeng Ding, Luciana Dini, Jörg Hw Distler, Abhinav Diwan, Mojgan Djavaheri-Mergny, Kostyantyn Dmytruk, Renwick Cj Dobson, Volker Doetsch, Karol Dokladny, Svetlana Dokudovskaya, Massimo Donadelli, X Charlie Dong, Xiaonan Dong, Zheng Dong, Terrence M Donohue, Kelly S Doran, Gabriella D'Orazi, Gerald W Dorn, Victor Dosenko, Sami Dridi, Liat Drucker, Jie Du, Li-Lin Du, Lihuan Du, André Du Toit, Priyamvada Dua, Lei Duan, Pu Duann, Vikash Kumar Dubey, Michael R Duchen, Michel A Duchosal, Helene Duez, Isabelle Dugail, Verónica I Dumit, Mara C Duncan, Elaine A Dunlop, William A Dunn, Nicolas Dupont, Luc Dupuis, Raúl V Durán, Thomas M Durcan, Stéphane Duvezin-Caubet, Umamaheswar Duvvuri, Vinay Eapen, Darius Ebrahimi-Fakhari, Arnaud Echard, Leopold Eckhart, Charles L Edelstein, Aimee L Edinger, Ludwig Eichinger, Tobias Eisenberg, Avital Eisenberg-Lerner, N Tony Eissa, Wafik S El-Deiry, Victoria El-Khoury, Zvulun Elazar, Hagit Eldar-Finkelman, Chris Jh Elliott, Enzo Emanuele, Urban Emmenegger, Nikolai Engedal, Anna-Mart Engelbrecht, Simone Engelender, Jorrit M Enserink, Ralf Erdmann, Jekaterina Erenpreisa, Rajaraman Eri, Jason L Eriksen, Andreja Erman, Ricardo Escalante, Eeva-Liisa Eskelinen, Lucile Espert, Lorena Esteban-Martínez, Thomas J Evans, Mario Fabri, Gemma Fabrias, Cinzia Fabrizi, Antonio Facchiano, Nils J Færgeman, Alberto Faggioni, W Douglas Fairlie, Chunhai Fan, Daping Fan, Jie Fan, Shengyun Fang, Manolis Fanto, Alessandro Fanzani, Thomas Farkas, Mathias Faure, Francois B Favier, Howard Fearnhead, Massimo Federici, Erkang Fei, Tania C Felizardo, Hua Feng, Yibin Feng, Yuchen Feng, Thomas A Ferguson, Álvaro F Fernández, Maite G Fernandez-Barrena, Jose C Fernandez-Checa, Arsenio Fernández-López, Martin E Fernandez-Zapico, Olivier Feron, Elisabetta Ferraro, Carmen Veríssima Ferreira-Halder, Laszlo Fesus, Ralph Feuer, Fabienne C Fiesel, Eduardo C Filippi-Chiela, Giuseppe Filomeni, Gian Maria Fimia, John H Fingert, Steven Finkbeiner, Toren Finkel, Filomena Fiorito, Paul B Fisher, Marc Flajolet, Flavio Flamigni, Oliver Florey, Salvatore Florio, R Andres Floto, Marco Folini, Carlo Follo, Edward A Fon, Francesco Fornai, Franco Fortunato, Alessandro Fraldi, Rodrigo Franco, Arnaud Francois, Aurélie François, Lisa B Frankel, Iain Dc Fraser, Norbert Frey, Damien G

Freyssenet, Christian Frezza, Scott L Friedman, Daniel E Frigo, Dongxu Fu, José M Fuentes, Juan Fueyo, Yoshio Fujitani, Yuuki Fujiwara, Mikihiro Fujiya, Mitsunori Fukuda, Simone Fulda, Carmela Fusco, Bozena Gabryel, Matthias Gaestel, Philippe Gailly, Malgorzata Gajewska, Sehamuddin Galadari, Gad Galili, Inmaculada Galindo, Maria F Galindo, Giovanna Galliciotti, Lorenzo Galluzzi, Luca Galluzzi, Vincent Galy, Noor Gammoh, Sam Gandy, Anand K Ganesan, Swamynathan Ganesan, Ian G Ganley, Monique Gannagé, Fen-Biao Gao, Feng Gao, Jian-Xin Gao, Lorena García Nannig, Eleonora García Véscovi, Marina Garcia-Macía, Carmen Garcia-Ruiz, Abhishek D Garg, Pramod Kumar Garg, Ricardo Gargini, Nils Christian Gassen, Damián Gatica, Evelina Gatti, Julie Gavard, Evripidis Gavathiotis, Liang Ge, Pengfei Ge, Shengfang Ge, Po-Wu Gean, Vania Gelmetti, Armando A Genazzani, Jiefei Geng, Pascal Genschik, Lisa Gerner, Jason E Gestwicki, David A Gewirtz, Saeid Ghavami, Eric Ghigo, Debabrata Ghosh, Anna Maria Giammarioli, Francesca Giampieri, Claudia Giampietri, Alexandra Giatromanolaki, Derrick J Gibbings, Lara Gibellini, Spencer B Gibson, Vanessa Ginet, Antonio Giordano, Flaviano Giorgini, Elisa Giovannetti, Stephen E Girardin, Suzana Gispert, Sandy Giuliano, Candece L Gladson, Alvaro Glavic, Martin Gleave, Nelly Godefroy, Robert M Gogal, Kuppan Gokulan, Gustavo H Goldman, Delia Goletti, Michael S Goligorsky, Aldrin V Gomes, Ligia C Gomes, Hernando Gomez, Candelaria Gomez-Manzano, Rubén Gómez-Sánchez, Dawit Ap Gonçalves, Ebru Goncu, Qingqiu Gong, Céline Gongora, Carlos B Gonzalez, Pedro Gonzalez-Alegre, Pilar Gonzalez-Cabo, Rosa Ana González-Polo, Ing Swie Goping, Carlos Gorbea, Nikolai V Gorbunov, Daphne R Goring, Adrienne M Gorman, Sharon M Gorski, Sandro Goruppi, Shino Goto-Yamada, Cecilia Gotor, Roberta A Gottlieb, Illana Gozes, Devrim Gozuacik, Yacine Graba, Martin Graef, Giovanna E Granato, Gary Dean Grant, Steven Grant, Giovanni Luca Gravina, Douglas R Green, Alexander Greenhough, Michael T Greenwood, Benedetto Grimaldi, Frédéric Gros, Charles Grose, Jean-Francois Groulx, Florian Gruber, Paolo Grumati, Tilman Grune, Jun-Lin Guan, Kun-Liang Guan, Barbara Guerra, Carlos Guillen, Kailash Gulshan, Jan Gunst, Chuanyong Guo, Lei Guo, Ming Guo, Wenjie Guo, Xu-Guang Guo, Andrea A Gust, Åsa B Gustafsson, Elaine Gutierrez, Maximiliano G Gutierrez, Ho-Shin Gwak, Albert Haas, James E Haber, Shinji Hadano, Monica Hagedorn, David R Hahn, Andrew J Halayko, Anne Hamacher-Brady, Kozo Hamada, Ahmed Hamai, Andrea Hamann, Maho Hamasaki, Isabelle Hamer, Qutayba

Hamid, Ester M Hammond, Feng Han, Weidong Han, James T Handa, John A Hanover, Malene Hansen, Masaru Harada, Ljubica Harhaji-Trajkovic, J Wade Harper, Abdel Halim Harrath, Adrian L Harris, James Harris, Udo Hasler, Peter Hasselblatt, Kazuhisa Hasui, Robert G Hawley, Teresa S Hawley, Congcong He, Cynthia Y He, Fengtian He, Gu He, Rong-Rong He, Xian-Hui He, You-Wen He, Yu-Ying He, Joan K Heath, Marie-Josée Hébert, Robert A Heinzen, Gudmundur Vignir Helgason, Michael Hensel, Elizabeth P Henske, Chengtao Her, Paul K Herman, Agustín Hernández, Carlos Hernandez, Sonia Hernández-Tiedra, Claudio Hetz, P Robin Hiesinger, Katsumi Higaki, Sabine Hilfiker, Bradford G Hill, Joseph A Hill, William D Hill, Keisuke Hino, Daniel Hofius, Paul Hofman, Günter U Höglinger, Jörg Höhfeld, Marina K Holz, Yonggeun Hong, David A Hood, Jeroen Jm Hoozemans, Thorsten Hoppe, Chin Hsu, Chin-Yuan Hsu, Li-Chung Hsu, Dong Hu, Guochang Hu, Hong-Ming Hu, Hongbo Hu, Ming Chang Hu, Yu-Chen Hu, Zhuo-Wei Hu, Fang Hua, Ya Hua, Canhua Huang, Huey-Lan Huang, Kuo-How Huang, Kuo-Yang Huang, Shile Huang, Shiqian Huang, Wei-Pang Huang, Yi-Ran Huang, Yong Huang, Yunfei Huang, Tobias B Huber, Patricia Huebbe, Won-Ki Huh, Juha J Hulmi, Gang Min Hur, James H Hurley, Zvenyslava Husak, Sabah Na Hussain, Salik Hussain, Jung Jin Hwang, Seungmin Hwang, Thomas Is Hwang, Atsuhiro Ichihara, Yuzuru Imai, Carol Imbriano, Megumi Inomata, Takeshi Into, Valentina Iovane, Juan L Iovanna, Renato V Iozzo, Nancy Y Ip, Javier E Irazoqui, Pablo Iribarren, Yoshitaka Isaka, Aleksandra J Isakovic, Harry Ischiropoulos, Jeffrey S Isenberg, Mohammad Ishaq, Hiroyuki Ishida, Isao Ishii, Jane E Ishmael, Ciro Isidoro, Ken-ichi Isobe, Erika Isono, Shohreh Issazadeh-Navikas, Koji Itahana, Eisuke Itakura, Andrei I Ivanov, Anand Krishnan V Iyer, José M Izquierdo, Yotaro Izumi, Valentina Izzo, Marja Jäättelä, Nadia Jaber, Daniel John Jackson, William T Jackson, Tony George Jacob, Thomas S Jacques, Chinnaswamy Jagannath, Ashish Jain, Nihar Ranjan Jana, Byoung Kuk Jang, Alkesh Jani, Bassam Janji, Paulo Roberto Jannig, Patric J Jansson, Steve Jean, Marina Jendrach, Ju-Hong Jeon, Niels Jessen, Eui-Bae Jeung, Kailiang Jia, Lijun Jia, Hong Jiang, Hongchi Jiang, Liwen Jiang, Teng Jiang, Xiaoyan Jiang, Xuejun Jiang, Xuejun Jiang, Ying Jiang, Yongjun Jiang, Alberto Jiménez, Cheng Jin, Hongchuan Jin, Lei Jin, Meiyan Jin, Shengkan Jin, Umesh Kumar Jinwal, Eun-Kyeong Jo, Terje Johansen, Daniel E Johnson, Gail Vw Johnson, James D Johnson, Eric Jonasch, Chris Jones, Leo Ab

Joosten, Joaquin Jordan, Anna-Maria Joseph, Bertrand Joseph, Annie M Joubert, Dianwen Ju, Jingfang Ju, Hsueh-Fen Juan, Katrin Juenemann, Gábor Juhász, Hye Seung Jung, Jae U Jung, Yong-Keun Jung, Heinz Jungbluth, Matthew J Justice, Barry Jutten, Nadeem O Kaakoush, Kai Kaarniranta, Allen Kaasik, Tomohiro Kabuta, Bertrand Kaeffer, Katarina Kågedal, Alon Kahana, Shingo Kajimura, Or Kakhlon, Manjula Kalia, Dhan V Kalvakolanu, Yoshiaki Kamada, Konstantinos Kambas, Vitaliy O Kaminskyy, Harm H Kampinga, Mustapha Kandouz, Chanhee Kang, Rui Kang, Tae-Cheon Kang, Tomotake Kanki, Thirumala-Devi Kanneganti, Haruo Kanno, Anumantha G Kanthasamy, Marc Kantorow, Maria Kaparakis-Liaskos, Orsolya Kapuy, Vassiliki Karantza, Md Razaul Karim, Parimal Karmakar, Arthur Kaser, Susmita Kaushik, Thomas Kawula, A Murat Kaynar, Po-Yuan Ke, Zun-Ji Ke, John H Kehrl, Kate E Keller, Jongsook Kim Kemper, Anne K Kenworthy, Oliver Kepp, Andreas Kern, Santosh Kesari, David Kessel, Robin Ketteler, Isis Do Carmo Kettelhut, Bilon Khambu, Muzamil Majid Khan, Vinoth Km Khandelwal, Sangeeta Khare, Juliann G Kiang, Amy A Kiger, Akio Kihara, Arianna L Kim, Cheol Hyeon Kim, Deok Ryong Kim, Do-Hyung Kim, Eung Kweon Kim, Hye Young Kim, Hyung-Ryong Kim, Jae-Sung Kim, Jeong Hun Kim, Jin Cheon Kim, Jin Hyoung Kim, Kwang Woon Kim, Michael D Kim, Moon-Moo Kim, Peter K Kim, Seong Who Kim, Soo-Youl Kim, Yong-Sun Kim, Yonghyun Kim, Adi Kimchi, Alec C Kimmelman, Tomonori Kimura, Jason S King, Karla Kirkegaard, Vladimir Kirkin, Lorrie A Kirshenbaum, Shuji Kishi, Yasuo Kitajima, Katsuhiko Kitamoto, Yasushi Kitaoka, Kaio Kitazato, Rudolf A Kley, Walter T Klimecki, Michael Klinkenberg, Jochen Klucken, Helene Knævelsrud, Erwin Knecht, Laura Knuppertz, Jiunn-Liang Ko, Satoru Kobayashi, Jan C Koch, Christelle Koechlin-Ramonatxo, Ulrich Koenig, Young Ho Koh, Katja Köhler, Sepp D Kohlwein, Masato Koike, Masaaki Komatsu, Eiki Kominami, Dexin Kong, Hee Jeong Kong, Eumorphia G Konstantakou, Benjamin T Kopp, Tamas Korcsmaros, Laura Korhonen, Viktor I Korolchuk, Nadya V Koshkina, Yanjun Kou, Michael I Koukourakis, Constantinos Koumenis, Attila L Kovács, Tibor Kovács, Werner J Kovacs, Daisuke Koya, Claudine Kraft, Dimitri Krainc, Helmut Kramer, Tamara Kravic-Stevovic, Wilhelm Krek, Carole Kretz-Remy, Roswitha Krick, Malathi Krishnamurthy, Janos Kriston-Vizi, Guido Kroemer, Michael C Kruer, Rejko Kruger, Nicholas T Ktistakis, Kazuyuki Kuchitsu, Christian Kuhn, Addanki Pratap Kumar, Anuj Kumar, Ashok Kumar, Deepak Kumar, Dhiraj Kumar, Rakesh Kumar, Sharad

Kumar, Mondira Kundu, Hsing-Jien Kung, Atsushi Kuno, Sheng-Han Kuo, Jeff Kuret, Tino Kurz, Terry Kwok, Taeg Kyu Kwon, Yong Tae Kwon, Irene Kyrmizi, Albert R La Spada, Frank Lafont, Tim Lahm, Aparna Lakkaraju, Truong Lam, Trond Lamark, Steve Lancel, Terry H Landowski, Darius Jr Lane, Jon D Lane, Cinzia Lanzi, Pierre Lapaquette, Louis R Lapierre, Jocelyn Laporte, Johanna Laukkarinen, Gordon W Laurie, Sergio Lavandero, Lena Lavie, Matthew J LaVoie, Betty Yuen Kwan Law, Helen Ka-wai Law, Kelsey B Law, Robert Layfield, Pedro A Lazo, Laurent Le Cam, Karine G Le Roch, Hervé Le Stunff, Vijittra Leardkamolkarn, Marc Lecuit, Byung-Hoon Lee, Che-Hsin Lee, Erinna F Lee, Gyun Min Lee, He-Jin Lee, Hsinyu Lee, Jae Keun Lee, Jongdae Lee, Ju-hyun Lee, Jun Hee Lee, Michael Lee, Myung-Shik Lee, Patty J Lee, Sam W Lee, Seung-Jae Lee, Shiow-Ju Lee, Stella Y Lee, Sug Hyung Lee, Sung Sik Lee, Sung-Joon Lee, Sunhee Lee, Ying-Ray Lee, Yong J Lee, Young H Lee, Christiaan Leeuwenburgh, Sylvain Lefort, Renaud Legouis, Jinzhi Lei, Qun-Ying Lei, David A Leib, Gil Leibowitz, Istvan Lekli, Stéphane D Lemaire, John J Lemasters, Marius K Lemberg, Antoinette Lemoine, Shuilong Leng, Guido Lenz, Paola Lenzi, Lilach O Lerman, Daniele Lettieri Barbato, Julia I-Ju Leu, Hing Y Leung, Beth Levine, Patrick A Lewis, Frank Lezoualc'h, Chi Li, Faqiang Li, Feng-Jun Li, Jun Li, Ke Li, Lian Li, Min Li, Min Li, Qiang Li, Rui Li, Sheng Li, Wei Li, Wei Li, Xiaotao Li, Yumin Li, Jiqin Lian, Chengyu Liang, Qiangrong Liang, Yulin Liao, Joana Liberal, Pawel P Liberski, Pearl Lie, Andrew P Lieberman, Hyunjung Jade Lim, Kah-Leong Lim, Kyu Lim, Raquel T Lima, Chang-Shen Lin, Chiou-Feng Lin, Fang Lin, Fangming Lin, Fu-Cheng Lin, Kui Lin, Kwang-Huei Lin, Pei-Hui Lin, Tianwei Lin, Wan-Wan Lin, Yee-Shin Lin, Yong Lin, Rafael Linden, Dan Lindholm, Lisa M Lindqvist, Paul Lingor, Andreas Linkermann, Lance A Liotta, Marta M Lipinski, Vitor A Lira, Michael P Lisanti, Paloma B Liton, Bo Liu, Chong Liu, Chun-Feng Liu, Fei Liu, Hung-Jen Liu, Jianxun Liu, Jing-Jing Liu, Jing-Lan Liu, Ke Liu, Leyuan Liu, Liang Liu, Quentin Liu, Rong-Yu Liu, Shiming Liu, Shuwen Liu, Wei Liu, Xian-De Liu, Xiangguo Liu, Xiao-Hong Liu, Xinfeng Liu, Xu Liu, Xueqin Liu, Yang Liu, Yule Liu, Zexian Liu, Zhe Liu, Juan P Liuzzi, Gérard Lizard, Mila Ljujic, Irfan J Lodhi, Susan E Logue, Bal L Lokeshwar, Yun Chau Long, Sagar Lonial, Benjamin Loos, Carlos López-Otín, Cristina López-Vicario, Mar Lorente, Philip L Lorenzi, Péter Lõrincz, Marek Los, Michael T Lotze, Penny E Lovat, Binfeng Lu, Bo Lu, Jiahong Lu, Qing Lu, She-Min Lu, Shuyan Lu, Yingying Lu, Frédéric

Luciano, Shirley Luckhart, John Milton Lucocq, Paula Ludovico, Aurelia Lugea, Nicholas W Lukacs, Julian J Lum, Anders H Lund, Honglin Luo, Jia Luo, Shouqing Luo, Claudio Luparello, Timothy Lyons, Jianjie Ma, Yi Ma, Yong Ma, Zhenyi Ma, Juliano Machado, Glaucia M Machado-Santelli, Fernando Macian, Gustavo C MacIntosh, Jeffrey P MacKeigan, Kay F Macleod, John D MacMicking, Lee Ann MacMillan-Crow, Frank Madeo, Muniswamy Madesh, Julio Madrigal-Matute, Akiko Maeda, Tatsuya Maeda, Gustavo Maegawa, Emilia Maellaro, Hannelore Maes, Marta Magariños, Kenneth Maiese, Tapas K Maiti, Luigi Maiuri, Maria Chiara Maiuri, Carl G Maki, Roland Malli, Walter Malorni, Alina Maloyan, Fathia Mami-Chouaib, Na Man, Joseph D Mancias, Eva-Maria Mandelkow, Michael A Mandell, Angelo A Manfredi, Serge N Manié, Claudia Manzoni, Kai Mao, Zixu Mao, Zong-Wan Mao, Philippe Marambaud, Anna Maria Marconi, Zvonimir Marelja, Gabriella Marfe, Marta Margeta, Eva Margittai, Muriel Mari, Francesca V Mariani, Concepcio Marin, Sara Marinelli, Guillermo Mariño, Ivanka Markovic, Rebecca Marquez, Alberto M Martelli, Sascha Martens, Katie R Martin, Seamus J Martin, Shaun Martin, Miguel A Martin-Acebes, Paloma Martín-Sanz, Camille Martinand-Mari, Wim Martinet, Jennifer Martinez, Nuria Martinez-Lopez, Ubaldo Martinez-Outschoorn, Moisés Martínez-Velázquez, Marta Martinez-Vicente, Waleska Kerllen Martins, Hirosato Mashima, James A Mastrianni, Giuseppe Matarese, Paola Matarrese, Roberto Mateo, Satoaki Matoba, Naomichi Matsumoto, Takehiko Matsushita, Akira Matsuura, Takeshi Matsuzawa, Mark P Mattson, Soledad Matus, Norma Maugeri, Caroline Mauvezin, Andreas Mayer, Dusica Maysinger, Guillermo D Mazzolini, Mary Kate McBrayer, Kimberly McCall, Craig McCormick, Gerald M McInerney, Skye C McIver, Sharon McKenna, John J McMahon, Iain A McNeish, Fatima Mechta-Grigoriou, Jan Paul Medema, Diego L Medina, Klara Megyeri, Maryam Mehrpour, Jawahar L Mehta, Yide Mei, Ute-Christiane Meier, Alfred J Meijer, Alicia Meléndez, Gerry Melino, Sonia Melino, Edesio Jose Tenorio De Melo, Maria A Mena, Marc D Meneghini, Javier A Menendez, Regina Menezes, Liesu Meng, Ling-hua Meng, Songshu Meng, Rossella Menghini, A Sue Menko, Rubem Fs Menna-Barreto, Manoj B Menon, Marco A Meraz-Ríos, Giuseppe Merla, Luciano Merlini, Angelica M Merlot, Andreas Meryk, Stefania Meschini, Joel N Meyer, Man-tian Mi, Chao-Yu Miao, Lucia Micale, Simon Michaeli, Carine Michiels, Anna Rita Migliaccio, Anastasia Susie Mihailidou, Dalibor Mijaljica, Katsuhiko Mikoshiba, Enrico Milan, Leonor Miller-Fleming, Gordon B Mills, Ian G Mills, Georgia Minakaki, Berge A

Minassian, Xiu-Fen Ming, Farida Minibayeva, Elena A Minina, Justine D Mintern, Saverio Minucci, Antonio Miranda-Vizuete, Claire H Mitchell, Shigeki Miyamoto, Keisuke Miyazawa, Noboru Mizushima, Katarzyna Mnich, Baharia Mograbi, Simin Mohseni, Luis Ferreira Moita, Marco Molinari, Maurizio Molinari, Andreas Buch Møller, Bertrand Mollereau, Faustino Mollinedo, Marco Mongillo, Martha M Monick, Serena Montagnaro, Craig Montell, Darren J Moore, Michael N Moore, Rodrigo Mora-Rodriguez, Paula I Moreira, Etienne Morel, Maria Beatrice Morelli, Sandra Moreno, Michael J Morgan, Arnaud Moris, Yuji Moriyasu, Janna L Morrison, Lynda A Morrison, Eugenia Morselli, Jorge Moscat, Pope L Moseley, Serge Mostowy, Elisa Motori, Denis Mottet, Jeremy C Mottram, Charbel E-H Moussa, Vassiliki E Mpakou, Hasan Mukhtar, Jean M Mulcahy Levy, Sylviane Muller, Raquel Muñoz-Moreno, Cristina Muñoz-Pinedo, Christian Münz, Maureen E Murphy, James T Murray, Aditya Murthy, Indira U Mysorekar, Ivan R Nabi, Massimo Nabissi, Gustavo A Nader, Yukitoshi Nagahara, Yoshitaka Nagai, Kazuhiro Nagata, Anika Nagelkerke, Péter Nagy, Samisubbu R Naidu, Sreejayan Nair, Hiroyasu Nakano, Hitoshi Nakatogawa, Meera Nanjundan, Gennaro Napolitano, Naweed I Naqvi, Roberta Nardacci, Derek P Narendra, Masashi Narita, Anna Chiara Nascimbeni, Ramesh Natarajan, Luiz C Navegantes, Steffan T Nawrocki, Taras Y Nazarko, Volodymyr Y Nazarko, Thomas Neill, Luca M Neri, Mihai G Netea, Romana T Netea-Maier, Bruno M Neves, Paul A Ney, Ioannis P Nezis, Hang Tt Nguyen, Huu Phuc Nguyen, Anne-Sophie Nicot, Hilde Nilsen, Per Nilsson, Mikio Nishimura, Ichizo Nishino, Mireia Niso-Santano, Hua Niu, Ralph A Nixon, Vincent Co Njar, Takeshi Noda, Angelika A Noegel, Elsie Magdalena Nolte, Erik Norberg, Koenraad K Norga, Sakineh Kazemi Noureini, Shoji Notomi, Lucia Notterpek, Karin Nowikovsky, Nobuyuki Nukina, Thorsten Nürnberger, Valerie B O'Donnell, Tracey O'Donovan, Peter J O'Dwyer, Ina Oehme, Clara L Oeste, Michinaga Ogawa, Besim Ogretmen, Yuji Ogura, Young J Oh, Masaki Ohmuraya, Takayuki Ohshima, Rani Ojha, Koji Okamoto, Toshiro Okazaki, F Javier Oliver, Karin Ollinger, Stefan Olsson, Daniel P Orban, Paulina Ordonez, Idil Orhon, Laszlo Orosz, Eyleen J O'Rourke, Helena Orozco, Angel L Ortega, Elena Ortona, Laura D Osellame, Junko Oshima, Shigeru Oshima, Heinz D Osiewacz, Takanobu Otomo, Kinya Otsu, Jing-hsiung James Ou, Tiago F Outeiro, Dong-yun Ouyang, Hongjiao Ouyang, Michael Overholtzer, Michelle A Ozbun, P Hande Ozdinler, Bulent Ozpolat, Consiglia Pacelli, Paolo Paganetti, Guylène Page, Gilles Pages,

Ugo Pagnini, Beata Pajak, Stephen C Pak, Karolina Pakos-Zebrucka, Nazzy Pakpour, Zdena Palková, Francesca Palladino, Kathrin Pallauf, Nicolas Pallet, Marta Palmieri, Søren R Paludan, Camilla Palumbo, Silvia Palumbo, Olatz Pampliega, Hongming Pan, Wei Pan, Theocharis Panaretakis, Aseem Pandey, Areti Pantazopoulou, Zuzana Papackova, Daniela L Papademetrio, Issidora Papassideri, Alessio Papini, Nirmala Parajuli, Julian Pardo, Vrajesh V Parekh, Giancarlo Parenti, Jong-In Park, Junsoo Park, Ohkmae K Park, Roy Parker, Rosanna Parlato, Jan B Parys, Katherine R Parzych, Jean-Max Pasquet, Benoit Pasquier, Kishore Bs Pasumarthi, Daniel Patschan, Cam Patterson, Sophie Pattingre, Scott Pattison, Arnim Pause, Hermann Pavenstädt, Flaminia Pavone, Zully Pedrozo, Fernando J Peña, Miguel A Peñalva, Mario Pende, Jianxin Peng, Fabio Penna, Josef M Penninger, Anna Pensalfini, Salvatore Pepe, Gustavo Js Pereira, Paulo C Pereira, Verónica Pérez-de La Cruz, María Esther Pérez-Pérez, Diego Pérez-Rodríguez, Dolores Pérez-Sala, Celine Perier, Andras Perl, David H Perlmutter, Ida Perrotta, Shazib Pervaiz, Maija Pesonen, Jeffrey E Pessin, Godefridus J Peters, Morten Petersen, Irina Petrache, Basil J Petrof, Goran Petrovski, James M Phang, Mauro Piacentini, Marina Pierdominici, Philippe Pierre, Valérie Pierrefite-Carle, Federico Pietrocola, Felipe X Pimentel-Muiños, Mario Pinar, Benjamin Pineda, Ronit Pinkas-Kramarski, Marcello Pinti, Paolo Pinton, Bilal Piperdi, James M Piret, Leonidas C Platanias, Harald W Platta, Edward D Plowey, Stefanie Pöggeler, Marc Poirot, Peter Polčic, Angelo Poletti, Audrey H Poon, Hana Popelka, Blagovesta Popova, Izabela Poprawa, Shibu M Poulose, Joanna Poulton, Scott K Powers, Ted Powers, Mercedes Pozuelo-Rubio, Krisna Prak, Reinhild Prange, Mark Prescott, Muriel Priault, Sharon Prince, Richard L Proia, Tassula Proikas-Cezanne, Holger Prokisch, Vasilis J Promponas, Karin Przyklenk, Rosa Puertollano, Subbiah Pugazhenthi, Luigi Puglielli, Aurora Pujol, Julien Puyal, Dohun Pyeon, Xin Qi, Wen-bin Qian, Zheng-Hong Qin, Yu Qiu, Ziwei Qu, Joe Quadrilatero, Frederick Quinn, Nina Raben, Hannah Rabinowich, Flavia Radogna, Michael J Ragusa, Mohamed Rahmani, Komal Raina, Sasanka Ramanadham, Rajagopal Ramesh, Abdelhaq Rami, Sarron Randall-Demllo, Felix Randow, Hai Rao, V Ashutosh Rao, Blake B Rasmussen, Tobias M Rasse, Edward A Ratovitski, Pierre-Emmanuel Rautou, Swapan K Ray, Babak Razani, Bruce H Reed, Fulvio Reggiori, Markus Rehm, Andreas S Reichert, Theo Rein, David J Reiner, Eric Reits, Jun Ren, Xingcong Ren, Maurizio Renna, Jane Eb Reusch, Jose L Revuelta,

Leticia Reyes, Alireza R Rezaie, Robert I Richards, Des R Richardson, Clémence Richetta, Michael A Riehle, Bertrand H Rihn, Yasuko Rikihisa, Brigit E Riley, Gerald Rimbach, Maria Rita Rippo, Konstantinos Ritis, Federica Rizzi, Elizete Rizzo, Peter J Roach, Jeffrey Robbins, Michel Roberge, Gabriela Roca, Maria Carmela Roccheri, Sonia Rocha, Cecilia Mp Rodrigues, Clara I Rodríguez, Santiago Rodriguez De Cordoba, Natalia Rodriguez-Muela, Jeroen Roelofs, Vladimir V Rogov, Troy T Rohn, Bärbel Rohrer, Davide Romanelli, Luigina Romani, Patricia Silvia Romano, M Isabel G Roncero, Jose Luis Rosa, Alicia Rosello, Kirill V Rosen, Philip Rosenstiel, Magdalena Rost-Roszkowska, Kevin A Roth, Gael Roué, Mustapha Rouis, Kasper M Rouschop, Daniel T Ruan, Diego Ruano, David C Rubinsztein, Edmund B Rucker, Assaf Rudich, Emil Rudolf, Ruediger Rudolf, Markus A Ruegg, Carmen Ruiz-Roldan, Avnika Ashok Ruparelia, Paola Rusmini, David W Russ, Gian Luigi Russo, Giuseppe Russo, Rossella Russo, Tor Erik Rusten, Victoria Ryabovol, Kevin M Ryan, Stefan W Ryter, David M Sabatini, Michael Sacher, Carsten Sachse, Michael N Sack, Junichi Sadoshima, Paul Saftig, Ronit Sagi-Eisenberg, Sumit Sahni, Pothana Saikumar, Tsunenori Saito, Tatsuya Saitoh, Koichi Sakakura, Machiko Sakoh-Nakatogawa, Yasuhito Sakuraba, María Salazar-Roa, Paolo Salomoni, Ashok K Saluja, Paul M Salvaterra, Rosa Salvioli, Afshin Samali, Anthony Mj Sanchez, José A Sánchez-Alcázar, Ricardo Sanchez-Prieto, Marco Sandri, Miguel A Sanjuan, Stefano Santaguida, Laura Santambrogio, Giorgio Santoni, Claudia Nunes Dos Santos, Shweta Saran, Marco Sardiello, Graeme Sargent, Pallabi Sarkar, Sovan Sarkar, Maria Rosa Sarrias, Minnie M Sarwal, Chihiro Sasakawa, Motoko Sasaki, Miklos Sass, Ken Sato, Miyuki Sato, Joseph Satriano, Niramol Savaraj, Svetlana Saveljeva, Liliana Schaefer, Ulrich E Schaible, Michael Scharl, Hermann M Schatzl, Randy Schekman, Wiep Scheper, Alfonso Schiavi, Hyman M Schipper, Hana Schmeisser, Jens Schmidt, Ingo Schmitz, Bianca E Schneider, E Marion Schneider, Jaime L Schneider, Eric A Schon, Miriam J Schönenberger, Axel H Schönthal, Daniel F Schorderet, Bernd Schröder, Sebastian Schuck, Ryan J Schulze, Melanie Schwarten, Thomas L Schwarz, Sebastiano Sciarretta, Kathleen Scotto, A Ivana Scovassi, Robert A Screaton, Mark Screen, Hugo Seca, Simon Sedej, Laura Segatori, Nava Segev, Per O Seglen, Jose M Seguí-Simarro, Juan Segura-Aguilar, Ekihiro Seki, Iban Seiliez, Christian Sell, Clay F Semenkovich, Gregg L Semenza, Utpal Sen, Andreas L Serra, Ana Serrano-Puebla, Hiromi Sesaki, Takao Setoguchi, Carmine Settembre, John J

Shacka, Ayesha N Shajahan-Haq, Irving M Shapiro, Shweta Sharma, Hua She, C-K James Shen, Chiung-Chyi Shen, Han-Ming Shen, Sanbing Shen, Weili Shen, Rui Sheng, Xianyong Sheng, Zu-Hang Sheng, Trevor G Shepherd, Junyan Shi, Qiang Shi, Qinghua Shi, Yuguang Shi, Shusaku Shibutani, Kenichi Shibuya, Yoshihiro Shidoji, Jeng-Jer Shieh, Chwen-Ming Shih, Yohta Shimada, Shigeomi Shimizu, Dong Wook Shin, Mari L Shinohara, Michiko Shintani, Takahiro Shintani, Tetsuo Shioi, Ken Shirabe, Ronit Shiri-Sverdlov, Orian Shirihai, Gordon C Shore, Chih-Wen Shu, Deepak Shukla, Andriy A Sibirny, Valentina Sica, Christina J Sigurdson, Einar M Sigurdsson, Puran Singh Sijwali, Beata Sikorska, Wilian A Silveira, Sandrine Silvente-Poirot, Gary A Silverman, Jan Simak, Thomas Simmet, Anna Katharina Simon, Hans-Uwe Simon, Cristiano Simone, Matias Simons, Anne Simonsen, Rajat Singh, Shivendra V Singh, Shrawan K Singh, Debasish Sinha, Sangita Sinha, Frank A Sinicrope, Agnieszka Sirko, Kapil Sirohi, Balindiwe Jn Sishi, Annie Sittler, Parco M Siu, Efthimios Sivridis, Anna Skwarska, Ruth Slack, Iva Slaninová, Nikolai Slavov, Soraya S Smaili, Keiran Sm Smalley, Duncan R Smith, Stefaan J Soenen, Scott A Soleimanpour, Anita Solhaug, Kumaravel Somasundaram, Jin H Son, Avinash Sonawane, Chunjuan Song, Fuyong Song, Hyun Kyu Song, Ju-Xian Song, Wei Song, Kai Y Soo, Anil K Sood, Tuck Wah Soong, Virawudh Soontornniyomkij, Maurizio Sorice, Federica Sotgia, David R Soto-Pantoja, Areechun Sotthibundhu, Maria João Sousa, Herman P Spaink, Paul N Span, Anne Spang, Janet D Sparks, Peter G Speck, Stephen A Spector, Claudia D Spies, Wolfdieter Springer, Daret St Clair, Alessandra Stacchiotti, Bart Staels, Michael T Stang, Daniel T Starczynowski, Petro Starokadomskyy, Clemens Steegborn, John W Steele, Leonidas Stefanis, Joan Steffan, Christine M Stellrecht, Harald Stenmark, Tomasz M Stepkowski, Stęphan T Stern, Craig Stevens, Brent R Stockwell, Veronika Stoka, Zuzana Storchova, Björn Stork, Vassilis Stratoulias, Dimitrios J Stravopodis, Pavel Strnad, Anne Marie Strohecker, Anna-Lena Ström, Per Stromhaug, Jiri Stulik, Yu-Xiong Su, Zhaoliang Su, Carlos S Subauste, Srinivasa Subramaniam, Carolyn M Sue, Sang Won Suh, Xinbing Sui, Supawadee Sukseree, David Sulzer, Fang-Lin Sun, Jiaren Sun, Jun Sun, Shi-Yong Sun, Yang Sun, Yi Sun, Yingjie Sun, Vinod Sundaramoorthy, Joseph Sung, Hidekazu Suzuki, Kuninori Suzuki, Naoki Suzuki, Tadashi Suzuki, Yuichiro J Suzuki, Michele S Swanson, Charles Swanton, Karl Swärd, Ghanshyam Swarup, Sean T Sweeney, Paul W Sylvester, Zsuzsanna Szatmari, Eva Szegezdi, Peter W Szlosarek, Heinrich

Taegtmeyer, Marco Tafani, Emmanuel Taillebourg, Stephen Wg Tait, Krisztina Takacs-Vellai, Yoshinori Takahashi, Szabolcs Takáts, Genzou Takemura, Nagio Takigawa, Nicholas J Talbot, Elena Tamagno, Jerome Tamburini, Cai-Ping Tan, Lan Tan, Mei Lan Tan, Ming Tan, Yee-Joo Tan, Keiji Tanaka, Masaki Tanaka, Daolin Tang, Dingzhong Tang, Guomei Tang, Isei Tanida, Kunikazu Tanji, Bakhos A Tannous, Jose A Tapia, Inmaculada Tasset-Cuevas, Marc Tatar, Iman Tavassoly, Nektarios Tavernarakis, Allen Taylor, Graham S Taylor, Gregory A Taylor, J Paul Taylor, Mark J Taylor, Elena V Tchetina, Andrew R Tee, Fatima Teixeira-Clerc, Sucheta Telang, Tewin Tencomnao, Ba-Bie Teng, Ru-Jeng Teng, Faraj Terro, Gianluca Tettamanti, Arianne L Theiss, Anne E Theron, Kelly Jean Thomas, Marcos P Thomé, Paul G Thomes, Andrew Thorburn, Jeremy Thorner, Thomas Thum, Michael Thumm, Teresa Lm Thurston, Ling Tian, Andreas Till, Jenny Pan-yun Ting, Vladimir I Titorenko, Lilach Toker, Stefano Toldo, Sharon A Tooze, Ivan Topisirovic, Maria Lyngaas Torgersen, Liliana Torosantucci, Alicia Torriglia, Maria Rosaria Torrisi, Cathy Tournier, Roberto Towns, Vladimir Trajkovic, Leonardo H Travassos, Gemma Triola, Durga Nand Tripathi, Daniela Trisciuoglio, Rodrigo Troncoso, Ioannis P Trougakos, Anita C Truttmann, Kuen-Jer Tsai, Mario P Tschan, Yi-Hsin Tseng, Takayuki Tsukuba, Allan Tsung, Andrey S Tsvetkov, Shuiping Tu, Hsing-Yu Tuan, Marco Tucci, David A Tumbarello, Boris Turk, Vito Turk, Robin Fb Turner, Anders A Tveita, Suresh C Tyagi, Makoto Ubukata, Yasuo Uchiyama, Andrej Udelnow, Takashi Ueno, Midori Umekawa, Rika Umemiya-Shirafuji, Benjamin R Underwood, Christian Ungermann, Rodrigo P. Ureshino, Ryo Ushioda, Vladimir N Uversky, Néstor L Uzcátegui, Thomas Vaccari, Maria I Vaccaro, Libuše Váchová, Helin Vakifahmetoglu-Norberg, Rut Valdor, Enza Maria Valente, Francois Vallette, Angela M Valverde, Greet Van Den Berghe, Ludo Van Den Bosch, Gijs R Van Den Brink, F Gisou Van Der Goot, Ida J Van Der Klei, Luc Jw Van Der Laan, Wouter G Van Doorn, Marjolein Van Egmond, Kenneth L Van Golen, Luc Van Kaer, Menno Van Lookeren Campagne, Peter Vandenabeele, Wim Vandenberghe, Ilse Vanhorebeek, Isabel Varela-Nieto, M Helena Vasconcelos, Radovan Vasko, Demetrios G Vavvas, Ignacio Vega-Naredo, Guillermo Velasco, Athanassios D Velentzas, Panagiotis D Velentzas, Tibor Vellai, Edo Vellenga, Mikkel Holm Vendelbo, Kartik Venkatachalam, Natascia Ventura, Salvador Ventura, Patrícia St Veras, Mireille Verdier, Beata G Vertessy, Andrea Viale, Michel Vidal, Helena La Vieira, Richard D Vierstra, Nadarajah Vigneswaran,

Neeraj Vij, Miquel Vila, Margarita Villar, Victor H Villar, Joan Villarroya, Cécile Vindis, Giampietro Viola, Maria Teresa Viscomi, Giovanni Vitale, Dan T Vogl, Olga V Voitsekhovskaja, Clarissa Von Haefen, Karin Von Schwarzenberg, Daniel E Voth, Valérie Vouret-Craviari, Kristina Vuori, Jatin M Vyas, Christian Waeber, Cheryl Lyn Walker, Mark J Walker, Jochen Walter, Lei Wan, Xiangbo Wan, Bo Wang, Caihong Wang, Chao-Yung Wang, Chengshu Wang, Chenran Wang, Chuangui Wang, Dong Wang, Fen Wang, Fuxin Wang, Guanghui Wang, Hai-jie Wang, Haichao Wang, Hong-Gang Wang, Hongmin Wang, Horng-Dar Wang, Jing Wang, Junjun Wang, Mei Wang, Mei-Qing Wang, Pei-Yu Wang, Peng Wang, Richard C Wang, Shuo Wang, Ting-Fang Wang, Xian Wang, Xiao-jia Wang, Xiao-Wei Wang, Xin Wang, Xuejun Wang, Yan Wang, Yanming Wang, Ying Wang, Ying-Jan Wang, Yipeng Wang, Yu Wang, Yu Tian Wang, Yuqing Wang, Zhi-Nong Wang, Pablo Wappner, Carl Ward, Diane McVey Ward, Gary Warnes, Hirotaka Watada, Yoshihisa Watanabe, Kei Watase, Timothy E Weaver, Colin D Weekes, Jiwu Wei, Thomas Weide, Conrad C Weihl, Günther Weindl, Simone Nardin Weis, Longping Wen, Xin Wen, Yunfei Wen, Benedikt Westermann, Cornelia M Weyand, Anthony R White, Eileen White, J Lindsay Whitton, Alexander J Whitworth, Joëlle Wiels, Franziska Wild, Manon E Wildenberg, Tom Wileman, Deepti Srinivas Wilkinson, Simon Wilkinson, Dieter Willbold, Chris Williams, Katherine Williams, Peter R Williamson, Konstanze F Winklhofer, Steven S Witkin, Stephanie E Wohlgemuth, Thomas Wollert, Ernst J Wolvetang, Esther Wong, G William Wong, Richard W Wong, Vincent Kam Wai Wong, Elizabeth A Woodcock, Karen L Wright, Chunlai Wu, Defeng Wu, Gen Sheng Wu, Jian Wu, Junfang Wu, Mian Wu, Min Wu, Shengzhou Wu, William Kk Wu, Yaohua Wu, Zhenlong Wu, Cristina Pr Xavier, Ramnik J Xavier, Gui-Xian Xia, Tian Xia, Weiliang Xia, Yong Xia, Hengyi Xiao, Jian Xiao, Shi Xiao, Wuhan Xiao, Chuan-Ming Xie, Zhiping Xie, Zhonglin Xie, Maria Xilouri, Yuyan Xiong, Chuanshan Xu, Congfeng Xu, Feng Xu, Haoxing Xu, Hongwei Xu, Jian Xu, Jianzhen Xu, Jinxian Xu, Liang Xu, Xiaolei Xu, Yangqing Xu, Ye Xu, Zhi-Xiang Xu, Ziheng Xu, Yu Xue, Takahiro Yamada, Ai Yamamoto, Koji Yamanaka, Shunhei Yamashina, Shigeko Yamashiro, Bing Yan, Bo Yan, Xianghua Yan, Zhen Yan, Yasuo Yanagi, Dun-Sheng Yang, Jin-Ming Yang, Liu Yang, Minghua Yang, Pei-Ming Yang, Peixin Yang, Qian Yang, Wannian Yang, Wei Yuan Yang, Xuesong Yang, Yi Yang, Ying Yang, Zhifen Yang, Zhihong Yang, Meng-Chao Yao, Pamela J Yao, Xiaofeng Yao, Zhenyu Yao, Zhiyuan

Yao, Linda S Yasui, Mingxiang Ye, Barry Yedvobnick, Behzad Yeganeh, Elizabeth S Yeh, Patricia L Yeyati, Fan Yi, Long Yi, Xiao-Ming Yin, Calvin K Yip, Yeong-Min Yoo, Young Hyun Yoo, Seung-Yong Yoon, Ken-Ichi Yoshida, Tamotsu Yoshimori, Ken H Young, Huixin Yu, Jane J Yu, Jin-Tai Yu, Jun Yu, Li Yu, W Haung Yu, Xiao-Fang Yu, Zhengping Yu, Junying Yuan, Zhi-Min Yuan, Beatrice Yjt Yue, Jianbo Yue, Zhenyu Yue, David N Zacks, Eldad Zacksenhaus, Nadia Zaffaroni, Tania Zaglia, Zahra Zakeri, Vincent Zecchini, Jinsheng Zeng, Min Zeng, Qi Zeng, Antonis S Zervos, Donna D Zhang, Fan Zhang, Guo Zhang, Guo-Chang Zhang, Hao Zhang, Hong Zhang, Hong Zhang, Hongbing Zhang, Jian Zhang, Jian Zhang, Jiangwei Zhang, Jianhua Zhang, Jing-pu Zhang, Li Zhang, Lin Zhang, Lin Zhang, Long Zhang, Ming-Yong Zhang, Xiangnan Zhang, Xu Dong Zhang, Yan Zhang, Yang Zhang, Yanjin Zhang, Yingmei Zhang, Yunjiao Zhang, Mei Zhao, Wei-Li Zhao, Xiaonan Zhao, Yan G Zhao, Ying Zhao, Yongchao Zhao, Yu-xia Zhao, Zhendong Zhao, Zhizhuang J Zhao, Dexian Zheng, Xi-Long Zheng, Xiaoxiang Zheng, Boris Zhivotovsky, Qing Zhong, Guang-Zhou Zhou, Guofei Zhou, Huiping Zhou, Shu-Feng Zhou, Xu-jie Zhou, Hongxin Zhu, Hua Zhu, Wei-Guo Zhu, Wenhua Zhu, Xiao-Feng Zhu, Yuhua Zhu, Shi-Mei Zhuang, Xiaohong Zhuang, Elio Ziparo, Christos E Zois, Teresa Zoladek, Wei-Xing Zong, Antonio Zorzano, and Susu M Zughaier. Guidelines for the use and interpretation of assays for monitoring autophagy (3rd edition). *Autophagy*, 12(1):1–222, January 2016.

[232] Mihee Ko, Kun Zou, Hirohisa Minagawa, Wenxin Yu, Jian-Sheng Gong, Katsuhiko Yanagisawa, and Makoto Michikawa. Cholesterol-mediated Neurite Outgrowth Is Differently Regulated between Cortical and Hippocampal Neurons. *Journal of Biological Chemistry*, 280(52):42759–42765, December 2005.

[233] Takayuki Kondo, Masashi Asai, Kayoko Tsukita, Yumiko Kutoku, Yutaka Ohsawa, Yoshihide Sunada, Keiko Imamura, Naohiro Egawa, Naoki Yahata, Keisuke Okita, Kazutoshi Takahashi, Isao Asaka, Takashi Aoi, Akira Watanabe, Kaori Watanabe, Chie Kadoya, Rie Nakano, Dai Watanabe, Kei Maruyama, Osamu Hori, Satoshi Hibino, Tominari Choshi, Tatsutoshi Nakahata, Hiroyuki Hioki, Takeshi Kaneko, Motoko Naitoh, Katsuhiro Yoshikawa, Satoko Yamawaki, Shigehiko Suzuki, Ryuji Hata, Shu-ichi Ueno, Tsuneyoshi Seki, Kazuhiro Kobayashi, Tatsushi Toda, Kazuma Murakami, Kazuhiro Irie, William L. Klein, Hiroshi Mori, Takashi Asada, Ryosuke Takahashi, Nobuhisa

Iwata, Shinya Yamanaka, and Haruhisa Inoue. Modeling Alzheimer's Disease with iPSCs Reveals Stress Phenotypes Associated with Intracellular Aβ and Differential Drug Responsiveness. *Cell Stem Cell*, 12(4):487–496, April 2013.

[234] Katherine J. Kopeikina, Susanne Wegmann, Rose Pitstick, George A. Carlson, Brian J. Bacskai, Rebecca A. Betensky, Bradley T. Hyman, and Tara L. Spires-Jones. Tau Causes Synapse Loss without Disrupting Calcium Homeostasis in the rTg4510 Model of Tauopathy. *PLoS ONE*, 8(11):e80834, November 2013.

[235] Gennady Korotkevich, Vladimir Sukhov, Nikolay Budin, Boris Shpak, Maxim N. Artyomov, and Alexey Sergushichev. Fast gene set enrichment analysis, June 2016.

[236] K S Kosik, C L Joachim, and D J Selkoe. Microtubule-associated protein tau (tau) is a major antigenic component of paired helical filaments in Alzheimer disease. *Proceedings of the National Academy of Sciences*, 83(11):4044–4048, June 1986.

[237] Kenneth S. Kosik, Lisa D. Orecchio, Shelley Bakalis, and Rachael L. Neve. Developmentally regulated expression of specific tau sequences. *Neuron*, 2(4):1389–1397, April 1989.

[238] Kevin P. Kotredes, Adrian Oblak, Ravi S. Pandey, Peter Bor-Chian Lin, Dylan Garceau, Harriet Williams, Asli Uyar, Rita O'Rourke, Sarah O'Rourke, Cynthia Ingraham, Daria Bednarczyk, Melisa Belanger, Zackary Cope, Kate E. Foley, Benjamin A. Logsdon, Lara M. Mangravite, Stacey J. Sukoff Rizzo, Paul R. Territo, Gregory W. Carter, Michael Sasner, Bruce T. Lamb, and Gareth R. Howell. Uncovering Disease Mechanisms in a Novel Mouse Model Expressing Humanized APOEε4 and Trem2*R47H. *Frontiers in Aging Neuroscience*, 13:735524, October 2021.

[239] Kevin P. Kotredes, Ravi S. Pandey, Scott Persohn, Kierra Elderidge, Charles P. Burton, Ethan W. Miner, Kathryn A. Haynes, Diogo Francisco S. Santos, Sean-Paul Williams, Nicholas Heaton, Cynthia M. Ingraham, Christopher Lloyd, Dylan Garceau, Rita O'Rourke, Sarah Herrick, Claudia Rangel-Barajas, Surendra Maharjan, Nian Wang, Michael Sasner, Bruce T. Lamb, Paul R. Territo, Stacey J. Sukoff Rizzo, Gregory W. Carter, Gareth R. Howell, and Adrian L. Oblak. Characterizing Molecular and Synaptic Signatures in mouse

models of Late-Onset Alzheimer's Disease Independent of Amyloid and Tau Pathology. *bioRxiv: The Preprint Server for Biology*, page 2023.12.19.571985, December 2023.

[240] Malamati Kourti and Athanasios Metaxas. A systematic review and meta-analysis of tau phosphorylation in mouse models of familial Alzheimer's disease. *Neurobiology of Disease*, 192:106427, March 2024.

[241] Neil W. Kowall and Kenneth S. Kosik. Axonal disruption and aberrant localization of tau protein characterize the neuropil pathology of Alzheimer's disease. *Annals of Neurology*, 22(5):639–643, November 1987.

[242] Ivan Koychev, Jennifer Lawson, Tharani Chessell, Clare Mackay, Roger Gunn, Barbara Sahakian, James B Rowe, Alan J Thomas, Lynn Rochester, Dennis Chan, Brian Tom, Paresh Malhotra, Clive Ballard, Iain Chessell, Craig W Ritchie, Vanessa Raymont, Iracema Leroi, Imre Lengyel, Matt Murray, David L Thomas, John Gallacher, and Simon Lovestone. Deep and Frequent Phenotyping study protocol: an observational study in prodromal Alzheimer's disease. *BMJ Open*, 9(3):e024498, 2019.

[243] Sonja Kriks, Jae-Won Shim, Jinghua Piao, Yosif M. Ganat, Dustin R. Wakeman, Zhong Xie, Luis Carrillo-Reid, Gordon Auyeung, Chris Antonacci, Amanda Buch, Lichuan Yang, M. Flint Beal, D. James Surmeier, Jeffrey H. Kordower, Viviane Tabar, and Lorenz Studer. Dopamine neurons derived from human ES cells efficiently engraft in animal models of Parkinson's disease. *Nature*, 480(7378):547–551, December 2011.

[244] Yu-Min Kuo, Mark R. Emmerling, Carmen Vigo-Pelfrey, Timothy C. Kasunic, Joel B. Kirkpatrick, Geoffrey H. Murdoch, Melvyn J. Ball, and Alex E. Roher. Water-soluble Aβ(N-40, N-42) Oligomers in Normal and Alzheimer Disease Brains. *Journal of Biological Chemistry*, 271(8):4077–4081, February 1996.

[245] Valentina N. Lagomarsino, Richard V. Pearse, Lei Liu, Yi-Chen Hsieh, Marty A. Fernandez, Elizabeth A. Vinton, Daniel Paull, Daniel Felsky, Shinya Tasaki, Chris Gaiteri, Badri Vardarajan, Hyo Lee, Christina R. Muratore, Courtney R. Benoit, Vicky Chou, Seeley B. Fancher, Amy He, Julie P. Merchant, Duc M. Duong, Hector Martinez, Monica Zhou, Fatmata Bah, Maria A. Vicent, Jonathan M.S. Stricker, Jishu Xu, Eric B. Dammer, Allan I. Levey, Lori B. Chibnik, Vilas Menon, Nicholas T. Seyfried, Philip L. De Jager, Scott Noggle,

Dennis J. Selkoe, David A. Bennett, and Tracy L. Young-Pearse. Stem cell-derived neurons reflect features of protein networks, neuropathology, and cognitive outcome of their aged human donors. *Neuron*, 109(21):3402–3420.e9, November 2021.

[246] Yann Le Guen, Michael E. Belloy, Benjamin Grenier-Boley, Itziar De Rojas, Atahualpa Castillo-Morales, Iris Jansen, Aude Nicolas, Céline Bellenguez, Carolina Dalmasso, Fahri Küçükali, Sarah J. Eger, Katrine Laura Rasmussen, Jesper Qvist Thomassen, Jean-François Deleuze, Zihuai He, Valerio Napolioni, Philippe Amouyel, Frank Jessen, Patrick G. Kehoe, Cornelia Van Duijn, Magda Tsolaki, Pascual Sánchez-Juan, Kristel Sleegers, Martin Ingelsson, Giacomina Rossi, Mikko Hiltunen, Rebecca Sims, Wiesje M. Van Der Flier, Alfredo Ramirez, Ole A. Andreassen, Ruth Frikke-Schmidt, Julie Williams, Agustín Ruiz, Jean-Charles Lambert, Michael D. Greicius, Members of the EADB, GR@ACE, DEGESCO, DemGene, GERAD, and EADI Groups, Beatrice Arosio, Luisa Benussi, Anne Boland, Barbara Borroni, Paolo Caffarra, Delphine Daian, Antonio Daniele, Stéphanie Debette, Carole Dufouil, Emrah Düzel, Daniela Galimberti, Vilmantas Giedraitis, Timo Grimmer, Caroline Graff, Edna Grünblatt, Olivier Hanon, Lucrezia Hausner, Stefanie Heilmann-Heimbach, Henne Holstege, Jakub Hort, Deckert Jürgen, Teemu Kuulasmaa, Aad Van Der Lugt, Carlo Masullo, Patrizia Mecocci, Shima Mehrabian, Alexandre De Mendonça, Susanne Moebus, Benedetta Nacmias, Gael Nicolas, Robert Olaso, Goran Papenberg, Lucilla Parnetti, Florence Pasquier, Oliver Peters, Yolande A. L. Pijnenburg, Julius Popp, Innocenzo Rainero, Inez Ramakers, Steffi Riedel-Heller, Nikolaos Scarmeas, Philip Scheltens, Norbert Scherbaum, Anja Schneider, Davide Seripa, Hilkka Soininen, Vincenzo Solfrizzi, Gianfranco Spalletta, Alessio Squassina, John Van Swieten, Thomas J. Tegos, Lucio Tremolizzo, Frans Verhey, Martin Vyhnalek, Jens Wiltfang, Mercè Boada, Pablo García-González, Raquel Puerta, Luis M. Real, Victoria Álvarez, María J. Bullido, Jordi Clarimon, José María García-Alberca, Pablo Mir, Fermin Moreno, Pau Pastor, Gerard Piñol-Ripoll, Laura Molina-Porcel, Jordi Pérez-Tur, Eloy Rodríguez-Rodríguez, Jose Luís Royo, Raquel Sánchez-Valle, Martin Dichgans, and Dan Rujescu. Association of Rare *APOE* Missense Variants V236E and R251G With Risk of Alzheimer Disease. *JAMA Neurology*, 79(7):652, July 2022.

[247] Hyo Lee, Aimee J. Aylward, Richard V. Pearse, Alexandra M. Lish, Yi-Chen Hsieh, Zachary M. Augur, Courtney R. Benoit, Vicky Chou, Allison Knupp, Cheryl Pan, Srilakshmi Goberdhan, Duc M. Duong, Nicholas T. Seyfried, David A. Bennett, Mariko F. Taga, Kevin Huynh, Matthias Arnold, Peter J. Meikle, Philip L. De Jager, Vilas Menon, Jessica E. Young, and Tracy L. Young-Pearse. Cell-type-specific regulation of APOE and CLU levels in human neurons by the Alzheimer's disease risk gene SORL1. *Cell Reports*, 42(8):112994, August 2023.

[248] Hyo Lee, Richard V. Pearse, Alexandra M. Lish, Cheryl Pan, Zachary M. Augur, Gizem Terzioglu, Pallavi Gaur, Meichen Liao, Masashi Fujita, Earvin S. Tio, Duc M. Duong, Daniel Felsky, Nicholas T. Seyfried, Vilas Menon, David A. Bennett, Philip L. De Jager, and Tracy L. Young-Pearse. Contributions of Genetic Variation in Astrocytes to Cell and Molecular Mechanisms of Risk and Resilience to Late-Onset Alzheimer's Disease. *Glia*, 73(6):1166–1187, June 2025.

[249] Jong Kil Lee, Hee Kyung Jin, Min Hee Park, Bo-ra Kim, Phil Hyu Lee, Hiromitsu Nakauchi, Janet E. Carter, Xingxuan He, Edward H. Schuchman, and Jae-sung Bae. Acid sphingomyelinase modulates the autophagic process by controlling lysosomal biogenesis in Alzheimer's disease. *Journal of Experimental Medicine*, 211(8):1551–1570, July 2014.

[250] Mark Lee, Eric Whitsel, Christy Avery, Timothy M. Hughes, Michael E. Griswold, Sanaz Sedaghat, Rebecca F. Gottesman, Thomas H. Mosley, Gerardo Heiss, and Pamela L. Lutsey. Variation in Population Attributable Fraction of Dementia Associated With Potentially Modifiable Risk Factors by Race and Ethnicity in the US. *JAMA Network Open*, 5(7):e2219672, July 2022.

[251] Suzee E. Lee, Maria C. Tartaglia, Görsev Yener, Sermin Genç, William W. Seeley, Pascual Sanchez-Juan, Fermin Moreno, Mario F. Mendez, Eric Klein, Rosa Rademakers, Adolfo López De Munain, Onofre Combarros, Joel H. Kramer, Robert O. Kenet, Adam L. Boxer, Michael D. Geschwind, Maria-Luisa Gorno-Tempini, Anna M. Karydas, Gil D. Rabinovici, Giovanni Coppola, Daniel H. Geschwind, and Bruce L. Miller. Neurodegenerative Disease Phenotypes in Carriers of MAPT p.A152T, A Risk Factor for Frontotemporal Dementia Spectrum Disorders and Alzheimer Disease. *Alzheimer Disease & Associated Disorders*, 27(4):302–309, October 2013.

[252] Virginia M.-Y. Lee, Brian J. Balin, Laszlo Otvos, and John Q. Trojanowski. A68: a Major Subunit of Paired Helical Filaments and Derivatized Forms of Normal Tau. *Science*, 251(4994):675–678, February 1991.

[253] Chommanad Lerdkrai, Nithi Asavapanumas, Bianca Brawek, Yury Kovalchuk, Nima Mojtahedi, Maria Olmedillas Del Moral, and Olga Garaschuk. Intracellular Ca^{2+} stores control in vivo neuronal hyperactivity in a mouse model of Alzheimer's disease. *Proceedings of the National Academy of Sciences*, 115(6), February 2018.

[254] Karelle Leroy, Kunie Ando, Vincent Laporte, Robert Dedecker, Valérie Suain, Michèle Authelet, Céline Héraud, Nathalie Pierrot, Zehra Yilmaz, Jean-Noël Octave, and Jean-Pierre Brion. Lack of Tau Proteins Rescues Neuronal Cell Death and Decreases Amyloidogenic Processing of APP in APP/PS1 Mice. *The American Journal of Pathology*, 181(6):1928–1940, December 2012.

[255] Suzanne Lesage, Valérie Drouet, Elisa Majounie, Vincent Deramecourt, Maxime Jacoupy, Aude Nicolas, Florence Cormier-Dequaire, Sidi Mohamed Hassoun, Claire Pujol, Sorana Ciura, Zoi Erpapazoglou, Tatiana Usenko, Claude-Alain Maurage, Mourad Sahbatou, Stefan Liebau, Jinhui Ding, Basar Bilgic, Murat Emre, Nihan Erginel-Unaltuna, Gamze Guven, François Tison, Christine Tranchant, Marie Vidailhet, Jean-Christophe Corvol, Paul Krack, Anne-Louise Leutenegger, Michael A. Nalls, Dena G. Hernandez, Peter Heutink, J. Raphael Gibbs, John Hardy, Nicholas W. Wood, Thomas Gasser, Alexandra Durr, Jean-François Deleuze, Meriem Tazir, Alain Destée, Ebba Lohmann, Edor Kabashi, Andrew Singleton, Olga Corti, Alexis Brice, Suzanne Lesage, François Tison, Marie Vidailhet, Jean-Christophe Corvol, Yves Agid, Mathieu Anheim, Anne-Marie Bonnet, Michel Borg, Emmanuel Broussolle, Philippe Damier, Alain Destée, Alexandra Dürr, Franck Durif, Paul Krack, Stephan Klebe, Ebba Lohmann, Maria Martinez, Pierre Pollak, Olivier Rascol, Christine Tranchant, Marc Vérin, François Viallet, Alexis Brice, Suzanne Lesage, Elisa Majounie, François Tison, Marie Vidailhet, Jean Christophe Corvol, Michael A. Nalls, Dena G. Hernandez, J. Raphael Gibbs, Alexandra Dürr, Sampath Arepalli, Roger A. Barker, Yoav Ben-Shlomo, Daniela Berg, Francesco Bettella, Kailash Bhatia, Rob M.A. de Bie, Alessandro Biffi, Bastiaan R. Bloem, Zoltan Bochdanovits, Michael Bonin, Suzanne Lesage, François Tison, Marie Vidailhet, Jean-Christophe Corvol, Yves Agid, Mathieu Anheim, Anne-Marie

Bonnet, Michel Borg, Emmanuel Broussolle, Philippe Damier, Alain Destée, Alexandra Dürr, Franck Durif, Paul Krack, Stephan Klebe, Ebba Lohmann, Maria Martinez, Pierre Pollak, Olivier Rascol, Christine Tranchant, Marc Vérin, Jose M. Bras, Kathrin Brockmann, Janet Brooks, David J. Burn, Gavin Charlesworth, Honglei Chen, Patrick F. Chinnery, Sean Chong, Carl E. Clarke, Mark R. Cookson, Carl Counsell, Philippe Damier, Jean-François Dartigues, Panos Deloukas, Günther Deuschl, David T. Dexter, Karin D. van Dijk, Allissa Dillman, Jing Dong, Frank Durif, Sarah Edkins, Valentina Escott-Price, Jonathan R. Evans, Thomas Foltynie, Jianjun Gao, Michelle Gardner, Alison Goate, Emma Gray, Rita Guerreiro, Clare Harris, Jacobus J. van Hilten, Albert Hofman, Albert Hollenbeck, Peter Holmans, Janice Holton, Michèle Hu, Xuemei Huang, Heiko Huber, Gavin Hudson, Sarah E. Hunt, Johanna Huttenlocher, Thomas Illig, Pálmi V. Jónsson, Laura L. Kilarski, Iris E. Jansen, Jean-Charles Lambert, Cordelia Langford, Andrew Lees, Peter Lichtner, Patricia Limousin, Grisel Lopez, Delia Lorenz, Steven Lubbe, Codrin Lungu, María Martinez, Walter Mätzler, Alisdair McNeill, Catriona Moorby, Matthew Moore, Karen E. Morrison, Ese Mudanohwo, Sean S. O'Sullivan, Michael J. Owen, Justin Pearson, Joel S. Perlmutter, Hjörvar Pétursson, Vincent Plagnol, Pierre Pollak, Bart Post, Simon Potter, Bernard Ravina, Tamas Revesz, Olaf Riess, Fernando Rivadeneira, Patrizia Rizzu, Mina Ryten, Mohamad Saad, Javier Simón-Sánchez, Stephen Sawcer, Anthony Schapira, Hans Scheffer, Claudia Schulte, Manu Sharma, Karen Shaw, Una-Marie Sheerin, Ira Shoulson, Joshua Shulman, Ellen Sidransky, Chris C.A. Spencer, Hreinn Stefánsson, Kári Stefánsson, Joanna D. Stockton, Amy Strange, Kevin Talbot, Carlie M. Tanner, Avazeh Tashakkori-Ghanbaria, Daniah Trabzuni, Bryan J. Traynor, André G. Uitterlinden, Daan Velseboer, Robert Walker, Bart van de Warrenburg, Mirdhu Wickremaratchi, Caroline H. Williams-Gray, Sophie Winder-Rhodes, Isabel Wurster, Nigel Williams, Huw R. Morris, Peter Heutink, John Hardy, Nicholas W. Wood, Thomas Gasser, Andrew B. Singleton, and Alexis Brice. Loss of VPS13C Function in Autosomal-Recessive Parkinsonism Causes Mitochondrial Dysfunction and Increases PINK1/Parkin-Dependent Mitophagy. *The American Journal of Human Genetics*, 98(3):500–513, March 2016.

[256] Antoine Leuzy, Claudia Cicognola, Konstantinos Chiotis, Laure Saint-Aubert, Laetitia Lemoine, Niels Andreasen, Henrik Zetterberg, Keqiang Ye, Kaj

Blennow, Kina Höglund, and Agneta Nordberg. Longitudinal tau and metabolic PET imaging in relation to novel CSF tau measures in Alzheimer's disease. *European Journal of Nuclear Medicine and Molecular Imaging*, 46(5):1152–1163, May 2019.

[257] Ephrat Levy-Lahad, Wilma Wasco, Parvoneh Poorkaj, Donna M. Romano, Junko Oshima, Warren H. Pettingell, Chang-en Yu, Paul D. Jondro, Stephen D. Schmidt, Kai Wang, Annette C. Crowley, Ying-Hui Fu, Suzanne Y. Guenette, David Galas, Ellen Nemens, Ellen M. Wijsman, Thomas D. Bird, Gerard D. Schellenberg, and Rudolph E. Tanzi. Candidate Gene for the Chromosome 1 Familial Alzheimer's Disease Locus. *Science*, 269(5226):973–977, August 1995.

[258] Jada Lewis, Dennis W. Dickson, Wen-Lang Lin, Louise Chisholm, Anthony Corral, Graham Jones, Shu-Hui Yen, Naruhiko Sahara, Lisa Skipper, Debra Yager, Chris Eckman, John Hardy, Mike Hutton, and Eileen McGowan. Enhanced Neurofibrillary Degeneration in Transgenic Mice Expressing Mutant Tau and APP. *Science*, 293(5534):1487–1491, August 2001.

[259] Cheryl E. G. Leyns, Jason D. Ulrich, Mary B. Finn, Floy R. Stewart, Lauren J. Koscal, Javier Remolina Serrano, Grace O. Robinson, Elise Anderson, Marco Colonna, and David M. Holtzman. TREM2 deficiency attenuates neuroinflammation and protects against neurodegeneration in a mouse model of tauopathy. *Proceedings of the National Academy of Sciences*, 114(43):11524–11529, October 2017.

[260] Ling Li, Jee Hoon Roh, Eun Hyuk Chang, Yoonkyung Lee, Suji Lee, Minchul Kim, Wonyoung Koh, Jong Wook Chang, Hee Jin Kim, Mahito Nakanishi, Roger A. Barker, Duk L. Na, and Jihwan Song. iPSC Modeling of Presenilin1 Mutation in Alzheimer's Disease with Cerebellar Ataxia. *Experimental Neurobiology*, 27(5):350–364, October 2018.

[261] Xiaoyu Li, Yatender Kumar, Hans Zempel, Eva-Maria Mandelkow, Jacek Biernat, and Eckhard Mandelkow. Novel diffusion barrier for axonal retention of Tau in neurons and its failure in neurodegeneration. *The EMBO Journal*, 30(23):4825–4837, November 2011.

[262] Yuan-Ta Lin, Jinsoo Seo, Fan Gao, Heather M. Feldman, Hsin-Lan Wen, Jay Penney, Hugh P. Cam, Elizabeta Gjoneska, Waseem K. Raja, Jemmie Cheng, Richard Rueda, Oleg Kritskiy, Fatema Abdurrob, Zhuyu Peng, Blerta Milo,

Chung Jong Yu, Sara Elmsaouri, Dilip Dey, Tak Ko, Bruce A. Yankner, and Li-Huei Tsai. APOE4 Causes Widespread Molecular and Cellular Alterations Associated with Alzheimer's Disease Phenotypes in Human iPSC-Derived Brain Cell Types. *Neuron*, 98(6):1141–1154.e7, June 2018.

[263] Alexandra M. Lish, Nancy Ashour, Richard V. Pearse, Paige C. Galle, Gwendolyn A. Orme, Sarah E. Heuer, Courtney R. Benoit, Kellianne D. Alexander, Elyssa F.L. Grogan, Gizem Terzioglu, Allegra Scarpa, Andrew M. Stern, Nicholas Seyfried, Vilas Menon, and Tracy L. Young-Pearse. Astrocyte induction of disease-associated microglia is suppressed by acute exposure to fAD neurons in human iPSC triple cultures. *Cell Reports*, 44(6):115777, June 2025.

[264] Chia-Chen Liu, Melissa E. Murray, Xia Li, Na Zhao, Na Wang, Michael G. Heckman, Francis Shue, Yuka Martens, Yonghe Li, Ana-Caroline Raulin, Cassandra L. Rosenberg, Sydney V. Doss, Jing Zhao, Melissa C. Wren, Lin Jia, Yingxue Ren, Tadafumi C. Ikezu, Wenyan Lu, Yuan Fu, Thomas Caulfield, Zachary A. Trottier, Joshua Knight, Yixing Chen, Cynthia Linares, Xue Wang, Aishe Kurti, Yan W. Asmann, Zbigniew K. Wszolek, Glenn E. Smith, Prashanthi Vemuri, Kejal Kantarci, David S. Knopman, Val J. Lowe, Clifford R. Jack, Joseph E. Parisi, Tanis J. Ferman, Bradley F. Boeve, Neill R. Graff-Radford, Ronald C. Petersen, Steven G. Younkin, John D. Fryer, Hu Wang, Xianlin Han, Carl Frieden, Dennis W. Dickson, Owen A. Ross, and Guojun Bu. *APOE3* -Jacksonville (V236E) variant reduces self-aggregation and risk of dementia. *Science Translational Medicine*, 13(613):eabc9375, September 2021.

[265] Li Liu, Valerie Drouet, Jessica W. Wu, Menno P. Witter, Scott A. Small, Catherine Clelland, and Karen Duff. Trans-Synaptic Spread of Tau Pathology In Vivo. *PLoS ONE*, 7(2):e31302, February 2012.

[266] Gill Livingston, Jonathan Huntley, Kathy Y Liu, Sergi G Costafreda, Geir Selbæk, Suvarna Alladi, David Ames, Sube Banerjee, Alistair Burns, Carol Brayne, Nick C Fox, Cleusa P Ferri, Laura N Gitlin, Robert Howard, Helen C Kales, Mika Kivimäki, Eric B Larson, Noeline Nakasujja, Kenneth Rockwood, Quincy Samus, Kokoro Shirai, Archana Singh-Manoux, Lon S Schneider, Sebastian Walsh, Yao Yao, Andrew Sommerlad, and Naaheed Mukadam.

Dementia prevention, intervention, and care: 2024 report of the Lancet standing Commission. *The Lancet*, 404(10452):572–628, August 2024.

[267] Daniel A. Llano, Genevieve Laforet, and Viswanath Devanarayan. Derivation of a New ADAS-cog Composite Using Tree-based Multivariate Analysis: Prediction of Conversion From Mild Cognitive Impairment to Alzheimer Disease. *Alzheimer Disease & Associated Disorders*, 25(1):73–84, January 2011.

[268] A Lomakin, D S Chung, G B Benedek, D A Kirschner, and D B Teplow. On the nucleation and growth of amyloid beta-protein fibrils: detection of nuclei and quantitation of rate constants. *Proceedings of the National Academy of Sciences*, 93(3):1125–1129, February 1996.

[269] Mariella Lopez Salon, Laura Morelli, Eduardo M. Castao, Eduardo F. Soto, and Juana M. Pasquini. Defective ubiquitination of cerebral proteins in Alzheimer's disease. *Journal of Neuroscience Research*, 62(2):302–310, October 2000.

[270] Michael I Love, Wolfgang Huber, and Simon Anders. Moderated estimation of fold change and dispersion for RNA-seq data with DESeq2. *Genome Biology*, 15(12):550, December 2014.

[271] Ying Luan, Weiyi Wang, Qi Huang, Yan Wang, Jana Nussbaumer, Jie Wang, Anna Steward, Sebastian N. Roemer-Cassiano, Yihui Guan, Michael Ewers, Michael Schöll, Ruiqing Ni, Binyin Li, Nicolai Franzmeier, and Fang Xie. Synaptic loss pattern is constrained by brain connectome and modulated by phosphorylated tau in Alzheimer's disease. *Nature Communications*, 16(1):6356, July 2025.

[272] Lih-Fen Lue, Yu-Min Kuo, Alex E. Roher, Libuse Brachova, Yong Shen, Lucia Sue, Thomas Beach, Janice H. Kurth, Russel E. Rydel, and Joseph Rogers. Soluble Amyloid β Peptide Concentration as a Predictor of Synaptic Change in Alzheimer's Disease. *The American Journal of Pathology*, 155(3):853–862, September 1999.

[273] Katie Lunnon, Aoife Keohane, Ruth Pidsley, Stephen Newhouse, Joanna Riddoch-Contreras, Elisabeth B. Thubron, Matthew Devall, Hikka Soininen, Iwona Kłoszewska, Patrizia Mecocci, Magda Tsolaki, Bruno Vellas, Leonard Schalkwyk, Richard Dobson, Afshan N. Malik, John Powell, Simon Lovestone, and Angela Hodges. Mitochondrial genes are altered in blood early in Alzheimer's disease. *Neurobiology of Aging*, 53:36–47, May 2017.

[274] Philip T.T. Ly, Yili Wu, Haiyan Zou, Ruitao Wang, Weihui Zhou, Ayae Kinoshita, Mingming Zhang, Yi Yang, Fang Cai, James Woodgett, and Weihong Song. Inhibition of GSK3β-mediated BACE1 expression reduces Alzheimer-associated phenotypes. *Journal of Clinical Investigation*, 123(1):224–235, January 2013.

[275] Courtney MacMullen, Neelam Sharma, and Ronald L Davis. Mitochondrial dynamics and bioenergetics in Alzheimer's induced pluripotent stem cell-derived neurons. *Brain*, 148(4):1405–1420, April 2025.

[276] Kira S Makarova, Nick V Grishin, Svetlana A Shabalina, Yuri I Wolf, and Eugene V Koonin. A putative RNA-interference-based immune system in prokaryotes: computational analysis of the predicted enzymatic machinery, functional analogies with eukaryotic RNAi, and hypothetical mechanisms of action. *Biology Direct*, 1(1):7, December 2006.

[277] Prashant Mali, Luhan Yang, Kevin M. Esvelt, John Aach, Marc Guell, James E. DiCarlo, Julie E. Norville, and George M. Church. RNA-Guided Human Genome Engineering via Cas9. *Science*, 339(6121):823–826, February 2013.

[278] Jan-Philipp Mallm, Jakob-Andreas Tschäpe, Meike Hick, Mikhail A. Filippov, and Ulrike C. Müller. Generation of conditional null alleles for *APP* and *APLP2*. *genesis*, 48(3):200–206, March 2010.

[279] Maria Manczak, Ramesh Kandimalla, David Fry, Hiromi Sesaki, and P. Hemachandra Reddy. Protective effects of reduced dynamin-related protein 1 against amyloid beta-induced mitochondrial dysfunction and synaptic damage in Alzheimer's disease. *Human Molecular Genetics*, page ddw330, September 2016.

[280] E.-M. Mandelkow and E. Mandelkow. Biochemistry and Cell Biology of Tau Protein in Neurofibrillary Degeneration. *Cold Spring Harbor Perspectives in Medicine*, 2(7):a006247–a006247, July 2012.

[281] Justine D. Manos, Christina N. Preiss, Nandini Venkat, Joseph Tamm, Peter Reinhardt, Taekyung Kwon, Jessica Wu, Allison D. Winter, Thomas R. Jahn, Kiran Yanamandra, Katherine Titterton, Eric Karran, and Xavier Langlois. Uncovering specificity of endogenous TAU aggregation in a human iPSC-neuron TAU seeding model. *iScience*, 25(1):103658, January 2022.

[282] Nicole Maphis, Guixiang Xu, Olga N. Kokiko-Cochran, Shanya Jiang, Astrid Cardona, Richard M. Ransohoff, Bruce T. Lamb, and Kiran Bhaskar. Reactive microglia drive tau pathology and contribute to the spreading of pathological tau in the brain. *Brain*, 138(6):1738–1755, June 2015.

[283] Soraia Martins, Andreas Müller-Schiffmann, Lars Erichsen, Martina Bohndorf, Wasco Wruck, Kristel Sleegers, Christine Van Broeckhoven, Carsten Korth, and James Adjaye. IPSC-Derived Neuronal Cultures Carrying the Alzheimer's Disease Associated TREM2 R47H Variant Enables the Construction of an Aβ-Induced Gene Regulatory Network. *International Journal of Molecular Sciences*, 21(12):4516, June 2020.

[284] Patricia Martín-Maestro, Ricardo Gargini, Andrew A. Sproul, Esther García, Luis C. Antón, Scott Noggle, Ottavio Arancio, Jesús Avila, and Vega García-Escudero. Mitophagy Failure in Fibroblasts and iPSC-Derived Neurons of Alzheimer's Disease-Associated Presenilin 1 Mutation. *Frontiers in Molecular Neuroscience*, 10, 2017.

[285] Patricia Martín-Maestro, Andrew Sproul, Hector Martinez, Dominik Paquet, Meri Gerges, Scott Noggle, and Anatoly A. Starkov. Autophagy Induction by Bexarotene Promotes Mitophagy in Presenilin 1 Familial Alzheimer's Disease iPSC-Derived Neural Stem Cells. *Molecular Neurobiology*, 56(12):8220–8236, December 2019.

[286] Amir T. Marvian, Tabea Strauss, Qilin Tang, Benjamin J. Tuck, Sophie Keeling, Daniel Rüdiger, Negar Mirzazadeh Dizaji, Hossein Mohammad-Beigi, Brigitte Nuscher, Pijush Chakraborty, Duncan S. Sutherland, William A. McEwan, Thomas Köglsperger, Stefan Zahler, Markus Zweckstetter, Stefan F. Lichtenthaler, Wolfgang Wurst, Sigrid Schwarz, and Günter Höglinger. Distinct regulation of Tau Monomer and aggregate uptake and intracellular accumulation in human neurons. *Molecular Neurodegeneration*, 19(1):100, December 2024.

[287] C L Masters, G Simms, N A Weinman, G Multhaup, B L McDonald, and K Beyreuther. Amyloid plaque core protein in Alzheimer disease and Down syndrome. *Proceedings of the National Academy of Sciences*, 82(12):4245–4249, June 1985.

[288] Hansruedi Mathys, Jose Davila-Velderrain, Zhuyu Peng, Fan Gao, Shahin Mohammadi, Jennie Z. Young, Madhvi Menon, Liang He, Fatema Abdurrob, Xueqiao Jiang, Anthony J. Martorell, Richard M. Ransohoff, Brian P. Hafler, David A. Bennett, Manolis Kellis, and Li-Huei Tsai. Single-cell transcriptomic analysis of Alzheimer's disease. *Nature*, 570(7761):332–337, June 2019.

[289] Hansruedi Mathys, Zhuyu Peng, Carles A. Boix, Matheus B. Victor, Noelle Leary, Sudhagar Babu, Ghada Abdelhady, Xueqiao Jiang, Ayesha P. Ng, Kimia Ghafari, Alexander K. Kunisky, Julio Mantero, Kyriaki Galani, Vanshika N. Lohia, Gabrielle E. Fortier, Yasmine Lotfi, Jason Ivey, Hannah P. Brown, Pratham R. Patel, Nehal Chakraborty, Jacob I. Beaudway, Elizabeth J. Imhoff, Cameron F. Keeler, Maren M. McChesney, Haishal H. Patel, Sahil P. Patel, Megan T. Thai, David A. Bennett, Manolis Kellis, and Li-Huei Tsai. Single-cell atlas reveals correlates of high cognitive function, dementia, and resilience to Alzheimer's disease pathology. *Cell*, 186(20):4365–4385.e27, September 2023.

[290] Eriko S. Matsuo, Ryong-Woon Shin, Melvin L. Billingsley, Andre Van deVoorde, Michael O'Connor, John Q. Trojanowski, and Virginia M.Y. Lee. Biopsy-derived adult human brain tau is phosphorylated at many of the same sites as Alzheimer's disease paired helical filament tau. *Neuron*, 13(4):989–1002, October 1994.

[291] Niklas Mattsson, Philip S Insel, Sebastian Palmqvist, Erik Portelius, Henrik Zetterberg, Michael Weiner, Kaj Blennow, Oskar Hansson, and the Alzheimer's Disease Neuroimaging Initiative. Cerebrospinal fluid tau, neurogranin, and neurofilament light in Alzheimer's disease. *EMBO Molecular Medicine*, 8(10):1184–1196, October 2016.

[292] Etuini Ma'u, Sarah Cullum, Gary Cheung, Gill Livingston, and Naaheed Mukadam. Differences in the potential for dementia prevention between major ethnic groups within one country: A cross sectional analysis of population attributable fraction of potentially modifiable risk factors in New Zealand. *The Lancet Regional Health - Western Pacific*, 13:100191, August 2021.

[293] Kwasi G. Mawuenyega, Wendy Sigurdson, Vitaliy Ovod, Ling Munsell, Tom Kasten, John C. Morris, Kevin E. Yarasheski, and Randall J. Bateman. Decreased Clearance of CNS β-Amyloid in Alzheimer's Disease. *Science*, 330(6012):1774–1774, December 2010.

[294] Joseph McInnes, Keimpe Wierda, An Snellinx, Laura Bounti, Yu-Chun Wang, Ilie-Cosmin Stancu, Nuno Apóstolo, Kris Gevaert, Ilse Dewachter, Tara L. Spires-Jones, Bart De Strooper, Joris De Wit, Lujia Zhou, and Patrik Verstreken. Synaptogyrin-3 Mediates Presynaptic Dysfunction Induced by Tau. *Neuron*, 97(4):823–835.e8, February 2018.

[295] Guy M. McKhann, David S. Knopman, Howard Chertkow, Bradley T. Hyman, Clifford R. Jack, Claudia H. Kawas, William E. Klunk, Walter J. Koroshetz, Jennifer J. Manly, Richard Mayeux, Richard C. Mohs, John C. Morris, Martin N. Rossor, Philip Scheltens, Maria C. Carrillo, Bill Thies, Sandra Weintraub, and Creighton H. Phelps. The diagnosis of dementia due to Alzheimer's disease: Recommendations from the National Institute on Aging-Alzheimer's Association workgroups on diagnostic guidelines for Alzheimer's disease. *Alzheimer's & Dementia*, 7(3):263–269, May 2011.

[296] Catriona A. McLean, Robert A. Cherny, Fiona W. Fraser, Stephanie J. Fuller, Margaret J. Smith, Konrad Vbeyreuther, Ashley I. Bush, and Colin L. Masters. Soluble pool of A? amyloid as a determinant of severity of neurodegeneration in Alzheimer's disease. *Annals of Neurology*, 46(6):860–866, December 1999.

[297] Shashwath A. Meda, Balaji Narayanan, Jingyu Liu, Nora I. Perrone-Bizzozero, Michael C. Stevens, Vince D. Calhoun, David C. Glahn, Li Shen, Shannon L. Risacher, Andrew J. Saykin, and Godfrey D. Pearlson. A large scale multivariate parallel ICA method reveals novel imaging–genetic relationships for Alzheimer's disease in the ADNI cohort. *NeuroImage*, 60(3):1608–1621, April 2012.

[298] Annika Mehr, Meike Hick, Susann Ludewig, Michaela Müller, Ulrike Herrmann, Jakob Von Engelhardt, David P Wolfer, Martin Korte, and Ulrike C Müller. Lack of APP and APLP2 in GABAergic Forebrain Neurons Impairs Synaptic Plasticity and Cognition. *Cerebral Cortex*, 30(7):4044–4063, June 2020.

[299] David A. Merle, Anja Witternigg, Carmen Tam-Amersdorfer, Christoph Hartlmüller, Emil Spreitzer, Evelyne Schrank, Sabine Wagner-Lichtenegger, Oliver Werzer, Klaus Zangger, Andreas J. Kungl, Tobias Madl, N. Helge Meyer, and S. Fabio Falsone. Increased Aggregation Tendency of Alpha-Synuclein in a Fully Disordered Protein Complex. *Journal of Molecular Biology*, 431(14):2581–2598, June 2019.

[300] Jerome Mertens, Apuã C.M. Paquola, Manching Ku, Emily Hatch, Lena Böhnke, Shauheen Ladjevardi, Sean McGrath, Benjamin Campbell, Hyungjun Lee, Joseph R. Herdy, J. Tiago Gonçalves, Tomohisa Toda, Yongsung Kim, Jürgen Winkler, Jun Yao, Martin W. Hetzer, and Fred H. Gage. Directly Reprogrammed Human Neurons Retain Aging-Associated Transcriptomic Signatures and Reveal Age-Related Nucleocytoplasmic Defects. *Cell Stem Cell*, 17(6):705–718, December 2015.

[301] Marsel Mesulam. The Cholinergic Lesion of Alzheimer's Disease: Pivotal Factor or Side Show? *Learning & Memory*, 11(1):43–49, January 2004.

[302] Michelle M. Mielke, Jeremy A. Syrjanen, Kaj Blennow, Henrik Zetterberg, Ingmar Skoog, Prashanthi Vemuri, Mary M. Machulda, Jonathan Graff-Radford, David S. Knopman, Clifford R. Jack, Ronald C. Petersen, and Silke Kern. Comparison of variables associated with cerebrospinal fluid neurofilament, total-tau, and neurogranin. *Alzheimer's & Dementia*, 15(11):1437–1447, November 2019.

[303] Marta Milà-Alomà, Nicholas J. Ashton, Mahnaz Shekari, Gemma Salvadó, Paula Ortiz-Romero, Laia Montoliu-Gaya, Andrea L. Benedet, Thomas K. Karikari, Juan Lantero-Rodriguez, Eugeen Vanmechelen, Theresa A. Day, Armand González-Escalante, Gonzalo Sánchez-Benavides, Carolina Minguillon, Karine Fauria, José Luis Molinuevo, Jeffrey L. Dage, Henrik Zetterberg, Juan Domingo Gispert, Marc Suárez-Calvet, and Kaj Blennow. Plasma p-tau231 and p-tau217 as state markers of amyloid-β pathology in preclinical Alzheimer's disease. *Nature Medicine*, August 2022.

[304] Marta Milà-Alomà, Ann Brinkmalm, Nicholas J. Ashton, Hlin Kvartsberg, Mahnaz Shekari, Grégory Operto, Gemma Salvadó, Carles Falcon, Juan Domingo Gispert, Natalia Vilor-Tejedor, Eider M. Arenaza-Urquijo, Oriol Grau-Rivera, Aleix Sala-Vila, Gonzalo Sanchez-Benavides, José María González-de Echávarri, Carolina Minguillon, Karine Fauria, Aida Niñerola-Baizán, Andrés Perissinotti, Gwendlyn Kollmorgen, Ivonne Suridjan, Henrik Zetterberg, José Luis Molinuevo, Kaj Blennow, Marc Suárez-Calvet, on behalf of the ALFA Study, Annabella Beteta, Raffaele Cacciaglia, Alba Cañas, Carme Deulofeu, Irene Cumplido, Ruth Dominguez, Maria Emilio, Sherezade Fuentes, Laura Hernandez, Gema Huesa, Jordi Huguet, Paula Marne, Tania Mench´on, Albina Polo, Sandra Pradas, Anna Soteras, and Marc Vilanova.

CSF Synaptic Biomarkers in the Preclinical Stage of Alzheimer Disease and Their Association With MRI and PET: A Cross-sectional Study. *Neurology*, 97(21), November 2021.

[305] Tomohiro Miyasaka, Maho Morishima-Kawashima, Rivka Ravid, Wouter Kamphorst, Kazuo Nagashima, and Yasuo Ihara. Selective Deposition of Mutant Tau in the FTDP-17 Brain Affected by the P301L Mutation. *Journal of Neuropathology & Experimental Neurology*, 60(9):872–884, September 2001.

[306] Thomas J. Montine, Brenna A. Cholerton, Maria M. Corrada, Steven D. Edland, Margaret E. Flanagan, Laura S. Hemmy, Claudia H. Kawas, and Lon R. White. Concepts for brain aging: resistance, resilience, reserve, and compensation. *Alzheimer's Research & Therapy*, 11(1):22, December 2019.

[307] Brenda D. Moore, Vijayaraghavan Rangachari, William M. Tay, Nicole M. Milkovic, and Terrone L. Rosenberry. Biophysical Analyses of Synthetic Amyloid-β(1-42) Aggregates before and after Covalent Cross-Linking. Implications for Deducing the Structure of Endogenous Amyloid-β Oligomers. *Biochemistry*, 48(49):11796–11806, December 2009.

[308] Estrella Morenas-Rodríguez, Yan Li, Brigitte Nuscher, Nicolai Franzmeier, Chengjie Xiong, Marc Suárez-Calvet, Anne M Fagan, Stephanie Schultz, Brian A Gordon, Tammie L S Benzinger, Jason Hassenstab, Eric McDade, Regina Feederle, Celeste M Karch, Kai Schlepckow, John C Morris, Gernot Kleinberger, Bengt Nellgard, Jonathan Vöglein, Kaj Blennow, Henrik Zetterberg, Michael Ewers, Mathias Jucker, Johannes Levin, Randall J Bateman, Christian Haass, Sarah Adams, Ricardo Allegri, Aki Araki, Nicolas Barthelemy, Jacob Bechara, Sarah Berman, Courtney Bodge, Susan Brandon, William (Bill) Brooks, Jared Brosch, Jill Buck, Virginia Buckles, Kathleen Carter, Lisa Cash, Charlie Chen, Jasmeer Chhatwal, Patricio Chrem, Jasmin Chua, Helena Chui, Carlos Cruchaga, Gregory S Day, Chrismary De La Cruz, Darcy Denner, Anna Diffenbacher, Aylin Dincer, Tamara Donahue, Jane Douglas, Duc Duong, Noelia Egido, Bianca Esposito, Marty Farlow, Becca Feldman, Colleen Fitzpatrick, Shaney Flores, Nick Fox, Erin Franklin, Nelly Friedrichsen, Hisako Fujii, Samantha Gardener, Bernardino Ghetti, Alison Goate, Sarah Goldberg, Jill Goldman, Alyssa Gonzalez, Susanne Gräber-Sultan, Neill Graff-Radford, Morgan Graham, Julia Gray, Emily Gremminger, Miguel Grilo, Alex Groves, Lisa Häsler, Cortaiga

Hellm, Elizabeth Herries, Laura Hoechst-Swisher, Anna Hofmann, David Holtzman, Russ Hornbeck, Yakushev Igor, Ryoko Ihara, Takeshi Ikeuchi, Snezana Ikonomovic, Kenji Ishii, Clifford Jack, Gina Jerome, Erik Johnson, Stephan Käser, Kensaku Kasuga, Sarah Keefe, William (Bill) Klunk, Robert Koeppe, Deb Koudelis, Elke Kuder-Buletta, Christoph Laske, Allan Levey, Oscar Lopez, Jacob Marsh, Rita Martinez, Ralph Martins, Neal Scott Mason, Colin Masters, Kwasi Mawuenyega, Austin McCullough, Arlene Mejia, James MountzMD, Cath Mummery, Neelesh Nadkarni, Akemi Nagamatsu, Katie Neimeyer, Yoshiki Niimi, James Noble, Joanne Norton, Brigitte Nuscher, Antoinette O'Connor, Ulricke Obermüller, Riddhi Patira, Richard Perrin, Lingyan Ping, Oliver Preische, Alan Renton, John Ringman, Stephen Salloway, Peter Schofield, Michio Senda, Nick Seyfried, Kristine Shady, Hiroyuki Shimada, Wendy Sigurdson, Jennifer Smith, Lori Smith, Beth Snitz, Hamid Sohrabi, Sochenda Stephens, Kevin Taddei, Sarah Thompson, Peter Wang, Qing Wang, Elise Weamer, Jinbin Xu, and Xiong Xu. Soluble TREM2 in CSF and its association with other biomarkers and cognition in autosomal-dominant Alzheimer's disease: a longitudinal observational study. *The Lancet Neurology*, 21(4):329–341, April 2022.

[309] Elena P. Moreno-Jiménez, Miguel Flor-García, Julia Terreros-Roncal, Alberto Rábano, Fabio Cafini, Noemí Pallas-Bazarra, Jesús Ávila, and María Llorens-Martín. Adult hippocampal neurogenesis is abundant in neurologically healthy subjects and drops sharply in patients with Alzheimer's disease. *Nature Medicine*, 25(4):554–560, April 2019.

[310] Yoshiyuki Morishima, Yukiko Gotoh, Janine Zieg, Tamera Barrett, Hiromichi Takano, Richard Flavell, Roger J. Davis, Yasufumi Shirasaki, and Michael E. Greenberg. β-Amyloid Induces Neuronal Apoptosis Via a Mechanism that Involves the c-Jun N-Terminal Kinase Pathway and the Induction of Fas Ligand. *The Journal of Neuroscience*, 21(19):7551–7560, October 2001.

[311] Maho Morishima-Kawashima, Masato Hasegawa, Koji Takio, Masami Suzuki, Hirotaka Yoshida, Koiti Titani, and Yasuo Ihara. Proline-directed and Non-proline-directed Phosphorylation of PHF-tau. *Journal of Biological Chemistry*, 270(2):823–829, January 1995.

[312] John E. Morley, Susan A. Farr, William A. Banks, Steven N. Johnson, Kelvin A. Yamada, and Lin Xu. A Physiological Role for Amyloid-β Protein:

Enhancement of Learning and Memory. *Journal of Alzheimer's Disease*, 19(2):441–449, January 2010.

[313] Lennart Mucke, Eliezer Masliah, Gui-Qiu Yu, Margaret Mallory, Edward M. Rockenstein, Gwen Tatsuno, Kang Hu, Dora Kholodenko, Kelly Johnson-Wood, and Lisa McConlogue. High-Level Neuronal Expression of $A\beta_{1–42}$ in Wild-Type Human Amyloid Protein Precursor Transgenic Mice: Synaptotoxicity without Plaque Formation. *The Journal of Neuroscience*, 20(11):4050–4058, June 2000.

[314] Elliott J. Mufson, Shuang Y. Ma, John Dills, Elizabeth J. Cochran, Sue Leurgans, Joanne Wuu, David A. Bennett, Syed Jaffar, Michelle L. Gilmor, Alan I. Levey, and Jeffrey H. Kordower. Loss of basal forebrain $P75^{ntr}$ immunoreactivity in subjects with mild cognitive impairment and Alzheimer's disease. *Journal of Comparative Neurology*, 443(2):136–153, February 2002.

[315] M. M. Mukaka. Statistics corner: A guide to appropriate use of correlation coefficient in medical research. *Malawi Medical Journal: The Journal of Medical Association of Malawi*, 24(3):69–71, September 2012.

[316] Michael Mullan, Henry Houlden, Fiona Crawford, Angus Kennedy, Penelope Rogues, and Martin Rossor. Age of onset in familial early onset Alzheimer's disease correlates with genetic aetiology. *American Journal of Medical Genetics*, 48(3):129–130, October 1993.

[317] Christina R. Muratore, Constance Zhou, Meichen Liao, Marty A. Fernandez, Walter M. Taylor, Valentina N. Lagomarsino, Richard V. Pearse, Heather C. Rice, Joseph M. Negri, Amy He, Priya Srikanth, Dana G. Callahan, Taehwan Shin, Monica Zhou, David A. Bennett, Scott Noggle, J. Christopher Love, Dennis J. Selkoe, and Tracy L. Young-Pearse. Cell-type Dependent Alzheimer's Disease Phenotypes: Probing the Biology of Selective Neuronal Vulnerability. *Stem Cell Reports*, 9(6):1868–1884, December 2017.

[318] Jill Murrell, Martin Farlow, Bernardino Ghetti, and Merrill D. Benson. A mutation in the Amyloid Precursor Protein Associated with Hereditary Alzheimer's Disease. *Science*, 254(5028):97–99, October 1991.

[319] Antonia Neubauer, Doris Weissenbrunner, Susanna Pekrun, Sigrun Roeber, Viktoria Ruf, Paul Feyen, Felix L. Strübing, and Jochen Herms. Alpha-synuclein deposition patterns in Alzheimer's disease: association with cortical amyloid beta and variable tau load. *Acta Neuropathologica*, 150(1):46, October 2025.

[320] Rachael L. Neve, Peter Harris, Kenneth S. Kosik, David M. Kurnit, and Timothy A. Donlon. Identification of cDNA clones for the human microtubule-associated protein tau and chromosomal localization of the genes for tau and microtubule-associated protein 2. *Molecular Brain Research*, 1(3):271–280, December 1986.

[321] David C. New, Kelvin Wu, Alice W. S. Kwok, and Yung H. Wong. G protein-coupled receptor-induced Akt activity in cellular proliferation and apoptosis. *The FEBS Journal*, 274(23):6025–6036, December 2007.

[322] Bryan Ng, Helen A Rowland, Tina Wei, Kanisa Arunasalam, Emma Mee Hayes, Ivan Koychev, Anne Hedegaard, Elena M Ribe, Dennis Chan, Tharani Chessell, Dominic ffytche, Roger N Gunn, Ece Kocagoncu, Jennifer Lawson, Paresh A Malhotra, Basil H Ridha, James B Rowe, Alan J Thomas, Giovanna Zamboni, Noel J Buckley, Zameel M Cader, Simon Lovestone, and Richard Wade-Martins. Neurons derived from individual early Alzheimer's disease patients reflect their clinical vulnerability. *Brain Communications*, page fcac267, October 2022.

[323] Bryan Ng, Jane Vowles, Dayne Beccano-Kelly, M. Irina Stefana, Darragh P. O'Brien, Nora Bengoa-Vergniory, Feodora Betherat, Ajantha Abey, Philippa Carling, Peter Kilfeather, John A. Todd, Tara M. Caffrey, Natalie Connor-Robson, Sally A. Cowley, and Richard Wade-Martins. Tau depletion in human neurons mitigates Aβ-driven toxicity. *bioRxiv*, 2022. _eprint: https://www.biorxiv.org/content/early/2022/12/23/2022.12.23.521772.full.pdf.

[324] Tiia Ngandu, Jenni Lehtisalo, Alina Solomon, Esko Levälahti, Satu Ahtiluoto, Riitta Antikainen, Lars Bäckman, Tuomo Hänninen, Antti Jula, Tiina Laatikainen, Jaana Lindström, Francesca Mangialasche, Teemu Paajanen, Satu Pajala, Markku Peltonen, Rainer Rauramaa, Anna Stigsdotter-Neely, Timo Strandberg, Jaakko Tuomilehto, Hilkka Soininen, and Miia Kivipelto. A 2 year multidomain intervention of diet, exercise, cognitive training, and vascular risk monitoring versus control to prevent cognitive decline in at-risk elderly people (FINGER): a randomised controlled trial. *The Lancet*, 385(9984):2255–2263, June 2015.

[325] Marta Nieto, Edwin S. Monuki, Hua Tang, Jaime Imitola, Nicole Haubst, Samia J. Khoury, Jim Cunningham, Magdalena Gotz, and Christopher A. Walsh. Expression of Cux-1 and Cux-2 in the subventricular zone and

upper layers II–IV of the cerebral cortex. *Journal of Comparative Neurology*, 479(2):168–180, November 2004.

[326] K Nieweg, A Andreyeva, B Van Stegen, G Tanriöver, and K Gottmann. Alzheimer's disease-related amyloid-β induces synaptotoxicity in human iPS cell-derived neurons. *Cell Death & Disease*, 6(4):e1709–e1709, April 2015.

[327] D. Nochlin, G. van Belle, T. D. Bird, and S. M. Sumi. Comparison of the severity of neuropathologic changes in familial and sporadic Alzheimer's disease. *Alzheimer Disease and Associated Disorders*, 7(4):212–222, 1993.

[328] Georgia L. Nolt, Lesley R. Golden, Shealee P. Thorpe, Jessica L. Funnell, Isaiah O. Stephens, Gabriela Hernandez, Steven M. MacLean, Chloe C. Lucido, Chesney R. Brock, Akhil V. Pallerla, Darcy R. Adreon, Holden C. Williams, Josh M. Morganti, and Lance A. Johnson. Microglia-derived APOE2 improves remyelination even in the presence of endogenous APOE4. *Journal of Neuroinflammation*, December 2025.

[329] Mercedes Novo, Sonia Freire, and Wajih Al-Soufi. Critical aggregation concentration for the formation of early Amyloid-β (1–42) oligomers. *Scientific Reports*, 8(1):1783, January 2018.

[330] Justin M. Nussbaum, Stephan Schilling, Holger Cynis, Antonia Silva, Eric Swanson, Tanaporn Wangsanut, Kaycie Tayler, Brian Wiltgen, Asa Hatami, Raik Rönicke, Klaus Reymann, Birgit Hutter-Paier, Anca Alexandru, Wolfgang Jagla, Sigrid Graubner, Charles G. Glabe, Hans-Ulrich Demuth, and George S. Bloom. Prion-like behaviour and tau-dependent cytotoxicity of pyroglutamylated amyloid-β. *Nature*, 485(7400):651–655, May 2012.

[331] Jan Näslund. Correlation Between Elevated Levels of Amyloid β-Peptide in the Brain and Cognitive Decline. *JAMA*, 283(12):1571, March 2000.

[332] Holly Oakley, Sarah L. Cole, Sreemathi Logan, Erika Maus, Pei Shao, Jeffery Craft, Angela Guillozet-Bongaarts, Masuo Ohno, John Disterhoft, Linda Van Eldik, Robert Berry, and Robert Vassar. Intraneuronal β-Amyloid Aggregates, Neurodegeneration, and Neuron Loss in Transgenic Mice with Five Familial Alzheimer's Disease Mutations: Potential Factors in Amyloid Plaque Formation. *The Journal of Neuroscience*, 26(40):10129–10140, October 2006.

[333] Adrian L. Oblak, Stefania Forner, Paul R. Territo, Michael Sasner, Gregory W. Carter, Gareth R. Howell, Stacey J. Sukoff-Rizzo, Benjamin A. Logsdon, Lara M. Mangravite, Ali Mortazavi, David Baglietto-Vargas, Kim N. Green, Grant R. MacGregor, Marcelo A. Wood, Andrea J. Tenner, Frank M. LaFerla, Bruce T. Lamb, and The MODEL-AD, and Consortium. Model organism development and evaluation for late-onset Alzheimer's disease: MODEL-AD. *Alzheimer's & Dementia: Translational Research & Clinical Interventions*, 6(1):e12110, January 2020.

[334] Anna Ochalek, Balázs Mihalik, Hasan X. Avci, Abinaya Chandrasekaran, Annamária Téglási, István Bock, Maria Lo Giudice, Zsuzsanna Táncos, Kinga Molnár, Lajos László, Jørgen E. Nielsen, Bjørn Holst, Kristine Freude, Poul Hyttel, Julianna Kobolák, and András Dinnyés. Neurons derived from sporadic Alzheimer's disease iPSCs reveal elevated TAU hyperphosphorylation, increased amyloid levels, and GSK3B activation. *Alzheimer's Research & Therapy*, 9(1):90, December 2017.

[335] Salvatore Oddo, Antonella Caccamo, Jason D Shepherd, M.Paul Murphy, Todd E Golde, Rakez Kayed, Raju Metherate, Mark P Mattson, Yama Akbari, and Frank M LaFerla. Triple-Transgenic Model of Alzheimer's Disease with Plaques and Tangles. *Neuron*, 39(3):409–421, July 2003.

[336] Sugako Oka, Julio Leon, Kunihiko Sakumi, Tomomi Ide, Dongchon Kang, Frank M. LaFerla, and Yusaku Nakabeppu. Human mitochondrial transcriptional factor A breaks the mitochondria-mediated vicious cycle in Alzheimer's disease. *Scientific Reports*, 6(1):37889, November 2016.

[337] Nicholas O'Neill, Thor D. Stein, Oluwatosin A. Olayinka, Jenny A. Empawi, Junming Hu, Tong Tong, Xiaoling Zhang, and Lindsay A. Farrer. Cognitive resilience to Alzheimer's disease characterized by cell-type abundance. *Alzheimer's & Dementia*, 20(10):6910–6921, October 2024.

[338] Adam L. Orr, Chaeyoung Kim, David Jimenez-Morales, Billy W. Newton, Jeffrey R. Johnson, Nevan J. Krogan, Danielle L. Swaney, and Robert W. Mahley. Neuronal Apolipoprotein E4 Expression Results in Proteome-Wide Alterations and Compromises Bioenergetic Capacity by Disrupting Mitochondrial Function. *Journal of Alzheimer's Disease*, 68(3):991–1011, April 2019.

[339] Maitane Ortiz-Virumbrales, Cesar L. Moreno, Ilya Kruglikov, Paula Marazuela, Andrew Sproul, Samson Jacob, Matthew Zimmer, Daniel Paull, Bin Zhang, Eric E. Schadt, Michelle E. Ehrlich, Rudolph E. Tanzi, Ottavio Arancio, Scott Noggle, and Sam Gandy. CRISPR/Cas9-Correctable mutation-related molecular and physiological phenotypes in iPSC-derived Alzheimer's PSEN2 N141I neurons. *Acta Neuropathologica Communications*, 5(1):77, December 2017.

[340] Rik Ossenkoppele, Emma M. Coomans, Liana G. Apostolova, Suzanne L. Baker, Henryk Barthel, Thomas G. Beach, Tammy L. S. Benzinger, Tobey Betthauser, Gérard N. Bischof, Michel Bottlaender, Pierick Bourgeat, Anouk Den Braber, Matthias Brendel, Adam M. Brickman, David M. Cash, Maria C. Carrillo, William Coath, Bradley T. Christian, Brad C. Dickerson, Vincent Dore, Alexander Drzezga, Azadeh Feizpour, Wiesje M. Van Der Flier, Nicolai Franzmeier, Giovanni B. Frisoni, Valentina Garibotto, Elsmarieke Van De Giessen, Juan Domingo-Gispert, Johannes Gnoerich, Yuna Gu, Yihui Guan, Bernard J. Hanseeuw, Theresa M. Harrison, Clifford R. Jack, Elena Jaeger, William J. Jagust, Willemijn J. Jansen, Renaud La Joie, Keith A. Johnson, Sterling C. Johnson, Ian A. Kennedy, Jun Pyo Kim, Koen Van Laere, Julien Lagarde, Patrick Lao, José A. Luchsinger, Silke Kern, William C. Kreisl, Vincent Malotaux, Maura Malpetti, Jennifer J. Manly, Xiaoxie Mao, Niklas Mattsson-Carlgren, Mayo Clinic Study on Aging, Ron C. Petersen, Konstantin Messerschmidt, Carolina Minguillon, Elizabeth M. Mormino, John T. O'Brien, Sebastian Palmqvist, Debora E. Peretti, Ron C. Petersen, Yolande A. L. Pijnenburg, Michael J. Pontecorvo, Judes Poirier, PREVENT-AD Research Group, Gil D. Rabinovici, Nesrine Rahmouni, Shannon L. Risacher, Pedro Rosa-Neto, Howard Rosen, Christopher C. Rowe, James B. Rowe, Michael Rullmann, Yasmine Salman, Marie Sarazin, Andrew J. Saykin, Julie A. Schneider, Michael Schöll, Jonathan M. Schott, Sang Won Seo, Geidy E. Serrano, Sergey Shcherbinin, Mahnaz Shekari, Ingmar Skoog, Ruben Smith, Reisa A. Sperling, Laure Spruyt, Erik Stomrud, Olof Strandberg, Joseph Therriault, Fang Xie, Rik Vandenberghe, Victor L. Villemagne, Sylvia Villeneuve, Pieter Jelle Visser, Hillary Vossler, Christina B. Young, Colin Groot, and Oskar Hansson. Tau PET positivity in individuals with and without cognitive impairment varies with age, amyloid-β status, APOE genotype and sex. *Nature Neuroscience*, 28(8):1610–1621, August 2025.

[341] Rik Ossenkoppele, Chul Hyoung Lyoo, Jonas Jester-Broms, Carole H. Sudre, Hanna Cho, Young Hoon Ryu, Jae Yong Choi, Ruben Smith, Olof Strandberg, Sebastian Palmqvist, Joel Kramer, Adam L. Boxer, Maria L. Gorno-Tempini, Bruce L. Miller, Renaud La Joie, Gil D. Rabinovici, and Oskar Hansson. Assessment of Demographic, Genetic, and Imaging Variables Associated With Brain Resilience and Cognitive Resilience to Pathological Tau in Patients With Alzheimer Disease. *JAMA Neurology*, 77(5):632, May 2020.

[342] Rik Ossenkoppele, Alexa Pichet Binette, Colin Groot, Ruben Smith, Olof Strandberg, Sebastian Palmqvist, Erik Stomrud, Pontus Tideman, Tomas Ohlsson, Jonas Jögi, Keith Johnson, Reisa Sperling, Vincent Dore, Colin L. Masters, Christopher Rowe, Denise Visser, Bart N. M. Van Berckel, Wiesje M. Van Der Flier, Suzanne Baker, William J. Jagust, Heather J. Wiste, Ronald C. Petersen, Clifford R. Jack, and Oskar Hansson. Amyloid and tau PET-positive cognitively unimpaired individuals are at high risk for future cognitive decline. *Nature Medicine*, 28(11):2381–2387, November 2022.

[343] Marcos Otero-Garcia, Sameehan U. Mahajani, Debia Wakhloo, Weijing Tang, Yue-Qiang Xue, Samuel Morabito, Jie Pan, Jane Oberhauser, Angela E. Madira, Tamara Shakouri, Yongning Deng, Thomas Allison, Zihuai He, William E. Lowry, Riki Kawaguchi, Vivek Swarup, and Inma Cobos. Molecular signatures underlying neurofibrillary tangle susceptibility in Alzheimer's disease. *Neuron*, 110(18):2929–2948.e8, September 2022.

[344] L. Otvos, L. Feiner, E. Lang, G. I. Szendrei, M. Goedert, and V. M-Y. Lee. Monoclonal antibody PHF-1 recognizes tau protein phosphorylated at serine residues 396 and 404. *Journal of Neuroscience Research*, 39(6):669–673, December 1994.

[345] Sarah Pahlke, Lara A. Kahale, Simin Mahinrad, Bernardo Sousa-Pinto, Rafael José Vieira, Mary Beth McAteer, Thomas Claessen, José Contador, Anna Hofmann, Lindsey A. Kuchenbecker, Luiza S. Machado, Noëlle Warmenhoven, Yara Yakoub, Sebastian Palmqvist, Suzanne E. Schindler, Charlotte Teunissen, Heather E. Whitson, Henrik Zetterberg, Rebecca Edelmayer, and Malavika P. Tampi. Blood-based biomarkers for detecting Alzheimer's disease pathology in cognitively impaired individuals within specialized care settings: A systematic review and meta-analysis. *Alzheimer's & Dementia*, 21(11):e70828, November 2025.

[346] Sebastian Palmqvist, Niklas Mattsson, Oskar Hansson, and for the Alzheimer's Disease Neuroimaging Initiative. Cerebrospinal fluid analysis detects cerebral amyloid-β accumulation earlier than positron emission tomography. *Brain*, 139(4):1226–1236, April 2016.

[347] Jorge J. Palop, Jeannie Chin, Erik D. Roberson, Jun Wang, Myo T. Thwin, Nga Bien-Ly, Jong Yoo, Kaitlyn O. Ho, Gui-Qiu Yu, Anatol Kreitzer, Steven Finkbeiner, Jeffrey L. Noebels, and Lennart Mucke. Aberrant Excitatory Neuronal Activity and Compensatory Remodeling of Inhibitory Hippocampal Circuits in Mouse Models of Alzheimer's Disease. *Neuron*, 55(5):697–711, September 2007.

[348] Peter K. Panegyres and Huei-Yang Chen. Differences between early and late onset Alzheimer's disease. *American Journal of Neurodegenerative Disease*, 2(4):300–306, 2013.

[349] Caroline B. Pantazis, Andrian Yang, Erika Lara, Justin A. McDonough, Cornelis Blauwendraat, Lirong Peng, Hideyuki Oguro, Jitendra Kanaujiya, Jizhong Zou, David Sebesta, Gretchen Pratt, Erin Cross, Jeffrey Blockwick, Philip Buxton, Lauren Kinner-Bibeau, Constance Medura, Christopher Tompkins, Stephen Hughes, Marianita Santiana, Faraz Faghri, Mike A. Nalls, Daniel Vitale, Shannon Ballard, Yue A. Qi, Daniel M. Ramos, Kailyn M. Anderson, Julia Stadler, Priyanka Narayan, Jason Papademetriou, Luke Reilly, Matthew P. Nelson, Sanya Aggarwal, Leah U. Rosen, Peter Kirwan, Venkat Pisupati, Steven L. Coon, Sonja W. Scholz, Theresa Priebe, Miriam Öttl, Jian Dong, Marieke Meijer, Lara J.M. Janssen, Vanessa S. Lourenco, Rik Van Der Kant, Dennis Crusius, Dominik Paquet, Ana-Caroline Raulin, Guojun Bu, Aaron Held, Brian J. Wainger, Rebecca M.C. Gabriele, Jackie M. Casey, Selina Wray, Dad Abu-Bonsrah, Clare L. Parish, Melinda S. Beccari, Don W. Cleveland, Emmy Li, Indigo V.L. Rose, Martin Kampmann, Carles Calatayud Aristoy, Patrik Verstreken, Laurin Heinrich, Max Y. Chen, Birgitt Schüle, Dan Dou, Erika L.F. Holzbaur, Maria Clara Zanellati, Richa Basundra, Mohanish Deshmukh, Sarah Cohen, Richa Khanna, Malavika Raman, Zachary S. Nevin, Madeline Matia, Jonas Van Lent, Vincent Timmerman, Bruce R. Conklin, Katherine Johnson Chase, Ke Zhang, Salome Funes, Daryl A. Bosco, Lena Erlebach, Marc Welzer, Deborah Kronenberg-Versteeg, Guochang Lyu, Ernest Arenas, Elena Coccia, Lily Sarrafha, Tim Ahfeldt, John C. Marioni,

William C. Skarnes, Mark R. Cookson, Michael E. Ward, and Florian T. Merkle. A reference human induced pluripotent stem cell line for large-scale collaborative studies. *Cell Stem Cell*, 29(12):1685–1702.e22, December 2022.

[350] Francesco Paonessa, Lewis D. Evans, Ravi Solanki, Delphine Larrieu, Selina Wray, John Hardy, Stephen P. Jackson, and Frederick J. Livesey. Microtubules Deform the Nuclear Membrane and Disrupt Nucleocytoplasmic Transport in Tau-Mediated Frontotemporal Dementia. *Cell Reports*, 26(3):582–593.e5, January 2019.

[351] Mercedes F. Paredes, Shawn F. Sorrells, Arantxa Cebrian-Silla, Kadellyn Sandoval, Dashi Qi, Kevin W. Kelley, David James, Simone Mayer, Julia Chang, Kurtis I. Auguste, Edward F. Chang, Antonio J. Gutierrez Martin, Arnold R. Kriegstein, Gary W. Mathern, Michael C. Oldham, Eric J. Huang, Jose Manuel Garcia-Verdugo, Zhengang Yang, and Arturo Alvarez-Buylla. Does Adult Neurogenesis Persist in the Human Hippocampus? *Cell Stem Cell*, 23(6):780–781, December 2018.

[352] Thomas D. Parker, David M. Cash, Christopher A. S. Lane, Kirsty Lu, Ian B. Malone, Jennifer M. Nicholas, Sarah-Naomi James, Ashvini Keshavan, Heidi Murray-Smith, Andrew Wong, Sarah M. Buchanan, Sarah E. Keuss, Carole H. Sudre, Marc Modat, David L. Thomas, Sebastian J. Crutch, Marcus Richards, Nick C. Fox, and Jonathan M. Schott. Hippocampal subfield volumes and pre-clinical Alzheimer's disease in 408 cognitively normal adults born in 1946. *PLOS ONE*, 14(10):e0224030, October 2019.

[353] Celeste Parra Bravo, Alice Maria Giani, Jesus Madero-Perez, Zeping Zhao, Yuansong Wan, Avi J. Samelson, Man Ying Wong, Alessandro Evangelisti, Ethan Cordes, Li Fan, Pearly Ye, Daphne Zhu, Tatyana Pozner, Maria Mercedes, Tark Patel, Allan Yarahmady, Gillian K. Carling, Fredrik H. Sterky, Virginia M.Y. Lee, Edward B. Lee, Michael DeTure, Dennis W. Dickson, Manu Sharma, Sue-Ann Mok, Wenjie Luo, Mingrui Zhao, Martin Kampmann, Shiaoching Gong, and Li Gan. Human iPSC 4R tauopathy model uncovers modifiers of tau propagation. *Cell*, 187(10):2446–2464.e22, May 2024.

[354] Tharick A. Pascoal, Andrea L. Benedet, Nicholas J. Ashton, Min Su Kang, Joseph Therriault, Mira Chamoun, Melissa Savard, Firoza Z. Lussier, Cécile Tissot, Thomas K. Karikari, Julie Ottoy, Sulantha Mathotaarachchi, Jenna

Stevenson, Gassan Massarweh, Michael Schöll, Mony J. De Leon, Jean-Paul Soucy, Paul Edison, Kaj Blennow, Henrik Zetterberg, Serge Gauthier, and Pedro Rosa-Neto. Microglial activation and tau propagate jointly across Braak stages. *Nature Medicine*, 27(9):1592–1599, September 2021.

[355] Rob Patro, Geet Duggal, Michael I Love, Rafael A Irizarry, and Carl Kingsford. Salmon provides fast and bias-aware quantification of transcript expression. *Nature Methods*, 14(4):417–419, April 2017.

[356] Jin-Jing Pei, Eva Braak, Heiko Braak, Inge Grundke-Iqbal, Khalid Iqbal, Bengt Winblad, and Richard F. Cowburn. Distribution of Active Glycogen Synthase Kinase 3β (GSK-3β) in Brains Staged for Alzheimer Disease Neurofibrillary Changes. *Journal of Neuropathology & Experimental Neurology*, 58(9):1010–1019, September 1999.

[357] Jin-Jing Pei, Cheng-Xin Gong, Wen-Lin An, Bengt Winblad, Richard F. Cowburn, Inge Grundke-Iqbal, and Khalid Iqbal. Okadaic-Acid-Induced Inhibition of Protein Phosphatase 2A Produces Activation of Mitogen-Activated Protein Kinases ERK1/2, MEK1/2, and p70 S6, Similar to That in Alzheimer's Disease. *The American Journal of Pathology*, 163(3):845–858, September 2003.

[358] Jin-Jing Pei, Inge Grundke-Iqbal, Khalid Iqbal, Nenad Bogdanovic, Bengt Winblad, and Richard F Cowburn. Accumulation of cyclin-dependent kinase 5 (cdk5) in neurons with early stages of Alzheimer's disease neurofibrillary degeneration. *Brain Research*, 797(2):267–277, June 1998.

[359] Jin-Jing Pei, Toshihisa Tanaka, Yunn-Chyn Tung, Eva Braak, Khalid Iqbal, and Inge Grundke-Iqbal. Distribution, Levels, and Activity of Glycogen Synthase Kinase-3 in the Alzheimer Disease Brain:. *Journal of Neuropathology and Experimental Neurology*, 56(1):70–78, January 1997.

[360] Joana B. Pereira, Shorena Janelidze, Olof Strandberg, Christopher D. Whelan, Henrik Zetterberg, Kaj Blennow, Sebastian Palmqvist, Erik Stomrud, Niklas Mattsson-Carlgren, and Oskar Hansson. Microglial activation protects against accumulation of tau aggregates in nondemented individuals with underlying Alzheimer's disease pathology. *Nature Aging*, 2(12):1138–1144, November 2022.

[361] Eleanor K. Pickett, Abigail G. Herrmann, Jamie McQueen, Kimberly Abt, Owen Dando, Jane Tulloch, Pooja Jain, Sophie Dunnett, Sadaf Sohrabi,

Maria P. Fjeldstad, Will Calkin, Leo Murison, Rosemary J. Jackson, Makis Tzioras, Anna Stevenson, Marie d'Orange, Monique Hooley, Caitlin Davies, Marti Colom-Cadena, Alejandro Anton-Fernandez, Declan King, Iris Oren, Jamie Rose, Chris-Anne McKenzie, Elizabeth Allison, Colin Smith, Oliver Hardt, Christopher M. Henstridge, Giles E. Hardingham, and Tara L. Spires-Jones. Amyloid Beta and Tau Cooperate to Cause Reversible Behavioral and Transcriptional Deficits in a Model of Alzheimer's Disease. *Cell Reports*, 29(11):3592–3604.e5, December 2019.

[362] Amy M Pooler, Emma C Phillips, Dawn H W Lau, Wendy Noble, and Diane P Hanger. Physiological release of endogenous tau is stimulated by neuronal activity. *EMBO reports*, 14(4):389–394, April 2013.

[363] Parvoneh Poorkaj, Murray Grossman, Ellen Steinbart, Haydeh Payami, Adele Sadovnick, David Nochlin, Takeshi Tabira, John Q. Trojanowski, Soo Borson, Douglas Galasko, Stephen Reich, Bruce Quinn, Gerard Schellenberg, and Thomas D. Bird. Frequency of Tau Gene Mutations in Familial and Sporadic Cases of Non-Alzheimer Dementia. *Archives of Neurology*, 58(3), March 2001.

[364] C Pottier, D Hannequin, S Coutant, A Rovelet-Lecrux, D Wallon, S Rousseau, S Legallic, C Paquet, S Bombois, J Pariente, C Thomas-Anterion, A Michon, B Croisile, F Etcharry-Bouyx, C Berr, J-F Dartigues, P Amouyel, H Dauchel, C Boutoleau-Bretonnière, C Thauvin, T Frebourg, J-C Lambert, D Campion, and PHRC GMAJ Collaborators. High frequency of potentially pathogenic SORL1 mutations in autosomal dominant early-onset Alzheimer disease. *Molecular Psychiatry*, 17(9):875–879, September 2012.

[365] Priya Prakash, Palak Manchanda, Evi Paouri, Kanchan Bisht, Kaushik Sharma, Jitika Rajpoot, Victoria Wendt, Ahad Hossain, Prageeth R. Wijewardhane, Caitlin E. Randolph, Yihao Chen, Sarah Stanko, Nadia Gasmi, Anxhela Gjojdeshi, Sophie Card, Jonathan Fine, Krupal P. Jethava, Matthew G. Clark, Bin Dong, Seohee Ma, Alexis Crockett, Elizabeth A. Thayer, Marlo Nicolas, Ryann Davis, Dhruv Hardikar, Daniela Allende, Richard A. Prayson, Chi Zhang, Dimitrios Davalos, and Gaurav Chopra. Amyloid-β induces lipid droplet-mediated microglial dysfunction via the enzyme DGAT2 in Alzheimer's disease. *Immunity*, 58(6):1536–1552.e8, June 2025.

[366] Darja Praprotnik, Mark A. Smith, Peggy L. Richey, Harry V. Vinters, and G. Perry. Filament heterogeneity within the dystrophic neurites of senile plaques suggests blockage of fast axonal transport in Alzheimer's disease. *Acta Neuropathologica*, 91(3):226–235, January 1996.

[367] Anita Pras, Bert Houben, Francesco A Aprile, Renée Seinstra, Rodrigo Gallardo, Leen Janssen, Wytse Hogewerf, Christian Gallrein, Matthias De Vleeschouwer, Alejandro Mata-Cabana, Mandy Koopman, Esther Stroo, Minke De Vries, Samantha Louise Edwards, Janine Kirstein, Michele Vendruscolo, Salvatore Fabio Falsone, Frederic Rousseau, Joost Schymkowitz, and Ellen A A Nollen. The cellular modifier MOAG-4/SERF drives amyloid formation through charge complementation. *The EMBO Journal*, 40(21):e107568, November 2021.

[368] V. P. Prasher, Matthew J. Farrer, Anna M. Kessling, Elizabeth M. C. Fisher, R. J. West, P. C. Barber, and A. C. Butler. Molecular mapping of alzheimer-type dementia in Down's syndrome. *Annals of Neurology*, 43(3):380–383, March 1998.

[369] Daniela Puzzo, Elentina K. Argyrousi, Agnieszka Staniszewski, Hong Zhang, Elisa Calcagno, Elisa Zuccarello, Erica Acquarone, Mauro Fa', Domenica D. Li Puma, Claudio Grassi, Luciano D'Adamio, Nicholas M. Kanaan, Paul E. Fraser, and Ottavio Arancio. Tau is not necessary for amyloid-β–induced synaptic and memory impairments. *Journal of Clinical Investigation*, 130(9):4831–4844, August 2020.

[370] Lei S. Qi, Matthew H. Larson, Luke A. Gilbert, Jennifer A. Doudna, Jonathan S. Weissman, Adam P. Arkin, and Wendell A. Lim. Repurposing CRISPR as an RNA-Guided Platform for Sequence-Specific Control of Gene Expression. *Cell*, 152(5):1173–1183, February 2013.

[371] Jing Qian, Rebecca A. Betensky, Bradley T. Hyman, and Alberto Serrano-Pozo. Association of *APOE* Genotype With Heterogeneity of Cognitive Decline Rate in Alzheimer Disease. *Neurology*, 96(19), May 2021.

[372] Qiang Qiang, Loren Skudder-Hill, Tomoko Toyota, Wenshi Wei, and Hiroaki Adachi. CSF GAP-43 as a biomarker of synaptic dysfunction is associated with tau pathology in Alzheimer's disease. *Scientific Reports*, 12(1):17392, October 2022.

[373] Giorgia Quadrato, Juliana Brown, and Paola Arlotta. The promises and challenges of human brain organoids as models of neuropsychiatric disease. *Nature Medicine*, 22(11):1220–1228, November 2016.

[374] Giorgia Quadrato, Tuan Nguyen, Evan Z. Macosko, John L. Sherwood, Sung Min Yang, Daniel R. Berger, Natalie Maria, Jorg Scholvin, Melissa Goldman, Justin P. Kinney, Edward S. Boyden, Jeff W. Lichtman, Ziv M. Williams, Steven A. McCarroll, and Paola Arlotta. Cell diversity and network dynamics in photosensitive human brain organoids. *Nature*, 545(7652):48–53, May 2017.

[375] Jasmin Rahimi and Gabor G Kovacs. Prevalence of mixed pathologies in the aging brain. *Alzheimer's Research & Therapy*, 6(9):82, December 2014.

[376] Waseem K. Raja, Alison E. Mungenast, Yuan-Ta Lin, Tak Ko, Fatema Abdurrob, Jinsoo Seo, and Li-Huei Tsai. Self-Organizing 3D Human Neural Tissue Derived from Induced Pluripotent Stem Cells Recapitulate Alzheimer's Disease Phenotypes. *PLOS ONE*, 11(9):e0161969, September 2016.

[377] Mark Rapoport, Hana N. Dawson, Lester I. Binder, Michael P. Vitek, and Adriana Ferreira. Tau is essential to β-amyloid-induced neurotoxicity. *Proceedings of the National Academy of Sciences*, 99(9):6364–6369, April 2002.

[378] Kristina Rehbach, Michael B. Fernando, and Kristen J. Brennand. Integrating CRISPR Engineering and hiPSC-Derived 2D Disease Modeling Systems. *The Journal of Neuroscience: The Official Journal of the Society for Neuroscience*, 40(6):1176–1185, February 2020.

[379] Luke Reilly, Erika Lara, Daniel Ramos, Ziyi Li, Caroline B. Pantazis, Julia Stadler, Marianita Santiana, Jessica Roberts, Faraz Faghri, Ying Hao, Mike A. Nalls, Priyanka Narayan, Yansheng Liu, Andrew B. Singleton, Mark R. Cookson, Michael E. Ward, and Yue A. Qi. A fully automated FAIMS-DIA mass spectrometry-based proteomic pipeline. *Cell Reports Methods*, 3(10):100593, October 2023.

[380] Eric M. Reiman, Joseph F. Arboleda-Velasquez, Yakeel T. Quiroz, Matthew J. Huentelman, Thomas G. Beach, Richard J. Caselli, Yinghua Chen, Yi Su, Amanda J. Myers, John Hardy, Jean Paul Vonsattel, Steven G. Younkin, David A. Bennett, Philip L. De Jager, Eric B. Larson, Paul K. Crane, C. Dirk Keene, M. Ilyas Kamboh, Julia K. Kofler, Linda Duque, John R. Gilbert,

Harry E. Gwirtsman, Joseph D. Buxbaum, Dennis W. Dickson, Matthew P. Frosch, Bernardino F. Ghetti, Kathryn L. Lunetta, Li-San Wang, Bradley T. Hyman, Walter A. Kukull, Tatiana Foroud, Jonathan L. Haines, Richard P. Mayeux, Margaret A. Pericak-Vance, Julie A. Schneider, John Q. Trojanowski, Lindsay A. Farrer, Gerard D. Schellenberg, Gary W. Beecham, Thomas J. Montine, Gyungah R. Jun, The Alzheimer's Disease Genetics Consortium, Erin Abner, Perrie M. Adams, Marilyn S. Albert, Roger L. Albin, Liana G. Apostolova, Steven E. Arnold, Sanjay Asthana, Craig S. Atwood, Clinton T. Baldwin, Robert C. Barber, Lisa L. Barnes, Sandra Barral, James T. Becker, Duane Beekly, Eileen H. Bigio, Thomas D. Bird, Deborah Blacker, Bradley F. Boeve, James D. Bowen, Adam Boxer, James R. Burke, Jeffrey M. Burns, Nigel J. Cairns, Laura B. Cantwell, Chuanhai Cao, Chris S. Carlson, Cynthia M. Carlsson, Regina M. Carney, Minerva M. Carrasquillo, Helena C. Chui, David H. Cribbs, Elizabeth A. Crocco, Carlos Cruchaga, Charles DeCarli, Malcolm Dick, Rachelle S. Doody, Ranjan Duara, Nilufer Ertekin-Taner, Denis A. Evans, Kelley M. Faber, Thomas J. Fairchild, Kenneth B. Fallon, David W. Fardo, Martin R. Farlow, Steven Ferris, Douglas R. Galasko, Marla Gearing, Daniel H. Geschwind, Valentina Ghisays, Alison M. Goate, Neill R. Graff-Radford, Robert C. Green, John H. Growdon, Hakon Hakonarson, Ronald L. Hamilton, Kara L. Hamilton-Nelson, Lindy E. Harrell, Lawrence S. Honig, Ryan M. Huebinger, Christine M. Hulette, Gail P. Jarvik, Lee-Way Jin, Anna Karydas, Mindy J. Katz, John S. K. Kauwe, Jeffrey A. Kaye, Ronald Kim, Neil W. Kowall, Joel H. Kramer, Brian W. Kunkle, Amanda P. Kuzma, Frank M. LaFerla, James J. Lah, Yuk Ye Leung, James B. Leverenz, Allan I. Levey, Ge Li, Andrew P. Lieberman, Richard B. Lipton, Oscar L. Lopez, Constantine G. Lyketsos, John Malamon, Daniel C. Marson, Eden R. Martin, Frank Martiniuk, Deborah C. Mash, Eliezer Masliah, Wayne C. McCormick, Susan M. McCurry, Andrew N. McDavid, Stefan McDonough, Ann C. McKee, Marsel Mesulam, Bruce L. Miller, Carol A. Miller, Joshua W. Miller, John C. Morris, Shubhabrata Mukherjee, Adam C. Naj, Sid O'Bryant, John M. Olichney, Joseph E. Parisi, Henry L. Paulson, Elaine Peskind, Ronald C. Petersen, Aimee Pierce, Wayne W. Poon, Huntington Potter, Liming Qu, Joseph F. Quinn, Ashok Raj, Murray Raskind, Barry Reisberg, Joan S. Reisch, Christiane Reitz, John M. Ringman, Erik D. Roberson, Ekaterina Rogaeva, Howard J. Rosen, Roger N. Rosenberg, Donald R. Royall, Mark A. Sager, Mary Sano, Andrew J. Saykin, Lon S. Schneider, William W. Seeley, Amanda G.

Smith, Joshua A. Sonnen, Salvatore Spina, Peter St George-Hyslop, Robert A. Stern, Russell H. Swerdlow, Rudolph E. Tanzi, Juan C. Troncoso, Debby W. Tsuang, Otto Valladares, Vivianna M. Van Deerlin, Linda J. Van Eldik, Badri N. Vardarajan, Harry V. Vinters, Sandra Weintraub, Kathleen A. Welsh-Bohmer, Kirk C. Wilhelmsen, Jennifer Williamson, Thomas S. Wingo, Randall L. Woltjer, Clinton B. Wright, Chuang-Kuo Wu, Chang-En Yu, Lei Yu, and Yi Zhao. Exceptionally low likelihood of Alzheimer's dementia in APOE2 homozygotes from a 5,000-person neuropathological study. *Nature Communications*, 11(1):667, February 2020.

[381] Christiane Reitz, Ekaterina Rogaeva, and Gary W. Beecham. Late-onset vs nonmendelian early-onset Alzheimer disease: A distinction without a difference? *Neurology Genetics*, 6(5):e512, October 2020.

[382] Fabiana Ribeiro, Ana C. Teixeira-Santos, Paulo Caramelli, and Anja K. Leist. Prevalence of dementia in Latin America and Caribbean countries: Systematic review and meta-analyses exploring age, sex, rurality, and education as possible determinants. *Ageing Research Reviews*, 81:101703, November 2022.

[383] Davide Risso, John Ngai, Terence P Speed, and Sandrine Dudoit. Normalization of RNA-seq data using factor analysis of control genes or samples. *Nature Biotechnology*, 32(9):896–902, September 2014.

[384] Karen Ritchie, Michael Ropacki, Bruce Albala, John Harrison, Jeffrey Kaye, Joel Kramer, Christopher Randolph, and Craig W. Ritchie. Recommended cognitive outcomes in preclinical Alzheimer's disease: Consensus statement from the European Prevention of Alzheimer's Dementia project. *Alzheimer's & Dementia*, 13(2):186–195, February 2017.

[385] Jacqueline P. Robbins, Leo Perfect, Elena M. Ribe, Marcello Maresca, Adrià Dangla-Valls, Evangeline M. Foster, Richard Killick, Paulina Nowosiad, Matthew J. Reid, Lucia Dutan Polit, Alejo J. Nevado, Daniel Ebner, Mohammad Bohlooly-Y, Noel Buckley, Menelas N. Pangalos, Jack Price, and Simon Lovestone. Clusterin Is Required for β-Amyloid Toxicity in Human iPSC-Derived Neurons. *Frontiers in Neuroscience*, 12:504, July 2018.

[386] Erik D. Roberson, Brian Halabisky, Jong W. Yoo, Jinghua Yao, Jeannie Chin, Fengrong Yan, Tiffany Wu, Patricia Hamto, Nino Devidze, Gui-Qiu Yu, Jorge J. Palop, Jeffrey L. Noebels, and Lennart Mucke. Amyloid-β/Fyn–Induced

Synaptic, Network, and Cognitive Impairments Depend on Tau Levels in Multiple Mouse Models of Alzheimer's Disease. *The Journal of Neuroscience*, 31(2):700–711, January 2011.

[387] Erik D. Roberson, Kimberly Scearce-Levie, Jorge J. Palop, Fengrong Yan, Irene H. Cheng, Tiffany Wu, Hilary Gerstein, Gui-Qiu Yu, and Lennart Mucke. Reducing Endogenous Tau Ameliorates Amyloid ß-Induced Deficits in an Alzheimer's Disease Mouse Model. *Science*, 316(5825):750–754, May 2007.

[388] John L Robinson, Edward B Lee, Sharon X Xie, Lior Rennert, EunRan Suh, Colin Bredenberg, Carrie Caswell, Vivianna M Van Deerlin, Ning Yan, Ahmed Yousef, Howard I Hurtig, Andrew Siderowf, Murray Grossman, Corey T McMillan, Bruce Miller, John E Duda, David J Irwin, David Wolk, Lauren Elman, Leo McCluskey, Alice Chen-Plotkin, Daniel Weintraub, Steven E Arnold, Johannes Brettschneider, Virginia M.-Y Lee, and John Q Trojanowski. Neurodegenerative disease concomitant proteinopathies are prevalent, age-related and APOE4-associated. *Brain*, 141(7):2181–2193, July 2018.

[389] Stephen R. Robinson and Glenda M. Bishop. Aβ as a bioflocculant: implications for the amyloid hypothesis of Alzheimer's disease. *Neurobiology of Aging*, 23(6):1051–1072, November 2002.

[390] E. I. Rogaev, R. Sherrington, E. A. Rogaeva, G. Levesque, M. Ikeda, Y. Liang, H. Chi, C. Lin, K. Holman, T. Tsuda, L. Mar, S. Sorbi, B. Nacmias, S. Piacentini, L. Amaducci, I. Chumakov, D. Cohen, L. Lannfelt, P. E. Fraser, J. M. Rommens, and P. H. St George-Hyslop. Familial Alzheimer's disease in kindreds with missense mutations in a gene on chromosome 1 related to the Alzheimer's disease type 3 gene. *Nature*, 376(6543):775–778, August 1995.

[391] Francieli Rohden, Pamela C. L. Ferreira, Bruna Bellaver, João Pedro Ferrari-Souza, Cristiano S. Aguzzoli, Carolina Soares, Sarah Abbas, Hussein Zalzale, Guilherme Povala, Firoza Z. Lussier, Douglas T. Leffa, Guilherme Bauer-Negrini, Nesrine Rahmouni, Cécile Tissot, Joseph Therriault, Stijn Servaes, Jenna Stevenson, Andrea L. Benedet, Nicholas J. Ashton, Thomas K. Karikari, Dana L. Tudorascu, Henrik Zetterberg, Kaj Blennow, Eduardo R. Zimmer, Diogo Souza, Pedro Rosa-Neto, and Tharick A. Pascoal. Glial reactivity correlates with synaptic dysfunction across aging and Alzheimer's disease. *Nature Communications*, 16(1):5653, July 2025.

[392] Arturo Romano, Annalucia Serafino, Ewa Krasnowska, Maria Teresa Ciotti, Pietro Calissano, Francesca Ruberti, and Cinzia Galli. Neuronal fibrillogenesis: amyloid fibrils from primary neuronal cultures impair long-term memory in the crab Chasmagnathus. *Behavioural Brain Research*, 147(1-2):73–82, December 2003.

[393] Baptiste Ronan, Odile Flamand, Lionel Vescovi, Christine Dureuil, Laurence Durand, Florence Fassy, Marie-France Bachelot, Annabelle Lamberton, Magali Mathieu, Thomas Bertrand, Jean-Pierre Marquette, Youssef El-Ahmad, Bruno Filoche-Romme, Laurent Schio, Carlos Garcia-Echeverria, Hélène Goulaouic, and Benoit Pasquier. A highly potent and selective Vps34 inhibitor alters vesicle trafficking and autophagy. *Nature Chemical Biology*, 10(12):1013–1019, December 2014.

[394] Mónica Rosselli, Alfredo Ardila, Sonia Moreno, Virginia Standish, Juan C. Arango-Lasprilla, Victoria Tirado, Jorge Ossa, Alison M. Goate, Kenneth S. Kosik, and Franciso Lopera. Cognitive Decline in Patients with Familial Alzheimer's Disease Associated with E280a Presenilin-1 Mutation: A Longitudinal Study. *Journal of Clinical and Experimental Neuropsychology*, 22(4):483–495, August 2000.

[395] Helen A Rowland, Georgina Miller, Qiang Liu, Shuhan Li, Nicola R Sharp, Bryan Ng, Tina Wei, Kanisa Arunasalam, Ivan Koychev, Anne Hedegaard, Elena M Ribe, Dennis Chan, Tharani Chessell, Ece Kocagoncu, Jennifer Lawson, Paresh Malhotra, Basil H Ridha, James B Rowe, Alan J Thomas, Giovanna Zamboni, Henrik Zetterberg, M Zameel Cader, Richard Wade-Martins, Simon Lovestone, Alejo Nevado-Holgado, Andrey Kormilitzin, and Noel J Buckley. Changes in iPSC-astrocyte morphology reflect Alzheimer's disease patient clinical markers. *Stem Cells*, 43(3), March 2025.

[396] Sean K. Ryan, Michael V. Gonzalez, James P. Garifallou, Frederick C. Bennett, Kimberly S. Williams, Nathaniel P. Sotuyo, Eugene Mironets, Kieona Cook, Hakon Hakonarson, Stewart A. Anderson, and Kelly L. Jordan-Sciutto. Neuroinflammation and EIF2 Signaling Persist despite Antiretroviral Treatment in an hiPSC Tri-culture Model of HIV Infection. *Stem Cell Reports*, 14(4):703–716, April 2020.

[397] Sean K. Ryan, Kelly L. Jordan-Sciutto, and Stewart A. Anderson. Protocol for Tri-culture of hiPSC-Derived Neurons, Astrocytes, and Microglia. *STAR Protocols*, 1(3):100190, December 2020.

[398] Christopher Sackmann and Martin Hallbeck. Oligomeric amyloid-β induces early and widespread changes to the proteome in human iPSC-derived neurons. *Scientific Reports*, 10(1):6538, April 2020.

[399] Takashi Saito, Yukio Matsuba, Naomi Mihira, Jiro Takano, Per Nilsson, Shigeyoshi Itohara, Nobuhisa Iwata, and Takaomi C Saido. Single App knock-in mouse models of Alzheimer's disease. *Nature Neuroscience*, 17(5):661–663, May 2014.

[400] Yasufumi Sakakibara, Michiko Sekiya, Takashi Saito, Takaomi C. Saido, and Koichi M. Iijima. Cognitive and emotional alterations in App knock-in mouse models of Aβ amyloidosis. *BMC Neuroscience*, 19(1):46, December 2018.

[401] Katterine Salazar, Nery Jara, Eder Ramírez, Isabelle De Lima, Javiera Smith-Ghigliotto, Valentina Muñoz, Luciano Ferrada, and Francisco Nualart. Role of vitamin C and SVCT2 in neurogenesis. *Frontiers in Neuroscience*, 17:1155758, June 2023.

[402] Gemma Salvadó, Kanta Horie, Nicolas R. Barthélemy, Jacob W. Vogel, Alexa Pichet Binette, Charles D. Chen, Andrew J. Aschenbrenner, Brian A. Gordon, Tammie L. S. Benzinger, David M. Holtzman, John C. Morris, Sebastian Palmqvist, Erik Stomrud, Shorena Janelidze, Rik Ossenkoppele, Suzanne E. Schindler, Randall J. Bateman, and Oskar Hansson. Disease staging of Alzheimer's disease using a CSF-based biomarker model. *Nature Aging*, 4(5):694–708, March 2024.

[403] Jose V. Sanchez-Mut, Ester Aso, Nicolas Panayotis, Ira Lott, Mara Dierssen, Alberto Rabano, Rocio G. Urdinguio, Agustin F. Fernandez, Aurora Astudillo, Jose I. Martin-Subero, Balazs Balint, Mario F. Fraga, Antonio Gomez, Cecile Gurnot, Jean-Christophe Roux, Jesus Avila, Takao K. Hensch, Isidre Ferrer, and Manel Esteller. DNA methylation map of mouse and human brain identifies target genes in Alzheimer's disease. *Brain*, 136(10):3018–3027, October 2013.

[404] David W. Sanders, Sarah K. Kaufman, Sarah L. DeVos, Apurwa M. Sharma, Hilda Mirbaha, Aimin Li, Scarlett J. Barker, Alex C. Foley, Julian R. Thorpe,

Louise C. Serpell, Timothy M. Miller, Lea T. Grinberg, William W. Seeley, and Marc I. Diamond. Distinct Tau Prion Strains Propagate in Cells and Mice and Define Different Tauopathies. *Neuron*, 82(6):1271–1288, June 2014.

[405] Sigrid B Sando, Stacey Melquist, Ashley Cannon, Michael L Hutton, Olav Sletvold, Ingvild Saltvedt, Linda R White, Stian Lydersen, and Jan O Aasly. APOE ε4 lowers age at onset and is a high risk factor for Alzheimer's disease; A case control study from central Norway. *BMC Neurology*, 8(1):9, December 2008.

[406] Kazuki Sato, Akiko Wakamiya, Tadakazu Maeda, Kaori Noguchi, Akihiko Takashima, and Kazutomo Imahori. Correlation among Secondary Structure, Amyloid Precursor Protein Accumulation, and Neurotoxicity of Amyloid β(25–35) Peptide as Analyzed by Single Alanine Substitution. *The Journal of Biochemistry*, 118(6):1108–1111, December 1995.

[407] A. M. Saunders, W. J. Strittmatter, D. Schmechel, P. H. St. George-Hyslop, M. A. Pericak-Vance, S. H. Joo, B. L. Rosi, J. F. Gusella, D. R. Crapper-MacLachlan, M. J. Alberts, C. Hulette, B. Crain, D. Goldgaber, and A. D. Roses. Association of apolipoprotein E allele 4 with late-onset familial and sporadic Alzheimer's disease. *Neurology*, 43(8):1467–1467, August 1993.

[408] Carlos A. Saura, Guiquan Chen, Seema Malkani, Se-Young Choi, Reisuke H. Takahashi, Dawei Zhang, Gunnar K. Gouras, Alfredo Kirkwood, Richard G. M. Morris, and Jie Shen. Conditional Inactivation of Presenilin 1 Prevents Amyloid Accumulation and Temporarily Rescues Contextual and Spatial Working Memory Impairments in Amyloid Precursor Protein Transgenic Mice. *The Journal of Neuroscience*, 25(29):6755–6764, July 2005.

[409] Carlos A Saura, Se-Young Choi, Vassilios Beglopoulos, Seema Malkani, Dawei Zhang, B.S.Shankaranarayana Rao, Sumantra Chattarji, Raymond J Kelleher, Eric R Kandel, Karen Duff, Alfredo Kirkwood, and Jie Shen. Loss of Presenilin Function Causes Impairments of Memory and Synaptic Plasticity Followed by Age-Dependent Neurodegeneration. *Neuron*, 42(1):23–36, April 2004.

[410] Faten A. Sayed, Lay Kodama, Li Fan, Gillian K. Carling, Joe C. Udeochu, David Le, Qingyun Li, Lu Zhou, Man Ying Wong, Rose Horowitz, Pearly Ye, Hansruedi Mathys, Minghui Wang, Xiang Niu, Linas Mazutis, Xueqiao Jiang, Xueting Wang, Fuying Gao, Matthew Brendel, Maria Telpoukhovskaia,

Tara E. Tracy, Georgia Frost, Yungui Zhou, Yaqiao Li, Yue Qiu, Zuolin Cheng, Guoqiang Yu, John Hardy, Giovanni Coppola, Fei Wang, Michael A. DeTure, Bin Zhang, Lei Xie, John Q. Trajnowski, Virginia M. Y. Lee, Shiaoching Gong, Subhash C. Sinha, Dennis W. Dickson, Wenjie Luo, and Li Gan. AD-linked R47H- *TREM2* mutation induces disease-enhancing microglial states via AKT hyperactivation. *Science Translational Medicine*, 13(622):eabe3947, December 2021.

[411] Lawrence M. Sayre, Dawn A. Zelasko, Peggy L. R. Harris, George Perry, Robert G. Salomon, and Mark A. Smith. 4-Hydroxynonenal-Derived Advanced Lipid Peroxidation End Products Are Increased in Alzheimer's Disease. *Journal of Neurochemistry*, 68(5):2092–2097, May 1997.

[412] Ari W. Schaler and Natura Myeku. Cilostazol, a phosphodiesterase 3 inhibitor, activates proteasome-mediated proteolysis and attenuates tauopathy and cognitive decline. *Translational Research*, 193:31–41, March 2018.

[413] Ari W. Schaler, Avery M. Runyan, Catherine L. Clelland, Eric J. Sydney, Stephanie L. Fowler, Helen Y. Figueroa, Seiji Shioda, Ismael Santa-Maria, Karen E. Duff, and Natura Myeku. PAC1 receptor–mediated clearance of tau in postsynaptic compartments attenuates tau pathology in mouse brain. *Science Translational Medicine*, 13(595):eaba7394, May 2021.

[414] D. Scheuner, C. Eckman, M. Jensen, X. Song, M. Citron, N. Suzuki, T.D. Bird, J. Hardy, M. Hutton, W. Kukull, E. Larson, L. Levy-Lahad, M. Viitanen, E. Peskind, P. Poorkaj, G. Schellenberg, R. Tanzi, W. Wasco, L. Lannfelt, D. Selkoe, and S. Younkin. Secreted amyloid β–protein similar to that in the senile plaques of Alzheimer's disease is increased in vivo by the presenilin 1 and 2 and APP mutations linked to familial Alzheimer's disease. *Nature Medicine*, 2(8):864–870, August 1996.

[415] A. Schneider, J. Biernat, M. Von Bergen, E. Mandelkow, and E.-M. Mandelkow. Phosphorylation that Detaches Tau Protein from Microtubules (Ser262, Ser214) Also Protects It against Aggregation into Alzheimer Paired Helical Filaments. *Biochemistry*, 38(12):3549–3558, March 1999.

[416] Hermann Schägger and Thomas Georg Ohm. Human Diseases with Defects in Oxidative Phosphorylation: 2. F_1 F_0 ATP-Synthase Defects in Alzheimer

Disease Revealed by Blue Native Polyacrylamide Gel Electrophoresis. *European Journal of Biochemistry*, 227(3):916–921, February 1995.

[417] Sathish Selvam, Roberta S. Dos Reis, Marc C. E. Wagner, Rishi Krishnakumar, Kamyar Keshavarz, Mo R. Ebrahimkhani, and Velpandi Ayyavoo. Vascularized human brain organoids as a model of the brain–peripheral axis in HIV-1 neuropathogenesis. *Scientific Reports*, January 2026.

[418] Diego Sepulveda-Falla, Justin S. Sanchez, Maria Camila Almeida, Daniela Boassa, Juliana Acosta-Uribe, Clara Vila-Castelar, Liliana Ramirez-Gomez, Ana Baena, David Aguillon, Nelson David Villalba-Moreno, Jessica Lisa Littau, Andres Villegas, Thomas G. Beach, Charles L. White, Mark Ellisman, Susanne Krasemann, Markus Glatzel, Keith A. Johnson, Reisa A. Sperling, Eric M. Reiman, Joseph F. Arboleda-Velasquez, Kenneth S. Kosik, Francisco Lopera, and Yakeel T. Quiroz. Distinct tau neuropathology and cellular profiles of an APOE3 Christchurch homozygote protected against autosomal dominant Alzheimer's dementia. *Acta Neuropathologica*, 144(3):589–601, September 2022.

[419] A. Serrano-Pozo, M. P. Frosch, E. Masliah, and B. T. Hyman. Neuropathological Alterations in Alzheimer Disease. *Cold Spring Harbor Perspectives in Medicine*, 1(1):a006189–a006189, September 2011.

[420] Lincoln M. P. Shade, Yuriko Katsumata, Erin L. Abner, Khine Zin Aung, Steven A. Claas, Qi Qiao, Bernardo Aguzzoli Heberle, J. Anthony Brandon, Madeline L. Page, Timothy J. Hohman, Shubhabrata Mukherjee, Richard P. Mayeux, Lindsay A. Farrer, Gerard D. Schellenberg, Jonathan L. Haines, Walter A. Kukull, Kwangsik Nho, Andrew J. Saykin, David A. Bennett, Julie A. Schneider, The National Alzheimer's Coordinating Center, Sarah Biber, Marilyn Albert, Sanjay Asthana, David Bennett, James Brewer, Helena Chui, Suzanne Craft, Charles DeCarli, Todd Golde, Thomas Grabowski, Victor Henderson, Bradley Hyman, Jeffrey Kaye, Neil Kowall, Frank LaFerla, Allan Levey, Oscar Lopez, Bruce Miller, John Morris, Henry Paulson, Ronald Petersen, Eric Reiman, Roger Rosenberg, Mary Sano, Andrew Saykin, Scott Small, Stephen Strittmatter, Russell Swerdlow, John Trojanowski, Linda Van Eldik, Robert Vassar, Thomas Wisniewski, Kari A. Stephens, Kwun C. G. Chan, Heather O'Connell, Kathryn Gauthreaux, Charles Mock, Yen-Chi Chen, Stacy Oswald, Zack Miller, Dean K. Shibata, Kyle Ormsby, Jessica Culhane, Sarah Yasuda, The Alzheimer's Disease Genetics Consortium, James D. Bowen,

Paul K. Crane, Gail P. Jarvik, C. Dirk Keene, Eric B. Larson, Wayne C. McCormick, Susan M. McCurry, Shubhabrata Mukherjee, Neil W. Kowall, Ann C. McKee, Robert A. Stern, Lawrence S. Honig, Jean Paul Vonsattel, Jennifer Williamson, Scott Small, James R. Burke, Christine M. Hulette, Kathleen A. Welsh-Bohmer, Marla Gearing, James J. Lah, Allan I. Levey, Thomas S. Wingo, Liana G. Apostolova, Martin R. Farlow, Bernardino Ghetti, Andrew J. Saykin, Salvatore Spina, Marilyn S. Albert, Constantine G. Lyketsos, Juan C. Troncoso, Matthew P. Frosch, Robert C. Green, John H. Growdon, Bradley T. Hyman, Rudolph E. Tanzi, Huntington Potter, Dennis W. Dickson, Nilufer Ertekin-Taner, Neill R. Graff-Radford, Joseph E. Parisi, Ronald C. Petersen, Ranjan Duara, Joseph D. Buxbaum, Alison M. Goate, Mary Sano, Arjun V. Masurkar, Thomas Wisniewski, Eileen H. Bigio, Marsel Mesulam, Sandra Weintraub, Robert Vassar, Jeffrey A. Kaye, Joseph F. Quinn, Randall L. Woltjer, Lisa L. Barnes, David A. Bennett, Julie A. Schneider, Lei Yu, Victor Henderson, Kenneth B. Fallon, Lindy E. Harrell, Daniel C. Marson, Erik D. Roberson, Charles DeCarli, Lee-Way Jin, John M. Olichney, Ronald Kim, Frank M. LaFerla, Edwin Monuki, Elizabeth Head, David Sultzer, Daniel H. Geschwind, Harry V. Vinters, Marie-Francoise Chesselet, Douglas R. Galasko, James B. Brewer, Adam Boxer, Anna Karydas, Joel H. Kramer, Bruce L. Miller, Howard J. Rosen, William W. Seeley, Jeffrey M. Burns, Russell H. Swerdlow, Erin Abner, David W. Fardo, Linda J. Van Eldik, Roger L. Albin, Andrew P. Lieberman, Henry L. Paulson, Steven E. Arnold, John Q. Trojanowski, Vivianna M. Van Deerlin, Ronald L. Hamilton, M. Ilyas Kamboh, Oscar L. Lopez, James T. Becker, Chuanhai Cao, Ashok Raj, Amanda G. Smith, Helena C. Chui, Carol A. Miller, John M. Ringman, Lon S. Schneider, Thomas D. Bird, Joshua A. Sonnen, Chang-En Yu, Elaine Peskind, Murray Raskind, Ge Li, Debby W. Tsuang, Craig S. Atwood, Cynthia M. Carlsson, Mark A. Sager, Nathaniel A. Chin, Suzanne Craft, Nigel J. Cairns, John C. Morris, Carlos Cruchaga, Stephen Strittmatter, Eric M. Reiman, Thomas G. Beach, Matthew J. Huentelman, John Hardy, Amanda J. Myers, John S. K. Kauwe, Hakon Hakonarson, Deborah Blacker, Thomas J. Montine, Clinton T. Baldwin, Lindsay A. Farrer, Gyungah Jun, Kathryn L. Lunetta, William S. Bush, Jonathan L. Haines, Alan J. Lerner, Xiongwei Zhou, Sandra Barral, Christiane Reitz, Badri N. Vardarajan, Richard Mayeux, Gary W. Beecham, Regina M. Carney, Michael L. Cuccaro, John R. Gilbert, Kara L. Hamilton-Nelson, Brian W. Kunkle, Eden R. Martin, Margaret A.

Pericak-Vance, Jeffery M. Vance, Laura B. Cantwell, Amanda P. Kuzma, John Malamon, Adam C. Naj, Liming Qu, Gerard D. Schellenberg, Otto Valladares, Li-San Wang, Yi Zhao, James B. Leverenz, Philip L. De Jager, Denis A. Evans, Mindy J. Katz, Richard B. Lipton, Bradley F. Boeve, Mariet Allen, Minerva M. Carrasquillo, Steven G. Younkin, Kelley M. Faber, Tatiana M. Foroud, Valory Pavlik, Paul Massman, Eveleen Darby, Monica Rodriguear, Aisha Khaleeq, Donald R. Royall, Alan Stevens, Marcia Ory, John C. DeToledo, Henrick Wilms, Kim Johnson, Victoria Perez, Michelle Hernandez, Kirk C. Wilhelmsen, Jeffrey Tilson, Scott Chasse, Robert C. Barber, Thomas J. Fairchild, Sid E. O'Bryant, Janice Knebl, James R. Hall, Leigh Johnson, Douglas Mains, Lisa Alvarez, Adriana Gamboa, David Paydarfar, John Bertelson, Martin Woon, Gayle Ayres, Alyssa Aguirre, Raymond Palmer, Marsha Polk, Perrie M. Adams, Ryan M. Huebinger, Joan S. Reisch, Roger N. Rosenberg, Munro Cullum, Benjamin Williams, Mary Quiceno, Linda Hynan, Janet Smith, Barb Davis, Trung Nguyen, Ekaterina Rogaeva, Peter St George-Hyslop, Mark T. W. Ebbert, Peter T. Nelson, and David W. Fardo. GWAS of multiple neuropathology endophenotypes identifies new risk loci and provides insights into the genetic risk of dementia. *Nature Genetics*, 56(11):2407–2421, November 2024.

[421] Ganesh M. Shankar, Brenda L. Bloodgood, Matthew Townsend, Dominic M. Walsh, Dennis J. Selkoe, and Bernardo L. Sabatini. Natural Oligomers of the Alzheimer Amyloid-β Protein Induce Reversible Synapse Loss by Modulating an NMDA-Type Glutamate Receptor-Dependent Signaling Pathway. *The Journal of Neuroscience*, 27(11):2866–2875, March 2007.

[422] R Sherrington. Alzheimer's disease associated with mutations in presenilin 2 is rare and variably penetrant. *Human Molecular Genetics*, 5(7):985–988, July 1996.

[423] R. Sherrington, E. I. Rogaev, Y. Liang, E. A. Rogaeva, G. Levesque, M. Ikeda, H. Chi, C. Lin, G. Li, K. Holman, T. Tsuda, L. Mar, J.-F. Foncin, A. C. Bruni, M. P. Montesi, S. Sorbi, I. Rainero, L. Pinessi, L. Nee, I. Chumakov, D. Pollen, A. Brookes, P. Sanseau, R. J. Polinsky, W. Wasco, H. A. R. Da Silva, J. L. Haines, M. A. Pericak-Vance, R. E. Tanzi, A. D. Roses, P. E. Fraser, J. M. Rommens, and P. H. St George-Hyslop. Cloning of a gene bearing missense mutations in early-onset familial Alzheimer's disease. *Nature*, 375(6534):754–760, June 1995.

[424] Richard Sherva, Congcong Zhu, Rui Zhang, Jesse Mez, Richard Hauger, Victoria C. Merritt, Matthew Panizzon, J. Michael Gaziano, Vidriana Catanzaro, Gerard D. Schellenberg, Margaret Pericak-Vance, Jonathan L. Haines, Li-San Wang, Richard Mayeux, VA Million Veteran Program, Sumitra Muralidhar, Jennifer Moser, Jennifer E. Deen, Philip S. Tsao, Sumitra Muralidhar, Elizabeth Hauser, Amy Kilbourne, Michael Matheny, Dave Oslin, Deepak Voora, Philip S. Tsao, Jessica V. Brewer, Mary T. Brophy, Kelly Cho, Lori Churby, Scott L. DuVall, Saiju Pyarajan, Robert Ringer, Luis E. Selva, Shahpoor Shayan, Brady Stephens, Stacey B. Whitbourne, Themistocles L. Assimes, Adriana Hung, Henry Kranzler, Lindsay A. Farrer, and Mark W. Logue. Genome-wide association studies of Alzheimer's disease and related disorders stratified by sex, onset age, and Apolipoprotein E genotype reveal novel risk loci in African Americans. *Alzheimer's Research & Therapy*, 17(1):171, July 2025.

[425] Yang Shi, Alexey G. Murzin, Benjamin Falcon, Alexander Epstein, Jonathan Machin, Paul Tempest, Kathy L. Newell, Ruben Vidal, Holly J. Garringer, Naruhiko Sahara, Makoto Higuchi, Bernardino Ghetti, Ming-Kuei Jang, Sjors H. W. Scheres, and Michel Goedert. Cryo-EM structures of tau filaments from Alzheimer's disease with PET ligand APN-1607. *Acta Neuropathologica*, 141(5):697–708, May 2021.

[426] Yang Shi, Wenjuan Zhang, Yang Yang, Alexey G. Murzin, Benjamin Falcon, Abhay Kotecha, Mike Van Beers, Airi Tarutani, Fuyuki Kametani, Holly J. Garringer, Ruben Vidal, Grace I. Hallinan, Tammaryn Lashley, Yuko Saito, Shigeo Murayama, Mari Yoshida, Hidetomo Tanaka, Akiyoshi Kakita, Takeshi Ikeuchi, Andrew C. Robinson, David M. A. Mann, Gabor G. Kovacs, Tamas Revesz, Bernardino Ghetti, Masato Hasegawa, Michel Goedert, and Sjors H. W. Scheres. Structure-based classification of tauopathies. *Nature*, 598(7880):359–363, October 2021.

[427] Yichen Shi, Peter Kirwan, and Frederick J Livesey. Directed differentiation of human pluripotent stem cells to cerebral cortex neurons and neural networks. *Nature Protocols*, 7(10):1836–1846, October 2012.

[428] Yichen Shi, Peter Kirwan, James Smith, Glenn MacLean, Stuart H. Orkin, and Frederick J. Livesey. A Human Stem Cell Model of Early Alzheimer's Disease

Pathology in Down Syndrome. *Science Translational Medicine*, 4(124), March 2012.

[429] O. A. Shipton, J. R. Leitz, J. Dworzak, C. E. J. Acton, E. M. Tunbridge, F. Denk, H. N. Dawson, M. P. Vitek, R. Wade-Martins, O. Paulsen, and M. Vargas-Caballero. Tau Protein Is Required for Amyloid -Induced Impairment of Hippocampal Long-Term Potentiation. *Journal of Neuroscience*, 31(5):1688–1692, 2011.

[430] John R. Sims, Jennifer A. Zimmer, Cynthia D. Evans, Ming Lu, Paul Ardayfio, JonDavid Sparks, Alette M. Wessels, Sergey Shcherbinin, Hong Wang, Emel Serap Monkul Nery, Emily C. Collins, Paul Solomon, Stephen Salloway, Liana G. Apostolova, Oskar Hansson, Craig Ritchie, Dawn A. Brooks, Mark Mintun, Daniel M. Skovronsky, TRAILBLAZER-ALZ 2 Investigators, Rafael Abreu, Pinky Agarwal, Puja Aggarwal, Marc Agronin, Alison Allen, Dario Altamirano, Gustavo Alva, James Andersen, Allan Anderson, Donald Anderson, Jennifer Arnold, Takashi Asada, Yasuhiro Aso, Vikram Atit, Ricardo Ayala, Michael Badruddoja, Hanna Badzio-jagiello, Michal Bajacek, David Barton, David Bear, Sabrina Benjamin, Richard Bergeron, Perminder Bhatia, Sandra Black, Allan Block, Mohammad Bolouri, Wendy Bond, Jean Bouthillier, Sharon Brangman, Bruce Brew, Sarah Brisbin, Toby Brisken, Amy Brodtmann, Mark Brody, Jared Brosch, Celia Brown, Paul Brownstone, Sylwia Bukowczan, Jeffrey Burns, Alicia Cabrera, Horace Capote, Angel Carrasco, Jose Cevallos Yepez, Eric Chavez, Howard Chertkow, Urszula Chyrchel-paszkiewicz, Anthony Ciabarra, Edward Clemmons, Daniel Cohen, Robert Cohen, Ian Cohen, Mauricio Concha, Brian Costell, Denis Crimmins, Yvette Cruz-pagan, Adolfo Cueli, Robert Cupelo, Maciej Czarnecki, David Darby, P.l.j. Dautzenberg, Peter De Deyn, Jose De La Gandara, Kenneth Deck, David Dibenedetto, Mark Dibuono, Eric Dinnerstein, Ahmet Dirican, Shanker Dixit, Jacek Dobryniewski, Ryan Drake, Peter Drysdale, Ranjan Duara, John Duffy, Aaron Ellenbogen, Victor Faradji, Marc Feinberg, Robert Feldman, Simon Fishman, Stephen Flitman, Concetta Forchetti, Ivonne Fraga, Andrew Frank, Benjamin Frishberg, Hiroto Fujigasaki, Hiroyuki Fukase, Ileana Fumero, Kenichi Furihata, Christopher Galloway, Rekha Gandhi, Kristi George, Marcel Germain, Darren Gitelman, Nicholas Goetsch, Danielle Goldfarb, Mark Goldstein, Lawrence Goldstick, Yaneicy Gonzalez Rojas, Ira Goodman, David Greeley, Carl Griffin, Eric Grigsby, Daniel Grosz,

Karl Hafner, David Hart, Sam Henein, Brad Herskowitz, Shinji Higashi, Yasuto Higashi, Gilbert Ho, Jonathan Hodgson, Mark Hohenberg, Larry Hollenbeck, Richard Holub, Tomokatsu Hori, Jakub Hort, Jan Ilkowski, K. Jennifer Ingram, Mitchell Isaac, Mitsunori Ishikawa, Lubos Janu, Mark Johnston, William Julio, William Justiz, Tomotsugu Kaga, Tatsuya Kakigi, Marvin Kalafer, Mikiko Kamijo, Jeffrey Kaplan, Michael Karathanos, Sadao Katayama, Siddharth Kaul, Andrew Keegan, Diana Kerwin, Uzma Khan, Arifulla Khan, Noriyuki Kimura, Gregory Kirk, Gabriela Klodowska, Hisatomo Kowa, Christen Kutz, Joseph Kwentus, Rosalyn Lai, Ayesha Lall, Mary Lawrence, Elly Lee, Ramon Leon, Gary Linker, Pawel Lisewski, Jonathan Liss, Collins Liu, Scott Losk, Ewelina Lukaszyk, Jennifer Lynch, Stephen Macfarlane, Josephine Macsweeney, Nicholas Mannering, Oto Markovic, Donald Marks, Joseph Masdeu, Yutaka Matsui, Kunitaka Matsuishi, Peter Mcallister, Brock Mcconnehey, Alvin Mcelveen, Lora Mcgill, Adam Mecca, Michael Mega, Jason Mensah, Anatol Mickielewicz, Artin Minaeian, Bharat Mocherla, Cynthia Murphy, Paul Murphy, Hirotaka Nagashima, Anil Nair, Malini Nair, John Nardandrea, Marshall Nash, Ziad Nasreddine, Yoshihiko Nishida, Jeffrey Norton, Lazaro Nunez, Jun Ochiai, Takuya Ohkubo, Yasuyuki Okamura, Eugene Okorie, Esteban Olivera, John O'mahony, Omid Omidvar, Desiree Ortiz-Cruz, Alexander Osowa, Michelle Papka, Alicia Parker, Paayal Patel, Ashok Patel, Meenakshi Patel, Claude Patry, Elizabeth Peckham, Michael Pfeffer, Alison Pietras, Michael Plopper, Anton Porsteinsson, Raphael Poulin Robitaille, Niels Prins, Orlando Puente, Marcin Ratajczak, Margaret Rhee, Angela Ritter, Ramon Rodriguez, Lilia Rodriguez Ables, Julio Rojas, Jeffrey Ross, Paule Royer, Jay Rubin, David Russell, Sterre Malou Rutgers, Stephanie Rutrick, Martin Sadowski, Beth Safirstein, Takafumi Sagisaka, Douglas Scharre, Lon Schneider, Curtis Schreiber, Michael Schrift, Paul Schulz, Harvey Schwartz, Julie Schwartzbard, John Scott, Lissette Selem, Pramod Sethi, Sharon Sha, Kenneth Sharlin, Sanjiv Sharma, Thomas Shiovitz, Rajinder Shiwach, Martin Sladek, Bart Sloan, Amanda Smith, Paul Solomon, Ehab Sorial, Evelio Sosa, Mary Stedman, Susan Steen, Lee Stein, Arkadiy Stolyar, John Stoukides, Shinji Sudoh, James Sutton, Junaid Syed, Kinga Szigeti, Hisatsugu Tachibana, Yuichi Takahashi, Amane Tateno, James Dale Taylor, Kelly Taylor, Oleg Tcheremissine, Adly Thebaud, Stephen Thein, Louise Thurman, Steven Toenjes, Hiromasa Toji, Misaki Toma, Duc Tran, Pilar Trueba, Masashi Tsujimoto, Raymond Turner, Akiyoshi Uchiyama,

Dorota Ussorowska, Sanjeev Vaishnavi, Elena Valor, Joel Vandersluis, Alberto Vasquez, Juan Velez, Cherian Verghese, Klaudia Vodickova-borzova, David Watson, David Weidman, David Weisman, Alexander White, Katherine Willingham, Izabela Winkel, Paul Winner, Jaron Winston, Adam Wolff, Hideo Yagi, Hideki Yamamoto, Sanjay Yathiraj, Yasumasa Yoshiyama, and Marzena Zboch. Donanemab in Early Symptomatic Alzheimer Disease: The TRAILBLAZER-ALZ 2 Randomized Clinical Trial. *JAMA*, 330(6):512, August 2023.

[431] Rebecca Sims, Matthew Hill, and Julie Williams. The multiplex model of the genetics of Alzheimer's disease. *Nature Neuroscience*, 23(3):311–322, March 2020.

[432] S S Sisodia. Beta-amyloid precursor protein cleavage by a membrane-bound protease. *Proceedings of the National Academy of Sciences*, 89(13):6075–6079, July 1992.

[433] S. S. Sisodia, E. H. Koo, K. Beyreuther, A. Unterbeck, and D. L. Price. Evidence that β-Amyloid Protein in Alzheimer's Disease Is Not Derived by Normal Processing. *Science*, 248(4954):492–495, April 1990.

[434] Carolina Soares, Bruna Bellaver, Pamela C. L. Ferreira, Guilherme Povala, Cristiano Schaffer Aguzzoli, João Pedro Ferrari-Souza, Hussein Zalzale, Firoza Z. Lussier, Francieli Rohden, Sarah Abbas, Guilherme Bauer-Negrini, Douglas Teixeira Leffa, Andréa Lessa Benedet, Rebecca Langhough, Tobey J. Betthauser, Bradley T. Christian, Rachael E. Wilson, Dana L. Tudorascu, Pedro Rosa-Neto, Thomas K. Karikari, Henrik Zetterberg, Kaj Blennow, Eduardo R. Zimmer, Sterling C. Johnson, and Tharick A. Pascoal. CSF total tau as a proxy of synaptic degeneration. *Nature Communications*, 16(1):8076, August 2025.

[435] Adedamola Saidi Soladogun and Li Zhang. Preexisting Genetic Background Primes the Responses of Human Neurons to Amyloid β. *International Journal of Molecular Sciences*, 26(19):9804, October 2025.

[436] Charlotte Soneson, Michael I. Love, and Mark D. Robinson. Differential analyses for RNA-seq: transcript-level estimates improve gene-level inferences. *F1000Research*, 4:1521, December 2015.

[437] Sheng-Kwei Song, Joong Hee Kim, Shiow-Jiuan Lin, Robert P. Brendza, and David M. Holtzman. Diffusion tensor imaging detects age-dependent white matter changes in a transgenic mouse model with amyloid deposition. *Neurobiology of Disease*, 15(3):640–647, April 2004.

[438] Kai-C. Sonntag, Woo-In Ryu, Kristopher M. Amirault, Ryan A. Healy, Arthur J. Siegel, Donna L. McPhie, Brent Forester, and Bruce M. Cohen. Late-onset Alzheimer's disease is associated with inherent changes in bioenergetics profiles. *Scientific Reports*, 7(1):14038, October 2017.

[439] Kirsty L. Spalding, Olaf Bergmann, Kanar Alkass, Samuel Bernard, Mehran Salehpour, Hagen B. Huttner, Emil Boström, Isabelle Westerlund, Céline Vial, Bruce A. Buchholz, Göran Possnert, Deborah C. Mash, Henrik Druid, and Jonas Frisén. Dynamics of Hippocampal Neurogenesis in Adult Humans. *Cell*, 153(6):1219–1227, June 2013.

[440] Brian R. Sperbera, Susan Leight, Michel Goedert, and V.M.-Y. Lee. Glycogen synthase kinase-3β phosphorylates tau protein at multiple sites in intact cells. *Neuroscience Letters*, 197(2):149–153, September 1995.

[441] Reisa A. Sperling, Paul S. Aisen, Laurel A. Beckett, David A. Bennett, Suzanne Craft, Anne M. Fagan, Takeshi Iwatsubo, Clifford R. Jack, Jeffrey Kaye, Thomas J. Montine, Denise C. Park, Eric M. Reiman, Christopher C. Rowe, Eric Siemers, Yaakov Stern, Kristine Yaffe, Maria C. Carrillo, Bill Thies, Marcelle Morrison-Bogorad, Molly V. Wagster, and Creighton H. Phelps. Toward defining the preclinical stages of Alzheimer's disease: Recommendations from the National Institute on Aging-Alzheimer's Association workgroups on diagnostic guidelines for Alzheimer's disease. *Alzheimer's & Dementia*, 7(3):280–292, May 2011.

[442] Maria Grazia Spillantini, Jill R. Murrell, Michel Goedert, Martin R. Farlow, Aaron Klug, and Bernardino Ghetti. Mutation in the tau gene in familial multiple system tauopathy with presenile dementia. *Proceedings of the National Academy of Sciences*, 95(13):7737–7741, June 1998.

[443] Teresa Sposito, Elisavet Preza, Colin J. Mahoney, Núria Setó-Salvia, Natalie S. Ryan, Huw R. Morris, Charles Arber, Michael J. Devine, Henry Houlden, Thomas T. Warner, Trevor J. Bushell, Michele Zagnoni, Tilo Kunath, Frederick J. Livesey, Nick C. Fox, Martin N. Rossor, John Hardy, and Selina

Wray. Developmental regulation of tau splicing is disrupted in stem cell-derived neurons from frontotemporal dementia patients with the 10 + 16 splice-site mutation in MAPT. *Human Molecular Genetics*, 24(18):5260–5269, September 2015.

[444] K. Stamer, R. Vogel, E. Thies, E. Mandelkow, and E.-M. Mandelkow. Tau blocks traffic of organelles, neurofilaments, and APP vesicles in neurons and enhances oxidative stress. *The Journal of Cell Biology*, 156(6):1051–1063, March 2002.

[445] Samuel H. Sternberg, Sy Redding, Martin Jinek, Eric C. Greene, and Jennifer A. Doudna. DNA interrogation by the CRISPR RNA-guided endonuclease Cas9. *Nature*, 507(7490):62–67, March 2014.

[446] Vicky Steubler, Susanne Erdinger, Michaela K Back, Susann Ludewig, Dominique Fässler, Max Richter, Kang Han, Lutz Slomianka, Irmgard Amrein, Jakob Von Engelhardt, David P Wolfer, Martin Korte, and Ulrike C Müller. Loss of all three APP family members during development impairs synaptic function and plasticity, disrupts learning, and causes an autism-like phenotype. *The EMBO Journal*, 40(12):e107471, June 2021.

[447] Anna Steward, Davina Biel, Anna Dewenter, Sebastian Roemer, Fabian Wagner, Amir Dehsarvi, Saima Rathore, Diana Otero Svaldi, Ixavier Higgins, Matthias Brendel, Martin Dichgans, Sergey Shcherbinin, Michael Ewers, and Nicolai Franzmeier. ApoE4 and Connectivity-Mediated Spreading of Tau Pathology at Lower Amyloid Levels. *JAMA Neurology*, 80(12):1295, December 2023.

[448] W. Blaine Stine, Karie N. Dahlgren, Grant A. Krafft, and Mary Jo LaDu. In Vitro Characterization of Conditions for Amyloid-β Peptide Oligomerization and Fibrillogenesis. *Journal of Biological Chemistry*, 278(13):11612–11622, March 2003.

[449] W. Blaine Stine, Lisa Jungbauer, Chunjiang Yu, and Mary Jo LaDu. Preparing Synthetic Aβ in Different Aggregation States. In Erik D. Roberson, editor, *Alzheimer's Disease and Frontotemporal Dementia*, volume 670, pages 13–32. Humana Press, Totowa, NJ, 2010. Series Title: Methods in Molecular Biology.

[450] W J Strittmatter, A M Saunders, D Schmechel, M Pericak-Vance, J Enghild, G S Salvesen, and A D Roses. Apolipoprotein E: high-avidity binding to beta-amyloid and increased frequency of type 4 allele in late-onset familial Alzheimer disease. *Proceedings of the National Academy of Sciences*, 90(5):1977–1981, March 1993.

[451] Hachiro Sugimoto, Hiroo Ogura, Yasuo Arai, Youichi Iimura, and Yoshiharu Yamanishi. Research and Development of Donepezil Hydrochloride, a New Type of Acetylcholinesterase Inhibitor. *Japanese Journal of Pharmacology*, 89(1):7–20, 2002.

[452] Audrey Sultan, Fabrice Nesslany, Marie Violet, Séverine Bégard, Anne Loyens, Smail Talahari, Zeyni Mansuroglu, Daniel Marzin, Nicolas Sergeant, Sandrine Humez, Morvane Colin, Eliette Bonnefoy, Luc Buée, and Marie-Christine Galas. Nuclear Tau, a Key Player in Neuronal DNA Protection. *Journal of Biological Chemistry*, 286(6):4566–4575, February 2011.

[453] L Sun, S.Y Liu, X.W Zhou, X.C Wang, R Liu, Q Wang, and J.Z Wang. Inhibition of protein phosphatase 2A- and protein phosphatase 1-induced tau hyperphosphorylation and impairment of spatial memory retention in rats. *Neuroscience*, 118(4):1175–1182, June 2003.

[454] Xiangyi Sun, Sili Pan, Dandan Li, Min Su, Honghua Zheng, Yun-wu Zhang, and Yanfang Li. Cell Adhesion Molecule Protocadherin-γC5 Ameliorates Aβ Plaque Pathogenesis by Modulating Astrocyte Function in Alzheimer's Disease. *The Journal of Neuroscience*, 45(10):e0967242025, March 2025.

[455] Hwan-Ching Tai, Bo Y Wang, Alberto Serrano-Pozo, Matthew P Frosch, Tara L Spires-Jones, and Bradley T Hyman. Frequent and symmetric deposition of misfolded tau oligomers within presynaptic and postsynaptic terminals in Alzheimer's disease. *Acta Neuropathologica Communications*, 2(1):146, December 2014.

[456] Kazutoshi Takahashi, Koji Tanabe, Mari Ohnuki, Megumi Narita, Tomoko Ichisaka, Kiichiro Tomoda, and Shinya Yamanaka. Induction of Pluripotent Stem Cells from Adult Human Fibroblasts by Defined Factors. *Cell*, 131(5):861–872, November 2007.

[457] Kazutoshi Takahashi and Shinya Yamanaka. Induction of Pluripotent Stem Cells from Mouse Embryonic and Adult Fibroblast Cultures by Defined Factors. *Cell*, 126(4):663–676, 2006.

[458] Hiroshi Takuma, Shigeki Arawaka, and Hiroshi Mori. Isoforms changes of tau protein during development in various species. *Developmental Brain Research*, 142(2):121–127, May 2003.

[459] Hiroshi Tanahashi, Yoshihiro Mitsunaga, Keikichi Takahashi, Hirokazu Tasaki, Shunzo Watanabe, and Takeshi Tabira. Missense mutation of S182 gene in Japanese familial Alzheimer's disease. *The Lancet*, 346(8972):440, August 1995.

[460] Hitoshi Tanimukai, Inge Grundke-Iqbal, and Khalid Iqbal. Up-regulation of inhibitors of protein phosphatase-2A in Alzheimer's disease. *The American Journal of Pathology*, 166(6):1761–1771, June 2005.

[461] Qing-Qing Tao, Xue Cai, Yan-Yan Xue, Weigang Ge, Liang Yue, Xiao-Yan Li, Rong-Rong Lin, Guo-Ping Peng, Wenhao Jiang, Sainan Li, Kun-Mu Zheng, Bin Jiang, Jian-Ping Jia, Tiannan Guo, and Zhi-Ying Wu. Alzheimer's disease early diagnostic and staging biomarkers revealed by large-scale cerebrospinal fluid and serum proteomic profiling. *The Innovation*, 5(1):100544, January 2024.

[462] Ran Tao, Chunmei Yue, Zhijie Guo, Wenke Guo, Yao Yao, Xianfa Yang, Zhen Shao, Chao Gao, Jianqing Ding, Lu Shen, Shengdi Chen, and Naihe Jing. Subtype-specific neurons from patient iPSCs display distinct neuropathological features of Alzheimer's disease. *Cell Regeneration*, 13(1):21, October 2024.

[463] Marta A Tarczyluk, David A Nagel, H Rhein Parri, Erin Hy Tse, James E Brown, Michael D Coleman, and Eric J Hill. Amyloid β 1-42 Induces Hypometabolism in Human Stem Cell-Derived Neuron and Astrocyte Networks. *Journal of Cerebral Blood Flow & Metabolism*, 35(8):1348–1357, August 2015.

[464] Julia Tcw, Lu Qian, Nina H. Pipalia, Michael J. Chao, Shuang A. Liang, Yang Shi, Bharat R. Jain, Sarah E. Bertelsen, Manav Kapoor, Edoardo Marcora, Elizabeth Sikora, Elizabeth J. Andrews, Alessandra C. Martini, Celeste M. Karch, Elizabeth Head, David M. Holtzman, Bin Zhang, Minghui Wang, Frederick R. Maxfield, Wayne W. Poon, and Alison M. Goate. Cholesterol and matrisome pathways dysregulated in astrocytes and microglia. *Cell*, 185(13):2213–2233.e25, June 2022.

[465] Julia Tcw, Minghui Wang, Anna A. Pimenova, Kathryn R. Bowles, Brigham J. Hartley, Emre Lacin, Saima I. Machlovi, Rawan Abdelaal, Celeste M. Karch, Hemali Phatnani, Paul A. Slesinger, Bin Zhang, Alison M. Goate, and Kristen J. Brennand. An Efficient Platform for Astrocyte Differentiation from Human Induced Pluripotent Stem Cells. *Stem Cell Reports*, 9(2):600–614, August 2017.

[466] Robert D. Terry, Eliezer Masliah, David P. Salmon, Nelson Butters, Richard DeTeresa, Robert Hill, Lawrence A. Hansen, and Robert Katzman. Physical basis of cognitive alterations in alzheimer's disease: Synapse loss is the major correlate of cognitive impairment. *Annals of Neurology*, 30(4):572–580, October 1991.

[467] Joseph Therriault, Marie Vermeiren, Stijn Servaes, Cécile Tissot, Nicholas J. Ashton, Andréa Lessa Benedet, Thomas K. Karikari, Juan Lantero-Rodriguez, Wagner S. Brum, Firoza Z. Lussier, Gleb Bezgin, Jenna Stevenson, Nesrine Rahmouni, Peter Kunach, Yi-Ting Wang, Jaime Fernandez-Arias, Kely Quispialaya Socualaya, Arthur C. Macedo, João Pedro Ferrari-Souza, Pâmela C. L. Ferreira, Bruna Bellaver, Douglas T. Leffa, Eduardo R. Zimmer, Paolo Vitali, Jean-Paul Soucy, Gallen Triana-Baltzer, Hartmuth C. Kolb, Tharick A. Pascoal, Paramita Saha-Chaudhuri, Serge Gauthier, Henrik Zetterberg, Kaj Blennow, and Pedro Rosa-Neto. Association of Phosphorylated Tau Biomarkers With Amyloid Positron Emission Tomography vs Tau Positron Emission Tomography. *JAMA Neurology*, 80(2):188, February 2023.

[468] Tiffany A. Thibaudeau, Raymond T. Anderson, and David M. Smith. A common mechanism of proteasome impairment by neurodegenerative disease-associated oligomers. *Nature Communications*, 9(1):1097, March 2018.

[469] Edda Thies and Eva-Maria Mandelkow. Missorting of Tau in Neurons Causes Degeneration of Synapses That Can Be Rescued by the Kinase MARK2/Par-1. *The Journal of Neuroscience*, 27(11):2896–2907, March 2007.

[470] Q Tian, Z.-Q Lin, X.-C Wang, J Chen, Q Wang, C.-X Gong, and J.-Z Wang. Injection of okadaic acid into the meynert nucleus basalis of rat brain induces decreased acetylcholine level and spatial memory deficit. *Neuroscience*, 126(2):277–284, January 2004.

[471] Ruilin Tian, Mariam A. Gachechiladze, Connor H. Ludwig, Matthew T. Laurie, Jason Y. Hong, Diane Nathaniel, Anika V. Prabhu, Michael S.

Fernandopulle, Rajan Patel, Mehrnoosh Abshari, Michael E. Ward, and Martin Kampmann. CRISPR Interference-Based Platform for Multimodal Genetic Screens in Human iPSC-Derived Neurons. *Neuron*, 104(2):239–255.e12, October 2019.

[472] Matthew K. Tobin, Kianna Musaraca, Ahmed Disouky, Aashutosh Shetti, Abdullah Bheri, William G. Honer, Namhee Kim, Robert J. Dawe, David A. Bennett, Konstantinos Arfanakis, and Orly Lazarov. Human Hippocampal Neurogenesis Persists in Aged Adults and Alzheimer's Disease Patients. *Cell Stem Cell*, 24(6):974–982.e3, June 2019.

[473] Kristine M. Tran, Shimako Kawauchi, Enikö A. Kramár, Narges Rezaie, Heidi Yahan Liang, Jasmine S. Sakr, Angela Gomez-Arboledas, Miguel A. Arreola, Celia Da Cunha, Jimmy Phan, Shuling Wang, Sherilyn Collins, Amber Walker, Kai-Xuan Shi, Jonathan Neumann, Ghassan Filimban, Zechuan Shi, Giedre Milinkeviciute, Dominic I. Javonillo, Katelynn Tran, Magdalena Gantuz, Stefania Forner, Vivek Swarup, Andrea J. Tenner, Frank M. LaFerla, Marcelo A. Wood, Ali Mortazavi, Grant R. MacGregor, and Kim N. Green. A Trem2R47H mouse model without cryptic splicing drives age- and disease-dependent tissue damage and synaptic loss in response to plaques. *Molecular Neurodegeneration*, 18(1):12, February 2023.

[474] Kerry Lee Tucker, Michael Meyer, and Yves-Alain Barde. Neurotrophins are required for nerve growth during development. *Nature Neuroscience*, 4(1):29–37, January 2001.

[475] Tomohiro Umeda, Satomi Maekawa, Tetsuya Kimura, Akihiko Takashima, Takami Tomiyama, and Hiroshi Mori. Neurofibrillary tangle formation by introducing wild-type human tau into APP transgenic mice. *Acta Neuropathologica*, 127(5):685–698, May 2014.

[476] Marija Usenovic, Shahriar Niroomand, Robert E. Drolet, Lihang Yao, Renee C. Gaspar, Nathan G. Hatcher, Joel Schachter, John J. Renger, and Sophie Parmentier-Batteur. Internalized Tau Oligomers Cause Neurodegeneration by Inducing Accumulation of Pathogenic Tau in Human Neurons Derived from Induced Pluripotent Stem Cells. *The Journal of Neuroscience*, 35(42):14234–14250, October 2015.

[477] L. A. Van De Pol, W. M. Van Der Flier, E.S.C. Korf, N. C. Fox, F. Barkhof, and P. Scheltens. Baseline predictors of rates of hippocampal atrophy in mild cognitive impairment. *Neurology*, 69(15):1491–1497, October 2007.

[478] Rik Van Der Kant, Vanessa F. Langness, Cheryl M. Herrera, Daniel A. Williams, Lauren K. Fong, Yves Leestemaker, Evelyne Steenvoorden, Kevin D. Rynearson, Jos F. Brouwers, J. Bernd Helms, Huib Ovaa, Martin Giera, Steven L. Wagner, Anne G. Bang, and Lawrence S.B. Goldstein. Cholesterol Metabolism Is a Druggable Axis that Independently Regulates Tau and Amyloid-β in iPSC-Derived Alzheimer's Disease Neurons. *Cell Stem Cell*, 24(3):363–375.e9, March 2019.

[479] Christopher H. Van Dyck, Chad J. Swanson, Paul Aisen, Randall J. Bateman, Christopher Chen, Michelle Gee, Michio Kanekiyo, David Li, Larisa Reyderman, Sharon Cohen, Lutz Froelich, Sadao Katayama, Marwan Sabbagh, Bruno Vellas, David Watson, Shobha Dhadda, Michael Irizarry, Lynn D. Kramer, and Takeshi Iwatsubo. Lecanemab in Early Alzheimer's Disease. *New England Journal of Medicine*, 388(1):9–21, January 2023.

[480] Tjakko J. Van Ham, Mats A. Holmberg, Annemieke T. Van Der Goot, Eva Teuling, Moises Garcia-Arencibia, Hyun-eui Kim, Deguo Du, Karen L. Thijssen, Marit Wiersma, Rogier Burggraaff, Petra Van Bergeijk, Jeroen van Rheenen, G. Jerre Van Veluw, Robert M.W. Hofstra, David C. Rubinsztein, and Ellen A.A. Nollen. Identification of MOAG-4/SERF as a Regulator of Age-Related Proteotoxicity. *Cell*, 142(4):601–612, August 2010.

[481] Mariana Vargas-Caballero, Franziska Denk, Heike J. Wobst, Emily Arch, Chrysia-Maria Pegasiou, Peter L. Oliver, Olivia A. Shipton, Ole Paulsen, and Richard Wade-Martins. Wild-Type, but Not Mutant N296H, Human Tau Restores Aβ-Mediated Inhibition of LTP in Tau-/- mice. *Frontiers in Neuroscience*, 11:201, April 2017.

[482] Tandis Vazin, K. Aurelia Ball, Hui Lu, Hyungju Park, Yasaman Ataeijannati, Teresa Head-Gordon, Mu-ming Poo, and David V. Schaffer. Efficient derivation of cortical glutamatergic neurons from human pluripotent stem cells: A model system to study neurotoxicity in Alzheimer's disease. *Neurobiology of Disease*, 62:62–72, February 2014.

[483] Prashanthi Vemuri and Clifford R Jack. Role of structural MRI in Alzheimer's disease. *Alzheimer's Research & Therapy*, 2(4):23, August 2010.

[484] Inge M W Verberk, Malika B Laarhuis, Karlijn A Van Den Bosch, Jarith L Ebenau, Mardou Van Leeuwenstijn, Niels D Prins, Philip Scheltens, Charlotte E Teunissen, and Wiesje M Van Der Flier. Serum markers glial fibrillary acidic protein and neurofilament light for prognosis and monitoring in cognitively normal older people: a prospective memory clinic-based cohort study. *The Lancet Healthy Longevity*, 2(2):e87–e95, February 2021.

[485] An Verheyen, Annick Diels, Joyce Dijkmans, Tutu Oyelami, Giulia Meneghello, Liesbeth Mertens, Sofie Versweyveld, Marianne Borgers, Arjan Buist, Pieter Peeters, and Miroslav Cik. Using Human iPSC-Derived Neurons to Model TAU Aggregation. *PLOS ONE*, 10(12):e0146127, December 2015.

[486] An Verheyen, Annick Diels, Joke Reumers, Kirsten Van Hoorde, Ilse Van Den Wyngaert, Constantin Van Outryve d'Ydewalle, An De Bondt, Jacobine Kuijlaars, Louis De Muynck, Ronald De Hoogt, Alexis Bretteville, Steffen Jaensch, Arjan Buist, Alfredo Cabrera-Socorro, Selina Wray, Andreas Ebneth, Peter Roevens, Ines Royaux, and Pieter J. Peeters. Genetically Engineered iPSC-Derived FTDP-17 MAPT Neurons Display Mutation-Specific Neurodegenerative and Neurodevelopmental Phenotypes. *Stem Cell Reports*, 11(2):363–379, August 2018.

[487] Michael Vershinin, Brian C. Carter, David S. Razafsky, Stephen J. King, and Steven P. Gross. Multiple-motor based transport and its regulation by Tau. *Proceedings of the National Academy of Sciences*, 104(1):87–92, January 2007.

[488] Matheus B. Victor, Noelle Leary, Xochitl Luna, Hiruy S. Meharena, Aine Ni Scannail, P. Lorenzo Bozzelli, George Samaan, Mitchell H. Murdock, Djuna Von Maydell, Audrey H. Effenberger, Oyku Cerit, Hsin-Lan Wen, Liwang Liu, Gwyneth Welch, Maeve Bonner, and Li-Huei Tsai. Lipid accumulation induced by APOE4 impairs microglial surveillance of neuronal-network activity. *Cell Stem Cell*, 29(8):1197–1212.e8, August 2022.

[489] Vanessa Vogelsberg-Ragaglia, Theresa Schuck, John Q Trojanowski, and Virginia M.-Y Lee. PP2A mRNA Expression Is Quantitatively Decreased in Alzheimer's Disease Hippocampus. *Experimental Neurology*, 168(2):402–412, April 2001.

[490] Dominic M. Walsh, Igor Klyubin, Julia V. Fadeeva, William K. Cullen, Roger Anwyl, Michael S. Wolfe, Michael J. Rowan, and Dennis J. Selkoe. Naturally secreted oligomers of amyloid β protein potently inhibit hippocampal long-term potentiation in vivo. *Nature*, 416(6880):535–539, April 2002.

[491] Dominic M. Walsh, Aleksey Lomakin, George B. Benedek, Margaret M. Condron, and David B. Teplow. Amyloid β-Protein Fibrillogenesis. *Journal of Biological Chemistry*, 272(35):22364–22372, August 1997.

[492] Chao Wang, Li Fan, Rabia R. Khawaja, Bangyan Liu, Lihong Zhan, Lay Kodama, Marcus Chin, Yaqiao Li, David Le, Yungui Zhou, Carlo Condello, Lea T. Grinberg, William W. Seeley, Bruce L. Miller, Sue-Ann Mok, Jason E. Gestwicki, Ana Maria Cuervo, Wenjie Luo, and Li Gan. Microglial NF-ϰB drives tau spreading and toxicity in a mouse model of tauopathy. *Nature Communications*, 13(1):1969, April 2022.

[493] Chao Wang, Michael E. Ward, Robert Chen, Kai Liu, Tara E. Tracy, Xu Chen, Min Xie, Peter Dongmin Sohn, Connor Ludwig, Anke Meyer-Franke, Celeste M. Karch, Sheng Ding, and Li Gan. Scalable Production of iPSC-Derived Human Neurons to Identify Tau-Lowering Compounds by High-Content Screening. *Stem Cell Reports*, 9(4):1221–1233, October 2017.

[494] Chengzhong Wang, Ramsey Najm, Qin Xu, Dah-eun Jeong, David Walker, Maureen E. Balestra, Seo Yeon Yoon, Heidi Yuan, Gang Li, Zachary A. Miller, Bruce L. Miller, Mary J. Malloy, and Yadong Huang. Gain of toxic apolipoprotein E4 effects in human iPSC-derived neurons is ameliorated by a small-molecule structure corrector. *Nature Medicine*, 24(5):647–657, May 2018.

[495] Jian-Zhi Wang, Cheng-Xin Gong, Tanweer Zaidi, Inge Grundke-Iqbal, and Khalid Iqbal. Dephosphorylation of Alzheimer Paired Helical Filaments by Protein Phosphatase-2A and -2B. *Journal of Biological Chemistry*, 270(9):4854–4860, March 1995.

[496] Jian-Zhi Wang, Inge Grundke-Iqbal, and Khalid Iqbal. Kinases and phosphatases and tau sites involved in Alzheimer neurofibrillary degeneration. *European Journal of Neuroscience*, 25(1):59–68, January 2007.

[497] Xiao-liang Wang, Qing Liu, Guo-Jun Chen, Mei-ling Li, and Yan-hui Ding. Overexpression of MTERF4 promotes the amyloidogenic processing of APP by

inhibiting ADAM10. *Biochemical and Biophysical Research Communications*, 482(4):928–934, January 2017.

[498] Yipeng Wang and Eckhard Mandelkow. Tau in physiology and pathology. *Nature Reviews Neuroscience*, 17(1):22–35, January 2016.

[499] Naoto Watamura, Martha S. Foiani, Sumi Bez, Mathieu Bourdenx, Alessia Santambrogio, Claire Frodsham, Elena Camporesi, Gunnar Brinkmalm, Henrik Zetterberg, Saisha Patel, Naoko Kamano, Mika Takahashi, Javier Rueda-Carrasco, Loukia Katsouri, Stephanie Fowler, Emir Turkes, Shoko Hashimoto, Hiroki Sasaguri, Takashi Saito, Afm Saiful Islam, Seico Benner, Toshihiro Endo, Katsuji Kobayashi, Chiho Ishida, Michele Vendruscolo, Masahito Yamada, Karen E. Duff, and Takaomi C. Saido. In vivo hyperphosphorylation of tau is associated with synaptic loss and behavioral abnormalities in the absence of tau seeds. *Nature Neuroscience*, 28(2):293–307, February 2025.

[500] Naoto Watamura, Kaori Sato, Gen Shiihashi, Ayami Iwasaki, Naoko Kamano, Mika Takahashi, Misaki Sekiguchi, Naomi Mihira, Ryo Fujioka, Kenichi Nagata, Shoko Hashimoto, Takashi Saito, Toshio Ohshima, Takaomi C. Saido, and Hiroki Sasaguri. An isogenic panel of *App* knock-in mouse models: Profiling β-secretase inhibition and endosomal abnormalities. *Science Advances*, 8(23):eabm6155, June 2022.

[501] Ian Weidling, Christina N. Preiss, Sarah E. Chancellor, Gyan Srivastava, Lauren Gibilisco, Gen Lin, Melanie Shackett Brennan, Janice Lee, Lindsay M. Roth, Olga Morozova, Kyong Nyon Nam, Nehal R. Patel, Qing Liu, J. K. Thomas, Peter Reinhardt, Ruven Wilkens, Dagmar E. Ehrnhoefer, Andreas Striebinger, Stefan Barghorn, Christina Xanthopoulos, Marie-Theres Weil, Sandra Biesinger, Miroslav Cik, Nandini Romanul, Kiran Yanamandra, Alessandra M. Welker, Jessica Wu, Laura Gasparini, Jan Stöhr, Xavier Langlois, and Justine D. Manos. hiPSC-neurons recapitulate the subtype-specific cell intrinsic nature of susceptibility to neurodegenerative disease-relevant aggregation. *Acta Neuropathologica Communications*, 13(1):108, May 2025.

[502] Michael W. Weiner, Dallas P. Veitch, Paul S. Aisen, Laurel A. Beckett, Nigel J. Cairns, Robert C. Green, Danielle Harvey, Clifford R. Jack, William Jagust, Enchi Liu, John C. Morris, Ronald C. Petersen, Andrew J. Saykin, Mark E.

Schmidt, Leslie Shaw, Li Shen, Judith A. Siuciak, Holly Soares, Arthur W. Toga, John Q. Trojanowski, and Alzheimer's Disease Neuroimaging Initiative. The Alzheimer's Disease Neuroimaging Initiative: A review of papers published since its inception. *Alzheimer's & Dementia*, 9(5), September 2013.

[503] M.J West, P.D Coleman, D.G Flood, and J.C Troncoso. Differences in the pattern of hippocampal neuronal loss in normal ageing and Alzheimer's disease. *The Lancet*, 344(8925):769–772, September 1994.

[504] Michalina Wezyk, Aleksandra Szybinska, Joanna Wojsiat, Marcelina Szczerba, Kelly Day, Harriet Ronnholm, Malin Kele, Mariusz Berdynski, Beata Peplonska, Jakub Piotr Fichna, Jan Ilkowski, Maria Styczynska, Anna Barczak, Marzena Zboch, Anna Filipek-Gliszczynska, Krzysztof Bojakowski, Magdalena Skrzypczak, Krzysztof Ginalski, Michal Kabza, Izabela Makalowska, Maria Barcikowska-Kotowicz, Urszula Wojda, Anna Falk, and Cezary Zekanowski. Overactive BRCA1 Affects Presenilin 1 in Induced Pluripotent Stem Cell-Derived Neurons in Alzheimer's Disease. *Journal of Alzheimer's Disease*, 62(1):175–202, February 2018.

[505] Pj Whitehouse, Dl Price, Rg Struble, Aw Clark, Jt Coyle, and Mahlon R. DeLong. Alzheimer's Disease and Senile Dementia: Loss of Neurons in the Basal Forebrain. *Science*, 215(4537):1237–1239, March 1982.

[506] Jennifer L. Whitwell. Progression of Atrophy in Alzheimer's Disease and Related Disorders. *Neurotoxicity Research*, 18(3-4):339–346, November 2010.

[507] Ayesha Wickramasinghe, Yiling Xiao, Naohiro Kobayashi, Songlin Wang, Kathryn P. Scherpelz, Toshio Yamazaki, Stephen C. Meredith, and Yoshitaka Ishii. Sensitivity-Enhanced Solid-State NMR Detection of Structural Differences and Unique Polymorphs in Pico- to Nanomolar Amounts of Brain-Derived and Synthetic 42-Residue Amyloid-β Fibrils. *Journal of the American Chemical Society*, 143(30):11462–11472, August 2021.

[508] Douglas P. Wightman, Iris E. Jansen, Jeanne E. Savage, Alexey A. Shadrin, Shahram Bahrami, Dominic Holland, Arvid Rongve, Sigrid Børte, Bendik S. Winsvold, Ole Kristian Drange, Amy E. Martinsen, Anne Heidi Skogholt, Cristen Willer, Geir Bråthen, Ingunn Bosnes, Jonas Bille Nielsen, Lars G. Fritsche, Laurent F. Thomas, Linda M. Pedersen, Maiken E. Gabrielsen, Marianne Bakke Johnsen, Tore Wergeland Meisingset, Wei Zhou, Petroula

Proitsi, Angela Hodges, Richard Dobson, Latha Velayudhan, Karl Heilbron, Adam Auton, 23andMe Research Team, Michelle Agee, Stella Aslibekyan, Elizabeth Babalola, Robert K. Bell, Jessica Bielenberg, Katarzyna Bryc, Emily Bullis, Briana Cameron, Daniella Coker, Gabriel Cuellar Partida, Devika Dhamija, Sayantan Das, Sarah L. Elson, Teresa Filshtein, Kipper Fletez-Brant, Pierre Fontanillas, Will Freyman, Pooja M. Gandhi, Barry Hicks, David A. Hinds, Karen E. Huber, Ethan M. Jewett, Yunxuan Jiang, Aaron Kleinman, Katelyn Kukar, Vanessa Lane, Keng-Han Lin, Maya Lowe, Marie K. Luff, Jey C. McCreight, Matthew H. McIntyre, Kimberly F. McManus, Steven J. Micheletti, Meghan E. Moreno, Joanna L. Mountain, Sahar V. Mozaffari, Priyanka Nandakumar, Elizabeth S. Noblin, Jared O'Connell, Aaron A. Petrakovitz, G. David Poznik, Morgan Schumacher, Anjali J. Shastri, Janie F. Shelton, Jingchunzi Shi, Suyash Shringarpure, Chao Tian, Vinh Tran, Joyce Y. Tung, Xin Wang, Wei Wang, Catherine H. Weldon, Peter Wilton, Julia M. Sealock, Lea K. Davis, Nancy L. Pedersen, Chandra A. Reynolds, Ida K. Karlsson, Sigurdur Magnusson, Hreinn Stefansson, Steinunn Thordardottir, Palmi V. Jonsson, Jon Snaedal, Anna Zettergren, Ingmar Skoog, Silke Kern, Margda Waern, Henrik Zetterberg, Kaj Blennow, Eystein Stordal, Kristian Hveem, John-Anker Zwart, Lavinia Athanasiu, Per Selnes, Ingvild Saltvedt, Sigrid B. Sando, Ingun Ulstein, Srdjan Djurovic, Tormod Fladby, Dag Aarsland, Geir Selbæk, Stephan Ripke, Kari Stefansson, Ole A. Andreassen, and Danielle Posthuma. A genome-wide association study with 1,126,563 individuals identifies new risk loci for Alzheimer's disease. *Nature Genetics*, 53(9):1276–1282, September 2021.

[509] Julian Daniel Sunday Willett, Mohammad Waqas, Younjung Choi, Tiffany Ngai, Kristina Mullin, Rudolph E. Tanzi, and Dmitry Prokopenko. Identification of 16 novel Alzheimer's disease loci using multi-ancestry meta-analyses. *Alzheimer's & Dementia*, 21(2):e14592, February 2025.

[510] Dylan M. Williams, Sami Heikkinen, Mikko Hiltunen, FinnGen, Neil M. Davies, and Emma L. Anderson. The proportion of Alzheimer's disease attributable to apolipoprotein E. *npj Dementia*, 2(1):1, January 2026.

[511] Thomas S. Wingo. Autosomal Recessive Causes Likely in Early-Onset Alzheimer Disease. *Archives of Neurology*, 69(1):59, January 2012.

[512] K. E. Wisniewski, H. M. Wisniewski, and G. Y. Wen. Occurrence of neuropathological changes and dementia of Alzheimer's disease in Down's syndrome. *Annals of Neurology*, 17(3):278–282, March 1985.

[513] Michael S. Wolfe. Tau Mutations in Neurodegenerative Diseases. *Journal of Biological Chemistry*, 284(10):6021–6025, March 2009.

[514] Michael S. Wolfe, Weiming Xia, Beth L. Ostaszewski, Thekla S. Diehl, W. Taylor Kimberly, and Dennis J. Selkoe. Two transmembrane aspartates in presenilin-1 required for presenilin endoproteolysis and γ-secretase activity. *Nature*, 398(6727):513–517, April 1999.

[515] Hongtao Wu, Dunyue Lu, Hao Jiang, Ye Xiong, Changsheng Qu, Bo Li, Asim Mahmood, Dong Zhou, and Michael Chopp. Simvastatin-Mediated Upregulation of VEGF and BDNF, Activation of the PI3K/Akt Pathway, and Increase of Neurogenesis Are Associated with Therapeutic Improvement after Traumatic Brain Injury. *Journal of Neurotrauma*, 25(2):130–139, February 2008.

[516] Jinsong Xiao, George Perry, Juan Troncoso, and Mervyn J. Monteiro. α-Calcium-Calmodulin-Dependent Kinase II is Associated with Paired Helical Filaments of Alzheimers Disease:. *Journal of Neuropathology and Experimental Neurology*, 55(9):954–963, September 1996.

[517] Xiaohong Xu, Ying Lei, Jie Luo, Jamie Wang, Shu Zhang, Xiu-Juan Yang, Mu Sun, Emile Nuwaysir, Guohuang Fan, Jing Zhao, Lei Lei, and Zhong Zhong. Prevention of β-amyloid induced toxicity in human iPS cell-derived neurons by inhibition of Cyclin-dependent kinases and associated cell cycle events. *Stem Cell Research*, 10(2):213–227, March 2013.

[518] Takuya Yagi, Daisuke Ito, Yohei Okada, Wado Akamatsu, Yoshihiro Nihei, Takahito Yoshizaki, Shinya Yamanaka, Hideyuki Okano, and Norihiro Suzuki. Modeling familial Alzheimer's disease with induced pluripotent stem cells. *Human Molecular Genetics*, 20(23):4530–4539, December 2011.

[519] Hyun-Sik Yang, Ling Teng, Daniel Kang, Vilas Menon, Tian Ge, Hilary K. Finucane, Aaron P. Schultz, Michael Properzi, Hans-Ulrich Klein, Lori B. Chibnik, Julie A. Schneider, David A. Bennett, Timothy J. Hohman, Richard P. Mayeux, Keith A. Johnson, Philip L. De Jager, and Reisa A. Sperling.

Cell-type-specific Alzheimer's disease polygenic risk scores are associated with distinct disease processes in Alzheimer's disease. *Nature Communications*, 14(1):7659, November 2023.

[520] Juan Yang, Hanzhi Zhao, Yu Ma, Guilai Shi, Jian Song, Yu Tang, Song Li, Ting Li, Nan Liu, Fan Tang, Junjie Gu, Lingling Zhang, Zhuohua Zhang, Xiaohui Zhang, Ying Jin, and Weidong Le. Early pathogenic event of Alzheimer's disease documented in iPSCs from patients with PSEN1 mutations. *Oncotarget*, 8(5):7900–7913, January 2017.

[521] Yang Yang, Diana Arseni, Wenjuan Zhang, Melissa Huang, Sofia Lövestam, Manuel Schweighauser, Abhay Kotecha, Alexey G. Murzin, Sew Y. Peak-Chew, Jennifer Macdonald, Isabelle Lavenir, Holly J. Garringer, Ellen Gelpi, Kathy L. Newell, Gabor G. Kovacs, Ruben Vidal, Bernardino Ghetti, Benjamin Ryskeldi-Falcon, Sjors H. W. Scheres, and Michel Goedert. Cryo-EM structures of amyloid-β 42 filaments from human brains. *Science*, 375(6577):167–172, January 2022.

[522] Yang Yang, Yasuhiro Ogawa, Kristian L. Hedstrom, and Matthew N. Rasband. βIV spectrin is recruited to axon initial segments and nodes of Ranvier by ankyrinG. *The Journal of Cell Biology*, 176(4):509–519, February 2007.

[523] Huakui Yu, Carlos A. Saura, Se-Young Choi, Linus D. Sun, Xudong Yang, Melissa Handler, Takeshi Kawarabayashi, Linda Younkin, Bogdan Fedeles, Matthew A. Wilson, Steve Younkin, Eric R. Kandel, Alfredo Kirkwood, and Jie Shen. APP Processing and Synaptic Plasticity in Presenilin-1 Conditional Knockout Mice. *Neuron*, 31(5):713–726, September 2001.

[524] Liping Yu, Rohinton Edalji, John E. Harlan, Thomas F. Holzman, Ana Pereda Lopez, Boris Labkovsky, Heinz Hillen, Stefan Barghorn, Ulrich Ebert, Paul L. Richardson, Laura Miesbauer, Larry Solomon, Diane Bartley, Karl Walter, Robert W. Johnson, Philip J. Hajduk, and Edward T. Olejniczak. Structural Characterization of a Soluble Amyloid β-Peptide Oligomer. *Biochemistry*, 48(9):1870–1877, March 2009.

[525] Yang Yu, Xiaoqin Run, Zhihou Liang, Yi Li, Fei Liu, Ying Liu, Khalid Iqbal, Inge Grundke-Iqbal, and Cheng-Xin Gong. Developmental regulation of tau phosphorylation, tau kinases, and tau phosphatases. *Journal of Neurochemistry*, 108(6):1480–1494, March 2009.

[526] Hans Zempel, Julia Luedtke, Yatender Kumar, Jacek Biernat, Hana Dawson, Eckhard Mandelkow, and Eva-Maria Mandelkow. Amyloid-β oligomers induce synaptic damage via Tau-dependent microtubule severing by TTLL6 and spastin. *The EMBO Journal*, 32(22):2920–2937, November 2013.

[527] Hans Zempel, Edda Thies, Eckhard Mandelkow, and Eva-Maria Mandelkow. Aβ Oligomers Cause Localized Ca^{2+} Elevation, Missorting of Endogenous Tau into Dendrites, Tau Phosphorylation, and Destruction of Microtubules and Spines. *The Journal of Neuroscience*, 30(36):11938–11950, September 2010.

[528] Henrik Zetterberg, Mona Pedersen, Karin Lind, Maria Svensson, Sindre Rolstad, Carl Eckerström, Steinar Syversen, Ulla-Britt Mattsson, Christina Ysander, Niklas Mattsson, Arto Nordlund, Hugo Vanderstichele, Eugeen Vanmechelen, Michael Jonsson, Åke Edman, Kaj Blennow, and Anders Wallin. Intra-Individual Stability of CSF Biomarkers for Alzheimer's Disease over Two Years. *Journal of Alzheimer's Disease*, 12(3):255–260, November 2007.

[529] Hua Zhang, the Alzheimer's Disease Neuroimaging Initiative, Min Su Kang, Kok Pin Ng, Tharick A. Pascoal, Pedro Rosa-Neto, and Serge Gauthier. Cerebrospinal fluid synaptosomal-associated protein 25 is a key player in synaptic degeneration in mild cognitive impairment and Alzheimer's disease. *Alzheimer's Research & Therapy*, 10(1):80, December 2018.

[530] Wenjuan Zhang, Benjamin Falcon, Alexey G Murzin, Juan Fan, R Anthony Crowther, Michel Goedert, and Sjors Hw Scheres. Heparin-induced tau filaments are polymorphic and differ from those in Alzheimer's and Pick's diseases. *eLife*, 8:e43584, February 2019.

[531] Wenjuan Zhang, Airi Tarutani, Kathy L. Newell, Alexey G. Murzin, Tomoyasu Matsubara, Benjamin Falcon, Ruben Vidal, Holly J. Garringer, Yang Shi, Takeshi Ikeuchi, Shigeo Murayama, Bernardino Ghetti, Masato Hasegawa, Michel Goedert, and Sjors H. W. Scheres. Novel tau filament fold in corticobasal degeneration. *Nature*, 580(7802):283–287, April 2020.

[532] Yingsha Zhang, ChangHui Pak, Yan Han, Henrik Ahlenius, Zhenjie Zhang, Soham Chanda, Samuele Marro, Christopher Patzke, Claudio Acuna, Jason Covy, Wei Xu, Nan Yang, Tamas Danko, Lu Chen, Marius Wernig, and Thomas C. Südhof. Rapid Single-Step Induction of Functional Neurons from Human Pluripotent Stem Cells. *Neuron*, 78(5):785–798, June 2013.

[533] Zhen Zhao, Abhay P Sagare, Qingyi Ma, Matthew R Halliday, Pan Kong, Kassandra Kisler, Ethan A Winkler, Anita Ramanathan, Takahisa Kanekiyo, Guojun Bu, Nelly Chuqui Owens, Sanket V Rege, Gabriel Si, Ashim Ahuja, Donghui Zhu, Carol A Miller, Julie A Schneider, Manami Maeda, Takahiro Maeda, Tohru Sugawara, Justin K Ichida, and Berislav V Zlokovic. Central role for PICALM in amyloid-β blood-brain barrier transcytosis and clearance. *Nature Neuroscience*, 18(7):978–987, July 2015.

[534] Lujia Zhou, Joseph McInnes, Keimpe Wierda, Matthew Holt, Abigail G. Herrmann, Rosemary J. Jackson, Yu-Chun Wang, Jef Swerts, Jelle Beyens, Katarzyna Miskiewicz, Sven Vilain, Ilse Dewachter, Diederik Moechars, Bart De Strooper, Tara L. Spires-Jones, Joris De Wit, and Patrik Verstreken. Tau association with synaptic vesicles causes presynaptic dysfunction. *Nature Communications*, 8(1):15295, May 2017.

[535] Yi Zhou, Yijing Su, Shiying Li, Benjamin C. Kennedy, Daniel Y. Zhang, Allison M. Bond, Yusha Sun, Fadi Jacob, Lu Lu, Peng Hu, Angela N. Viaene, Ingo Helbig, Sudha K. Kessler, Timothy Lucas, Ryan D. Salinas, Xiaosong Gu, H. Isaac Chen, Hao Wu, Joel E. Kleinman, Thomas M. Hyde, David W. Nauen, Daniel R. Weinberger, Guo-li Ming, and Hongjun Song. Molecular landscapes of human hippocampal immature neurons across lifespan. *Nature*, 607(7919):527–533, July 2022.

[536] Yingyue Zhou, Wilbur M. Song, Prabhakar S. Andhey, Amanda Swain, Tyler Levy, Kelly R. Miller, Pietro L. Poliani, Manuela Cominelli, Shikha Grover, Susan Gilfillan, Marina Cella, Tyler K. Ulland, Konstantin Zaitsev, Akinori Miyashita, Takeshi Ikeuchi, Makoto Sainouchi, Akiyoshi Kakita, David A. Bennett, Julie A. Schneider, Michael R. Nichols, Sean A. Beausoleil, Jason D. Ulrich, David M. Holtzman, Maxim N. Artyomov, and Marco Colonna. Human and mouse single-nucleus transcriptomics reveal TREM2-dependent and TREM2-independent cellular responses in Alzheimer's disease. *Nature Medicine*, 26(1):131–142, January 2020.

[537] C. Zimmer. Dynamics of Cux2 Expression Suggests that an Early Pool of SVZ Precursors is Fated to Become Upper Cortical Layer Neurons. *Cerebral Cortex*, 14(12):1408–1420, May 2004.

[538] Benedikt Zott, Manuel M. Simon, Wei Hong, Felix Unger, Hsing-Jung Chen-Engerer, Matthew P. Frosch, Bert Sakmann, Dominic M. Walsh, and Arthur Konnerth. A vicious cycle of β amyloid–dependent neuronal hyperactivation. *Science*, 365(6453):559–565, August 2019.